

**Synthetic receptors as sensors**

Guest editor: Eric V. Anslyn

Department of Chemistry and Biochemistry, 1 Longhorn Way, A5300 The University of Texas,  
Austin, TX 78712, USA

**Contents**

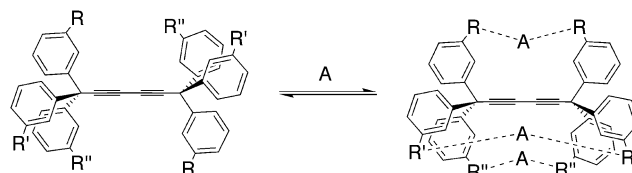
Announcement: Tetrahedron Symposia-in-Print  
Preface

pp 11051–11053  
pp 11055–11056

**ARTICLES**

Exploring the effects of cooperative interactions on affinity using a pinwheel sensor system  
Paul D. Jones and Timothy E. Glass\*

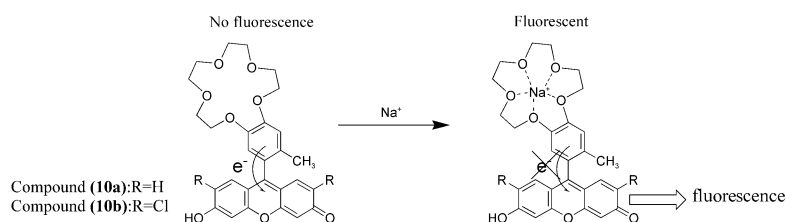
pp 11057–11065



Rational design of novel photoinduced electron transfer type fluorescent  
probes for sodium cation

pp 11067–11073

Suguru Kenmoku, Yasuteru Urano, Koujiro Kanda, Hirotatsu Kojima, Kazuya Kikuchi  
and Tetuso Nagano\*

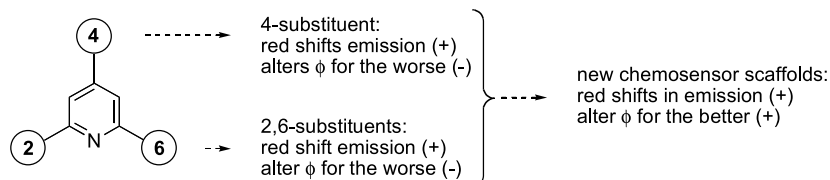


## Structural studies of biarylpyridines fluorophores lead to the identification of promising long wavelength emitters for use in fluorescent chemosensors

pp 11075–11087

A. G. Fang, J. V. Mello and N. S. Finney\*

Study of polyarylpyridine fluorophores:

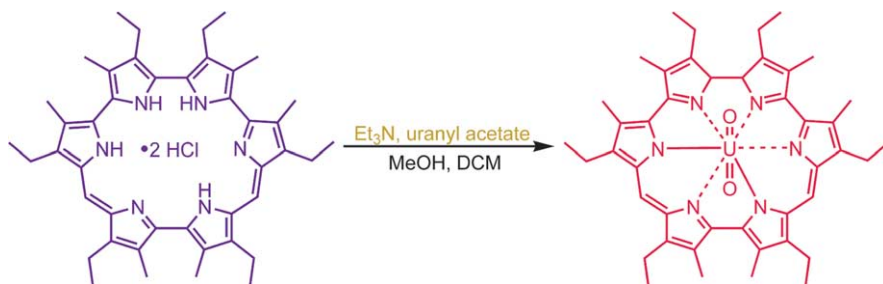


## Hexaphyrin(1.0.1.0.0.0). A new colorimetric actinide sensor

pp 11089–11097

Jonathan L. Sessler,\* Patricia J. Melfi, Daniel Seidel, Anne E. V. Gorden, Doris K. Ford, Philip D. Palmer and C. Drew Tait

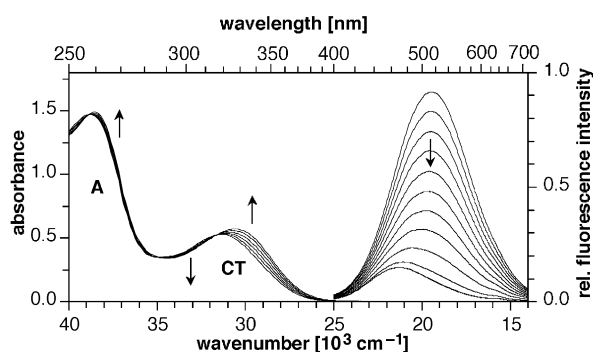
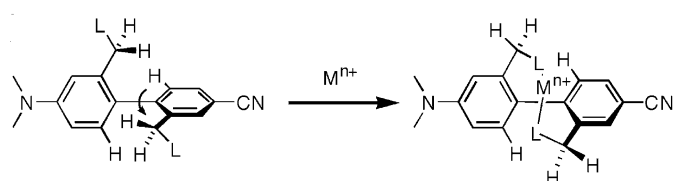
Hexaphyrin(1.0.1.0.0.0) changes color upon complexation with the dioxo actinide cations,  $\text{UO}_2^{2+}$ ,  $\text{NpO}_2^{2+}$  and  $\text{PuO}_2^{2+}$ , while initial studies indicate it only weakly interacts with transition metals or lanthanides, making it attractive as a colorimetric actinide sensor. Semi-quantitative studies carried out in  $\text{MeOH}-\text{CH}_2\text{Cl}_2$  (95:5, v/v), reveal a naked eye detection limit for  $\text{UO}_2^{2+}$  sensing of ca. 5.8 ppm.



## Fluorescence sensing based on cation-induced conformational switching: copper-selective modulation of the photoinduced intramolecular charge transfer of a donor–acceptor biphenyl fluorophore

pp 11099–11107

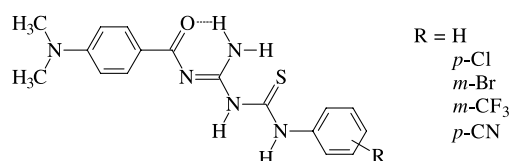
John Cody and Christoph J. Fahrni\*



## Ratiometric dual fluorescent receptors for anions under intramolecular charge transfer mechanism

pp 11109–11115

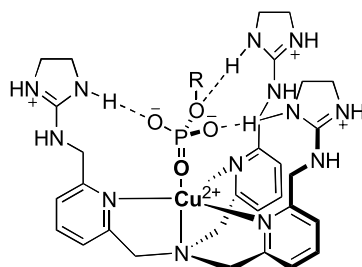
Zhen-Chang Wen and Yun-Bao Jiang\*



**Molecular recognition and indicator-displacement assays for phosphoesters**

pp 11117–11124

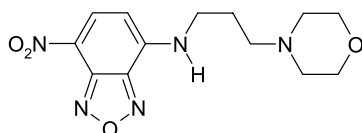
Tianzhi Zhang and Eric V. Anslyn\*



**Fluorescent photoionic devices with two receptors and two switching mechanisms: applications to pH sensors and implications for metal ion detection**

pp 11125–11131

John F. Callan, A. Prasanna de Silva,\* Joanne Ferguson, Allen J. M. Huxley and Aoife M. O'Brien

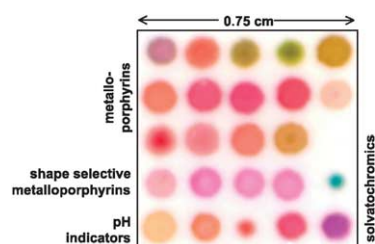


4-(Dialkylaminoalkylamino)-7-nitrobenzo-2-oxa-1,3-diazoles are fluorescent pH sensors which combine internal charge transfer (ICT) and photoinduced electron transfer (PET) ideas.

**Colorimetric sensor arrays for molecular recognition**

pp 11133–11138

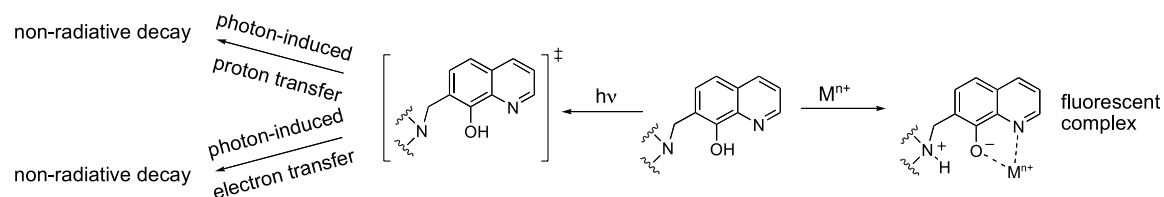
Kenneth S. Suslick,\* Neal A. Rakow and Avijit Sen



**Origins of ‘on-off’ fluorescent behavior of 8-hydroxyquinoline containing chemosensors**

pp 11139–11144

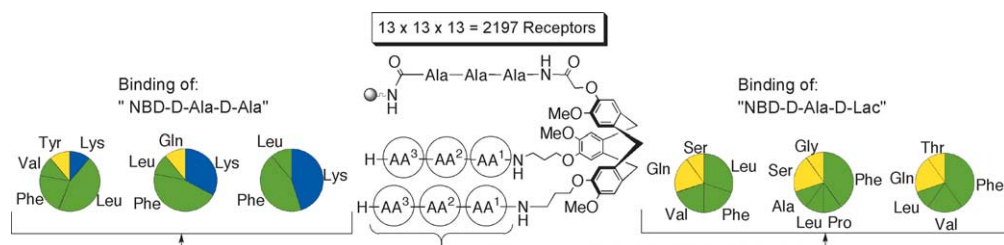
R. Todd Bronson, Marco Montalti, Luca Prodi,\* Nelsi Zaccheroni, Randy D. Lamb, N. Kent Dalley, Reed M. Izatt, Jerald S. Bradshaw and Paul B. Savage\*



### Selection of synthetic receptors capable of sensing the difference in binding of D-Ala-D-Ala or D-Ala-D-Lac ligands by screening of a combinatorial CTV-based library

pp 11145–11157

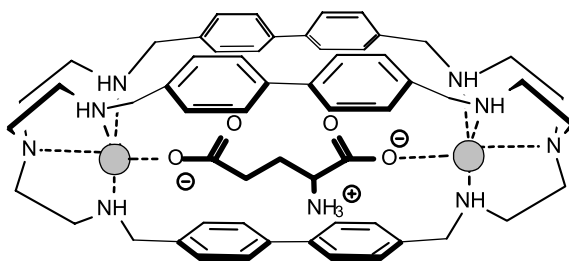
Cristina Chamorro and Rob M. J. Liskamp\*



### Fluorescent detection of glutamate with a dicopper(II) polyamine cage

pp 11159–11162

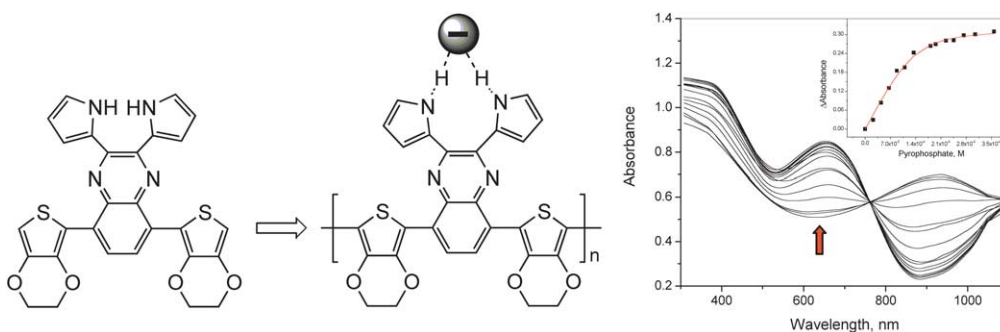
Marco Bonizzoni, Luigi Fabbrizzi,\* Giulio Piovani and Angelo Taglietti



### Materials chemistry approach to anion-sensor design

pp 11163–11168

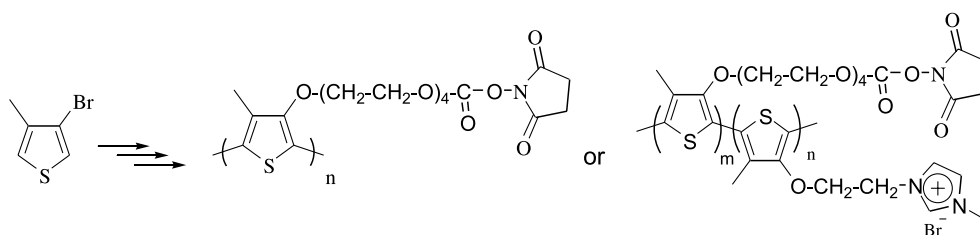
Pavel Anzenbacher, Jr.,\* Karolina Jursikova, Dmitry Aldakov, Manuel Marquez and Radek Pohl



### Functional polythiophenes as optical chemo- and biosensors

pp 11169–11173

Maité Béra-Abérem, Hoang-Anh Ho and Mario Leclerc\*

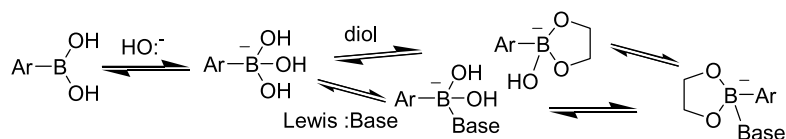




**Binary and ternary phenylboronic acid complexes with saccharides and Lewis bases**

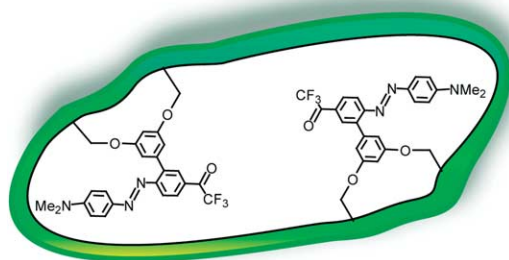
pp 11175–11190

L. I. Bosch, T. M. Fyles\* and T. D. James\*

**Integrating chemosensors for amine-containing compounds into cross-linked dendritic hosts**

pp 11191–11204

Eric Mertz, Stephanie L. Elmer, Amy M. Balija and Steven C. Zimmerman\*

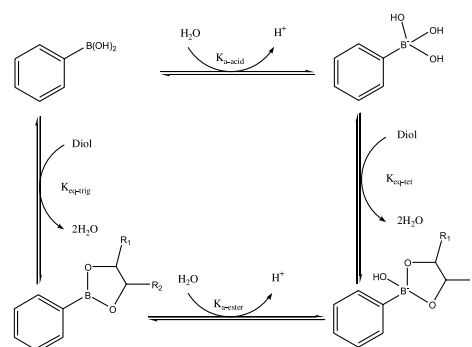


Cross-linked dendrimeric host for 2-point covalent binding of diamines.

**The relationship among  $pK_a$ , pH, and binding constants in the interactions between boronic acids and diols—it is not as simple as it appears**

pp 11205–11209

Jun Yan, Greg Springsteen, Susan Deeter and Binghe Wang\*

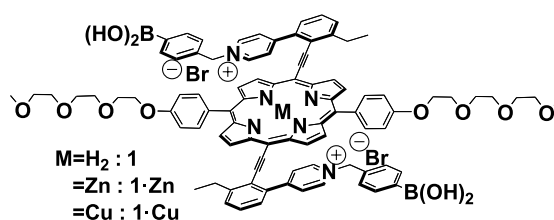


i+

**Mono- and oligosaccharide sensing by phenylboronic acid-appended 5,15-bis(diarylethynyl)porphyrin complexes**

pp 11211–11218

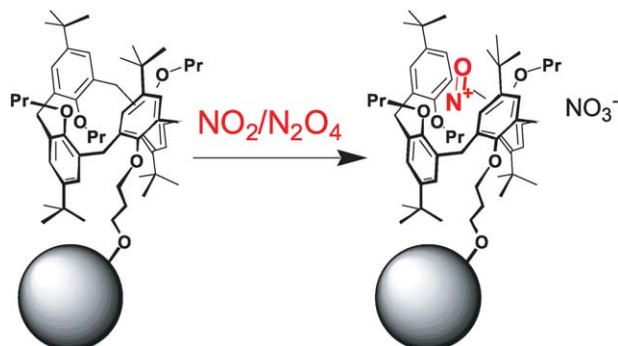
Osamu Hirata, Yohei Kubo, Masayuki Takeuchi\* and Seiji Shinkai\*



**Polymer-supported calix[4]arenes for sensing and conversion of  $\text{NO}_2/\text{N}_2\text{O}_4$** 

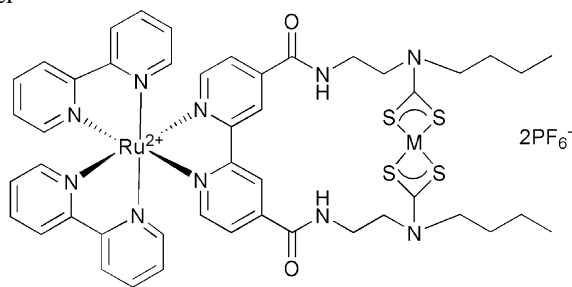
pp 11219–11225

Yanlong Kang and Dmitry M. Rudkevich\*

**Heterodinuclear ruthenium(II) bipyridyl-transition metal dithiocarbamate macrocycles for anion recognition and sensing**

pp 11227–11238

Michelle D. Pratt and Paul D. Beer\*

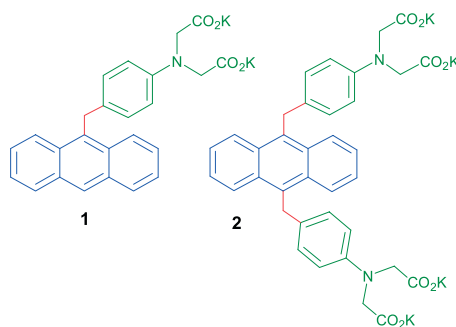


M = Ni(II), Cu(II), or Zn(II)

**Highly selective fluorescent chemosensors for cadmium in water**

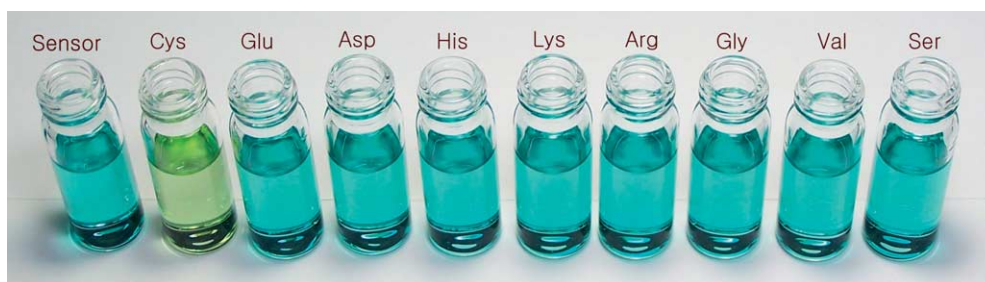
pp 11239–11249

Thorfinnur Gunnlaugsson,\* T. Clive Lee and Raman Parkesh

**Rationally designed chromogenic chemosensor that detects cysteine in aqueous solution with remarkable selectivity**

pp 11251–11257

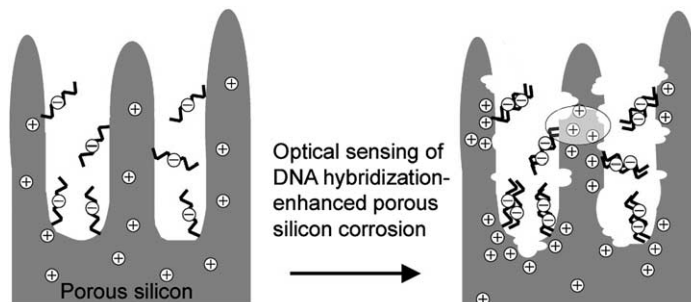
Min Su Han and Dong H. Kim\*



**DNA hybridization-enhanced porous silicon corrosion: mechanistic investigations and prospect for optical interferometric biosensing**

pp 11259–11267

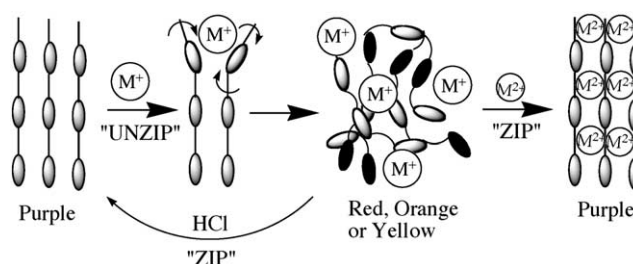
Claudia Steinem, Andreas Janshoff, Victor S.-Y. Lin, Nicolas H. Völcker and M. Reza Ghadiri\*

**Regioregular poly(thiophene-3-alkanoic acid)s: water soluble conducting polymers suitable for chromatic chemosensing in solution and solid state**

pp 11269–11275

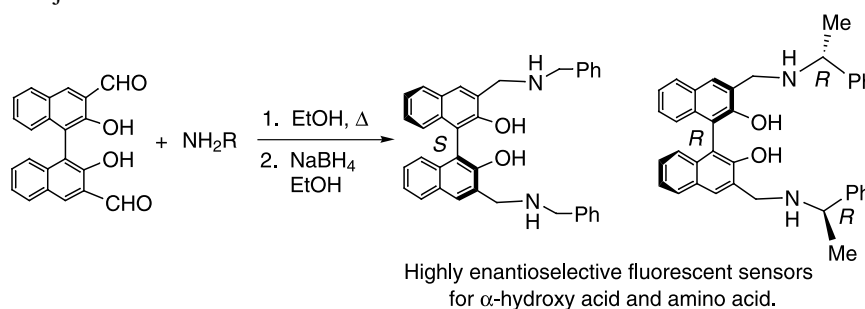
Paul C. Ewbank, Robert S. Loewe, Lei Zhai, Jerry Reddinger, Geneviève Sauvé and Richard D. McCullough\*

The self-assembly and disassembly of regioregular poly(thiophene-3-alkanoic acid)s were driven by the analytes. The conformational changes resulted in clear visual color changes. These polymers show great potential in the development of sensors.

**Enantioselective fluorescent recognition of chiral acids by 3- and 3,3'-aminomethyl substituted BINOLs**

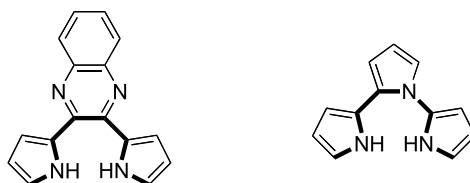
pp 11277–11281

Jing Lin, Amaresh R. Rajaram and Lin Pu\*

**A new terpyrrolic analogue of dipyrrolylquinoxalines: an efficient optical-based sensor for anions in organic media**

pp 11283–11291

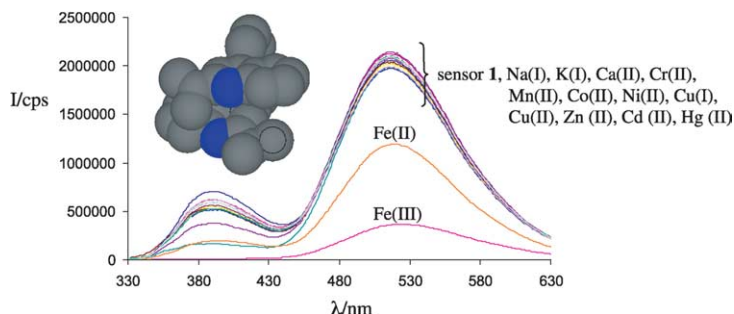
Sergiy V. Shevchuk, Vincent M. Lynch and Jonathan L. Sessler\*



### Selective metal ion recognition using a fluorescent 1,8-diquinolnaphthalene-derived sensor in aqueous solution

pp 11293–11297

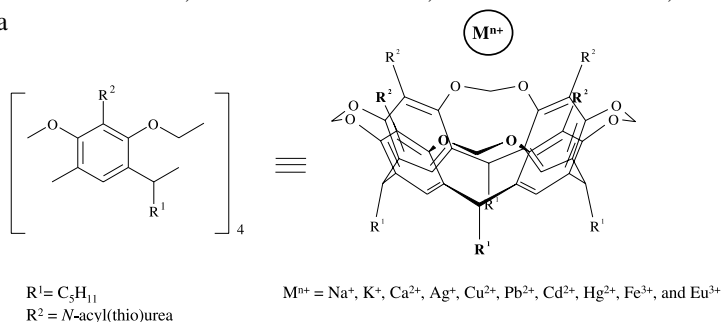
Gilbert E. Tumambac, Charlene M. Rosencrance and Christian Wolf\*



### Heavy metal complexation by *N*-acyl(thio)urea-functionalized cavitands: synthesis, extraction and potentiometric studies

pp 11299–11306

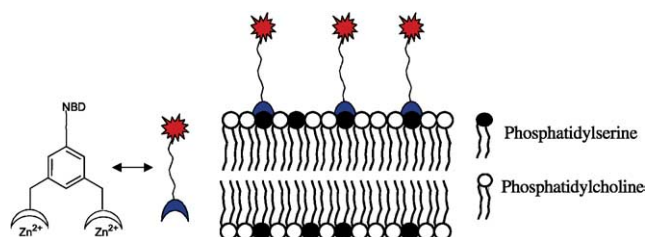
Marta M. Reinoso García, Willem Verboom,\* David N. Reinhoudt, Elzbieta Malinowska, Mariusz Pietrzak and Dorota Wojciechowska



### Fluorophore-linked zinc(II)dipicolylamine coordination complexes as sensors for phosphatidylserine-containing membranes

pp 11307–11315

C. Lakshmi, Roger G. Hanshaw and Bradley D. Smith\*




**OTHER CONTENTS**

**Contributors to this issue**  
**Instructions to contributors**

**p I**  
**pp III–VI**

\*Corresponding author

+ Supplementary data available via ScienceDirect

**COVER**

The traditional approach to the creation of a molecular sensor involves communication between a receptor and a reporter. Upon binding of the analyte to the receptor, communication occurs with the reporter, which in turn creates an optical or electrochemical signal. The structures on the cover highlight a few of the examples reported in this Symposium-in-Print. *Tetrahedron* **2004**, *60*, 11041–11316.

© 2004 Eric V. Anslyn. Published by Elsevier Ltd.



Full text of this journal is available, on-line from **ScienceDirect**. Visit [www.sciencedirect.com](http://www.sciencedirect.com) for more information.

---

**CONTENTS**  
**Direct**

This journal is part of **ContentsDirect**, the *free* alerting service which sends tables of contents by e-mail for Elsevier books and journals. You can register for **ContentsDirect** online at: <http://contentsdirect.elsevier.com>

---

Indexed/Abstracted in: AGRICOLA, Beilstein, BIOSIS Previews, CAB Abstracts, Chemical Abstracts. Current Contents: Life Sciences, Current Contents: Physical, Chemical and Earth Sciences, Current Contents Search, Derwent Drug File, Ei Compendex, EMBASE/Excerpta Medica, Medline, PASCAL, Research Alert, Science Citation Index, SciSearch



ELSEVIER

ISSN 0040-4020

# Tetrahedron Symposia-in-Print

## Series Editor

Professor H. H. Wasserman, Department of Chemistry, Yale University, P.O. Box 208107, New Haven, CT 06520-8107, U.S.A.

*Tetrahedron Symposia-in-Print* comprise collections of original research papers covering timely areas of organic chemistry.

Each symposium is organized by a Symposium Editor who will invite authors, active in the selected field, to submit original articles covering current research, complete with experimental sections. These papers will be rapidly reviewed and processed for publication by the Symposium Editor under the usual refereeing system.

Authors who have not already been invited, and who may have obtained recent significant results in the area of the announced symposium, may also submit contributions for Editorial consideration and possible inclusion. Before submitting such papers authors should send an abstract to the Symposium Editor for preliminary evaluation. Firm deadlines for receipt of papers will allow sufficient time for completion and presentation of ongoing work without loss of the freshness and timeliness of the research results.

## Symposia-in-Print—already published

1. Recent trends in organic photochemistry, Albert Padwa, Ed. *Tetrahedron* **1981**, *37*, 3227–3420.
2. New general synthetic methods, E. J. Corey, Ed. *Tetrahedron* **1981**, *37*, 3871–4119.
3. Recent developments in polycyclopentanoid chemistry, Leo A. Paquette, Ed. *Tetrahedron* **1981**, *37*, 4357–4559.
4. Biradicals, Josef Michl, Ed. *Tetrahedron* **1982**, *38*, 733–867.
5. Electron-transfer initiated reactions, Gary B. Schuster, Ed. *Tetrahedron* **1982**, *38*, 1025–1122.
6. The organic chemistry of animal defense mechanisms, Jerrold Meinwald, Ed. *Tetrahedron* **1982**, *38*, 1853–1970.
7. Recent developments in the use of silicon in organic synthesis, Hans Reich, Ed. *Tetrahedron* **1983**, *39*, 839–1009.
8. Linear tetrapyrroles, Ray Bonnett, Ed. *Tetrahedron* **1983**, *39*, 1837–1954.
9. Heteroatom-directed metallations in heterocyclic synthesis, George R. Newkome, Ed. *Tetrahedron* **1983**, *39*, 1955–2091.
10. Recent aspects of the chemistry of  $\beta$ -lactams, J. E. Baldwin, Ed. *Tetrahedron* **1983**, *39*, 2445–2608.
11. New spectroscopic techniques for studying metabolic processes, A. I. Scott, Ed. *Tetrahedron* **1983**, *39*, 3441–3626.
12. New developments in indole alkaloids, Martin E. Kuehne, Ed. *Tetrahedron* **1983**, *39*, 3627–3780.
13. Recent aspects of the chemistry of nucleosides, nucleotides and nucleic acids, Colin B. Reese, Ed. *Tetrahedron* **1984**, *40*, 1–164.
14. Bioorganic studies on receptor sites, Koji Nakanishi, Ed. *Tetrahedron* **1984**, *40*, 455–592.
15. Synthesis of chiral non-racemic compounds, A. I. Meyers, Ed. *Tetrahedron* **1984**, *40*, 1213–1418.
16. Control of acyclic stereochemistry, Teruaki Mukaiyama, Ed. *Tetrahedron* **1984**, *40*, 2197–2344.
17. Recent aspects of anthracycline chemistry, T. Ross Kelly, Ed. *Tetrahedron* **1984**, *40*, 4537–4794.
18. The organic chemistry of marine products, Paul J. Scheuer, Ed. *Tetrahedron* **1985**, *41*, 979–1108.
19. Recent aspects of carbene chemistry, Matthew Platz, Ed. *Tetrahedron* **1985**, *41*, 1423–1612.
20. Recent aspects of singlet oxygen chemistry of photooxidation, Isao Saito and Teruo Matsuura, Eds. *Tetrahedron* **1985**, *41*, 2037–2236.
21. Synthetic applications of dipolar cycloaddition reactions, Wolfgang Oppolzer, Ed. *Tetrahedron* **1985**, *41*, 3447–3568.
22. Selectivity and synthetic applications of radical reactions, Bernd Giese, Ed. *Tetrahedron* **1985**, *41*, 3887–4302.
23. Recent aspects of organoselenium chemistry, Dennis Liotta, Ed. *Tetrahedron* **1985**, *41*, 4727–4890.
24. Application of newer organometallic reagents to the total synthesis of natural products, Martin Semmelhack, Ed. *Tetrahedron* **1985**, *41*, 5741–5900.
25. Formal transfers of hydride from carbon–hydrogen bonds, James D. Wuest, Ed. *Tetrahedron* **1986**, *42*, 941–1208.
26. Synthesis of non-natural products: challenge and reward, Philip E. Eaton, Ed. *Tetrahedron* **1986**, *42*, 1549–1916.
27. New synthetic methods—II, F. E. Ziegler, Ed. *Tetrahedron* **1986**, *42*, 2777–3028.
28. Structure and reactivity of organic radical ions, Heinz D. Roth, Ed. *Tetrahedron* **1986**, *42*, 6097–6350.
29. Organic chemistry in anisotropic media, V. Ramamurthy, J. R. Scheffer and N. J. Turro, Eds. *Tetrahedron* **1987**, *43*, 1197–1746.
30. Current topics in sesquiterpene synthesis, John W. Huffman, Ed. *Tetrahedron* **1987**, *43*, 5467–5722.
31. Peptide chemistry: design and synthesis of peptides, conformational analysis and biological functions, Victor J. Hruby and Robert Schwyzer, Eds. *Tetrahedron* **1988**, *44*, 661–1006.
32. Organosilicon chemistry in organic synthesis, Ian Fleming, Ed. *Tetrahedron* **1988**, *44*, 3761–4292.
33.  $\alpha$ -Amino acid synthesis, Martin J. O'Donnell, Ed. *Tetrahedron* **1988**, *44*, 5253–5614.
34. Physical-organic/theoretical chemistry: the Dewar interface, Nathan L. Bauld, Ed. *Tetrahedron* **1988**, *44*, 7335–7626.
35. Recent developments in organocopper chemistry, Bruce H. Lipshutz, Ed. *Tetrahedron* **1989**, *45*, 349–578.
36. Organotin compounds in organic synthesis, Yoshinori Yamamoto, Ed. *Tetrahedron* **1989**, *45*, 909–1230.



37. Mycotoxins, Pieter S. Steyn, Ed. *Tetrahedron* **1989**, *45*, 2237–2464.
38. Strain-assisted syntheses, Léon Ghosez, Ed. *Tetrahedron* **1989**, *45*, 2875–3232.
39. Covalently linked donor–acceptor species for mimicry of photosynthetic electron and energy transfer, Devens Gust and Thomas A. Moore, Eds. *Tetrahedron* **1989**, *45*, 4669–4912.
40. Aspects of modern carbohydrate chemistry, S. Hanessian, Ed. *Tetrahedron* **1990**, *46*, 1–290.
41. Nitroalkanes and nitroalkenes in synthesis, Anthony G. M. Barrett, Ed. *Tetrahedron* **1990**, *46*, 7313–7598.
42. Synthetic applications of anodic oxidations, John S. Swenton and Gary W. Morrow, Eds. *Tetrahedron* **1991**, *47*, 531–906.
43. Recent advances in bioorganic chemistry, Dale L. Boger, Ed. *Tetrahedron* **1991**, *47*, 2351–2682.
44. Natural product structure determination, R. B. Bates, Ed. *Tetrahedron* **1991**, *47*, 3511–3664.
45. Frontiers in natural products biosynthesis. Enzymological and molecular genetic advances, D. E. Cane, Ed. *Tetrahedron* **1991**, *47*, 5919–6078.
46. New synthetic methods—III, S. E. Denmark, Ed. *Tetrahedron* **1992**, *48*, 1959–2222.
47. Organotitanium reagents in organic chemistry, M. T. Reetz, Ed. *Tetrahedron* **1992**, *48*, 5557–5754.
48. Total and semi-synthetic approaches to taxol, J. D. Winkler, Ed. *Tetrahedron* **1992**, *48*, 6953–7056.
49. Synthesis of optically active compounds—prospects for the 21st century, Kenji Koga and Takayuki Shioiri, Eds. *Tetrahedron* **1993**, *49*, 1711–1924.
50. Peptide secondary structure mimetics, Michael Kahn, Ed. *Tetrahedron* **1993**, *49*, 3433–3689.
51. Transition metal organometallics in organic synthesis, Anthony J. Pearson, Ed. *Tetrahedron* **1993**, *49*, 5415–5682.
52. Palladium in organic synthesis, Jan-E. Bäckvall, Ed. *Tetrahedron* **1994**, *50*, 285–572.
53. Recent progress in the chemistry of enediyne antibiotics, Terrence W. Doyle and John F. Kadow, Eds. *Tetrahedron* **1994**, *50*, 1311–1538.
54. Catalytic asymmetric addition reactions, Stephen F. Martin, Ed. *Tetrahedron* **1994**, *50*, 4235–4574.
55. Mechanistic aspects of polar organometallic chemistry, Manfred Schlosser, Ed. *Tetrahedron* **1994**, *50*, 5845–6128.
56. Molecular recognition, Andrew D. Hamilton, Ed. *Tetrahedron* **1995**, *51*, 343–648.
57. Recent advances in the chemistry of zirconocene and related compounds, Ei-ichi Negishi, Ed. *Tetrahedron* **1995**, *51*, 4255–4570.
58. Fluoroorganic chemistry: synthetic challenges and biomedical rewards, Giuseppe Resnati and Vadim A. Soloshonok, Eds. *Tetrahedron* **1996**, *52*, 1–330.
59. Novel applications of heterocycles in synthesis, A. R. Katritzky, Ed. *Tetrahedron* **1996**, *52*, 3057–3374.
60. Fullerene chemistry, Amos B. Smith III, Ed. *Tetrahedron* **1996**, *52*, 4925–5262.
61. New synthetic methods—IV. Organometallics in organic chemistry, István E. Markó, Ed. *Tetrahedron* **1996**, *52*, 7201–7598.
62. Cascade reactions, Ron Grigg, Ed. *Tetrahedron* **1996**, *52*, 11385–11664.
63. Applications of solid-supported organic synthesis in combinatorial chemistry, James A. Bristol, Ed. *Tetrahedron* **1997**, *53*, 6573–6706.
64. Recent applications of synthetic organic chemistry, Stephen F. Martin, Ed. *Tetrahedron* **1997**, *53*, 8689–9006.
65. Chemical biology, Gregory L. Verdine and Julian Simon, Eds. *Tetrahedron* **1997**, *53*, 11937–12066.
66. Recent aspects of S, Se, and Te chemistry, Richard S. Glass and Renji Okazaki, Eds. *Tetrahedron* **1997**, *53*, 12067–12318.
67. Modern organic chemistry of polymerization, H. K. Hall Jr., Ed. *Tetrahedron* **1997**, *53*, 15157–15616.
68. New synthetic methods—V, John L. Wood, Ed. *Tetrahedron* **1997**, *53*, 16213–16606.
69. New developments in organonickel chemistry, Bruce H. Lipshutz and Tien-Yau Luh, Eds. *Tetrahedron* **1998**, *54*, 1021–1316.
70. Solution phase combinatorial chemistry, David L. Coffen, Ed. *Tetrahedron* **1998**, *54*, 3955–4150.
71. Heterocycles in asymmetric synthesis, Alexandre Alexakis, Ed. *Tetrahedron* **1998**, *54*, 10239–10554.
72. Recent advances of phase-transfer catalysis, Takayuki Shioiri, Ed. *Tetrahedron* **1999**, *55*, 6261–6402.
73. Olefin metathesis in organic synthesis, Marc L. Snapper and Amir H. Hoveyda, Eds. *Tetrahedron* **1999**, *55*, 8141–8262.
74. Stereoselective carbon–carbon bond forming reactions, Harry H. Wasserman, Stephen F. Martin and Yoshinori Yamamoto, Eds. *Tetrahedron* **1999**, *55*, 8589–9006.
75. Applications of combinatorial chemistry, Miles G. Siegel and Stephen W. Kaldor, Eds. *Tetrahedron* **1999**, *55*, 11609–11710.
76. Advances in carbon–phosphorus heterocyclic chemistry, François Mathéy, Ed. *Tetrahedron* **2000**, *56*, 1–164.
77. Transition metal organometallics in organic synthesis, Kenneth M. Nicholas, Ed. *Tetrahedron* **2000**, *56*, 2103–2338.
78. Organocopper chemistry II, Norbert Krause, Ed. *Tetrahedron* **2000**, *56*, 2727–2904.
79. Carbene complexes in organic chemistry, James W. Herndon, Ed. *Tetrahedron* **2000**, *56*, 4847–5044.
80. Recent aspects of the chemistry of  $\beta$ -lactams—II, Marvin J. Miller, Ed. *Tetrahedron* **2000**, *56*, 5553–5742.
81. Molecular assembly and reactivity of organic crystals and related structures, Miguel A. Garcia-Garibay, Vaidhyanathan Ramamurthy and John R. Scheffer, Eds. *Tetrahedron* **2000**, *56*, 6595–7050.
82. Protein engineering, Richard Chamberlin, Ed. *Tetrahedron* **2000**, *56*, 9401–9526.
83. Recent advances in peptidomimetics, Jeffrey Aubé, Ed. *Tetrahedron* **2000**, *56*, 9725–9842.
84. New synthetic methods—VI, George A. Kraus, Ed. *Tetrahedron* **2000**, *56*, 10101–10282.
85. Oxidative activation of aromatic rings: an efficient strategy for arene functionalization, Stéphane Quideau and Ken S. Feldman, Eds. *Tetrahedron* **2001**, *57*, 265–424.
86. Lewis acid control of asymmetric synthesis, Keiji Maruoka, Ed. *Tetrahedron* **2001**, *57*, 805–914.
87. Novel aromatic compounds, Lawrence T. Scott and Jay S. Siegel, Eds. *Tetrahedron* **2001**, *57*, 3507–3808.
88. Asymmetric synthesis of novel sterically constrained amino acids, Victor J. Hruby and Vadim A. Soloshonok, Eds. *Tetrahedron* **2001**, *57*, 6329–6650.
89. Recognition-mediated self-assembly of organic systems, Vincent M. Rotello, Ed. *Tetrahedron* **2002**, *58*, 621–844.
90. Synthesis of marine natural products containing polycyclic ethers, Masahiro Hirama and Jon D. Rainier, Eds. *Tetrahedron* **2002**, *58*, 1779–2040.

91. Fluorous chemistry, John A. Gladysz and Dennis P. Curran, Eds. *Tetrahedron* **2002**, 58, 3823–4132.
92. Recent developments in chiral lithium amide base chemistry, Peter O'Brien, Ed. *Tetrahedron* **2002**, 58, 4567–4734.
93. Beyond natural product synthesis (Tetrahedron Prize for Creativity in Organic Chemistry 2001 - Yoshito Kishi), Harry H. Wasserman and Stephen F. Martin, Eds. *Tetrahedron* **2002**, 58, 6223–6602.
94. Strained heterocycles as intermediates in organic synthesis, Amy R. Howell, Ed. *Tetrahedron* **2002**, 58, 6979–7194.
95. Molecular design of Lewis and Brønsted acid catalysts—the key to environmentally benign reagents (Tetrahedron Chair 2002), Hisashi Yamamoto, Ed. *Tetrahedron* **2002**, 58, 8153–8364.
96. Recent developments in dendrimer chemistry, David K. Smith, Ed. *Tetrahedron* **2003**, 59, 3787–4024.
97. Art, science and technology in total synthesis (Tetrahedron Prize for Creativity in Organic Chemistry 2002 - K. C. Nicolaou), Stephen F. Martin and Harry H. Wasserman, Eds. *Tetrahedron* **2003**, 59, 6667–7070.
98. New synthetic methods—VII, Brian M. Stoltz, Ed. *Tetrahedron* **2003**, 59, 8843–9030.
99. Oxiranyl and aziridinyl anions as reactive intermediates in synthetic organic chemistry, S. Florio, Ed. *Tetrahedron* **2003**, 59, 9683–9864.
100. Recent advances in rare earth chemistry, Shū Kobayashi, Ed. *Tetrahedron* **2003**, 59, 10339–10598.
101. Biocatalysts in synthetic organic chemistry, S. M. Roberts, Ed. *Tetrahedron* **2004**, 60, 483–806.
102. Recent advances in the chemistry of zirconocenes, Keisuke Suzuki and Peter Wipf, Eds. *Tetrahedron* **2004**, 60, 1257–1424.
103. Atropisomerism, Jonathan Clayden, Ed. *Tetrahedron* **2004**, 60, 4325–4558.
104. Chemistry of biologically and physiologically intriguing phenomena, Daisuke Uemura, Ed. *Tetrahedron* **2004**, 60, 6959–7098.
105. Olefin metathesis: a powerful and versatile instrument for organic synthesis (Tetrahedron prize for creativity in organic chemistry 2003 – R. H. Grubbs), Stephen F. Martin and Harry H. Wasserman, Eds. *Tetrahedron* **2004**, 60, 7099–7438.
106. From synthetic methodology to biomimetic target assembly (Tetrahedron prize for creativity in organic chemistry 2003 – D. Seebach), Léon A. Ghosez, Ed. *Tetrahedron* **2004**, 60, 7439–7794.
107. Solid and solution phase combinatorial chemistry, Rolf Breinbauer and Herbert Waldmann, Eds. *Tetrahedron* **2004**, 60, 8579–8738.
108. Catalytic tools enabling total synthesis (Tetrahedron Chair 2004), Alois Fürstner, Ed. *Tetrahedron* **2004**, 60, 9529–9784.
109. Synthesis and applications of non-racemic cyanohydrins and  $\alpha$ -amino nitriles, Michael North, Ed. *Tetrahedron* **2004**, 60, 10371–10568.
110. Synthetic receptors as sensors, Eric V. Anslyn, Ed. *Tetrahedron* **2004**, 60, 11041–11316.





## Preface

**Synthetic receptors as sensors**

Synthetic receptors have been studied for decades. The Nobel Prize given to Cram, Lehn, and Petersen represented recognition of the importance of studying supramolecular chemistry using synthetic receptors. The driving force for these early studies, as well as many current endeavors, was to decipher the underlying principles that Nature uses for complex molecular assemblies and catalysis. However, since its inception, the field of molecular recognition using synthetic receptors has also been focused on practical applications. In fact, many of the crown ether and cryptand structures created by Cram, Lehn, and Petersen, as well as variations inspired by their designs, have been put to practical use. One such application is in the field of molecular sensing.

In analytical chemistry, a sensor is defined as an instrument that can detect and quantify the concentration of an analyte. Hence, an HPLC instrument in an EPA lab, a mass spec instrument at an airport, or even of course, a simple pH meter and electrode, are considered sensors. In supramolecular chemistry, as well as biochemistry and molecular biology, the term sensor is more closely associated with a molecule or a molecular event. When a chemical receptor gives a measurable signal in response to binding of an analyte, the receptor itself is called the sensor. Incorporation of this sensor into a device leads to an analytical protocol.

Some of the earliest organic sensors are simple pH indicators. In fact, the use of synthetic receptors as sensors commenced when chemists branched away from natural products as pH indicators, and synthesized their own designed pH indicators. Further, when chemists created the complexone agents (indicators conjugated to metal binding sites) for the optical signaling of metal cations, the field of using designed synthetic receptors as sensors took another leap forward. In addition, ion-selective electrodes incorporating receptors such as crown ethers, polyaza macrocycles, and calixarenes, took the field even further. Therefore, the use of synthetic receptors to create measurable responses has a very long history.

However, with the greatest respect to the importance of the contributions mentioned above, as well as others, I would name four individuals whose design notions supramolecular chemists now most closely associate with sensors: Anthony Czarnek at Sensors for Medicine and Science, A. Prasanna de Silva at Queen's College Belfast, Roger Tsien at U.C.S.D., and Seiji Shinkai at Kyushu University. In my opinion, these four individuals took leading roles in the 1980's and 1990's to advance the notions of combining

synthetic receptors with signaling elements to detect and quantify various analytes. Drs. Czarnek, DeSilva, and Shinkai showed how photo induced electron transfer (PET) mechanisms could be built into a wide variety of synthetic receptors to detect various cations, anions, and neutral analytes. Further, Anthony Czarnek coined the term 'chemosensor' to accentuate the difference between designed chemical receptors and biosensors. The term is now pervasive in the literature. Lastly, Dr. Tsien showed that exquisitely designed complexone agents could achieve the required specificity and sensitivity for analytes of biological interest, even within a cellular environment. Two of these individuals have contributed papers on their recent advances to this Symposium in Print.

In the early twenty first century, the field of sensing using synthetic receptors is exploding. A variety of synthetic receptor designs with no resemblance to the early crown and complexone agents dominate the field. In this symposium in print we find work on cavities carved into dendritic hosts from Steven Zimmerman, quinolyl-based receptors from Christian Wolf and Paul Savage, membrane-bound bimetallic receptors from Bradley Smith, chiral clefts from Lin Pu, polymeric structures from Mario Leclerc, Richard McCullough, and Pavel Anzenbacher, boronic-acid based receptors from Tony James, Masayuki Takeuchi, and Seiji Shinkai, as well as Binghe Wang, terpyrrole derivatives from Jonathan Sessler, and trityl pinwheels from Timothy Glass. Combinatorial chemical synthesis also now plays an important role in creating receptors for sensing applications, as was demonstrated early on by Clark Still. A very nice contribution from Rob Liskamp herein shows the great potential for this avenue of investigation. Clearly the creation of synthetic receptors for sensing applications is fertile ground for the creativity of supramolecular chemists.

However, just as important as receptor design is to a sensing method, so is the signaling protocol. Because synthesis allows chemists to incorporate their own novel and imaginative concepts, there are a large number of protocols being adapted to chemosensors. For example, in this symposium in print alone there are numerous signaling protocols successfully combined with synthetic receptors. We find papers reporting on PET-based methods for sodium and cadmium from Tetsuo Nagano and Thorfinn Gunnlaugsson respectively, intramolecular charge transfer from Yun-Bao Jiang, a combination of PET and internal charge transfer from A.P. de Silva, electrochemical techniques being exploited by Willem Verboom and Paul Beer, colorimetric methods for heavy metals from Jonathan

Sessler, indicator-displacement assays for phosphoesters from our group, Fabry-Perot interference patterns explored by Reza Ghadiri, and conformational changes to modulate emission from Nathaniel Finney and Christoph Fahrni. The sampling of methods in the symposium in print does not give justice to the plethora of methods supramolecular chemists are applying to sensing applications. There will surely be increasingly novel approaches developed for the signaling of molecular recognition events, and this represents an important growth area for our field.

In addition, the use of synthetic receptors within array sensing platforms is catching significant attention from the groups of Thomas Schrader, Benjamin Miller, Andrew Hamilton, Amit Basu, Ken Shimizu, our group, as well as numerous others. The inherent cross reactivity and differential binding characteristics of synthetic receptors makes them idea candidates for a variety of practical applications in the analysis of complex mixtures. In this regard, a nice contribution from Kenneth Suslick is found in this symposium in print.

An important frontier for synthetic receptors as sensors is the targeting of bio-relevant analytes. For example, Robert Strongin has recently targeted cysteine and homo-cysteine. In this symposium in print Dong Kim reports an alternative approach to the creation of a selective sensor for cysteine, Dmitry Rudkevick reports a method to detect NO, and Luigi Fabbrizzi gives a method to detect glutamate. Irrespective of such advances, it is still predominately true that researchers

in molecular biology turn to antibodies, enzymes, and possibly aptamers, rather than considering synthetic receptors, for their own sensing needs. As mentioned earlier, Roger Tsien has made good progress in ‘breaking the ice’ in this regard. However, it is of paramount importance that supramolecular chemistry principles continue to be directed toward this goal, because this is the context in which synthetic receptors will make their greatest impact on advances in science and medicine.

In summary, this Symposium in Print simply scratches the surface of the incredible creativity applied to sensors derived from synthetic receptors. The symposium has only included a handful of the leading research groups in this field, but with even this small sampling, it is evident that the ingenuity of supramolecular chemists will increasingly lead to novel receptor designs and fascinating signaling protocols. As Anthony Czarnik first challenged the supramolecular chemistry field in his pioneering paper ‘Desperately Seeking Sensors’, I continue to challenge our field to work towards practical analytical protocols using synthetic receptors - the field is truly just beginning to blossom.

Eric V. Anslyn  
*Department of Chemistry and Biochemistry,*  
*1 Longhorn Way,*  
*A5300 The University of Texas,*  
*Austin, TX 78712,*  
*USA*  
*E-mail address:* [anslyn@ccwf.cc.utexas.edu](mailto:anslyn@ccwf.cc.utexas.edu)

Available online 30 September 2004

# Exploring the effects of cooperative interactions on affinity using a pinwheel sensor system

Paul D. Jones and Timothy E. Glass\*

Department of Chemistry, The Pennsylvania State University, University Park, PA 16802, USA

Received 5 February 2004; revised 7 July 2004; accepted 19 August 2004

Available online 21 September 2004

**Abstract**—A series of three pinwheel sensors were constructed with 1, 2, and 3 binding sites. Binding of  $Zn^{+2}$  and  $Cd^{+2}$  was monitored by fluorescence over a range of temperatures. The data demonstrate that cooperative interactions generally increase the effective affinity of the sensor. This effect is more pronounced in systems which have lower inherent affinity for the analyte.  
 © 2004 Elsevier Ltd. All rights reserved.

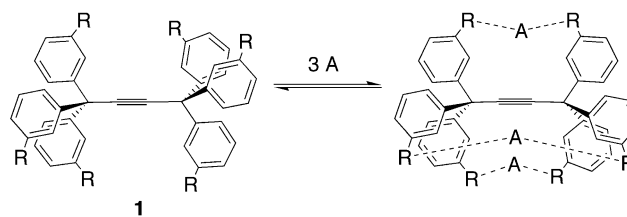
## 1. Introduction

Fluorescent chemical sensors are becoming an increasingly valuable tool for the detection of many analytes in a wide range of applications.<sup>1</sup> As part of an ongoing project geared toward creating more effective chemical sensors, we have been exploring a novel class of cooperative receptors based on bistrityl acetylene compounds, termed pinwheel receptors (Scheme 1).<sup>2</sup> The recognition elements appended to the trityl skeleton bind the analyte across the receptor framework producing three identical binding pockets. Cooperative recognition is seen because binding of the first analyte preorganizes the symmetrical receptor into a conformation in which the second and third analyte can bind more strongly. This mechanism of cooperativity is conceptually similar to the restricted rotational freedom employed by Rebek's cooperative biphenyl bis-crown ether<sup>3</sup> and Shinkai's cooperative porphyrin sandwich complexes.<sup>4</sup>

In fact, several artificial cooperative receptors have been developed,<sup>5</sup> though few have been applied toward chemical sensor applications.<sup>6</sup> From a design perspective, this method of recognizing a guest is attractive. Many elegant (non-cooperative) receptor designs have been developed over the years in which two or more recognition elements are displayed in a convergent fashion for binding of a guest. Strong binding is most often observed when the recognition elements are held rigidly apart such that there is little entropic loss to the receptor upon binding the guest.<sup>7</sup> The

challenge of receptor design becomes one of creating the optimal spacing and orientation of the recognition elements in a rigid fashion.<sup>8</sup> For receptors of the class depicted in Scheme 1, there is a range of distances which the recognition elements can span owing to free rotation about the acetylenic axis. Binding of the first analyte rigidly sets the correct distance between the remaining pairs of binding groups. Thus, the entropic loss upon binding the analyte is effectively averaged over three consecutive binding events, diminishing the overall entropic penalty to binding. This receptor design should be general for a range of analytes of varying size within the outer limits of receptor framework. The spacing between the recognition elements need only be roughly adjusted to the size of the desired guest. Upon binding of the first guest, the receptor is then fully organized to match the size of the guest.

We have previously argued that the type of cooperative recognition described above increases the affinity and selectivity of a sensor for its analyte relative to a similar non-cooperative sensor.<sup>2a</sup> These points were initially addressed using sensors for metal ions<sup>2b</sup> and dicarboxylates.<sup>9</sup> In this report, we explore these issues using a series of



R=Recognition element; A=Analyte

Scheme 1.

**Keywords:** Sensor; Allosteric; Cooperative.

\* Corresponding author. Address: Department of Chemistry, University of Missouri, Columbia, MO 65211, USA. Tel.: +1-573-882-3813; fax: +1-573-882-2754; e-mail: [glasst@missouri.edu](mailto:glasst@missouri.edu)

metal ion sensors with varying numbers of binding sites. Comparison of the recognition properties of sensors with varying degrees of cooperativity provides insight into the advantages and disadvantages of the cooperative recognition method.

## 2. Results

The sensors used for this study are shown in Figure 1. Compounds **2a–c** are based on a bis-acetylene bis-trityl system for ease of synthesis.<sup>10</sup> The amino-methoxyquinoline groups would serve not only as recognition elements, but also as the fluorescent readout mechanism. Two recognition elements (R) should bind a metal ion between them, across the bisacetylene axis in a tetrahedral fashion (as per Fig. 1). The benzylic amine will participate in photoelectron transfer (PET)<sup>1b</sup> quenching of the fluorophore in the unbound state. Upon metal chelation the amine will no longer be able to quench the fluorophore and a significant increase in fluorescence is anticipated. Receptor **2a**, with one set of binding groups, was designed to be a non-cooperative receptor while receptors **2b** and **2c** were designed to be two-fold and three-fold cooperative receptors, respectively. Assuming that the binding pockets in the three molecules are similar, this series of sensors should provide information on the effect of cooperativity on the recognition properties of the system.

### 2.1. Synthesis

The synthesis of receptors **2a–c** is shown in Scheme 2. The fluorophore portion was prepared by bromination of methoxyquinoline followed by substitution with methylamine to give **5**. Trityl chlorides **6a–c** were reacted with ethynyl Grignard to yield alkynes **7a–c**. Dimerization of the

alkynes was effected by copper chloride and *N*-methyl pyrrolidine or TMEDA under aerobic conditions. Treatment of butadiyne **8a–c** with excess titanium tetrachloride and  $\alpha,\alpha$ -dichloromethyl methyl ether regioselectively formylated only the anisole rings, yielding aldehydes **9a–c**. Reductive amination of the aldehydes with amine **5** using triacetoxy sodium borohydride yielded sensors **2a–c**.

### 2.2. Metal ion binding studies

**2.2.1. UV/vis studies.** Metal ion binding was first studied by titrating sensors **2a–c** with metal ions and following changes in the UV/vis absorptions. All three sensors appeared to bind many metals tightly including  $\text{Ni}^{+2}$ ,  $\text{Cd}^{+2}$ ,  $\text{Zn}^{+2}$ ,  $\text{Mn}^{+2}$ ,  $\text{Hg}^{+2}$ , and  $\text{Ag}^{+1}$ . Figure 2 shows a representative example of the titrations of sensors **2a–c** with  $\text{Cd}(\text{ClO}_4)_2$  in acetonitrile. All metals produced a red-shift in the major UV band centered at 325 nm. With the exception of extinction coefficient, which varied as per the number of chromophores per molecule, all three sensors had similar UV behavior indicating that the binding pockets are similar between the various sensors.

Unfortunately, all of the binding constants were too high to derive useful data from the UV/vis titrations. In fact, titration curves based on Figure 2 showed near linear responses which saturated at approximately the stoichiometric point for each sensor (1, 2, and 3 equiv of  $\text{Cd}^{+2}$  for sensors **2a**, **2b**, and **2c**, respectively). These results verify the expected stoichiometry of the sensors.

**2.2.2. Fluorescence studies.** The fluorescence titrations of the sensors were much more informative as the concentration of sensor required for such analysis was significantly lower (0.3  $\mu\text{M}$ ). Of all of the metals tested, only zinc and cadmium produced well behaved fluorescence modulation

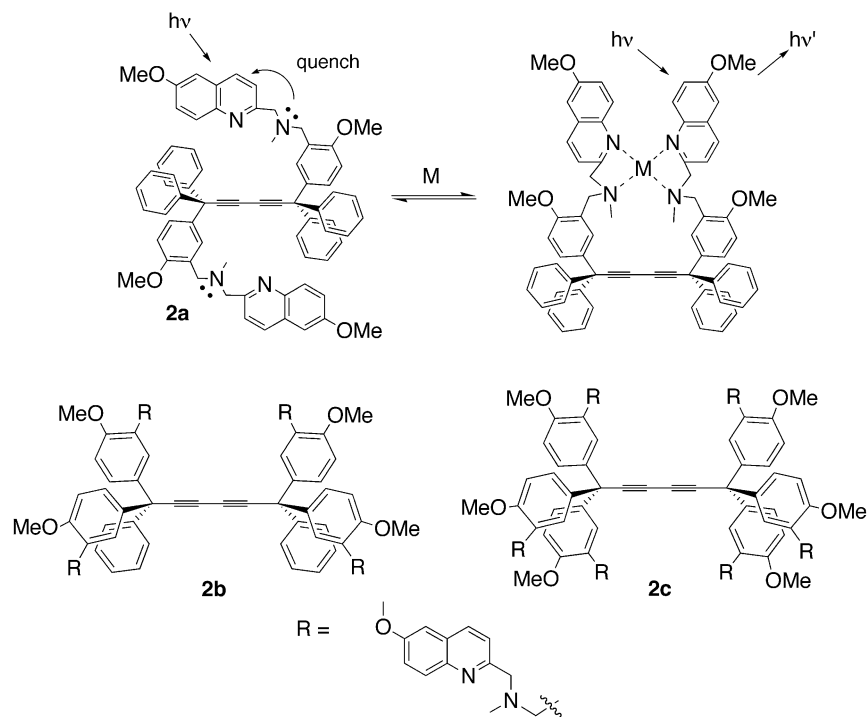
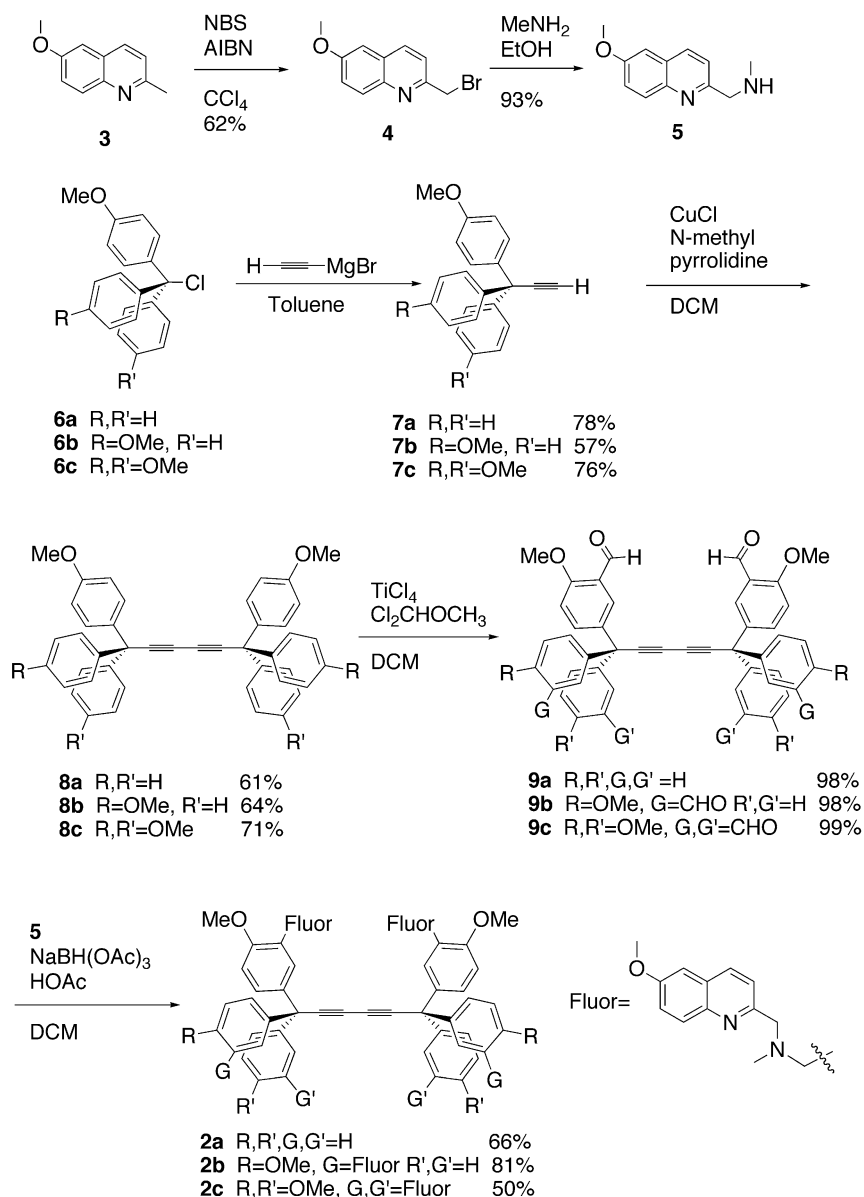


Figure 1. A series of three bis-trityl receptors.



Scheme 2.

when added to the sensor. Figure 3 shows a representative example in which **2a** is titrated with  $\text{Zn}^{+2}$  in acetonitrile. As anticipated, the sensor has little native fluorescence due to the PET quenching of the benzylic amines. Binding of the metal ions produced a substantial increase in fluorescence. Generally, cadmium produced a 3–4 fold increase in emission at 393 nm (excited at 336 nm) and zinc produced a 7–9 fold increase in emission at the same wavelength. It is likely that quenching metal ions such as silver did not give a good response with this sensor because they quench the fluorophore as they bind, retaining an ‘off’ state of the sensor.

The binding isotherms for all three sensors with zinc are shown in Figure 4. While the fluorescence experiment allows the concentration of host to be very low, the apparent dissociation constants of the receptors are still close to the concentration of host. This implies that the concentration of added guest does not really approximate the concentration

of free guest in solution very well. Since the binding isotherms used to calculate the dissociation constants rely on free guest concentrations, the data were corrected using the known concentration of sensor so that the  $x$ -axis reflects the equilibrium concentration of free zinc in solution. Using this correction, more accurate dissociation constants and Hill coefficients could be obtained. Therefore, this correction was applied to all titration data.

Binding constants for the three sensors with  $\text{Zn}^{+2}$  and  $\text{Cd}^{+2}$  were determined by fitting the experimental data to the Hill equation (Table 1). For the purpose of internal consistency, sensor **2a** was fitted to the Hill equation and in all cases gave a Hill coefficient of very near 1.0, which is consistent with a non-cooperative sensor.

The UV/vis titration data was used to determine the stoichiometry of the sensors. In order to verify this in the fluorescence mode, job plots were prepared. As expected,

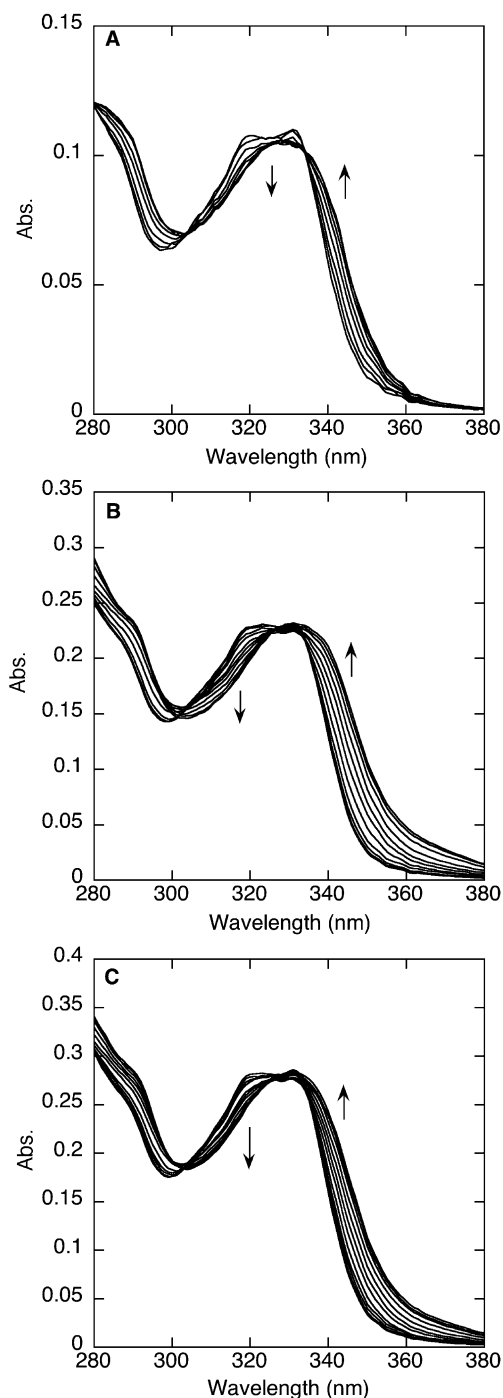


**Figure 2.** UV/Vis titration of sensors **2a–c** ( $[2] = 10 \mu\text{M}$ ) with  $\text{Cd}(\text{ClO}_4)_2$  in  $\text{CH}_3\text{CN}$  with  $0.5 \text{ mM NaClO}_4$  as a supporting electrolyte. (A) Sensor **2a**. (B) Sensor **2b**. (C) Sensor **2c**.

each sensor gave a maximum change in fluorescence close to its stoichiometric point for both metals tested. The Job plot for the three sensors and  $\text{Cd}^{+2}$  are overlaid in **Figure 5**. Sensor **2a** had maximal change in fluorescence at 48 mol% fraction of  $\text{Cd}^{+2}$ , sensor **2b** at 67% and sensor **2c** at 73%. Interestingly, sensors **2b** and **2c** show suppressed changes in fluorescence at low mole fraction of metal, in keeping with the cooperative nature of these receptors.

**2.2.3. Variable temperature studies.** Fluorescence titrations were then conducted with receptors **2a–c** and

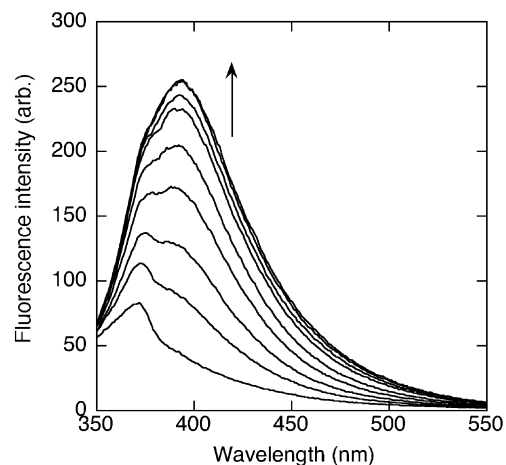


**Figure 3.** Fluorescence titration of compound **2a** with  $\text{Zn}(\text{ClO}_4)_2$  at  $25^\circ\text{C}$ .  $[\mathbf{2a}] = 0.3 \mu\text{M}$  in  $\text{CH}_3\text{CN}$  with  $0.50 \text{ mM NaClO}_4$  as a supporting electrolyte.  $\lambda_{\text{ex}} = 336 \text{ nm}$ .

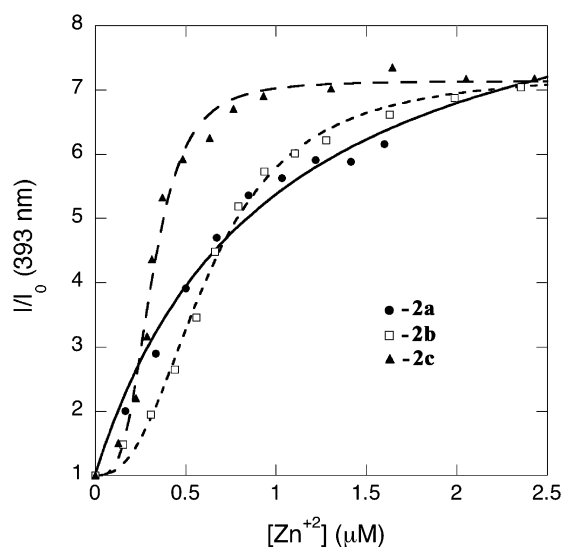


**Figure 4.** Binding isotherms for receptors **2a–c** with  $\text{Zn}(\text{ClO}_4)_2$  at  $393 \text{ nm}$  in acetonitrile with  $0.50 \text{ mM NaClO}_4$  as a supporting electrolyte. Concentration of  $\text{Zn}^{+2}$  is given as the equilibrium concentration of free zinc in solution. (A) Receptor **2a**. The best fit line (solid) is to a single site isotherm. (B) Receptor **2b**. The best fit line (short dash) is to a Hill equation. (C) Receptor **2c**. The best fit line (long dash) is to a Hill equation.

$\text{Zn}(\text{ClO}_4)_2$  at different temperatures to investigate the effect of cooperativity on apparent  $K_d$ . **Figure 6** summarizes these experiments. Generally, the  $K_d$  of the non-cooperative sensor increased with increasing temperature, while the  $K_d$  of the cooperative sensors was relatively unaffected.

### 3. Discussion

Shinkai has described a detailed study of five receptors based on his cooperative cerium sandwich complexes with 1, 2, 3, and 4 sites.<sup>11</sup> While the Hill coefficient correlated nicely with the number of sites, the binding pockets communicated with each other electronically such that it was not possible to compare association constants in a meaningful way. In this study, we attempted to make comparisons of dissociation constants between sensors with

**Table 1.** Hill coefficients and dissociation constants for sensors **2a–c** under conditions listed in Figure 4

Sensor	Analyte	Hill coeff.	$K_d$ ( $\mu\text{M}$ ) <sup>a</sup>	$I/I_0$ max. <sup>b</sup>
<b>2a</b>	$\text{Zn}^{+2}$	0.97	0.85	9.2
<b>2b</b>	$\text{Zn}^{+2}$	1.9	0.54	7.3
<b>2c</b>	$\text{Zn}^{+2}$	2.9	0.33	7.2
<b>2a</b>	$\text{Cd}^{+2}$	0.99	0.42	4.8
<b>2b</b>	$\text{Cd}^{+2}$	2.0	0.26	4.7
<b>2c</b>	$\text{Cd}^{+2}$	2.9	0.26	7.6

<sup>a</sup> Error in  $K_d$  is approximately  $\pm 15\%$ .

<sup>b</sup> The maximum fluorescence change of each sensor at saturation.

different numbers of binding pockets. It has been shown previously for a related pinwheel sensor, that two sets of binding groups on one trityl unit cannot interact to bind a metal, therefore binding must occur across the acetylene axis as shown in Figure 1. In the case of sensors **2a–c**, the similarity of the three sets of UV titration data indicates that the binding sites are similar between the three sensors. This result is supported by NMR titrations of the three sensors with metal ions (data not shown) in which similar behavior is observed between all three sensors. Therefore, to a first approximation, the binding pocket in **2a** appears to be equivalent to those of **2b** and **2c**.

To compare affinity between sensors, binding constants were determined in terms of apparent dissociation constants ( $K_d$ ). This value is the half saturation value of the sensor, a value that is commonly used in biological systems when the number of binding sites is unknown.<sup>12</sup> In this case, it allows direct comparison of affinity between sensors with different numbers of sites, since the actual association constants of the three sensors have different units. This type of analysis is also convenient in cases where the Hill coefficient is non-integral implying a mixture of species of varying analyte occupancy. Ultimately, this value is the most useful measure of binding as it describes the concentration of analyte that the sensor is capable of recognizing.

Visual inspection of the binding isotherms in Figure 4 supports our assertion that cooperativity enhances binding. The cooperative sensors have steeper binding isotherms and saturate much more quickly giving an overall lower apparent  $K_d$  (higher binding) than the non-cooperative

sensor. Moreover, the 3-fold cooperative system (**2c**) has a lower apparent  $K_d$  than the 2-fold cooperative sensor (**2b**). Similarly, the effective range of analyte over which the sensor is useful is larger for the non-cooperative system (**2a**) than **2b** which is again larger than the **2c**. Thus, the advantages and disadvantages of cooperativity are immediately evident.

As expected, the hill coefficients for sensors **2b** and **2c** correlated to the number of binding sites indicating that the multi-site sensors are binding in a cooperative mode. It is evident from Figure 4 and Table 1 that for zinc, the cooperative sensors bind more tightly than the non-cooperative sensors. However, the differences in this case (ca. 2.5-fold decrease in  $K_d$  for **2c** vs. **2a**) are small compared to what we have observed previously (50-fold).<sup>2a</sup> We believe that the difference arises from the high inherent affinity of **2** for metal ions. The contribution of cooperativity arises from the freezing out of rotational entropy upon binding of the first metal ion. The higher affinity of the second metal ion can be viewed in terms of free energy of association in which the total free energy is a combination of the inherent free energy of the recognition elements for the metal plus the free energy of cooperativity<sup>12</sup> (which stems from preorganization of the sensor upon the first binding event). Therefore, it stands to reason that in this system where the inherent affinity of the sensor for zinc is quite high (large free energy of association) the added free energy of cooperativity makes less of an impact in terms of higher affinity compared to a system with lower inherent affinity for the analyte. This assertion is qualitatively supported by the cadmium binding data (Table 1) in which **2a** binds  $\text{Cd}^{+2}$  even more tightly than  $\text{Zn}^{+2}$  and

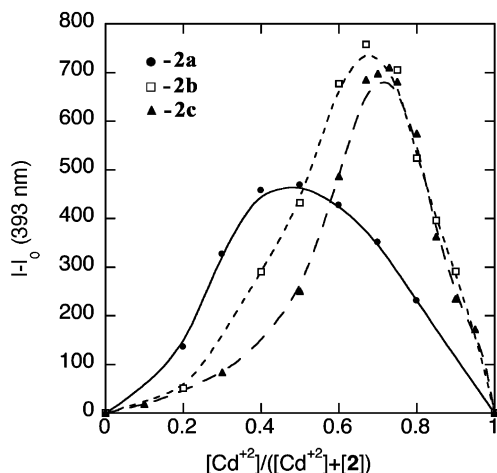


**Figure 5.** Job plot for receptors **2a–c** with  $\text{Cd}(\text{ClO}_4)_2$ .  $[\text{Cd}^{2+}] + [\text{host}] = 20 \mu\text{M}$  in  $\text{CH}_3\text{CN}$  with  $0.50 \text{ M NaClO}_4$  as a supporting electrolyte. The lines are merely illustrative and do not represent a fit to the data.

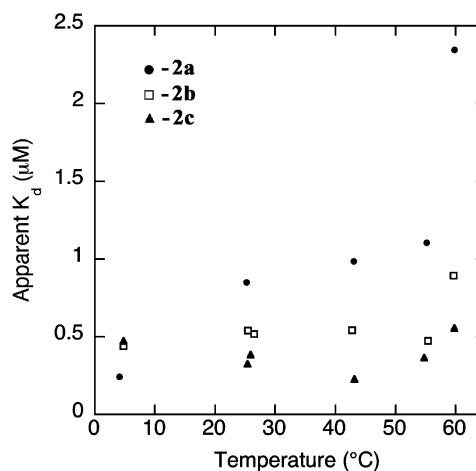


**Figure 6.** Apparent  $K_d$  of sensors **2a–c** with  $\text{Zn}(\text{ClO}_4)_2$  as a function of temperature.



the ratio of  $K_d$  for **2c** and **2a** is smaller. Thus, it is reasonable to expect that cooperativity will have the biggest impact on association in systems with relatively low inherent free energy of association.

To explore these effects further, we examined the effect of temperature on  $K_d$ . The plot of  $K_d$  versus temperature (Fig. 6) has some scatter due to the error inherent in calculation of  $K_d$ , however, the trends are very informative. The non-cooperative sensor demonstrated the greatest variability in  $K_d$  over the relatively small range of temperatures explored. The increase in  $K_d$  (decrease in affinity) as temperature increased is in agreement with expectation since the organization of the sensor to bind the metal is entropically disfavored. At higher temperatures, binding affinity should be decreased. Interestingly, the cooperative sensors showed little variation in apparent  $K_d$  over the temperature range. Again this is consistent with the picture of a sensor architecture in which the entropic loss in organizing the system for binding is averaged over multiple binding events. Thus the binding of the cooperative receptors is expected to be dominated by the enthalpic contribution of the metal–ligand bonds. It is evident that as the binding affinity of the non-cooperative system decreases (at higher temperature), the effect of cooperativity is more pronounced. Thus the cooperative sensor **2c** has a five-fold greater effective binding constant for zinc than **2a** at the higher temperatures.

#### 4. Conclusions

A series of three sensors for metal ions has been synthesized which vary by the number of binding sites. The sensors incorporate an amino-methoxyquinaldine moiety which functions not only as a recognition unit but also as a PET based fluorescent readout. Fluorescence studies were performed at various temperatures and association was measured in terms of apparent  $K_d$ . Binding data for zinc and cadmium ions indicated that cooperative interactions produced an increase in affinity by lowering the entropic penalty for organizing the receptor for tight binding. The extent of the increase in affinity depended on the inherent strength of the recognition elements for the analyte. Taken together, these studies highlight the advantages of cooperative recognition.

#### 5. Experimental

##### 5.1. General procedures

NMR spectra were recorded on a Bruker WP-200, AC-200, DPX-300, AMX-360, DRX-400 in  $\text{CDCl}_3$  with residual protonated solvent or tetramethylsilane (TMS) as an internal reference unless otherwise noted. Fluorescence titrations were conducted on a Shimadzu 5301PC spectrofluorimeter using 0.5 or 1.0 mL sample volumes with 0.3  $\mu\text{M}$  sensor and 0.5 mM  $\text{NaClO}_4$  as a supporting electrolyte. UV/vis titrations were conducted on a Cary 1E spectrophotometer using 1.0 mL sample volumes and 10  $\mu\text{M}$  sensor and 0.5 mM  $\text{NaClO}_4$  as a supporting electrolyte. Dissociation constants and Hill coefficients were determined by fitting

the experimentally determined binding isotherms to the Hill equation using Kaleidagraph or by the standard linearization techniques for cooperative systems.<sup>13</sup>

##### 5.2. Synthesis

**5.2.1. 2-Bromomethyl-6-methoxy-quinoline 4.** A mixture of 6-methoxyquinaldine (820 mg, 4.7 mmol) and NBS (838 mg, 4.7 mmol) was refluxed in  $\text{CCl}_4$  (100 mL). AIBN (40 mg, 0.24 mmol) was added to the solution. The reaction was refluxed for an additional 3 h then cooled to 10 °C. The reaction mixture was filtered and the filtrate was concentrated in vacuo. The resultant residue was purified via chromatography ( $\text{SiO}_2$  1:1 DCM–hexanes) to give compound **4** as a pink solid (732 mg, 62%). Mp=98–100 °C dec.  $^1\text{H}$  NMR (300 MHz,  $\text{CDCl}_3$ ): 8.05 (d,  $J=8.5$  Hz, 1H), 7.96 (d,  $J=9.2$  Hz, 1H), 7.52 (d,  $J=8.5$  Hz, 1H), 7.37 (dd,  $J=9.2, 2.8$  Hz, 1H), 7.12 (d,  $J=2.8$  Hz, 1H), 4.69 (s, 2H), 3.93 (s, 3H).  $^{13}\text{C}$  NMR (50 MHz,  $\text{CDCl}_3$ ): 159.2, 155.3, 144.5, 136.9, 131.5, 129.2, 123.5, 122.3, 105.7, 55.9, 34.8. FTIR (neat): 2938, 1625, 1599, 1503, 1482, 1380, 1254, 1225, 1163, 1117, 1030  $\text{cm}^{-1}$ . HRMS ( $m/z$ ): calculated for  $\text{C}_{11}\text{H}_{11}\text{BrNO}$   $[\text{M}+\text{H}]^+$ : 252.0019, found: 252.0017.

**5.2.2. (6-Methoxy-quinolin-2-yl-methyl)-methylamine 5.** Bromide **4** (362 mg, 1.4 mmol) was dissolved in THF (2.0 mL) and added via syringe to a solution of  $\text{MeNH}_2$  in EtOH (24.2 g, 5.7 mmol  $\text{MeNH}_2/\text{g}$  solution) over 1 hr at room temperature. It was found that using the commercially available solutions of methylamine (40% in water or 1 M in THF) gave poorer results. The reaction was stirred for an additional 2 h. The solvent was removed and DCM (50 mL) was added to the resultant solid. Aqueous NaOH (2.0 M) was added via syringe to the stirred DCM suspension until all solids were dissolved (ca. 800  $\mu\text{L}$ ). The organic layer was separated and dried with  $\text{MgSO}_4$ . The solvent was removed and the remaining oil purified by chromatography ( $\text{SiO}_2$ , 15% TEA in EtOAc) to give compound **5** as a yellow oil (262 mg, 93%).  $^1\text{H}$  NMR (360 MHz,  $\text{CDCl}_3$ ): 7.99 (d,  $J=8.5$  Hz, 1H), 7.95 (d,  $J=9.3$  Hz, 1H), 7.39 (d,  $J=8.5$  Hz, 1H), 7.34 (dd,  $J=9.2, 2.8$  Hz, 1H), 7.05 (d,  $J=2.8$  Hz, 1H), 4.01 (s, 2H), 3.90 (s, 3H), 2.53 (s, 3H), 2.26 (br, 1H).  $^{13}\text{C}$  NMR (90 MHz,  $\text{CDCl}_3$ ): 157.6, 157.4, 143.8, 135.1, 130.3, 128.1, 121.9, 120.8, 105.1, 57.7, 55.4, 36.3. FTIR (neat): 3321, 2937, 2837, 1622, 1601, 1568, 1501, 1461, 1380, 1233, 1163, 1111, 1030  $\text{cm}^{-1}$ . HRMS ( $m/z$ ): calculated for  $\text{C}_{12}\text{H}_{15}\text{N}_2\text{O}$   $[\text{M}+\text{H}]^+$ : 203.1179, found: 203.1189.

**5.2.3. 4-Methoxytrityl alkyne 7a.** Chloride **6a** (2.5 g, 8.1 mmol) was dissolved in argon-sparged toluene (300 mL) and cooled to  $-78$  °C. To this was added ethynylmagnesium bromide (32 mL, 0.5 M in THF) via syringe over 10 min. The reaction was allowed to warm to room temperature and was stirred an additional 3 h. The reaction was quenched with saturated aqueous  $\text{NH}_4\text{Cl}$  and extracted with EtOAc. The organic layer was dried with  $\text{MgSO}_4$ , filtered, and concentrated in vacuo. The residue was purified via chromatography ( $\text{SiO}_2$ , 1:5 DCM–hexanes) to give compound **7a** as a white solid (1.889 g, 78%). Mp=100–103 °C.  $^1\text{H}$  NMR (300 MHz,  $\text{CDCl}_3$ ): 7.29–7.15 (m, 10H), 7.17–7.14 (m, 2H), 6.82–6.79 (m, 2H), 3.77 (s, 3H), 2.67 (s, 1H).  $^{13}\text{C}$  NMR (75 MHz,  $\text{CDCl}_3$ ): 158.4, 145.0,



136.9, 130.1, 129.0, 127.9, 126.8, 113.3, 90.0, 73.2, 55.2, 54.8. FTIR (neat): 3301, 3054, 2986, 2306, 1606, 1509, 1490, 1445, 1421, 1264, 1180  $\text{cm}^{-1}$ . HRMS ( $m/z$ ): calculated for  $\text{C}_{23}\text{H}_{19}\text{O}$  [ $\text{M}+\text{H}$ ] $^{+}$ : 299.1430, found: 299.1424.

**5.2.4. 1,4-Bis-(4-methoxytrityl)-butadiyne 8a.** Alkyne **7a** (1.02 g, 3.40 mmol) and CuCl (3.36 g, 34.0 mmol) were added to DCM (35 mL) at room temperature. *N*-methyl pyrrolidine (7.0 mL, 68 mmol) was added drop wise to the reaction.  $\text{O}_2$  was bubbled through the reaction via a dispersion tube for 8 h. The reaction was filtered through a  $\text{SiO}_2$  plug with EtOAc to remove the copper salts. The filtrate was concentrated and the residue purified via chromatography ( $\text{SiO}_2$ , 15% v/v DCM in hexanes) to give compound **8a** as an off white solid (626.7 mg, 61%). Mp = 187–188 °C.  $^1\text{H}$  NMR (360 MHz,  $\text{CD}_2\text{Cl}_2$ ): 7.32–7.23 (m, 20H), 7.15–7.13 (m, 4H), 6.86–6.82 (m, 4H), 3.78 (s, 6H).  $^{13}\text{C}$  NMR (75 MHz,  $\text{CD}_2\text{Cl}_2$ ): 159.1, 145.0, 136.7, 130.5, 129.3, 128.5, 127.4, 113.8, 84.9, 70.0, 56.0, 55.6. FTIR (neat): 3057, 2954, 2835, 2037, 1954, 1901, 1605, 1582, 1508, 1489, 1462, 1445, 1298, 1251, 1178  $\text{cm}^{-1}$ . HRMS ( $m/z$ ): calculated for  $\text{C}_{44}\text{H}_{35}\text{O}_2$  [ $\text{M}+\text{H}$ ] $^{+}$ : 594.2553, found: 594.2564.

**5.2.5. 1,4-Bis-(4-methoxytrityl-3-carboxaldehyde)-butadiyne 9a.** Bis-trityl **8a** (280 mg, 0.47 mmol) and  $\alpha,\alpha$ -dichloromethyl methyl ether (460  $\mu\text{L}$ , 5.0 mmol) were dissolved in DCM (60 mL) and the resulting solution cooled to  $-5$  °C.  $\text{TiCl}_4$  (660  $\mu\text{L}$ , 6.0 mmol) was added drop wise via syringe over 2 min. The reaction was allowed to warm to room temperature and was stirred an additional 1 hr. The reaction was poured into aqueous HCl (100 mL, 2.0 M) and stirred for 2 min. The aqueous suspension was extracted with EtOAc ( $3 \times 100$  mL). The organic extracts were combined, dried with  $\text{MgSO}_4$  and concentrated. The resultant residue was purified via column chromatography ( $\text{SiO}_2$ , 1:1 DCM–EtOAc) to give compound **9a** as an off white amorphous solid (300 mg, 98%).  $^1\text{H}$  NMR (300 MHz,  $\text{CD}_2\text{Cl}_2$ ): 10.4 (s, 2H), 7.56 (dd,  $J=8.7$ , 2.7 Hz, 2H), 7.51 (d,  $J=2.5$  Hz, 2H), 7.35–7.20 (m, 20H), 7.01 (d,  $J=8.7$  Hz, 2H), 3.93 (s, 6H).  $^{13}\text{C}$  NMR (75 MHz,  $\text{CD}_2\text{Cl}_2$ ): 189.4, 161.4, 144.2, 137.1, 136.8, 129.2, 128.7, 128.6, 127.7, 124.5, 112.3, 84.6, 70.4, 56.3, 56.0. FTIR (neat): 3058, 2942, 2861, 1684, 1604, 1579, 1490, 1446, 1417, 1393, 1282, 1254, 1205, 1180, 1110, 1025  $\text{cm}^{-1}$ . HRMS ( $m/z$ ): calculated for  $\text{C}_{46}\text{H}_{35}\text{O}_4$  [ $\text{M}+\text{H}$ ] $^{+}$ : 651.2530, found: 651.2555.

**5.2.6. 1,1,4,4-Tetraphenyl-1,4-bis(2-methoxy-benz-4-yl-(6-methoxyquinolin-2-ylmethyl) methylamino)-butadiyne 2a.** Aldehyde **9a** (60 mg, 0.077 mmol) and amine **5** (60 mg, 0.30 mmol) were dissolved in DCM (3.0 mL). To this was added HOAc (14  $\mu\text{L}$ , 0.22 mmol) and  $\text{NaBH}(\text{OAc})_3$  (61 mg, 0.30 mmol). The reaction was allowed to stir for 10 h. Aqueous NaOH (1 M, 2 mL) was added and the reaction was stirred for 5 min. The organic layer was separated and dried with  $\text{MgSO}_4$ . The solvent was removed and the resultant residue was purified via chromatography twice ( $\text{SiO}_2$ , 2% TEA/EtOAc then 2% MeOH( $\text{NH}_3$ )/DCM) to give compound **2a** as an amorphous yellow solid (53 mg, 66%).  $^1\text{H}$  NMR (300 MHz,  $\text{CD}_3\text{CN}/\text{CD}_2\text{Cl}_2$ ): 7.82 (d,  $J=8.5$  Hz, 2H), 7.78 (d,  $J=9.2$  Hz, 2H),

7.45 (d,  $J=2.5$  Hz, 2H), 7.32 (d,  $J=8.5$  Hz, 2H), 7.30–7.20 (m, 22H), 6.98 (d,  $J=2.7$  Hz, 2H), 6.97 (dd,  $J=8.6$ , 2.5 Hz, 2H), 6.78 (d,  $J=8.7$  Hz, 2H), 3.83 (s, 6H), 3.73 (s, 6H), 3.69 (s, 4H), 3.55 (s, 4H), 2.14 (s, 6H).  $^{13}\text{C}$  NMR (75 MHz,  $\text{CDCl}_3$ ): 158.3, 157.2, 156.6, 144.8, 143.3, 136.1, 135.1, 131.1, 130.2, 129.0, 128.4, 128.2, 128.0, 126.9, 126.6, 121.5, 121.3, 109.6, 105.2, 84.5, 69.8, 64.1, 55.7, 55.5, 55.3, 42.5. FTIR (neat): 2939, 2836, 1623, 1601, 1558, 1498, 1456, 1377, 1310, 1234, 1161, 1110, 1031  $\text{cm}^{-1}$ . HRMS ( $m/z$ ): calculated for  $\text{C}_{70}\text{H}_{64}\text{N}_4\text{O}_4$  [ $\text{M}+2\text{H}$ ] $^{2+}$ : 512.2458, found: 512.2439.

**5.2.7. 4,4'-Dimethoxytrityl-alkyne 7b.** Chloride **6b** (2.5 g, 7.4 mmol) was dissolved in argon sparged toluene (300 mL) and cooled to  $-78$  °C. To this was added ethynylmagnesium bromide (20 mL, 0.5 M in THF) via syringe over 10 min. The reaction was allowed to warm to room temperature and was stirred an additional 3 h. The reaction was quenched with saturated aqueous  $\text{NH}_4\text{Cl}$  and extracted with EtOAc. The organic layer was dried with  $\text{MgSO}_4$ , filtered, and concentrated in vacuo. The residue was purified via chromatography ( $\text{SiO}_2$ , 1:4 DCM–hexanes) to give compound **7b** as a white solid (1.400 g, 57%). Mp = 107–108 °C.  $^1\text{H}$  NMR (300 MHz,  $\text{CDCl}_3$ ): 7.35–7.25 (m, 5H), 7.22–7.19 (m, 4H), 6.87–6.84 (m, 4H), 3.83 (s, 6H), 2.72 (s, 1H).  $^{13}\text{C}$  NMR (75 MHz,  $\text{CDCl}_3$ ): 158.3, 145.3, 137.2, 130.1, 128.9, 128.0, 126.8, 113.3, 90.2, 73.0, 55.2, 54.1. FTIR (neat): 3053, 2986, 2305, 1607, 1509, 1421, 1422, 1265, 1179, 1034  $\text{cm}^{-1}$ . HRMS ( $m/z$ ): calculated for  $\text{C}_{23}\text{H}_{21}\text{O}_2$  [ $\text{M}+\text{H}$ ] $^{+}$ : 329.1536, found: 329.1515.

**5.2.8. 1,4-Bis-(4,4'-dimethoxytrityl)-butadiyne 8b.** Alkyne **7b** (691 mg, 2.1 mmol) and CuCl (2.0 g, 21 mmol) were added to DCM (20 mL) at room temperature. *N*-methyl pyrrolidine (4.4 mL, 42 mmol) was added drop wise to the reaction.  $\text{O}_2$  was bubbled through the reaction via a dispersion tube for 8 h. The reaction was poured into 100 mL dilute aqueous HCl and extracted with DCM. The organic layer was dried with  $\text{MgSO}_4$ , concentrated in vacuo and the residue purified via chromatography ( $\text{SiO}_2$ , 20% v/v DCM in hexanes) to give compound **8b** as an off white solid (420 mg, 64%). Mp = 172–173 °C.  $^1\text{H}$  NMR (360 MHz,  $\text{CD}_2\text{Cl}_2$ ): 7.35–7.23 (m, 10H), 7.18–7.16 (m, 4H), 6.86–6.84 (m, 4H), 3.80 (s, 6H).  $^{13}\text{C}$  NMR (75 MHz,  $\text{CD}_2\text{Cl}_2$ ): 159.1, 145.4, 137.1, 130.5, 129.3, 128.5, 127.3, 113.8, 85.2, 69.9, 55.6, 55.4. FTIR (neat): 3055, 2955, 2836, 2042, 1960, 1894, 1734, 1606, 1583, 1507, 1464, 1444, 1415, 1300, 1251, 1177, 1033  $\text{cm}^{-1}$ . HRMS ( $m/z$ ): calculated for  $\text{C}_{46}\text{H}_{39}\text{O}_4$  [ $\text{M}+\text{H}$ ] $^{+}$ : 655.2843, found: 655.2831.

**5.2.9. 1,4-Bis-(4,4'-dimethoxytrityl-3,3'-di-carboxaldehyde)-butadiyne 9b.** Bis-trityl **8b** (420 mg, 0.64 mmol) and  $\alpha,\alpha$ -dichloromethyl methyl ether (574  $\mu\text{L}$ , 6.4 mmol) were dissolved in DCM (60 mL) and the resulting solution cooled to  $-5$  °C.  $\text{TiCl}_4$  (840  $\mu\text{L}$ , 7.6 mmol) was added drop wise via syringe over 2 min. The reaction was allowed to warm to room temperature and was stirred an additional 20 min. The reaction was poured into aqueous HCl (100 mL, 2.0 M) and stirred for 2 min. The aqueous suspension was extracted with EtOAc ( $3 \times 100$  mL). The organic extracts were combined, dried with  $\text{MgSO}_4$  and concentrated. The resultant residue was purified via chromatography ( $\text{SiO}_2$ , 1:1 DCM–EtOAc) to give compound **9b** as a pink

amorphous solid (505 mg, 98%).  $^1\text{H}$  NMR (300 MHz,  $\text{CD}_2\text{Cl}_2$ ): 10.45 (s, 4H), 7.61 (dd,  $J=8.6$ , 2.7 Hz, 4H), 7.58 (d,  $J=2.3$  Hz, 4H), 7.45–7.25 (m, 10H), 7.08 (d, 8.6 Hz, 4H), 4.00 (s, 12H).  $^{13}\text{C}$  NMR (75 MHz,  $\text{CD}_2\text{Cl}_2$ ): 189.4, 161.5, 143.8, 136.7, 129.9, 129.1, 128.8, 128.5, 127.9, 124.6, 112.4, 84.5, 70.1, 56.3, 55.3. FTIR (neat): 3057, 2943, 2864, 1683, 1604, 1578, 1491, 1463, 1418, 1393, 1282, 1255, 1205, 1180, 1112, 1023  $\text{cm}^{-1}$ . HRMS ( $m/z$ ): calculated for  $\text{C}_{50}\text{H}_{39}\text{O}_8$   $[\text{M}+\text{H}]^+$ : 767.2640, found: 767.2612.

**5.2.10. 1,4-Diphenyl-1,1,4,4-tetra(2-methoxy-benz-4-yl)-(6-methoxyquinolin-2-ylmethyl)-methylamino)-butadiyne 2b.** Aldehyde **9b** (17 mg, 0.026 mmol), amine **5** (43 mg, 0.21 mmol) were dissolved in DCM (2.0 mL). To this was added HOAc (10  $\mu\text{L}$ , 0.17 mmol) and  $\text{NaBH}(\text{OAc})_3$  (45 mg, 0.21 mmol). The reaction was allowed to stir for 10 h. Aqueous NaOH (1 M, 2 mL) was added and the reaction was stirred for 5 min. The organic layer was separated and dried with  $\text{MgSO}_4$ . The solvent was removed and the resultant residue was purified via chromatography twice ( $\text{SiO}_2$ , 2% TEA/EtOAc then 2% MeOH( $\text{NH}_3$ )/DCM) to give compound **2b** as an amorphous yellow solid (30 mg, 81%).  $^1\text{H}$  NMR (300 MHz,  $\text{CDCl}_3$ ): 7.86 (d,  $J=9.2$  Hz, 4H), 7.73 (d,  $J=8.6$  Hz, 4H), 7.44 (d,  $J=2.2$  Hz, 4H), 7.40 (d,  $J=7.8$  Hz, 4H), 7.35–7.15 (m, 14H), 7.06 (dd,  $J=8.4$ , 2.4 Hz, 4H), 6.83 (d,  $J=2.7$  Hz, 4H), 6.66 (d,  $J=8.7$  Hz, 4H), 3.83 (s, 12H), 3.75 (s, 8H), 3.69 (s, 12H), 3.56 (s, 8H), 2.13 (s, 12H).  $^{13}\text{C}$  NMR (75 MHz,  $\text{CDCl}_3$ ): 158.2, 157.2, 156.5, 145.2, 143.3, 136.5, 135.1, 131.0, 130.2, 129.0, 128.4, 128.2, 127.9, 126.7, 126.5, 121.5, 121.2, 109.6, 105.2, 84.8, 69.7, 64.0, 55.4, 55.3, 55.2, 42.5. FTIR (neat): 2940, 2836, 1623, 1601, 1497, 1456, 1378, 1310, 1235, 1161, 1110, 1031  $\text{cm}^{-1}$ . HRMS ( $m/z$ ): calculated for  $\text{C}_{98}\text{H}_{96}\text{N}_8\text{O}_2$   $[\text{M}+2\text{H}]^{2+}$ : 756.3670, found: 756.3661.

**5.2.11. 4,4',4''-Trimethoxytrityl alkyne 7c.** Chloride **6c** (2.66 g, 7.14 mmol) was dissolved in argon sparged toluene (200 mL) and cooled to  $-78^\circ\text{C}$ . To this was added ethynyl-magnesium bromide (30 mL, 0.5 M in ether) via syringe over 10 min. The reaction was allowed to warm to room temperature and was stirred an additional 3 h. The reaction was quenched with saturated aqueous  $\text{NH}_4\text{Cl}$  and extracted with EtOAc. The organic layer was dried with  $\text{MgSO}_4$ , filtered, and concentrated in vacuo. The residue was purified via chromatography ( $\text{SiO}_2$ , 40% DCM/hexanes) to give compound **6c** as a white solid (1.97 g, 76%). Mp = 126–128  $^\circ\text{C}$ .  $^1\text{H}$  NMR (300 MHz,  $\text{CDCl}_3$ ): 7.23–7.20 (m, 6H), 6.87–6.84 (m, 6H), 3.82 (s, 9H), 2.71 (s, 1H).  $^{13}\text{C}$  NMR (75 MHz,  $\text{CD}_2\text{Cl}_2$ ): 158.3, 137.5, 130.0, 113.2, 90.3, 72.7, 55.2, 53.4. FTIR (neat): 3305, 3154, 2958, 2838, 2253, 1794, 1606, 1583, 1507, 1464, 1381, 1297, 1250, 1178, 1095  $\text{cm}^{-1}$ . HRMS ( $m/z$ ): calculated for  $\text{C}_{24}\text{H}_{22}\text{O}_3$   $[\text{M}]^+$ : 358.1564, found: 358.1560.

**5.2.12. 1,4-Bis-(4,4',4''-trimethoxytrityl)-butadiyne 8c.** Alkyne **7c** (500 mg, 1.39 mmol) and  $\text{CuCl}$  (3.45 g, 34.8 mmol) were suspended in DCM (5.0 mL). To this was added TMEDA (5.85 mL, 38.7 mmol) via syringe over 10 min. The reaction was stirred for 2 days while being vented to the atmosphere via an 18 gauge needle. The reaction was quenched with saturated aqueous  $\text{NH}_4\text{Cl}$  and then extracted with DCM. The organic layer dried with  $\text{MgSO}_4$  and the solvent removed. The residue was purified via

chromatography ( $\text{SiO}_2$ , gradient elution from 30% DCM/hexanes to 100% DCM then to 100% EtOAc) to give compound **8c** as an off white solid (355 mg, 71%). Mp = 265–266  $^\circ\text{C}$ .  $^1\text{H}$  NMR (360 MHz,  $\text{CDCl}_3$ ): 7.14–7.12 (m, 12H), 6.83–6.80 (m, 12H), 3.79 (s, 18H).  $^{13}\text{C}$  NMR (50 MHz,  $\text{CDCl}_3$ ): 158.4, 137.2, 130.1, 113.3, 84.6, 69.4, 55.2, 54.3. FTIR (KBr): 2932, 2836, 2055, 2896, 1742, 1606, 1582, 1502, 1461, 1414, 1300, 1246, 1176, 1114, 1031  $\text{cm}^{-1}$ . HRMS ( $m/z$ ): calculated for  $\text{C}_{48}\text{H}_{42}\text{O}_6$   $[\text{M}]^+$ : 714.2976, found: 715.2971.

**5.2.13. 1,4-Bis-(4,4',4''-trimethoxytrityl 3,3',3''-tricarboxaldehyde)-butadiyne 9c.** Bis-trityl **8c** (243 mg, 0.339 mmol) and  $\alpha,\alpha$ -dichloromethyl methyl ether (570  $\mu\text{L}$ , 6.1 mmol) were dissolved in DCM (30 mL) and the resulting solution cooled to  $0^\circ\text{C}$ .  $\text{TiCl}_4$  (872  $\mu\text{L}$ , 7.7 mmol) was added drop wise via syringe over 2 min. The reaction was allowed to warm to room temperature and was stirred an additional 2 hr. The reaction was poured into aqueous HCl (100 mL, 2.0 M) and stirred for 2 min. The aqueous suspension was extracted with EtOAc ( $3 \times 100$  mL). The organic extracts were combined, dried with  $\text{MgSO}_4$  and concentrated. The resultant residue was purified via column chromatography ( $\text{SiO}_2$ , 1:1 DCM–EtOAc) to give compound **9c** as an off white amorphous solid (300 mg, 99%).  $^1\text{H}$  NMR (300 MHz,  $\text{CDCl}_3$ ): 10.39 (s, 6H), 7.55 (d,  $J=2.6$  Hz, 6H), 7.49 (dd,  $J=8.7$ , 2.6 Hz, 6H), 6.98 (d,  $J=8.8$  Hz, 6H), 3.93 (s, 18H).  $^{13}\text{C}$  NMR (75 MHz,  $\text{CDCl}_3$ ): 189.4, 161.1, 136.4, 136.0, 128.3, 124.2, 112.0, 83.9, 70.5, 55.8, 54.1. FTIR (neat): 3157, 2944, 2868, 2041, 1682, 1603, 1494, 1462, 1418, 1393, 1281, 1258, 1181, 1113, 1023  $\text{cm}^{-1}$ . HRMS ( $m/z$ ): calculated for  $\text{C}_{54}\text{H}_{43}\text{O}_{12}$   $[\text{M}+\text{H}]^+$ : 883.2749, found: 883.2716.

**5.2.14. 1,1,1,4,4,4-Hexa-(2-methoxybenz-4-yl)-(6-methoxyquinolin-2-yl-methyl) methylamino)-butadiyne 2c.** Aldehyde **9c** (30 mg, 0.033 mmol), amine **5** (81 mg, 0.40 mmol) were dissolved in DCM (2.0 mL). To this was added HOAc (23  $\mu\text{L}$ , 0.40 mmol) and  $\text{NaBH}(\text{OAc})_3$  (85 mg, 0.40 mmol). The reaction was allowed to stir for 10 h. Aqueous NaOH (1 M, 2 mL) was added and the reaction was stirred for 5 min. The organic layer was separated and dried with  $\text{MgSO}_4$ . The solvent was removed and the resultant residue was purified via chromatography twice on using ( $\text{SiO}_2$ , 2% TEA/EtOAc then 2% MeOH( $\text{NH}_3$ )/DCM) to give compound **2c** as an amorphous yellow solid (33 mg, 50%).  $^1\text{H}$  NMR (360 MHz,  $\text{CDCl}_3$ ): 7.84 (d,  $J=9.2$  Hz, 6H), 7.67 (d,  $J=8.4$  Hz, 6H), 7.47 (d,  $J=2.3$  Hz, 6H), 7.37 (d,  $J=8.8$  Hz, 6H), 7.24 (dd,  $J=9.2$ , 2.8 Hz, 6H), 7.10 (dd,  $J=8.3$ , 2.2 Hz, 6H), 6.77 (d,  $J=2.5$  Hz, 6H), 6.60 (d,  $J=8.7$  Hz, 6H), 3.81 (s, 18H), 3.69 (s, 12H), 3.63 (s, 18H), 3.52 (s, 12H), 2.09 (s, 18H).  $^{13}\text{C}$  NMR (90 MHz,  $\text{CDCl}_3$ ): 158.3, 157.2, 156.5, 143.3, 137.1, 135.0, 131.0, 130.3, 128.4, 128.1, 126.5, 121.4, 121.2, 109.7, 105.4, 85.2, 69.7, 64.0, 55.4, 55.3, 55.2, 54.7, 42.5. FTIR (neat): 2935, 2836, 2049, 1681, 1624, 1601, 1499, 1462, 1378, 1310, 1235, 1162, 1110, 1031  $\text{cm}^{-1}$ . HRMS ( $m/z$ ): calculated for  $\text{C}_{126}\text{H}_{128}\text{N}_{12}\text{O}_{12}$   $[\text{M}+2\text{H}]^{2+}$ : 1000.4882, found: 1000.4865.

#### Acknowledgements

This work was supported by the National Institutes of Health (GM 59245).

## References and notes

1. (a) *Chemosensors of Ion and Molecule Recognition*; Desvergne, J. P., Czarnik, A. W., Eds.; NATO ASI Series C: 492; Kluwer: Dordrecht, 1997. (b) de Silva, A. P.; Gunaratne, H. Q. N.; Gunnlaugsson, T.; Huxley, A. J. M.; McCoy, C. P.; Radermacher, J. T.; Rice, T. E. *Chem. Rev.* **1997**, *97*, 1515–1566. (c) Czarnik, A. W. *Chem. and Bio.* **1995**, *2*, 423. (d) Wiskur, S. L.; Ait-Haddou, H.; Lavigne, J. J.; Anslyn, E. V. *Acc. Chem. Res.* **2001**, *34*, 963–972.
2. (a) Glass, T. E. *J. Am. Chem. Soc.* **2000**, *122*, 4522–4523. (b) Raker, J.; Glass, T. E. *J. Org. Chem.* **2001**, *66*, 6505–6512.
3. Rebek, J.; Costello, T.; Marshall, L.; Wattle, R.; Gadwood, R. C.; Onan, K. *J. Am. Chem. Soc.* **1985**, *107*, 7481–7487.
4. Shinkai, S.; Ikeda, M.; Sugasaki, A.; Takeuchi, M. *Acc. Chem. Res.* **2001**, *34*, 494–503. Takeuchi, M.; Ikeda, M.; Sugasaki, A.; Shinkai, S. *Acc. Chem. Res.* **2001**, *34*, 865–873.
5. (a) Wipf, P.; Venkatraman, S.; Miller, C. P.; Geib, S. *J. Angew. Chem., Int. Ed. Engl.* **1994**, *33*, 1516–1518. (b) Blanc, S.; Yakirevitch, P.; Leize, E.; Meyer, M.; Libman, J.; Van Dorsselaer, A.; Albrecht-Gary, A.-M.; Shanzer, A. *J. Am. Chem. Soc.* **1997**, *119*, 4934–4944. (c) Takeuchi, M.; Shioya, T.; Swager, T. M. *Angew. Chem., Int. Ed.* **2001**, *40*, 3372–3376.
6. (a) Marquis, K.; Desvergne, J.-P.; Bouas-Laurent, H. *J. Org. Chem.* **1995**, *60*, 7984–7996. (b) Chen, C.-T.; Huang, W. *J. Am. Chem. Soc.* **2002**, *124*, 6246–6247.
7. (a) Williams, D. H.; Westwell, M. S. *Chem. Soc. Rev.* **1998**, *57*. (b) Williams, D. H.; Searle, M.; Mackay, J. P.; Gerhard, U.; Maplestone, R. A. *Proc. Natl. Acad. Sci. U.S.A.* **1993**, *90*, 1172–1178.
8. Yang, W.; He, H.; Drueckhammer, D. G. *Angew. Chem., Int. Ed. Engl.* **2001**, *40*, 1714–1718.
9. Raker, J.; Glass, T. E. *J. Org. Chem.* **2002**, *67*, 6113–6116.
10. Raker, J.; Glass, T. E. *Tetrahedron* **2001**, *57*, 10233–10240.
11. Ikeda, M.; Takeuchi, M.; Sugasaki, A.; Robertson, A.; Imada, T.; Shinkai, S. *Supramol. Chem.* **2000**, *12*, 321.
12. Wyman, J.; Gill, S. J. *Binding and Linkage: Functional Chemistry of Biological Macromolecules*; University Science Books: Mill Valley, CA, 1990.
13. Connors, K. A. *Binding Constants*; Wiley: New York, 1987.

# Rational design of novel photoinduced electron transfer type fluorescent probes for sodium cation

Suguru Kenmoku,<sup>a</sup> Yasuteru Urano,<sup>a</sup> Koujirou Kanda,<sup>a</sup> Hirotatsu Kojima,<sup>a</sup> Kazuya Kikuchi<sup>a,b</sup> and Tetuso Nagano<sup>a,\*</sup>

<sup>a</sup>Graduate School of Pharmaceutical Sciences, The University of Tokyo, 7-3-1 Hongo, Bunkyo-ku, Tokyo 113-0033, Japan

<sup>b</sup>Presto, JST Corporation, 4-8-1 Honcho, Kawaguchi, Saitama 332-0012, Japan

Received 31 January 2004; accepted 22 June 2004

Available online 23 August 2004

**Abstract**—We have developed novel fluorescence probes for sodium cation based on photoinduced electron transfer (PeT). In this study, we rationally designed new probes and succeeded in achieving fluorescence enhancement upon sodium ion binding by reducing the HOMO energy level of the chelator group within the probe molecule. Our new probes show low pH dependency, possibly because of their simple structures. Our results confirm the value of rational probe design based on PeT.

© 2004 Elsevier Ltd. All rights reserved.

## 1. Introduction

Fluorescein is highly fluorescent in aqueous media and emits longer wavelength light upon excitation at 490 nm. For these reasons, various fluorescein derivatives have been used as fluorescent tags<sup>1</sup> or fluorescence probes.<sup>2</sup> For example, many fluorescein-based fluorescence probes are available for various cations, such as Fluo-3,<sup>3</sup> ZnAF-2<sup>4</sup> and CoroNa Red<sup>5</sup> (Fig. 1). Most of these probes are based on an aminofluorescein structure containing a selective chelator for the target cation. Why has this structure been retained in so many cation probes? One answer is that many chelators consist of nitrogen atoms.<sup>6</sup> However, another and more important reason is that aminofluorescein is non-fluorescent and becomes fluorescent upon formation of the amidoderi-

vative.<sup>7</sup> In this sense, design of these fluorescence probes is largely empirical, and this limits the design flexibility.

Recently, we showed that the fluorescein molecule is a directly conjugated electron donor and acceptor system.<sup>8</sup> Furthermore, the fluorescence properties of fluorescein derivatives can be controlled by intramolecular photoinduced electron transfer (PeT). PeT is a well-known mechanism through which the fluorescence of a fluorophore is quenched by electron transfer from the donor to the acceptor.<sup>9</sup> In a molecule in which two groups, a fluorophore (electron acceptor) and its fluorescence quencher (electron donor) are located in close proximity and have no ground state interaction with each other, when the fluorophore is photochemically excited, a single electron is transferred

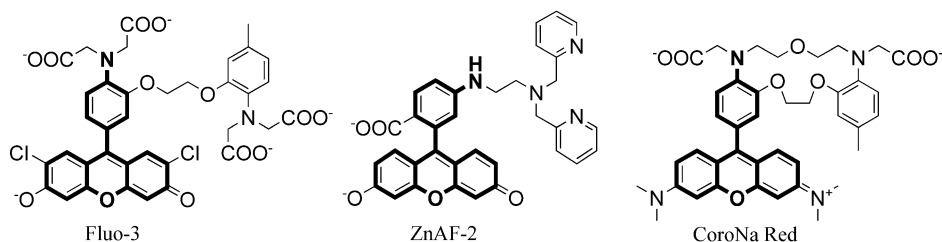


**Figure 1.** Cation probes based on PeT. Solid lines indicate the aminofluorescein or aminorhodamine platform.

**Keywords:** Photoinduced electron transfer; Rational design; Fluorescence probe; Sodium cation.

\* Corresponding author. Tel.: +81358414854; fax: +81358414855; e-mail: [ff26014@mail.ecc.u-tokyo.ac.jp](mailto:ff26014@mail.ecc.u-tokyo.ac.jp)

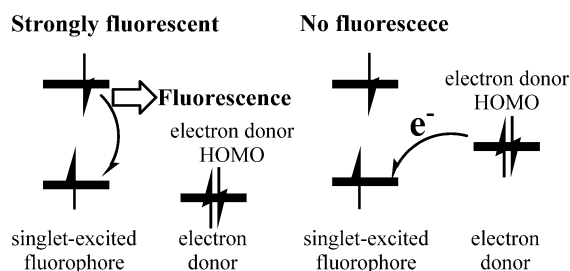


**Figure 2.** On the left, the HOMO energy level of the electron donor moiety is too low to allow electron transfer. Consequently, emission from the singlet-excited fluorophore is not affected. On the right, the HOMO energy level is enough high to allow electron transfer, so the fluorescence decreases.

from the electron donor to the excited fluorophore. Consequently, the fluorophore loses its energy thermally instead of by emitting fluorescence (Fig. 2).

Indeed, many fluorescence probes for cations as (Fig. 1) are based on PeT. Furthermore, almost all probes that detect cations are structurally based on aminofluorescein. The aniline moiety within aminofluorescein quenches the fluorescence of the singlet excited xanthene dye. However, is aminofluorescein necessary for developing novel probes? Our recent work suggests that the answer to this question is no.

Our report<sup>8</sup> revealed that the rate of intramolecular PeT in the fluorescein molecule follows the Marcus and Rehm–Weller equations and that fluorescein derivatives have characteristically small  $\lambda$  and  $V$  values.

Marcus equation:

$$k_{\text{PeT}} = \left( \frac{4\pi^3}{h^2 \lambda k_B T} \right)^{1/2} V^2 \exp \left[ \frac{-(\Delta G_{\text{PeT}}^0 + \lambda)^2}{4\lambda k_B T} \right] \quad (1)$$

$\lambda$ , reorganization energy;  $V$ , electronic coupling matrix element between electron donor and acceptor;  $\Delta G_{\text{PeT}}^0$ , free energy of electron transfer reaction.

Rehm–Weller equation:

$$\Delta G_{\text{PeT}}^0 = E_{\text{ox}} - E_{\text{red}} - \Delta E_{00} - w_p \quad (2)$$

$E_{\text{ox}}$ , oxidation potential of electron donor;  $E_{\text{red}}$ , reduction potential of electron acceptor;  $\Delta E_{00}$ , singlet excitation energy of fluorophore;  $w_p$ , work term for charge separation state.

We very recently found that the carboxyl group of fluorescein molecule can be replaced with other substituents such as methyl or methoxyl<sup>10</sup> (Fig. 3). For example, the methyl-substituted derivative called 2-MeTokyoGreen (2-MeTG) was as fluorescent as the traditional fluorescein molecule (Fig. 3). We synthesized many derivatives, and found an excellent relationship<sup>10</sup> between the HOMO energy levels of the benzene moiety (electron donor) and the quantum efficiency (QE) of TGs: a higher-HOMO-energy-level benzene moiety diminishes the fluorescence of xanthene more efficiently (Fig. 3), and the threshold HOMO energy level for fluorescence off/on switching could be precisely determined. Those findings enabled us to control the fluorescence properties of xanthene without an aniline moiety and gave great flexibility in designing novel probes. Using these findings, we tried to develop novel cation probes bearing only O atoms as ligands.

## 2. Results and discussion

We chose benzo-15-crown-5-ether derivatives as candidates for the electron donor. We calculated the HOMO energy levels of *o*-dimethoxybenzenes as analogues of the benzo-crown-ether moiety. As shown in Figure 3, 3,4-dimethoxybenzoic acid (compound (1), whose HOMO energy level is  $-0.220$  hartrees, solid line) seems not to be a good electron donor group; on the other hand, 3,4-dimethoxytoluene ((2),  $-0.206$  hartrees, dashed line) seems to be a good donor. So compound (3) should emit strong fluorescence (in other words, retention of the carboxyl group has prevented the development of cation probes with a plain benzo-crown-ether), while compound (4) should emit little fluorescence. Thus, we synthesized the novel sodium probes, (10a) and (10b) shown in Scheme 1. In general, the  $pK_a$  value of the phenolic hydroxyl group of xanthene is about 6<sup>11</sup> and that of 2,7-dichloroxanthene is about 4.5, so it is likely that (10b) will be a better probe than (10a) under acidic conditions.

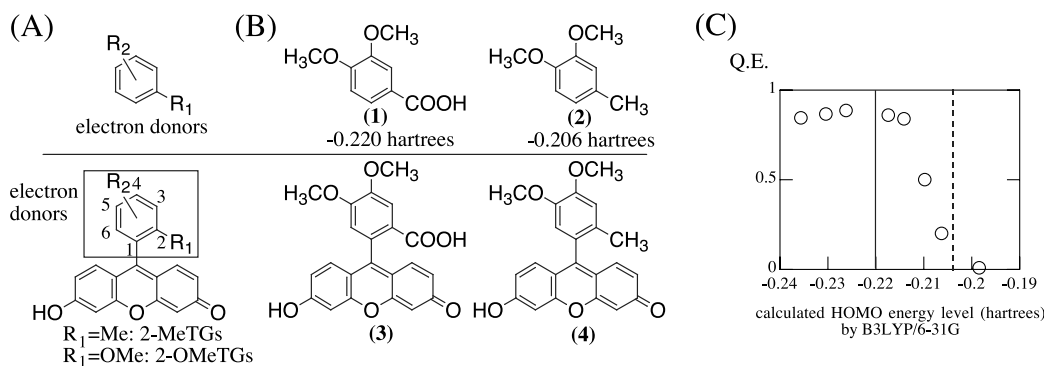
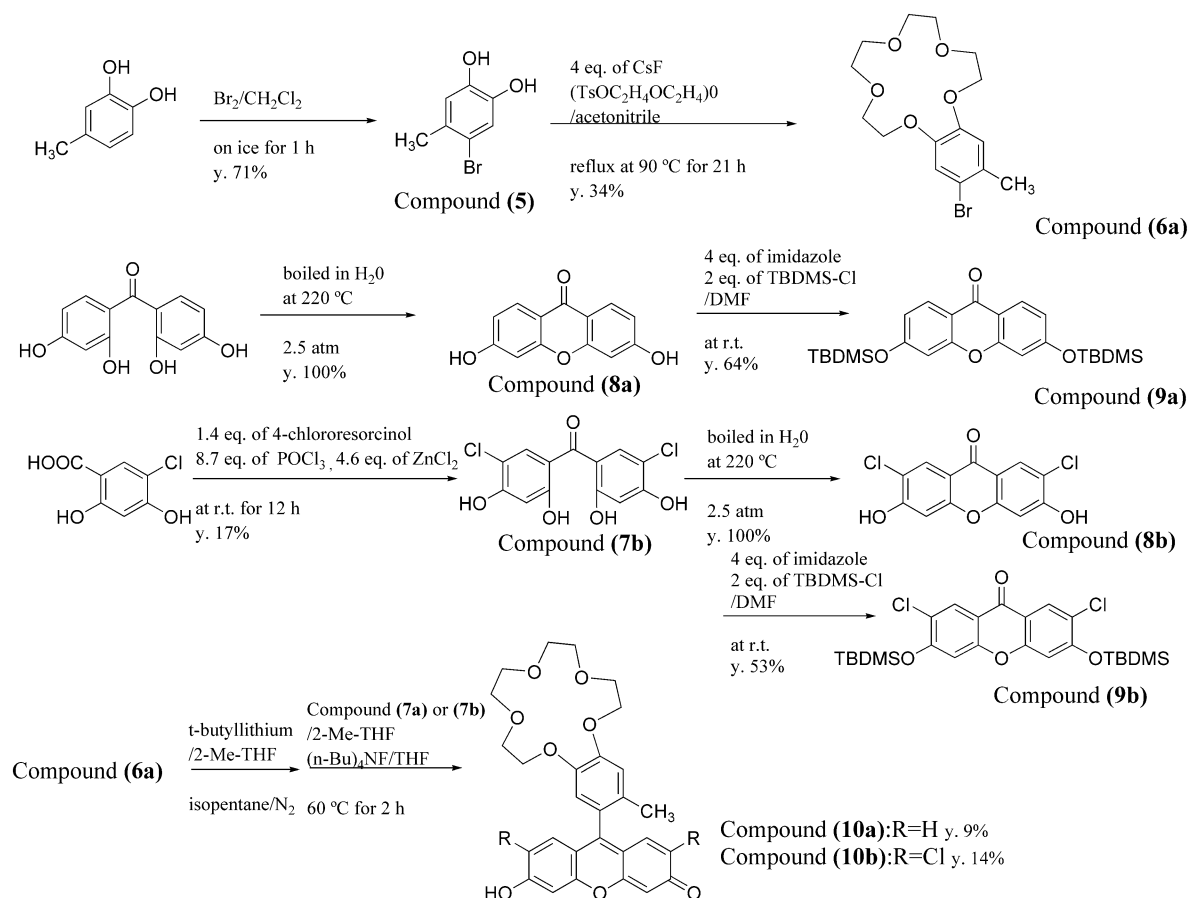


**Figure 3.** (A) Electron donors and TokyoGreens. (B) Tested analogues for rational design of novel probes. (C) The graph is a plot of the HOMO level of the benzene moiety (electron donor) versus the QE of TGs. HOMO energy levels were calculated by B3LYP/6-31G. The points represent 2-MeTG, 2,4-diMeTG, 2,5-diMeTG, 2-OMeTG, 2-Me, 4-OMeTG, 2-OMe,5-MeTG, 2,4-diOMeTG, and 2,5-diOMeTG, from left to right. The solid line and dashed line indicate the calculated HOMO energy levels of compounds (1) and (2), respectively. QE of (3) and (4) can be estimated from the intersection of the respective lines with the best fit to the points on the graph.



Scheme 1. Synthesis of compounds (10a) and (10b).

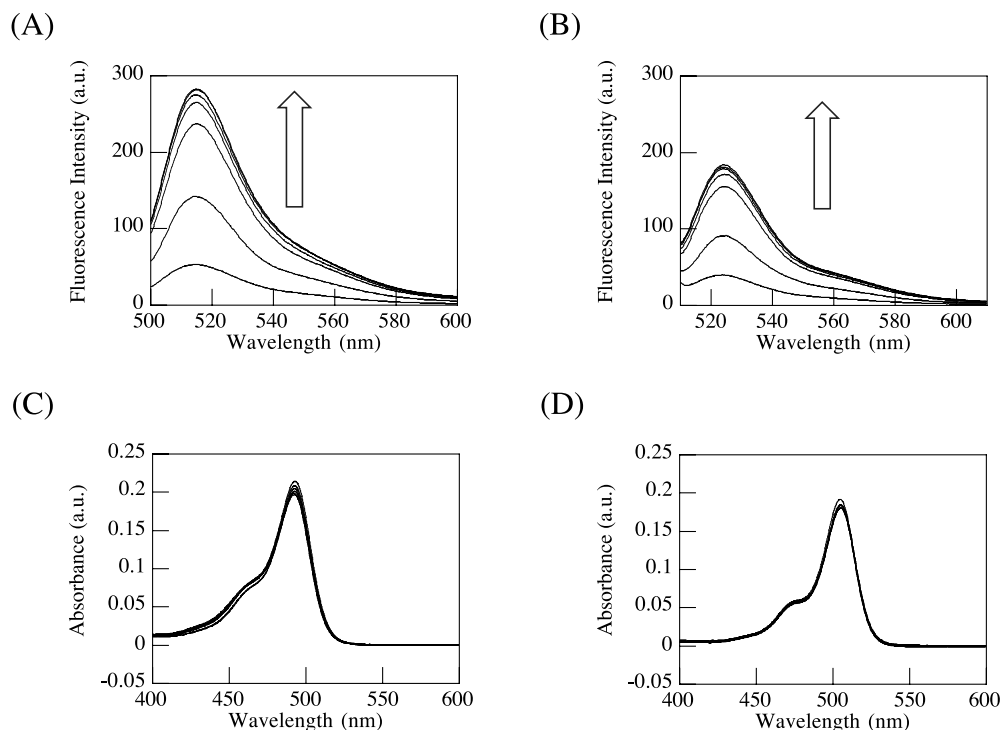


**Figure 4.** Panels A and B are emission spectra of **(10a)** and **(10b)** excited at 492 and 506 nm, respectively. Panel C and D are absorbance spectra of **(10a)** and **(10b)**, respectively. Each sample was measured in aqueous MOPS buffer, pH 7.0, containing 0.5% DMF as a cosolvent. Probes were added as stock solution in DMF, finally 3  $\mu\text{M}$ .  $[\text{NaClO}_4]$  was 0, 200, 700, 1000, 1500, 2000 or 3000 mM. In panel A,  $\Phi_{\text{fl}}([\text{NaClO}_4] = 3000 \text{ mM}) = 0.041$ ,  $\Phi_{\text{fl}}([\text{NaClO}_4] = 0 \text{ mM}) = 0.008$ . In panel B,  $\Phi_{\text{fl}}([\text{NaClO}_4] = 3000 \text{ mM}) = 0.025$ ,  $\Phi_{\text{fl}}([\text{NaClO}_4] = 0 \text{ mM}) = 0.005$ .

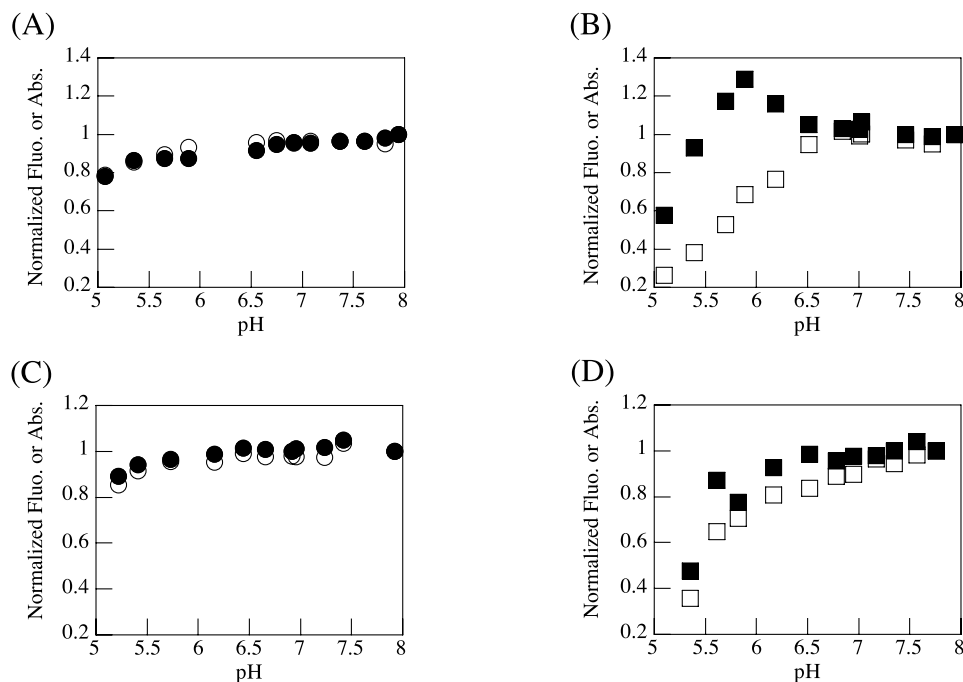


**Figure 5.** Fluorescence intensity and absorbance were normalized to those at pH 8. Each sample was measured in aqueous MOPS buffer of various pH values, adjusted with trimethylammonium hydroxide, containing 0 or 1000 mM NaClO<sub>4</sub>, and 0.1% DMF as a cosolvent. The final concentrations of (**10b**) and Sodium Green are 3 and 0.5  $\mu$ M, respectively. Panels A and C are normalized absorbance (open circle) and normalized fluorescence (closed circle) of (**10b**) in 0 and 1000 mM NaClO<sub>4</sub>, respectively. Panels B and D are normalized absorbance (open square) and normalized fluorescence (closed square) of Sodium Green in 0 and 1000 mM NaClO<sub>4</sub>, respectively.

Absorption and emission spectra of (**10a**) and (**10b**) are shown in Figure 4. For both probes, the fluorescence intensity was enhanced by the addition of sodium perchlorate while there was little change in the absorption spectrum, which means that the fluorescence increases of (**10a**) and (**10b**) resulted from increases of QE. The QE of (**10a**) increased from 0.008 to 0.041, that is, about 5-fold, upon binding Na<sup>+</sup>. The QE of (**10b**) also increased from 0.005 to 0.025, that is, also 5-fold. Quite similar results were obtained in the case of NaCl addition, so the photochemical properties of (**10a**) and (**10b**) are independent of the counter anion. These fluorescence enhancements are large compared with that of benzo (Böens et al.<sup>12</sup>), which has a plain benzo-crown-ether as the chelator. Benzo may become more or less fluorescent upon binding cations, but PeT-type probes such as (**10a**) and (**10b**) always become more fluorescent. The  $K_d$  values for Na<sup>+</sup> are about 0.38 and 0.44 M for (**10a**) and (**10b**), respectively. Fluorescence of (**10a**) and (**10b**), which are distinct from aminofluorescein, could thus be controlled through rational design based on TGs.

We compared the pH dependency of the fluorescence intensity and absorbance of (**10b**) with those of a well-known Na<sup>+</sup> probe, Sodium Green.<sup>13</sup> In panels A and C in Figure 5, in the presence of 0 and 1 M NaClO<sub>4</sub>, (**10b**) showed plateau profiles in the range of pH 5–8. On the other hand, as shown in panels B and D, the absorbance of Sodium Green decreased drastically below pH 6.5. This pH profile of Sodium Green is distinct from that of dichlorofluorescein, whose  $pK_a$  was reported to be below 5; this indicates the existence of the intramolecular stacking of the two fluorophores. The pH dependency of Sodium Green's

fluorescence is more complex. In panel B, the fluorescence intensity peaked at pH 5.8 and decreased at lower pH. In panel D, the fluorescence intensity tended to decrease in lower pH. These data clearly show that the fluorescence intensity of Sodium Green is dependent not only on the concentration of Na<sup>+</sup>, but also on the pH. Some fluorescent cation probes consist of one chelator and two fluorophores, for example Calcium Green-2<sup>14</sup> and SBFI.<sup>15</sup> The main aim of using two fluorophores in one molecule is to achieve greater fluorescence enhancement by unstacking of the fluorophores upon cation binding. Indeed, Sodium Green has two absorption peaks at 492 and 506 nm, of which the former is thought to correspond to the molecule with intramolecular stacking and the latter to the unstacked molecule. Higher Na<sup>+</sup> concentration makes Abs<sub>492</sub> lower and Abs<sub>506</sub> higher. This fluorescence enhancement mechanism provides a low detection limit, but may cause unexpected effects, for example undesirable pH dependency. Our probe design is so simple that there is little possibility of unexpected effects.

We obtained similar results in the case of adding potassium ion (shown in Fig. 6). We employed potassium chloride as the potassium salt. The  $K_d$  values for K<sup>+</sup> are 0.29 M for (**10a**) and 0.25 M for (**10b**).

The cation affinity did not differ much between (**10a**) and (**10b**) because the chelator moiety and the xanthene dye are orthogonal and resonantly independent of each other. The  $K_d$  values described above imply that the affinities of (**10a**) and (**10b**) for K<sup>+</sup> are higher than those for Na<sup>+</sup>, and that full binding to Na<sup>+</sup> enhances the fluorescence of (**10a**) and (**10b**) about 5-fold while full binding to K<sup>+</sup> does so by only



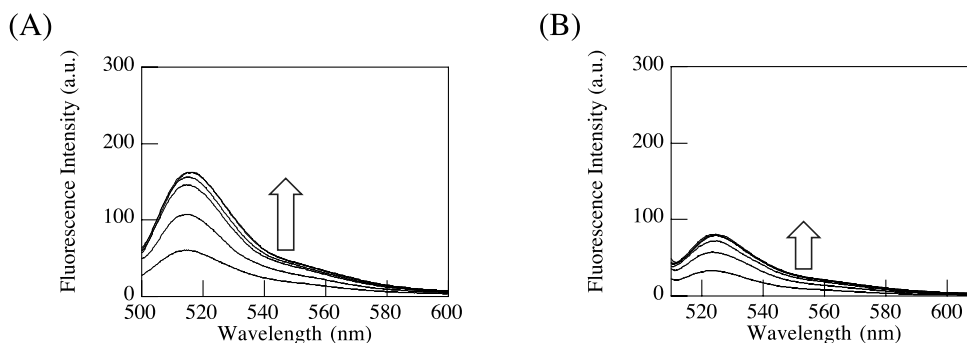


**Figure 6.** Panels A and B are emission spectra of **(10a)** and **(10b)** excited at 492 and 506 nm, respectively. Each sample was measured in aqueous MOPS buffer, pH 7.0, containing 0.5% DMF as a cosolvent. Probes were added as stock solution in DMF, finally 3  $\mu\text{M}$ .  $[\text{NaClO}_4]$  was 0, 200, 700, 1000, 1800 or 2700 mM. In panel A,  $\phi_{\text{fl}}([\text{NaClO}_4]=2700 \text{ mM})=0.021$ ,  $\phi_{\text{fl}}([\text{NaClO}_4]=0 \text{ mM})=0.008$ . In panel B,  $\phi_{\text{fl}}([\text{NaClO}_4]=2700 \text{ mM})=0.010$ ,  $\phi_{\text{fl}}([\text{NaClO}_4]=0 \text{ mM})=0.005$ .

**Table 1.** Comparison of  $\text{Na}^+$  addition and  $\text{K}^+$  addition to **(10a)** and **(10b)**.

	$K_d$ (M)		$F_{\text{max}}/F_{\text{min}}$	
	For $\text{Na}^+$	For $\text{K}^+$	$\text{Na}^+$	$\text{K}^+$
Compound <b>(10a)</b>	0.38	0.29	5.3	2.4
Compound <b>(10b)</b>	0.44	0.25	4.6	2.4

$F_{\text{max}}/F_{\text{min}}$ , fluorescence saturated with  $\text{M}^+$ /fluorescence in  $\text{M}^+$ -free condition

2–3-fold. Although **(10a)** and **(10b)** have higher affinity for  $\text{K}^+$  than  $\text{Na}^+$ , the electron-withdrawing effect of  $\text{Na}^+$  is stronger than that of  $\text{K}^+$ , so the oxidation potentials of sodium-bound benzo-crown-ether are higher than those of potassium-bound benzo-crown-ether. Consequently, **(10a)** and **(10b)** are more fluorescent in the presence of  $\text{Na}^+$  than in the presence of the same concentration of  $\text{K}^+$  (Table 1).

To confirm the change of HOMO energy level of the benzo-crown moiety as an electron donor upon  $\text{Na}^+$  binding, we measured  $E_{\text{ox}}$  of 2,3,5,6,8,9,11,12-octahydro-16-methyl-1,4,7,10,13-benzopentaoxacyclopentadecin (**6b**) in acetonitrile containing various concentrations of sodium perchlorate (Fig. 7). The oxidation potential of **(6b)** was shifted to the more positive with the increase of sodium perchlorate content. This indicates that the oxidation potential of **(6b)** was raised upon binding  $\text{Na}^+$ . The oxidation potential difference between the  $\text{Na}^+$ -free form and occupied form was about 0.10 V. Thus, we obtained the evidence that the oxidation potential of the electron donors within **(10a)** and **(10b)** was raised upon binding  $\text{Na}^+$ .

### 3. Conclusion

By predicting QE from the HOMO energy level of the electron donor, we succeeded in easily designing reasonable PeT-type cation probes. Compounds **(10a)** and **(10b)** become more fluorescent upon binding  $\text{Na}^+$ , and **(10b)** shows a good pH profile (low pH-dependency). These rationally designed probes are simple, having one chelator as the electron donor and one fluorophore, so that stacking should not be a problem. This strategy can be applied for designing molecules containing other fluorescent dyes, for example, BODIPY<sup>16</sup> and rhodamine.<sup>17</sup> Our strategy should be useful not only for developing new probes, but also for improving existing probes because the key factors for obtaining better probes, for example, the extent of the change of HOMO energy level upon the binding the target and the selectivity of chelator itself, can be controlled by means of minor structural modifications. We intend to search for good pairs of electron donors and fluorophores based on the estimated HOMO levels of electron donor candidates and thereby to develop novel probes for various biomolecules.

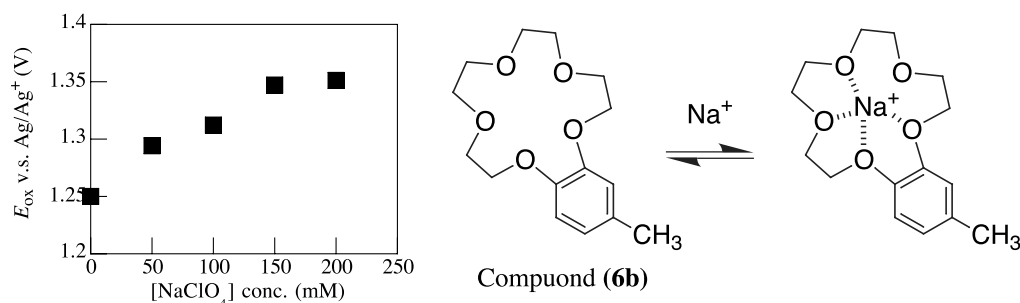


**Figure 7.** Cyclic voltammetry of compound **(6b)** in acetonitrile containing various concentrations of  $\text{NaClO}_4$ . Ionic strength was kept the same for all solutions with tetrabutylammonium perchlorate.



## 4. Experimental

### 4.1. Materials and general instrumentation

General chemicals were of the best grade available, supplied by Tokyo Chemical Industries, Wako Pure Chemical or Aldrich Chemical Company, and were used without further purification. Special chemicals consisted of dimethyl sulfoxide (DMSO, fluorometric grade, Dojindo) and tetrabutylammonium perchlorate (TBAP, electrochemical grade, dried over P<sub>2</sub>O<sub>5</sub> before use, Fluka). Acetonitrile, acetone, *N,N*-dimethylformamide (DMF), tetrahydrofuran (THF), methanol, and ethanol were used after appropriate distillation or purification. NMR spectra were recorded on a JNM-LA300 (JEOL) instrument at 300 MHz for <sup>1</sup>H NMR. Mass spectra (MS) were measured with a JMS-DX300 (JEOL), for EI, an MS700 (JEOL) for FAB and a JMS-T100LC (JEOL) for ESI-TOF. All experiments were carried out at 298 K, unless otherwise specified.

### 4.2. Fluorescence properties and quantum efficiency of fluorescence

Steady-state fluorescence spectroscopic studies were performed on an F4500 (Hitachi). UV–visible spectra were obtained on a UV-1600 (Shimadzu), with 0.1 mol L<sup>-1</sup> NaOHaq (pH 13) as the solvent, unless otherwise specified. Each solution contained up to 0.1% (v/v) DMF as a cosolvent. For determination of the fluorescence ( $\Phi_{fl}$ ), fluorescein in 0.1 mol L<sup>-1</sup> NaOHaq ( $\Phi_{fl}=0.85$ ) was used as a fluorescence standard.<sup>18</sup> The quantum efficiencies of fluorescence were obtained with the following equation ( $F$  denotes fluorescence intensity at each wavelength and  $\sum[F]$  was calculated by summation).

$$\Phi_{fl}^{(\text{sample})} = \Phi_{fl}^{(\text{standard})} \text{Abs}^{(\text{standard})} / \text{Abs}^{(\text{sample})} \\ * \sum [F^{(\text{sample})}] / \sum [F^{(\text{standard})}]$$

### 4.3. Cyclic voltammetry

Cyclic voltammetry was performed on a 600A electrochemical analyzer (ALS). A three-electrode arrangement in a single cell was used for the measurements: a Pt wire as the auxiliary electrode, a glassy carbon electrode as the working electrode, and an Ag/Ag<sup>+</sup> electrode as the reference electrode. The sample solutions contained 1.0 × 10<sup>-3</sup> M sample and 0.1 M tetrabutylammonium perchlorate (TBAP) as a supporting electrolyte in acetonitrile, and argon was bubbled through the solution for 10 min before each measurement.

### 4.4. Preparation

**4.4.1. 4-Bromo-5-methylcatechol (3).** To a solution of 4-methylcatechol (28 mmol) in CH<sub>2</sub>Cl<sub>2</sub> (100 ml), a mixture of bromine (31 mmol) and CH<sub>2</sub>Cl<sub>2</sub> (20 ml) was added dropwise at -80 °C. When a white solid precipitate appeared, addition was stopped to avoid formation of the dibromoderivative (about 15 mmol of bromine was added).

The reaction mixture was washed with 100 ml of satd ascorbic acid solution in water, and 100 ml of brine. The organic layer was dried over Na<sub>2</sub>SO<sub>4</sub> and concentrated under reduced pressure to give 4.1 g of white solid (yield 71%). <sup>1</sup>H NMR (300 MHz, CDCl<sub>3</sub>)  $\delta$  7.05 (1H, s, aromatic H), 6.76 (1H, s, aromatic H), 5.16 (1H, s, OH), 5.14 (1H, s, OH), 2.27 (3H, s, CH<sub>3</sub>); MS (EI) *m/z* (%) 204 [M+2], 202 [M+], 18 (100).

**4.4.2. 2,3,5,6,8,9,11,12-Octahydro-15-bromo-16-methyl-1,4,7,10,13-benzopentaoxacyclopentadecin (4a).** A mixture of 3-bromo-4-methylcatechol (5 mmol), tetra(ethylene glycol) di-*p*-tosylate (5 mmol), CsF (33 mmol), and dry acetonitrile (100 ml) was refluxed at 90 °C for 22 h. Acetonitrile was removed under reduced pressure and the residue was suspended in AcOEt, filtered to remove CsF, and concentrated. The resulting residue was chromatographed (NH-silica gel, AcOEt/MeOH = 20/1) to give 0.6 g of white solid (yield 34%). <sup>1</sup>H NMR (300 MHz, CDCl<sub>3</sub>)  $\delta$  7.01 (1H, s, 17-H), 6.74 (1H, s, 14-H), 4.1 (4H, m, 2, 12-H), 3.9 (4H, m, 3, 11-H), 3.7 (8H, m, 5, 6, 8, 9-H), 2.30 (3H, s, CH<sub>3</sub>); MS (EI) *m/z* (%) 362 [M+2], 360 [M], 228 (100).

**4.4.3. 2,3,5,6,8,9,11,12-Octahydro-15-methyl-1,4,7,10,13-benzopentaoxacyclopentadecin (6b).** The synthesis of (6b) followed that of (6a).

**4.4.4. 3,3'-Dichloro-2,2',4,4'-tetrahydroxybenzophenone (7b).** Compound 7b was prepared according to the literature.<sup>19</sup>

**4.4.5. 3,6-Dihydroxyxanth-9-one (8a).** Compound 8a was prepared according to the literature.<sup>20</sup>

**4.4.6. 2,7-Dichloro-3,6-dihydroxyxanth-9-one (8b).** Compound 8b was prepared according to the literature.<sup>20</sup>

**4.4.7. O,O'-Bis(*tert*-butyldimethylsilyl)-3,6-dihydroxyxanth-9-one (9a).** Compound 9a was prepared according to the literature.<sup>21</sup>

**4.4.8. O,O'-Bis(*tert*-butyldimethylsilyl)-2,7-dichloro-3,6-dihydroxyxanth-9-one (9b).** Compound 9b was prepared according to the literature.<sup>21</sup>

**4.4.9. 9-(2',3',5',6',8',9',11',12'-Octahydro-16'-methyl-1',4',7',10',13'-benzopentaoxacyclopentadecin-15'-yl)-6-hydroxy-3*H*-xanthen-3-one (10a).** To a solution of (6a) (150 mg) in dry 2-methyltetrahydrofuran (15 ml), a portion of *tert*-butyllithium in *n*-pentane (1.54 N, 1 ml) was added dropwise via a syringe at below -150 °C over 10 min. The mixture was stirred for 30 min at below -150 °C, then a solution of (9a) in dry 2-methyltetrahydrofuran (3 ml) was added dropwise via a syringe over 10 min, and the reaction mixture was allowed to warm to room temperature over 1 h. A portion of 2 N HCl<sub>aq</sub> was added, a solution of tetra(*n*-butyl)ammonium fluoride in THF was added, and the reaction mixture was refluxed at 80 °C for 1 h. The mixture was evaporated under reduced pressure. The residue was dissolved in CH<sub>2</sub>Cl<sub>2</sub>, and the solution was washed with a portion of 2 N HCl<sub>aq</sub>. The organic layer was extracted with five portions of 2 N NaOH<sub>aq</sub>, and then the aqueous solution was acidified with 2 N HCl<sub>aq</sub>, and

extracted with CH<sub>2</sub>Cl<sub>2</sub>. The organic layer was dried over Na<sub>2</sub>SO<sub>4</sub>, and evaporated under reduced pressure. The resulting residue was chromatographed (silica gel, CH<sub>2</sub>Cl<sub>2</sub>/methanol=10/2) to give orange-colored solid (yield 8.0%). <sup>1</sup>H NMR (300 MHz, CDCl<sub>3</sub>) δ 7.09 (2H, d, 1, 8-H, *J*=1.9 Hz), 7.05 (2H, d, 4, 5-H, *J*=9.2 Hz), 6.91 (1H, dd, 2, 7-H, *J*=1.9, 9.2 Hz), 6.86 (2H, s, 1, 14'-H), 6.66 (1H, s, 17'-H), 4.2 (2H, m, 12'-H), 4.1 (2H, m, 2'-H), 4.0 (2H, m, 11'-H), 3.9 (2H, m, 3'-H), 3.8 (4H, m, 5', 9'-H), 3.77 (4H, s, 6', 8'-H), 1.95 (3H, s, CH<sub>3</sub>) (%). <sup>13</sup>C NMR (300 MHz, CDCl<sub>3</sub>) δ 19.4, 68.2, 68.8, 69.6, 70.2, 103.1, 114.2, 115.4, 116.0, 121.5, 132.5, 159.0, 207.1; MS (FAB) *m/z* 515 [MNa<sup>+</sup>]; HRMS (ESI-Tof) [MNa<sup>+</sup>] 515.16819, found 515.16644 (−1.75 mmu).

**4.4.10. 9-(2',3',5',6',8',9',11',12'-Octahydro-16'-methyl-1',4',7',10',13'-benzopentaoxacyclopentadecin-15'-yl)-2,7-dichloro-6-hydroxy-3*H*-xanthen-3-one (10b).** The synthesis of (10b) followed that of (10a) (yield 10%). <sup>1</sup>H NMR (300 MHz, DMSO) δ 7.04 (1H, s, 14'-H), 6.84 (1H, s, 17'-H), 6.81 (2H, s, 1, 8-H), 6.26 (2H, s, 4, 5-H), 4.2 (2H, m, 12'-H), 4.0 (2H, m, 2'-H), 3.8 (2H, m, 11'-H), 3.7 (2H, m, 3'-H), 3.6 (4H, m, 5', 9'-H), 3.6 (4H, s, 6', 8'-H) 1.94 (3H, s, CH<sub>3</sub>). <sup>13</sup>C NMR (300 MHz, CDCl<sub>3</sub>) δ 18.6, 68.0, 68.4, 68.5, 69.3, 70.1, 103.6, 109.3, 114.4, 115.3, 124.3, 126.9, 127.0, 128.1, 132.9, 146.1, 148.6, 149.8, 156.2; MS (FAB) *m/z* 583 [MNa<sup>+</sup>], 585 ([M+2]Na<sup>+</sup>); HRMS (ESI-Tof) [MNa<sup>+</sup>] 583.09024, found 583.08912 (−1.12 mmu).

### Acknowledgements

This study was supported in part by the Advanced and Innovational Research Program in Life Sciences from the Ministry of Education, Culture, Sports, Science and Technology, the Japanese Government, by Takeda Science Foundation, by Nagase Science and Technology Foundation, by research grants from the Ministry of Education, Science, Sports and Culture of Japan (Grant Nos. 12771349, 13557209, and 14030023 to Y.U.), and by Kowa Life Science Foundation to Y.U.

### References and notes

- (a) Dirks, R. W.; van Gijlswijk, R. P.; Tullis, R. H.; Smit, A. B.; van Minnen, J.; van der Ploeg, M.; Raap, A. K. *J. Histochem. Cytochem.* **1990**, *38*, 467–473. (b) Lau, S. K.; Zaccardo, F.; Little, M.; Banks, P. *J. Chromatogr. A* **1998**, *809*, 203–210.
- (a) Shoda, T.; Kikuchi, K.; Kojima, H.; Urano, Y.; Komatsu, H.; Suzuki, K.; Nagano, T. *Analyst* **2003**, *128*, 719–723. (b) Takakusa, H.; Kikuchi, K.; Urano, Y.; Kojima, H.; Nagano, T. *Chem. Eur. J.* **2003**, *9*, 1479–1485. (c) Setsukinai, K.;

- Urano, Y.; Kakinuma, K.; Majima, H. J.; Nagano, T. *J. Biol. Chem.* **2003**, *278*, 3170–3175. (d) Kojima, H.; Urano, Y.; Kikuchi, K.; Higuchi, T.; Nagano, T. *Angew. Chem. Int. Ed.* **1999**, *38*, 3209–3212. (e) Kojima, H.; Sakurai, K.; Kikuchi, K.; Kawahara, S.; Kirino, Y.; Nagoshi, H.; Hirata, Y.; Akaike, T.; Maeda, H.; Nagano, T. *Biol. Pharm. Bull.* **1997**, *20*, 1229–1232. (f) Tanaka, K.; Miura, T.; Umezawa, N.; Urano, Y.; Kikuchi, K.; Higuchi, T.; Nagano, T. *J. Am. Chem. Soc.* **2001**, *123*, 2530–2536.
- Kao, J. P. Y.; Harootunian, A. T.; Tsien, R. Y. *J. Biol. Chem.* **1989**, *264*, 8179–8184.
- (a) Hirano, T.; Kikuchi, K.; Urano, Y.; Nagano, T. *J. Am. Chem. Soc.* **2002**, *124*, 6555–6562. (b) Hirano, T.; Kikuchi, K.; Urano, Y.; Higuchi, T.; Nagano, T. *Angew. Chem. Int. Ed.* **2000**, *39*, 1052–1054. (c) Hirano, T.; Kikuchi, K.; Urano, Y.; Higuchi, T.; Nagano, T. *J. Am. Chem. Soc.* **2000**, *122*, 12399–12400.
- Haugland, R. P. *Handbook of Fluorescent Probes and Research Products*, 9th ed. Molecular Probes, Inc.: Eugene, 2002.
- Martell, A. E.; Hancock, R. D. *Metal Complexes in Aqueous Solutions*; Plenum: New York, 1996.
- Munkholm, C.; Parkinson, D. R.; Walt, D. R. *J. Am. Chem. Soc.* **1990**, *112*, 2608–2612.
- Miura, T.; Urano, Y.; Tanaka, K.; Nagano, T.; Ohkubo, K.; Fukuzumi, S. *J. Am. Chem. Soc.* **2003**, *125*, 8666–8671.
- (a) de Silva, A. P.; Gunaratne, H. Q. N.; Gunlaugsson, T.; Huxley, A. J. M.; McCoy, C. P.; Rademacher, J. T.; Rice, T. E. *Chem. Rev.* **1997**, *97*, 1515–1566. (b) Marcus, R. A.; Sutin, N. *Biochim. Biophys. Acta* **1985**, *811*, 265–322.
- Urano, Y.; Kanda, K.; Kamiya, M.; Ueno, T.; Hirose, K.; Nagano, T. Submitted for publication.
- Chen, S.; Nakamura, H.; Tamura, Z. *Chem. Pharm. Bull.* **1979**, *27*, 475–479.
- Cielen, E.; Tahri, A.; Ver Heyen, K.; Hoornaert, G. J.; De Schryver, F. C.; Böens, N. *J. Chem. Soc., Perkin Trans. 2*, **1998**, *7*, 1573–1580.
- (a) Kuhn, M. A.; Haugland, P. R. U.S. Patent 5,405,975, 1995. (b) Kuhn, M. A.; Haugland, P. R. U.S. Patent 5,516,864, 1996.
- Kuhn, M. A.; Haugland, P. R. U.S. Patent 5,453,517, 1995.
- Minta, A.; Tsien, R. Y. *J. Biol. Chem.* **1989**, *264*, 19449–19457.
- Gabe, Y.; Urano, Y.; Kikuchi, K.; Kojima, H.; Nagano, T. *J. Am. Chem. Soc.* **2004**, *126*, 3357–3367.
- Kojima, H.; Hirotani, M.; Nakatsubo, N.; Kikuchi, K.; Urano, Y.; Higuchi, T.; Hirata, Y.; Nagano, T. *Anal. Chem.* **2001**, *73*, 1967–1973.
- Nishikawa, Y.; Hiraki, K. *Analytical Methods of Fluorescence and Phosphorescence*; Kyoritsu: Tokyo, 1984, pp 76–80.
- Kurduker, R.; Subba Rao, N. V. *Proc. Indian Acad. Sci. Sect. A.* **1963**, *57*, 280–287.
- Grover, P. K.; Shah, G. D.; Shah, R. C. *J. Chem. Sci. (Lond)* **1955**, 3982–3985.
- Minta, A.; Tsien, R. Y. *J. Biol. Chem.* **1989**, *264*, 8171–8178.

# Structural studies of biarylpyridines fluorophores lead to the identification of promising long wavelength emitters for use in fluorescent chemosensors

A. G. Fang, J. V. Mello and N. S. Finney\*

Department of Chemistry and Biochemistry, University of California, San Diego, 9500 Gilman Dr., La Jolla, CA 92093-0358, USA

Received 15 April 2004; revised 24 June 2004; accepted 19 August 2004

Available online 22 September 2004

**Abstract**—Fluorescent chemosensors—molecules whose fluorescence emission changes in response to a reversible binding event—require both a substrate binding domain and a reporting fluorophore. Our approach to chemosensor development is based on a combination of a new signaling mechanism and a modular fluorophore synthesis. The latter feature has facilitated detailed study of the properties of polyarylpyridine fluorophores, and has led to the identification of a visibly-emissive pyridine as a promising lead structure for chemosensor development. The results of this study are described herein.

© 2004 Elsevier Ltd. All rights reserved.

## 1. Introduction

Fluorescent chemosensors—molecules whose fluorescence emission changes in response to a reversible binding event—require a substrate binding domain, a reporting fluorophore and a signaling mechanism that allows the two to communicate. We have previously described the development of fluorescent chemosensors that rely on conformational restriction as signaling mechanism.<sup>1–4</sup> This effort was driven by the hypothesis that it would combine two important and often mutually-exclusive features of other systems: simplicity of molecular architecture and generality of signaling mechanism. While we have conducted extensive photophysical studies on chemosensors based on biphenyl and biarylacetylene fluorophores, the most promising of our systems are the biarylpyridine, which exhibit several of desirable properties:

- (1) Visible emission from a locally excited (LE) state that is highly responsive to ion-binding induced conformational restriction.
- (2) A second, longer-wavelength visible emission band arising from a charge transfer (CT) state induced by coordination of an ion to the pyridine nitrogen.
- (3) Modular synthetic assembly.

- (4) Tuning of the emission wavelength by remote substituents on the pyridine ring.

The simple architecture of these systems is self-evident (Fig. 1).<sup>2</sup> The generality of the signaling mechanism is attested to by the perfect correlation between metal–ion binding detected by <sup>1</sup>H NMR and observed fluorescence response—in all cases to date, ion binding produces a detectable change in fluorescence emission.

In parallel with efforts to widen the variation of ligand structure, we have synthesized numerous new arylpyridine fluorophores with the objective of shifting both LE and CT emission further into the visible region.<sup>2</sup> We provide here a detailed description of these efforts, including identification of important structure–emission relationships, discovery of a potentially serious limitation to our fluorophore design, and a solution to this problem guided by an understanding of structure–emission relationships.

## 2. Background

Fluorescent chemosensors allow fluorescence detection, with all the associated benefits, of non-fluorescent analytes.<sup>1</sup> The importance of fluorescent chemosensors in applications as diverse as environmental monitoring, cellular imaging and biomedical device construction is increasingly widely appreciated. The majority of established chemosensors fall into one of 3 categories:

- (1) Systems based on direct interaction between the analyte

*Keywords:* Fluorescence; Chemosensor; Pyridine; Synthesis; Spectroscopy.

\* Corresponding author. Present address: Organisch-chemisches Institut, Universität Zürich, Winterthurer-strasse 190, CH-8057 Zürich, Switzerland. Tel.: +41 (01) 635 4283; e-mail: [finney@unizh.ch](mailto:finney@unizh.ch)

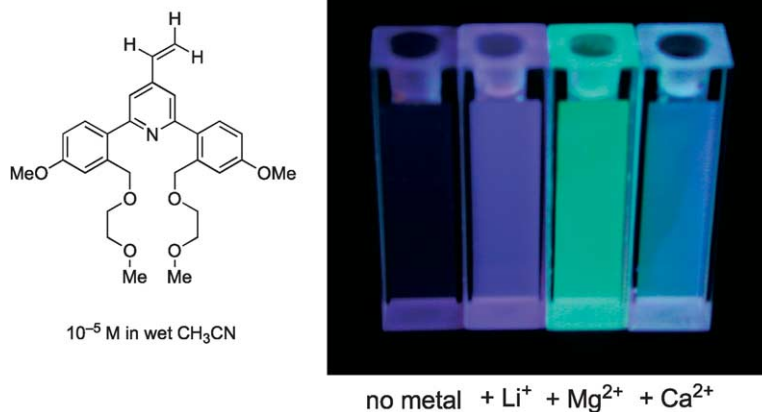


**Figure 1.** An arylpyridine fluorescent chemosensor with dual visible emission.

- (almost always a metal ion) and a nitrogen atom lone pair that is ‘wired into’ the fluorophore (Fig. 2-1).<sup>1,5</sup>
- (2) Systems in which analyte binding displaces a fluorophore or changes its microenvironment (Fig. 2-2).<sup>1,6</sup>
  - (3) Systems in which analyte binding alters the energy transfer between a fluorophore/acceptor pair, where the acceptor is either another fluorophore or a quencher (Fig. 2-3).<sup>1,7,8</sup>

The first category, which represents the statistical majority of reported fluorescent chemosensors, has the significant advantage of relying on relatively simple molecular architecture. Important examples of this approach include  $\text{Ca}^{2+}$ - and  $\text{Zn}^{2+}$ -responsive chemosensors with applicability for cellular imaging.<sup>5c,d</sup> The central limitation of this approach is the requirement for

lone-pair coordination. This generally constrains the substrate scope to metal ions and dictates that the fluorophore/receptor hybrid contain benzylic or anilinic nitrogen atoms, which in turn restricts the design of new fluorophores and/or binding domains.

In contrast, the third category, often based on fluorescence resonant energy transfer (FRET) between donor and acceptor fluorophores, typically relies on substantially complex molecular architecture—polypeptides, oligonucleotides or fusion proteins.<sup>7,8</sup> Important embodiments of this strategy include fusions of green fluorescent protein (GFP) analogs and calmodulin that can be expressed *in vivo* to facilitate  $\text{Ca}^{2+}$  imaging in cells.<sup>7a</sup> Offsetting the limitation of complexity is the generality of the signaling mechanism, which places no constraint on the structure of the binding

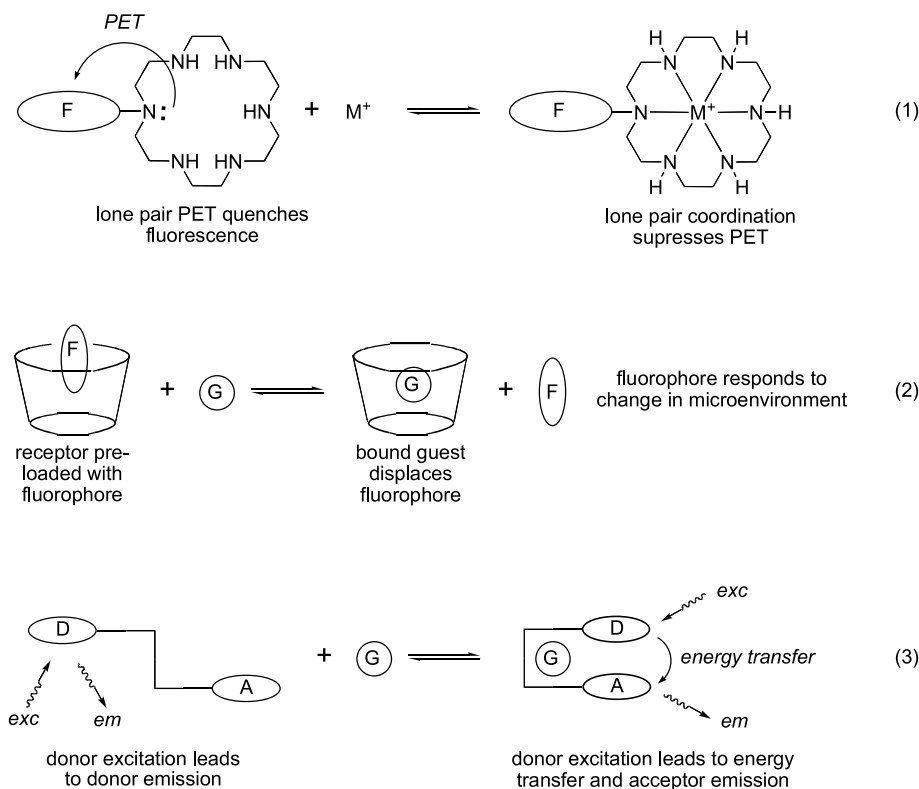


**Figure 2.** Broad overview of fluorescent chemosensor strategies.

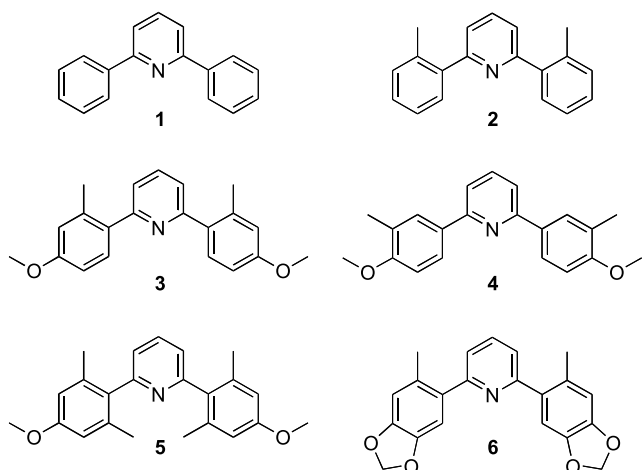


Figure 3. Biarylpyridines with varying substituents at the 2 and 6-positions.

domain beyond a requirement that binding induce a large change in interchromophore distance.

The second category, initially based primarily on displacement of covalently-tethered fluorophores from the cavity of cyclodextrin hosts, are appropriately intermediate between the first and third categories in terms of complexity and generality.<sup>6</sup> Embodiments typically rely on structures no more complicated than cyclodextrin, and generality is limited only by the requirement that there be sufficient similarity between the fluorophore and the analyte that the analyte can effectively compete with the fluorophore in binding to the receptor. Important recent examples of this strategy include systems for sensing ATP.<sup>6b</sup>

### 3. Results

#### 3.1. Structural studies on ‘fourth category’ fluorophores

Fluorescent chemosensors based on conformational

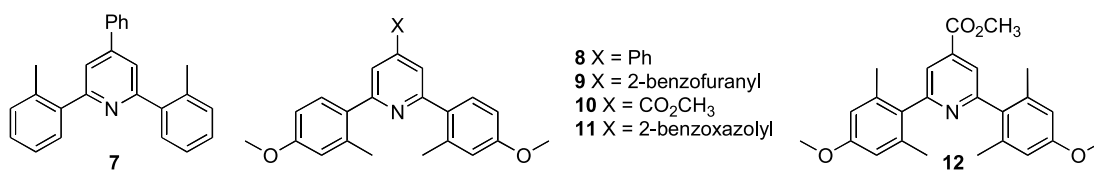


Figure 4. Biarylpyridines with varying substituents at the 4-position.

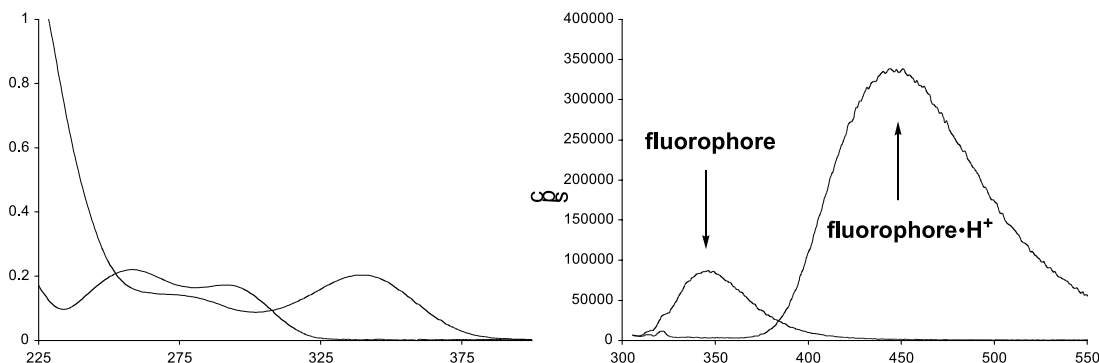


Figure 5. Absorption and emission spectra of the chemosensor from Figure 1.

restriction represent a fourth category addition to the above list. As mentioned above, the modular nature of biarylpyridine fluorophores (our preferred member of this fourth category) simplifies structure–property studies.<sup>2</sup> The goals of the present work were gaining a greater understanding of substituent effects and red-shifting the LE and CT emission wavelengths. We initially focused on the nature of the aryl substituents at the 2- and 6-positions (Fig. 3), and subsequently investigated fluorophores with varied 4-substituents in greater detail (Fig. 4). With regard to LE and CT emission, the default emission of biarylpyridines is that from the LE state. However, CT emission can be induced by simple protonation of the pyridine (Fig. 5). For both states, the longest wavelength absorption maximum correlates with the excitation maximum for fluorescence emission. In cases where the CT state is non-emissive (vide infra) the formation of the CT state can still be verified by characteristic changes in the absorption spectrum (Fig. 5).

#### 3.2. Synthesis of arylpyridine fluorophores

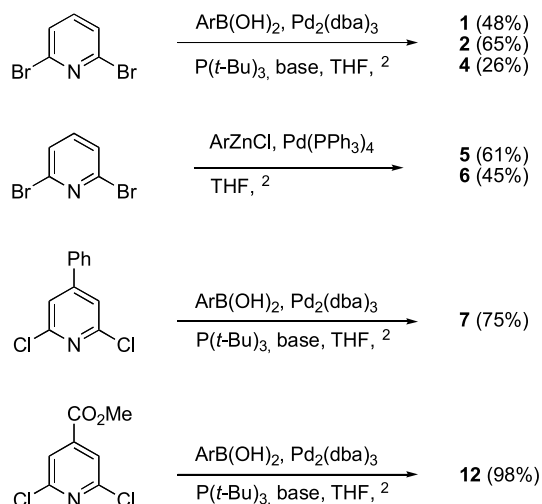
The syntheses of compounds 3 and 8–11 have been described previously.<sup>2</sup> Fluorophores 1, 2 and 4–6 were prepared from 2,6-dibromopyridine, while 7 and 12 were prepared from 2,6-dichloro-4-phenylpyridine and 2,6-dichloro-4-carboxymethylpyridine, respectively (Scheme 1). Central to all of these syntheses is the efficiency of palladium catalyzed cross coupling of the required halopyridines.<sup>2,9,10</sup>

## 4. Discussion

#### 4.1. Influence of the 2,6-substituents on optical properties

Our first generation biarylpyridine chemosensors (cf. Fig. 1) all contained as common features *o,o'*-alkyl and *p,p'*-OCH<sub>3</sub> substituents on the aryl groups at the 2 and 6 positions. The presence of the *o,o'* groups was presumed to be essential





Scheme 1. Synthesis of arylpyridine fluorophores.

based on our previous study of biphenyl systems. However, the properties of biarylpyridines and biphenyls are sufficiently different that this presumption warranted direct evaluation. The *p,p'*-substituents were initially included based on the ready availability of the precursor aryl fragments rather than deliberate design, and the inclusion of these groups even more clearly required evaluation.

The spectroscopic properties of **1–6** (Table 1) reveal that both the alkyl and OCH<sub>3</sub> substituents are essential to the function of our system. The inclusion of the *o,o'*-alkyl substituents is essential for lowering the LE quantum yield to the point where it is subject to modulation by conformational restriction. For instance, the fluorophore in Figure 1 has an LE quantum yield of ~0.02; in contrast, fluorophores with LE quantum yields >0.10 no longer respond strongly to binding-induced conformational restriction. (This is one of the ironies inherent in an approach based on using substrate binding to turn a poor fluorophore into a good fluorophore—it is essential to start with a poor fluorophore.) The presence of the polarizing OCH<sub>3</sub> substituents provides a desirable red-shift in absorption and emission but what would be, in the absence of the alkyl substituents, an undesirable increase in LE quantum yield.

The addition of *o,o'*-CH<sub>3</sub> groups to 2,6-biphenylpyridine (**1** vs **2**) leads to a slight reduction in extinction coefficient and quantum efficiency of emission from both the LE and CT

states. The reduction in LE emission parallels that seen when comparing biphenyl ( $\phi=0.18$ ) to the more twisted derivative 2,2'-dimethylbiphenyl ( $\phi=0.01$ ).<sup>11</sup> Based on previous work with biphenyls, we conclude that this reduction in quantum yield is in large part due to the increased efficiency of spin-orbit coupling (SOC) in twisted biaryl excited states.<sup>12</sup> While factors independent of biaryl torsion might be considered, such as C–C twisting and C–H stretching-mediated deactivation of the excited state, the similarity of the quantum yields of biphenyl and 3,3'-dimethylbiphenyl ( $\phi=0.21$ ) argues against this.<sup>11</sup> The 'gap rule'—the empirical observation that the rate of IC decreases as excited state energy increases—also argues against this possibility, in that the excited state energy is in excess of 100 kcal/mol.<sup>3a,13,14</sup> An additional consequence of introducing *o,o'*-CH<sub>3</sub> groups is an undesirable blue shift in both the LE (20 nm) and CT (5 nm) emission. This is also consistent with reduced planarity and thus reduced conjugation in the excited state.

The addition of *p,p'*-OCH<sub>3</sub> substituents (**2** vs **3**) has a dramatic impact on the efficiency of both absorption and emission, almost completely compensating for the reduction in quantum yield caused by introduction of the *o,o'*-CH<sub>3</sub> groups. In addition, it has a pronounced effect on the absorption and emission wavelengths. Notably, the emission maximum for the LE state shifts more than 20 nm to the red, while that of the CT state shifts by more than 60 nm. The emission shifts are accompanied by smaller but still significant red shifts in the LE and CT excitation maxima. These indicate that both the LE and CT excited states are highly polarized, with the flanking aromatic rings serving as electron donors and the pyridine ring, consistent with its electron deficient nature relative to a hydrocarbon, serving as an electron acceptor. While this polarization is present in the ground state, it is clearly more pronounced in the excited states: the near doubling of  $\epsilon$  reflects a large increase in the transition dipole for the excitation from ground to excited state.<sup>15</sup> A corresponding increase in the efficiency of radiative decay of the LE state, shown by the increase in  $\phi$ , is expected based on the proportionality of the Einstein A and B coefficients (which govern emission and excitation) for fluorophores of very similar structure.<sup>16</sup> The red shifts in emission wavelength indicate that the *p*-OCH<sub>3</sub> groups serve to stabilize both the LE and CT excited states, effectively lowering their energy and reducing the energy gap between excited and ground state. The effects on absorption and emission are much more pronounced in the CT state, as

Table 1. Salient optical properties of **1–6**

Compound	$\epsilon$ ( $\times 10^3$ ) <sup>a</sup>	$\Phi$ (LE) <sup>a,b</sup>	$\Phi$ (CT) <sup>c</sup>	LE <sub>exc</sub> <sup>d</sup>	LE <sub>em</sub> <sup>e</sup>	CT <sub>exc</sub> <sup>f</sup>	CT <sub>em</sub> <sup>g</sup>
<b>1</b>	10.2	0.037	0.951	302	338	322	393
<b>2</b>	8.1	0.004	0.831	280	320	307	388
<b>3</b>	14.8	0.031	0.177	290	352	342	449
<b>4</b>	11.6	0.560	0.544	315	359	366	459
<b>5</b>	9.3	0.003	0.021	272	342	324	450
<b>6</b>	13.5	0.059	0.004	303	378	359	480

<sup>a</sup> Measured at LE excitation maximum.

<sup>b</sup> Quantum yield of LE emission.

<sup>c</sup> Quantum yield of CT emission.

<sup>d</sup> Excitation maximum for LE state.

<sup>e</sup> Emission maximum for LE state.

<sup>f</sup> Excitation maximum for CT state.

<sup>g</sup> Emission maximum for CT state.

expected based on its greater charge separation relative to the LE state.

The importance of the *o,o'*-CH<sub>3</sub> groups is underscored by comparison to the corresponding *m,m'*-dimethyl case (**3** vs **4**). Relocation of the flanking CH<sub>3</sub> groups lowers the absorptivity of the molecule while simultaneously increasing the LE quantum yield by an order of magnitude and doubling the CT quantum yield. In addition, the excitation maxima for the *m,m'* isomer are significantly red shifted, although there are only very small changes in the emission wavelengths. The decreased absorptivity indicates that removal of the *o,o'*-CH<sub>3</sub> groups leads to greatly increased conjugation—and thus polarization—in the ground state, while the smaller changes in the emission wavelengths indicate smaller changes in the degree of polarization in the excited state. The lower value of  $\epsilon$  for **4** is thus explained, as  $\epsilon$  should scale with the transition dipole which should in turn vary with the difference in polarization of the ground and excited states.<sup>15</sup> That is, increasing the polarization of the ground state without altering the polarization of the transition state would be expected to decrease  $\epsilon$ , in the absence of other effects. The smaller red shifts in the emission wavelengths are consistent with greater excited state planarization, and the effect of removing the *o,o'*-CH<sub>3</sub> groups is similar in comparing **3** vs **4** and **2** vs **1**.

The influence of deplanarization is further delineated by the addition of a second pair of flanking CH<sub>3</sub> groups (**3** vs **5**). While deplanarization and polarization offset one another in **3**, in **5** deplanarization almost fully compensates for the ground state influence of polarization, and the values for  $\epsilon$  (reduced by  $\sim 4 \times 10^{-3}$ ) and the absorption maxima (reduced by  $\sim 20$  nm) of **5** are even lower than those of **2**, which lacks both the OCH<sub>3</sub> and additional CH<sub>3</sub> groups. Similarly, the quantum yield of both the LE and CT states descend to values similar to those of **2**. The emission maxima provide valuable structural information. The wavelength of LE emission shows a  $\sim 20$  nm blue shift relative to **3**, while that the CT emission remains unchanged within measurement error. This indicates that the ground and LE states of **5** are less planar and thus less conjugated than those of **3**, as would be expected based on increased steric congestion. That this congestion does not influence the CT emission wavelength suggests that the CT state is

twisted, such that the additional CH<sub>3</sub> groups have relatively little influence on the conformation and thus energetic separation of the CT state and the corresponding twisted conformation of the ground state. While this evidence is indirect, it is consistent with the extensive literature on twisted intramolecular charge transfer (TICT) states.<sup>17,18</sup>

There are two significant aspects of the spectroscopic properties of bis(piperonyl) compound **6**. First, the further increase in polarization induced by two additional alkoxy substituents (**6** vs **3**) leads to the longest LE and CT emission wavelengths in the series (380 and 480 nm, respectively, compared to 350 and 450 nm for **3**).<sup>19</sup> Second, and of great practical importance, emission from **6** is a presage of a trend that is more fully illustrated by **7–12**: as emission from biarylpyridines moves farther to the red, the quantum yield of the CT state begins to drop off. The first of these observations may be rationalized much as the difference between **2** and **3**, with electron donating substituents stabilizing the polarized excited states and reducing the energetic separation from the ground state. The second and more problematic observation is again consistent with the gap rule.<sup>14</sup> For **6**, the 480 nm CT emission is equivalent to an energy gap of almost exactly 60 kcal/mol, which correlates with significant decrease in CT quantum yield ( $\phi = 0.06$ , vs 0.28 for **3**). This energy (ca. 60 kcal/mol) is apparently the upper limit at which IC begins to contribute to nonradiative decay.

#### 4.2. Influence of the 4-substituent on optical properties

The influence of the 4-substituent on the emission of biarylpyridines is delineated by compounds **7–12** (Table 2). Three prominent trends can be seen. First, increasing the chromophore surface or polarization by substitution at the 4-position can lead to a significant red shift in LE emission, and in one case can alter the identity of the core fluorescing unit. Second, the quantum yield for LE emission increases as emission moves to longer wavelengths. Third, CT emission decreases over the same series, leading quickly to molecules with non-emissive CT states.

By itself, comparison of 2,6-bis(*o*-tolyl)pyridine and its 4-phenyl counterpart (**7** vs **2**) would suggest that the 4-substituent has a modest influence on most of the properties

**Table 2.** Salient optical properties of **7–12** (with **2**, **3** and **5** for comparison)

Compound	$\epsilon (\times 10^3)^a$	$\Phi$ (LE) <sup>b</sup>	$\Phi$ (CT) <sup>c</sup>	LE <sub>exc</sub> <sup>d</sup>	LE <sub>em</sub> <sup>e</sup>	CT <sub>exc</sub> <sup>f</sup>	CT <sub>em</sub> <sup>g</sup>
<b>7</b>	4.9	0.005	0.803	295	349	302	399
<b>8</b>	9.3	0.200	0.182	310	379	350	483
<b>9</b>	38.3	0.210	0.016	310	400	370	505
<b>10</b>	4.4	0.230	—	324	424	379	—
<b>11</b>	14.6	0.140	—	300	440	—	—
<b>12</b>	4.7	0.070	—	300	457	360	—
<b>2</b>	8.1	0.004	0.051	280	320	307	388
<b>3</b>	14.8	0.031	0.282	290	352	342	449
<b>5</b>	9.3	0.003	0.021	272	342	324	450

<sup>a</sup> Measured at LE absorption/excitation maximum.

<sup>b</sup> Quantum yield of LE emission.

<sup>c</sup> Quantum yield of CT emission.

<sup>d</sup> Excitation maximum for LE emission.

<sup>e</sup> Emission maximum for LE excitation.

<sup>f</sup> Excitation maximum for LE state.

<sup>g</sup> Emission maximum for CT excitation.

of these fluorophores. The quantum yields are virtually identical, the extinction coefficient is actually slightly reduced, and the emission wavelengths for the LE and CT states shift to longer wavelength by 30 and 15 nm, respectively. The longer emission wavelength is expected based on the increase in fluorophore surface area, thus delocalization and stabilization of the excited state. It is not immediately obvious why the LE emission wavelength responds more strongly than the CT state to the increased delocalization, or why the CT quantum yield responds more strongly than that of the LE.

Addition of a 4-phenyl group to the chromophore bearing both *o*-CH<sub>3</sub> and *p*-OCH<sub>3</sub> groups (**3**) leads to a much more dramatic change in spectroscopic properties (**8** vs **3**). The extinction coefficient decreases, indicative of a lower transition dipole that presumably results from an increase in ground state polarization relative to the LE state. The LE quantum yield increases substantially ( $\phi=0.20$  vs  $\phi=0.03$  for **3**) while the CT quantum yield decreases ( $\phi=0.09$  vs  $\phi=0.28$  for **3**). Absorption and emission wavelengths for both states shift to longer wavelength, the LE emission now approaching the visible region of the spectrum. The reduced CT emission efficiency is a consequence of the gap rule, as described above. The increased LE efficiency must result from the extended conjugation of the chromophore surface, and we take this as evidence that the 2,6-substituents—and their conformation mediated nonradiative decay—contribute less, proportionally, to the properties of more extended chromophores. (This is substantiated by **9** and **11**; vide infra.)

Replacing the phenyl group with a benzofuran provides further evidence that increased chromophore delocalization diminishes the impact of nonradiative decay mediated by the 2,6-aryl substituents (**9** vs **3**). Extension with benzofuran leads to a large increase in extinction coefficient, a further increase in LE quantum yield and a further reduction in CT quantum yield. In addition, the LE emission maximum moves into the visible region (400 nm), and the CT emission maximum moves from green into the green-yellow (505 nm). The emission and quantum yield effects may be rationalized as were those for **8**. The near quintupling of extinction coefficient is surprising but, like the increased LE quantum yield, shows that the 4-substituent makes an increased contribution to the character of the excited state. This can be seen most readily by comparing the absorption spectra of **8** and **9** (Fig. 6). The

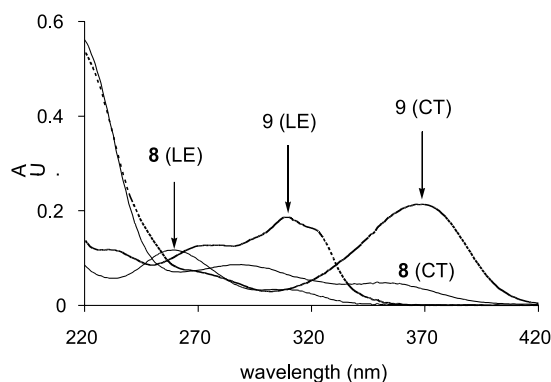


Figure 6. Absorption spectra of **8** and **9**.

absorption spectrum of **8** is similar to that of **3** and the 4-vinyl derivative (Fig. 3). Immediate differences in peak shape and the number and relative intensity of the absorption maxima can be seen for **9**. This demonstrates that the benzofuran substituent is a powerful determinant of the nature of the excited states, with commensurate deemphasis of the 2,6-aryl groups.

Installation of a benzoxazole at the 4-position yields a chromophore with absorption properties that no longer resemble those of **1–10** (Fig. 7), and the absorption and emission of which do not change noticeably upon addition of excess TFA. This structural variation has thus altered the fluorophore identity to the point that a CT excited state—radiative or nonradiative—simply no longer exists.

As a counterpart to increasing the chromophoric surface, placing a methyl carboxylate (which extends conjugation by only 2 atoms) at the 4-position shows that direct polarization of the pyridine, like polarization of the 2,6-biaryl groups, also influences fluorophore behavior (**10** vs **3**). The extinction coefficient decreases, consistent with a more polarized ground state and less difference in polarization between the ground and excited states. The LE emission becomes slightly more efficient and moves further into the visible, the 425 nm maximum representing a 100 nm Stokes shift. The CT state—which can still be observed by absorbance—is non-emissive.

The final variant on 4-substitution, **12**, is the tetramethyl analog of **10**. It is notable in that while it has a shorter wavelength LE absorption, as would be predicted by sterically decreased conjugation, it has a longer emission wavelength. The red shifted emission, which corresponds to ~62 kcal/mol, now runs afoul of the gap rule and accounts for the reduced quantum yield. That a longer emission wavelength results from increased deplanarization suggests that the optimal conformation of the LE state is no longer as near planar as was the case for **3**. Although this suggests an optimal geometry more suited to the CT state, which is nonradiative and expected to be twisted, the CT state can clearly be identified by the absorption spectrum and is distinct from the LE state. The apparent change in optimal LE state geometry remains unexplained, but coupled with the reduced quantum yield it provides an opportunity for the development of fluorescent chemosensors with visible

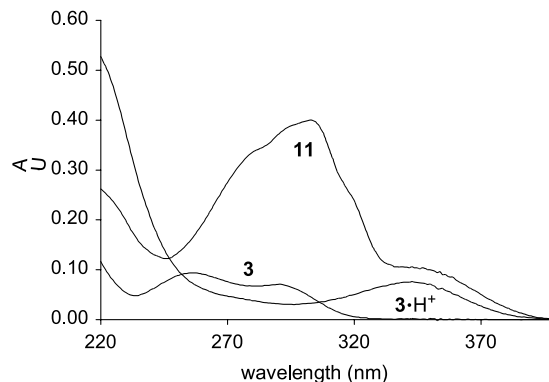


Figure 7. Comparison of the absorption spectra of **3** and **11**.



emission and geometrical constraints different from those associated with **3**.

### 4.3. The limitations of longer wavelength fluorophores

The properties of the pyridine fluorophores with visible LE emission constitute a potential problem for the development of fluorescent chemosensors based on conformational control. The approach hinges on being able to start with a poor fluorophore and induce increased LE emission efficiency via binding induced conformational restriction. This, in turn, means the approach is best suited for fluorophores with low initial quantum yields—unlike the visibly-emissive **8–11**. In addition, the loss of the second signaling channel—the CT emission—is a setback, in that dual emission provided an additional level of discrimination for distinguishing between bound metal ions.

The first of these concerns, reduced sensitivity at longer LE emission wavelength, is ameliorated to an extent by the observation that **13**, the 4-carboxymethyl analog of the chemosensor shown in Figure 1, still provides a visible response to the presence of metal ions (Fig. 8). The ~4-fold increase in emission intensity translates to a  $\phi \geq 0.90$ , which is a record among the systems we have studied, and is easily observed by eye. Offsetting this promising result are the lack of response to  $\text{Mg}^{2+}$  and  $\text{Ca}^{2+}$  (cf. Fig. 1), which had previously induced formation of the radiative CT state. While treatment with TFA indicates that  $\mathbf{13} \cdot \text{H}^+$  possesses a nonemissive CT state, neither  $\text{Mg}^{2+}$  nor  $\text{Ca}^{2+}$  induce formation of this state, indicating that the pyridine ring is now sufficiently electron deficient that the nitrogen atom serves as a poor Lewis base. Related studies with the podand derived from the 4-phenyl fluorophore (**9**) showed only minimal metal ion response, an observation which suggests that the response of **13** to  $\text{Li}^+$  is the exception rather than the rule. That said, it is worth noting that **13** still provides a visible emissive readout of the presence of  $\text{Li}^+$ .

## 5. Conclusion and recent progress

In summary, variation of the substituents at the 2, 4 and 6-positions of polyaryl pyridines can have a profound effect

on the absorbance and emission of these fluorophores. With regard to the 2,6-aryl groups, *o,o'*-alkyl substitution was shown to be essential for maintaining low initial quantum yields, while *p,p'*-alkoxy substitution was shown to provide a beneficial red shift in emission without untoward increase in emission efficiency. The influence of the 4-substituent on absorption and emission wavelengths was dramatic, with LE emission in the green region of the visible spectrum being possible. An unfortunate side effect of increased LE and CT emission wavelengths is the accompanying variation in quantum yields. LE emission efficiency (ideally low) increases with wavelength, while CT emission efficiency (ideally high) decreases with wavelength. While in certain cases we have found that fluorescent chemosensors with relatively high initial quantum yields (e.g.,  $\phi = 0.23$  for **13**) retain useful metal ion response, this is not generally the case.

Two recent observations represent promising leads for the development of the next generation of pyridine-derived fluorescent chemosensors. The first of these arose from juxtaposing the 4-carboxylate substituent found in **10** and **13** with the 4-vinyl group found in the chemosensor from Figure 1. By preparing vinylogous amide **14** (Fig. 9), we have found a fluorophore that benefits from a red shift induced by the carboxylate substituent, but does not suffer from the increase in quantum yield seen in **10** or **13**. The second, and more belated, observation is that the importance of the *p,p'*-methoxy groups may have been overestimated. Podand **15**—similar to **13** and the podand of Figure 1—responds strongly to presence of metal ions (Fig. 10). While the absence of the methoxy groups leads to emission wavelengths that are much shorter than desirable, the lower initial quantum yield ( $\phi \leq 0.01$ ) allows for a much greater dynamic range for the fluorescence response.

Our ongoing efforts focus on gaining a greater understanding the properties of **14**, exploiting this fluorophore for the development of fluorescent chemosensors, and turning the luminescence of long wavelength CT emission back on. In addition, based on evaluation of **15**, it is clearly necessary to reinvestigate the influence of the 4-substituent in the series of fluorophores lacking the *p,p'*-methoxy groups.

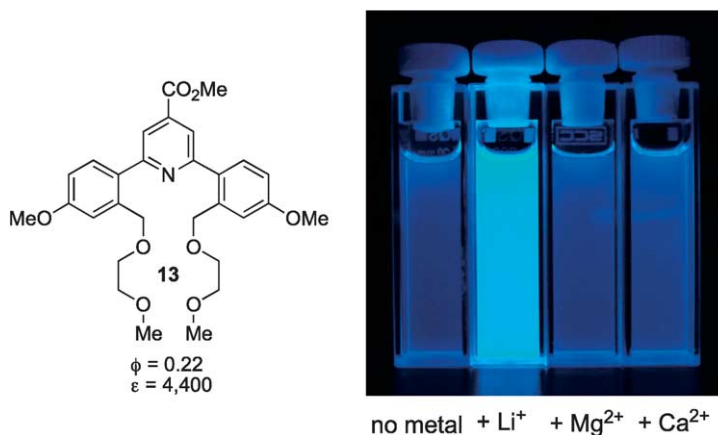


Figure 8. Titration of **13** ( $10^{-5}$  M in  $\text{CH}_3\text{CN}$ ) with  $\text{Li}^+$ .

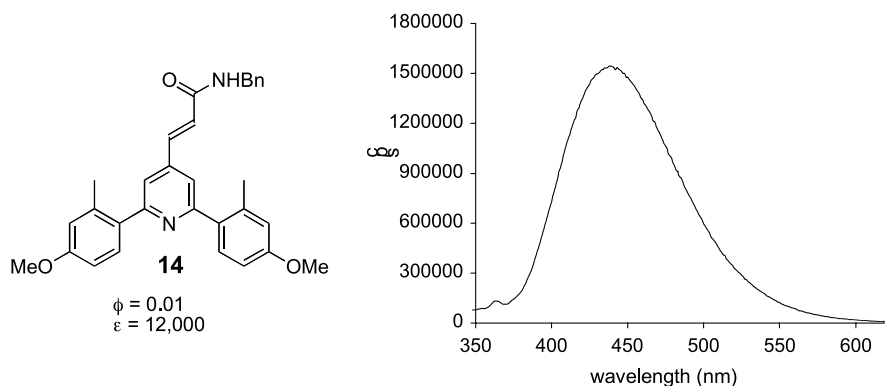


Figure 9. Vinylogous amide **14** has desirable visible LE emission.

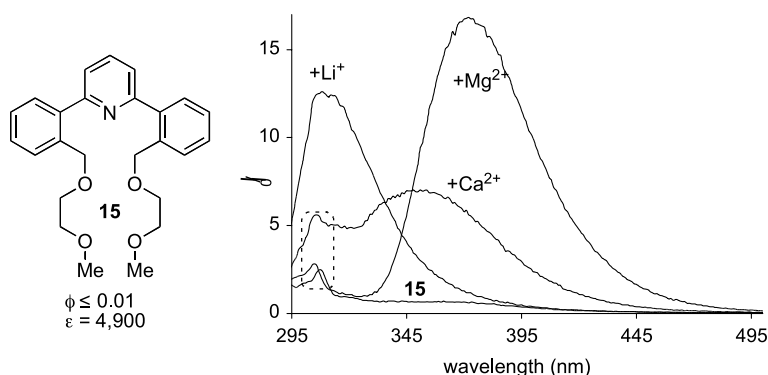


Figure 10. Titration of podand **15** ( $10^{-5}$  M in  $\text{CH}_3\text{CN}$ ) with metal ions. Emission maxima in broken box are Raman scattering from  $\text{CH}_3\text{CN}$ .

## 6. Experimental

### 6.1. General notes

Melting points were obtained in open capillary tubes with a Thomas Scientific Uni-Melt melting point apparatus and are uncorrected.  $^1\text{H}$  NMR spectra were obtained on Varian HG-400 (400 MHz) spectrometers. Chemical shifts ( $\delta$ ) are reported in parts per million (ppm) relative to residual solvent ( $\text{CHCl}_3$ ), s,  $\delta$ , 7.26). Multiplicities are given as: s (singlet), d (doublet), t (triplet), q (quartet), dd (doublet of doublets), ddd (doublet of doublet of doublets), dt (doublet of triplets) and m (multiplet). Proton-decoupled  $^{13}\text{C}$  NMR spectra were obtained on Varian HG-400 (100 MHz) spectrometers.  $^{13}\text{C}$  chemical shifts are reported relative to  $\text{CDCl}_3$  (t,  $\delta$ , 77.0). IR stretches are given in  $\text{cm}^{-1}$ ; spectra were obtained on a Nicolet 550 Series II Spectrophotometer. MALDI-FT mass spectroscopic analyses were provided by the facility at The Scripps Research Institute; all other mass spectroscopic analyses were provided by the facility at UCLA.

Fluorescence measurements were carried out in spectroscopic grade  $\text{CH}_3\text{CN}$  on a PTI Quantmaster 2000, with flash lamp excitation and 2 nm excitation and emission slit widths. Solutions of fluorophore were prepared by successive dilution and were typically  $1 \times 10^{-5}$  M in  $\text{CH}_3\text{CN}$ . Solutions of metal perchlorate salts were prepared by successive dilution and were typically 1 M. Fluorescence titrations were carried out by sequentially adding 0.005 or 0.010 mL aliquots of metal solution via micropipette to 2.500 mL of fluorophore solution in a quartz cuvette. The

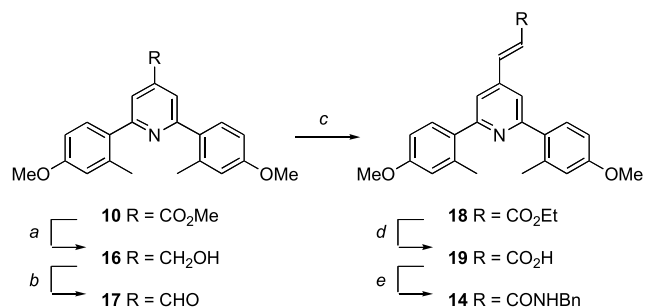
solutions were equilibrated by stirring prior to acquiring fluorescence spectra. No efforts were made to exclude water or air. Quantum yields and extinction coefficients were determined by standard methods.<sup>20</sup>

Chromatographic purifications were performed by flash chromatography with silica gel (Fisher Scientific, 32–63  $\mu\text{m}$ ) packed in glass columns; eluting solvent for each purification was determined by thin layer chromatography (TLC). Analytical TLC was performed on glass plates coated with 0.25 mm silica gel 60 F<sub>254</sub> (EM Science) using UV light for visualization.

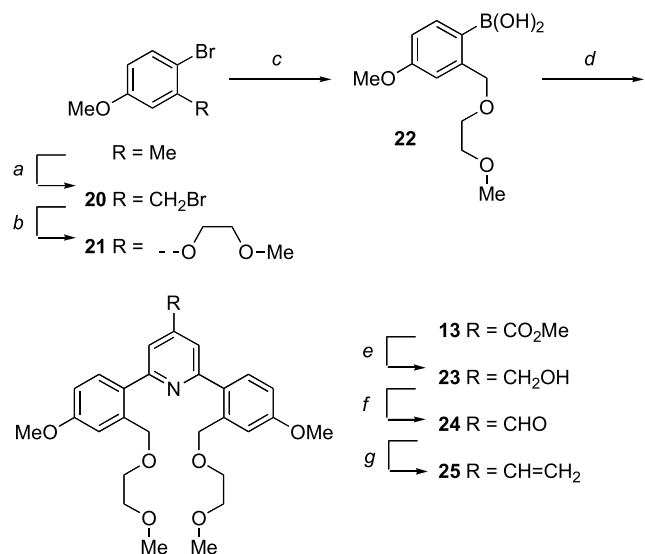
Synthetic procedures were carried out under an inert atmosphere, using standard Schlenk line techniques. Where noted, solutions were degassed by evacuating and backfilling with  $\text{N}_2$  several times. THF,  $\text{CH}_2\text{Cl}_2$ , and benzene were dried by passage through a column of activated alumina.<sup>21</sup> Pyridine was distilled from  $\text{CaH}_2$ . All other reagents and solvents were used as received unless otherwise specified.

### 6.2. Experimental procedures<sup>9,10</sup>

Compounds **3** and **8–11** were prepared as described previously.<sup>2</sup> Compound **1** is commercially available but was prepared as described below for convenience. Compound **14** was prepared in 5 steps and good yield from ester **10** (Scheme 2). Compound **13** and the fluorescent chemosensor shown in Figure 1 (**25**) were prepared from 2-bromo-5-methoxytoluene (Scheme 3). Compound **15** was prepared in analogy to **2** by variation of the boronic acid.



**Scheme 2.** Preparation of vinylogous amide **14**. Reagents and conditions: (a) DiBAL/THF,  $-78^{\circ}\text{C}$ , 89%; (b) DMSO, (COCl)<sub>2</sub>, NEt<sub>3</sub>, CH<sub>2</sub>Cl<sub>2</sub>,  $-78^{\circ}\text{C}$ , 94%; (c) (EtO)<sub>2</sub>P(O)CH<sub>2</sub>CO<sub>2</sub>Et, <sup>t</sup>BuO<sup>-</sup>K<sup>+</sup>, THF,  $0^{\circ}\text{C}$ , 100%; (d) LiOH·2H<sub>2</sub>O, THF, RT 85%; (e) BnNH<sub>2</sub>, DEPBT, THF, RT, 94%.



**Scheme 3.** Preparation of **13** and the chemosensor from Figure 1 (**25**). Reagents and conditions: (a) NBS, AIBN, PhH, 86%;<sup>2</sup> (b) CH<sub>3</sub>OCH<sub>2</sub>CH<sub>2</sub>OCH<sub>2</sub>OH, NaH, THF, 80%; (c) BuLi, B(O<sup>i</sup>Pr)<sub>3</sub>, THF; NaOH, 70%; (d) 2,6-dichloro-4-carboxy-methylpyridine, Pd<sub>2</sub>(dba)<sub>3</sub>, P<sup>t</sup>Bu<sub>3</sub>, CsF, THF,<sup>2</sup> 52%; (e) DiBALiH, THF,  $-78^{\circ}\text{C}$ , 99%; (f) DMSO, (COCl)<sub>2</sub>, NEt<sub>3</sub>, CH<sub>2</sub>Cl<sub>2</sub>,  $-78^{\circ}\text{C}$ , 90%; (g) Ph<sub>3</sub>PCH<sub>3</sub><sup>+</sup>I<sup>-</sup>, BuLi, THF,  $0^{\circ}\text{C}$ , 60%.

**6.2.1. Compound 1.** 2,6-Dibromopyridine (0.100 g, 0.422 mmol, 1 equiv), phenylboronic acid (0.155 g, 1.27 mmol, 3.00 equiv), [HP<sup>t</sup>Bu<sub>3</sub>]<sup>+</sup>BF<sub>4</sub><sup>-</sup> (0.012 g, 0.040 mmol, 0.10 equiv), Pd<sub>2</sub>(dba)<sub>3</sub> (0.019 g, 0.021 mmol, 0.050 equiv), and CsCO<sub>3</sub> (0.756 g, 2.320 mmol, 5.50 equiv) was suspended in THF (10 mL). The reaction mixture was degassed and refluxed for 16 h. After cooling to room temperature, H<sub>2</sub>O (50 mL) was added and the mixture extracted with methylene chloride (2×50 mL). The combined organic extracts were dried over Na<sub>2</sub>SO<sub>4</sub> and concentrated. Purification by column chromatography (20% toluene/hexanes) produced 0.098 g (0.422 mmol, 48%) of **1** as a white solid, mp  $78\text{--}80^{\circ}\text{C}$ . <sup>1</sup>H NMR (400 MHz, CDCl<sub>3</sub>):  $\delta$ =8.18 (m, 4H), 7.82 (dd, 6.8,  $J$ =7.0 Hz, 1H), 7.71 (d,  $J$ =7.6 Hz, 2H), 7.52 (m, 4H), 7.46 (m, 2H). IR (KBr):  $\nu$ =3056, 2925, 1588, 1449, 758, 697. TLC ( $R_f$ )=0.11 (20% toluene/hexanes).

**6.2.2. Compound 2.** Procedure as for **1**, except P<sup>t</sup>Bu<sub>3</sub> in THF was used as the phosphine source. White solid, mp  $68\text{--}70^{\circ}\text{C}$ , 65%. <sup>1</sup>H NMR (400 MHz, CDCl<sub>3</sub>):  $\delta$ =7.81 (t,  $J$ =7.6 Hz, 1H), 7.45 (m, 2H), 7.36 (d,  $J$ =7.6 Hz, 2H), 7.27

(m, 6H), 2.43 (s, 6H). <sup>13</sup>C NMR (100 MHz, CDCl<sub>3</sub>):  $\delta$ =159.24, 140.48, 136.11, 135.62, 130.50, 129.67, 128.01, 125.67, 121.83, 20.69. IR (KBr):  $\nu$ =3030, 2951, 1562, 1457, 767. HRMS (EI): calcd for C<sub>19</sub>H<sub>16</sub>N [M<sup>+</sup>] 259.1361; found 259.1349. TLC ( $R_f$ )=0.4 (5% acetone/hexanes).

**6.2.3. Compound 4.** Procedure as for **2**. White solid, mp  $140\text{--}141^{\circ}\text{C}$ , 26%. <sup>1</sup>H NMR (400 MHz, CDCl<sub>3</sub>):  $\delta$ =7.95 (m, 4H), 7.72 (t,  $J$ =7.6 Hz, 1H), 7.56 (d,  $J$ =8.0 Hz, 2H), 6.94 (d,  $J$ =8.8 Hz, 2H), 3.91 (s, 6H), 2.34 (s, 6H). <sup>13</sup>C NMR (100 MHz, CDCl<sub>3</sub>):  $\delta$ =158.42, 156.41, 136.95, 131.74, 129.16, 126.56, 125.50, 117.06, 109.82, 55.47, 16.58. IR (KBr):  $\nu$ =2943, 1615, 1562, 1510, 1449, 1256, 1143, 1029. HRMS (EI): calcd for C<sub>21</sub>H<sub>21</sub>NO<sub>2</sub> [M<sup>+</sup>] 319.1572; found 319.1569. TLC ( $R_f$ )=0.20 (10% EtOAc/hexanes).

**6.2.4. Compound 5.** 4-Bromo-3,5-dimethylanisole (0.25 g, 1.17 mmol, 2.00 equiv) was cooled to  $-78^{\circ}\text{C}$  in THF (5 mL). *n*-BuLi (1.22 mL 1.20 M in hexanes, 1.46 mmol, 2.50 equiv) was added dropwise and stirred at  $-78^{\circ}\text{C}$  for 15 min. ZnCl<sub>2</sub> (0.40 g, 2.92 mmol, 5.00 equiv) was transferred via cannula into the reaction mixture as a THF solution (10 mL), and the reaction was stirred for an additional 15 min. The reaction mixture was transferred via cannula into a flask containing 2,6-dibromopyridine (0.14 g, 0.58 mmol, 1 equiv) and Pd(PPh<sub>3</sub>)<sub>4</sub> (0.03 g, 0.03 mmol, 0.05 equiv). The reaction mixture was degassed then refluxed for 20 h. The reaction was allowed to cool to room temperature, H<sub>2</sub>O (25 mL) was added, and the mixture was extracted with EtOAc (3×25 mL). The combined organic fractions were washed with brine (1×25 mL), dried over Na<sub>2</sub>SO<sub>4</sub>, filtered, and concentrated under vacuum. Purification by column chromatography (20% EtOAc/hexanes) produced 0.09 g (0.27 mmol, 46%) of **5** as a pale yellow solid, mp  $167\text{--}168^{\circ}\text{C}$ .  $R_f$ =0.24 (20% EtOAc/hexanes). IR (KBr):  $\nu$ =2961, 1602, 1575, 1463, 1315, 1194, 1160, 1074, and 838 cm<sup>-1</sup>. <sup>1</sup>H NMR (CDCl<sub>3</sub>):  $\delta$ =7.80 (t,  $J$ =8 Hz, 1H), 7.17 (d,  $J$ =8 Hz, 2H), 6.64 (s, 4H), 3.80 (s, 6H), and 2.06 ppm (s, 12H). <sup>13</sup>C NMR (CDCl<sub>3</sub>):  $\delta$ =159.7, 158.7, 137.1, 136.4, 122.7, 112.9, 112.7, 55.2, and 20.7 ppm. HRMS (DEI): calculated for C<sub>23</sub>H<sub>24</sub>NO<sub>2</sub> (M-H<sup>+</sup>): 346.180704, found 346.181374.

**6.2.5. Compound 6.** 2-Bromo-4,5-methylenedioxytoluene (0.25 g, 1.16 mmol, 3.00 equiv) was cooled to  $-78^{\circ}\text{C}$  in THF (5 mL). *n*-BuLi (0.67 mL/1.8 M, 1.20 mmol 3.10 equiv) was added and the reaction stirred for 5 min, ZnCl<sub>2</sub> (0.181 g, 1.65 mmol, 3.50 equiv) in THF (3.0 mL) was added. The arylzinc chloride so generated was transferred via cannula into a degassed solution of 2,6-dibromopyridine (0.0920 g, 0.387 mmol, 1 equiv), Pd<sub>2</sub>(dba)<sub>3</sub> (0.018 g, 0.019 mmol, 0.050 equiv, P<sup>t</sup>Bu<sub>3</sub> (0.56 mL, 0.14 M in THF, 0.077 mmol, 0.20 equiv), and refluxed for 16 h. Upon cooling to room temperature, the reaction mixture was diluted with EtOAc (1×50 mL), washed with H<sub>2</sub>O (1×250 mL) and saturated NaCl (1×50 mL). The organic layer was dried over Na<sub>2</sub>SO<sub>4</sub>, concentrated, and chromatographed on silica gel (10% EtOAc/hexanes) to afford a white solid (0.047 g, 35%), mp  $149\text{--}151^{\circ}\text{C}$ . <sup>1</sup>H NMR (400 MHz, CDCl<sub>3</sub>):  $\delta$ =7.75 (t,  $J$ =7.6 Hz, 1H), 7.28 (d,  $J$ =7.6 Hz, 2H), 6.96 (s, 2H), 6.74 (s, 2H), 5.95 (s, 4H), 2.33 (s, 6H). <sup>13</sup>C NMR (100 MHz, CDCl<sub>3</sub>):  $\delta$ =158.83, 147.20, 145.50, 135.98, 133.73, 129.43, 121.75, 110.45, 109.91, 100.85, 20.59. IR

(KBr):  $\nu=2925, 1562, 1510, 1449, 1047, 933$ . HRMS (EI): calcd for  $C_{21}H_{16}NO_4 [(M-H)^+]$  346.1079; found 346.1084. TLC ( $R_f$ )=0.20 (12% EtOAc/hexanes).

**6.2.6. Compound 7.** Procedure as for **2**. White solid, mp 129–130 °C, 75%.  $^1H$  NMR (400 MHz,  $CDCl_3$ ):  $\delta=7.72$  (dd,  $J=1.6, 6.8$  Hz, 2H), 7.60 (s, 2H), 7.51 (m, 5H), 7.29 (m, 6H), 2.48 (s, 3H).  $^{13}C$  NMR (100 MHz,  $CDCl_3$ ):  $\delta=159.84, 148.55, 140.51, 138.27, 135.71, 130.52, 129.67, 128.95, 128.85, 128.07, 126.95, 125.68, 119.94, 20.75$ . IR (KBr):  $\nu=3039, 2925, 1588, 1545, 1396, 767$ . HRMS (EI): calcd for  $C_{25}H_{20}N [(M-H)^+]$  334.1596; found 334.1592. TLC ( $R_f$ )=0.34 (5% EtOAc/hexanes).

**6.2.7. Compound 12.** 4-Bromo-3,5-dimethylanisole (0.25 g, 1.17 mmol, 2.00 equiv) was cooled to  $-78$  °C in THF (5 mL). *n*-BuLi (1.22 mL 1.2 M in hexanes, 1.46 mmol, 2.5 equiv) was added dropwise and stirred at  $-78$  °C for 15 min.  $ZnCl_2$  (0.40 g, 2.92 mmol, 5.00 equiv) was transferred via cannula into the reaction mixture as a THF solution (10 mL), and the reaction was stirred for an additional 15 min. The reaction mixture was transferred via cannula into a flask containing 2,6-dichloroisonicotinic acid methyl ester (0.120 g, 0.58 mmol, 1 equiv) and  $Pd(PPh_3)_4$  (0.03 g, 0.03 mmol, 0.05 equiv). The reaction mixture was degassed then refluxed for 16 h. The reaction was allowed to cool to room temperature,  $H_2O$  (25 mL) was added, and the mixture was extracted with EtOAc ( $3 \times 25$  mL). The combined organic fractions were washed with brine ( $1 \times 25$  mL), dried over  $Na_2SO_4$ , filtered, and concentrated under vacuum. Purification by column chromatography (20% EtOAc/hexanes) produced 0.02 g (0.06 mmol, 10%) of **12** as a yellow solid, mp 189 °C.  $R_f=0.20$  (20% EtOAc/hexanes). IR (KBr):  $\nu=2960, 1732, 1607, 1439, 1396, 1345, 1316, 1245, \text{ and } 1157$   $cm^{-1}$ .  $^1H$  NMR ( $CDCl_3$ ):  $\delta=7.75$  (s, 2H), 6.64 (s, 4H), 3.96 (s, 3H), 3.80 (s, 6H), and 2.05 ppm (s, 12H).  $^{13}C$  NMR ( $CDCl_3$ ):  $\delta=165.7, 160.9, 158.9, 138.1, 137.0, 132.7, 122.1, 112.8, 55.3, 52.8, \text{ and } 20.7$  ppm. HRMS (DEI): calculated for  $C_{25}H_{26}NO_4 (M-H)^+$ : 404.186184, found 404.187089.

**6.2.8. Compound 13.** Procedure as for **1** except **22** was used as the boronic acid,  $P^tBu_3$  in THF as the phosphine and  $CsF$  as the base. Colorless oil, 52%.  $^1H$  NMR (400 MHz,  $CDCl_3$ ):  $\delta=7.99$  (s, 2H), 7.54 (d, 2H,  $J=8.4$  Hz), 7.20 (d, 2H,  $J=2.8$  Hz), 6.93 (dd, 2H,  $J=2.8, 8.4$  Hz), 4.72 (s, 4H), 3.98 (s, 3H), 3.87 (s, 6H), 3.57–3.54 (m, 8H), 3.35 (s, 6H).  $^{13}C$  NMR (100 MHz,  $CDCl_3$ ):  $\delta=165.83, 160.12, 159.22, 142.50, 137.73, 131.55, 131.42, 120.07, 114.26, 113.45, 71.85, 71.40, 69.61, 59.17, 55.42, 52.73$ . IR (neat):  $\nu=2890, 1737$  (s), 1606, 1248, 1099. HRMS (MALDI): calcd for  $C_{29}H_{36}NO_8 [(M-H)^+]$  548.2255; found 548.2271. TLC ( $R_f$ )=0.20 (45% EtOAc/hexanes).

**6.2.9. Compound 14.** Carboxylic acid **19**, (0.054 g, 0.139 mmol, 1 equiv), *N,N'*-diisopropyl-*N*-ethylamine (0.048 mL, 0.278 mmol, 2.00 equiv), and 3-(diethoxyphosphoryloxy)-1,2,3-benzotriazin-4(3*H*)-one (DEPBT)<sup>22</sup> (0.083 g, 0.278 mmol, 2.00 equiv) was suspended in THF (2.5 mL). After stirring for 5 min, benzylamine (0.018 mL, 0.167 mmol, 1.20 equiv) was added and the resulting solution was stirred for 3 h at 23 °C. The solution was diluted with  $CH_2Cl_2$  (50 mL) and washed with  $H_2O$  ( $2 \times$

50 mL), and saturated NaCl ( $1 \times 25$  mL). The organic phase was dried over  $Na_2SO_4$  and was concentrated. Purification by flash column chromatography (30% EtOAc/hexanes) provided 0.063 g (0.131 mmol, 94%) of a yellow solid.  $^1H$  NMR ( $CDCl_3$ ):  $\delta=7.69$  (d, 1H,  $J=15.6$  Hz), 7.35 (m, 9H), 6.82 (m, 4H), 6.60 (d, 1H,  $J=15.6$  Hz), 5.98 (t, 1H,  $J=5.6$  Hz), 4.60 (d, 2H,  $J=5.6$  Hz), 3.84 (s, 6H), 2.44 (s, 6H). IR (KBr):  $\nu=3283$  (b), 2934, 1676 (s), 1615, 1239, 1047, 741. HRMS (EI): calcd for  $C_{31}H_{30}N_2O_3 [M^+]$  478.2256; found 478.2266. TLC ( $R_f$ )=0.33 (35% EtOAc/hexanes).

**6.2.10. Compound 15.** Procedure as for **1**. Pale yellow viscous oil, 90%.  $^1H$  NMR (400 MHz,  $CD_3CN$ ):  $\delta=7.89$  (t, 1H,  $J=7.6$  Hz), 7.57 (s, 2H), 7.54 (m, 4H), 7.42 (m, 4H), 4.62 (s, 4H), 3.49–3.39 (m, 8H), 3.23 (s, 6H).  $^{13}C$  NMR (100 MHz,  $CDCl_3$ ):  $\delta=158.28, 140.10, 136.50, 135.99, 129.92, 129.00, 128.39, 127.59, 122.23, 71.86, 71.11, 69.41, 58.96$ . IR (neat):  $\nu=2895, 1731, 1579, 1442, 1107$ . HRMS (EI): calcd for  $C_{25}H_{29}NO_4 [M^+]$  407.2097; found 407.2086. TLC ( $R_f$ )=0.30 (30% acetone/hexanes).

**6.2.11. Compound 16.** DiBALH (5.43 mL, 1.0 M in hexanes, 5.43 mmol, 3.00 equiv) was added dropwise to a solution of methyl ester **10** (0.656 g, 1.81 mmol, 1 equiv) in THF (10 mL) at  $-78$  °C. After stirring for 5 min at  $-78$  °C, the reaction mixture was warmed to room temperature and quenched by the addition of methanol ( $\sim 2.5$  mL), followed by  $H_2O$  (40 mL). After stirring for 10 min, the reaction was extracted with EtOAc ( $3 \times 40$  mL) and the combined organic extracts washed with saturated NaCl ( $1 \times 25$  mL). The organic phase was dried over  $Na_2SO_4$  and was concentrated. Purification by flash column chromatography (30% EtOAc/hexanes) provided 0.56 g (1.61 mmol, 89%) of **16** as a white solid, mp 149–151 °C.  $^1H$  NMR ( $CDCl_3$ ):  $\delta=7.34$  (dd, 2H,  $J=0.8, 8.4$  Hz), 7.18 (s, 2H), m (6.77, 4H), 4.62 (d, 2H,  $J=4.4$  Hz), 3.84 (s, 6H), 2.75 (b, 1H), 2.38 (s, 6H).  $^{13}C$  NMR ( $CDCl_3$ ):  $\delta=159.13, 158.92, 150.25, 137.27, 133.22, 130.95, 119.01, 115.85, 110.99, 63.55, 55.25, 21.04$ . IR (KBr):  $\nu=3214$  (b), 2934, 2838, 1606, 1457, 1300. HRMS (EI): calcd for  $C_{22}H_{23}NO_3 [M^+]$  349.1678; found 349.1665. TLC ( $R_f$ )=0.15 (30% EtOAc/hexanes).

**6.2.12. Compound 17.** DMSO (0.25 mL, 3.50 mmol, 2.40 equiv) was added to oxalyl chloride (0.25 mL, 2.90 mmol, 2.00 equiv) in  $CH_2Cl_2$  (15 mL) at  $-78$  °C. After stirring for 5 min, alcohol **16** (0.51 g, 1.45 mmol, 1 equiv) in  $CH_2Cl_2$  (2.5 mL) was added via syringe and the reaction stirred for 5 min at  $-78$  °C. Triethylamine (1.01 mL, 7.25 mmol, 5.00 equiv) was then added and the reaction warmed to room temperature. Upon warming, the solution was diluted with  $CH_2Cl_2$  (50 mL) and washed with  $H_2O$  ( $2 \times 50$  mL) and saturated NaCl ( $1 \times 25$  mL). The organic phase was dried over  $Na_2SO_4$  and was concentrated. Purification by flash column chromatography (25% EtOAc/hexanes) provided 0.474 g (1.37 mmol, 94%) of a viscous yellow oil.  $^1H$  NMR ( $CDCl_3$ ):  $\delta=10.15$  (s, 1H), 7.71 (s, 2H), 7.46 (d, 2H,  $J=9.2$  Hz), 6.85 (m, 4H), 3.86 (s, 6H), 2.45 (s, 6H).  $^{13}C$  NMR ( $CDCl_3$ ):  $\delta=191.77, 160.52, 159.61, 142.10, 137.47, 132.21, 131.18, 119.91, 116.18, 111.32, 55.31, 21.20$ . IR (neat):  $\nu=2969, 2838, 2733, 1711$  (s), 1606, 1239, 1178, 1047. HRMS (EI): calcd for  $C_{22}H_{20}NO_3$



$[(M-H)^+]$  346.1443; found 346.1444. TLC ( $R_f$ )=0.47 (30% EtOAc/hexanes).

**6.2.13. Compound 18.** Aldehyde **19** (0.046 g, 0.132 mmol, 1 equiv) and triethylphosphonoacetate (0.033 mL, 0.165 mmol, 1.25 equiv) was suspended in THF (5 mL) and cooled to 0 °C. KO<sup>t</sup>Bu (0.165 mL, 1.0 M in THF, 0.165 mmol, 1.25 equiv) was added via syringe and the reaction stirred for 10 min at 0 °C. Upon warming to room temperature, the solution was diluted with EtOAc (30 mL) and washed with H<sub>2</sub>O (2 × 25 mL) and saturated NaCl (1 × 15 mL). The organic phase was dried over Na<sub>2</sub>SO<sub>4</sub> and was concentrated. Purification by flash column chromatography (25% EtOAc/hexanes) provided 0.055 g (0.132 mmol, 100%) of a highly viscous green/yellow oil. <sup>1</sup>H NMR (CDCl<sub>3</sub>): δ=7.69 (d, 1H, *J*=15.6 Hz), 7.41 (d, 2H, *J*=9.2 Hz), 7.38 (s, 2H), 6.83 (m, 4H), 6.64 (d, 1H, *J*=16.0 Hz), 4.30 (q, 2H, *J*=6.8 Hz), 3.85 (s, 6H), 2.46 (s, 6H), 1.37 (t, 3H, *J*=6.8 Hz). <sup>13</sup>C NMR (CDCl<sub>3</sub>): δ=165.97, 159.82, 159.36, 142.22, 141.73, 137.33, 132.80, 131.00, 122.27, 119.61, 116.02, 111.16, 60.92, 55.28, 21.11, 14.39. IR (neat): ν=2960, 2838, 1711 (s), 1606, 1239, 1178, 1047. HRMS (MALDI): calcd for C<sub>26</sub>H<sub>28</sub>NO<sub>4</sub> [(M-H)<sup>+</sup>] 418.2018; found 418.2024. TLC ( $R_f$ )=0.37 (25% EtOAc/hexanes).

**6.2.14. Compound 19.** Ester **18** (0.115 g, 0.275 mmol, 1 equiv) was suspended in THF (4 mL), LiOH·2H<sub>2</sub>O (0.017 g, in 1.0 mL of H<sub>2</sub>O, 0.413 mmol, 1.50 equiv) was added and the reaction stirred for 30 min at 23 °C. The reaction mixture was neutralized by the addition of 1 M HCl (0.413 mL, 0.413 mmol, 1.50 equiv) and extracted with CH<sub>2</sub>Cl<sub>2</sub> (3 × 25 mL). The organic phase was dried over Na<sub>2</sub>SO<sub>4</sub> and was concentrated to afford 0.091 g (0.234 mmol, 85%) of a pure yellow solid. <sup>1</sup>H NMR (CDCl<sub>3</sub>): δ=7.78 (d, 1H, *J*=16.4 Hz), 7.42 (d, 2H, *J*=9.2 Hz), 7.39 (s, 2H), 6.83 (m, 4H), 6.65 (d, 1H, *J*=16.0 Hz), 3.85 (s, 6H), 2.46 (s, 6H). <sup>13</sup>C NMR (CDCl<sub>3</sub>): δ=170.58, 159.96, 159.48, 144.43, 141.42, 137.39, 132.61, 131.03, 121.51, 119.85, 116.08, 111.23, 55.32, 21.10. IR (KBr): ν=2934, 2838, 2593, 1711, 1615, 1291, 1248, 1047. HRMS (MALDI): calcd for C<sub>24</sub>H<sub>24</sub>NO<sub>4</sub> [(M-H)<sup>+</sup>] 390.1705; found 390.1684.

**6.2.15. Compound 20.** 2-Bromo-5-methoxytoluene (5.00 g, 24.00 mmol, 1 equiv), *N*-bromosuccinimide (5.13 g, 28.8 mmol, 1.20 equiv), and AIBN (0.08 g, 0.48 mmol, 0.02 equiv) was suspended in benzene (100 mL). The reaction mixture was heated to reflux for 1 h and then cooled to 23 °C. The resulting mixture was filtered and the filtrate was diluted with diethyl ether (75 mL) and washed with H<sub>2</sub>O (2 × 100 mL) and saturated NaCl (1 × 50 mL). The organic phase was dried over Na<sub>2</sub>SO<sub>4</sub> and was concentrated. The crude solid was triturated with diethyl ether/hexanes (1:4) and filtered to yield 5.50 g (19.60 mmol, 86%) of a white solid, mp 80–82 °C. <sup>1</sup>H NMR (400 MHz, CDCl<sub>3</sub>): δ=7.45 (d, 1H, *J*=8.8 Hz), 6.99 (d, 1H, *J*=3.2 Hz), 6.74 (dd, 1H *J*=2.8, 8.8 Hz), 4.55 (s, 2H), 3.80 (s, 3H). IR (KBr): ν=2943, 2847, 1483, 1291, 1256, 1012, 811. TLC ( $R_f$ )=0.58 (10% EtOAc/hexanes).

**6.2.16. Compound 21.** 2-Methoxyethanol (1.13 mL, 14.30 mmol, 2.00 equiv) was added dropwise to a solution of NaH (0.8, 60% w/w in mineral oil, 21.40 mmol,

3.00 equiv) in THF (50 mL) at 0 °C. After stirring for 10 min, benzyl bromide **20** (2.00 g, 7.14 mmol, 1 equiv) in THF (3.0 mL) was added via syringe. The reaction mixture was warmed to RT and stirred for 18 h. The solvent was removed on the rotary evaporator and the residue dissolved in diethyl ether (50 mL), which was subsequently washed with H<sub>2</sub>O (2 × 50 mL) and saturated NaCl (1 × 25 mL). The organic phase was dried over Na<sub>2</sub>SO<sub>4</sub> and was concentrated. Purification by flash column chromatography (25% EtOAc/hexanes) provided 1.56 g (5.67 mmol, 80%) of a clear oil. <sup>1</sup>H NMR (400 MHz, CDCl<sub>3</sub>): δ=7.40 (d, 1H, *J*=8.8 Hz), 7.10 (d, 1H, *J*=3.2 Hz), 6.70 (dd, 1H, *J*=8.8, 3.2 Hz), 4.60 (s, 2H), 3.80 (s, 3H), 3.71 (m, 2H), 3.62 (m, 2H), 3.42 (s, 3H). <sup>13</sup>C NMR (100 MHz, CDCl<sub>3</sub>): δ=158.79, 138.30, 132.72, 114.56, 113.92, 112.40, 72.24, 71.79, 69.92, 59.08, 55.41. IR (neat): ν=2890, 1580, 1475, 1291, 1108. HRMS (MALDI): calcd for C<sub>11</sub>H<sub>15</sub>O<sub>3</sub> [(M-Na<sup>+</sup>)] 297.0097; found 297.0094. TLC ( $R_f$ )=0.25 (10% EtOAc/hexanes).

**6.2.17. Compound 22.** *n*-BuLi (5.40 mL, 1.6 M solution in hexanes, 8.60 mmol, 1.20 equiv) was added dropwise to a solution of aryl bromide **21** (1.96 g, 7.14 mmol, 1 equiv) in THF (50 mL) at -78 °C, and the resulting solution stirred for 5 min. Triisopropyl borate (2.16 mL, 9.30 mmol, 1.30 equiv) was added via syringe and the flask warmed to RT. The majority (~75%) of the solvent was removed with the rotary evaporator and 1 M HCl (50 mL) was added and the resulting solution was stirred for 4 h. The mixture was extracted with ether (3 × 33 mL) and the combined organic fractions were extracted with 1 M NaOH (3 × 15 mL). The aqueous extracts were combined and neutralized with HCl (conc.) until acidic to litmus. The aqueous layer was then extracted with EtOAc (3 × 33 mL) and the combined organic phases were dried over Na<sub>2</sub>SO<sub>4</sub> and concentrated. This produced a colorless oil (1.20 g, 5.00 mmol, 70%) that hardened upon standing. This material was used in subsequent reactions without further purification. <sup>1</sup>H NMR (400 MHz, CDCl<sub>3</sub>): δ=7.88 (d, 1H, *J*=8.4 Hz), 6.89 (dd, 1H, *J*=8.4, 2.4 Hz), 6.81 (d, 1H, *J*=2.4 Hz), 6.27 (b, 2H), 4.63 (s, 2H), 3.83 (s, 3H), 3.65 (m, 2H), 3.55 (m, 2H), 3.37 (s, 3H). IR (KBr): ν=3362 (b), 2917, 1606, 1370, 1265, 1073.

**6.2.18. Compound 23.** Procedure as for **1** except **22** was used as the boronic acid, P<sup>t</sup>Bu<sub>3</sub> in THF as the phosphine and CsF as the base. Colorless oil, 52%. <sup>1</sup>H NMR (400 MHz, CDCl<sub>3</sub>): δ=7.99 (s, 2H), 7.54 (d, 2H, *J*=8.4 Hz), 7.20 (d, 2H, *J*=2.8 Hz), 6.93 (dd, 2H, *J*=2.8, 8.4 Hz), 4.72 (s, 4H), 3.98 (s, 3H), 3.87 (s, 6H), 3.57–3.54 (m, 8H), 3.35 (s, 6H). <sup>13</sup>C NMR (100 MHz, CDCl<sub>3</sub>): δ=165.83, 160.12, 159.22, 142.50, 137.73, 131.55, 131.42, 120.07, 114.26, 113.45, 71.85, 71.40, 69.61, 59.17, 55.42, 52.73. IR (neat): ν=2890, 1737 (s), 1606, 1248, 1099. HRMS (MALDI): calcd for C<sub>29</sub>H<sub>36</sub>NO<sub>8</sub> [(M+H)<sup>+</sup>] 548.2255; found 548.2271. TLC ( $R_f$ )=0.20 (45% EtOAc/hexanes).

**6.2.19. Compound 23.** Procedure as for **16**. Colorless oil, 99%. <sup>1</sup>H NMR (400 MHz, CDCl<sub>3</sub>): δ=7.57 (d, 2H, *J*=8.4 Hz), 7.55 (s, 2H), 7.12 (d, 2H, *J*=2.4 Hz), 6.93 (dd, 2H, *J*=2.4, 8.4 Hz), 4.72 (d, 2H, *J*=6.8 Hz), 4.61 (s, 4H), 3.91 (b, 1H), 3.86 (s, 6H), 3.65–3.60 (m, 8H), 3.40 (s, 6H). <sup>13</sup>C NMR (100 MHz, CDCl<sub>3</sub>): δ=159.53, 157.65, 150.80, 136.88, 133.21, 131.36, 119.64, 114.47, 113.59, 72.08, 71.60, 69.60,

63.99, 59.12, 55.41. IR (neat):  $\nu=3441$  (b), 2908, 1606, 1431, 1239, 1082, 872. HRMS (MALDI): calcd for  $C_{28}H_{36}NO_7 [(M-H)^+]$  498.2486; found 498.2475. TLC ( $R_f$ )=0.19 (60% THF/hexanes).

**6.2.20. Compound 24.** Procedure as for **17**. Colorless oil, 90%.  $^1H$  NMR (400 MHz,  $CDCl_3$ ):  $\delta=10.18$  (s, 1H), 7.93 (s, 2H), 7.58 (d, 2H,  $J=8.4$  Hz), 7.18 (d, 2H,  $J=2.8$  Hz), 6.95 (dd, 2H,  $J=2.8, 8.4$  Hz), 4.69 (s, 4H), 3.88 (s, 6H), 3.61–3.54 (m, 8H), 3.36 (s, 6H).  $^{13}C$  NMR (100 MHz,  $CDCl_3$ ):  $\delta=192.30, 159.98, 159.32, 142.51, 137.62, 131.64, 131.39, 120.06, 114.26, 113.48, 71.89, 71.36, 69.63, 59.08, 55.45$ . IR (neat):  $\nu=2908, 1711$  (s), 1615, 1553, 1248, 1099, 889. HRMS (MALDI): calcd for  $C_{28}H_{34}NO_7 [(M-H)^+]$  496.2330; found 496.2318. TLC ( $R_f$ )=0.33 (35% EtOAc/hexanes).

**6.2.21. Compound 25.** A suspension of methyl triphenylphosphonium iodide (0.175 g, 0.433 mmol, 2.90 equiv) in THF (5 mL) was cooled to 0 °C. *n*-BuLi (0.271 mL, 1.60 M in hexanes, 0.433 mmol, 2.90 equiv) was added via syringe and the mixture stirred for 30 min. Aldehyde **24** (0.075 g, 0.151 mmol, 1 equiv) in THF (1 mL) was added via syringe and the reaction stirred for an additional 30 min. The reaction was warmed to RT and stirred for 5 h. The solution was diluted with  $CH_2Cl_2$  (20 mL) and washed with  $H_2O$  ( $2 \times 25$  mL) and saturated NaCl ( $1 \times 10$  mL). The organic phase was dried over  $Na_2SO_4$  and was concentrated. Purification by flash column chromatography (45% EtOAc/hexanes) afforded 0.045 g (0.091 mmol, 60%) of **25** as a pale yellow viscous oil.  $^1H$  NMR (400 MHz,  $CDCl_3$ ):  $\delta=7.50$  (d, 2H,  $J=8.4$  Hz), 7.44 (s, 2H), 7.18 (d, 2H,  $J=2.4$  Hz), 6.91 (dd, 2H,  $J=2.4, 8.4$  Hz), 6.77 (dd, 1H,  $J=11.2, 17.6$  Hz), 6.06 (d, 1H,  $J=17.6$  Hz), 5.51 (d, 1H,  $J=11.2$  Hz), 4.71 (s, 4H), 3.86 (s, 6H), 3.60–3.52 (m, 8H), 3.36 (s, 6H).  $^{13}C$  NMR (100 MHz,  $CDCl_3$ ):  $\delta=159.55, 158.17, 145.12, 137.51, 135.06, 132.58, 131.10, 118.79, 118.31, 113.62, 113.21, 71.89, 71.19, 69.50, 59.05, 55.39$ . IR (neat):  $\nu=2882, 1597, 1501, 1248, 1099, 1038, 881, 811$ . HRMS (MALDI): calcd for  $C_{29}H_{36}NO_6 [(M-H)^+]$  494.2537; found 494.2560. TLC ( $R_f$ )=0.20 (35% EtOAc/hexanes).

## References and notes

- For representative reviews of the chemosensor field, see: (a) Rurack, K.; Resch-Genger, U. *Chem. Soc. Rev.* **2002**, *31*, 116–127. (b) Lavigne, J. J.; Anslyn, E. V. *Angew. Chem. Int. Ed.* **2001**, *40*, 3118–3130. (c) Valeur, B.; Leray, I. *Coord. Chem. Rev.* **2000**, *205*, 3–40. (d) de Silva, A. P.; Eilers, J.; Zlokarnik, G. *Proc. Natl. Acad. Sci. U.S.A.* **1999**, *96*, 8336–8337. (e) Snowden, T. S.; Anslyn, E. V. *Curr. Opin. Chem. Biol.* **1999**, *3*, 740–746. (f) de Silva, A. P.; Gunaratne, H. Q. N.; Gunnlaugsson, T.; Huxley, A. J. M.; McCoy, C. P.; Rademacher, J. T.; Rice, T. E. *Chem. Rev.* **1997**, *97*, 1515–1566. (g) Fabbri, L.; Licchelli, M.; Pallavicini, P.; Sacchi, D.; Taglietti, A. *Analyst* **1996**, *121*, 1763–1768. (h) *Fluorosensors for Ion and Molecule Recognition*. Czarnik, A. W., Ed.; American Chemical Society: Washington, DC, 1994.
- For our previous work on pyridine derived fluorescent chemosensors, see: (a) Mello, J. V.; Finney, N. S. *Angew. Chem. Int. Ed.* **2001**, *40*, 1536–1538. (b) Mello, J. V.; Finney, N. S. *Org. Lett.* **2001**, *3*, 4263–4265. (c) Fang, A. G.; Mello, J. V.; Finney, N. S. *Org. Lett.* **2003**, *5*, 967–970.
- For our previous work on hydrocarbon and Ru(II)bpy<sub>3</sub><sup>2+</sup> derived chemosensors, see: (a) McFarland, S. A.; Finney, N. S. *J. Am. Chem. Soc.* **2001**, *123*, 1260–1261. (b) McFarland, S. A.; Finney, N. S. *J. Am. Chem. Soc.* **2002**, *124*, 1178–1179. (c) McFarland, S. A.; Finney, N. S. *Chem. Commun.* **2003**, 388–389.
- For an early example of the use of conformational restriction of a binaphthyl to provide a fluorescent response to binding, see: Takeuchi, M.; Yoda, S.; Imada, T.; Shinkai, S. *Tetrahedron* **1997**, *53*, 8335–8348. Note that in this case the maximum reported  $III_0$  was <1.3.
- For recent representative examples, see: (a) Guo, X.; Qian, X.; Jia, L. *J. Am. Chem. Soc.* **2004**, *126*, 2272–2273. (b) Nolan, E. M.; Lippard, S. J. *J. Am. Chem. Soc.* **2003**, *125*, 14270–14271. (c) Walkup, G. K.; Burdette, S. C.; Lippard, S. J.; Tsien, R. Y. *J. Am. Chem. Soc.* **2000**, *122*, 5644–5645.
- For representative examples, see: (a) Ueno, A.; Ikeda, A.; Ikeda, H.; Ikeda, T.; Toda, F. *J. Org. Chem.* **1999**, *64*, 382–387. (b) Metzger, A.; Anslyn, E. V. *Angew. Chem. Int. Ed.* **1998**, *37*, 649–652. (c) Corradini, R.; Dossena, A.; Galaverna, G.; Marchelli, R.; Panagia, A.; Sartor, G. *J. Org. Chem.* **1997**, *62*, 6283–6289. (d) Hamasaki, K.; Usui, S.; Ikeda, H.; Ikeda, T.; Ueno, A. *Supramol. Chem.* **1997**, *8*, 125–135.
- For representative examples of protein/macromolecule FRET based chemosensors, see: (a) Truong, K.; Sawano, A.; Mizuno, H.; Hama, H.; Tong, K. I.; Mal, T. K.; Miyawaki, A.; Ikura, M. *Nat. Struct. Biol.* **2001**, *8*, 1069–1073. (b) Miyawaki, A.; Llopis, J.; Heim, R.; McCaffery, J. M.; Adams, J. A.; Ikura, M.; Tsien, R. Y. *Nature* **1997**, *388*, 882. (c) Adams, S. R.; Harootyan, A. T.; Buechler, Y. J.; Taylor, S. S.; Tsien, R. Y. *Nature* **1991**, *349*, 694. Note that there are numerous FRET based assays for enzymatic activity, etc. that are of great value but do not meet the definition of a chemosensor (see Ref. 1h).
- For representative examples of small molecule FRET based chemosensors, see: (a) Arduini, M.; Felluga, F.; Mancin, F.; Rossi, P.; Tecilla, P.; Tonellato, U.; Valentinuzzi, N. *Chem. Commun.* **2003**, 1606–1607. (b) Schneider, S. E.; O’Neil, S. N.; Anslyn, E. V. *J. Am. Chem. Soc.* **2000**, *122*, 542–543. (c) Pearce, D. A.; Walkup, G. K.; Imperiali, B. *Biorg. Med. Chem. Lett.* **1998**, *8*, 1963–1968. (d) Godwin, H. A.; Berg, J. M. *J. Am. Chem. Soc.* **1996**, *118*, 6514–6515.
- For relevant reviews of Pd-catalyzed cross coupling reactions, see: (a) Miyaura, N.; Suzuki, A. *Chem. Rev.* **1995**, *95*, 2457–2483. (b) Negishi, E.-i. In *Metal-Catalyzed Cross Coupling Reactions*. Diederich, F. Stang, P. J., Eds.; Wiley: New York, 1998. Chapter 1. (c) Suzuki, A. *J. Organomet. Chem.* **1999**, *576*, 147–168.
- While not always required, we find the use of P(*t*-Bu)<sub>3</sub> typically provides the best yields for Suzuki coupling to 2,6-dichloropyridine derivatives. For early reports of the utility of this phosphine, see: (a) Old, D. W.; Wolfe, J. P.; Buchwald, S. L. *J. Am. Chem. Soc.* **1998**, *120*, 9722–9723. (b) Littke, A. F.; Fu, G. C. *Angew. Chem. Int. Ed.* **1997**, *37*, 3387–3388. For the more recent use of this phosphine as its HBF<sub>4</sub> salt, see: Netherton, M. R.; Fu, G. C. *Org. Lett.* **2001**, *3*, 4295–4298.



11. Berlman, I. *Handbook of Fluorescence Spectra of Aromatic Molecules*; Academic: New York, 1971.
12. For the empirical correlation between biaryl dihedral angle and nonradiative decay, see: (a) Fujii, T.; Suzuki, S.; Komatsu, S. *Chem. Phys. Lett.* **1978**, *57*, 175–178. (b) Fujii, T.; Suzuki, S.; Komatsu, S. *Bull. Chem. Soc. Jpn* **1982**, *55*, 2516–2520 and references therein.
13. For general treatments of nonradiative decay, see: (a) Freed, K. F. *Acc. Chem. Res.* **1978**, *11*, 74–80. (b) Klessinger, M.; Michl, J. *Excited States and Photochemistry of Organic Molecules*; VCH: New York, 1995; pp 252–260.
14. For select early derivations of the inverse exponential relationship between energy gap and relaxation rate, see: (a) Engleman, R.; Jortner, J. *Mol. Phys.* **1970**, *18*, 145. (b) Freed, K. F.; Jortner, J. *J. Chem. Phys.* **1970**, *52*, 6272–6291. (c) Siebrand, W. *J. Chem. Phys.* **1967**, *46*, 440–447. This can also be regarded as a restatement of Ermolaev's Rule: Ermolaev, V. L. *Sov. Phys. Usp.* **1963**, *80*, 333–358. *Usp. Fiz. Nauk* **1963**, *80*, 3–40. More quantitatively,  $k_{IC} \approx 10^{13} e^{-\alpha \Delta E} \approx 10^{13} f_v$  (where  $\alpha$  is a proportionality constant and  $f_v$  is the Franck–Condon factor for the transition in question). For energy gaps ( $\Delta E$ ) of  $\sim 50$  kcal/mol, Franck–Condon factors are  $\sim 10^5$ , leading to  $k_{IC} \sim (10^8 \text{ s}^{-1})$ . This is slow relative to typical rates of fluorescence emission and ISC, leading to the qualitative  $\Delta E \approx 50$ –60 kcal/mol cutoff for ignoring IC. See: Turro, N. *Modern Molecular Photochemistry*; University Science Books: Sausalito, CA, 1991; pp 180–185.
15. The assertion that the transition dipole should correlate with ground or excited state dipole moment is incorrect at the quantum mechanical level, and inconsistent with some observations (for instance, hexatriene, which has centrosymmetric ground and excited states and thus no net dipole in either state, still has a large  $\epsilon$ ). However, the classical model for oscillator strength equates the transition dipole to the polarizability of a molecule in an applied electric field, which qualitatively relates the ground and excited state dipole moments. As we are comparing molecules of very similar structure, we believe that our argument is at least qualitatively valid. See: Turro, N. *Modern Molecular Photochemistry*; University Science Books: Sausalito, CA, 1991; pp 81–90.
16. The UV spectra suggest that the Einstein coefficient for absorption, and thus the rate of radiative decay, are unchanged. See: Calvert, J. G.; Pitts, J. N. *Photochemistry*; Wiley: New York, 1996; pp 173–174.
17. (a) Rettig, W. *Angew. Chem. Int. Ed.* **1986**, *25*, 971–988. (b) Bhattacharyya, K.; Chowdhury, M. *Chem. Rev.* **1993**, *93*, 507–535.
18. For recent work on the TICT states of simple pyridine derivatives, see: Dobkowski, J.; Wojcik, J.; Kozminski, W.; Kolos, R.; Waluk, J.; Michl, J. *J. Am. Chem. Soc.* **2002**, *124*, 2406–2407 and references therein.
19. While *m*-alkoxy groups are generally considered electron withdrawing due to  $\sigma$  polarization, this generalization is based on ground state phenomena such as electrophilic aromatic substitution. The fact that the excited states are dominantly  $\pi^*$  in nature apparently leads to the *m*-alkoxy groups being moderately electron donating.
20. Lakowicz, J. R. *Principles of Fluorescence Spectroscopy*, 2nd ed.; Kluwer Academic: New York, 1999.
21. Pangborn, A. B.; Giardello, M. A.; Grubbs, R. H.; Rosen, R. K.; Timmers, F. J. *Organometallics* **1996**, *15*, 1518–1520.
22. Li, H.; Jiang, X.; Ye, Y. H.; Fan, C.; Romoff, T.; Goodman, M. *Org. Lett.* **1999**, *1*, 91–93.

# Hexaphyrin(1.0.1.0.0.0). A new colorimetric actinide sensor

Jonathan L. Sessler,<sup>a,\*</sup> Patricia J. Melfi,<sup>a</sup> Daniel Seidel,<sup>a,†</sup> Anne E. V. Gorden,<sup>a,‡</sup> Doris K. Ford,<sup>b</sup> Philip D. Palmer<sup>b</sup> and C. Drew Tait<sup>b</sup>

<sup>a</sup>Department of Chemistry and Biochemistry, Institute for Cellular and Molecular Biology, 1 University Station A5300, The University of Texas at Austin, Austin, TX 78712-0165, USA

<sup>b</sup>C—Chemistry and NMT—Nuclear Materials Technology Divisions, Los Alamos National Laboratory, Los Alamos, NM 87545, USA

Received 25 March 2004; revised 23 July 2004; accepted 19 August 2004

Available online 17 September 2004

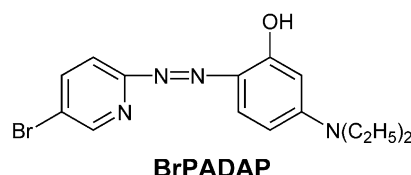
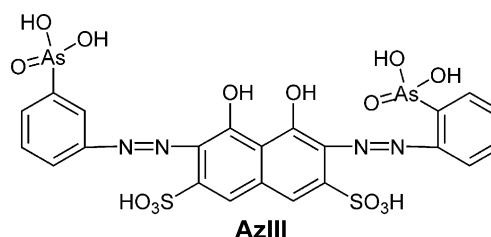
**Abstract**—Hexaphyrin(1.0.1.0.0.0) (isoamethyrin) undergoes a significant color change in the presence of  $\text{UO}_2^{2+}$ ,  $\text{PuO}_2^{2+}$ , and  $\text{NpO}_2^{2+}$ . The complexation of the first of these dioxo actinide cations was studied in semi-quantitative fashion in 1:1 MeOH– $\text{CH}_2\text{Cl}_2$ . Under these conditions, the detection limit for  $\text{UO}_2^{2+}$  was found to be ca. 5.8 ppm by naked eye monitoring and <28 ppb by UV–vis spectroscopy. Isoamethyrin does not undergo a color change in the presence of most transition metals or when exposed to Gd(III). Isoamethyrin thus constitutes an attractive alternative to 2,2'-(1,8-dihydroxy-3,6-disulfonaphthylene-2,7-bisazo)-bisbenzenearsonic acid (AzIII) and 2-(5-bromo-2-pyridylazo)-5-(diethylamino)phenol (BrPADAP), systems currently used as actinide cation sensors.

© 2004 Elsevier Ltd. All rights reserved.

## 1. Introduction

Nuclear weapon production and the use of nuclear electricity have created a high amount of enriched uranium and plutonium worldwide. Weapons programs in the United States and Russia for instance, have led to the production of nearly 200 metric tons of purified plutonium.<sup>1</sup> Likewise, nuclear energy production, accounting for 25–30% of the world's electrical power supply, has generated something in the order of 7000 metric tons of plutonium and uranium, with a large portion of it as spent reactor fuel.<sup>1</sup> In addition to any concerns associated with stockpiling and transporting this radioactive material, the prospects for nuclear weapons smuggling between countries, arms proliferation and the threat of a 'dirty bomb' has made the possibility of uranium or plutonium being released into the environment a frightening possibility. In the event of a spill or an accident, a fast, easy, and accurate method of uranium and plutonium detection would be beneficial. At present, detection of plutonium and uranium is mainly effected via  $\alpha$ -scintillation counting methods. However, these techniques rely on instrumentation, such as Geiger counters, that may not be suitable in certain situations. Hence, a colorimetric sensor

system based on chemical principles is expected to be particularly useful. It could provide an easily deployable alternative to more conventional scintillation counting based approaches, provided it showed little in the way of false positives due to other species. Currently, such a sensor does not exist, although two generalized metal sensing systems, 2,2'-(1,8-dihydroxy-3,6-disulfonaphthylene-2,7-bisazo)-bisbenzenearsonic acid (AzIII)<sup>2,3</sup> and 2-(5-bromo-2-pyridylazo)-5-(diethylamino)phenol (BrPADAP)<sup>4,5</sup> have been used to sense uranyl and plutonyl. While both dyes, AzIII and BrPADAP, display relatively low limits of  $\text{UO}_2^{2+}$  detection (46 ppb for AzIII<sup>2</sup> and 200 ppb for BrPADAP<sup>4</sup> in aqueous media and ethanol, respectively, at a standard >3:1 UV–vis spectroscopic signal-to-noise level), both suffer from drawbacks that do not make them ideal candidates for actinide detection.



**Keywords:** Expanded porphyrins; Isoamethyrin; Uranium; Colorimetric sensor.

\* Corresponding author. Tel.: +1-512-471-5009; fax: +1-512-471-7550; e-mail: [ssessler@mail.utexas.edu](mailto:ssessler@mail.utexas.edu)

<sup>†</sup> Present address: Department of Chemistry, University of California, Berkeley, CA 94720, USA.

<sup>‡</sup> Present address: Department of Chemistry and Chemical Biology, Harvard University, Cambridge, MA 02138, USA.

For instance, AzIII has a low selectivity for the actinides and displays similar molar absorptivities for Th(IV) and the trivalent lanthanides. In fact, it has a lower detection limit for the lanthanides (20 ppb with Gd(III)) than for  $\text{UO}_2^{2+}$ . This is problematic since the lighter lanthanides are produced in fission events.<sup>6</sup> Thus, to avoid detection of the lanthanides rather than actinides, under simple ‘field use’ conditions, a pre-purification step to remove the lanthanides is necessary.<sup>2</sup> BrPADAP also complexes Th(IV) strongly and displays reduced detection accuracy for uranium and plutonium in the presence of Th(IV).<sup>4</sup> Also, this dye is not water-soluble and gives rise to only a very slight color change upon metal complexation. Clearly, there exists a need for better actinide-sensing dyes. Such improvements could come from an increased understanding of the chemistry of the actinides.

As a result of 50 years of study, a significant amount has been discovered about the chemistry of the actinides, even though much of the chemistry remains far from understood. Upon exposure to air, for instance, U commonly forms the (VI) dioxo cation (uranyl,  $\text{UO}_2^{2+}$ ), while Pu prefers the IV, V or VI oxidation state, with the latter being mobile in water.<sup>7</sup> Thus, an efficient sensor must be able to ‘sense’ these dioxo, or ‘yl’ cations. It is known that the actinides, hard Lewis acids, interact strongly with hard donor atoms such as O or F, but interact in a more covalent fashion with softer donor atoms such as N, S and Cl.<sup>8,9</sup> By exploiting the weaker interaction produced with nitrogen, we have been able to characterize a number of expanded porphyrin-actinide complexes.<sup>10–12</sup> Some of these expanded porphyrin complexes displayed dramatic color changes upon complexation of the metal, with hexaphyrin(1.0.1.0.0.0) (‘isoamethyrin’; **1**) producing the most dramatic change.

This impressive color change came as no surprise to us as porphyrins and expanded porphyrins are known for the range of colors their complexes produce. Indeed, since the early 1990’s metalloporphyrins have been employed as part of arrays designed to act as ‘electronic noses’ and ‘electronic tongues’. In the context of this work, they have demonstrated their utility in the detection of numerous analytes.<sup>13,14</sup> Most notably, Rakow and Suslick have used metalloporphyrin dyes to detect vapors ranging from alcohols to phosphates to halocarbons.<sup>13</sup> Also, Di Natalie and co-workers have demonstrated the utility of metalloporphyrins in analytical applications ranging from food freshness<sup>14a,b</sup> to wine.<sup>14c</sup> However, metal cations have remained relatively unexplored as targeted analytes in the porphyrin-based sensor field. This is especially true for the actinides.

Figure 1 shows the color change observed when uranium is added to isoamethyrin. In this particular system, it was observed that the molar absorptivity increases roughly by a factor of five upon addition of this metal cation.<sup>11</sup> This has led us to consider that this species could serve as an excellent actinide sensor. In this paper, we report the results of studies that provide support for this hypothesis. In particular, we show that isoamethyrin allows for the so-called naked eye detection of the uranyl, neptunyl, and plutonyl cations under appropriately chosen solution phase conditions. We also report the result of more quantitative



**Figure 1.** Color change seen upon addition of uranyl acetate to solutions of isoamethyrin. Left: acid salt of isoamethyrin; Middle: after addition of 10 equiv  $\text{Et}_3\text{N}$ ; Right:  $\text{UO}_2^{2+}$  complex. Both solutions ( $\text{UO}_2^{2+}$  and isoamethyrin) were made up using a 3:4 (v/v) mixture of methanol and dichloromethane.

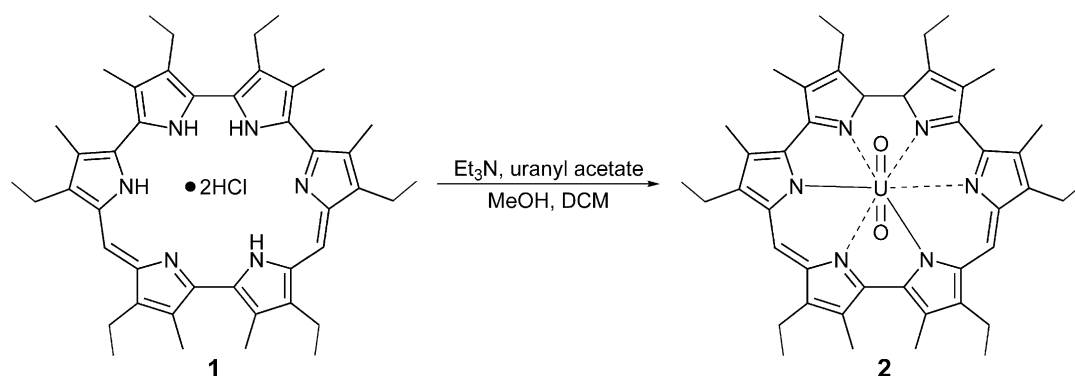
studies carried out in 95:5  $\text{MeOH-CH}_2\text{Cl}_2$  (v/v) in the presence of the uranyl cation that have allowed the dynamic range of this prospective sensor system to be assessed.

## 2. Results and discussion

### 2.1. Qualitative analysis

Previously, we have characterized the interactions of isoamethyrin with uranyl ( $\text{UO}_2^{2+}$ ), neptunyl ( $\text{NpO}_2^{2+}$ ) and plutonyl ( $\text{PuO}_2^{2+}$ ) and reported the solid state crystal structures of the uranyl and neptunyl complexes as proof of complex formation.<sup>11,12</sup> It was also reported that the acid salt of isoamethyrin exhibits three Soret-like bands 384 nm ( $\epsilon = 24,000 \text{ dm}^3 \text{ mol}^{-1} \text{ cm}^{-1}$ ), 497 nm ( $\epsilon = 59,000 \text{ dm}^3 \text{ mol}^{-1} \text{ cm}^{-1}$ ) and 597 nm ( $\epsilon = 25,000 \text{ dm}^3 \text{ mol}^{-1} \text{ cm}^{-1}$ ). Upon complexation with uranium, the macrocycle undergoes spontaneous oxidation. This results in a change in the overall electronic structure from antiaromatic to aromatic (Scheme 1). This process, which is believed to be air based, causes a significant change in the UV–vis spectra. In particular, one sharp, Soret-like transition at 530 nm ( $\epsilon = 330,000 \text{ dm}^3 \text{ mol}^{-1} \text{ cm}^{-1}$ ) and two smaller Q-like bands at 791 nm ( $\epsilon = 56,000 \text{ dm}^3 \text{ mol}^{-1} \text{ cm}^{-1}$ ) and 832 nm ( $\epsilon = 81,000 \text{ dm}^3 \text{ mol}^{-1} \text{ cm}^{-1}$ ) are seen for the uranyl complex (**2**). The intensity (molar absorptivity) of the single Soret-like band in the uranium complex increases by a factor of 5 when compared with the acid salt of isoamethyrin. The free base form of isoamethyrin, the species that coordinates uranyl cation, has been found to have a molar absorptivity of  $50,000 \text{ dm}^3 \text{ mol}^{-1} \text{ cm}^{-1}$  (472 nm), which is more than six times lower than that of the uranyl complex. This sharp difference has engendered the present study, leading us, in particular, to suggest that it could be used to detect actinide complexation, both by UV–vis spectroscopy and, more importantly, the naked eye.

As might be expected, similar color changes are observed when the Np(VI) or Pu(VI) cations are added to 1:1 (v/v)  $\text{MeOH-CH}_2\text{Cl}_2$  solutions of isoamethyrin, as shown in Figure 2. Unfortunately, as a result of limitations associated with highly radioactive species, we were not able to obtain molar absorptivities of these complexes. On the other hand,



**Scheme 1.** Addition of uranyl acetate to hexaphyrin(1.0.1.0.0.0) and subsequent oxidation of the ring.

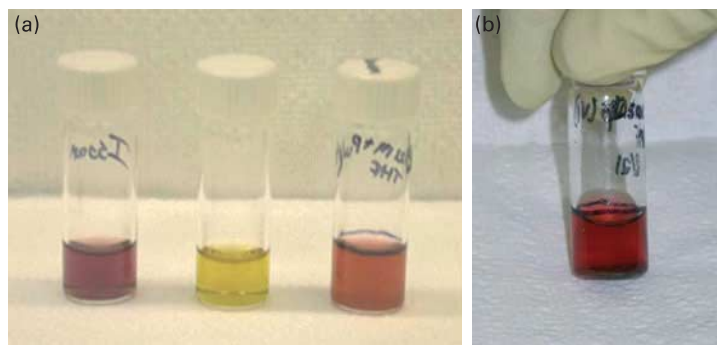


**Figure 2.** Color change seen upon addition of  $\text{NpO}_2^{2+}$  and  $\text{PuO}_2^{2+}$  to solutions of isoamethyrin. Far left: acid salt of isoamethyrin; 2nd from left: solution after addition of 10 equiv  $\text{Et}_3\text{N}$  3rd from left: after the further addition of plutonyl chloride; Far right: after addition of neptunyl chloride to a solution of isoamethyrin containing  $\text{Et}_3\text{N}$ . All solutions consist of 1:1 (v/v) methanol–dichloromethane.

it was noted that complexation was extremely facile. In particular, while the  $\text{U(VI)}$  complex requires about 24 h to show a significant color change, the addition of  $\text{Pu(VI)}$  or  $\text{Np(VI)}$  to a solution of isoamethyrin and  $\text{Et}_3\text{N}$  induces an instant color change, producing essentially the same rose color seen in the case of the uranium–isoamethyrin complex.

For storage and stability, the plutonyl and neptunyl species were stored as the chloride salts in 1 M  $\text{HClO}_4$ . The plutonyl salt was used in the form of a 0.2 M solution while the neptunyl salt was available as a 0.3 M solution. It is believed that the isoamethyrin system is pH sensitive, coordinating cations effectively only at higher pH. Since we were forced to add plutonyl and neptunyl salts at a pH of 0, more than 10 equiv of  $\text{Et}_3\text{N}$  were added to these solutions. Despite the lower pH, both the neptunyl and plutonyl complexes form immediately upon addition of the metal, further supporting the assertion that isoamethyrin may serve as an actinide sensor.

The increased rate of colorimetric response (and presumably complexation) has been attributed to the fact that neptunyl and plutonyl cations are stable in the (V) oxidation state, while the (VI) state is preferred in the case of uranyl.<sup>15</sup> It is believed that upon addition of the metal, the  $\text{Np(VI)}$  and  $\text{Pu(VI)}$  'yl' cations are readily reduced to the corresponding (V) oxidation state, thus facilitating oxidation of the isoamethyrin ligand, either in a stoichiometric or catalytic sense (i.e. by shuttling between the (VI) and (V) oxidation state). Consistent with this hypothesis is the finding that

although it is the  $\text{Np(V)}$  complex that is obtained regardless of the oxidation state of the metal before addition (V or VI)<sup>12</sup> the rates of metal complex formation differ. In the case of the uranyl, such a presumed metal cation redox enhanced insertion process is not possible and oxidation of the ring most likely occurs via direct air-based oxidation. This, it is proposed, results in a slower overall reaction time.

## 2.2. Quantitative analysis

### 2.2.1. Interactions of isoamethyrin with uranyl acetate.

In an attempt to understand isoamethyrin better and to compare it to previously reported actinide sensors, we set out to determine an effective 'dynamic range' associated with the formation of its actinide complexes. Due to the limitations inherent when working with radioactive material, such as neptunyl and plutonyl, the associated quantitative studies (see below) were made using depleted uranium acetate, which can be easily studied on the benchtop.

Prior to analyzing in detail the uranyl–isoamethyrin complex and its formation, the stability of the macrocycle itself was investigated. It has been shown that the uranyl complex may exist for many weeks in solution without decomposition,<sup>11</sup> and when the macrocycle exists as the acid salt (containing two HCl molecules in its core) a similar stability has been observed. However, as inspection of Figure 3 reveals, this is not the case for the free base form of isoamethyrin. In fact, slow decomposition occurs over 5 days as judged from a bleaching of the UV–vis

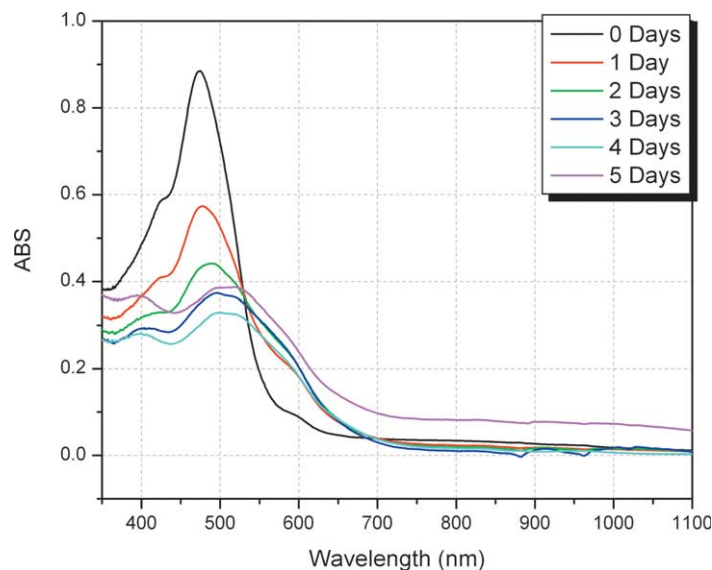


**Figure 3.** Changes in the UV–vis spectral features of a solution of free-base isoamethyrin ( $2.0 \times 10^{-5}$  M) that occur over time. The isoamethyrin solution in question was made up in methanol–dichloromethane 95:5 (v/v) and contained 4 equiv of  $\text{Et}_3\text{N}$ . It was stored in the dark when not being subject to UV–vis spectral analysis.

spectroscopic features. Unfortunately, since it is the free base form of isoamethyrin that complexes the uranyl cation, any metal insertion reaction requiring more than 1 day to complete has to be considered against a ‘background’ of possible macrocycle decomposition. Evidence for such a competition may be seen by comparing Figures 4 and 5.

As can be seen from Figure 4, the addition of 0.5 equiv of uranyl acetate dihydrate to a solution of **1** leads to formation of the uranyl-complexed isoamethyrin, as is evidenced by the slight red shift in the Soret band from 473 to 525 nm, as well as the growth of a Q-like band at 830 nm. However,

these spectral changes are also accompanied by decomposition, as is evidenced by the bleaching of the Soret band. The extinction coefficient of the uranyl–isoamethyrin complex is 6 times greater than that of the free base aromatic form of isoamethyrin ( $\epsilon = 330,000$  vs.  $52,000 \text{ dm}^3 \text{ mol}^{-1} \text{ cm}^{-1}$ ). For this reason, a growth in the Soret band intensity is expected to accompany complexation. This is in fact observed in the presence of 3 (as opposed to 0.5) equiv of uranyl acetate (Fig. 5). In this case, not only is the intensity of the Soret band increased, a new Q-like band is seen to grow in that is nearly three times as large as that seen in the presence of 0.5 equiv ( $\epsilon = 18,000$  vs.

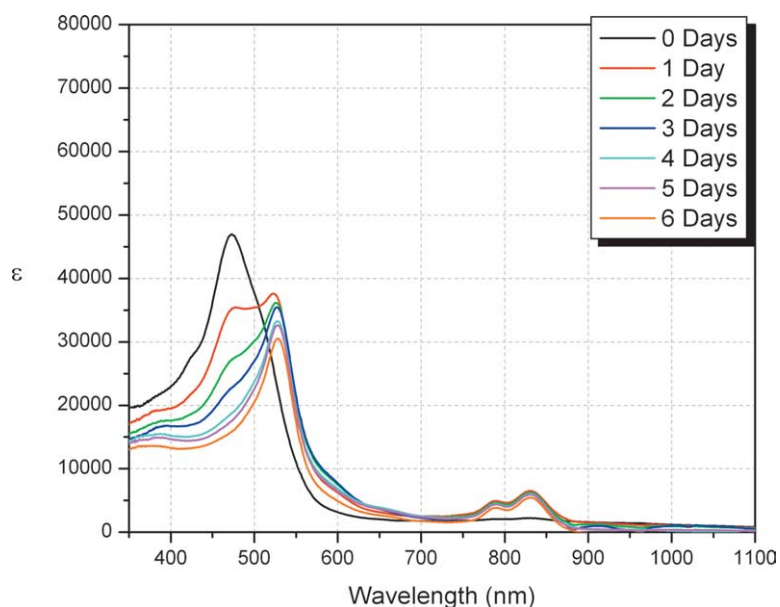


**Figure 4.** Changes in the UV–vis spectral features of a solution of isoamethyrin containing 0.5 equiv uranyl acetate observed over the course of six days. The isoamethyrin solution in question was made up in methanol–dichloromethane 95:5 (v/v) and contained 4 equiv of  $\text{Et}_3\text{N}$ . It was stored in the dark when not being subject to UV–vis spectral analysis. The isoamethyrin concentration is  $2.0 \times 10^{-5}$  M and the uranyl concentration is  $1.0 \times 10^{-5}$  M.



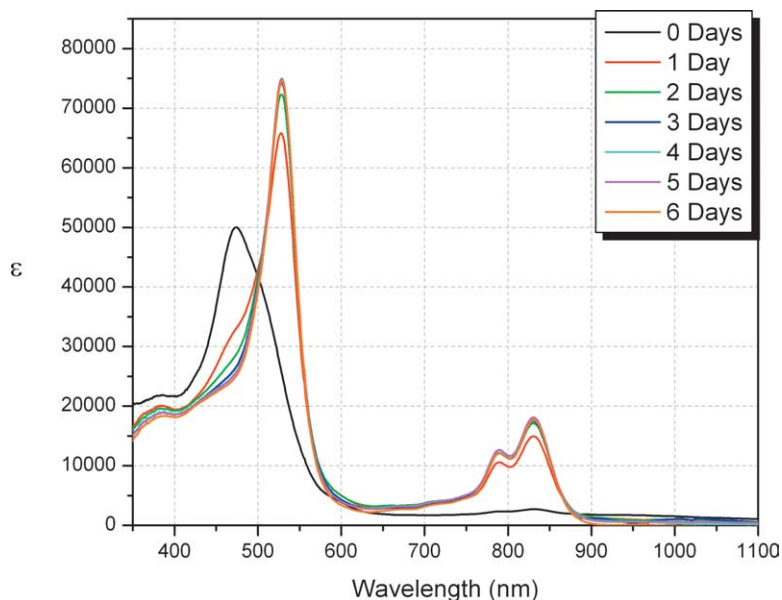


**Figure 5.** Changes in the UV-vis spectral features of a solution of isoamethyrin containing 3 equiv of uranyl acetate as observed over the course of six days. The isoamethyrin solution in question was made up in methanol-dichloromethane 95:5 (v/v) and contained 4 equiv of  $\text{Et}_3\text{N}$ . It was stored in the dark when not being subject to UV-vis spectral analysis. The isoamethyrin concentration is  $2.0 \times 10^{-5}$  M and the uranyl concentration is  $6.0 \times 10^{-5}$  M. The molar absorptivity ( $\epsilon$ ) is in units of  $\text{dm}^3 \text{mol}^{-1} \text{cm}^{-1}$ .

$6500 \text{ dm}^3 \text{mol}^{-1} \text{cm}^{-1}$ ). This confirms, as expected, that more of the uranyl-isoamethyrin complex is formed in the presence of an increased uranyl cation concentration.

**2.2.2. Dynamic range of uranyl detection.** In order to identify the dynamic range for uranium detection by naked-eye-detectable visual response, titrations of the uranyl cation into an isoamethyrin solution were carried out; the results are shown in Figure 6. Both the Soret and Q-like bands increase with increasing concentrations of uranium. For this experiment, an isoamethyrin concentration of

$1.69 \times 10^{-5}$  M was chosen so as to produce a solution with an absorptivity (1 cm cuvette) that was optimal for UV-vis spectroscopic study. As can be seen from an inspection of Figure 6, significant changes were seen in both the Soret and Q-band regions. While the first of these bands is more intense and hence more sensitive to uranium concentration, it does not allow for a unique determination since it appears at the same wavelength in the case of both the complexed and uncomplexed forms, albeit at different molar absorptivities. The Q-like band, however, only appears when uranyl is present, and, based on independent

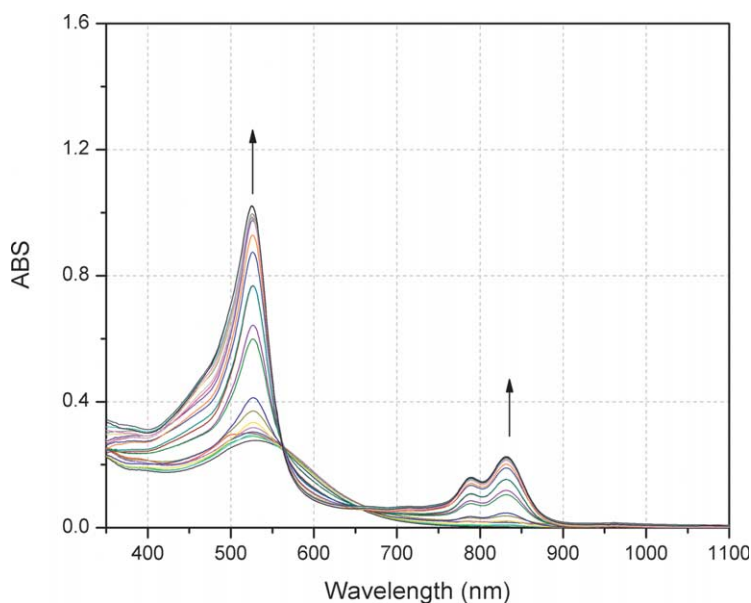


**Figure 6.** Growth of the Soret and Q-like bands with increasing equivalents of uranyl acetate. The isoamethyrin solution in question was made up in methanol-dichloromethane 95:5 (v/v) and contained 4 equiv of  $\text{Et}_3\text{N}$ . Twenty-four individual samples were made up and stored in the dark for 1 week before being subject to UV-vis spectral analysis. The isoamethyrin concentration remained constant at  $1.686 \times 10^{-5}$  M. Over the course of this 'titration', the uranyl concentration was increased from 0 to 17 equiv, with the specific concentrations being: 0 M,  $8.71 \times 10^{-7}$ ,  $1.74 \times 10^{-6}$ ,  $2.61 \times 10^{-6}$ ,  $4.34 \times 10^{-6}$ ,  $6.06 \times 10^{-6}$ ,  $8.64 \times 10^{-6}$ ,  $1.12 \times 10^{-5}$ ,  $1.63 \times 10^{-5}$ ,  $2.13 \times 10^{-5}$ ,  $2.75 \times 10^{-5}$ ,  $3.36 \times 10^{-5}$ ,  $4.15 \times 10^{-5}$ ,  $4.94 \times 10^{-5}$ ,  $6.09 \times 10^{-5}$ ,  $7.20 \times 10^{-5}$ ,  $8.64 \times 10^{-5}$ ,  $1.00 \times 10^{-4}$ ,  $1.20 \times 10^{-4}$ ,  $1.45 \times 10^{-4}$ ,  $1.69 \times 10^{-4}$ ,  $1.96 \times 10^{-4}$ ,  $2.26 \times 10^{-4}$ ,  $2.58 \times 10^{-4}$  and  $2.91 \times 10^{-4}$  M.





**Figure 7.** Color change observed in the presence of varying concentrations of uranyl acetate. The solutions in question have an isoamethyrin concentration of  $1.686 \times 10^{-5}$  M and contain 4 equiv of  $\text{Et}_3\text{N}$ ; they were made up in methanol–dichloromethane 95:5 (v/v). The vials were stored in the dark for 9 days before the photo. The uranyl cation concentrations in the vials shown, labeled 4, 5, 6, 7, 8, 9, 10, 11, 12, 13, and 14, were  $4.34 \times 10^{-6}$ ,  $6.06 \times 10^{-6}$ ,  $8.64 \times 10^{-6}$ ,  $1.12 \times 10^{-5}$ ,  $1.63 \times 10^{-5}$ ,  $2.13 \times 10^{-5}$ ,  $2.75 \times 10^{-5}$ ,  $3.36 \times 10^{-5}$ ,  $4.16 \times 10^{-5}$ ,  $4.94 \times 10^{-5}$  and  $6.09 \times 10^{-5}$ , respectively.

synthesis and characterization,<sup>11</sup> is believed to indicate complexation of uranyl by the oxidized form of isoamethyrin. An easily discernible change in the Q-like band occurs after the addition of 0.1 equiv of uranyl have been added, or at a concentration of  $1.74 \times 10^{-6}$  M  $\text{UO}_2^{2+}$ . At a uranyl concentration of  $7.2 \times 10^{-5}$  M uranyl, or after roughly 4.3 equiv have been added, the spectral changes are maximal. Adding additional uranyl acetate does not increase the height of the Q-like band, leading us to suggest that under these conditions the equilibrium between the complexed and uncomplexed species now fully favors the uranyl complex. Therefore, the dynamic range for complexation of uranium can be set at 0.1–4.3 equiv uranyl. For isoamethyrin at a concentration of  $1.69 \times 10^{-5}$  M, this translates to a dynamic range of  $1.74 \times 10^{-6}$  M through  $7.2 \times 10^{-5}$  M uranyl, or a detection limit of 2.3 ppm, as judged by UV–vis spectroscopic analysis at this wavelength. If the Soret band ( $\epsilon = 330,000$ ) is used instead of the Q-like band, and a  $> 10$ :1 signal-to-noise detection standard is applied, an isoamethyrin concentration as low as  $1.02 \times 10^{-7}$  M produces a response in the presence of 1 equiv of  $\text{UO}_2^{2+}$ . This translates to a UV–vis spectroscopic detection of 27.5 ppb. However, if the current, more ‘favorable’  $> 3$ :1 signal-to-noise detection standard used by others<sup>2</sup> is applied, a detection limit approaching 9 ppb could be expected.

As would be anticipated, detection by the naked eye is less sensitive, and a color change, indicating the formation of the complexed species, is not seen until roughly 1.3 equiv of uranium have been added, or for an isoamethyrin concentration of  $1.686 \times 10^{-5}$  M in methanol–dichloromethane 95:5 (v/v) containing 4 equiv of  $\text{Et}_3\text{N}$ ,  $2.13 \times 10^{-5}$  M in  $\text{UO}_2^{2+}$ , yielding an uranyl detection limit of roughly 5.8 ppm. This color change can be seen in Figure 7, between vials 8 and 9.

To test further the limits of detection, a solution of isoamethyrin with an absorbance of 0.1 (1 cm cuvette) was prepared. This solution, at a concentration of  $5.012 \times 10^{-6}$  M, is a barely visible peach color. With the addition of 1.4 equiv of uranyl acetate ( $6.785 \times 10^{-6}$  M or 1.8 ppm) in the same solvent mixture, a pink hue first becomes evident within a day and then more so over time, as shown in Figure 8a.

Figure 8b shows the growth in the Soret band observed over time (indicating complex formation). While it would be difficult to detect uranium with the naked eye at any lower isoamethyrin concentrations, the use of a standard UV–vis spectrophotometer as above is expected to permit much lower concentrations to be detected. In any event, as would be expected, more dilute samples were found to slow the

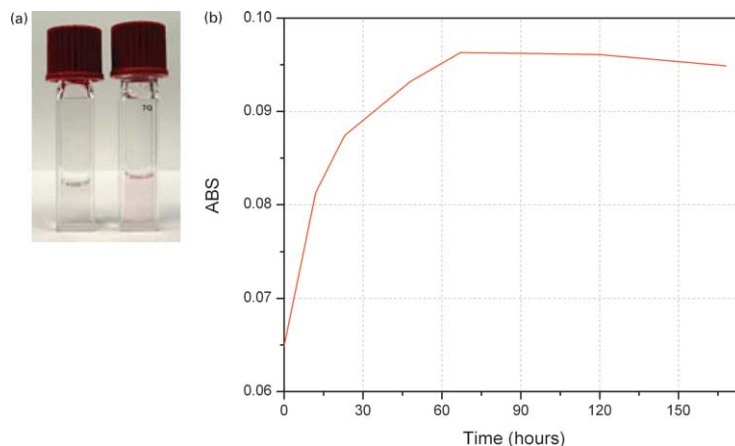


**Figure 8.** (a) Picture of the color change observed upon the addition of uranyl cation to isoamethyrin. The vial on left shows the free-base form of isoamethyrin and the vial on the right shows an equivalent solution after the addition of 1.4 equiv of uranyl acetate. The solutions were stored in the dark for 6 days prior to recording the photographs. The isoamethyrin concentration is  $5.012 \times 10^{-6}$  M in both cases and the uranyl concentration is  $6.785 \times 10^{-6}$  M. (b) Increase in absorbance at 524 nm observed with time after the addition of 1.4 equiv uranyl acetate. The isoamethyrin solution in question was made up in methanol–dichloromethane 95:5 (v/v) and contained 4 equiv of  $\text{Et}_3\text{N}$ . It was stored in the dark when not being subject to UV–vis spectral analysis.

**Table 1.** Reactivity of isoamethyrin with metal salts

Metal	Equivalents	Color	$\lambda_{\max}$ <sup>a</sup>	ESI-MS
UO <sub>2</sub> <sup>2+</sup>	2	Pink	530, 791, 832	Yes
Cu(II)	2	Pink	494, 525, 800, 880	Possible <sup>b</sup>
Gd(III)	2	Orange	497, 719	No
Zn(II)	2	Orange	497, 719	No
Cd(II)	2	Orange	490, 836 (br)	Yes
Mn(II)	2	Brown/orange	500	Yes
Ni(II)	2	Orange	493, 749 (br), 979 (br)	Slight
Ce(IV)	10	Purple	527, 438	No
Cr(VI)	20	Orange	356	Possible <sup>b</sup>
Fe(III)	10	Orange	433	No
Mg(II)	2	Purple/brown	394, 488, 956	No
La(III)	2	Red/brown	485, 956	No
Sm(III)	2	Purple/pink	493	No
Pb(IV)	2	Red	498, 811 (br)	Yes

<sup>a</sup> All UV–vis spectra were recorded in 95:5 (v/v) MeOH–CH<sub>2</sub>Cl<sub>2</sub>.

<sup>b</sup> In the case of Cu(II) and Cr(VI), a high degree of fragmentation accompanied the peak assumed to represent an isoamethyrin complex containing one copper or chromium atom.

complexation process. As can be inferred from an inspection of Figure 8b, complexation appears complete after roughly 65 h. However, at higher concentrations of isoamethyrin, regardless of the uranyl concentration, formation of the uranyl–isoamethyrin complex appears complete after only 24 h, as judged by the absence of further time-dependent spectral changes.

**2.2.3. Isoamethyrin complexation with other metals.** In order to assess more fully the ability of isoamethyrin to serve as an actinide sensor, the spectroscopic changes (if any) produced by other cations were briefly investigated. Complexation was determined by UV–vis spectroscopic and ESI-mass spectrometric analysis. A range of transition metals was chosen. In addition the lanthanide species Ce(IV), Sm(III), La(III) and Gd(III), were tested, since these cations are known to compete with other actinide sensors.<sup>2–5</sup> The observed color changes,  $\lambda_{\max}$  values, and ESI results are presented in Table 1. As a quick assessment, a large excess of the metal was added to solution of isoamethyrin. The metal cations that induced a color change or produced any sign of complexation as judged from ESI-MS analysis were taken and subject to a more precise study wherein 2 equiv of the cation in question were added to a similar isoamethyrin solution.

Figure 9 displays the color changes observed upon the addition of each metal cation. As can be seen from inspection of this figure, the only species that might be

construed as giving a false positive is Cu(II). While the color produced upon the addition of 2 equiv of uranyl acetate and Cu(II) acetate is very similar, the uranyl species displays more of a pink color and the copper appears more purple. According to UV–vis spectroscopic analysis, a Q-like band is seen after addition of not only the copper acetate but also cadmium nitrate, nickel acetate and lead tetraacetate to solutions of isoamethyrin, (as well as, of course, uranyl acetate). However, the Q-like band for the presumed Cu(II), Cd(II), Ni(II) and Pb(IV) complexes is very different from that of the uranyl–isoamethyrin complex and could represent not only complex formation, but also production of oxidized, protonated species as the result of, e.g., metal-based solvolysis. In any case, the spectra produced by the addition of these metal cations are distinct from those seen in the case of the uranyl cation. For instance, the spectra produced upon addition of Cd(II) is characterized by a broad peak between 700 and 900 nm, while the spectra produced with Cu(II) contains a somewhat shifted Q-like band as compared to the spectra of the uranyl complex ( $\lambda_{\max}$  = 800 and 880 nm). In addition, while 525 nm, the Soret band seen upon addition of Cu(II) ( $\lambda_{\max}$  = 525 nm) appears to overlap the Soret band of U(VI) spectra at 530 nm, it possesses only half the height as the uranyl complex. In fact, the only spectra with Soret bands similar to that of the uranyl complex are those generated upon the addition of Gd(III) and Zn(II). However, with only a minor peak at 719 nm, neither of these spectra displays a Q-like band, thus making them easily distinguishable from



**Figure 9.** Colors of solutions of isoamethyrin ( $1.02 \times 10^{-4}$  M) containing 4 equiv of Et<sub>3</sub>N in a MeOH–CH<sub>2</sub>Cl<sub>2</sub> (95:5 v/v) solution. Far left: the acid salt of isoamethyrin and then from left to right after the addition of 2 equiv of, respectively, uranyl(VI) acetate, copper(II) nitrate, gadolinium(III) acetate, zinc(II) acetate, nickel(II) acetate, lead(IV) tetraacetate, manganese(II) acetylacacetate, and cadmium(II) nitrate. The vial on the far right contains the free base form of isoamethyrin.

those recorded for the uranyl complex. These preliminary results show that isoamethyryn can act as a selective colorimetric sensor for the actinides as judged both from the color change produced upon addition of the metal cations and the UV–vis spectra of the complexes that are presumably formed. A more detailed analysis of these latter species is currently ongoing.

### 3. Conclusions

Nuclear weapons production and the use of nuclear powered electricity has increased the possibility of radioactive elements, such as uranium or plutonium, being released into the environment. For this reason, a simple, fast and accurate means of identifying these elements is important. The current ‘dyes’ found to change color in the presence of uranium or plutonium suffer from a number of drawbacks including low selectivity for the actinides. However, as reported here, the expanded porphyrin, isoamethyryn (hexaphyryn(1.0.1.0.0.0)), could provide an attractive alternative. It undergoes a readily discernable color change in the presence of the uranyl, neptunyl and plutonyl cations.<sup>11,12</sup> Semi-quantitative studies carried out with uranyl–acetate in a 1:1 mixture of methanol and dichloromethane (v/v) indicate a detection limit of less than 28 ppb as judged from UV–vis spectroscopic analysis of the Soret-like band, and ca. 5.8 ppm using one’s naked eye. These detection limits are competitive with those of AzIII and BrPADAP, dyes currently used as colorimetric sensors for the actinides (detection limits of 46 and 200 ppb, respectively). Further, and as importantly, preliminary results indicate that hexaphyryn(1.0.1.0.0.0) is not as sensitive to other metals that may be present in actinide-rich samples. This latter attribute means that the risk of a ‘false positive’ would be potentially reduced were the present expanded porphyrin used to analyze sample under field use conditions. Further development of isoamethyryn and related species as potential actinide sensors is thus actively underway.

### 4. Experimental

#### 4.1. General data

All chemicals (obtained from Aldrich Chemical Co. and Strem Chemical) and solvents were of reagent grade quality and used without further purification unless otherwise stated. Neptunyl chloride and plutonyl chloride solutions were prepared as previously reported.<sup>16</sup> Isoamethyryn was synthesized as previously reported.<sup>11</sup> Spectroscopic grade methanol and dichloromethane were used for the uranyl titrations and used without further purification. Electronic absorption spectra were recorded on a Beckman DU-7 spectrophotometer, using 1 cm quartz cells. Mass spectra were measured with either a Finnigan-MAT 4023, Bell and Howell 21-491 or VG Analytical ZAB E/SE instrument.

#### 4.2. UV–vis titration experiments

UV–vis titrations analogous to those of the present study have been previously described by the Sessler group.<sup>17</sup> While the general procedures as reported were followed,

rather than recording the spectrum of the same solution before and after uranyl addition, identical solutions containing both host and guest were prepared one week prior to recording the spectra. This procedure was required due to the slow coordination of the uranyl with isoamethyryn. Thus, for the study shown in Figure 6, 24 vials containing 1.5 mL of an isoamethyryn solution in 95:5 (v/v) methanol–dichloromethane solution with 4 equiv of Et<sub>3</sub>N were prepared. Concentrations of uranyl acetate ranging from  $8.9 \times 10^{-7}$  M to  $2.9 \times 10^{-4}$  M were added to the above solution, while keeping the isoamethyryn concentration constant at  $1.68 \times 10^{-5}$  M. The vials were sealed and stored in the dark for 1 week in order to allow for complete complexation. At this juncture, the UV–vis spectra of all vials were recorded.

#### 4.3. Metalation of isoamethyryn

Initial ‘quick and dirty’ experiments were performed with a number of different metal salts in high excess in order to assess the ability of isoamethyryn to coordinate the metal. Those found worthy of further investigation were subject to more precise study. Two equivalent of the metal solution were added to a solution of isoamethyryn containing 4 equiv of Et<sub>3</sub>N in 95:5 dichloromethane–methanol (v/v) solution. The solutions were monitored by UV–vis spectroscopy until no further changes were observed. All metalations were found to be complete within 24 h. For the UV–vis spectra, 20  $\mu$ L of the presumed isoamethyryn–metal complex was added to 2.0 mL methanol to produce a final solution with an absorptivity suitable for study. ( $1.02 \times 10^{-5}$  M).

### Acknowledgements

This work was supported by the Department of Energy, Office of Basic Energy Sciences (grant DEFG03-01ER-15186 to J.L.S.). P.J.M. expresses her appreciation to the Seaborg Institute for Transactinium Science for a Summer Fellowship. The work carried out at Los Alamos National Laboratory was funded by the Department of Energy, Office of Basic Energy Sciences and the Defense Programs Education Office. Los Alamos National Laboratory is operated by the University of California under contract W-7405-ENG-36.

### References and notes

1. Draganic, G. R.; Draganic, Z. D.; Adloff, J.-P. *Radiation and Radioactivity on Earth and Beyond*; CRC: Boca Raton, FL, 1990.
2. Collins, G. E.; Lu, Q. *Anal. Chim. Acta* **2001**, *436*, 181–189.
3. Rohwer, H.; Rheeder, N.; Hosten, E. *Anal. Chim. Acta* **1997**, *341*, 263–268.
4. Suresh, A.; Patre, D. K.; Srinivasan, T. G.; Rao, P. R. V. *Spectrochim. Acta A* **2002**, *58*, 341–347.
5. Gray, H. N.; Jorgensen, B.; McClaugherty, D. L.; Kippenberger, A. *Ind. Eng. Chem. Res.* **2001**, *40*, 3540–3546.
6. Cotton, S. *Lanthanides and Actinides*; Oxford University Press: New York, 1991.

7. Runde, W. H. In *Los Alamos Science: Challenges in Plutonium Science*, 26, 2000; Vol. 2, p 26
8. Clark, D. L.; Hobart, D. E.; Neu, M. P. *Chem. Rev.* **1995**, 95, 25–48.
9. Choppin, G. R. *Radiochim. Acta* **1983**, 45–53.
10. Sessler, J. L.; Vivian, A. E.; Seidel, D.; Burrell, A. K.; Hoehner, M.; Mody, T. D.; Gebauer, A.; Weghorn, S. J.; Lynch, V. *Cord. Chem. Rev.* **2000**, 216–217, 411–434 and references therein.
11. Sessler, J. L.; Seidel, D.; Vivian, A. E.; Lynch, V.; Scott, B. L.; Keogh, D. W. *Angew. Chem., Int. Ed. Engl.* **2001**, 40, 591–594.
12. Sessler, J. L.; Gordon, A. E. V.; Seidel, D.; Hannah, S.; Lynch, V.; Gordon, P. L.; Donohoe, R. J.; Tait, C. D.; Keogh, D. W. *Inorg. Chim. Acta* **2002**, 341, 54–70.
13. (a) Rakow, N. A.; Suslick, K. S. *Nature* **2000**, 406, 710–713. (b) Suslick, K. S.; Rakow, N. A.; Kosal, M. E.; Chou, J. H. *J. Porphyr. Phthaocyal.* **2000**, 4, 407–413.
14. (a) Brunink, J.; Di Natale, C.; Bungaro, F.; Davide, F.; D'Amico, A.; Paolesse, R.; Boschi, T.; Faccio, M.; Ferri, G. *Anal. Chim. Acta* **1996**, 325, 53–64. (b) Di Natale, C.; Macagnano, A.; Repole, G.; Saggio, G.; D'Amico, A.; Paolesse, R.; Boschi, T. *Mat. Sci. Eng. C* **1998**, 5, 209–215. (c) Di Natale, C.; Paolesse, R.; Burgio, M.; Martinelli, E.; Pennazza, G.; D'Amico, A. *Anal. Chim. Acta* **2004**, 513, 49–56.
15. Kaltsoyannis, N.; Scott, P. *The f Elements from Oxford Chemistry Primers*; Evans, J., Ed.; Oxford Science Publications, Oxford University Press: New York, 1999.
16. Newton, T. W.; Hobart, D. E.; Palmer, P. D.; Report; LA-UR-86-967; Los Alamos National Laboratory, 1986.
17. Sessler, J. L.; Pantos, G. D.; Katayev, E.; Lynch, V. *Org. Lett.* **2003**, 5, 4141–4144; see supporting information.

# Fluorescence sensing based on cation-induced conformational switching: copper-selective modulation of the photoinduced intramolecular charge transfer of a donor–acceptor biphenyl fluorophore

John Cody and Christoph J. Fahrni\*

*School of Chemistry and Biochemistry, Georgia Institute of Technology, 770 State Street, Atlanta, GA 30332, USA*

Received 2 February 2004; revised 27 July 2004; accepted 19 August 2004

Available online 15 September 2004

**Abstract**—The fluorescence emission energy of donor–acceptor substituted biphenyls is highly sensitive towards conformational changes of the interannular twist angle. By integrating 4-dimethylamino-4'-cyano-biphenyl into the ligand backbone of a thioether-rich metal receptor we designed a fluorescence sensor that exhibits high selectivity towards copper. Upon metal binding the ligand undergoes a significant conformational change, which induces a strong hypsochromic shift of the photoinduced charge-transfer emission. Steady-state absorption and fluorescence spectroscopy revealed a high affinity towards Cu(I) with a well-defined 1:1 metal–ligand complex stoichiometry. The nature of the conformational changes upon Cu(I) coordination were analyzed in detail by <sup>1</sup>H NMR and 2D NOESY experiments. The spectroscopic data provide a coherent picture, which is consistent with a Boltzmann ground-state distribution of several rotamers that are locked into a more flattened geometry upon coordination of Cu(I).

© 2004 Elsevier Ltd. All rights reserved.

## 1. Introduction

Cation-specific fluorescence sensors are powerful tools for the measurement of metal ion concentrations in environmental and biological samples. They typically combine high optical sensitivity with excellent cation selectivity, and are therefore particularly well suited for the non-invasive visualization of labile metal pools in a biological environment.<sup>1</sup> Perhaps the largest class of fluorescence sensors function as simple cation-responsive switches.<sup>2</sup> The linear relationship between intensity and cation concentration allows for quantitative measurements; however, the emission intensity depends also on the sensor concentration, which is often not known with sufficient accuracy in biological samples. Fluorescence sensors which undergo a spectral shift upon binding of the cation inherently provide concentration information of the metal-free sensor and are principally suitable for accurate quantitative measurements via ratiometric fluorescence imaging.<sup>3</sup> Despite their usefulness, only a handful of ratiometric sensors have been

developed, indicating the considerable challenges in the probe design.<sup>4</sup>

Upon excitation into a charge transfer state the electronic structure of the fluorophore is significantly altered, which typically gives rise to considerable structural changes such as alteration of bond angles and distances, or twisting of conformationally flexible bonds.<sup>5</sup> In particular the latter relaxation mode could be effectively utilized to achieve a spectral shift, either via cation-induced changes of the ground-state geometry or through interference with an excited-state conformational relaxation pathway. Despite being a promising approach for the design of ratiometric probes, there are currently only few sensors which are based on a cation-induced conformational switching mechanism.<sup>6</sup>

Among suitable fluorophore platforms 4-dimethylamino-4'-cyanobiphenyl derivatives stand out due to their spectral sensitivity towards conformational changes of the interannular C–C bond (Chart 1).<sup>7,8</sup> For example, the methyl substituents in **DMDCB** enforce a near perpendicular ground-state geometry, which results in a large bathochromic shift compared to the more flattened unsubstituted fluorophore **DCB**.<sup>7</sup> To take advantage of this conformational sensitivity we thought to integrate the **DCB** fluorophore structure into a ligand backbone, such that cation binding

*Keywords:* Fluorescence sensor; Copper; Photoinduced charge transfer; Ligand design; Donor–acceptor fluorophores.

\* Corresponding author. Tel.: +1-404-385-1164; fax: +1-404-894-2295; e-mail: [fahrni@chemistry.gatech.edu](mailto:fahrni@chemistry.gatech.edu)



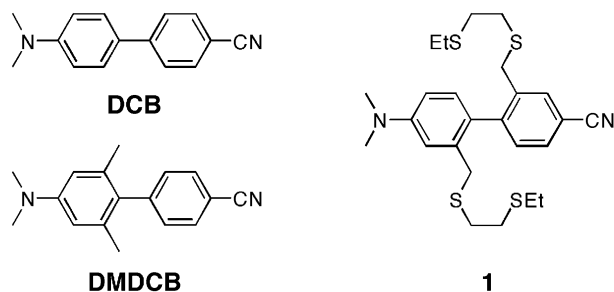
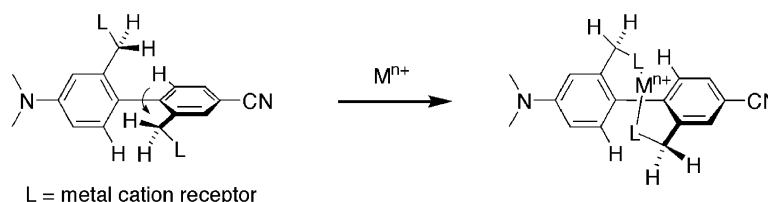
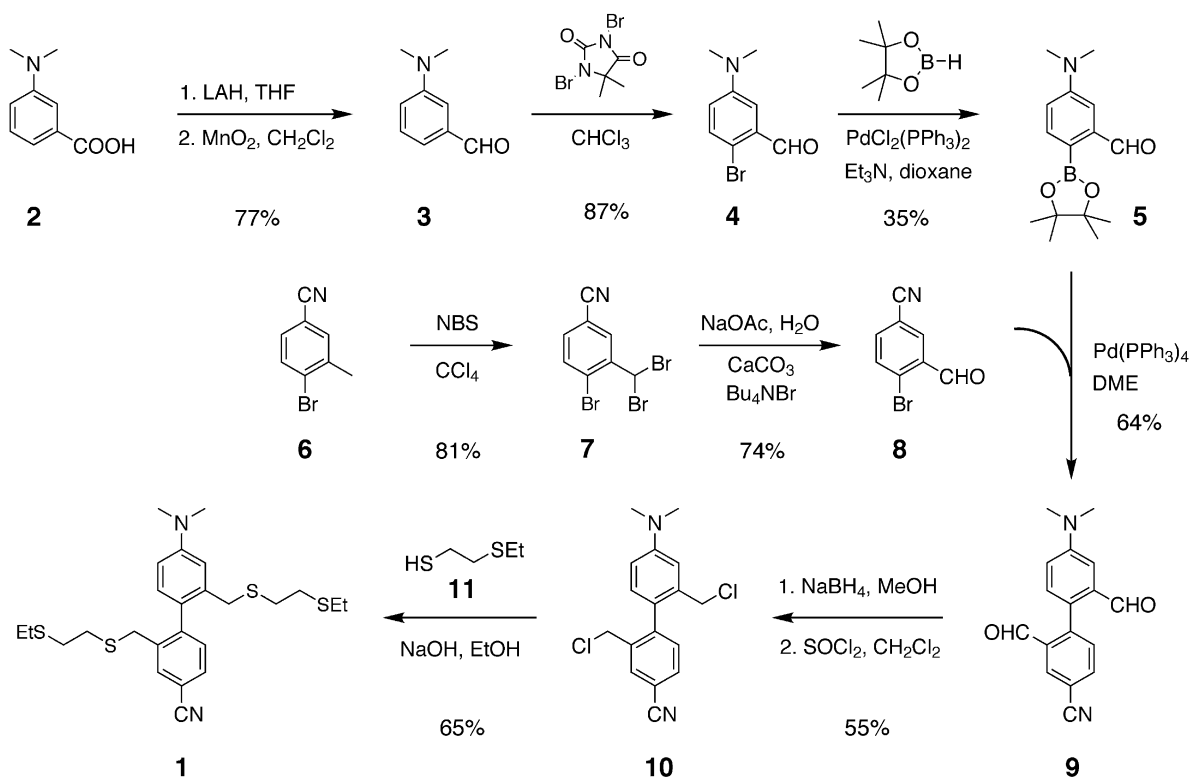


Chart 1.

would induce a significant conformational change of the interannular twist angle (Scheme 1). Because our current interest is focusing on the development of copper-selective fluorescence sensors, we used a thioether-rich ligand environment as metal-receptor for the design of chemosensor **1**. However, this approach could be readily adapted for selective fluorescence sensing of other metal cations by attaching different coordinating motifs.



Scheme 1.



Scheme 2.

## 2. Results and discussion

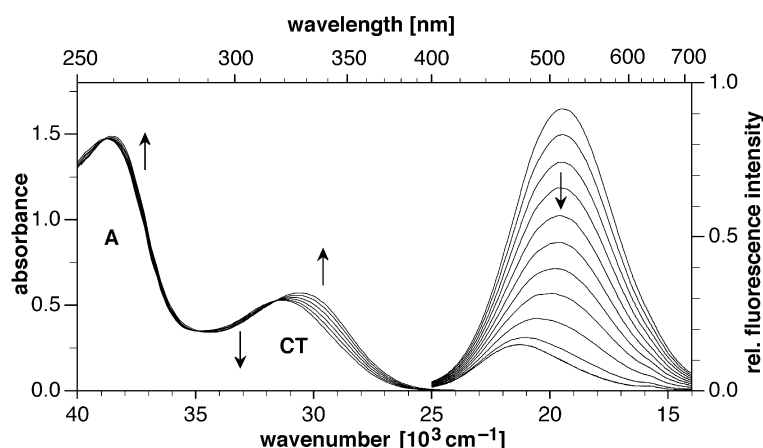
### 2.1. Synthesis

While symmetrically substituted biphenyl derivatives are accessible from a single precursor via reductive coupling,<sup>9</sup> the synthesis of unsymmetrically substituted donor–acceptor biphenyls such as **1** requires two different building blocks and is therefore significantly more laborious. To achieve sufficient synthetic flexibility, we were looking for a suitable precursor that could be functionalized with a wide range of metal-coordinating motifs. Key intermediate **9** fulfills these requirements and is readily obtained via palladium-catalyzed Suzuki-coupling of the corresponding reaction partners **5** and **8** (Scheme 2). While the aldehyde group is stable towards Suzuki-coupling conditions,<sup>10</sup> it is readily functionalized via reductive amination or condensation with amines to yield the corresponding Schiff bases. Furthermore, upon reduction and conversion to the corresponding halide or tosylate, it can serve as a versatile precursor for substitution with a wide range of nitrogen, sulfur or oxygen nucleophiles. For the synthesis of ligand **1**



**Table 1.** Spectroscopic data for **1**, **1-Cu(I)**, **DCB**,<sup>a</sup> and **DMDCB**<sup>a</sup> in anhydrous EtOH at 298 K

	Absorption $\lambda_{\max}$ (nm), $\epsilon$ ( $M^{-1} \text{cm}^{-1}$ ) <sup>b</sup>	Emission $\lambda_{\max}$ (nm)	Quantum yield <sup>c</sup> $\Phi_f$	Stokes' shift ( $\text{cm}^{-1}$ )	$\text{HW}_{\text{em}}$ <sup>d</sup> ( $\text{cm}^{-1}$ )
Ligand <b>1</b>	319 (CT), 4630 239 (A)	512	0.08	11,800	5000
<b>1</b> + 2 equiv $[\text{Cu}(\text{CH}_3\text{CN})_4]\text{PF}_6$	326 (CT), 5770 240 (A)	473	0.026	9550	4300
<b>DCB</b> <sup>a</sup>	345 (CT)	456	0.81	7100	3400
<b>DMDCB</b> <sup>a</sup>	312 (CT)	535	0.04	13,400	6200

<sup>a</sup> From Ref. 7.<sup>b</sup> Molar extinction coefficient.<sup>c</sup> Aerated solution, quinine sulfate in 1 N  $\text{H}_2\text{SO}_4$  as quantum yield standard.<sup>12</sup><sup>d</sup> Fluorescence emission band half-width.**Figure 1.** Absorption (left) and fluorescence emission (right, excitation at isosbestic point) spectra for the titration of ligand **1** (100  $\mu\text{M}$  in EtOH, 298 K) with 0.1 molar equiv aliquots of  $[\text{Cu}(\text{CH}_3\text{CN})_4]\text{PF}_6$ . For clarity the absorption spectra are only shown for 0.2 molar equiv aliquots.

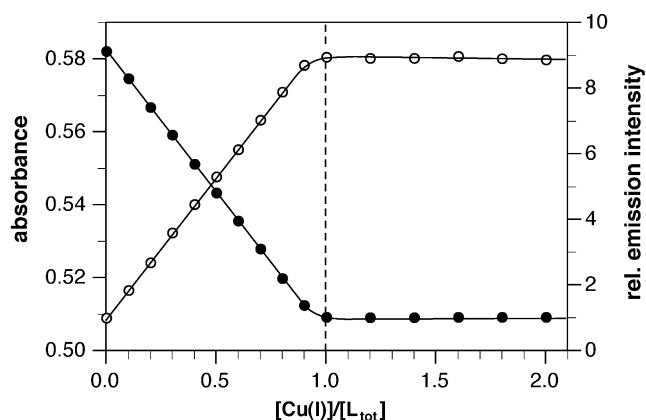
the aldehyde groups were reduced with sodium borohydride, chlorinated with thionyl chloride, and finally substituted with thiol **11**. The donor building block **5** was synthesized in four steps starting from commercially available 3-(dimethylamino)-benzoic acid **2**. Aldehyde **3** was obtained in 77% overall yield via reduction with lithium aluminum hydride followed by oxidation with manganese dioxide in anhydrous dichloromethane. The regioselective ortho-bromination of aldehyde **3** was accomplished in 87% yield using 1,3-dibromo-5,5-dimethylhydantoin as reagent. Finally, palladium-catalyzed borylation<sup>11</sup> of aryl-bromide **4** provided the boronate **5** in 35% yield. For the synthesis of the acceptor moiety **8** commercially available 4-bromo-3-methyl-benzonitrile was converted via radical bromination to the dibromomethyl derivative **7**, which was then hydrolyzed under mild conditions to give **8** in 60% overall yield. Although the current study is focusing on thioether ligand **1**, the synthetic strategy outlined in Scheme 2 should be suitable to provide access to a wide range of other donor-acceptor substituted biphenyl ligands.

## 2.2. Complexation studies with $[\text{Cu}(\text{I})(\text{CH}_3\text{CN})_4]\text{PF}_6$

### 2.2.1. Steady state absorption and emission spectra.

A compilation of the photophysical data for ligand **1** and its Cu(I) complex are given in Table 1. Because the absorption and emission properties of D–A substituted biphenyls are

strongly dependent on the interannular twist angle  $\Phi$ , the published photophysical data<sup>7</sup> for **DCB** ( $\Phi_{\text{gas}} = 39^\circ$ ) and **DMDCB** ( $\Phi_{\text{gas}} = 78^\circ$ ) provide a valuable reference for the interpretation of the photophysical properties of ligand **1**. The absorption spectrum of the free ligand in absolute ethanol shows two broad feature-less bands centered around 239 and 319 nm (Fig. 1, left). Using **DCB** and **DMDCB** as reference compounds, the bands can be unambiguously assigned to a locally excited state of the  $^1\text{L}_a$  type (A), and a charge-transfer state ( $^1\text{CT}$ ), which involves  $\pi$ -electron

**Figure 2.** Mol-ratio plot of the UV-vis absorbance at 326 nm (○) and the fluorescence intensity at 512 nm (●) for the titration shown in Figure 1.

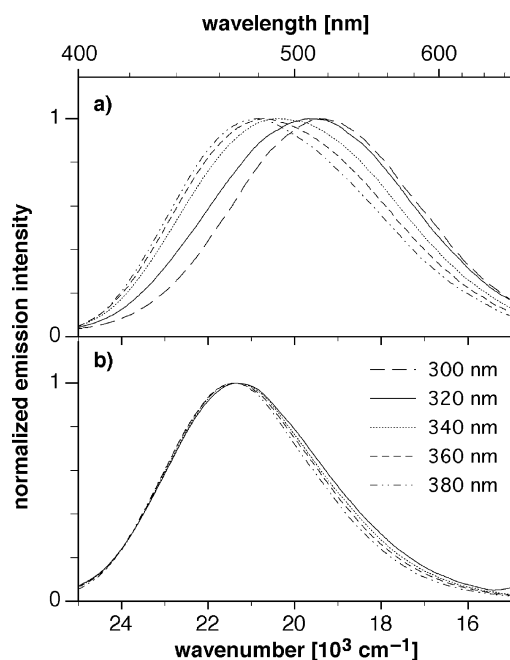


**Figure 3.** Normalized fluorescence emission spectra of **1** and **1-Cu(I)** as a function of the excitation wavelength (300–380 nm; 100  $\mu$ M **1** in EtOH, 298 K). (a) Free ligand; (b) ligand **1** in the presence of 2 molar equiv of  $[\text{Cu}(\text{CH}_3\text{CN})_4]\text{PF}_6$ .

delocalization from the dimethylamino to the cyano group. The relative intensities and positions of the two bands resembles strongly the published absorption spectrum for **DMDCB**,<sup>7</sup> suggesting a similar twist angle of approximately  $80^\circ$  for the ground state equilibrium geometry. The highly Stokes' shifted fluorescence emission of the free ligand exhibits a peak wavelength of 512 nm (Fig. 1, right), which is only slightly higher in energy compared to the published value of 535 nm for the peak emission of **DMDCB** in ethanol.<sup>7</sup> The Stokes' shift of the fluorescence emission of **1** is by  $1600\text{ cm}^{-1}$  smaller compared to the value for **DMDCB**, suggesting a slightly smaller degree of geometrical reorganization in the emissive  $^1\text{CT}$  state.

Upon addition of  $[\text{Cu}(\text{I})(\text{CH}_3\text{CN})_4]\text{PF}_6$  the CT absorption band of ligand **1** undergoes a bathochromic shift by 7 nm ( $670\text{ cm}^{-1}$ ), whereas the peak emission moves to

significantly higher energy by 39 nm ( $1600\text{ cm}^{-1}$ ) and decreases in intensity (Fig. 1). The UV–vis absorption traces form a set of sharp isosbestic points throughout the entire titration range, indicating a stoichiometrically well-defined equilibrium which involves only two UV–vis active species, the free ligand and its Cu(I)-coordinated form.

The mol-ratio plot of the absorbance at 326 and the fluorescence emission at 510 nm reveals for both saturation after addition of 1 molar equiv of Cu(I), which is consistent with a 1:1 complex stoichiometry (Fig. 2). Furthermore, the linearity of the absorbance increase and emission decrease up to 1 molar equiv of Cu(I) suggests a high binding affinity with near-quantitative fractional saturation at each copper concentration. Because reliable binding constants can be only obtained from titration data with a fractional saturation of less than 80%,<sup>13</sup> the mol-ratio plot is not suitable to extract an accurate binding affinity. A comparison of the fluorescence emission band half-width shows a significant decrease by  $700\text{ cm}^{-1}$  for the Cu(I)-bound ligand (Table 1) and directly reflects the reduced conformational flexibility upon complexation. The greater band half-width of the free ligand is presumably due to the presence of several energetically similar rotamer conformations, which comprise a dynamic ground-state Boltzmann distribution. This interpretation is further corroborated by the observation that the peak emission position depends strongly on the excitation wavelength in the case of the free but not the Cu(I)-bound ligand (Fig. 3). The free ligand shows a broad distribution of the peak emission wavelength, which undergoes a hypsochromic shift by more than 30 nm when excited at increasingly lower energy. In contrast, the fluorescence emission of the Cu(I)-bound ligand is essentially independent of the excitation energy, thus suggesting conformational 'locking' upon Cu(I) coordination.

To gain further insights into the energetics of the ground-state rotamer equilibrium, we performed density functional calculations at the B3LYP/6-31G\* level of theory with model compound **12** (Fig. 4). The gas-phase ground-state potential curve for rotation about the inter-annular C–C bond reveals indeed a very shallow well with a minimum at  $\Phi=82.0^\circ$ . Although compared to **DMDCB** the *ortho*-substituted methyl groups in **12** are expected to generate a

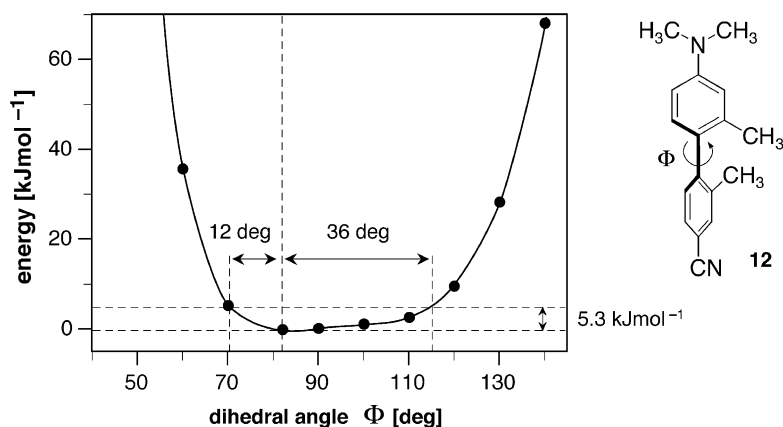


**Figure 4.** Unrelaxed gas-phase ground-state potential energy curve for **12** as a function of the biphenyl dihedral angle  $\Phi$  (B3LYP/6-31G\*). The potentials represent single point energies of the corresponding unrelaxed molecular geometries, which were obtained from the geometry-optimized structure ( $\Phi=82.0^\circ$ ) by variation of  $\Phi$ . The vertical dotted line indicates the dihedral angle of the lowest-energy rotamer.

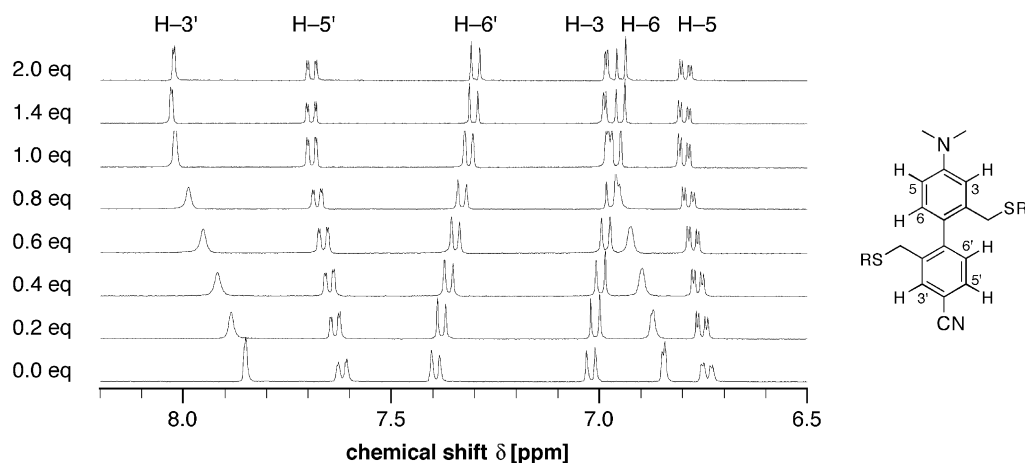


**Figure 5.** Aromatic region of the  $^1\text{H}$  NMR spectra for the titration of ligand **1** (20 mM in  $\text{CD}_3\text{OD}$ ) with  $[\text{Cu}(\text{CH}_3\text{CN})_4]\text{PF}_6$  at 298 K. The concentration of added Cu(I) is indicated as molar equivalents of total ligand present. The proton numbering scheme is provided with the structure to the right.

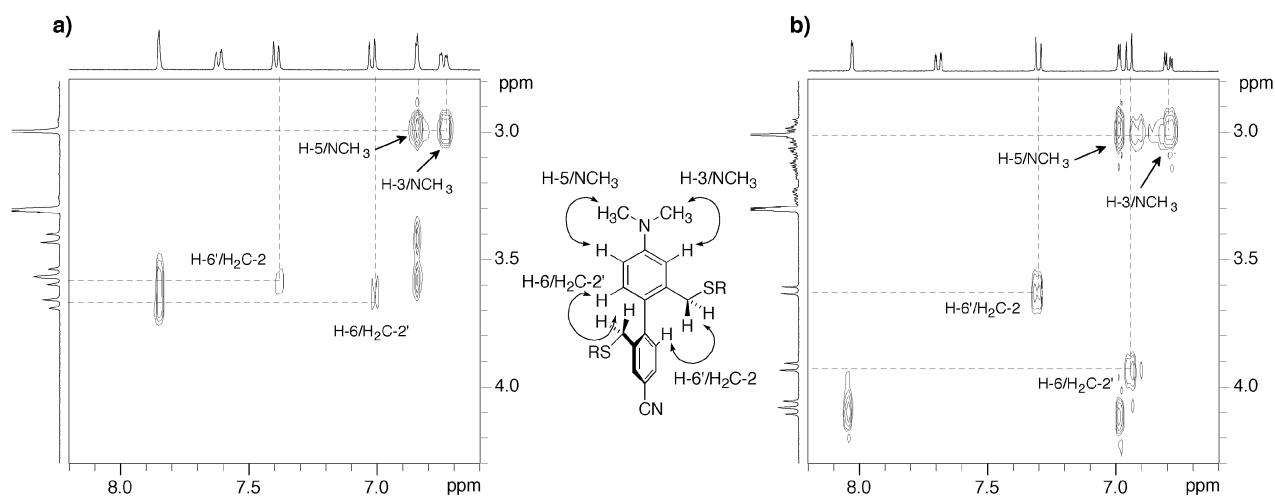


**Figure 6.** NOESY spectra of (a) ligand **1** and (b) ligand **1** in the presence of 2 molar equiv of  $[\text{Cu}(\text{CH}_3\text{CN})_4]\text{PF}_6$  in  $\text{CD}_3\text{OD}$  at 298 K. For clarity the graph is reduced to the spectrum section which shows the cross-correlation signals between the benzylic ( $\text{H}_2\text{C}-2/2'$ ), the dimethylamino ( $\text{N}(\text{CH}_3)_2$ ), and the aromatic ring protons ( $\text{H}-6/6'$ ).

similar energy barrier for rotation about the interannular C–C bond, the potential curve for **12** is not symmetrical. As illustrated in Figure 4 rotation by  $12^\circ$  from the equilibrium geometry towards a more acute dihedral angle increases the potential energy by  $5.3 \text{ kJ mol}^{-1}$ , whereas a rotation of  $36^\circ$  is necessary to create an isoenergetic potential in the opposite direction. Nevertheless, the calculated dihedral angle of the lowest-energy conformation is very similar compared to **DMDCB**, for which a lowest energy conformation with  $\Phi=78^\circ$  has been reported based on semi-empirical AM1 calculations.<sup>7</sup> Hence, the spectroscopic data combined with the computational study suggests that the ground-state equilibrium is dominated by rotamers with a near perpendicular dihedral angle. At the same time, the observed hypsochromic shift of the peak emission is consistent with the presence of a subpopulation of rotamers with a more flattened geometry ( $\Phi > 90^\circ$ ). With increasing flattening of the biphenyl ring-system, the CT absorption energy moves gradually towards lower energy. Upon excitation at the red-edge of the UV–vis CT band, the contribution of the flattened rotamers to the emission

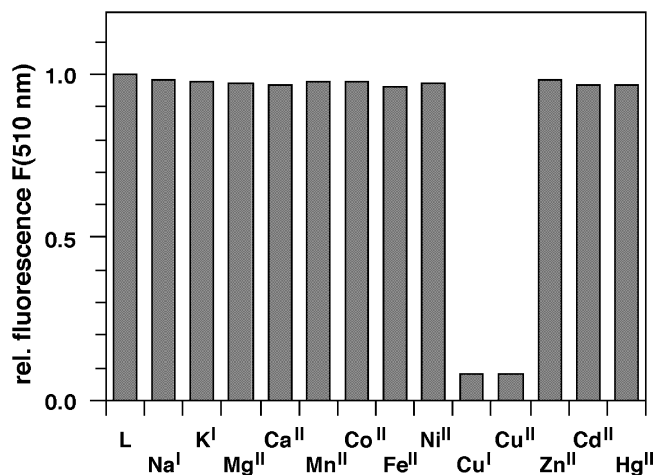


**Figure 7.** Emission intensity of ligand **1** at 510 nm (excitation at 320 nm) in response to various metal cations (100  $\mu\text{M}$  in EtOH, 2 molar equiv metal, 298 K).

spectrum becomes increasingly important due to their increased cross-section at lower energy.

**2.2.2. NMR studies.** To explore the ground-state structural changes of the ligand backbone upon coordination of Cu(I), we performed a series of NMR experiments. The  $^1\text{H}$  NMR spectra for titration of ligand **1** with  $[\text{Cu}(\text{I})(\text{CH}_3\text{CN})_4]\text{PF}_6$  in  $\text{CD}_3\text{OD}$  revealed significant changes in the chemical shift of the aromatic proton resonances of the biphenyl ring system (Fig. 5). Throughout the entire titration range a single set of sharp resonances was observed, indicating fast metal exchange kinetics compared to the NMR time scale. Therefore, the chemical shifts reflect directly the fractional contribution of free and Cu(I)-bound ligand. As already observed for the UV–vis and fluorescence titrations the resonances shift linearly up to 1 molar equiv of Cu(I) and undergo no further changes at higher concentrations. It is noteworthy that the slope of the chemical shift changes is essentially identical for the corresponding *ortho*-(H-6/6') and *meta*-proton (H-3/3' and H-5/5') resonances, thus suggesting a symmetrical coordination of Cu(I) to both thioether branches and no involvement of the dimethylamino group in metal coordination.

### 2.3. NOESY (Nuclear Overhauser Enhancement Spectroscopy) experiment

The NOESY experiment is the two-dimensional equivalent of a NOE difference experiment and yields correlation signals which are caused by dipolar cross-relaxation between nuclei in a close spatial relationship. Because the intensities of the cross-peaks are proportional to the sixth power of the proton–proton distances, this technique is well suited to investigate structural differences between the free and Cu(I)-bound ligand. As shown in Figure 6 the conformational differences of the biphenyl backbone are best reflected in the changes of the cross-correlation signal intensities of the benzylic ( $\text{H}_2\text{C}-2/2'$ ) and *ortho*-protons (H-6/6'). If the integrated intensities are normalized for each spectra using the correlation signals between the H-5/H-3 and dimethylamino protons, qualitative information of the distance changes associated with Cu(I) coordination can be directly extracted from the spectra. Hence, upon addition of excess Cu(I) the cross correlation signals for  $\text{H}_2\text{C}-2/\text{H}-6'$  and  $\text{H}_2\text{C}-2'/\text{H}-6$  increase by a factor of 2, whereas the signal for the cross-relaxation of H-6/H-6' decreases by a factor of 10 (not included in Fig. 6). These data unambiguously indicate that upon Cu(I) coordination the dihedral angle of the biphenyl backbone increases ( $\Phi > 90^\circ$ ) to yield a more flattened conformation.

**2.3.1. Selectivity.** To evaluate the selectivity of ligand **1** we measured its fluorescence response in the presence of various metal cations (Fig. 7). Among the tested mono- and divalent metal cations only Cu(I) and Cu(II) induced a significant change of the emission intensity. Although Cd(II) and Hg(II) are both members of the 'copper triangle', neither metal resulted in a change of the emission intensity. Similarly, the UV–vis spectra displayed no changes upon addition of either cation (data not shown), suggesting a surprisingly weak interaction with the thioether ligand.

## 3. Conclusions

The absorption and emission spectroscopic data combined with the  $^1\text{H}$  NMR and 2D NOESY experiments provide a coherent picture of the conformational changes which occur in the ground-state equilibrium upon coordination of Cu(I) to ligand **1** at room temperature. While the free ligand shows an equilibrium distribution of rotamers in the ground-state, Cu(I) complexation imposes conformational locking and results in a flattened geometry with respect to the two aryl moieties. Detailed studies by Maus et al. unequivocally established that the photoinduced charge transfer state of **DMDCB** undergoes flattening distortion in non-polar solvents, but adopts a near perpendicular geometry in polar solvents such as acetonitrile or ethanol.<sup>7,8,14</sup> The similarities of the emission quantum yield and the spectroscopic data of **1** compared to **DMDCB** suggests, that the free ligand **1** might also adopt a near-perpendicular geometry in the charge transfer state. However, it is important to keep in mind that the different positioning of the *ortho*-substituents on the biphenyl ring system results in an unsymmetrical potential energy surface for ligand **1**, thus providing a better opportunity for relaxation of the charge transfer state towards a more open dihedral angle. In either case, conformational locking by Cu(I) would inhibit this rotational relaxation pathway and result in reduced geometrical distortion, which is consistent with the smaller Stokes' shift and higher emission energy for the Cu(I)-complex. The reduced quantum yield of the Cu(I) bound form might be due to the presence of an additional non-emissive excited state ( $^1\text{ET}$ ), which could be accessed via reductive electron transfer from Cu(I) to the biphenyl fluorophore. At present, conclusions regarding the excited state conformational dynamics and non-radiative deactivation pathways remain rather speculative and require more detailed photophysical studies.

In summary, this study demonstrates that cation-induced conformational locking of the ground or excited state can yield substantial shifts of the emission energy and represents therefore an attractive strategy for the design of ratiometric cation-responsive fluorescence sensors.

## 4. Experimental

### 4.1. Materials and reagents

All starting materials, reagents and solvents were purchased from Aldrich (Milwaukee, WI) or Fisher Scientific (Pittsburgh, PA) and used without further purification. NMR:  $\delta$  in ppm vs.  $\text{SiMe}_4$  (0 ppm,  $^1\text{H}$ , 400 MHz). MS: selected peaks;  $m/z$ . Melting points are uncorrected. Flash chromatography: Merck silica gel (240–400 mesh). TLC: 0.25 mm, Merck silica gel 60 F<sub>254</sub>, visualizing at 254 nm or with 2%  $\text{KMnO}_4$  solution.

### 4.2. Synthesis

**4.2.1. 2-Bromo-5-(dimethylamino)-benzaldehyde (4).** Solid lithium aluminum hydride (5.75 g, 152 mmol) was added in portions to a stirring solution of acid **2** (10.0 g, 61 mmol) in anhydrous THF at 0 °C. The reaction mixture

was stirred for 1 h at room temperature and then quenched by addition of H<sub>2</sub>O (4 equiv relative to LAH). The precipitate was filtered off, washed with THF, and the combined filtrates were concentrated under reduced pressure to yield 3-(dimethylamino)-benzylalcohol as a yellow oil (8.22 g, 90%). *R<sub>f</sub>* 0.15 (hexane/EtOAc 4:1); <sup>1</sup>H NMR (CDCl<sub>3</sub>, 400 MHz) δ 2.62 (s, 1H broad), 2.90 (s, 6H), 4.55 (s, 2H), 6.62–6.71 (m, 3H), 7.19 (t, *J* = 7.7 Hz, 1H); <sup>13</sup>C NMR (CDCl<sub>3</sub>, 100 MHz) δ 40.6, 65.5, 111.2, 111.9, 115.2, 129.0, 141.8, 150.7; MS (70 eV) 150.1 (M<sup>+</sup>, 25), 148.1 (100), 77 (25); FAB HRMS *m/e* calcd for (M+H) C<sub>9</sub>H<sub>11</sub>NO 149.0841, found 149.0827.

A mixture of the crude alcohol (5.15 g, 34 mmol) and activated MnO<sub>2</sub> (35.5 g, 409 mmol) in anhydrous CH<sub>2</sub>Cl<sub>2</sub> was stirred for 4 h at room temperature. The solid was filtered off (Celite) and washed with CH<sub>2</sub>Cl<sub>2</sub>. The combined filtrates were extracted with aq NaHCO<sub>3</sub>, dried over anhydrous MgSO<sub>4</sub>, and concentrated under reduced pressure to yield aldehyde **3** as a yellow-green oil (4.32 g, 85%). *R<sub>f</sub>* 0.34 (8:1 hexane/EtOAc); <sup>1</sup>H NMR (CDCl<sub>3</sub>, 400 MHz) δ 2.99 (s, 6H), 6.94 (dd, *J* = 2.2, 1.6 Hz, 1H), 6.97 (dd, *J* = 2.7, 1.1 Hz, 1H), 7.17 (d, *J* = 1.6 Hz, 1H), 7.37 (t, *J* = 7.7 Hz, 1H), 9.94 (s, 1H); <sup>13</sup>C NMR (CDCl<sub>3</sub>, 100 MHz) δ 40.3, 111.5, 118.2, 118.8, 129.5, 137.1, 150.7, 193.2; MS (70 eV) 149.1 (M<sup>+</sup>, 97), 148.1 (100), 77 (25). FAB HRMS *m/e* calcd for (M+H) C<sub>9</sub>H<sub>11</sub>NO 149.0841, found 149.0827.

To the crude benzaldehyde (4.36 g, 29 mmol) in CH<sub>2</sub>Cl<sub>2</sub> was added 1,3-dibromo-5,5-dimethylhydantoin (3.77 g, 13 mmol). The mixture was then allowed to reflux overnight and subsequently diluted with H<sub>2</sub>O and extracted with CH<sub>2</sub>Cl<sub>2</sub>. The organic layers were then dried with MgSO<sub>4</sub>, filtered and concentrated under reduced pressure. The reaction mixture was purified on silica gel (8:1 hexanes/EtOAc) to yield **4** as a bright yellow solid (5.80 g, 87%) with an overall yield from **2** of 67%. Mp 55–58 °C; *R<sub>f</sub>* 0.39 (8:1 hexanes/EtOAc); <sup>1</sup>H NMR (CDCl<sub>3</sub>, 400 MHz) δ 2.98 (s, 6H), 6.80 (dd, *J* = 8.8, 3.3 Hz, 1H), 7.19 (d, *J* = 3.3 Hz, 1H), 7.43 (d, *J* = 8.8 Hz, 1H), 10.31 (s, 1H); <sup>13</sup>C NMR (CDCl<sub>3</sub>, 100 MHz) δ 40.4, 112.1, 113.0, 119.0, 119.2, 133.2, 133.9, 192.7, MS (70 eV) 228 (M<sup>+</sup>, 98), 227 (100), 156 (24). EI HRMS *m/e* calcd for (M+H) C<sub>9</sub>H<sub>10</sub>BrNO 226.9946, found 226.9950.

**4.2.2. 5-Dimethylamino-2-(4,4,5,5-tetramethyl-[1,3,2]-dioxaborolan-2-yl)-benzaldehyde (5).** 4,4,5,5-Tetramethyl-[1,3,2]-dioxaborolane (950 μL, 6.55 mmol) was added to a Schlenk tube containing a solution of bromide **4** (0.5 g, 2.18 mmol) in dioxane. Triethylamine (950 μL, 6.82 mmol) and PdCl<sub>2</sub>(PPh<sub>3</sub>)<sub>2</sub> (46 mg, 3 mol%) were added and the solution was flushed with a light stream of argon. The tube was then heated for 3 h at 100 °C. The reaction mixture was then diluted with H<sub>2</sub>O and extracted with EtOAc. The organic layers were dried with MgSO<sub>4</sub>, filtered, and concentrated under reduced pressure. The product was purified on silica gel (hexane/EtOAc 10:1) to yield boronate ester **5** as a yellow oil (209 mg, 35%). *R<sub>f</sub>* 0.35 (8:1 hexane/EtOAc); <sup>1</sup>H NMR (CDCl<sub>3</sub>, 400 MHz) δ 1.35 (s, 12H), 3.03 (s, 6H), 6.86 (dd, *J* = 8.8, 2.7 Hz, 1H), 7.28 (d, *J* = 2.7 Hz, 1H), 7.80 (d, *J* = 8.8 Hz, 1H), 10.68 (s, 1H); <sup>13</sup>C NMR (CDCl<sub>3</sub>, 100 MHz) δ 24.9, 40.1, 83.6, 108.9, 115.7, 137.7, 142.7, 151.8, 195.8; MS (70 eV) 275.2 (M<sup>+</sup>, 63), 261.0

(18), 217.2 (100), 176.1 (16). EI HRMS *m/e* calcd for (M+H) C<sub>15</sub>H<sub>22</sub>BNO<sub>3</sub> 275.1693, found 275.1759.

**4.2.3. 4-Bromo-3-formyl-benzonitrile (8).** A solution of 4-bromo-3-methylbenzonitrile **6** (4.0 g, 20 mmol), *N*-bromosuccinimide (7.63 g, 43 mmol), and benzoyl peroxide (250 mg, 1.0 mmol) was heated at reflux for 4 h. The reaction mixture was diluted with H<sub>2</sub>O and extracted with EtOAc. The organic layers were dried over anhydrous MgSO<sub>4</sub>, filtered, and concentrated under reduced pressure. The product was purified on silica gel (hexane/Et<sub>2</sub>O 20:1) to yield 5.85 g of dibromide **7** as a white powder (17 mmol, 81%). Mp 149–151 °C; *R<sub>f</sub>* 0.17 (20:1 hexane/Et<sub>2</sub>O); <sup>1</sup>H NMR (CDCl<sub>3</sub>, 400 MHz) δ 7.00 (s, 1H), 7.44 (dd, *J* = 8.2, 1.6 Hz, 1H), 7.66 (d, *J* = 8.2 Hz, 1H), 8.31 (d, *J* = 1.6 Hz, 1H); MS (70 eV) 354.8 (M<sup>+</sup>, 9), 273.9 (100), 114.0 (46). EI HRMS *m/e* calcd for (M+H) C<sub>8</sub>H<sub>4</sub>Br<sub>2</sub>N 350.7894, found 350.7892.

The crude bromide **7** (5.85 g, 17 mmol) was added to a solution of sodium acetate (5.98 g, 73 mmol), calcium carbonate (3.70 g, 37 mmol), and tetrabutyl ammonium bromide (1.26 g, 3.9 mmol) in 500 mL of H<sub>2</sub>O. The reaction mixture was heated under reflux for 12 h, cooled to room temperature, and extracted with CH<sub>2</sub>Cl<sub>2</sub>. The organic layers were dried with MgSO<sub>4</sub>, filtered, and concentrated under reduced pressure. The product was purified on silica gel to yield aldehyde **8** as a white powder (2.57 g, 12 mmol, 74%) with an overall yield from **6** of 60%. Mp 124–126 °C; *R<sub>f</sub>* 0.12 (hexane/Et<sub>2</sub>O 20:1); <sup>1</sup>H NMR (CDCl<sub>3</sub>, 400 MHz) δ 7.72 (dd, *J* = 8.2, 2.2 Hz, 1H), 7.84 (d, *J* = 8.2 Hz, 1H), 8.18 (d, *J* = 2.2 Hz, 1H), 10.35 (s, 1H); <sup>13</sup>C NMR (CDCl<sub>3</sub>, 100 MHz) δ 112.6, 116.8, 131.5, 133.3, 134.2, 135.1, 137.2, 189.5; MS (70 eV) 210 (M<sup>+</sup>, 100), 129.1 (30), 101 (42), 50 (38). EI HRMS *m/e* calcd for (M+H) C<sub>8</sub>H<sub>4</sub>BrNO 208.9476, found 208.9476.

**4.2.4. 4-Dimethylamino-2,2'-diformyl-4'-cyano-1,1'-biphenyl (9).** 4-Bromo-3-formylbenzonitrile **8** (161 mg, 0.77 mmol) was added to a Schlenk tube containing a solution of boronate ester **5** (209 mg, 0.76 mmol), CsF (281 mg, 1.9 mmol), and Pd(PPh<sub>3</sub>)<sub>4</sub> (5 mol%) in 8 mL of dimethoxyethane. The mixture was heated under reflux overnight at which point a bright orange precipitate was formed. The reaction mixture was diluted with H<sub>2</sub>O and extracted with CH<sub>2</sub>Cl<sub>2</sub>. The organic layers were dried over anhydrous MgSO<sub>4</sub>, filtered, and concentrated under reduced pressure. The crude product was purified on silica gel (CH<sub>2</sub>Cl<sub>2</sub>/MeOH 4:1) to yield 135 mg of the coupling product **9** as an orange crystalline solid (0.49 mmol, 64%). Mp 189–191 °C; *R<sub>f</sub>* 0.33 (hexane/EtOAc 2:1); <sup>1</sup>H NMR (CDCl<sub>3</sub>, 400 MHz) δ 3.11 (s, 6H), 6.97 (dd, *J* = 8.2, 2.7 Hz, 1H), 7.14 (d, *J* = 8.8 Hz, 1H), 7.28 (d, *J* = 2.7 Hz, 1H), 7.44 (d, *J* = 8.2 Hz, 1H), 7.84 (dd, *J* = 7.7, 1.7 Hz, 1H), 8.28 (d, *J* = 1.7 Hz, 1H), 9.80 (s, 1H), 9.81 (s, 1H); <sup>13</sup>C NMR (CDCl<sub>3</sub>, 100 MHz) δ 40.6, 112.3, 113.1, 116.6, 117.9, 125.0, 131.8, 133.0, 133.3, 135.0, 135.5, 135.6, 147.0, 150.9, 189.7, 191.4; MS (70 eV) 278.1 (M<sup>+</sup>, 88), 249.2 (100), 221.2 (25) EI HRMS *m/e* calcd for (M+H) C<sub>17</sub>H<sub>14</sub>N<sub>2</sub>O<sub>2</sub> 278.1055, found 278.1058.

**4.2.5. 2,2'-Bis(chloromethyl)-4-(dimethylamino)-4'-cyano-1,1'-biphenyl (10).** A solution of the aldehyde



(55 mg, 0.20 mmol) in MeOH was added slowly to a solution of NaBH<sub>4</sub> (17 mg, 0.45 mmol) in MeOH. The solution was then allowed to stir at room temperature for 1 h. The reaction mixture was then quenched with H<sub>2</sub>O and extracted with Et<sub>2</sub>O. The organic layers were dried with MgSO<sub>4</sub>, filtered, and concentrated under reduced pressure. The product was purified on silica gel (2:1 hexane/EtOAc) to yield 4'-(dimethylamino)-2,2'-bis(hydroxymethyl)-1,1'-biphenyl-4-carbonitrile as a yellow solid (0.16 mmol, 81%). Mp 132–135 °C; R<sub>f</sub> 0.21 (2:1 hexane/EtOAc); <sup>1</sup>H NMR (CDCl<sub>3</sub>, 400 MHz) δ 3.09 (s, 6H), 4.98 (s, 2H broad), 6.71 (d, J=2.7 Hz, 1H), 6.82 (dd, J=8.2, 2.7 Hz, 1H), 6.98 (dd, J=8.8, 2.7 Hz, 1H), 7.44 (d, J=8.8 Hz, 1H), 7.79 (dd, J=8.2, 1.7 Hz), 8.20 (d, J=1.7 Hz, 1H); <sup>13</sup>C NMR (CDCl<sub>3</sub>, 100 MHz) δ 40.8, 68.8, 70.6, 112.0, 114.9, 116.6, 118.9, 130.3, 130.5, 131.9, 132.3, 133.7, 135.2, 136.7, 142.6, 151.1; MS (70 eV) 282.2 (M<sup>+</sup>, 100), 263.2 (23), 233.1 (33), 190.1 (17). EI HRMS *m/e* calcd for (M+H) C<sub>17</sub>H<sub>18</sub>N<sub>2</sub>O<sub>2</sub> 282.1368, found 282.1378.

Thionyl chloride (31 μL, 0.42 mmol) was added cautiously to a solution of the alcohol (30 mg, 0.11 mmol) in CH<sub>2</sub>Cl<sub>2</sub>. The reaction was then allowed to stir for 1.5 h at room temperature. The reaction mixture was then diluted with CH<sub>2</sub>Cl<sub>2</sub> and washed with sat. NaHCO<sub>3</sub>. The organic layers were dried with MgSO<sub>4</sub>, filtered, and concentrated under reduced pressure. No further purification was necessary and the chloride **10** was isolated as a pale yellow solid (0.07 mmol, 68%). Mp 115–117 °C; R<sub>f</sub> 0.25 (1:1 hexane/EtOAc); <sup>1</sup>H NMR (CDCl<sub>3</sub>, 400 MHz) δ 2.97 (s, 6H), 4.12–4.36 (m, 4H), 6.67 (dd, J=8.2, 2.7 Hz, 1H), 6.75 (d, J=2.7 Hz, 1H), 6.98 (d, J=8.8 Hz, 1H), 7.32 (d, J=7.7 Hz, 1H), 7.57 (dd, J=7.7, 1.7 Hz, 1H), 7.80 (d, J=1.7 Hz, 1H); <sup>13</sup>C NMR (CDCl<sub>3</sub>, 100 MHz) δ 40.2, 43.1, 44.8, 112.0, 112.2, 113.3, 118.3, 124.9, 130.3, 131.3, 131.9, 133.5, 135.6, 138.1, 144.8, 150.7; MS (70 eV) 318.1 (M<sup>+</sup>, 100), 234.2 (48), 190.1 (19). EI HRMS *m/e* calcd for (M+H) C<sub>17</sub>H<sub>16</sub>Cl<sub>2</sub>N<sub>2</sub> 318.0691, found 318.0704.

**4.2.6. 2-Mercaptoethylethyl sulfide (11).** A mixture of thiourea (2.0 g, 26 mmol) and 2-chloroethylethyl sulfide (3.2 g, 26 mmol) was heated at 100 °C under N<sub>2</sub> atmosphere. After all thiourea had dissolved a very viscous fluid was formed at which point the reaction was allowed to cool to room temperature. The mixture was hydrolyzed by addition of 5 mL of 5 M NaOH and then stirred overnight. The mixture was acidified with 6 M HCl to pH 3 and extracted with ether. The organic extract was dried over anhydrous MgSO<sub>4</sub> and concentrated in vacuo yielding 2.14 g of thiol **11** as a colorless liquid (17.5 mmol, 68%). <sup>1</sup>H NMR (CDCl<sub>3</sub>, 400 MHz) δ 1.27 (t, J=7.1 Hz, 3H), 2.53–2.62 (m, 2H), 2.71–2.78 (m, 4H), 5.31 (s, 1H); <sup>13</sup>C NMR (CDCl<sub>3</sub>, 100 MHz) δ 14.7, 24.6, 25.7, 35.6; MS (EI) 122 (M<sup>+</sup>, 90), 75 (100), 61 (54), 47 (50). EI HRMS *m/e* calculated for (M<sup>+</sup>) C<sub>4</sub>H<sub>10</sub>S<sub>2</sub> 122.0224, found 122.0225.

**4.2.7. 4-Dimethylamino-2,2'-bis-(2-ethylsulfanyl-ethyl-sulfanylmethyl)-4'-cyano-1,1'-biphenyl (1).** A solution of the chloride **10** (52 mg, 0.16 mmol) in EtOH was added dropwise to a solution of the thiol **11** (58 mg, 0.48 mmol) in EtOH containing NaOH (20 mg, 0.50 mmol). The reaction mixture was then allowed to stir at room temperature for 1 h. The reaction mixture was then diluted with H<sub>2</sub>O and

extracted with CH<sub>2</sub>Cl<sub>2</sub>. The organic layers were dried with MgSO<sub>4</sub>, filtered, and concentrated under reduced pressure. The product was purified via Chromatron (1:1 hexane/EtOAc) to yield **1** as a viscous yellow oil (0.11 mmol, 65%). R<sub>f</sub> 0.22 (1:1 hexane/EtOAc); <sup>1</sup>H NMR (CD<sub>3</sub>CN, 400 MHz) δ 1.20–1.30 (m, 6H), 2.47–2.61 (m, 12H), 3.02 (s, 6H), 3.36–3.63 (m, 4H), 6.67 (dd, J=8.8, 2.7 Hz, 1H), 6.76 (d, J=2.7 Hz, 1H), 7.00 (d, J=8.2 Hz, 1H), 7.35 (d, J=7.7 Hz, 1H), 7.55 (dd, J=7.7, 1.7 Hz, 1H), 7.83 (d, J=1.7 Hz, 1H); <sup>13</sup>C NMR (CDCl<sub>3</sub>, 100 MHz) δ 14.7, 25.9, 30.2, 30.9, 31.2, 31.3, 32.0, 33.5, 34.7, 38.5, 40.3, 110.9, 111.1, 113.1, 118.7, 125.8, 129.9, 130.3, 131.8, 132.9, 136.0, 138.8, 145.6, 150.2; MS (70 eV) 490.2 (M<sup>+</sup>, 76), 247.2 (100), 89.1 (87). EI HRMS *m/e* calcd for (M+H) C<sub>25</sub>H<sub>34</sub>N<sub>2</sub>S<sub>4</sub> 490.1605, found 490.1605.

### 4.3. Steady state absorption and fluorescence spectroscopy

All sample stock solutions and buffer solutions were filtered through 0.2 μm Nylon membrane filters to remove interfering dust particles or fibers. UV–vis absorption spectra were recorded at 25 °C using a Varian Cary Bio50 UV–vis spectrometer with constant-temperature accessory. Steady-state emission and excitation spectra were recorded with a PTI fluorimeter and FELIX software. Throughout the titration the sample solution was stirred with a magnetic stirring device. For all titrations the path length was 1 cm with a cell volume of 3.0 mL. All fluorescence spectra have been corrected for the spectral response of the detection system (emission correction file provided by instrument manufacturer) and for the spectral irradiance of the excitation channel (via calibrated photodiode). Quantum yields were determined in aerated, anhydrous ethanol using quinine sulfate dihydrate in 1.0 N H<sub>2</sub>SO<sub>4</sub> (Φ<sub>F</sub>=0.507 ± 0.03 as fluorescence standard.<sup>12</sup>

### 4.4. NMR spectroscopy

All NMR spectra (<sup>1</sup>H, <sup>13</sup>C, <sup>1</sup>H–<sup>1</sup>H NOESY) were recorded on either a Bruker DRX 500 or Mercury VX 400. For all titrations the total sample volume was 700 μL containing 20 mM ligand solution in CD<sub>3</sub>OD. The titrations were performed by adding 0.1 molar equiv aliquots of a solution of [Cu(I)(CH<sub>3</sub>CN)<sub>4</sub>]PF<sub>6</sub> in CD<sub>3</sub>CN to a solution of ligand **1** in CD<sub>3</sub>OD.

### 4.5. Quantum chemical calculations

The geometry of the ground-state structure for **12** was optimized by the density functional method using the B3LYP hybrid functional with the split-valence polarized 6-31G\* (6-31G(d)) basis set as implemented in the Q-Chem<sup>15</sup> electronic structure calculation suite of programs. The calculation of the ground-state potential curve is based on unrelaxed geometries using the corresponding dihedral angles for rotation around the interannular C–C bond.

### Acknowledgements

Financial support from the National Institutes of Health



(R01GM67169) and the Georgia Institute of Technology is gratefully acknowledged. Computations were supported by the Center for Computational Molecular Science and Technology at the Georgia Institute of Technology and partially funded through a Shared University Research (SUR) grant from IBM and the Georgia Institute of Technology. We also thank D. Bostwick for mass spectral data and Dr. L. Gelbaum for performing the NOESY experiments.

### References and notes

- Mason, W. T. *Fluorescent and Luminescent Probes for Biological Activity*, 2nd ed.; Academic: San Diego, 1999. For recent reports on the visualization of labile Zn(II) in mammalian cells see for example: Zalewski, P. D.; Millard, S. H.; Forbes, I. J.; Kapaniris, O.; Slavotinek, A.; Betts, W. H.; Ward, A. D.; Lincoln, S. F.; Mahadevan, I. *J. Histochem. Cytochem.* **1994**, *42*, 877. Budde, T.; Minta, A.; White, J. A.; Kay, A. R. *Neuroscience* **1997**, *79*, 347. Nasir, M. S.; Fahrni, C. J.; Suhy, D. A.; Kolodsick, K. J.; Singer, C. P.; O'Halloran, T. V. *J. Biol. Inorg. Chem.* **1999**, *4*, 775. Pearce, D. A.; Jotterand, N.; Carrico, I. S.; Imperiali, B. *J. Am. Chem. Soc.* **2001**, *123*, 5160. Hirano, T.; Kikuchi, K.; Urano, Y.; Nagano, T. *J. Am. Chem. Soc.* **2002**, *124*, 6555. Burdette, S. C.; Frederickson, C. J.; Bu, W.; Lippard, S. J. *J. Am. Chem. Soc.* **2003**, *125*, 1778. Kimura, E.; Aoki, S.; Kikuta, E.; Koike, T. *Proc. Natl Acad. Sci. U.S.A.* **2003**, *100*, 3731.
- DeSilva, A. P.; Gunaratne, H. Q. N.; Gunnlaugsson, T.; Huxley, A. J. M.; McCoy, C. P.; Rademacher, J. T.; Rice, T. E. *Chem. Rev.* **1997**, *97*, 1515.
- Gryniewicz, G.; Poenie, M.; Tsien, R. Y. *J. Biol. Chem.* **1985**, *260*, 3440.
- Haugland, R. P. *Handbook of Fluorescent Probes and Research Products*; Molecular Probes: Eugene, OR, 2002. Recent developments for ratiometric measurement of Zn(II): Maruyama, S.; Kikuchi, K.; Hirano, T.; Urano, Y.; Nagano, T. *J. Am. Chem. Soc.* **2002**, *124*, 10650. Gee, K. R.; Zhou, Z. L.; Ton-That, D.; Sensi, S. L.; Weiss, J. H. *Cell Calcium* **2002**, *31*, 245. Henary, M. M.; Fahrni, C. J. *J. Phys. Chem. A*, **2004**, *108*, 5210. Taki, M.; Wolford, J. L.; O'Halloran, T. V. *J. Am. Chem. Soc.* **2004**, *126*, 712. Chang, C. J.; Jaworski, J.; Nolan, E. M.; Sheng, M.; Lippard, S. J. *Proc. Natl Acad. Sci. U.S.A.* **2004**, *101*, 1129.
- Rettig, W.; Maus, M. *Conformational Changes Accompanying Intramolecular Excited State Electron Transfer*; Waluk, J., Ed.; Wiley: New York, 2000; p 1.
- McFarland, S. A.; Finney, N. S. *J. Am. Chem. Soc.* **2001**, *123*, 1260. Mello, J. V.; Finney, N. S. *Angew. Chem. Int. Ed. Engl.* **2001**, *40*, 1536. Morozumi, T.; Anada, T.; Nakamura, H. *J. Phys. Chem. B* **2001**, *105*, 2923. Costero, A. M.; Andreu, R.; Monrabal, E.; Martinez-Manez, R.; Sancenon, F.; Soto, J. *J. Chem. Soc. Dalton Trans.* **2002**, 1769. Lee, D. H.; Im, J. H.; Lee, J. H.; Hong, J. I. *Tetrahedron Lett.* **2002**, *43*, 9637. McFarland, S. A.; Finney, N. S. *J. Am. Chem. Soc.* **2002**, *124*, 1178. McFarland, S. A.; Finney, N. S. *Chem. Commun.* **2003**, 388.
- Maus, M.; Rettig, W.; Bonafoux, D.; Lapouyade, R. *J. Phys. Chem. A* **1999**, *103*, 3388.
- Maus, M.; Rettig, W. *Chem. Phys.* **2000**, *261*, 323.
- Hassan, J.; Sevignon, M.; Gozzi, C.; Schulz, E.; Lemaire, M. *Chem. Rev.* **2002**, *102*, 1359.
- Kumar, S. *J. Chem. Soc. Perkin Trans. 1* **2001**, 1018.
- Murata, M.; Oyama, T.; Watanabe, S.; Masuda, Y. *J. Org. Chem.* **2000**, *65*, 164.
- Demas, J. N.; Crosby, G. A. *J. Phys. Chem.* **1971**, *75*, 991.
- Deranleau, D. A. *J. Am. Chem. Soc.* **1969**, *91*, 4044.
- Maus, M.; Rettig, W. *J. Phys. Chem. A* **2002**, *106*, 2104. Maus, M.; Rettig, W. *Phys. Chem. Chem. Phys.* **2001**, *3*, 5430. Maus, M.; Rettig, W. *Chem. Phys. Lett.* **2000**, *324*, 57. Maus, M.; Rettig, W. *Chem. Phys.* **1997**, *218*, 151.
- Kong, J.; White, C. A.; Krylov, A. I.; Sherrill, C. D.; Adamson, R. D.; Furlani, T. R.; Lee, M. S.; Lee, A. M.; Gwaltney, S. R.; Adams, T. R.; Ochsenfeld, C.; Gilbert, A. T. B.; Kedziora, G. S.; Rassolov, V. A.; Maurice, D. R.; Nair, N.; Shao, Y.; Besley, N. A.; Maslen, P. E.; Dombroski, J. P.; Dachsel, H.; Zhang, W. M.; Korambath, P. P.; Baker, J.; Byrd, E. F. C.; Voorhis, T. V.; Oumi, M.; Hirata, S.; Hsu, C. P.; Ishikawa, N.; Florian, J.; Warshel, A.; Johnson, B. G.; Gill, P. M. W.; Head-Gordon, M.; Pople, J. A. *Q-Chem*; 2.0 ed.; Q-Chem Inc.: PA, 2000.



# Ratiometric dual fluorescent receptors for anions under intramolecular charge transfer mechanism

Zhen-Chang Wen and Yun-Bao Jiang\*

Department of Chemistry and the MOE Key Laboratory of Analytical Sciences, Xiamen University, Xiamen 361005, China

Received 29 January 2004; revised 5 July 2004; accepted 19 August 2004

Available online 15 September 2004

**Abstract**—A series of the intramolecular charge transfer (ICT) dual fluorescent receptors with anion binding site in the electron acceptor were designed and synthesized. These receptors exhibited dual fluorescence in acetonitrile and the charge transfer (CT) emission energy was found to correlate linearly with the Hammett constant of the substituent existing in the electron acceptor, which is the basis for anion sensing. Dual fluorescence of these receptors was found to be sensitive to the presence of anions such as fluoride and acetate and the receptors can be employed as ratiometric fluorescent sensors for anions.

© 2004 Elsevier Ltd. All rights reserved.

## 1. Introduction

Anion recognition and sensing have received increasing recent attention in supramolecular, organic and inorganic chemistry.<sup>1</sup> Because of the high sensitivity of fluorescence detection, many fluorescent receptors for anions have been developed. Similar to a cation fluorescent receptor,<sup>2</sup> an anion receptor includes two important moieties, i.e. a recognition binding site and a signal reporter that are either integrated directly or connected by a flexible spacer. A major fluorescent signaling mechanism hitherto employed is photo-induced electron transfer,<sup>3</sup> while other mechanisms such as competitive binding,<sup>4</sup> metal-to-ligand charge transfer,<sup>5</sup> excimer or exciplex formation,<sup>6</sup> excited-state proton transfer (ESPT)<sup>7</sup> and proton coupled electron transfer (PCET)<sup>8</sup> have also been reported.

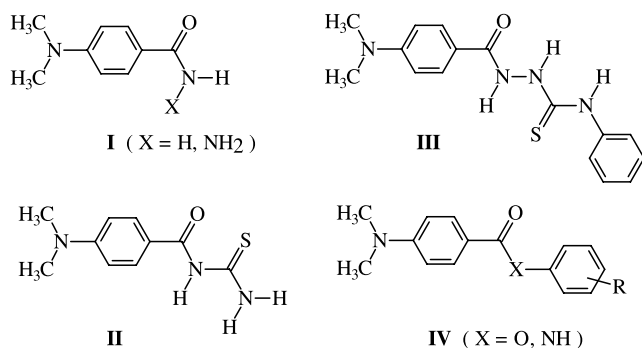
It is known that the ICT photophysics and emission are highly dependent of the electron donor/acceptor strength and in many cases dual fluorescence can be observed with the ICT fluorophores.<sup>9</sup> This suggests that a sensitive ratiometric dual fluorescent anion receptor could be constructed if the dual fluorescent ICT fluorophore is appropriately linked to an anion-binding site. This is significant for a fluorescent sensor since normal fluorescent sensing based on intensity change suffers from the excitation source fluctuation as the emission intensity is

proportional to the excitation intensity. It should be pointed out that receptors operating under the ICT signaling mechanism for cation sensing, either single<sup>2,10</sup> or dual fluorescent,<sup>11</sup> have been exploited, whereas received much less attention in anion sensing.<sup>8</sup>

We understand that a ratiometric ICT dual fluorescent anion receptor relies heavily on the choice of a spacer that links the ICT fluorophore and the anion binding site to allow for a highly efficient communication of the anion binding messages to the fluorophore. As with the ICT fluorophore the photophysics and emission of the CT state are subject to the electron donor/acceptor strength, the anion binding site is assumed to be better incorporated in either electron donor or acceptor moiety. We have been investigating to employ the ICT photophysics of *p*-dimethylaminobenzonitrile (DMABN) and its family molecules in constructing anion receptors. We showed that, with *p*-dimethylaminobenzamide (**I**, Scheme 1),<sup>8a</sup> *N*-(*p*-dimethylaminobenzoyl)thiourea (**II**, Scheme 1),<sup>8b</sup> and *N*-(*p*-dimethylaminobenzamido)thiourea (**III**, Scheme 1)<sup>8c</sup> in which the anion binding sites incorporated in the electron acceptors are amide and thiourea, respectively, their ICT dual fluorescence was sensitive to the presence of anions such as AcO<sup>-</sup>, F<sup>-</sup>, and H<sub>2</sub>PO<sub>4</sub><sup>-</sup> etc. In those cases, however, the CT emission band position showed essentially no shift upon anion binding. This might suggest that the sensing is not due to the variation in the electron accepting strength of the acceptor. We therefore continue to search for ICT dual fluorescent receptors that respond to anions due to variations of the electron donor/acceptor strength as would be indicated by shifted CT emission upon anion binding. Previously we

**Keywords:** Receptor; Anion sensing; Thiourea; Intramolecular charge transfer; Dual fluorescence; Ratiometric.

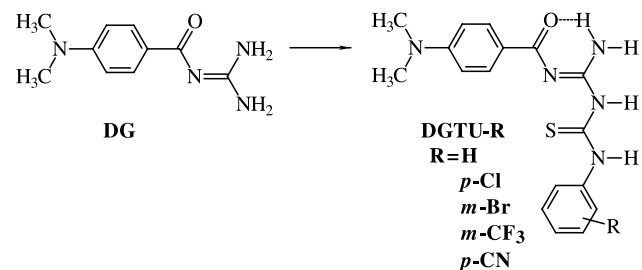
\* Corresponding author. Tel./fax: +86-592-2185662;  
e-mail: ybjiang@xmu.edu.cn



**Scheme 1.** Molecular structures of *p*-dimethylaminobenzamide and *p*-dimethylaminobenzoate derivatives.

showed that, with substituted phenyl *p*-dimethylaminobenzoates (**IV**, X=O, **Scheme 1**)<sup>12a</sup> and *p*-dimethylaminobenzalinides (**IV**, X=NH, **Scheme 1**)<sup>12c</sup> the CT fluorescence depends on the substituent at the ester and amido phenyl moieties, respectively. In the former case a linear correlation was found between the CT emission energy and the Hammett constant of the substituent but the dependence was weak in particular in highly polar solvent, whereas in the latter case an additional benzalide-like CT channel complicated the charge transfer photophysics. These results, however, suggested that new ICT dual fluorescent receptors for anions could be constructed within this framework.

We therefore, came to **DGTU-Rs** (**Scheme 2**) in which the *p*-dimethylaminobenzamide moiety is the ICT fluorophore with dual fluorescence emission while the thiourea moiety is a well-known anion binding site. These two parts are conjugated by an iminoyl group, hopefully to enhance the substituent (R) effect than in their ester counterparts (**IV**, X=O, **Scheme 1**). Substituent was introduced in the phenylthiourea moiety of **DGTU-R** for the purposes of understanding the sensing mechanism and modulating the acidity of the thioureido –NH protons<sup>3c,d</sup> important for anion binding.



**Scheme 2.** Synthesis of **DGTU-Rs**. Reagents and conditions: substituted isothiocyanate, CH<sub>2</sub>Cl<sub>2</sub>, room temperature.

## 2. Results and discussion

**DGTU-Rs** were easily prepared from the reactions of **DG** with isothiocyanates at room temperature (**Scheme 2**), while **DG** was obtained according the reported method.<sup>13</sup> It was expected that in **DGTU-Rs** with an iminoyl linker the thiourea anion-binding site was electronically conjugated to the ICT fluorophore, *p*-dimethylaminobenzamide. Substituent effect on the NMR signals of the four –NH protons in

**DGTU-Rs** was examined and linear correlations were found with varied slopes, **Figure 1**. It was found that with three of the –NH protons the NMR signals were correlated with Hammett substituent constant<sup>14</sup> with positive slopes of 0.311, 0.401, and 0.538, respectively. The NMR signal of the fourth –NH proton, however, appeared at far downfield and showed a negative linear dependence of the Hammett substituent constant by a slope of –0.388. These observations suggested a completely different electronic environment of this –NH proton that it is involved in an intramolecular six-membered ring hydrogen bond<sup>15</sup> (**Scheme 2**). This was also supported by the AM1 calculations. This negative yet sensitive dependence of the chemical shift indicated that the substituent effect could indeed be communicated into the carbonyl oxygen atom, meaning that the thiourea moiety is conjugated with the ICT fluorophore, the dual fluorescence signal reporter in the anion receptors.

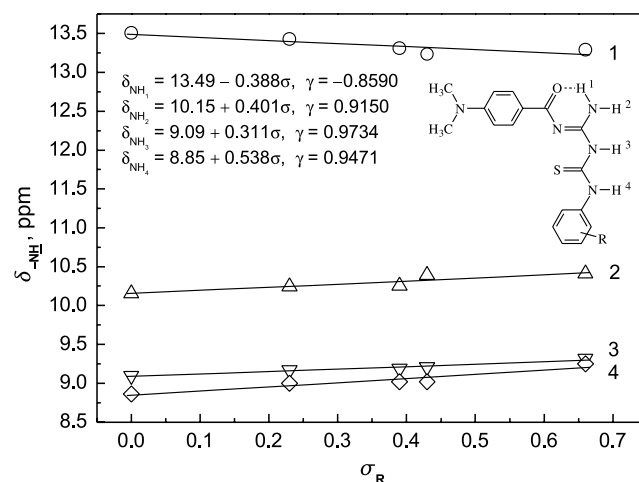


**Figure 1.** Plots of –NH proton chemical shifts against Hammett constants of the substituent,  $\sigma_R$ .<sup>14</sup>

The absorption and fluorescence spectra of **DGTU-Rs** were recorded. It was found that the absorption spectra were independent of the substituent within the series with maximum wavelength of 344 nm and molar absorption coefficients of  $10^4 \text{ M}^{-1} \text{ cm}^{-1}$  order of magnitude (**Table 1**). The transitions responsible for the absorption could then be assigned as of the ( $\pi, \pi^*$ ) character. Dual fluorescence typical of the occurrence of the ICT with electron donor/acceptor *para*-substituted benzenes, such as *p*-dimethylaminobenzonitrile<sup>9</sup> and *p*-dimethylamino-benzamide,<sup>8a</sup> was observed with all of the **DGTU-Rs** in highly polar solvents such as acetonitrile. As an example, fluorescence spectra of **DGTU-*m*-CF<sub>3</sub>** in ethyl acetate–acetonitrile binary solvents are shown in **Figure 2**. It was noted that, while the short-wavelength LE (locally excited state) emission showed very weak dependence on the solvent composition, a continuous red-shift occurred in the long-wavelength emission with increasing solvent polarity, which is in line of the CT nature of its emissive state. Similar observations were made with other **DGTU-Rs** and detailed spectral parameters are summarized in **Table 1**.

Different from the absorption spectra of the **DGTU-R**

**Table 1.** Absorption and fluorescence spectral parameters of **DGTU-Rs** in acetonitrile in the absence and presence of anions

R	$\lambda_{\text{abs}}^{\text{max}}$ (nm)	$\epsilon$ ( $10^4 \text{ M}^{-1} \text{ cm}^{-1}$ )	$\lambda_{\text{LE}}$ (nm)	$\lambda_{\text{CT}}$ (nm)	$I_{\text{CT}}/I_{\text{LE}}$	$\Phi$
H	344/326 <sup>a</sup> /336 <sup>b</sup>	3.47/4.28 <sup>a</sup> /3.40 <sup>b</sup>	385/385 <sup>a</sup> /385 <sup>b</sup>	507/501 <sup>a</sup> /501 <sup>b</sup>	0.43/0.04 <sup>a</sup> /0.34 <sup>b</sup>	0.0051
<i>p</i> -Cl	344/329/339	4.18/5.00/4.23	388/388/388	516/510/514	1.03/0.05/0.69	0.0045
<i>m</i> -Br	344/327/336	3.39/4.44/3.45	388/388/388	526/516/522	2.62/0.08/1.26	0.0031
<i>m</i> -CF <sub>3</sub>	344/327/329	3.47/4.54/4.12	388/388/388	530/520/524	1.31/0.04/0.29	0.0026
<i>p</i> -CN	344/330/332	3.74/4.39/4.12	385/385/385	550/524/535	0.85/0.07/0.20	0.0021

<sup>a</sup> In the presence of fluoride anion.

<sup>b</sup> In the presence of acetate anion.

series, the fluorescence emission in particular the long-wavelength CT emission showed a sensitive dependence on the substituent at thiourea moiety. As can be seen in Figure 3a, the CT emission of **DGTU-R** in acetonitrile shifted to the red when the substituent (R) became increasingly electron-withdrawing from H to *p*-CN, which is in the same trend as that observed with substituted-phenyl *p*-dimethylaminobenzoates.<sup>12a</sup> This observation also confirms that the substituent is located in the electron acceptor moiety.

We previously established<sup>12</sup> that, in case of a series of CT fluorophores of similar structure and practically the same absorption spectra, the CT emission energy correlated linearly with the Hammett constant of the substituent existing in the electron donor/acceptor. Obviously these criteria were fulfilled with the **DGTU-R** series. As seen in Figure 3b, a linear correlation indeed existed between the CT emission energies of **DGTU-Rs** and the Hammett substituent constants. This indicated that the electron acceptor strength was monotonically enhanced with increasing electron-withdrawing ability of the substituent in the phenylthiourea moiety. The slope in acetonitrile of  $-0.273 \text{ eV}$  was much higher in its absolute value than those observed with substituted-phenyl *p*-dimethylaminobenzoates in solvents of much lower polarity, for example,  $-0.180$ ,  $-0.169$ , and  $-0.138 \text{ eV}$  in DEE, THF, and ethyl acetate, respectively.<sup>12a</sup> This means that a higher substituent effect on the CT emission occurs with **DGTU-Rs** than that in their ester counterparts. This can be readily ascribed to the higher conjugating efficiency of the iminoyl linker in comparison with the oxygen bridge ( $-\text{O}-$ ) present in the ester molecules.<sup>12a</sup> Also noted in Table 1 and Figure 3a was that the CT to LE intensity ratio ( $I_{\text{CT}}/I_{\text{LE}}$ ) became lower in

case of lower electron acceptor strength. It was therefore expected that sensitive receptors for anions could be achieved based on the dual fluorescent **DGTU-Rs**, since it has been shown that anion binding to the thiourea moiety increases its electron donating ability<sup>3c,d</sup> which will consequently decrease the strength of electron acceptors in these dual fluorescent receptors.

The ICT dual fluorescence of all **DGTU-Rs** was found to be sensitive to the presence of anions such as  $\text{F}^-$  and  $\text{AcO}^-$ , to extents depending on the substituent R. Figure 4a shows the fluorescence spectra of **DGTU-*m*-CF<sub>3</sub>** in ACN in the presence of  $\text{F}^-$ . It was found that addition of  $\text{F}^-$  resulted in a substantial quenching of the long-wavelength CT emission and an obvious blue shift in its band position, for instance, from 530 to 520 nm in the presence of 3 equiv of  $\text{F}^-$ . Meanwhile, only small changes were observed in the LE emission in both its position and intensity. An isoemissive point at 425 nm was noted, which means that

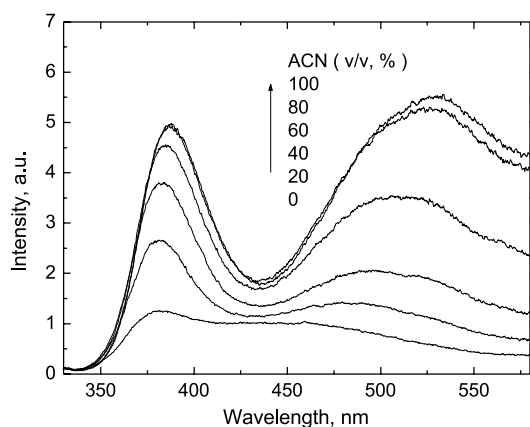


**Figure 2.** Fluorescence spectra of **DGTU-*m*-CF<sub>3</sub>** in ethyl acetate-acetonitrile binary solvents. Excitation wavelength was 298 nm. [**DGTU-*m*-CF<sub>3</sub>**] =  $2.0 \times 10^{-5} \text{ M}$ .

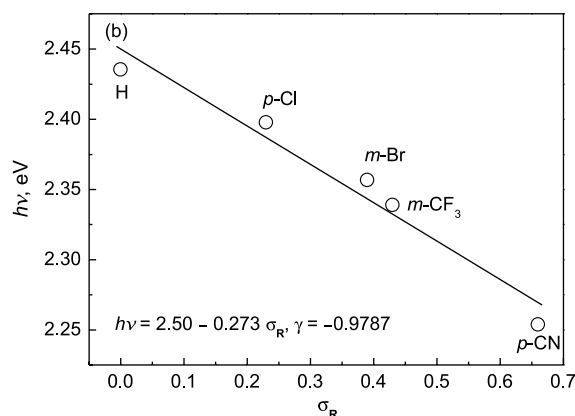
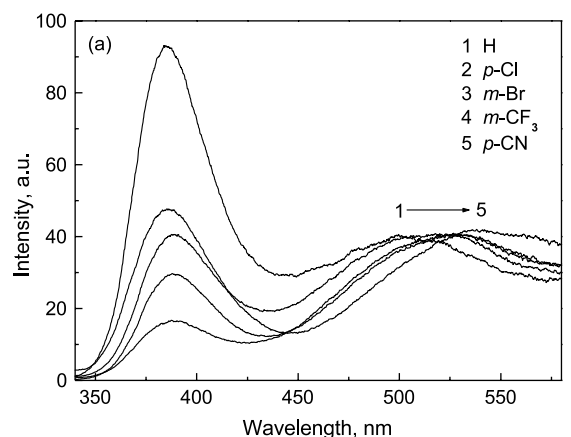


**Figure 3.** (a) The CT-emission normalized fluorescence spectra of **DGTU-Rs** in acetonitrile with excitation wavelength of 298 nm and (b) plot of the CT emission energy against Hammett substituent constant.

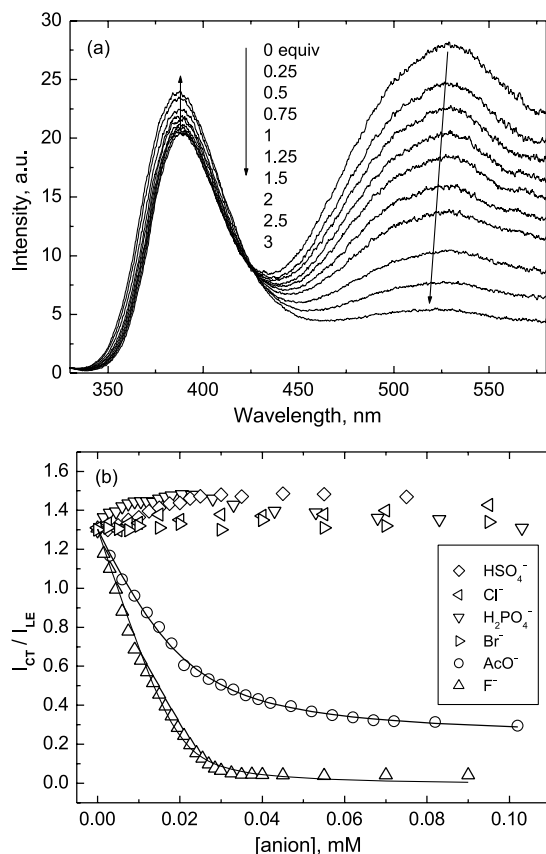
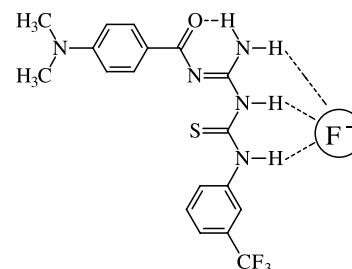


**Figure 4.** (a) Fluorescence spectra of **DGTU-*m*-CF<sub>3</sub>** in ACN ( $2.0 \times 10^{-5}$  M) in the presence of  $F^-$  with excitation wavelength of 298 nm, an isosbestic wavelength, and (b) plot of the  $I_{CT}/I_{LE}$  ratio versus anion concentration. Data points in (b) are experimental results and the lines through them are nonlinearly fitted curves.

the excited-state LE to CT reaction equilibrium was shifted upon anion binding. Similar variation but to a less extent was observed when  $AcO^-$  was introduced, whereas other anions such as  $H_2PO_4^-$ ,  $HSO_4^-$ ,  $Cl^-$  and  $Br^-$  led to much less change or no change in the fluorescence spectrum of **DGTU-*m*-CF<sub>3</sub>**. Within **DGTU-R** series there are four  $-NH$  proton donors, of which the one with its NMR signal appears at far downfield of around 13.2 ppm is involved in an intramolecular hydrogen bond with the carbonyl oxygen<sup>15</sup> (Fig. 1 and Scheme 2). There are hence three  $-NH$  protons in **DGTU-Rs** available for hydrogen bonding with anions. Inspection of the structure of the receptors it can be supposed that **DGTU-Rs** may bind anions via two thioureido  $-NH$  protons and/or two guanidino  $-NH$  protons.<sup>3c,d,8,13,16</sup> Control molecule **DG** (Scheme 2) that has only guanidino  $-NH$  protons, however, showed not any response to anion in both its absorption and fluorescence spectra. It was therefore assumed that **DGTU-Rs** bind anions such as  $F^-$  via two thioureido  $-NH$  protons with additional contribution from the other free guanidino  $-NH$  proton (Scheme 3). Job plot (Fig. 5) supported this by confirming a 1:1 stoichiometry between **DGTU-*m*-CF<sub>3</sub>** and  $F^-$ . Further evidence for this binding was obtained from <sup>1</sup>H NMR data. In  $DMSO-d_6$ , the NMR signals of thioureido  $-NH$  protons in **DGTU-*m*-CF<sub>3</sub>**, originally appeared at 9.020 and 9.209 ppm, were shifted and broadened in the presence of 0.25 equiv of  $AcO^-$  to appear as a broad band peaked at 9.201 ppm, whereas those of the guanidino  $-NH$



**Scheme 3.** Schematic diagram for the binding of **DGTU-*m*-CF<sub>3</sub>** with  $F^-$ .

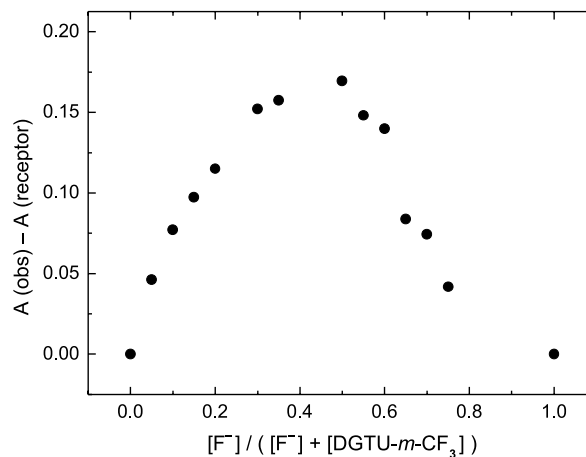


**Figure 5.** Job plot for binding of  $F^-$  to **DGTU-*m*-CF<sub>3</sub>** in acetonitrile.  $A(\text{obs})$  and  $A(\text{receptor})$  are absorbances at 327 nm of the anion/receptor mixture and receptor, respectively. The total concentration of  $F^-$  and **DGTU-*m*-CF<sub>3</sub>** is  $4.0 \times 10^{-5}$  M.

protons experienced much less changes. Variation in the absorption spectra confirmed the formation of well-defined binding complexes between receptors and anions. Figure 6a shows the absorption spectra of **DGTU-*m*-CF<sub>3</sub>** in acetonitrile in the presence of  $F^-$ . The absorption spectrum of **DGTU-*m*-CF<sub>3</sub>**, originally peaked at 344 nm, was blue shifted to 327 nm with increasing  $F^-$  concentration, which was accompanied by the appearance of three distinct isosbestic points at 336, 298, and 277 nm, respectively.

The fluorescence response observed here can be accounted for under the ICT mechanism that the CT photophysics and emission are highly subject to the electron donor/acceptor strength.<sup>9,11,12</sup> In Figure 3 it is shown that with **DGTU-Rs** a decrease in the electron acceptor strength results in a blue shift in the CT emission and a lowered CT to LE intensity ratio. Indeed, anion binding to the thioureido moiety in the electron acceptor of **DGTU-Rs** led to a blue shift in the CT emission and a decrease in the CT to LE intensity ratio (Table 1 and Fig. 4). Accordingly, the CT to LE intensity ratio of the **DGTU-R-*F*<sup>-</sup>** complex was found lower than that of the **DGTU-R-*AcO*<sup>-</sup>** complex (Table 1), which is obviously due to the higher charge density of  $F^-$  because of its smaller size.

Sensing of anions such as  $AcO^-$ ,  $F^-$ ,  $H_2PO_4^-$ ,  $HSO_4^-$ ,  $Br^-$ , and  $Cl^-$  using **DGTU-R** receptors was then examined via both the ICT dual fluorescence intensity ratio and absorption titrations. Figures 4b and 6b show the titration curves of the spectral parameters of **DGTU-*m*-CF<sub>3</sub>** against anion



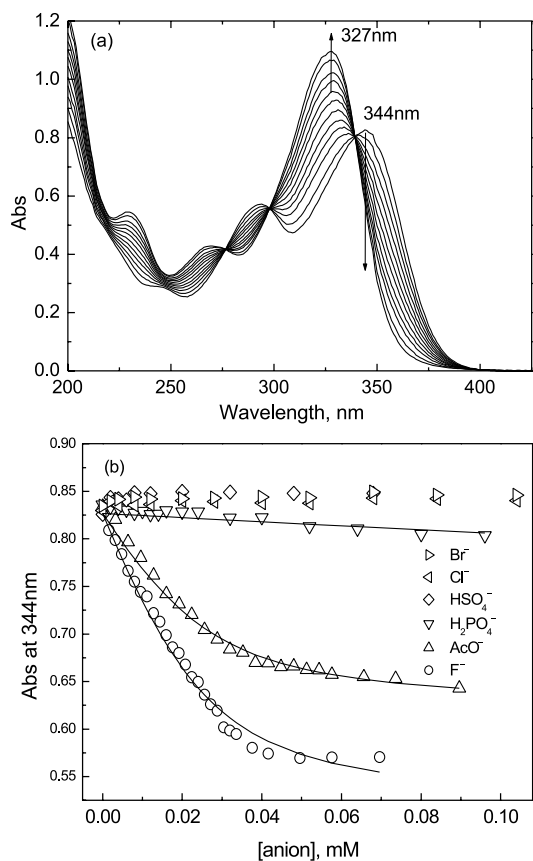


**Figure 6.** (a) Trace of absorption spectra of **DGTU-*m*-CF<sub>3</sub>** in ACN ( $2.4 \times 10^{-5}$  M) upon addition of increasing concentration of F<sup>-</sup> and (b) plot of the absorbance at 344 nm versus anion concentration. Data points in (b) are experimental results and the lines through them are nonlinearly fitted curves.

concentrations in acetonitrile. Sensitive and selective sensing of anions can be achieved with this receptor. With other receptors anion sensing was also possible. The anion binding constants of **DGTU-Rs** were evaluated by nonlinear fitting of the plots of the CT to LE intensity ratio and the absorbance at 344 nm of the receptor against anion concentration,<sup>7c,8c,17</sup> assuming a 1:1 stoichiometry. The latter was confirmed by the nice fitting shown in **Figures 4b and 6b** as examples. The obtained binding constants are listed in **Table 2**. The binding constants ranging from  $10^4$  to  $10^6$  M<sup>-1</sup> varied in general in the order of F<sup>-</sup> > AcO<sup>-</sup> > H<sub>2</sub>PO<sub>4</sub><sup>-</sup> ≫ HSO<sub>4</sub><sup>-</sup>, Br<sup>-</sup>, Cl<sup>-</sup>, in agreement with that observed with other neutral thiourea-based receptors.<sup>3c,d,8b-d</sup> With the same anion, the binding constants varied in the order of **DGTU** < **DGTU-*p*-Cl** < **DGTU-*m*-Br** < **DGTU-*p*-CF<sub>3</sub>** < **DGTU-*p*-CN**, as

expected from the increasing acidity of the thioureido -NH protons.

### 3. Conclusion

In summary, we developed a series of the ICT dual fluorescent anion receptors in which the phenylthiourea anion-binding site was electronically conjugated via an iminoyl linker to the electron acceptor moiety of the CT fluorophore *p*-dimethylaminobenzamide. With the aid of substitution at the phenylthiourea moiety it was established that the substituent electronic effect could be efficiently transmitted to the CT fluorophore and hence influenced its CT dual fluorescence. This formed the basis of anion sensing by these receptors. The anion sensing was signaled by a blue shift in the CT emission and by a decrease in the CT to LE intensity ratio. The CT dual fluorescent receptors (**I–III**, **Scheme 1**) previously reported from this group responded anions with decreases in the CT to LE intensity ratio, but no shift in both the CT and LE band positions.<sup>8</sup> The present receptors therefore represent, to the best of our knowledge, the first set of ratiometric CT dual fluorescent anion receptors with emissive CT state that sense anions due to variations in the electron acceptor strength. The ICT signaling mechanism outlined here could be applicable for extended investigations of optimal combinations of the CT fluorophore, anion-binding site, and conjugating linker between them.

### 4. Experimental

#### 4.1. Materials

Solvents employed in organic syntheses were market available AR reagents. Solvents used for spectral study were of spectroscopic grade and were further purified before use so that no fluorescent impurity was detected at the employed excitation wavelength of 298 nm. Tetra(*n*-butyl) ammonium salts of anions were prepared by neutralizing the corresponding acids by tetra(*n*-butyl)ammonium hydroxide. DG was synthesized according to a reported method<sup>13</sup> and it further reacted with substituted phenylisothiocyanate in CH<sub>2</sub>Cl<sub>2</sub> at room temperature afforded individual receptor, **DGTU-R** (**Scheme 1**). The crude products were purified on silica-gel column chromatography using petroleum ether (m.p.60–90 °C) and ethyl acetate mixture (2:1, v/v) as eluent and the purified products were fully characterized. <sup>1</sup>H

**Table 2.** Binding constants ( $K_b$ ) of anions with **DGTU-Rs** in acetonitrile from absorption (344 nm) and fluorescence ( $I_{CT}/I_{LE}$ ) titrations<sup>a</sup>

R	$K_b$ (abs), $10^5$ M <sup>-1b</sup>		$K_b$ (flu), $10^5$ M <sup>-1c</sup>	
	F <sup>-</sup>	AcO <sup>-</sup>	F <sup>-</sup>	AcO <sup>-</sup>
H	0.12 ± 0.02	nd <sup>d</sup>	0.22 ± 0.03	nd <sup>d</sup>
<i>p</i> -Cl	0.18 ± 0.03	nd <sup>d</sup>	0.40 ± 0.04	nd <sup>d</sup>
<i>m</i> -Br	0.24 ± 0.03	nd <sup>d</sup>	4.73 ± 0.55	1.33 ± 0.11
<i>m</i> -CF <sub>3</sub>	1.47 ± 0.32	1.58 ± 0.14	9.74 ± 1.57	1.95 ± 0.36
<i>p</i> -CN	25.8 ± 7.1	3.60 ± 0.80	16.8 ± 5.2	8.41 ± 1.55

<sup>a</sup> Anions exist in their tetrabutylammonium salts.

<sup>b</sup> Binding constant obtained from absorption titration.

<sup>c</sup> Binding constant obtained from fluorescence titration.

<sup>d</sup> Not determined because of minor spectral change that did not allow for an accurate evaluation of the binding constant. This was also the case with other anions examined such as H<sub>2</sub>PO<sub>4</sub><sup>-</sup>, HSO<sub>4</sub><sup>-</sup>, Br<sup>-</sup>, and Cl<sup>-</sup>.



(500 MHz) and  $^{13}\text{C}$  (125 MHz) NMR data were acquired in DMSO- $d_6$  on a Varian Unity<sup>+</sup> 500 MHz NMR spectrometer using TMS as the internal reference. ESI-MS data were obtained on a Bruker ESQUIRE-3000plus LC-MS/MS spectrometer and HRMS data obtained on a Micromass LCT time-of-flight mass spectrometer configured with a standard Z-spray electrospray interface.

**4.1.1. DGTU.**  $^1\text{H}$  NMR,  $\delta$  (ppm): 3.036 (6H, s), 6.818 (2H, d,  $J=9$  Hz), 7.045 (1H, s), 7.272 (2H, s), 7.679 (2H, s), 7.925 (2H, d,  $J=9$  Hz), 8.863 (1H, s, NH), 9.099 (1H, s, NH), 10.156 (1H, s, NH), 13.507 (1H, s, NH).  $^{13}\text{C}$  NMR,  $\delta$  (ppm): 39.985, 111.087, 117.557, 121.903, 123.295, 123.935, 128.209, 129.893, 139.751, 153.545, 157.029, 167.085. ESI-MS:  $m/z$  342.0 ( $\text{M}+\text{H}^+$ , MeOH). HRMS found:  $m/z$  342.1387; calcd for  $[\text{C}_{17}\text{H}_{20}\text{N}_5\text{OS}^+]$ : 342.1389.

**4.1.2. DGTU-*p*-Cl.**  $^1\text{H}$  NMR,  $\delta$  (ppm): 3.038 (6H, s), 6.820 (2H, d,  $J=8.5$  Hz), 7.295 (2H, d,  $J=6.5$  Hz), 7.748 (2H, d,  $J=9$  Hz), 7.929 (2H, d,  $J=8$  Hz), 8.997 (1H, s, NH), 9.169 (1H, s, NH), 10.245 (1H, s, NH), 13.426 (1H, s, NH).  $^{13}\text{C}$  NMR,  $\delta$  (ppm): 40.009, 111.081, 117.492, 123.366, 125.749, 126.815, 128.019, 129.919, 138.678, 153.564, 157.264, 167.108. ESI-MS:  $m/z$  375.9 ( $\text{M}+\text{H}^+$ , MeOH). HRMS found:  $m/z$  376.0999; calcd for  $[\text{C}_{17}\text{H}_{19}\text{ClN}_5\text{OS}^+]$ : 376.0999.

**4.1.3. DGTU-*m*-Br.**  $^1\text{H}$  NMR,  $\delta$  (ppm): 3.041 (6H, s), 6.844 (2H, d,  $J=9$  Hz), 7.221 (2H, s), 7.828 (2H, s), 7.928 (2H, d,  $J=8$  Hz), 9.020 (1H, s, NH), 9.188 (1H, s, NH), 10.254 (1H, s, NH), 13.311 (1H, s, NH).  $^{13}\text{C}$  NMR,  $\delta$  (ppm): 39.997, 111.090, 117.475, 121.012, 123.873, 125.886, 129.949, 130.214, 141.277, 153.572, 157.337, 167.125. ESI-MS:  $m/z$  421.8 ( $\text{M}+\text{H}^+$ , MeOH). HRMS found:  $m/z$  420.0490; calcd for  $[\text{C}_{17}\text{H}_{19}\text{BrN}_5\text{OS}^+]$ : 420.0494.

**4.1.4. DGTU-*m*-CF<sub>3</sub>.**  $^1\text{H}$  NMR,  $\delta$  (ppm): 3.040 (6H, s), 6.820 (2H, d,  $J=8.5$  Hz), 7.369 (1H, s), 7.495 (H, d,  $J=7.5$  Hz), 7.918 (1H, s), 7.934 (2H, d,  $J=9$  Hz), 8.164 (1H, s), 9.020 (1H, s, NH), 9.209 (1H, s, NH), 10.392 (1H, s, NH), 13.233 (1H, s, NH).  $^{13}\text{C}$  NMR,  $\delta$  (ppm): 40.002, 111.053, 111.095, 117.445, 123.042, 125.205, 128.837, 129.433, 129.918, 140.322, 153.568, 157.364, 167.109. ESI-MS:  $m/z$  409.9 ( $\text{M}+\text{H}^+$ , MeOH). HRMS found:  $m/z$  410.1265; calcd for  $[\text{C}_{18}\text{H}_{19}\text{F}_3\text{N}_5\text{OS}^+]$ : 410.1262.

**4.1.5. DGTU-*p*-CN.**  $^1\text{H}$  NMR,  $\delta$  (ppm): 3.043 (6H, s), 6.826 (2H, d,  $J=9.5$  Hz), 7.684 (2H, d,  $J=8.5$  Hz), 7.926 (2H, d,  $J=9$  Hz), 8.005 (2H, d,  $J=8.5$  Hz), 9.250 (1H, s, NH), 9.315 (1H, s, NH), 10.441 (1H, s, NH), 13.290 (1H, s, NH).  $^{13}\text{C}$  NMR,  $\delta$  (ppm): 40.002, 111.058, 117.352, 118.788, 119.236, 121.420, 123.788, 129.949, 132.587, 143.655, 153.591, 157.932, 167.156. ESI-MS:  $m/z$  366.9 ( $\text{M}+\text{H}^+$ , MeOH). HRMS found:  $m/z$  367.1338; calcd for  $[\text{C}_{18}\text{H}_{19}\text{N}_6\text{OS}^+]$ : 367.1341.

## 4.2. Absorption and fluorescence spectral studies

The absorption and fluorescence spectra were recorded on Varian Cary 300 absorption spectrophotometer and Hitachi F-4500 fluorescence spectrophotometer, respectively. Solutions were measured in 1-cm quartz cell. The solvent employed for spectral titrations was acetonitrile (ACN).

Fluorescence quantum yields were measured using quinine sulfate as a standard (0.546 in 0.5 M  $\text{H}_2\text{SO}_4$ ).<sup>18</sup>

Spectral titrations were carried out by introducing aliquot of anion solution into the receptor solution of fixed concentration.

## 4.3. Determination of anion-receptor binding constants

The binding constants of anions with receptors were evaluated by nonlinearly fitting both the variations of the absorbance at 344 nm and the CT to LE fluorescence intensity ratio of the receptors against anion concentration, assuming a 1:1 binding stoichiometry.

## Acknowledgements

This work was supported by the Natural Science Foundation of China (20175020), the Ministry of Education (MOE) of China, the Natural Science Foundation of Fujian Province (D0220001), and VolkswagenStiftung (I/77 072). We thank Professor E. V. Anslyn for his kind invitation of this contribution.

## References and notes

- (a) Schmidtchen, F. P.; Berger, M. *Chem. Rev.* **1997**, *97*, 1609–1646. (b) Snowden, T. S.; Anslyn, E. V. *Curr. Opin. Chem. Biol.* **1999**, *3*, 740–746. (c) Gale, P. A. *Coord. Chem. Rev.* **2000**, *199*, 181–233. (d) Beer, P. D.; Gale, P. A. *Angew. Chem., Int. Ed.* **2001**, *40*, 486–516. (e) Gale, P. A. *Coord. Chem. Rev.* **2001**, *213*, 79–128. (f) Sessler, J. L.; Davis, J. M. *Acc. Chem. Res.* **2001**, *34*, 989–997. (g) Martínez-Máñez, R.; Sancenón, F. *Chem. Rev.* **2003**, *103*, 4419–4476.
- (a) de Silva, A. P.; Gunaratne, H. Q. N.; Gunnlaugsson, T.; Huxley, A. J. M.; McCoy, C. P.; Rademacher, J. T.; Rice, T. E. *Chem. Rev.* **1997**, *97*, 1515–1566. (b) de Silva, A. P.; Fox, D. B.; Huxley, A. J. M.; Moody, T. S. *Coord. Chem. Rev.* **2000**, *205*, 41–57.
- (a) Vance, D. H.; Czarnik, A. W. *J. Am. Chem. Soc.* **1994**, *116*, 9397–9398. (b) Kubo, Y.; Tsukahara, M.; Ishihara, S.; Tokita, S. *Chem. Commun.* **2000**, 653–654. (c) Gunnlaugsson, T.; Davis, A. P.; Glynn, M. *Chem. Commun.* **2001**, 2556–2557. (d) Gunnlaugsson, T.; Davis, A. P.; O'Brien, J. E.; Glynn, M. *Org. Lett.* **2002**, *4*, 2449–2452.
- (a) Niikura, K.; Metzger, A.; Anslyn, E. V. *J. Am. Chem. Soc.* **1998**, *120*, 8533–8534. (b) Metzger, A.; Anslyn, E. V. *Angew. Chem., Int. Ed.* **1998**, *37*, 649–652. (c) Wiskur, S. L.; Ait-Haddou, H.; Anslyn, E. V.; Lavigne, J. J. *Acc. Chem. Res.* **2001**, *34*, 963–972.
- Beer, P. D. *Acc. Chem. Res.* **1998**, *31*, 71–80.
- (a) Nishizawa, S.; Kaneda, H.; Uchida, T.; Teramae, N. *J. Chem. Soc., Perkin Trans. 2* **1998**, 2325–2327. (b) Nishizawa, S.; Kato, Y.; Teramae, N. *J. Am. Chem. Soc.* **1999**, *121*, 9463–9464. (c) Liao, J. H.; Chen, C. T.; Fang, J. M. *Org. Lett.* **2002**, *4*, 561–564.
- (a) Yoshida, H.; Saigo, K.; Hiratani, K. *Chem. Lett.* **2000**, 116–117. (b) Choi, K.; Hamilton, A. D. *Angew. Chem., Int. Ed.* **2001**, *40*, 3912–3915. (c) Zhang, X.; Guo, L.; Wu, F. Y.; Jiang,

- Y. B. *Org. Lett.* **2003**, *5*, 2667–2670. (d) Tong, H.; Zhou, G.; Wang, L.; Jing, X.; Wang, F.; Zhang, J. *Tetrahedron Lett.* **2003**, *44*, 131–134.
8. (a) Wu, F. Y.; Jiang, Y. B. *Chem. Phys. Lett.* **2002**, *355*, 438–444. (b) Wu, F. Y.; Ma, L. H.; Jiang, Y. B. *Anal. Sci.* **2001**, *17*(Suppl.), i801–i803. (c) Wu, F. Y.; Li, Z.; Wen, Z. C.; Zhou, N.; Zhao, Y. F.; Jiang, Y. B. *Org. Lett.* **2002**, *4*, 3203–3205. (d) Wu, F. Y.; Zhang, X.; Jiang, Y. B. *Chem. J. Chinese Univ.* **2003**, *24*, 1990–1992.
9. (a) Rettig, W. *Angew. Chem., Int. Ed. Engl.* **1986**, *25*, 971–988. (b) Rotkiewicz, K.; Grabowski, Z. R.; Rettig, W. *Chem. Rev.* **2003**, *103*, 3899–4031.
10. (a) Rurack, K.; Rettig, W.; Resch-Genger, U. *Chem. Commun.* **2000**, 407–408. (b) Crochet, P.; Malval, J. P.; Lapouyade, R. *Chem. Commun.* **2000**, 289–290.
11. (a) Létard, J. F.; Delmond, S.; Lapouyade, R.; Braun, D.; Rettig, W.; Kreissler, M. *Recl. Trav. Chim. Pays-Bas* **1995**, *114*, 517–527. (b) Collins, G. E.; Choi, L. S.; Callahan, J. H. *J. Am. Chem. Soc.* **1998**, *120*, 1474–1478. (c) Malval, J. P.; Lapouyade, R. *Helv. Chim. Acta* **2001**, *84*, 2439–2451. (d) Malval, J. P.; Lapouyade, R.; Létard, J. F.; Jarry, C. *Photochem. Photobiol. Sci.* **2003**, *2*, 259–266. (e) Wen, Z.-C.; Jiang, Y.-B. *Chin. Chem. Lett.* **2004**, *15*, 551–554.
12. (a) Huang, W.; Zhang, X.; Ma, L. H.; Wang, C. J.; Jiang, Y. B. *Chem. Phys. Lett.* **2002**, *352*, 401–407. (b) Zhang, X.; Sun, X. Y.; Wang, C. J.; Jiang, Y. B. *J. Phys. Chem. A* **2002**, *106*, 5577–5581. (c) Zhang, X.; Wang, C. J.; Liu, L. H.; Jiang, Y. B. *J. Phys. Chem. B* **2002**, *106*, 12432–12440.
13. Hennrich, G.; Sonnenschein, H.; Resch-Genger, U. *Tetrahedron Lett.* **2001**, *42*, 2805–2808.
14. Hansch, C.; Leo, A.; Taft, R. W. *Chem. Rev.* **1991**, *91*, 165–195.
15. (a) Jubian, V.; Dixon, R. P.; Hamilton, A. D. *J. Am. Chem. Soc.* **1992**, *114*, 1120. (b) Cunha, S.; Costa, M. B.; Napolitano, H. B.; Lariucci, C.; Vencato, I. *Tetrahedron* **2001**, *57*, 1671–1675.
16. Schmuck, C. *Chem. Eur. J.* **2000**, *6*, 709–718.
17. Valeur, B.; Pouget, J.; Bourson, J.; Kaschke, M.; Ernsting, N. P. *J. Phys. Chem.* **1992**, *96*, 6545–6549.
18. Demas, J. N.; Crobys, G. A. *J. Phys. Chem.* **1971**, *75*, 991–1024.



# Molecular recognition and indicator-displacement assays for phosphoesters

Tianzhi Zhang and Eric V. Anslyn\*

Department of Chemistry and Biochemistry, 1 Longhorn Way, A5300 The University of Texas, Austin, TX 78712, USA

Received 16 April 2004; revised 21 July 2004; accepted 19 August 2004

Available online 21 September 2004

**Abstract**—The binding affinities of host **1** towards different phosphoesters were studied. An indicator-displacement assay was also performed, which was able to detect the host–guest interactions with a small visual color change. The degree of substitutions of the phosphate, the functionality of the substituents, and the steric bulk of the substituents, all affect the phosphoester affinities with the host molecule.

© 2004 Elsevier Ltd. All rights reserved.

## 1. Introduction

Phosphate esters play a dominant role in the physiology of cells, and hence are essential to many organisms. They are structural and functional elements in DNA, RNA, and their monomeric building blocks. Further, they participate in post-translational signaling in proteins and as a head group in phospholipids.<sup>1,2</sup> Therefore, the design and synthesis of receptors that have high selectivities and affinities for phosphate esters in aqueous media is a current goal of molecular recognition studies. Receptors functionalized with guanidinium groups,<sup>3–8</sup> polyaza groups,<sup>9–27</sup> amides,<sup>28</sup> and ureas (including thiourea)<sup>29–31</sup> have been found to have high affinities towards phosphate esters through multiple hydrogen bonding and ion-pairing interactions. However, most of the previously reported receptors either lack high affinities or have low selectivities towards these guest molecules in aqueous media at neutral pH. To design an effective phosphate ester receptor that would have both high selectivities and high affinities at biological pH in water provides the impetus for the work described herein. As a secondary goal, we demonstrate that an indicator-displacement assay makes for a simple optical technique for detecting phosphoesters.

Our group previously reported the design and synthesis of the  $C_{3v}$  metallo-host molecule **1**.<sup>32–34</sup> Via a combination of electrostatic interactions, hydrogen bonding interactions, coordination bonds, and geometrical complementarity in the

receptor design, the binding properties of the host showed both high affinities and selectivities towards tetrahedral inorganic anions in aqueous solutions at neutral pH (Table 1). Specifically, phosphate and arsenate were the guests of choice.

Herein, we report binding affinities of this receptor towards organic phosphate esters. Indicator-displacement assays gave us a more sensitive analysis technique than direct UV–vis spectral changes of **1** upon phosphoester binding, giving a more sensitive detection limit for determining phosphoester binding constants. Our goal with these studies was to expand the possible targets for **1**, and to determine to what extent phosphoesters would enhance or diminish binding relative to phosphate. Our long term goal is to create specific receptors that can signal mono-phosphorylation events by kinases in biological systems.

## 2. Results and discussions

### 2.1. Synthesis

A synthesis of **1** has been previously reported.<sup>33</sup> However, in the previous route several low yielding steps and difficult chromatographic separations were involved. Due to interest our group has in expanding the capabilities of **1** and future analogous designs, we sought a higher yielding and easier route. We now report such a route (Scheme 1).

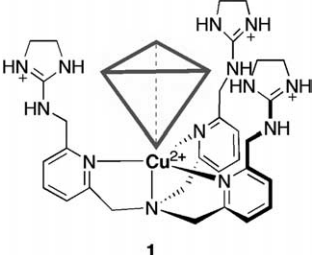
The synthesis of receptor **1** started with commercially available 2,6-dihydroxymethyl pyridine **2**. A  $CH_2Cl_2$  suspension of **2**, silver oxide, and potassium iodide was brought to  $-20\text{ }^\circ\text{C}$ , followed by addition of tosyl chloride as

**Keywords:** Molecular recognition; Phosphoester; Indicator displacement assay.

\* Corresponding author. Tel.: +1-5124710068; fax: +1-5124717791; e-mail: [anslyn@ccwf.utexas.edu](mailto:anslyn@ccwf.utexas.edu)

**Table 1.** Design of host **1**, and previously reported affinity constants in buffered water at pH 7.4

Guests	Binding constants ( $K_a$ ) ( $M^{-1}$ )
$HPO_4^{2-}$	$1.5 \times 10^4$
$HAsO_4^{2-}$	$1.7 \times 10^4$
$ReO_4^-$ , $AcO^-$ , $NO_3^-$ , $HCO_3^-$ , $Cl^-$	< 100

**1**

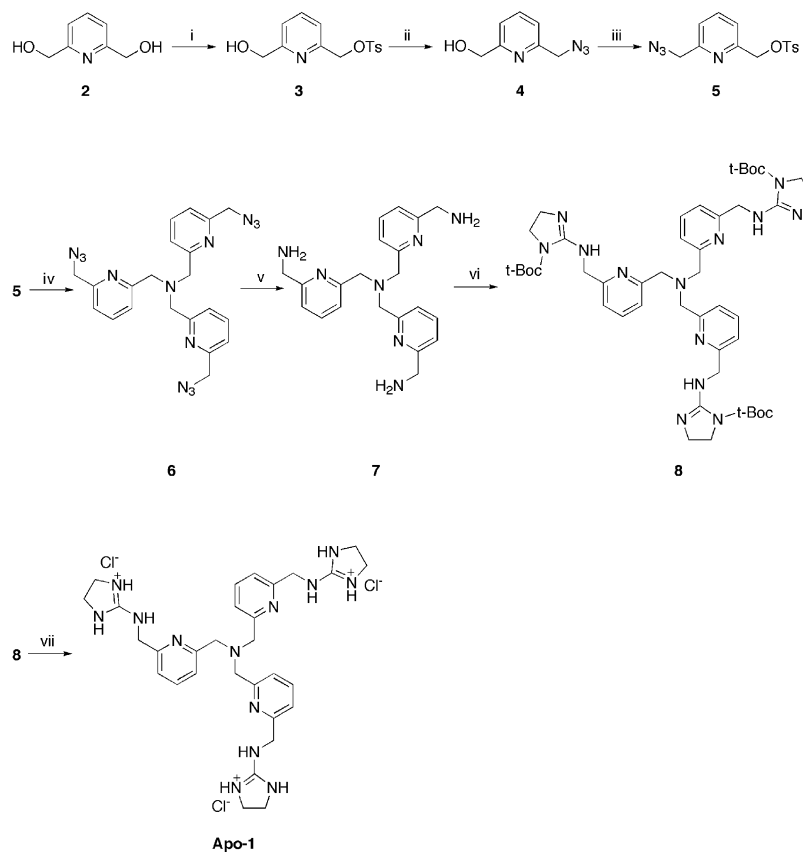
All data were measured at  $[1] = 1.17$  mM.

a solid. The reaction system was slowly warmed to room temperature and stirred for 3 h. The mixture was filtered through a pad of silica gel, and the filtrate was washed with EtOAc.<sup>35</sup> A flash column, first with  $CH_2Cl_2$ , then EtOAc, gave monosubstituted **3** at a 75% yield as a pink solid. To compound **3** was then added  $NaN_3$  in DMF, and the solution was heated at 80 °C for 5 h. A greenish yellow solid of **4** was obtained. The second tosylation was carried out using  $NaOH$ <sup>36</sup> as a base. Compound **5** was obtained as a yellow oil in 93% yield (using the reagents in step (i) gave near a 100% yield).  $Na_2CO_3$  was found to be the better reagent than  $K_2CO_3$  in the amine alkylation step to obtain the pale yellow

oil **6**, in a 72% yield. The rest of the steps were the same as previously reported to afford **apo-1**.<sup>32</sup> The complexation of cupric ion occurred upon addition of 1 equiv of cupric chloride into a water solution of **apo-1**. Compound **1** was then obtained in situ.

## 2.2. Binding studies

Eleven different phosphate esters were studied in pure water solution. Their binding affinities to **1** were monitored by UV–vis absorbance changes (Table 2). UV–vis titration studies were based on the modulations of the cupric ion



**Scheme 1.** New synthetic route to **1**. (i) 1.5 equiv  $Ag_2O$ , 0.1 equiv  $KI$ , 1.1 equiv  $TsCl$ ,  $CH_2Cl_2$ ,  $-20$  °C to rt, 3 h, 75%; (ii)  $NaN_3$ , DMF, 80 °C, 5 h, 100%; (iii)  $NaOH$ ,  $TsCl$ , THF,  $H_2O$ , 0 °C, 4 h, 93%; (iv)  $NH_4OAc$ ,  $Na_2CO_3$ ,  $CH_3CN$ , rt, 2 days, 72%; (v)  $PPh_3$ , THF,  $H_2O$ , rt, 4 h, 70%; (vi) *N*-(*t*-Boc)-2-thiomethyl-2-imidazoline, EtOH, HOAc, 50 °C, 4 h, 45%; (vii) a. TFA,  $CH_2Cl_2$ , rt, 12 h; b.  $Cl^-$  column exchange.

**Table 2.** Association constants obtained by UV-titrations at different temperatures

Guest	$K_a$ ( $1 \times 10^3 \text{ M}^{-1}$ ) 25 °C
<b>9</b>	$5.7 \pm 0.4$
<b>10</b>	$1.0 \pm 0.1$
<b>11</b>	—
<b>12</b>	$2.5 \pm 0.3$
<b>13</b>	$4.5 \pm 0.8$
<b>14</b>	$6.3 \pm 0.8$
<b>15</b>	$2.3 \pm 0.2$
<b>16</b>	$2.1 \pm 0.3$
<b>17</b>	$1.3 \pm 0.2$
<b>18</b>	$4.6 \pm 0.6$
<b>19</b>	$3.9 \pm 0.5$
<b>20</b>	$11.4 \pm 2.9$

All data were measured at  $[1] = 1.92 \text{ mM}$ .

absorptions at 775 nm. Small but reproducible changes in the molar absorptivities of the host were observed for all the phosphate esters due to modulations of the d–d forbidden transitions. All phosphate esters showed distinct 1:1 binding curves (see Fig. 1 for one example).

Clear trends are evident in Table 2 indicating the differences in the ability of **1** to bind various phosphoesters. We first examined 4-nitrophenyl phosphate esters. Unsubstituted inorganic phosphate **9** binds the strongest, whereas 4-nitrophenyl phosphate **10** shows reduced binding.

Phosphodiesters, such as bis(4-nitrophenyl) phosphate **11** show no evidence of binding.

These differences were attributed to three possible effects. One is the lower charge on a phosphomonoester than with phosphate, and even a further decrease in charge with a diester. A second effect derives from the electron withdrawing nature of nitrophenyl ring, which further reduces the charge density on the phosphate group itself. A third possible effect derives from sterics between the host and the guest. The phenyl rings on the 4-nitrophenyl esters might not fit into the cavity of the host, and hence lower the association constant. We probed these various issues by examining parent phenyl groups, alkyl phosphoesters, and primary and secondary alkyl groups.

Monosubstituted phenyl phosphate **12** showed stronger binding than monosubstituted 4-nitrophenyl phosphate **10**. Therefore, the strong electron withdrawing nitro group on the *para* position of **10** did indeed lower the electron density on the phosphate oxygen, thus weakening the ion-pairing driven association with **1**.

To examine alkyl phosphoesters, a handful of biologically relevant phosphate monoesters were studied. The binding affinities of D-glucose 6-phosphate and adenosine 5'-monophosphate were particularly interesting. Importantly, these primary phosphate esters showed almost as strong

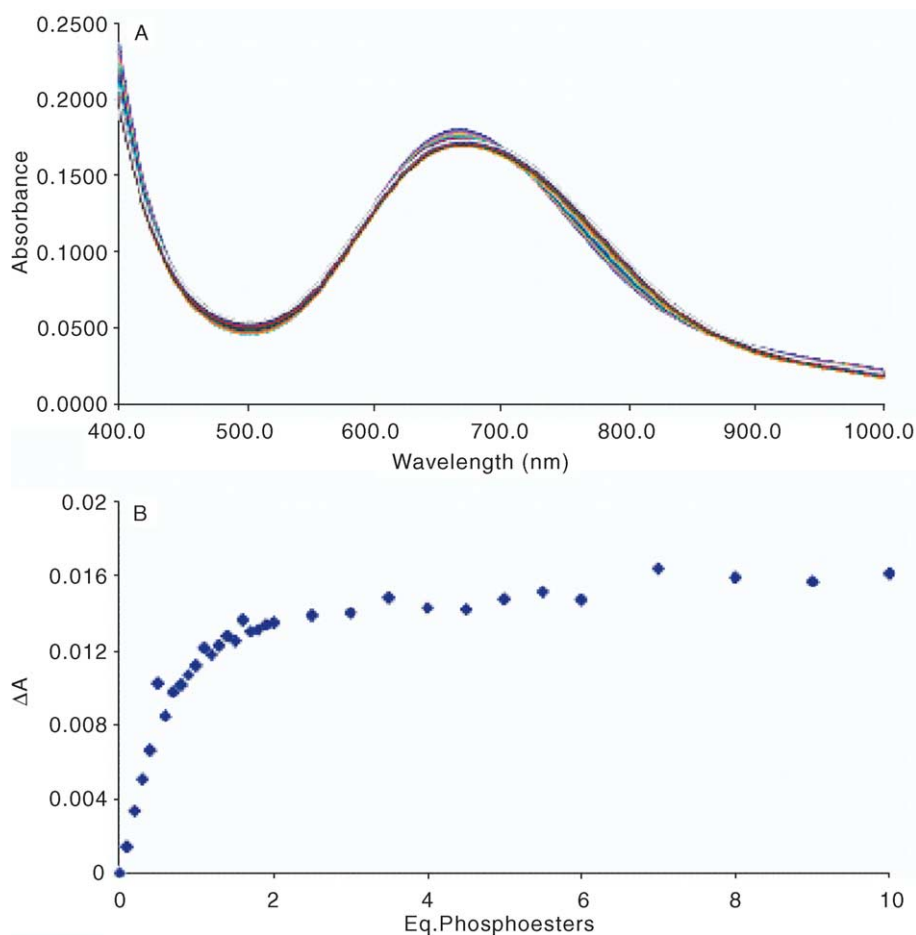


**Figure 1.** (A) Small but reproducible changes in the UV–vis spectra upon addition of phosphoesters. (B) Example of the titration data used to determine affinity constants.

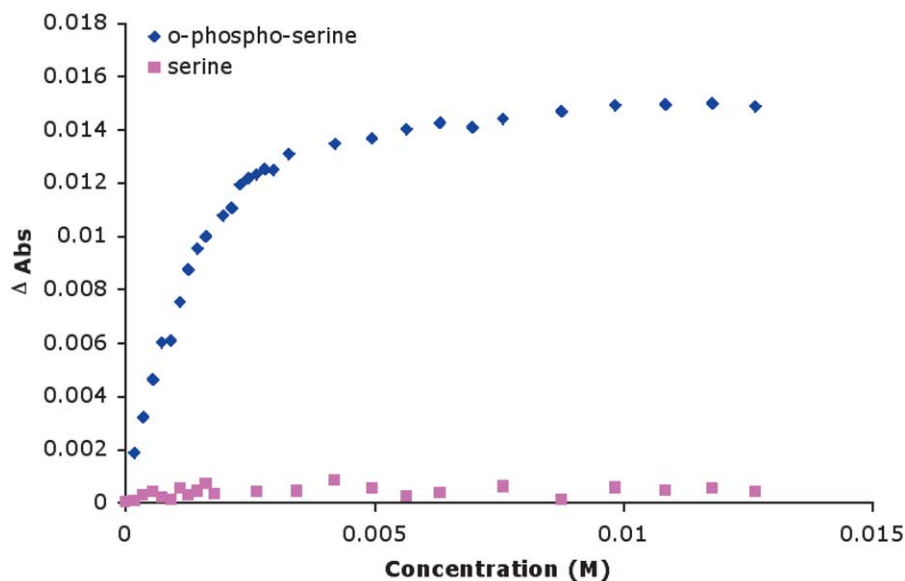


**Figure 2.** UV-vis titration data of *o*-phospho-L-serine and serine.

binding as inorganic phosphate. Apparently, the sterics introduced by a single primary alkyl group does not influence the binding. This is consistent with previous evidence that indicated inorganic phosphate binds to **1** in primary its dianionic form,<sup>34</sup> and hence  $\text{HPO}_4^{2-}$  is analogous to a phosphomonoester ( $\text{RPO}_4^{2-}$ ).

The branching of the alkyl groups also affected the binding

strengths. Primary phosphate esters had stronger binding than those with secondary alkyl groups (**15**, **16**, **17**). This must be a steric effect, indicating that the host does not accommodate branching in the alkyl groups when burying the phosphate group in the cavity. This discovery prompted us to examine the binding difference between phosphoserine **18**, phosphothreonine **19**, and phosphotyrosine **20**.

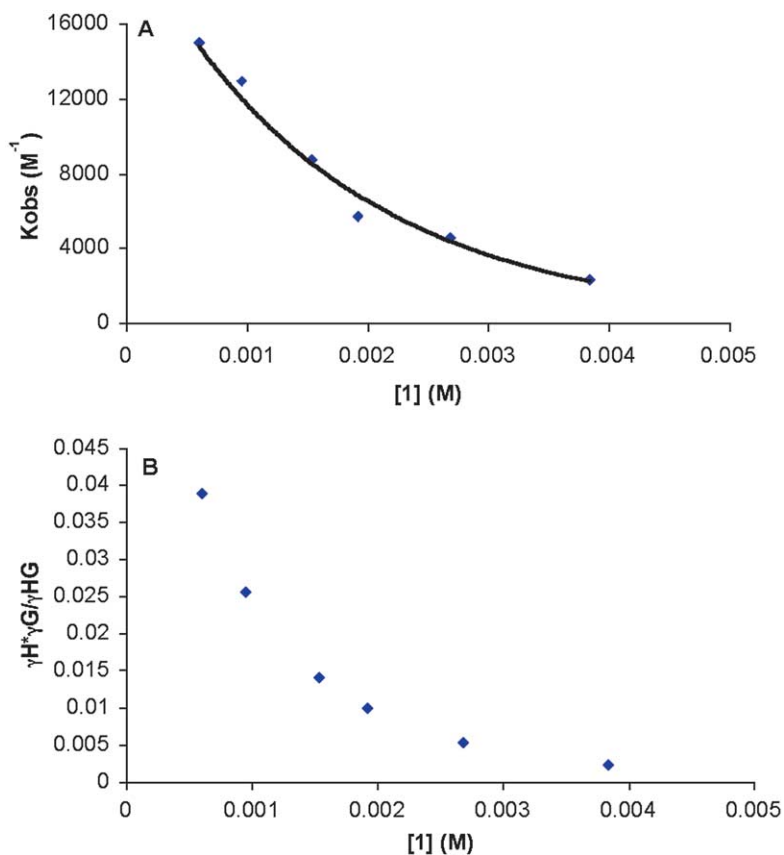


**Figure 3.** (A) Binding affinity changes with host **1** concentrations. (B) Calculated activity coefficients dependence on the host concentrations in the presence of 10 mM Tris buffer.



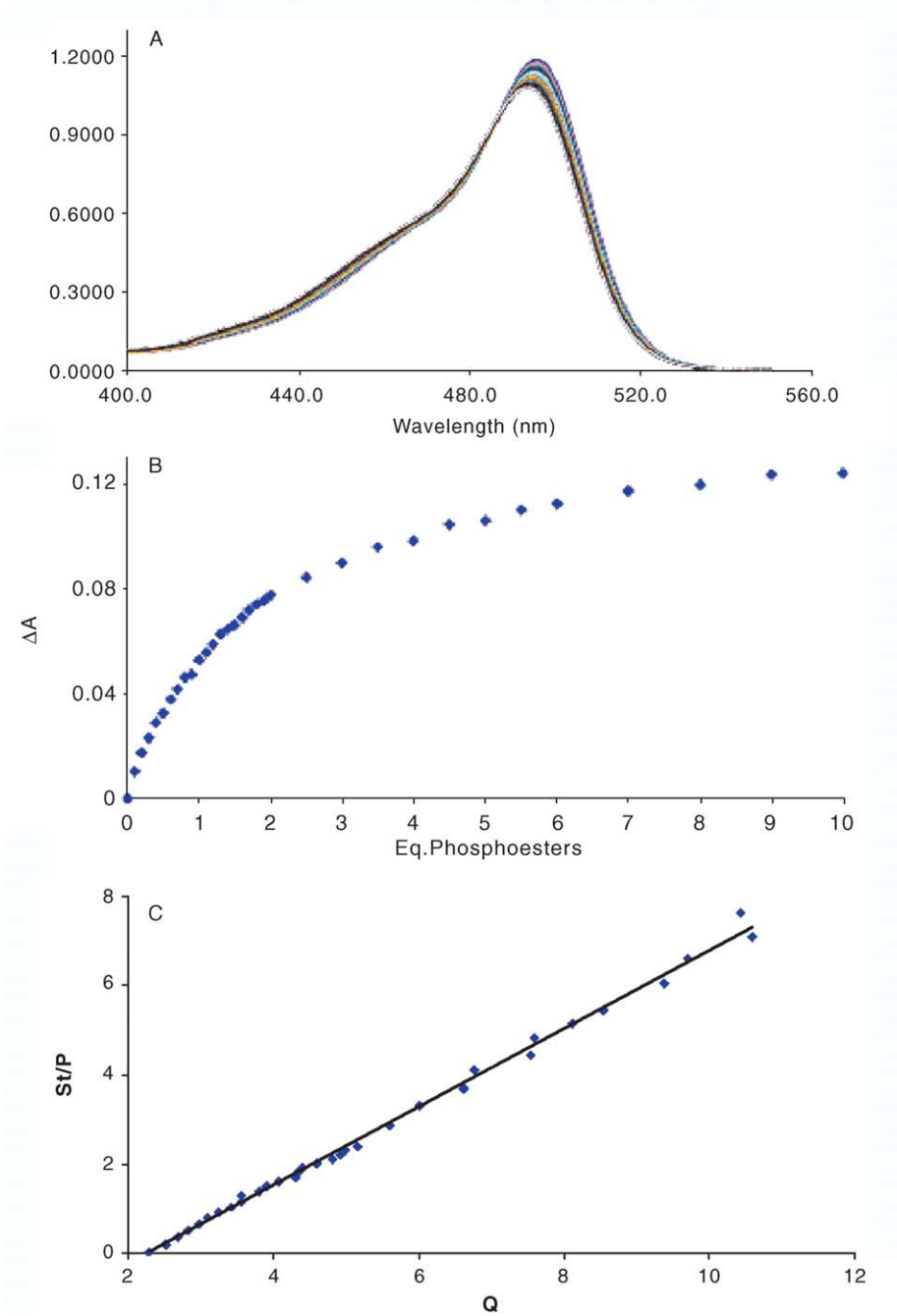
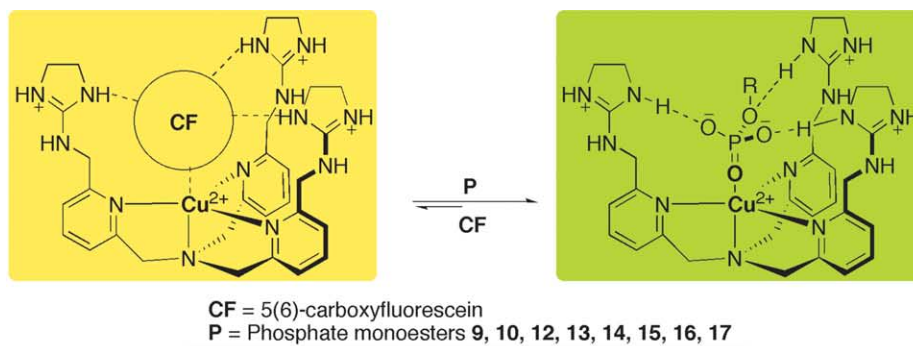


**Figure 4.** (A) Reproducible changes in the UV-vis spectra of host-indicator solution upon addition of phosphoesters. (B) Example of the titration data used to determine the competing affinity constant. (C) Competition displacement algorithm.<sup>37</sup>

We first determined the binding site of these three compounds, because all of these three have terminal amine and carboxyl groups that could also coordinate to the cupric center. Serine as a control was chosen for UV–vis titration to investigate the binding to the host molecule (Fig. 2). It is clear from the figure that serine was not bound to the host **1**. Thus, phosphate is the binding site to **1**, even it is known that cupric ion has a strong affinity to ligands with lone pair nitrogen atoms.

The affinities of these three amino acid phosphates for **1** were similar but not identical compared to our previous discussion. *o*-Phospho-L-threonine binds less effective than *o*-phospho-L-serine, again reflecting a steric influence. However, *o*-phospho-L-tyrosine **20** showed the strongest binding compared to the other two amino acid phosphates (**18** and **19**).

A concentration dependence of the  $K_a$  values was also studied. The binding constants at different concentrations of host molecule (3.84, 2.69, 1.92, 1.54, 0.96, 0.61 mM) towards inorganic phosphate anion were measured at room temperature. It was clear that the lower the host concentration, the larger the binding constants. Because the accuracy of our UV–vis studies is dependent upon the detection limit of the UV–vis spectrometer, at the lower host concentrations there is a larger error. Yet, this is not the source of the concentration trend.

The trend was unexpected at first, but can be readily explained by an effect of ionic strength. The Debye–Huckel equation 1 for determining ionic strength has a large dependence on multiply charged species. The host is formally positive five, with five negative chloride counterions. The activity coefficient ( $\gamma$ ) for a specific ion can be calculated by Eq. 2. The size of each ion ( $\alpha$ ) is not known in this case. However, with concentrations in millimolar range or less, the denominator of Eq. 2 would be near 1. Therefore, Eq. 2 can be simplified as shown in Eq. 3. The host–guest binding equation 4 and its dependence upon concentrations and activity coefficients 5 are shown. The observed binding constant ( $K_{\text{obs}}$ ), which was calculated in our study, is proportional to the activity coefficients of those three species in Eq. 4 since the theoretical binding constant ( $K$ ) does not change with concentrations (Eq. 6). Therefore, the activity coefficient dependence upon host concentration should have the same trend as the  $K_{\text{obs}}$  dependence upon host concentration. Similar trends were obtained from  $K_{\text{obs}}$  versus **[1]** (Fig. 3A) and  $\gamma_{\text{H}}\gamma_{\text{G}}/\gamma_{\text{HG}}$  versus **[1]** (Fig. 3B). This supports the notion that host concentration decreases, a smaller binding constant should be obtained.

$$\mu = (1/2) \sum C_z^2 \quad (1)$$

$$\log \gamma = \frac{-0.51z^2\mu^{1/2}}{1 + (\alpha\mu^{1/2}/305)} \quad (2)$$

$$\log \gamma = -0.51z^2\mu^{1/2} \quad (3)$$



$$K = \frac{[\text{HG}]^{3+}\gamma_{\text{HG}}}{[\text{H}]^{5+}\gamma_{\text{H}}[\text{G}]^{2-}\gamma_{\text{G}}} = \frac{[\text{HG}]^{3+}}{[\text{H}]^{5+}[\text{G}]^{2-}} \frac{\gamma_{\text{HG}}}{\gamma_{\text{H}}\gamma_{\text{G}}} \\ = K_{\text{obs}} \frac{\gamma_{\text{HG}}}{\gamma_{\text{H}}\gamma_{\text{G}}} \quad (5)$$

$$K_{\text{obs}} = K \frac{\gamma_{\text{H}}\gamma_{\text{G}}}{\gamma_{\text{HG}}} \quad (6)$$

To create optical sensing methods for detecting the phosphoesters, we turned to indicator-displacement assays. We previously reported the use 5(6)-carboxyfluorescein as an indicator in a 50:50 methanol/water (v:v) solution to quantitate inorganic phosphate in serum and saliva using **1** as the host.<sup>32</sup> In a similar manner to this previous report, clear color changes of light orange to bright yellow were observed upon addition of the phosphate esters **9**, **10**, **12**, **13**, **14**, **15**, **16**, **17** into a solution of a host–indicator complex (Fig. 4). Compounds **13** and **14** were chosen for quantitative indicator displacement UV–titrations because they showed strong binding in the other UV–vis titrations. In each case, the indicator-displacement by phosphoesters proceeded with a 1:1 stoichiometry. The binding constants calculated from the curving fitting results were  $1.2 \times 10^5$  and  $1.1 \times 10^5 \text{ M}^{-1}$ , respectively, at **[1]** = 25.0  $\mu\text{M}$ . They are comparable to those obtained from host only titrations:  $3.6 \times 10^4$  and  $1.5 \times 10^4 \text{ M}^{-1}$ , respectively, at **[1]** = 1.92 mM, but we observed a much larger absorbance change. These results confirmed that the binding strength between host and guest were dependent upon both the host concentrations and the solvents. Also, the indicator-displacement assay gave us an opportunity to detect the guests at lower concentrations and with a higher optical response.

### 3. Conclusion

In summary, the binding affinities of the host **1** towards different phosphoesters were studied. An indicator-displacement assay was also performed, which was able to detect the host–guest interactions with small visual color changes. The degree of substitution of the phosphate, the functionality of the substituents, and the size of the substituents, all affected their interactions with the host molecule. The success of using this  $\text{C}_{3v}$  host to bind the phosphomonoesters has given us the opportunity to further exploit this host to monitor phosphorylated organic molecules in vivo, which is the direction we are pursuing.

### 4. Experimental

#### 4.1. General considerations

All chemicals used were obtained from Aldrich or Acros and were used without purifications unless noted. Flash chromatography was performed on Whatman 60 Å 230–400 mesh silica gel.  $^1\text{H}$  (400 MHz) and  $^{13}\text{C}$  (75 MHz) spectra were measured by Varian Unity Plus spectrometer. Mass spectra were recorded on a Finnigan VG analytical ZAB2-E spectrometer. UV–vis spectra were collected on a Beckman DU-640 at various temperatures.

## 4.2. Synthesis

**4.2.1. Compound 3.** A  $\text{CH}_2\text{Cl}_2$  (50 mL) suspension of 2,6-dihydroxymethyl pyridine **2** (1.00 g, 7.19 mmol), silver oxide (2.84 g, 10.78 mmol), potassium iodide (0.24 g, 1.44 mmol) was brought to  $-20^\circ\text{C}$ , tosyl chloride (1.51 g, 7.91 mmol) was then added as a solid. The reaction system was slowly warmed up to room temperature and stirred for 3 h. The reaction mixture was filtered through a pad of silica gel, and washed with ethyl acetate. A flash column, first with  $\text{CH}_2\text{Cl}_2$ , then ethyl acetate, gave mono-substituted pink solid **3** (1.58 g, 75%). Mp  $56\text{--}57.5^\circ\text{C}$ .  $^1\text{H}$  NMR ( $\text{CDCl}_3$ , 300 Hz)  $\delta$  2.44 (3H, s),  $\delta$  4.68 (2H, s),  $\delta$  5.13 (2H, s),  $\delta$  7.21 (1H, d),  $\delta$  7.32 (3H, m),  $\delta$  7.69 (1H, t),  $\delta$  7.83 (2H, d).  $^{13}\text{C}$  NMR ( $\text{CDCl}_3$ , 75 Hz)  $\delta$  21.54,  $\delta$  63.69,  $\delta$  71.30,  $\delta$  120.15,  $\delta$  120.49,  $\delta$  127.93,  $\delta$  129.84,  $\delta$  132.60,  $\delta$  137.70,  $\delta$  145.08,  $\delta$  152.41,  $\delta$  158.89. HRCI  $\text{C}_{14}\text{H}_{16}\text{NO}_4\text{S}$  (M+1) 294.079214 (calcd 294.079214).

**4.2.2. Compound 4.** To compound **3** (1.58 g, 5.38 mmol) was added  $\text{NaN}_3$  (1.05 g, 16.16 mmol) in a DMF (40 mL) solution, and the solution was heated at  $80^\circ\text{C}$  for 5 h. The DMF was removed by high vac. The residue was redissolved in ethyl acetate. The precipitate was removed via filtration through a pad of celite. Evaporation of the solvent gave a pure greenish yellow solid **4** (0.88 g, 100%).  $^1\text{H}$  NMR ( $\text{CDCl}_3$ , 300 Hz)  $\delta$  4.35 (2H, s),  $\delta$  4.66 (2H, s),  $\delta$  7.15 (1H, d),  $\delta$  7.20 (1H, d),  $\delta$  7.62 (1H, t).  $^{13}\text{C}$  NMR ( $\text{CDCl}_3$ , 75 Hz)  $\delta$  54.92,  $\delta$  63.89,  $\delta$  119.63,  $\delta$  120.25,  $\delta$  137.57,  $\delta$  154.50,  $\delta$  159.54. HRCI  $\text{C}_7\text{H}_9\text{N}_4\text{O}$  (M+1) 165.078323 (calcd 165.078323).

**4.2.3. Compound 5.** Compound **4** (0.54 g, 3.29 mmol) was dissolved in THF (1.6 mL) and  $\text{H}_2\text{O}$  (1.6 mL), and brought to  $0^\circ\text{C}$ .  $\text{NaOH}$  (0.39 g, 9.87 mmol) was added. A THF (2.7 mL) solution of tosyl chloride (0.69 g, 3.62 mmol) was added to the previous suspension dropwise while stirring. The system was kept at  $0^\circ\text{C}$  and stirred for 4 h, and then extracted with  $\text{CH}_2\text{Cl}_2$ . The combined organic layer was washed with brine and dried with  $\text{Na}_2\text{SO}_4$ . Evaporation of the solvent gave compound **5** as a yellow oil (0.97 g, 93%).  $^1\text{H}$  NMR ( $\text{CDCl}_3$ , 300 Hz)  $\delta$  2.37 (3H, s),  $\delta$  4.33 (2H, s),  $\delta$  5.07 (2H, s),  $\delta$  7.21 (1H, d),  $\delta$  7.33 (3H, m),  $\delta$  7.65 (1H, t),  $\delta$  7.77 (2H, d).  $^{13}\text{C}$  NMR ( $\text{CDCl}_3$ , 75 Hz)  $\delta$  21.39,  $\delta$  54.94,  $\delta$  71.35,  $\delta$  120.77,  $\delta$  121.37,  $\delta$  127.81,  $\delta$  129.74,  $\delta$  132.44,  $\delta$  137.77,  $\delta$  144.96,  $\delta$  153.56,  $\delta$  155.28. HRCI  $\text{C}_{14}\text{H}_{15}\text{N}_4\text{O}_3\text{S}$  (M+1) 319.85414 (calcd 319.85414).

## 4.3. UV-vis titrations

A typical titration is described below, through concentrations varied from experiment to experiment. A stock solution of receptor (15.37 mM) was prepared, and buffered with Tris (10.04 mM) at  $\text{pH}=7.4$ . A similar solution of the guest ( $\sim 50$  mM) was also prepared and buffered with Tris (10.04 mM). To a quartz cuvette was added 875  $\mu\text{L}$  of a Tris (10.04 mM) solution and scanned as the blank reading. 125  $\mu\text{L}$  of the stock solution was introduced to the same cuvette (receptor concentration after dilution 1.92 mM), and the absorbance was recorded. Aliquots of a solution containing the receptor (1.92 mM) and each guest ( $\sim 38$  mM) in Tris buffer were then added to the cuvette and the absorbance was recorded after each addition. At a

chosen wavelength of cupric d–d transition, the delta absorbances were calculated relative to the first absorbance reading. These values were then plotted versus the concentration of the added guest for each aliquot. The binding isotherm from this raw data was curve fit using a 1:1 binding algorithm in Origin.

## 4.4. Indicator-displacement assay

All titration solutions contained 10.90 mM Tris buffer in 50/50 (v:v) methanol/water. A stock solution of receptor (99.8  $\mu\text{M}$ ), and 5(6)-carboxyfluorescein (99.8  $\mu\text{M}$ ) was prepared in Tris (10.90 mM) buffered at  $\text{pH}=7.4$ . A similar solution of the guest ( $\sim 2.5$  mM) was also prepared and buffered with Tris (10.90 mM). To a quartz cuvette was added 750  $\mu\text{L}$  of a Tris (10.90 mM) solution and scanned as the blank reading. 250  $\mu\text{L}$  of the stock solution was introduced to the same cuvette (receptor and 5(6)-carboxyfluorescein concentrations after dilution 25.0  $\mu\text{M}$ ), and the absorbance was recorded. Aliquots of a solution containing the receptor (25.0  $\mu\text{M}$ ), 5(6)-carboxyfluorescein (25.0  $\mu\text{M}$ ) and each guest (499  $\mu\text{M}$ ) in Tris buffer were then added to the cuvette and the absorbance was recorded after each addition. At a chosen wavelength of 5(6)-carboxyfluorescein absorptions, the delta absorbances were calculated relative to the first absorbance reading. These values were then plotted versus the concentration of the added guest for each aliquot. The binding isotherm from this raw data was curve fit using the 1:1 binding equation in Origin.<sup>32</sup>

## Acknowledgements

We would like to thank Dr. Suzanne L. Tobey for her previous contributions to this project. We gratefully acknowledge the financial support from the NIH (EB00549-5).

## References and notes

- Schultz, C. *Bioorg. Med. Chem.* **2003**, *11*, 885–898.
- Aoki, S.; Kimura, E. *Rev. Mol. Biotech.* **2002**, *90*, 129–155.
- Dixon, R. P.; Geib, S. J.; Hamilton, A. D. *J. Am. Chem. Soc.* **1992**, *114*, 365–366.
- Jubian, V.; Dixon, R. P.; Hamilton, A. D. *J. Am. Chem. Soc.* **1992**, *114*, 1120–1121.
- Jubian, V.; Veronese, A.; Dixon, R. P.; Hamilton, A. D. *Angew. Chem., Int. Ed. Engl.* **1995**, *34*, 1237–1239.
- Schneider, S. E.; O'Neil, S. N.; Anslyn, E. V. *J. Am. Chem. Soc.* **2000**, *122*, 542–543.
- McCleskey, S. C.; Griffin, M. J.; Schneider, S. E.; McDevitt, J. T.; Anslyn, E. V. *J. Am. Chem. Soc.* **2003**, *125*, 1114–1115.
- Zhong, Z.; Anslyn, E. V. *Angew. Chem., Int. Ed.* **2003**, *26*, 3005–3008.
- Kimura, E.; Kodama, M.; Yatsunami, T. *J. Am. Chem. Soc.* **1982**, *104*, 3182–3187.
- Kimura, E.; Koike, T. *Chem. Commun.* **1998**, *15*, 1495–1599.
- Dietrich, B.; Guilhem, J.; Lehn, J.; Pascard, C.; Sonveaux, E. *Helv. Chim. Acta* **1984**, *67*, 91–104.

12. Marecek, J. F.; Fischer, P. A.; Burrows, C. J. *Tetrahedron Lett.* **1988**, 29, 6231–6234.
13. Bianchi, A.; Micheloni, M.; Paolett, P. *Coord. Chem. Rev.* **1991**, 110, 17–113.
14. Aguilar, J. A.; Garcia-Espana, E.; Guerrero, J. A.; Luis, S. V.; Llinares, J. M.; Miraver, J. F.; Ramirez, J. A.; Soriano, C. *J. Chem. Soc., Chem. Commun.* **1995**, 2237–2239.
15. Andres, A.; Bazzicalupi, C.; Bencini, A.; Bianchi, A. F.; Garcia-Espana, E.; Giorgi, C.; Nardi, N.; Paoletti, P.; Ramirez, J. A.; Baltancoli, B. *J. Chem. Soc., Perkin Trans. 2* **1994**, 2367–2373.
16. Schneider, H.; Blatter, T.; Eliseev, A.; Rudiger, V.; Raevsky, O. A. *Pure Appl. Chem.* **1993**, 65, 2329–2334.
17. Andres, A.; Burguete, M. I.; Garcia-Espana, E.; Luis, S. V.; Miravet, J. F.; Soriano, C. *J. Chem. Soc., Perkin Trans. 2* **1993**, 749–755.
18. Bencini, A.; Bianchi, A.; Giorgi, C.; Paoletti, P.; Valtancoli, B.; Fusi, V.; García-España, E.; Llinares, J. M.; Ramírez, J. A. *Inorg. Chem.* **1996**, 35, 1114–1120.
19. Bazzicalupi, C.; Bencini, A.; Bianchi, A.; Fusi, V.; Giorgi, C.; Granchi, A.; Paoletti, P.; Valtancoli, B. *J. Chem. Soc., Perkin Trans. 2* volume 4 **1997**, 775–781.
20. Bazzicalupi, C.; Beconcini, A.; Bencini, A.; Fusi, V.; Giorgi, C.; Masotti, A.; Valtancoli, B. *J. Chem. Soc., Perkin Trans. 2* **1999**, 8, 1675–1682.
21. Menger, F. M.; Catlin, K. K. *Angew. Chem., Int. Ed. Engl.* **1995**, 34, 2147–2150.
22. Hartley, J. H.; James, T. D.; Ward, C. J. *J. Chem. Soc., Perkin Trans. 1* **2000**, 3155–3184.
23. Powell, D.; Bowman-James, K. *Coord. Chem. Rev.* **2003**, 240(1–2), 57–75.
24. Chu, F.; Flatt, L. S.; Anslyn, E. V. *J. Am. Chem. Soc.* **1994**, 116, 4194–4204.
25. Flatt, L. S.; Lynch, V.; Anslyn, E. V. *Tetrahedron Lett.* **1992**, 33, 2785–2788.
26. Tohda, K.; Tange, M.; Odashima, K.; Umezawa, Y.; Furuta, H.; Sessler, J. L. *Anal. Chem.* **1992**, 64, 960–964.
27. Furuta, H.; Magda, D.; Sessler, J. L. *J. Am. Chem. Soc.* **1991**, 113, 978–985.
28. Das, G.; Onouchi, H.; Yashima, E.; Sakai, N.; Matile, S. *ChemBioChem* **2002**, 3(11), 1089–1096.
29. Kelly, T. R.; Kim, M. H. *J. Am. Chem. Soc.* **1994**, 116, 7072–7080.
30. Yeo, W.; Hong, J. *Tetrahedron Lett.* **1998**, 39, 3769–3772.
31. Gale, P. A. *Coord. Chem. Rev.* **2000**, 199(1), 181–233.
32. Tobey, S. L.; Anslyn, E. V. *Org. Lett.* **2003**, 5, 2029–2031.
33. Tobey, S. L.; Jones, B. D.; Anslyn, E. V. *J. Am. Chem. Soc.* **2003**, 125, 4026–4027.
34. Tobey, S. L.; Anslyn, E. V. *J. Am. Chem. Soc.* **2003**, 125, 14807–14815.
35. Bouzide, A.; Sauve, G. *Org. Lett.* **2002**, 4, 2329–2332.
36. Cabezon, B.; Cao, J.; Raymo, F. M.; Stoddart, J. F.; White, A. J. P.; William, D. J. *Chem. Eur. J.* **2000**, 6, 2262–2273.
37. Connors, K. A. *Binding Constants*; John Wiley and Sons: New York, 1987.

# Fluorescent photoionic devices with two receptors and two switching mechanisms: applications to pH sensors and implications for metal ion detection

John F. Callan, A. Prasanna de Silva,\* Joanne Ferguson, Allen J. M. Huxley and Aoife M. O'Brien

*School of Chemistry, Queen's University, Belfast BT9 5AG, Northern Ireland, UK*

Received 14 November 2003; revised 8 August 2004; accepted 19 August 2004

Available online 11 September 2004

**Abstract**—Two leading designs of fluorescent sensors are combined to yield the novel hybrid system of the 'Fluorophore–Receptor<sub>1</sub>–Spacer–Receptor<sub>2</sub>' format. We use 4-(dialkylaminoalkylamino)-7-nitrobenzo-2-oxa-1,3-diazoles as examples. The emission from internal charge transfer excited states in the present instances are highly responsive to N–H deprotonation as well as being quenched by intramolecular tertiary amine groups via photoinduced electron transfer (PET). When applied to pH sensing, this leads in favourable cases to two steps in the fluorescence–pH profile which can be viewed as a multi-stable photoionic device, even though single steps are more usual. The former situation is favoured when the two proton-associated equilibria are sufficiently separated on the pH scale and when the PET process is of moderate efficiency. These systems have the added feature of excitation/emission wavelengths in the visible region. As a secondary theme, we point out that caution is required when designing sensors for transition metal ions from systems with intrinsically proton-sensitive fluorescence due to receptors either integrated with or spaced from the fluorophore.

© 2004 Elsevier Ltd. All rights reserved.

## 1. Introduction

Fluorescence sensors and switches are proving to be useful across the range of sciences from medicine to materials.<sup>1</sup> The sensing of chemical species via fluorescence is growing rapidly thanks to two distinct design principles.<sup>2</sup> One of these is based on the integrated 'Fluorophore–Receptor' format where the two components overlap considerably and give rise to internal charge transfer (ICT) excited states. The energy of these states can be perturbed by guest species complexed nearby and guest-induced wavelength shifts are produced.<sup>3</sup> The other design principle employs the supramolecular<sup>4</sup> 'Fluorophore–Spacer–Receptor' format where the two terminal components largely preserve their properties, that is, predictability of many parameters is built-in. Nevertheless, photoinduced electron transfer (PET) can be arranged between the terminal components to switch 'off' fluorescence emission. The PET process can be further arranged to stop upon guest complexation and fluorescence can be recovered.<sup>5</sup> These two design principles have complementary strengths and it would be profitable to

combine them within a single sensor system. At a conceptual level this would be a novel 'Fluorophore–Receptor<sub>1</sub>–Spacer–Receptor<sub>2</sub>' format<sup>6</sup> (Fig. 1) which is quite different from 'Lumophore–Receptor<sub>1</sub>–Spacer–Receptor<sub>2</sub>' systems involving lanthanide complexes.<sup>7</sup> This would also be quite distinct from the 'Fluorophore–Spacer<sub>1</sub>–Receptor<sub>1</sub>–Spacer<sub>2</sub>–Receptor<sub>2</sub>' format where both receptors participate according to PET mechanisms.<sup>8</sup> Importantly, 'Fluorophore–Receptor<sub>1</sub>–Spacer–Receptor<sub>2</sub>' systems can give rise to photochemical molecular devices<sup>9</sup> which display two distinct 'on' states besides the 'off' state. Such multi-state systems are of current interest.<sup>10</sup> Absorptometric photoionic devices with two receptors have been recently shown to have unusual computational capabilities.<sup>11</sup>

At a more specific level, we choose simple amines as receptors (for protons) and the 4-amino-7-nitrobenzo-2-oxa-1,3-diazole fluorophore for the sensors **1**. Even though the classical amine–proton pairing is perhaps the simplest possible receptor–target combination, they allow the simplest demonstration of new possibilities in sensor design.<sup>2</sup> The choice of fluorophore has several underlying reasons. First, this will allow us to build sensors with visible excitation and emission wavelengths which are much sought after for reduced interference from the matrix,

**Keywords:** Fluorescent sensors; Photoinduced electron transfer; pH sensors; Internal charge transfer; Metal ion sensors.

\* Corresponding author. Tel.: +44-2890274422; fax: +44-2890382117; e-mail: a.desilva@qub.ac.uk



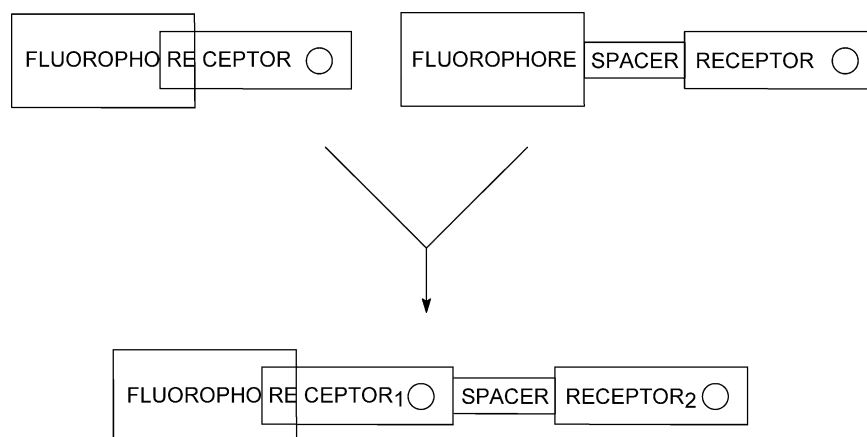


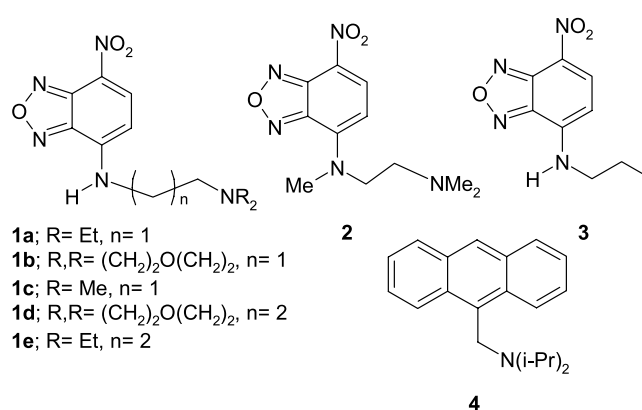
**Figure 1.** The ‘Fluorophore–Receptor<sub>1</sub>–Spacer–Receptor<sub>2</sub>’ format of fluorescent sensors and its parentage.

especially if such excitation can be provided by inexpensive light emitting diode sources<sup>12</sup> increasingly used in sensor equipment.<sup>13</sup> Second, 4-amino-7-nitrobenzo-2-oxa-1,3-diazoles have been known to show polarity-sensitive emission spectra.<sup>14</sup> Therefore the potential exists for developing two-dimensional fluorescent sensors<sup>15</sup> which allow simultaneous monitoring of properties like polarity via emission wavelength and chemical species such as protons via emission quantum yield.<sup>16</sup> Third, **1c** has been recently proposed as a fluorescent PET sensor for several transition metal ions, for example, chromium(III).<sup>17</sup> This work and some related studies<sup>18,19</sup> are very interesting since fluorescence switching ‘on’ with d-block metal ions is reported. Now we demonstrate that the sensitivity of the fluorescence of these systems to protons demands caution concerning the interpretation of these observations.

## 2. Results and discussion

4-Amino-7-nitrobenzo-2-oxa-1,3-diazoles have seen extensive use as fluorescent labels in biology<sup>20</sup> besides being a suitable fluorescent derivative of amines for analytical purposes.<sup>21</sup> The photophysics of these fluorophores has also received attention.<sup>14</sup> Ion sensors based on 4-amino-7-nitrobenzo-2-oxa-1,3-diazoles are also available. Shanzer’s extensive program uses such sensors which respond to Fe(III) with fluorescence switching ‘off’.<sup>22</sup> Street and Krause<sup>23</sup> as well as Forst and Pacey,<sup>24</sup> and more recently, Resch et. al.<sup>25a</sup> and Boiocchi et al.<sup>25b</sup> have elaborated the 4-amino nitrogen into azacrown ether or cyclam receptors for the purpose of ion capture. **1c** is included within a large series of compounds examined by Onoda et al.<sup>26</sup> to elucidate the influence of spacer length on PET efficiency.

The thermodynamic driving force for PET ( $\Delta G_{\text{PET}}$ ) from triethylamine to 4-amino-7-nitrobenzo-2-oxa-1,3-diazole fluorophore is  $-1.1$  eV,<sup>17b</sup> according to the Weller equation.<sup>27</sup> Corresponding amines when protonated will naturally give rise to a large positive  $\Delta G_{\text{PET}}$  value. So we can expect the fluorescence to be weak for compounds **1** and strong for protonated **1**.



The absorption spectra of compounds **1** are slightly but significantly dependent on pH in the acidic/neutral pH range. They are strongly dependent on pH in the alkaline range. The case of **1b** in these two pH ranges is shown in Figures 2 and 3, respectively. The behaviour in the acidic/neutral range is as expected of a fluorescent PET sensor for protons,<sup>28</sup> but the behaviour in the alkaline range is more typical of an ICT sensor.<sup>1a</sup> The resulting parameters are given in Table 1. Bearing in mind that multiple protonation–deprotonation equilibria may be involved, these absorbance (*A*) changes can be analyzed according to Eq. (1)<sup>29</sup> to give the  $pK_a$  values shown.

$$\log[(A_{\text{max}} - A)/(A - A_{\text{min}})] = \text{pH} - \text{p}K_a \quad (1)$$

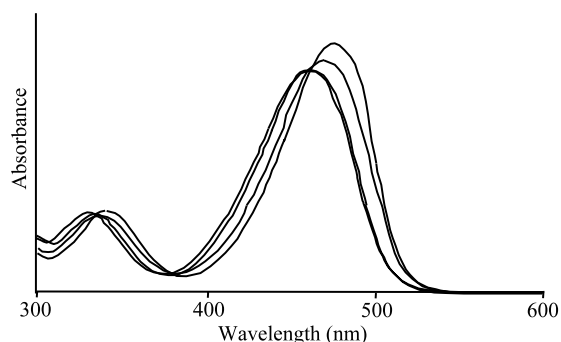


**Figure 2.** pH dependence of electronic absorption spectra of **1b** in the acidic/neutral pH range. The pH values in order of decreasing absorbance at 470 nm are: 7.1, 5.6, 5.0 and 4.5.



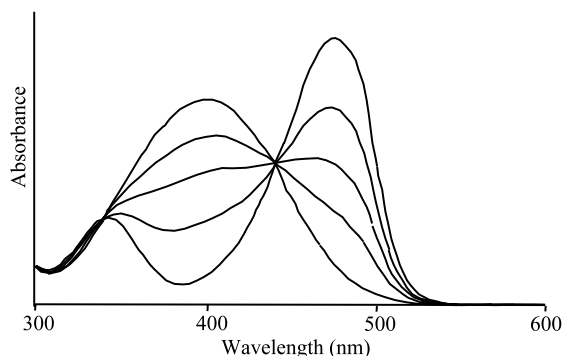


**Figure 3.** pH dependence of electronic absorption spectra of **1b** in the alkaline pH range. The pH values in order of decreasing absorbance at 470 nm are: 7.4, 9.0, 9.4, 9.7 and 11.5.

The pH dependence of fluorescence intensity ( $I_F$ ) (e.g., for **1d** in Figs. 4 and 5) can also be analyzed with equation 2<sup>28</sup> to give the  $pK_a$  values listed in Table 1.

$$\log\left[\frac{(I_{F_{\max}} - I_F)/(I_F - I_{F_{\min}})}{1}\right] = \text{pH} - pK_a \quad (2)$$

The  $pK_a$  value of receptors unconjugated with the fluorophore are expected to be similar whether determined absorptometrically or fluorimetrically. Such similarity is not expected when the receptor is integrated with the fluorophore.<sup>30</sup>

The massed data in Table 1 show many notable features. The absorption maxima ( $\lambda_{\max, \text{Abs}}$ ) are determined by the energy of the ICT excited state which carries significant positive charge on the 4-amino unit. So it is gratifying to find that the tertiary nitrogen at the 4-position (within **2**) gives the highest value (500 nm). This also implies that methylation of the 4-N does not introduce steric crowding which could have caused twisting of the 4-N-aromatic C bond leading to blue-shifts. Within the 4-NH series, a propyl side-chain (within **3**) produces the highest value (480 nm). The next highest value (471–474 nm) is seen for **1d** and **1e** where the  $\sigma$ -electron-withdrawing amino terminal is three

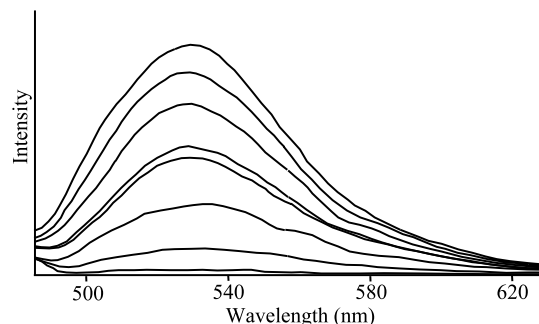


**Figure 4.** pH dependence of fluorescence emission spectra of **1d**. The pH values in order of decreasing intensity at 535 nm are: 5.4, 6.3, 6.7, 7.4, 8.0, 9.1, 9.7 and 10.6. The excitation wavelength is 441 nm.

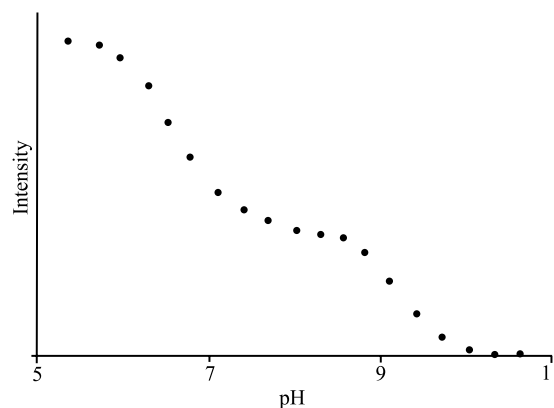


**Figure 5.** Fluorescence intensity (at 535 nm)—pH profile of **1d**. The excitation wavelength is 441 nm.

methylene units away from the 4-amino unit. The last in line is the set **1a–c** (465–470 nm) where the amino terminal is only separated by two methylene units from the 4-amino unit. Similar trends (**2** > **1d,e** > **1a–c**) can be discerned in the absorption maxima of the protonated series ( $\lambda_{\max, \text{Abs-H}}$ ). The presence of a protonated amine two (or three) methylene groups away from the 4-amino unit gives blue shifts of

**Table 1.** Optical and acid/base properties of systems **1a–e**, **2–4**<sup>a</sup>

Property	<b>1a</b>	<b>1b</b>	<b>1c</b>	<b>1d</b>	<b>1e</b>	<b>2</b>	<b>3</b>	<b>4</b>
$\lambda_{\max, \text{Abs+H}^+}$ (nm)	461	459	456	466	471	479	— <sup>b</sup>	354,371,393
$\lambda_{\max, \text{Abs}}$ (nm)	467	470	465	474	471	500	480	349,366,388
$\lambda_{\max, \text{Abs-H}^+}$ (nm)	399	400	401	397	394	— <sup>b</sup>	391	— <sup>b</sup>
$\lambda_{\text{isobestic}}$ (nm)	436,486 <sup>c</sup>	379,459 <sup>c</sup>	416,460 <sup>c</sup>	394,470 <sup>c</sup>	— <sup>d</sup>	391,476 <sup>c</sup>	439 <sup>c</sup>	351,360, 368,381,390
$pK_{a, \text{side-chain(Abs)}}$	439 <sup>e</sup>	441 <sup>c</sup>	440 <sup>e</sup>	441 <sup>c</sup>	— <sup>d</sup>	—	—	—
$pK_{a, \text{side-chain(Flu)}}$	8.1	5.3	6.9	6.8	ca. 9.2	8.0	— <sup>b</sup>	8.1
$pK_{a, \text{N-H(Abs)}}$	9.9	9.3	9.3	9.2	ca. 9.2	— <sup>b</sup>	9.3	— <sup>b</sup>
$\lambda_{\max, \text{Flu}}$ (nm)	524	526 <sup>f</sup> 530 <sup>g</sup>	523	535 <sup>f</sup> 535 <sup>g</sup>	530	532	534	398,420,443
$pK_{a, \text{side-chain(Flu)}}$	7.5	5.6	7.5	6.7	ca. 8.9	7.5	— <sup>b</sup>	8.2
FE	>100	10	40	2.7	80	7.7	— <sup>b</sup>	45
$pK_{a, \text{N-H(Flu)}}$	— <sup>h</sup>	9.0	— <sup>h</sup>	9.3	ca. 8.9	— <sup>b</sup>	8.8	— <sup>b</sup>
FE	— <sup>h</sup>	10	— <sup>h</sup>	30	80	— <sup>b</sup>	45	— <sup>b</sup>

<sup>a</sup> In MeOH–H<sub>2</sub>O (1:4, v/v) solution. Unless noted otherwise the fluorescence emission is so low in basic solution that a  $\lambda_{\max, \text{Flu}}$  value cannot be determined. Fluorescence experiments are performed with excitation at a suitable isobestic wavelength.

<sup>b</sup> Not present and not expected.

<sup>c</sup> Protonation equilibrium.

<sup>d</sup> No sharp isobestic points.

<sup>e</sup> De-protonation equilibrium.

<sup>f</sup> Protonated form.

<sup>g</sup> Neutral form.

<sup>h</sup> Not observed.

6–11 nm. Similar, though larger, effects are seen upon side-chain protonation of 4-(2'-aminoethyl)amino-1,8-naphthalimides<sup>31</sup> for the same reasons. The exception of no blue shift for **1e** is clearly a combination of (a) the larger distance from the 4-amino unit to the protonated amine and (b) the low charge density on the aliphatic amino terminal due to the presence of the two ethyl groups.

The 4-NH series show a large blue-shift in sufficiently basic media which can be ascribed to deprotonation of this rather acidic proton. Considerable redistribution of electron density is to be expected in such an event. The absorption maximum in all cases (**1a–e**, **3**) lie in the range 391–401 nm. Unsurprisingly, such a base-induced blue-shift is absent for **2** lacking a 4-NH group. This deprotonation of the 4-NH group naturally introduces an extra proton-associated equilibrium into the spectral studies. The observation of sharp isosbestic points therefore required that the pH variations be conducted in two separate pH ranges. Furthermore, the determination of pK<sub>a</sub> values involved larger uncertainties than usual ( $\pm 0.1$ ) in some cases owing to this complication.

The pK<sub>a</sub> values of the 4-NH group is largely constant in all cases (**1a–e**, **3**). The deviation seen in **1a** is probably because its side-chain pK<sub>a</sub> value is close enough to cause some interference. The pK<sub>a</sub> values of the side-chains largely follow the trend seen in simpler amines<sup>32</sup> and expected in physical organic chemistry.<sup>33</sup> The electron releasing tendency of Et<sub>2</sub>N > Me<sub>2</sub>N > morpholino is borne out in the two series of pK<sub>a</sub> values: **1a** > **1c** > **1b** and **1e** > **1d**. The chromophore acts as an electron withdrawing unit which is naturally more effective if only two methylene groups away, hence the pK<sub>a</sub> orders: **1e** > **1a** and **1d** > **1b**. The electron withdrawing ability of the chromophore is somewhat attenuated with methylation of the 4-N, hence the larger pK<sub>a</sub> value of **2** (8.0) c.f. **1c** (6.9).

Being a simple hydrocarbon chromophore, **4** is expected to possess a  $\pi\pi^*$  excited state with no ICT contribution. However, protonation of the aminomethyl side-chain induces a noticeable degree of ICT character which is evidenced by the 5 nm red-shift. This red-shift permitted the determination of a pK<sub>a</sub> value (8.1), a feat which is not possible for several fluorescent PET sensors with hydrocarbon chromophores.<sup>2,34</sup>

The examination of fluorescence spectra of these compounds as a function of pH showed the fluorescence switching 'on' upon protonation of the side-chain amine as commonly expected. Large proton-induced fluorescence enhancement (FE) factors (2.7–>100) are found. The smallest FE value is naturally seen for **1d** with the longer three-methylene spacer which retards PET rates compared to the cases with dimethylene spacers (Figs. 4 and 5). Also, the influence of the electron withdrawing substituents on the electron donor side-chain amine makes PET thermodynamically less favourable. Hence the FE order: **1a** > **1c** > **1b**. The case of **1e** is complicated by the overlap of the side-chain protonation and the 4-NH deprotonation equilibria. The fluorescence quenching process arising from the 4-NH deprotonation may be attributable to strong coupling

of the deprotonated fluorophore with solvent O–H oscillators.<sup>15</sup>

As expected, the fluorimetrically determined pK<sub>a</sub> values of the side-chain amines are not much different from those obtained absorptiometrically. The pK<sub>a</sub> values of the 4-NH group is not always determinable in this way because the fluorescence is already quenched when the alkaline pH range suitable for 4-NH deprotonation is reached. The clearest case where both equilibria are seen by fluorescence switching is that of **1d**. In this case, the pK<sub>a</sub> value of the side-chain amine is moved into the acidic range due to the electron withdrawing oxygen within the morpholine group. Additionally, the fluorescence quenching by the PET process is only moderate owing to the longer spacer. Thus there is sufficient fluorescence left to be quenched by the 4-NH deprotonation. This fluorescence–pH profile thus displays three plateaux which can be interpreted as a three-state molecular photoionic device.<sup>10</sup>

A second theme of this paper emerged for the following reason. Samanta et al. have observed large fluorescence enhancements for **1c** when treated with chromium(III) chloride hexahydrate and other hydrated transition metal salts in acetonitrile.<sup>17</sup> Many other related reports<sup>18,19</sup> have accumulated since then. Samanta et al. immediately noted the significance of this observation since d-block ions often open deexcitation pathways via electronic energy transfer (EET) and/or PET involving the metal centre. In fact, Fabbri's team have an extensive catalogue of sensors whose luminescence is switched 'off' upon encountering d-block ions or other redox-active species for some of which  $\Delta G_{\text{PET}}$  rationalizations are available.<sup>5c,1c</sup>

During their analysis, Samanta et al. have carefully discussed the possibility of protonation arising from adventitious protons since these cause powerful fluorescence switching 'on' in **1** as we have detailed above. However it is also important to analyze the possibility of protonation arising from the hydration shell of transition metal ions. So we have examined this possibility carefully. The acidity of the water molecules in the hydration shell of highly charged metal ions is well appreciated.<sup>35</sup> Thus chromium(III) chloride hexahydrate can potentially switch 'on' the fluorescence of **1c** by transfer of a proton from the coordinated waters to the dimethylamino side chain. To test this hypothesis, we synthesized a sterically hindered tertiary monoamine **4** which would signal local proton sources via fluorescence enhancement. Importantly, the fluorophore within **4** is a simple anthracene unit which is nowhere as electron deficient as that in **1c**. The reduction potentials of **4** and **1c** are  $-2.0$ <sup>36</sup> and  $-0.6$  V<sup>17b</sup> (vs. SCE) respectively. Compound **4** is a simple fluorescent PET sensor for protons. Its pK<sub>a</sub> value in H<sub>2</sub>O–MeOH (4:1, v/v) is 9.2, which is to be compared with the side-chain of **1c** (7.5). It should be a rather poorer ligand for Cr<sup>III</sup> than **1c** given the lack of chelation possibilities and the congested nature of the amine centre. Nevertheless, as Figures 6 and 7 show, **4** is about as efficient as **1c** in responding to chromium(III) chloride hexahydrate in acetonitrile solution. Thus we can conclude that protonation can give rise to the observation of fluorescence enhancement in **1c** with chromium(III) chloride hexahydrate. A referee has also pointed out the

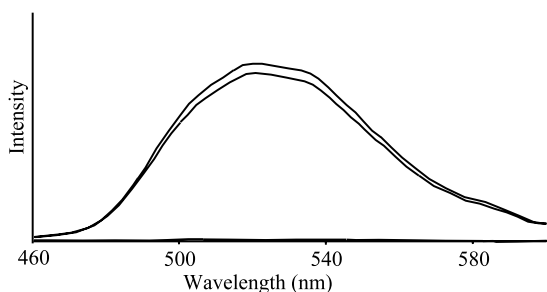


**Figure 6.** Fluorescence emission spectra of **1c** with and without added chromium(III) chloride hexahydrate. The concentrations of chromium(III) chloride hexahydrate in order of decreasing intensity at 523 nm are:  $5 \times 10^{-5}$ ,  $5 \times 10^{-5}$  and 0.0 M. The excitation wavelength is 440 nm.

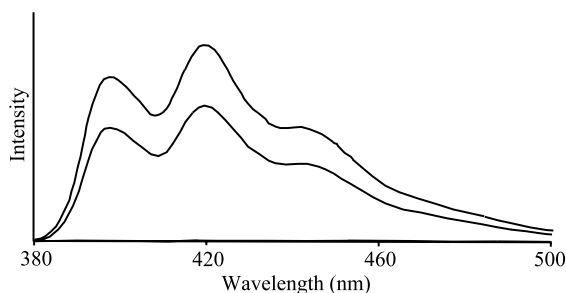


**Figure 7.** Fluorescence emission spectra of **4** with and without added chromium(III) chloride hexahydrate. The concentrations of chromium(III) chloride hexahydrate in order of decreasing intensity at 420 nm are:  $5 \times 10^{-5}$ ,  $5 \times 10^{-5}$  and 0.0 M. The excitation wavelength is 368 nm.

long-known kinetic inertness<sup>35</sup> of chromium(III) which would prevent ligation of **1c** to the Cr<sup>III</sup> centre.

Fe<sup>III</sup> is even less likely than Cr<sup>III</sup> to bind to amine ligands, especially when water is present.<sup>35</sup> So we have tested the response of **4** and **1c** to iron(III) chloride hexahydrate. The fluorescence enhancements are as large as those seen with the chromium version. Evidently, protons arising from the hydration shell are again exerting their influence by binding to the strongly basic aliphatic amine units and retarding PET from these groups to the two fluorophores. Care is warranted in this kind of situation because related problems have emerged in boric acid sensors.<sup>37,38</sup>

Nevertheless, there are a few examples of redox-active guests unequivocally switching ‘on’ fluorescence where the fear of proton-induced effects is less likely. The oldest of these is Verhoeven’s acridinium-phenylazacrown system from 1989<sup>39</sup> whose behaviour we rationalized in a 1993 review.<sup>5a</sup> When metal-free, **5** suffers PET from the phenylazacrown receptor to the acridinium fluorophore. Cation entry suppresses this particular PET process. The Ag<sup>+</sup> guest would encourage a new PET towards itself whereas the electron deficient acridinium fluorophore opposes this and vice versa. Deexcitation based on guest-centred PET is therefore energetically expensive. Additionally the d<sup>10</sup> ion is bereft of low-lying excited states to induce EET processes. Much more recently, Kollmansberger et al.<sup>40</sup> report a closely related case which responds to Hg<sup>2+</sup> with a large fluorescence enhancement. Several more papers have appeared on this topic very recently.<sup>41</sup> Kubo et al. have also reported a case of luminescence enhancement in the

presence of redox-active pyridinium guests.<sup>42</sup> The rationalization is probably similar to that of **5**.

A sensor based on an anthracene-cryptand system due to Bharadwaj and coworkers also possesses easily protonatable amino groups which can lead to fluorescence enhancements.<sup>43</sup> Nevertheless, after several control experiments, they concluded that the metal ion effects were not artifactual. Importantly, they also found that the transition metal ion was electrochemically inactive once buried in the cryptand cavity. The distance from the fluorophore of an easily protonatable amino group precludes rapid PET and hence, any significant proton-controlled fluorescence effects. This argument has also been nicely applied by Reymond et al. to design a ‘on-off’ fluorescent Cu<sup>2+</sup> sensor.<sup>44</sup> Samanta et al. have also used persuasive arguments to rule out protonation from being responsible for metal-induced fluorescence ‘off-on’ and ‘on-off’ switching of a pyridine derivative<sup>45</sup> of lower basicity than those encountered among the amine cases such as **1**. Generally, higher the basicity the more caution is required, that is, aromatic amines or pyridines will be less problematic (though not zero) than aliphatic amines. The fears about coordinated waters are expected to disappear when the studies in the field shift from organic solvents to pH-buffered water.

### 3. Conclusion

Fluorescent sensors **1** of the ‘Fluorophore–Receptor<sub>1</sub>–Spacer–Receptor<sub>2</sub>’ type give insights into the overlapping of PET and ICT mechanisms. The pH sensing involves overlapping of two protonation/deprotonation equilibria in some of these instances. In others, fluorescence-pH profiles with two steps is found. The pH response can cloud the ability of **1** to accurately measure hydrated transition metal ions in aprotic media.

## 4. Experimental

### 4.1. General

UV–visible absorption and fluorescence emission spectra were recorded on Perkin–Elmer Lambda 9 and Perkin–Elmer LS-5B instruments. The general conditions are given under Table 1. A General Electric GNQ500 nuclear magnetic resonance spectrometer and VG MS902 mass spectrometer were also employed. Compounds **1c**<sup>17</sup> and **3**<sup>46</sup> are known.

**4.1.1. *N,N*-Diethyl-*N'*-(7-nitrobenzo-2-oxa-1,3-diazol-4-yl)-1,2-ethanediamine (**1a**).** To a solution of 4-chloro-7-nitrobenzo-2-oxa-1,3-diazole (0.49 g, 2.5 mmol) in ethanol (30 mL) at 0 °C, *N,N*-diethyl-1,2-ethanediamine (0.31 g, 2.7 mmol) was added over 30 min. The solvent was evaporated under vacuum. The residue was re-dissolved in dichloromethane and washed with saturated aqueous sodium bicarbonate solution. The aqueous layer was further extracted with dichloromethane and the combined organic layers were dried (MgSO<sub>4</sub>) and concentrated when the \*\*\*product crystallized. Yield 29%. Mp 94–95 °C. <sup>1</sup>H NMR

(CDCl<sub>3</sub>):  $\delta$  = 8.43 (d,  $J$  = 8 Hz, 1H, ArH), 6.12 (d,  $J$  = 8 Hz, 1H, ArH), 3.44 (b, 2H, NHCH<sub>2</sub>), 2.82 (t,  $J$  = 6 Hz, 2H, NHCH<sub>2</sub>CH<sub>2</sub>), 2.60 (q,  $J$  = 7 Hz, 4H, N(CH<sub>2</sub>CH<sub>3</sub>)<sub>2</sub>), 1.11 (t,  $J$  = 7 Hz, 4H, N(CH<sub>2</sub>CH<sub>3</sub>)<sub>2</sub>); MS:  $m/z$ (%): 279(3%)[M<sup>+</sup>], 264(2), 144(2), 131(5), 117(10), 103(7), 86(100); HRMS  $m/z$  calcd for C<sub>12</sub>H<sub>17</sub>N<sub>5</sub>O<sub>3</sub> 279.1331; found 279.1335.

**4.1.2. *N*-(2'-Morpholinoethyl)-*N*-(7-nitrobenzo-2-oxa-1,3-diazol-4-yl)amine (1b).** The preparative procedure was the same as that for **1a** except that 2-morpholino-1-ethanamine was the amine used. The work-up was different in that the residue was chromatographed on a silica column with hexane–dichloromethane (1:6, v/v). Yield 36%. Mp 140–141 °C. <sup>1</sup>H NMR (CDCl<sub>3</sub>):  $\delta$  = 8.50 (d,  $J$  = 9 Hz, 1H, ArH), 6.15 (d,  $J$  = 9 Hz, 1H, ArH), 3.80 (t,  $J$  = 4.5 Hz, 4H, N(CH<sub>2</sub>CH<sub>2</sub>)<sub>2</sub>), 3.55 (b, 2H, NHCH<sub>2</sub>), 2.82 (t,  $J$  = 6 Hz, 2H, NHCH<sub>2</sub>CH<sub>2</sub>), 2.58 (b, 4H, N(CH<sub>2</sub>CH<sub>2</sub>)<sub>2</sub>); MS:  $m/z$ (%): 293(2%)[M<sup>+</sup>], 250(3), 243(2), 219(1), 180(12), 165(7), 117(3), 108(17), 100(100); HRMS  $m/z$  calcd for C<sub>12</sub>H<sub>15</sub>N<sub>5</sub>O<sub>4</sub> 293.1124; found 293.1120.

**4.1.3. *N*-(3'-Morpholinopropyl)-*N*-(7-nitrobenzo-2-oxa-1,3-diazol-4-yl)amine (1d).** The preparative procedure was largely the same as that for **1a** except that 2-morpholino-1-propanamine was the amine used and it was added over 1 h at room temperature followed by stirring for a further 24 h. The work-up was different in that the residue was crystallized from ethanol. Yield 68%. Mp 251–252 °C. <sup>1</sup>H NMR (CDCl<sub>3</sub>):  $\delta$  = 9.88 (b, 1H, NH), 8.47 (dd,  $J$  = 9, 0.6 Hz, 1H, ArH), 6.03 (d,  $J$  = 9 Hz, 1H, ArH), 3.93 (t,  $J$  = 4.5 Hz, 4H, O(CH<sub>2</sub>CH<sub>2</sub>)<sub>2</sub>), 3.60 (d,  $J$  = 1 Hz, 2H, NHCH<sub>2</sub>), 2.72 (t,  $J$  = 5 Hz, 2H, NHCH<sub>2</sub>CH<sub>2</sub>CH<sub>2</sub>), 2.61 (b, 4H, O(CH<sub>2</sub>CH<sub>2</sub>)<sub>2</sub>), 1.99 (m, 2H, NHCH<sub>2</sub>CH<sub>2</sub>); MS:  $m/z$ (%): 307(21%)[M<sup>+</sup>], 291(13), 263(5), 249(5), 217(6), 151(7), 119(19), 91(43), 57(100); HRMS  $m/z$  calcd for C<sub>13</sub>H<sub>17</sub>N<sub>5</sub>O<sub>4</sub> 307.3070; found 307.3064.

**4.1.4. *N,N*-Diethyl-*N'*-(7-nitrobenzo-2-oxa-1,3-diazol-4-yl)-1,3-propanediamine (1e).** The preparative procedure was largely the same as that for **1a** except that *N,N*-diethyl-1,3-propanediamine was the amine used and it was added over 1 h at room temperature. The work-up was different in that the residue was crystallized from ethanol. Yield 57%. Mp 182–183 °C. <sup>1</sup>H NMR [(CD<sub>3</sub>)<sub>2</sub>CO]:  $\delta$  = 8.50 (d,  $J$  = 9 Hz, 1H, ArH), 6.53 (d,  $J$  = 9 Hz, 1H, ArH), 3.88 (b, 2H, NHCH<sub>2</sub>), 3.57 (q,  $J$  = 7 Hz, 4H, N(CH<sub>2</sub>CH<sub>3</sub>)<sub>2</sub>), 3.21 (t,  $J$  = 6 Hz, 4H, NHCH<sub>2</sub>CH<sub>2</sub>CH<sub>2</sub>), 2.38 (m, 2H, NHCH<sub>2</sub>CH<sub>2</sub>), 1.15 (t,  $J$  = 7 Hz, 4H, N(CH<sub>2</sub>CH<sub>3</sub>)<sub>2</sub>); MS:  $m/z$ (%): 293(42%)[M<sup>+</sup>], 278(5), 256(3), 193(3), 117(6), 100(7), 86(100); HRMS  $m/z$  calcd for C<sub>13</sub>H<sub>19</sub>N<sub>5</sub>O<sub>3</sub> 293.1487; found 293.1496.

**4.1.5. *N,N,N'*-Trimethyl-*N'*-(7-nitrobenzo-2-oxa-1,3-diazol-4-yl)-1,2-ethanediamine (2).** The preparative procedure was largely the same as that for **1a** except that *N,N,N'*-trimethyl-1,2-ethanediamine was the amine used and it was added over 1 h at room temperature followed by refluxing for 1 h. The work-up was different in that the residue was chromatographed on a silica column with hexane–ethyl acetate (2:3, v/v). Yield 85%. Mp 129–130 °C. <sup>1</sup>H NMR [(CD<sub>3</sub>)<sub>2</sub>SO]:  $\delta$  = 8.62 (d,  $J$  = 8 Hz, 1H, ArH), 6.63 (d,  $J$  = 8 Hz, 1H, ArH), 4.39 (t,  $J$  = 6 Hz, 2H, CH<sub>3</sub>NCH<sub>2</sub>CH<sub>2</sub>), 3.61 (t,  $J$  = 6 Hz, 2H, CH<sub>3</sub>NCH<sub>2</sub>CH<sub>2</sub>),

2.74 (s, 6H, N(CH<sub>3</sub>)<sub>2</sub>), 2.60 (s, 3H, CH<sub>3</sub>NCH<sub>2</sub>CH<sub>2</sub>); MS:  $m/z$ (%): 265(46%)[M<sup>+</sup>], 243(8), 218(12), 160(43), 152(40), 119(18), 91(9), 58(100); HRMS  $m/z$  calcd for C<sub>11</sub>H<sub>15</sub>N<sub>5</sub>O<sub>3</sub> 265.1175; found 265.1185.

**4.1.6. 9-*N,N*-Di(prop-2'-yl)-aminomethylanthracene (4).** 9-Bromomethylanthracene<sup>47</sup> (0.5 g, 1.9 mmol) was refluxed with diisopropylamine (15 ml, 109 mmol) for 8 h. The reaction mixture was concentrated and partitioned between toluene and dilute aqueous HCl. The product was precipitated from the aqueous layer with NaOH and crystallized from ethanol. Yield 28%. Mp 130–130.5 °C. <sup>1</sup>H NMR (CDCl<sub>3</sub>):  $\delta$  = 8.75 (d,  $J$  = 8 Hz, 2H, ArH), 8.4 (s, 1H, ArH), 8.00 (d,  $J$  = 8 Hz, 2H, ArH), 7.49 (m, 4H, ArH), 4.71 (s, 2H, ArCH<sub>2</sub>N), 3.02 (m, 2H, (CH(CH<sub>3</sub>)<sub>2</sub>)<sub>2</sub>), 1.23 (d,  $J$  = 7 Hz, 12H, (CH(CH<sub>3</sub>)<sub>2</sub>)<sub>2</sub>); MS:  $m/z$ (%): 291(20%)[M<sup>+</sup>], 276(10), 249(20), 191(100).

### Acknowledgements

We thank The European Social Fund, The Department of Employment and Learning in Northern Ireland, Invest NI (RTD COE 40) and the European Union (HPRN-CT-2000-00029) for support. Professor Anunay Samanta (University of Hyderabad, India) is specially thanked for a robust debate about some of the issues. A referee is also thanked for a valuable input.

### References and notes

- (a) de Silva, A. P.; Gunaratne, H. Q. N.; Gunnlaugsson, T.; Huxley, A. J. M.; McCoy, C. P.; Rademacher, J. T.; Rice, T. R. **1997**, *Chem. Rev.* **97**, 1515. (b) *Chemosensors of Ion and Molecule Recognition*; Desvergne, J.-P., Czarnik, A. W., Eds.; Kluwer: Dordrecht, 1997. (c) *Luminescent Sensors*; Fabbri, L., Ed.; *Coord. Chem. Rev.*; 2000, 1. (d) Valeur, B. *Molecular Fluorescence*; Wiley: Weinheim, 2002. (e) Rurack, K.; Resch-Genger, U. **2002**, *Chem. Soc. Rev.* **31**, 116.
- Bissell, R. A.; de Silva, A. P.; Gunaratne, H. Q. N.; Lynch, P. L. M.; Maguire, G. E. M.; Sandanayake, K. R. A. S. *Chem. Soc. Rev.* **1992**, **21**, 187.
- (a) Tsien, R. Y. *Chem. Eng. News*, **1994**, July 18, 34. (b) Valeur, B. In *Topics in Fluorescence Spectroscopy*; Lakowicz, J. R., Ed.; Probe Design and Chemical Sensing; Plenum: New York, 1994; Vol. 4, p 21.
- Lehn, J.-M. *Supramolecular Chemistry*; VCH: Weinheim, 1995.
- (a) Bissell, R. A.; de Silva, A. P.; Gunaratne, H. Q. N.; Lynch, P. L. M.; Maguire, G. E. M.; McCoy, C. P.; Sandanayake, K. R. A. S. *Top. Curr. Chem.* **1993**, **168**, 223. (b) Czarnik, A. W. *Acc. Chem. Res.* **1994**, **27**, 302. (c) Fabbri, L.; Poggi, A. *Chem. Soc. Rev.* **1995**, **24**, 197.
- Mei, M. H.; Wu, S. K. *New J. Chem.* **2001**, **25**, 471.
- de Silva, A. P.; Gunaratne, H. Q. N.; Rice, T. E. *Angew. Chem., Int. Ed. Engl.* **1996**, **35**, 2116.
- (a) de Silva, A. P.; Gunaratne, H. Q. N.; McCoy, C. P. *Chem. Commun.* **1996**, 2399. (b) de Silva, A. P.; Gunaratne, H. Q. N.; McCoy, C. P. *Nature (London)* **1993**, **364**, 42.



9. Balzani, V.; Scandola, F. *Supramolecular Photochemistry*; Ellis-Horwood: Chichester, 1991.
10. (a) Grigg, R.; Norbert, W. D. J. A. *J. Chem. Soc., Chem. Commun.* **1992**, 1298. (b) Di Pietro, C.; Guglielmo, G.; Campagna, S.; Diotti, M.; Manfredi, A.; Quici, S. *New J. Chem.* **1998**, 22, 1037. (c) Fabbri, L.; Licchelli, M.; Pallavicini, P. *Angew. Chem., Int. Ed. Engl.* **1998**, 37, 800. (d) Pina, F.; Melo, M. J.; Bernardo, M. A.; Luis, S. V.; Garcia-Espana, E. *J. Photochem. Photobiol., A: Chem.* **1999**, 126, 65. (e) Dilek, G.; Akkaya, E. U. *Tetrahedron Lett.* **2000**, 41, 3721.
11. de Silva, A. P.; McClenaghan, N. D. *Chem. Eur. J.* **2002**, 8, 4935.
12. Daffy, L. M.; de Silva, A. P.; Gunaratne, H. Q. N.; Huber, C.; Lynch, P. L. M.; Werner, T.; Wolfbeis, O. S. *Chem. Eur. J.* **1998**, 4, 1810.
13. *Fibre Optic Chemical Sensors and Biosensors*; Wolfbeis, O. S., Ed.; CRC: Boca Raton, 1991; Vols 1 and 2.
14. Mukherjee, S.; Chattopadhyay, A.; Samanta, A.; Soujanya, T. *J. Phys. Chem.* **1994**, 98, 2809. Saha, S.; Samanta, A. *J. Phys. Chem., A* **1998**, 102, 7903.
15. de Costa, M. D. P.; de Silva, A. P.; Pathirana, S. T. *Can. J. Chem.* **1987**, 69, 1416.
16. Roiron, J.; Fox, D. B., Work in progress at Queen's University.
17. (a) Ramachandram, B.; Samanta, A. *Chem. Phys. Lett.* **1998**, 290, 9. (b) Ramachandram, B.; Samanta, A. *J. Phys. Chem., A* **1998**, 102, 10579.
18. (a) Mitchell, K. A.; Brown, R. G.; Yuan, D.; Chang, S.-C.; Utecht, R. E.; Lewis, D. E. *J. Photochem. Photobiol., A: Chem.* **1998**, 115, 157. (b) Badugu, R. *Chem. Lett.* **2002**, 106, 5572. (c) Grabchev, I.; Qian, X. H.; Xiao, Y.; Zhang, R. *New J. Chem.* **2002**, 26, 920. (d) Grabchev, I.; Chovelon, J. M.; Qian, X. H. *New J. Chem.* **2003**, 27, 337.
19. (a) Ramachandram, B.; Samanta, A. *Chem. Commun.* **1997**, 1037. (b) Banthia, S.; Samanta, A. *J. Phys. Chem., B* **2002**, 106, 5572.
20. See for example, Dekkers, D. W. C.; Comfurius, P.; Schroit, A. J.; Bevers, E. M.; Zwaal, R. F. A. *Biochemistry* **1998**, 37, 14833.
21. See for example, (a) Al Dirbashi, O.; Kuroda, N.; Nakashima, K. *Anal. Chim. Acta* **1998**, 365, 169. (b) Uzu, S.; Kanda, S.; Nakashima, K.; Imai, K. *Analyst* **1990**, 115, 1477.
22. (a) Lytton, S. D.; Cabantchik, Z. I.; Libman, J.; Shanzer, A. *Mol. Pharmacol.* **1991**, 40, 584. (b) Chen, Y.; Shanzer, A. *J. Am. Chem. Soc.* **1996**, 118, 12386. (c) Meijler, M. M.; Arad-Yellin, R.; Cabantchik, Z. I.; Shanzer, A. *J. Am. Chem. Soc.* **2002**, 124, 12666.
23. Street, K. W.; Krause, S. A. *Anal. Lett.* **1986**, 19, 735.
24. Forst, H.; Pacey, R. E. *Talanta* **1989**, 36, 335.
25. (a) Resch, U.; Rurack, K.; Bricks, J. L.; Slominski, J. L. *J. Fluoresc.* **1997**, 7, 231S. (b) Boiocchi, M.; Fabbri, L.; Licchelli, M.; Sacchi, D.; Vasquez, M.; Zampa, C. *Chem. Commun.* **2003**, 1812.
26. Onoda, M.; Uchiyama, S.; Santa, T.; Imai, K. *Luminescence* **2002**, 17, 11.
27. Weller, A. *Pure Appl. Chem.* **1968**, 16, 115.
28. de Silva, A. P.; Gunaratne, H. Q. N.; Lynch, P. L. M.; Patty, A. L.; Spence, G. L. *J. Chem. Soc., Perkin Trans. 2* **1993**, 1611.
29. Connors, K. *Binding Constants: the Measurement of Molecular Complex Stability*; Wiley: New York, 1987.
30. Klopfer, W. *Adv. Photochem.* **1977**, 10, 311.
31. de Silva, A. P.; Gunaratne, H. Q. N.; Habib-Jiwan, J.-L.; McCoy, C. P.; Rice, T. E.; Soumillion, J.-P. *Angew. Chem., Int. Ed. Engl.* **1995**, 34, 1728.
32. (a) Serjeant, E. P.; Dempsey, B. *Ionization Constants of Organic Acids in Aqueous Solution*; Pergamon: New York, 1979. (b) Perrin, D. D. *Dissociation Constants of Organic Bases in Aqueous Solution*; Butterworths: London, 1972.
33. Isaacs, N. S. *Physical Organic Chemistry*; Longman: Harlow, 1995.
34. de Silva, A. P.; Rupasinghe, R. A. D. D. *J. Chem. Soc., Chem. Commun.* **1985**, 1669.
35. Cotton, F. A.; Wilkinson, G. *Advanced Inorganic Chemistry*; Wiley: New York, 1966.
36. (a) Mann, C. K.; Barnes, K.K. *Electrochemical Reactions in Nonaqueous Systems*; Dekker: New York, 1970. (b) Siegeman, H. In *Technique of Electroorganic Synthesis*; Weinberg, N. L., Ed.; Wiley: New York, 1975.
37. Wang, W.; Springsteen, G.; Gao, S. H.; Wang, B. H. *Chem. Commun.* **2000**, 1283.
38. Arimori, S.; Ward, C. J.; James, T. D. *Chem. Commun.* **2001**, 2018.
39. (a) Jonker, S. A.; Ariese, F.; Verhoeven, J. W. *Recl. Trav. Chim. Pays-Bas* **1989**, 108, 109. (b) Jonker, S. A.; Verhoeven, J. W.; Reiss, C. A.; Goubitz, K.; Heijdenrijk, D. *Recl. Trav. Chim. Pays-Bas* **1990**, 109, 154.
40. Rurack, K.; Kollmannsberger, M.; Resch-Genger, U.; Daub, J. *J. Am. Chem. Soc.* **2000**, 122, 968.
41. (a) Prodi, L.; Bargossi, C.; Montalti, M.; Zaccaroni, N.; Su, N.; Bradshaw, J.; Izatt, R. M.; Savage, P. B. *J. Am. Chem. Soc.* **2000**, 122, 6769. (b) Nolan, E. M.; Lippard, S. J. *J. Am. Chem. Soc.* **2003**, 125, 14270. (c) Guo, X.; Qian, X.; Jia, L. *J. Am. Chem. Soc.* **2004**, 126, 2272.
42. Kubo, Y.; Tozawa, T.; Maruyama, S.; Tokita, S. *Abstr. Int. Conf. Supramol. Sci. Technol.* **1998**, 1, 96.
43. Ghosh, P.; Bharadwaj, P. K.; Mandal, S.; Ghosh, S. *J. Am. Chem. Soc.* **1996**, 118, 1553. Ghosh, P.; Bharadwaj, P. K.; Roy, J.; Ghosh, S. *J. Am. Chem. Soc.* **1997**, 119, 11903.
44. Klein, G.; Kaufmann, D.; Schürch, S.; Reymond, J.-L. *Chem. Commun.* **2001**, 561.
45. Sankaran, N. B.; Banthia, S.; Das, A.; Samanta, A. *New J. Chem.* **2002**, 26, 1529.
46. Matsushita, Y.; Takahashi, M.; Moriguchi, I. *Chem. Pharm. Bull.* **1986**, 34, 333.
47. Clements, J. H.; Webber, S. E. *J. Phys. Chem.* **1999**, 103, 9366.

# Colorimetric sensor arrays for molecular recognition

Kenneth S. Suslick,\* Neal A. Rakow and Avijit Sen

*Department of Chemistry, University of Illinois at Urbana-Champaign, 600 S. Mathews Av., Urbana, IL 61801, USA*

Received 28 July 2004; accepted 3 September 2004

Available online 1 October 2004

**Abstract**—The development of colorimetric sensor arrays for the detection of volatile organic compounds is reported. Using an array of chemo-responsive dyes, enormous discriminatory power is created in a simple device that can imaged easily with an ordinary flat-bed scanner. High sensitivities (ppb) have been demonstrated for the detection of biologically important analytes, including amines, carboxylic acids, and thiols. By the proper choice of dyes and substrate, the array can be made essentially non-responsive to changes in humidity. © 2004 Elsevier Ltd. All rights reserved.

## 1. Introduction

The generalized detection of volatile organic compounds (VOCs) is often referred to as electronic nose technology, and has generally been based on sensors that detect adsorption into a set of polymers or on electrochemical oxidations at a set of heated metal oxides.<sup>1,2</sup> In spite of some successes with such systems, the discrimination of compounds at low concentrations or within a given chemical class and the absence of interference from changes in humidity remain challenging goals. We have previously reported the colorimetric array detection of a wide range of odorants using metalloporphyrins.<sup>3–6</sup> The importance of including Lewis acids in such an array is emphasized by the recent indications that the mammalian olfactory receptors are in fact metalloproteins.<sup>7</sup> Here we review extensions of that concept to the development of an expanded colorimetric array detector.

## 2. The colorimetric sensor array

Fundamentally, molecular recognition involves the interactions between molecules: i.e. bond formation, acid–base interactions, hydrogen-bonding, dipolar and multipolar interactions,  $\pi$ – $\pi$  molecular complexation, and last and not least, van der Waals interaction and physical adsorption. Nearly all prior sensor technology relies essentially exclusively on van der Waals and physical adsorption, the weakest and least selective of forces between molecules. We

believe this to be a fundamental flaw in the development of sensors with both high sensitivity and high selectivity. In many ways, our colorimetric sensor array revisits the earlier, pre-electronic era of analytical chemistry,<sup>8</sup> with the addition of modern digital imaging.

The design of the colorimetric sensor array is based on two fundamental requirements: (1) the chemo-responsive dye must contain a center to interact strongly with analytes, and (2) this interaction center must be strongly coupled to an intense chromophore. The first requirement implies that the interaction must not be simple physical adsorption, but rather must involve other, stronger chemical interactions. Chemo-responsive dyes are those dyes that change color, in either reflected or absorbed light, upon changes in their chemical environment. The consequent dye classes from these requirements are (1) Lewis acid/base dyes (i.e. metal ion containing dyes), (2) Brønsted acidic or basic dyes (i.e. pH indicators), and (3) dyes with large permanent dipoles (i.e. zwitterionic solvatochromic dyes) (Fig. 2). In addition, we have incorporated our own bis-pocketed metalloporphyrins<sup>9</sup> to provide an aspect of shape-selective sensing to the array.

Disposable colorimetric arrays of chemo-responsive dyes have been created by printing the dyes on various inert solid supports, e.g. reverse phase silica gel plates, acid-free paper, or porous membranes of various polymers (e.g. nylon, PVDF). The specific array used in this work (Fig. 1) was spotted on C2 reverse phase silica gel plates using 0.1  $\mu$ L microcapillary pipettes. Arrays are commercially available from ChemSensing, Inc., Northbrook, Illinois ([www.chemsensing.com](http://www.chemsensing.com)), part number CSI.042 (Fig. 2).

For recognition of analytes with Lewis acid/base

*Keywords:* Sensors; Volatile organic compounds; VOC; Metalloporphyrins; Dyes; Electronic nose.

\* Corresponding author. Tel.: +1 217 333 2794; fax: +1 217 333 2685; e-mail: [ksuslick@uiuc.edu](mailto:ksuslick@uiuc.edu)



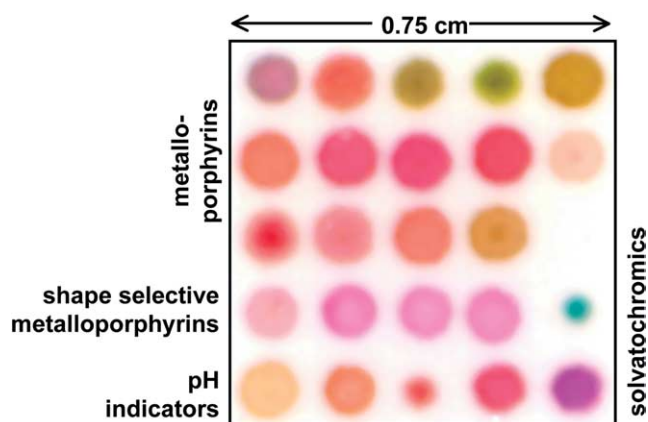


Figure 1. A colorimetric sensor array.

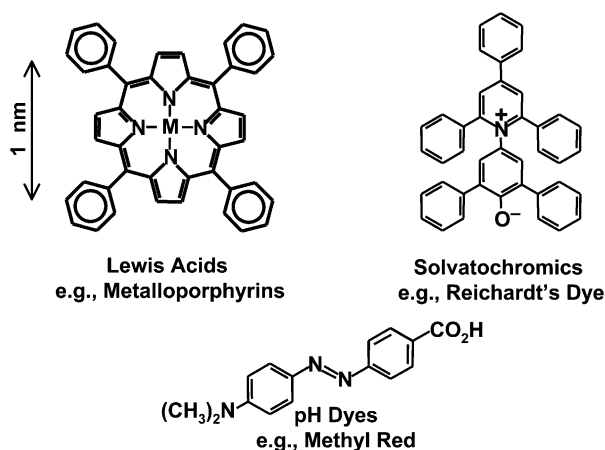


Figure 2. The components of colorimetric sensor arrays are inherently nanoscale.

capabilities, the use of porphyrins and their metal complexes are a natural choice. Metalloporphyrins are nearly ideal for the detection of metal-ligating vapors because of their open coordination sites for axial ligation, their large spectral shifts upon ligand binding, and their intense coloration. A series of metalated tetraphenylporphyrins (TPP) was used to provide differentiation based on metal-selective coordination.

Common pH indicator dyes change color in response to changes in the proton (Brønsted) acidity or basicity of their environment. Solvatochromic dyes change color in response to changes in the general polarity of their environment, primarily through strong dipole–dipole interactions. To some extent, all dyes inherently are solvatochromic, although some are much more responsive than others; among the most responsive are Reichardt's Dye and Nile Red.

In addition, our array incorporates a series of Zn-substituted, bis-pocketed porphyrins, based on *ortho*-substitution of the tetraphenylporphyrin core to differentiate analytes based on size and shape. These compounds include a family of silylether porphyrins with large, medium, and small pockets on both faces of the porphyrin (Figs. 3 and 4). These have been previously shown to exhibit extremely selective binding of organic ligands (Fig. 5).<sup>9</sup>

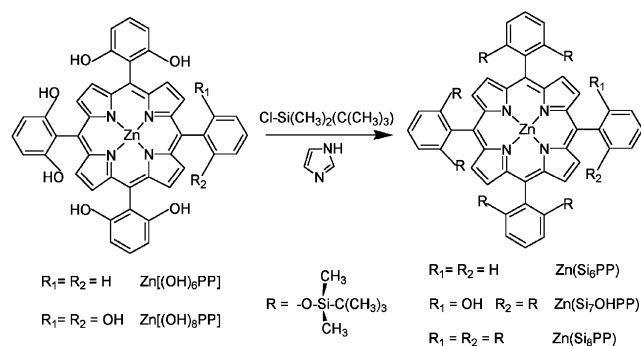


Figure 3. Silylether bis-pocket porphyrin synthesis.

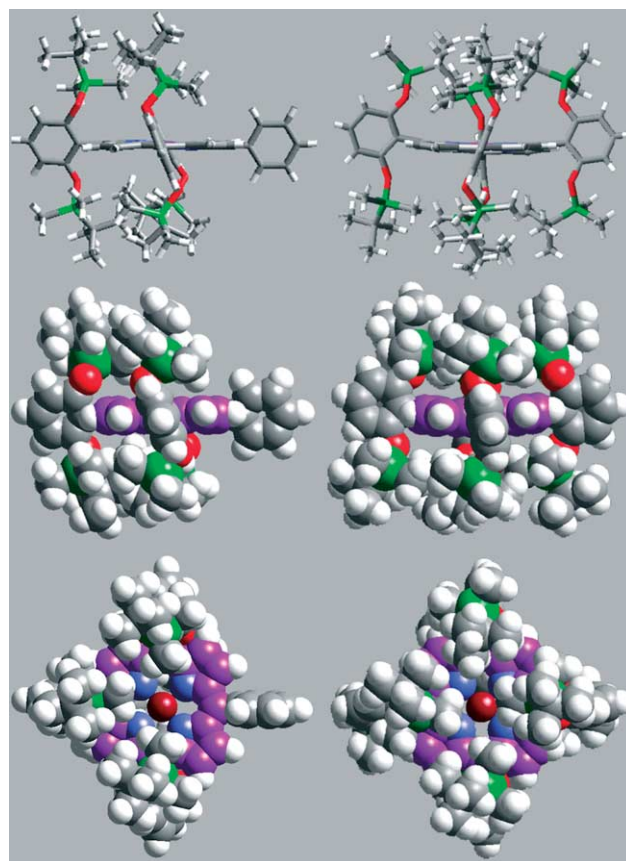
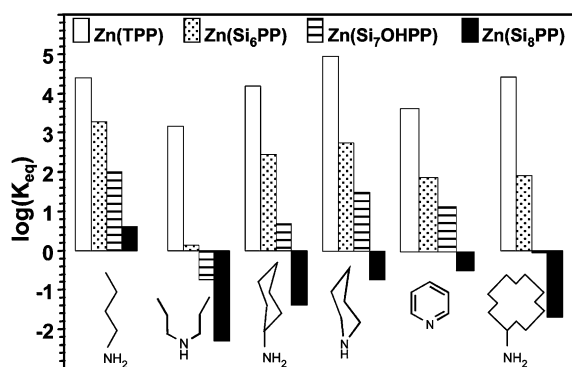


Figure 4. Molecular models of Zn(Si<sub>6</sub>PP) (left column) and Zn(Si<sub>8</sub>PP) (right column). The pairs of images from top to bottom are cylinder side-views, side-views, and top-views, respectively; space filling shown at 70% van der Waals radii; with the porphyrin carbon atoms shown in purple, oxygen atoms in red, silicon atoms in green, and Zn in dark red. The X-ray single crystal structure of Zn(Si<sub>8</sub>PP) is shown;<sup>9</sup> for Zn(Si<sub>6</sub>PP), an energy-minimized structure was obtained using Cerius 2 from MSI.

### 3. Discrimination of VOCs

In order to demonstrate the ability of the sensor array to discriminate among different volatile organics, the sensor array responses were determined for a series of different volatiles representing the common organic functionalities: amines, arenes, alcohols, aldehydes, carboxylic acids, esters, halocarbons, ketones, phosphines, sulfides, and thiols. These patterns are shown in Figure 6. Excellent discrimination among these analytes is observed even without any chemometric manipulations.



**Figure 5.** Ligand binding constants for siloxyl porphyrins compared to Zn(TPP) for a series of amines. The binding constants of silylether porphyrins are remarkably sensitive to the shape and size of the substrates relative to Zn(TPP) and can be controlled over a range of  $10^1$  to  $10^7$  relative to Zn(TPP). These selectivities originate from strong steric repulsions created by the *t*-butyldimethylsiloxyl substituents. The steric congestion caused by these bulky silylether groups is pronounced even for linear amines and small cyclic amines.

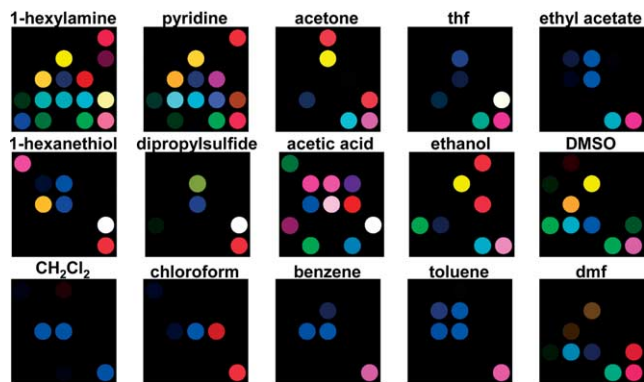


**Figure 6.** Colorimetric array responses for 18 common volatile organic compounds at saturation vapor pressure at 300 K.

An Epson Perfection 1250 flatbed scanner was used for scanning. The ‘before’ image was first acquired on the flatbed scanner; an array was then exposed to a flowing stream of  $N_2$  containing the analyte of interest, and the array was then scanned again after equilibration. The center of each dye spot ( $\sim 700$  pixels, 15 pixel radius) was averaged and the value from the before image subtracted; this can be done with Photoshop™ or with a customized software package, ChemEye™ (ChemSensing, Inc.). The arrays are disposable and are not meant for re-use, especially after exposure to high analyte concentrations.

Gas streams containing the vapor of interest were generated by flowing nitrogen through the neat liquid analyte in a thermostated, glass-fritted bubbler. To vary analyte concentrations, serial dilution in nitrogen using digital mass-flow controllers was utilized. Vapor pressures were calculated using published data.<sup>10</sup> All liquid analytes were obtained from Aldrich or Fisher Scientific and used as received.

Each analyte response is represented as the red, green, and blue values of each of the 24 dyes, i.e. a 72 dimensional vector. To examine the multivariate distances between the analyte responses in this 72-dim. RGB color space, a hierarchical cluster analysis (HCA) was performed; this analysis makes use of only the digital data representing the observed difference maps—no chemical information is included. The resulting dendrogram for the responses to saturated analyte vapors is shown in Figure 7. Remarkably, the clusters formed are in keeping with the qualitative structural and electronic properties of the VOCs. The familial similarities among compounds of the same functionality are exceptional: amines, alcohols, aldehydes, esters, etc. are all easily distinguished from each other. The only exception to this appears to be the pair of ketones, methyl ethyl ketone and 4-hexanone (methyl amyl ketone), which overlap into the ester and ether subgroups, respectively. This slight intergroup confusion may reflect the inclusion of too few ketones (i.e. two) to form a recognizable class out of sample of 32 VOCs.

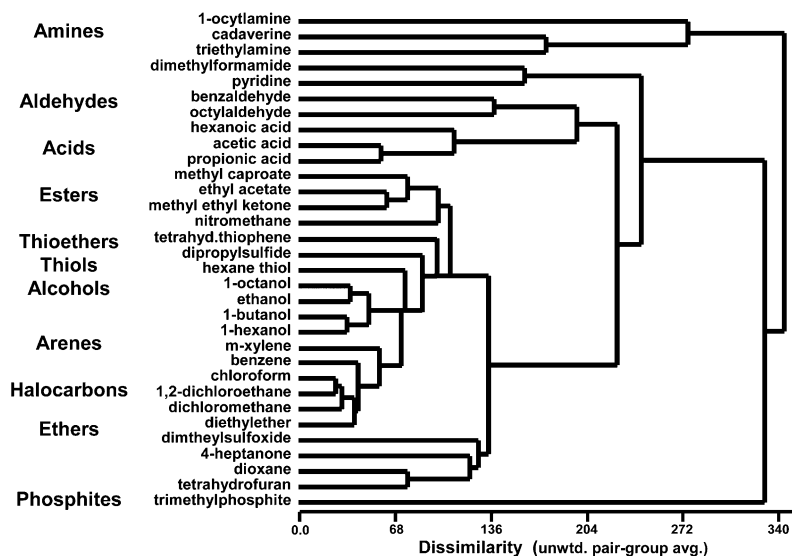


**Figure 7.** Dendrogram of the colorimetric array responses to 32 common organic compounds at full vapor pressure at 300 K. XLStat analysis package, v. 5.1, unweighted pair-group average agglomerative hierarchical cluster analysis.

A principal component analysis (PCA) of the full set of the VOC patterns reveals a surprisingly high degree of dispersion among the independent dimensions created by linear combinations of the RGB responses of the 24 dyes used in these arrays. The PCA shows that 95% of the discriminatory range requires 12 dimensions and 99% requires 20 dimensions. This extremely high dispersion reflects the very wide range of chemical-properties space being probed by our choice of chemoresponsive dyes. In comparison, most prior electronic nose technology is dominated by only a two or three independent dimensions (one of which, hydrophobicity, often accounts for 90% of the discrimination);<sup>1,2</sup> this is the inherent result of relying on van der Waals interactions for molecular recognition.

With a 24-dye array, each of the 72 dimensions (i.e. 24 RGB's) can take on one of 256 possible values (for inexpensive 8 bit scanners or digital cameras). The theoretical limit of discrimination, then, would be the number of possible patterns, i.e.  $(256)^{72}$ . Realistically, however, the RGB vector components do not range over the full 256 possible values; we do observe R, G, and B values vary over a range of 40. To discriminate patterns, let us assume a change of at least four is needed in the R, G, or B value (we can actually easily discriminate with changes of two). From the PCA, not all of the 75 dimensions are equally important. In fact, roughly 95% of all information is contained in  $\sim 12$  specific dimensions (i.e. linear combinations of the 72 different R, G, and B values). This implies a 'practical' limit of discrimination that is still immensely large:  $(40/4)^{12} = 10^{12}$  distinct patterns should be recognizable in a 24-dye colorimetric sensor array.

#### 4. Interference from humidity

One of the most serious weaknesses in current electronic nose technology is sensitivity to changes in humidity. Water vapor ranges in the environment from  $<2000$  to  $>20,000$  ppm; if one is interested in few ppm concentrations of VOCs, even a very low level of interference from water is therefore intolerable. Because the colorimetric array has been selected from hydrophobic, water insoluble dyes, these arrays are essentially impervious to changes in relative humidity. As shown in Figure 8, the dyes are essentially unresponsive to water vapor. The water–vapor

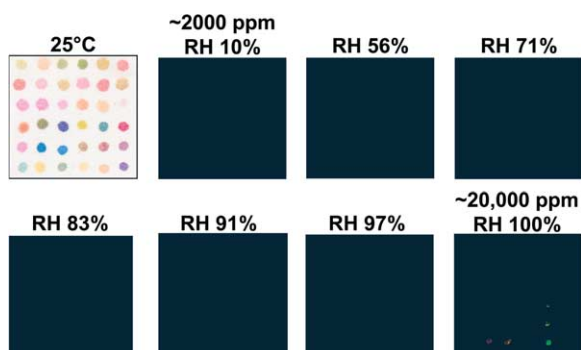


**Figure 8.** The colorimetric array is insensitive to changes in relative humidity. Similarly, changes in humidity do not significantly affect the color fingerprints of other analytes.

insensitivity of our technology gives it a substantial advantage.

#### 5. Sensitivity

Our colorimetric array sensor technology is based on strong and relatively specific interactions between the analytes and a chemoresponsive dye library. This is in marked contrast to prior electronic nose technology that relies on weak and extremely non-specific interactions (e.g. physical adsorption into polymers) between the analytes and the detectors. For example, the prior use of adsorption into polymer arrays (e.g. conductive polymer arrays, quartz microbalance or surface acoustic wave detectors coated with a variety of polymers, or polymers doped with single indicating fluorophore) depends upon weak matrix–analyte interactions to provide limited selectivity and relatively poor sensitivity. A major advantage of our sensor arrays is that they are able to provide unique patterns for the identification of odors even at extremely low vapor concentrations because we rely on strong interactions between analyte and sensor dyes for molecular recognition.

Metal–ligand (i.e. metal–analyte) bonds range in their bond enthalpies from  $\sim 40$  to  $\sim 200$  kJ/mol. In non-coordinating solvents (e.g. alkanes), equilibrium binding constants are often  $>10^6 \text{ M}^{-1}$ . For pyridine, the vapor pressure is 0.02 atm at room temperature, so we have a Raoult's constant of  $\sim 2 \times 10^{-3} \text{ atm M}^{-1}$ . For a binding constant of  $\sim 10^6 \text{ M}^{-1}$ , this is equivalent to  $\sim 2$  ppb vapor. In contrast, the enthalpy of physical adsorption (e.g. into polymers) is only  $\sim 5$  to 20 kJ/mol (i.e. roughly a tenth of a metal bond). Therefore, the equilibrium constant for adsorption will typically be only about  $5 \times 10^{-5}$  as large as that for ligation to metal ions. Therefore, ligation is intrinsically  $\sim 20,000$ -fold more sensitive than adsorption into polymers. Differences in the sensitivity of detection techniques, of course, can either enhance or diminish this intrinsic advantage of ligation and other strong interactions over physical adsorption and other weak interactions (e.g. van der Waals).

As shown in Figure 9, this expectation of improved sensitivities is realized experimentally. Even GC-MS achieves typically only ppm to 100 ppb sensitivities for VOCs in the absence of pre-concentration. Figure 9 shows, however, that sub-ppm discrimination is not a problem with our colorimetric array detection for functionalized analytes such as thiols, amines and carboxylic acids. In fact, we can extend our sensitivities down to the low ppb regime for many such analytes. Extension of sensitivity by improved imaging technology (e.g. true 16-bit or 24-bit color resolution in place of our currently used 8-bit scanners) may improve our sensitivity by a thousand-fold.

It is worth noting that for these colorimetric arrays, every analyte at a different concentration is best thought of as a different analyte. For each analyte, a specific dye will begin to change color at some concentration and as the concentration of the analyte increases, the color change will saturate asymptotically; some dyes change at low concentrations of any given analyte but some only at very high concentrations. Quantitative analysis of single analytes



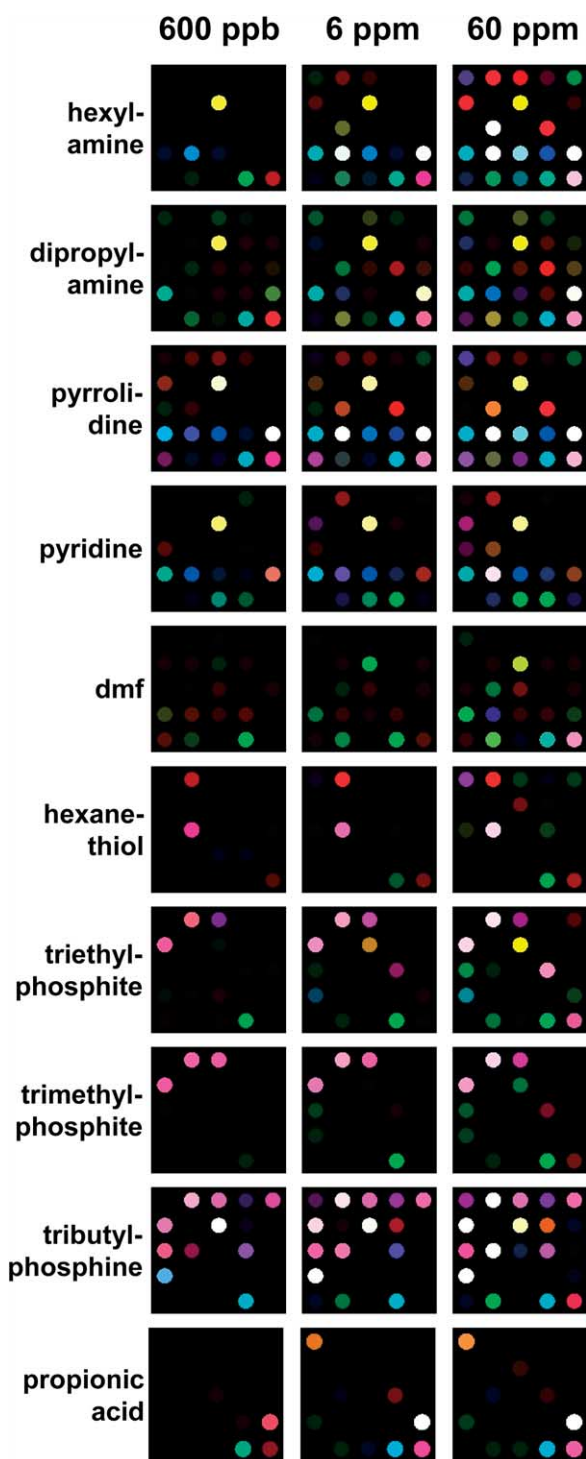


**Figure 9.** Colorimetric array sensitivity to low molecular weight analytes. Limits of recognition are well below 1 ppm.

(or of a single analyte changing in a constant background) can be done easily by comparison with a library of analyte patterns as a function of concentration.

## 6. Complex mixtures

Electronic nose techniques, in general, give a composite response to complex mixtures, as indeed does the mammalian olfactory system. Chemists very naturally

tend to assume that for any complex mixture, the single analytical goal is a complete component-by-component analysis. But in fact, multiple analytic goals for complex mixtures are conceivable: comparison to a standard (e.g. quality control, counterfeit detection), identification of chemical class or family of an unknown VOC, correlation of odors to properties (e.g. ‘good smelling’ as determined by a human sensory evaluation panel), changes in concentrations of a few components against a constant background, and of course, a complete component by component (CBC) analysis. Separation techniques (e.g. GC, HPLC, CE, etc.) excel at CBC analyses. For many other applications, however, a composite response may not only be sufficient, but actually preferred. Too much data is often only slightly better than not enough.

For rapid determination of identity of a complex mixture, for example, we find that colorimetric array sensors can fill an important niche. As a closing example, consider the results of Figure 10 as an interesting comparison among complex odorants.

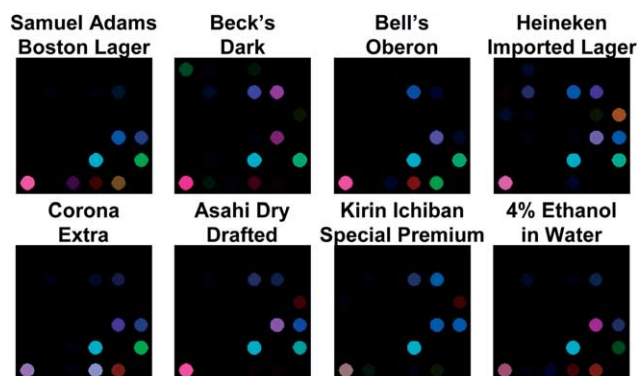


**Figure 10.** Colorimetric array analysis of a complex mixture: headspace analysis of various beers compared to 4% ethanol in water.

## Acknowledgements

This work was supported by the US NIH (HL 25934) and in part by the DOE Seitz Materials Research Laboratory under Grant DEFG02-91-ER45439. The authors are particularly grateful to the students who have and are continuing the development of this work: William B. McNamara III, Margaret A. Kosal, Jennifer Wilson, Chen Zhang, and Michael Janzen.

## References and notes

1. Albert, K. J.; Lewis, N. S.; Schauer, C. L.; Sotzing, G. A.; Stitzel, S. E.; Vaid, T. P.; Walt, D. R. *Chem. Rev.* **2000**, *100*, 2595.
2. Gardner, J. W.; Bartlett, P. N. *Electronic Noses: Principles and Applications*; Oxford University Press: New York, 1999.
3. Rakow, N. A.; Suslick, K. S. *Nature* **2000**, *406*, 710.
4. Rakow, N. A.; Suslick, K. S. *Artificial Chemical Sensing: Olfaction and the Electronic Nose*; Stetter, J. R., Pensrose,

- W. R., Eds.; Electrochem. Soc.: Pennington, NJ, 2001; pp 8–14.
5. Suslick, K. S.; Rakow, N. A. U.S. Patent 6,368,558, Apr 9, 2002.
  6. Suslick, K. S.; Rakow, N. A.; Sen, A. U.S. Patent 6,495,102 B1, Dec 17, 2002.
  7. Wang, J.; Luthey-Schulten, Z.; Suslick, K. S. *Proc. Natl. Acad. Sci. U.S.A.* **2003**, *100*, 3035.
  8. Kolthoff, I. M. *Acid Base Indicators*, Rosenblum, C., Trans.; Macmillan: New York, 1937.
  9. Sen, A.; Suslick, K. S. *J. Am. Chem. Soc.* **2000**, *122*, 11565.
  10. Yaws, C. L. *Handbook of Vapor Pressure*; Gulf: Houston, 1994.



# Origins of ‘on–off’ fluorescent behavior of 8-hydroxyquinoline containing chemosensors

R. Todd Bronson,<sup>a</sup> Marco Montalti,<sup>b</sup> Luca Prodi,<sup>b,\*</sup> Nelsi Zaccheroni,<sup>b</sup> Randy D. Lamb,<sup>a</sup>  
 N. Kent Dalley,<sup>a</sup> Reed M. Izatt,<sup>a</sup> Jerald S. Bradshaw<sup>a</sup> and Paul B. Savage<sup>a,\*</sup>

<sup>a</sup>Department of Chemistry and Biochemistry, Brigham Young University, C100 BNSN, Provo, UT 84602, USA

<sup>b</sup>Dipartimento di Chimica ‘G. Ciamician’, Università degli studi di Bologna, Via Selmi 2, I 40126, Bologna, Italy

Received 9 February 2004; revised 26 July 2004; accepted 20 August 2004

Available online 22 September 2004

**Abstract**—Derivatives of 8-hydroxyquinoline were used as model compounds to probe the pathways of non-radiative relaxation of fluorophores in two fluorescent chemosensors. Results suggest that both photo-induced proton transfer and photo-induced electron transfer contribute to quenching the fluorescence of the chemosensors. Crystal structures of an 8-hydroxyquinoline-containing chemosensor complexed to various metal ions indicate that a proton shift occurs concomitant with complex formation. This proton shift precludes both photo-induced proton and electron transfer allowing fluorescence emission from chemosensor-metal ion complexes.

© 2004 Elsevier Ltd. All rights reserved.

## 1. Introduction

The realization of the potential hazardous effects that specific metal ions can play on human health has led,<sup>1</sup> in part, to the development of ion-selective chemosensors for transition and post-transition metal ions.<sup>2</sup> Chemosensors are molecules that associate with a target analyte and provide a measurable response indicative of binding. Particular attention has been paid to fluorescent chemosensors, because fluorescence modulation may provide a means of detecting very low concentrations of targeted metal ions.<sup>3</sup>

Multiple strategies have been used in the development of chemosensors that modulate their fluorescence upon association with metal ions. One of the most successful methods takes advantage of photo-induced electron transfer (PET) from an amino group to an excited fluorophore.<sup>2</sup> While an amino group appended to a fluorophore retains its lone pair of electrons, it effectively quenches fluorescence. However, upon complexation with a metal cation, the lone pair is no longer free to quench fluorescence and chelation-enhanced fluorescence<sup>4</sup> is observed. This approach is advantageous because it provides an ‘off–on’ sensing response to metal ion binding, which decreases the likelihood of false positive results. Another strategy that

has been used by us<sup>5</sup> and others,<sup>6</sup> involves appending 8-hydroxyquinoline (8-HQ) derivatives to metal ion chelating groups. Alone, 8-HQ is only very weakly fluorescent; in its excited state, intramolecular proton transfer (oxygen to nitrogen) provides a route for non-radiative relaxation.<sup>7</sup> Chelation of metal ions can decrease the pK<sub>a</sub> values of the hydroxyl proton, and once this proton is lost, 8-HQ becomes highly fluorescent.<sup>8</sup> Consequently, chemosensors using 8-HQ also provide an ‘off–on’ sensing response to metal ion binding.

The first potential chemosensor we reported that contains 8-HQ displayed very high affinity for Ba<sup>2+</sup>;<sup>9</sup> however, the pK<sub>a</sub> of the hydroxyl group on 8-HQ in the Ba<sup>2+</sup> complex was not sufficiently lowered to allow deprotonation below pH = 8.<sup>8</sup> Consequently, this compound did not prove to be a useful chemosensor. In contrast, compounds **1** and **2** (Fig. 1) proved to be effective chemosensors for Mg<sup>2+</sup> and Hg<sup>2+</sup>,

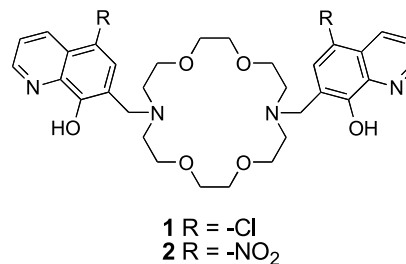


**Figure 1.** Structures of chemosensors **1** and **2**.

**Keywords:** Chemosensor; Fluorescence; Photophysical; General base; Quinoline.

\* Corresponding authors. Tel.: +1-801-422-4020; fax: +1-801-422-0153 (P.B.S.); e-mail addresses: paul\_savage@byu.edu; luca.prodi@unibo.it

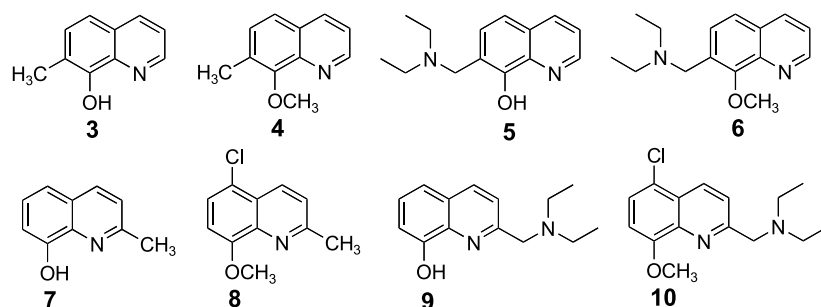


Figure 2. Structures of model compounds 3–10.

respectively, because they not only display high affinity for their target metal ion, but in their metal ion complexes the  $pK_a$ s of the hydroxyl groups on 8-HQ moieties are lowered sufficiently that the complexes become fluorescent even in slightly acidic solutions.<sup>5a,d</sup>

In chemosensors **1** and **2**, the 8-HQ groups and the amines to which they are appended are in an arrangement similar to that found in chemosensors that employ PET to ‘turn off’ fluorescence in the uncomplexed forms.<sup>4</sup> Therefore, we became interested in discovering if the amino groups in **1** and **2** play a role in quenching fluorescence and how they are involved in complex formation. To study the roles of these amino groups, we prepared a series of model compounds (**3–10**, Fig. 2), from which we were able to establish the relative roles of the amine and hydroxyl groups in **1** and **2** in quenching fluorescence. We also were able to determine the crystal structures of **2** complexed with  $Hg^{2+}$ ,  $Mg^{2+}$ , and  $Zn^{2+}$ . These structures preclude direct involvement of the amino groups in complex formation, but suggest that the amino groups act as general bases and facilitate formation of fluorescent complexes by deprotonating the hydroxyl groups on the fluorophores.

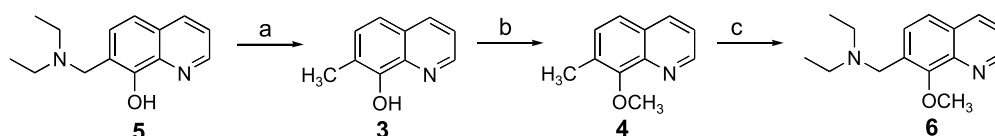
## 2. Results and discussion

The rationale for the use of model compounds was to determine the relative roles of 8-hydroxyl groups and 2-aminomethyl and 7-aminomethyl groups on the quenching of fluorescence of substituted quinolines and to use this information for a better understanding of the fluorescent properties of the chemosensors **1** and **2**. The photophysical properties of 8-HQ and 8-methoxyquinoline (8-MeOQ) derivatives have been studied in some detail.<sup>7,10</sup> In their fluorescence spectra, 8-HQ and 8-MeOQ present a non-structured fluorescence band in the 360–460 nm region, whose intensity and wavelength are strongly affected by the nature of the solvent.<sup>7</sup> As discussed, 8-HQ derivatives are weakly fluorescent, due to intermolecular photo-induced proton transfer (PPT). In addition, in protic media intermolecular PPT processes involving solvent molecules

can also occur, further decreasing the fluorescence quantum yield. Typically, 8-MeOQ derivatives show higher quantum yields, since intermolecular PPT is not possible. Nevertheless, in protic solvents intermolecular PPT processes can occur. It was anticipated that aminomethyl groups at either C2 or C7 in 8-HQ or 8-MeOQ derivatives would also quench fluorescence via PET. Because fluorescence of chemosensors **1** and **2** could potentially be quenched by both PPT and PET, the key question was: how do both of these methods of fluorescence quenching become inactive in the formation of their fluorescent metal ion complexes? The model compounds were expected to provide a clear picture of the roles of PPT and PET in fluorescent quenching.

Methods used in the syntheses of the model compounds were largely developed in the syntheses of chemosensors reported previously.<sup>5</sup> Compound **5** was prepared according to literature procedure.<sup>11</sup> Attempts to selectively methylate the hydroxyl group in **5** to generate **6** failed, and a more circuitous route to **6** was required (Scheme 1). Reduction of the quinolinyl C–N bond in **5** gave **3** in modest yield, followed by methylation of the hydroxyl group to give **4**. Radical bromination of **4** and nucleophilic displacement of the bromide by diethylamine gave **6** in only very small amounts. However, only milligram quantities of **6** were required, and the conversion of **4** to **6** was not optimized. Compound **7** is commercially available, and **8–10** were prepared using reported methods.<sup>9</sup>

On going from **3** to **4** or **7** to **8**, no large changes were expected in the absorption spectra, and they are in fact qualitatively very similar (see  $\lambda_{max}$  and  $\epsilon$  values in Table 1). As expected, on going from **3** to **4** or **7** to **8** significant increases in quantum yields (Table 1) were observed in both protic and aprotic solvents presumably due to PPT effects in **3** and **7**. There is also a notable difference in the fluorescence behaviors of **3** and **7** in methanol, with a 40-fold loss of fluorescence in **7**. These two compounds differ in the position of methyl group substitution with **3** substituted at C7 and **7** substituted at C2, but the source of this loss of fluorescence is unclear. Nevertheless, it should



Scheme 1. Synthesis of model compounds **3**, **4**, and **6**. Reagents (yields in parentheses): a) Pd/C,  $H_2$ , MeOH (43%); b) MeI, KOH, THF (93%); c) NBS, hv,  $CCl_4$ ;  $Et_2MJ$ ,  $K_2CO_3$ , MeCN (2% overall).

**Table 1.** Photophysical properties of **3–10**

	Solvent	Absorbance		Fluorescence		
		$\lambda_{\max}$ (nm)	$\epsilon$ ( $M^{-1} \text{ cm}^{-1}$ )	$\lambda_{\max}$ (nm)	$\Phi$	$\tau$ (ns)
<b>3</b>	CH <sub>3</sub> CN	307	2350	408	$2.7 \times 10^{-2}$	1.3
<b>3</b>	MeOH	306	2200	415	$4.5 \times 10^{-2}$	3.0
<b>4</b>	CH <sub>3</sub> CN	295	2900	410	$7.6 \times 10^{-2}$	1.2
<b>4</b>	MeOH	294	3200	410	$1.0 \times 10^{-1}$	3.0
<b>5</b>	CH <sub>3</sub> CN	315	3200	505	$2.0 \times 10^{-1}$	11.5
<b>5</b>	MeOH	315	2500	506	$5.0 \times 10^{-4}$	2.4
<b>6</b>	CH <sub>3</sub> CN	286	3200	390	$1.0 \times 10^{-3}$	0.7
<b>6</b>	MeOH	290	3800	390	$1.3 \times 10^{-3}$	0.6
<b>7</b>	CH <sub>3</sub> CN	304	2600	388	$9.3 \times 10^{-3}$	9.5
<b>7</b>	MeOH	305	2400	420	$1.2 \times 10^{-3}$	<0.5
<b>8</b>	CH <sub>3</sub> CN	307	4400	401	$3.9 \times 10^{-1}$	7.4
<b>8</b>	MeOH	309	4550	410	$1.3 \times 10^{-1}$	2.6
<b>9</b>	CH <sub>3</sub> CN	300	2900	398	$<1 \times 10^{-4}$	0.7
<b>9-H<sup>+</sup></b>	CH <sub>3</sub> CN	318	2100	435	$3.2 \times 10^{-4}$	0.8
<b>9</b>	MeOH	308	2550	438	$5.4 \times 10^{-4}$	0.6
<b>10</b>	CH <sub>3</sub> CN	306	4550	445	$3.0 \times 10^{-2}$	2.2
<b>10</b>	MeOH	311	4900	440	$4.6 \times 10^{-2}$	7.7

be taken into account during the design of chemosensors based on 8-HQ.

Due to PPT, **3** and **7** are only weakly fluorescent (see  $\Phi$  in Table 1), and if PET occurs in the excited state, quantum yields of **5** and **9** would be expected to decrease as compared to **3** and **7**. Indeed, upon addition of an aminomethyl group to **7** (giving **9**), a significant decrease in fluorescence is observed, and among these control compounds, the weakest fluorescence is observed with **9**. In addition, protonation of the amine (addition of 1 equiv of triflic acid) leads to an increase in quantum yield in acetonitrile. Comparison of the quantum yields of **3** and **5** is more complicated. Among all of the control compounds, the photophysical behavior of **5** is unique. For example, in the absorption spectrum the  $\lambda_{\max}$  is red-shifted, as is, to a much higher extent, the fluorescence band. This unique behavior may be rationalized in terms of the formation in the ground state of an intramolecular hydrogen bond involving the nitrogen of the amine and the hydroxy group, thus resulting in a six-membered, hydrogen bond-containing ring. Formation of this ring is expected to stabilize the charge transfer transition responsible for the lower energy absorption band and the fluorescence band, as observed. In addition, this process should decrease the effects of PPT involving the quinoline nitrogen, and the experimental results are consistent with this idea as evidenced by the high quantum yield of **5** in acetonitrile where the hydrogen bond is expected to be the strongest. The results obtained upon addition of triflic acid to **5** give additional support to the

hypothesis of formation of ground state hydrogen bond. The addition of 1 equiv of acid alters the absorption spectrum leading to a blue shift of the charge transfer band. A shift of the fluorescence band at ca. 500 nm in both methanol and acetonitrile to the 360–440 nm region is also observed, and the quantum yields are lowered by protonation. These findings suggest that the first protonation, occurring on the amine, causes the photophysical properties of **5** to become similar to those of **3**, as a result of interference with formation of the hydrogen bonded ring. The second protonation, that involves the quinoline nitrogen, leads to spectra that are similar to those found for the protonated form of **3**.

While the above comparisons support the hypothesis that both PPT and PET quenching can occur with substituted quinolines, the key comparisons are the quantum yields of **4** to **6** and **8** to **10**. In these compounds, intramolecular PPT is not possible, so the effects of PET should be clearly manifest. The fluorescence quantum yield of **6** is much lower than that of **4**, suggesting that PET is operative. Similarly, **10** is much less fluorescent than **8**.

Results from studies of the photophysical behaviors of **3–10** are consistent with the hypothesis that both PPT and PET processes can quench fluorescence of substituted quinolines and confirm earlier studies on quinoline-containing calixarenes. Chemosensors **1** and **2** are only weakly fluorescent alone, yet become highly fluorescent in the presence of their target metal ions ( $Mg^{2+}$  and  $Hg^{2+}$ , respectively). Therefore, both PPT and PET processes must be inhibited in the fluorescent complexes. Information indicating how this may occur comes from crystal structures of **2** complexed to  $Hg^{2+}$ ,  $Zn^{2+}$ , and  $Mg^{2+}$  and the behavior of **5** discussed previously.

X-ray quality crystals of **2** were grown in the presence of salts of either  $Hg^{2+}$ ,  $Zn^{2+}$ , or  $Mg^{2+}$  by slow evaporation of acetonitrile solutions. Coordinates for these structures have been archived at the Cambridge Crystallographic Data Center. The structures are shown in Figures 3–5. Initial inspection of these structures reveals a notable feature: the macrocyclic rings are not directly involved in complex formation (i.e. they are not chelated to the metal ions).

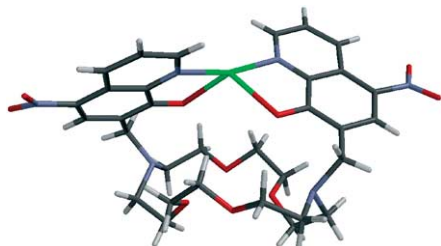


**Figure 3.** Crystal structure of **2-Hg<sup>2+</sup>** (two perchlorate ions have been removed for clarity). Colors: white = H; gray = C; violet = N; red = oxygen; green = Hg.

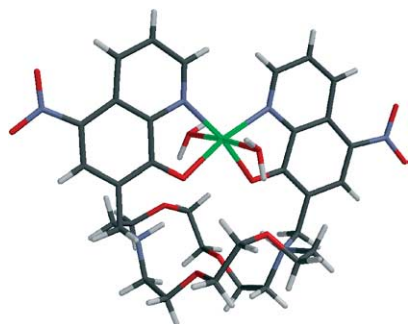


**Figure 4.** Crystal structure of  $2\text{-Zn}^{2+}$  (two perchlorate ions have been removed for clarity). Colors: white = H; gray = C; violet = N; red = oxygen; green = Zn.

Rather, it appears that the macrocyclic rings serve as a scaffold for the quinolines to impinge upon the metal ions. In the case of  $\text{Hg}^{2+}$ , a pseudotetrahedral coordination sphere is generated, and in the cases of  $\text{Zn}^{2+}$  and  $\text{Mg}^{2+}$  octahedral coordination spheres are formed with water molecules at the apical positions.

Upon closer inspection, a key role for the amino groups in the macrocyclic ring becomes apparent. These amino groups act as general bases and serve to deprotonate the 8-HQ hydroxyl group in the metal ion complexes. This deprotonation inhibits both PPT and PET processes and yields fluorescent complexes. In the  $2\text{-Zn}^{2+}$  and  $2\text{-Mg}^{2+}$  structures the protons in question were found on the nitrogen atoms of the amino groups in the macrocycle. It should be noted that the structures shown are dicationic (two perchlorate counterions have been deleted for clarity), and therefore, the hydroxyl protons must be found within the complex. Proton exchange, from the hydroxyl group to the amine, results in a significant decrease in the length of the C–O bond in the 8-HQ groups as compared to 8-HQ in uncomplexed **1** or a closely related 8-HQ containing compound. The averages of the two 8-HQ C–O bond lengths in the  $2\text{-Zn}^{2+}$  and  $2\text{-Mg}^{2+}$  structures are 1.283 and 1.284 Å, respectively, while the length of those in the free ligand (**1**) are 1.365 Å. The protons in question were not identified in the  $2\text{-Hg}^{2+}$  complex, although the complex is dicationic. Nevertheless, the 8-HQ C–O bond length is 1.269 Å, comparable to the C–O bond lengths in structures in which the protons were found on the amino groups in the macrocycles, suggesting that proton transfer occurred.

Results from the crystal structures in Figures 3–5 are

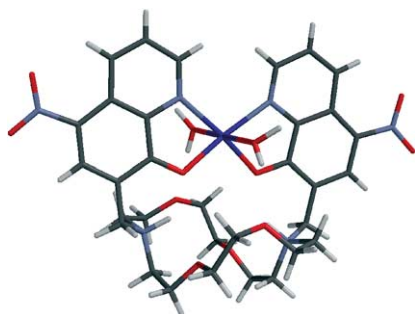


**Figure 5.** Crystal structure of  $2\text{-Mg}^{2+}$  (two perchlorate ions have been removed for clarity). Colors: white = H; gray = C; violet = N; red = oxygen; blue = Mg.

consistent with the unique behavior of **5** among the control compounds described. That is, the amino groups in **5** and in chemosensors **1** and **2** are well situated to engage in hydrogen bonding to the hydroxyl groups in 8-HQ derivatives, and, as metal chelation lowers the  $\text{pK}_a$  values of these hydrogens, these amino groups can act as general bases and deprotonate the hydroxyl groups.

### 3. Conclusions

We have demonstrated that both PPT and PET processes can cause fluorescence quenching in aminomethyl-substituted 8-HQ, and that these processes likely play an important role in the ‘on-off’ sensing properties of chemosensors **1** and **2**. In addition, crystal structure data suggest that proton transfer concomitant with complex formation inhibits both of these quenching mechanisms in cases where the aminomethyl group is at C7 in 8-HQ derivatives and can readily access the hydroxyl proton. As chemosensors incorporating 8-HQ are further developed, the relative roles of these quenching mechanisms will necessarily be taken into account and used to improve the responses of chemosensors to their target metal ions.

### 4. Experimental

#### 4.1. General methods

$^1\text{H}$  NMR,  $^{13}\text{C}$  NMR spectra were recorded on Varian Unity 500 MHz, Varian Unity 300 MHz, or Varian Gemini 200 MHz instruments. Mass spectrometric data were obtained on a JEOL SX 102 A spectrometer. Tetrahydrofuran (THF) and  $\text{CH}_2\text{Cl}_2$  were dried over  $\text{Na}^\circ$  or  $\text{CaH}_2$ . Chemicals were obtained from Fluka, Aldrich, and Sigma and were used as received unless otherwise noted.

**4.1.1. 8-Hydroxy-7-methylquinoline (3).** In methanol (125 mL) 7-diethylaminomethyl-8-hydroxyquinoline (**5**) (5.98 g, 26.0 mmol) and Pd/C (1.00 g, 10%, 9.40 mmol) were stirred under hydrogen gas atmosphere (3 one liter balloons) at room temperature for 6 h. After filtering and removal of solvent, **3** (1.79 g, 43%) was isolated using flash chromatography on silica gel (100:1 of  $\text{CH}_2\text{Cl}_2/\text{Et}_3\text{N}$ ) as a white solid (mp = 69–70 °C);  $^1\text{H}$  NMR  $\delta$  8.73 (d,  $J$  = 4.4 Hz, 1H), 8.8–8.2 (brs, 1H), 8.06 (d,  $J$  = 8.4 Hz, 1H), 7.4–7.2 (m, 3H), 2.47 (s, 3H);  $^{13}\text{C}$  NMR  $\delta$  149.6, 148.0, 138.2, 136.1, 130.8, 127.0, 120.9, 119.9, 117.2, 15.9; HRMS (EI) calcd for  $\text{C}_{10}\text{H}_9\text{ON}$  ( $\text{M}^+$ ): 159.0684, found: 159.0682.

**4.1.2. 8-Methoxy-7-methylquinoline (4).** Compound **3** (1.81 g, 10.4 mmol), KOH (2.53 g, 45.0 mmol), MeI (2.24 g, 15.7 mmol), and THF (100 mL) were stirred at room temperature for 12 h. After filtration and solvent removal, **4** (1.81 g, 93%) was isolated following flash chromatography on silica gel (2:1 of Hex/EtOAc) as a clear yellow oil.  $R_f$  = 0.3 (2:1 of Hex/EtOAc);  $^1\text{H}$  NMR  $\delta$  8.91 (dd,  $J_1$  = 4.0 Hz,  $J_2$  = 1.8 Hz, 1H), 8.07 (dd,  $J_1$  = 8.4 Hz,  $J_2$  = 1.8 Hz, 1H), 7.5–7.3 (m, 3H), 4.09 (s, 3H), 2.49 (s, 3H);  $^{13}\text{C}$  NMR  $\delta$  153.7, 149.6, 142.9, 136.1, 130.6, 130.0, 128.4, 122.9, 120.4, 61.7, 16.4; HRMS (EI) calcd for  $\text{C}_{11}\text{H}_{11}\text{ON}$  ( $\text{M}^+$ ): 173.0840, found: 173.0840.



**4.1.3. 7-Diethylaminomethyl-8-methoxyquinoline (6).**

Compound **4** (1.81 g, 10.4 mmol), *N*-bromosuccinimide (1.86 g, 10.4 mmol), and carbon tetrachloride (25 mL) were stirred at reflux while irradiated by two 250 W infrared lamps for 1.5 h. After filtration, the solvent was removed by evaporation. The crude mixture was partly purified by flash chromatography on silica gel (2:1 of Hex/EtOAc) resulting in a mixture of two compounds both having an  $R_f$  of  $\sim 0.5$  (2:1 of Hex/EtAOc). This mixture (890 mg) was then dissolved in  $\text{CH}_2\text{Cl}_2$  along with diethylamine (2.56 g, 35.0 mmol) and stirred at room temperature for 12 h. The solvent was then evaporated and product purified by flash chromatography on silica gel (100:5:1 of  $\text{CH}_2\text{Cl}_2/\text{MeOH}/\text{NH}_4\text{OH}$ ) to give **2-13** (45 mg, 2%) as a white solid.  $R_f = 0.5$ ; mp = 193–94 °C;  $^1\text{H NMR}$   $\delta$  9.81 (brs, 1H), 8.95 (dd,  $J_1 = 4.4$  Hz,  $J_2 = 1.8$  Hz, 1H), 8.20 (dd,  $J_1 = 8.4$  Hz,  $J_2 = 1.8$  Hz, 1H), 8.09 (d,  $J = 8.8$  Hz, 1H), 7.65 (d,  $J = 8.8$  Hz, 1H), 7.48 (dd,  $J_1 = 8.8$  Hz,  $J_2 = 4.4$  Hz, 1H), 4.36 (s, 2H), 4.25 (s, 3H), 3.04 (q,  $J = 7.2$  Hz, 4H), 1.41 (t,  $J = 7.4$  Hz, 6H);  $^{13}\text{C NMR}$   $\delta$  155.4, 149.8, 142.1, 136.4, 130.3, 129.3, 123.8, 123.5, 122.0, 63.2, 50.1, 46.6, 9.6; HRMS (EI) calcd for  $\text{C}_{15}\text{H}_{21}\text{ON}_2$  ( $\text{M} + \text{H}^+$ ): 245.1654, found: 245.1666.

**4.1.4. 2-Diethylaminomethyl-8-hydroxyquinoline (9).**

8-Hydroxyquinoline-2-carboxaldehyde (500 mg, 2.89 mmol), diethylamine (233 mg, 3.18 mmol),  $\text{NaBH}(\text{OAc})_3$  (674 mg, 3.18 mmol) were stirred at room temperature in 1,2-dichloroethane (25 mL) for 12 h. After filtering, solvent was evaporated and the crude product purified by flash chromatography on silica gel (100:5:1 of  $\text{CH}_2\text{Cl}_2/\text{MeOH}/\text{NH}_4\text{OH}$ ) to give **9** (396 mg, 60%) as an orange solid; mp = 82–83 °C.  $R_f = 0.5$ ;  $^1\text{H NMR}$   $\delta$  8.4–7.8 (brs, 1H), 8.05 (d,  $J = 8.8$  Hz, 1H), 7.64 (d,  $J = 8.4$  Hz, 1H), 7.38 (dd,  $J_1 = 8.4$  Hz,  $J_2 = 7.2$  Hz, 1H), 7.26 (dd,  $J_1 = 8.0$  Hz,  $J_2 = 1.4$  Hz, 1H), 7.14 (dd,  $J_1 = 7.4$  Hz,  $J_2 = 1.0$  Hz, 1H), 3.85 (s, 2H), 2.58 (q,  $J = 7.1$  Hz, 4H), 1.05 (t,  $J = 7.1$  Hz, 6H);  $^{13}\text{C NMR}$   $\delta$  159.4, 152.1, 137.5, 136.3, 127.6, 127.1, 122.1, 117.7, 110.0, 59.9, 47.7, 12.1; HRMS (FAB) calcd for  $\text{C}_{10}\text{H}_{10}\text{ON}$  ( $\text{MH}^+$ ): 160.0762, found: 160.0762.

**4.1.5. 5-Chloro-2-diethylaminomethyl-8-methoxyquinoline (10).**

2-Bromomethyl-5-chloro-8-methoxyquinoline (250 mg, 0.87 mmol), diethylamine (70 mg, 0.96 mmol), and  $\text{Na}_2\text{CO}_3$  (184 mg, 1.74 mmol) were stirred in  $\text{CH}_3\text{CN}$  at reflux for 12 h. After filtering, solvent was evaporated and the crude product purified by flash chromatography on silica gel (100:1 of  $\text{CH}_2\text{Cl}_2/\text{Et}_3\text{N}$ ) as a yellow oil to give **10** (210 mg, 91%).  $R_f = 0.5$  (100:10:1 of  $\text{CH}_2\text{Cl}_2/\text{MeOH}/\text{NH}_4\text{OH}$ );  $^1\text{H NMR}$   $\delta$  8.47 (d,  $J = 8.8$  Hz, 1H), 7.92 (d,  $J = 8.8$  Hz, 1H), 7.46 (d,  $J = 8.4$  Hz, 1H), 6.93 (d,  $J = 8.4$  Hz, 1H), 4.06 (s, 3H), 3.99 (s, 2H), 2.61 (q,  $J = 7.2$  Hz, 4H), 1.06 (t,  $J = 7.2$  Hz, 6H);  $^{13}\text{C NMR}$   $\delta$  161.8, 154.4, 140.1, 133.4, 126.2, 125.8, 122.4, 122.2, 107.6, 60.5, 56.4, 47.7, 12.2; HRMS (FAB) calcd for  $\text{C}_{15}\text{H}_{20}\text{ClON}_2$  ( $\text{MH}^+$ ): 279.1264, found: 279.1262.

**4.2. Photophysical measurements**

UV–vis absorption spectra were taken with a Perkin–Elmer lambda 40 spectrophotometer. Uncorrected emission and corrected excitation spectra were obtained with a Perkin–Elmer LS 50 spectrofluorimeter. The fluorescence lifetimes (uncertainty  $\pm 5\%$ ) were obtained with an Edinburgh

single-photon counting apparatus, in which the flash lamp was filled with  $\text{D}_2$ . Luminescence quantum yields (uncertainty  $\pm 15\%$ ) were determined using quinine sulphate in 0.5 M  $\text{H}_2\text{SO}_4$  aqueous solution ( $\Phi = 0.546^{12}$ ). In order to allow comparison of emission intensities, corrections for instrumental response, inner filter effects,<sup>13</sup> and phototube sensitivity were performed. Spectrophotometric and fluorimetric titrations and data analysis were carried out as previously described.<sup>14</sup>

**4.3. X-ray structure determination**

Single crystals suitable for X-ray structural studies were prepared by slow evaporation of acetonitrile from solutions of **2** with perchlorate salts of the indicated metal ions. Crystal and intensity data were obtained using a Siemens R3m/V automated diffractometer which utilized  $\text{Mo K}\alpha$  radiation. The lattice parameters and orientation matrix for each compound were obtained using a least squares procedure involving several carefully centered reflections for each crystal. Specific information about structures is given in the structures archived at the Cambridge Crystallographic Data Centre.

**References and notes**

- For example see: (a) National Research Council (U.S.) Board on Environmental Studies and Toxicology, *Toxicological Effects of Methylmercury*; National Academy Press: Washington, DC, 2000. (b) Chaney, R. L.; Ryan, J. A. *Risk Based Standards for Arsenic, Lead and Cadmium in Urban Soils*; Dechema: Frankfurt, 1994. (c) *Cadmium in the Human Environment: Toxicity and Carcinogenicity*; Nordberg, G. F., Herber, R. F. M., Alessio, L., Eds.; Oxford University Press: Oxford, 1992.
- (a) Valeur, B.; Leray, I. *Coord. Chem. Rev.* **2000**, *205*, 3–40. (b) Prodi, L.; Bolletta, F.; Montalti, M.; Zaccheroni, N. *Coord. Chem. Rev.* **2000**, *205*, 59–83.
- de Silva, A. P.; Gunaratne, H. Q. N.; Gunnlaugsson, T.; Huxley, A. J. M.; McCoy, C. P.; Rademacher, J. T.; Rice, T. E. *Chem. Rev.* **1997**, *97*, 1515.
- Huston, H. E.; Haider, K. W.; Czarnik, A. W. *J. Am. Chem. Soc.* **1988**, *110*, 4460.
- For examples see (a) Prodi, L.; Montalti, M.; Zaccheroni, N.; Bradshaw, J. S.; Izatt, R. M.; Savage, P. B. *Tetrahedron Lett.* **2001**, *42*, 2941. (b) Bronson, R. T.; Bradshaw, J. S.; Savage, P. B.; Fuangwasdi, S.; Lee, S. C.; Krakowiak, K. E.; Izatt, R. M. *J. Org. Chem.* **2001**, *66*, 4752. (c) Lee, S. C.; Izatt, R. M.; Zhang, X. X.; Nelsen, E. G.; Lamb, J. D.; Savage, P. B.; Bradshaw, J. S. *Inorg. Chim. Acta* **2001**, *317*, 174. (d) Prodi, L.; Bargossi, C.; Montalti, M.; Zaccheroni, N.; Su, N.; Bradshaw, J. S.; Izatt, R. M.; Savage, P. B. *J. Am. Chem. Soc.* **2000**, *122*, 6769. (e) Prodi, L.; Bolletta, F.; Montalti, M.; Zaccheroni, N.; Savage, P. B.; Bradshaw, J. S.; Izatt, R. M. *Tetrahedron Lett.* **1998**, *39*, 5451–5454.
- For examples see: (a) Moon, S. Y.; Cha, N. R.; Kim, Y. H.; Chang, S.-K. *J. Org. Chem.* **2004**, *69*, 181. (b) Casnati, A.; Sansone, F.; Sartori, A.; Prodi, L.; Montalti, M.; Zaccheroni, N.; Ugozzoli, F.; Ungaro, R. *Eur. J. Org. Chem.* **2003**, 1475. (c) Shults, M. D.; Pearce, D. A.; Imperiali, B. *J. Am. Chem. Soc.* **2003**, *125*, 10536. (d) Pearce, D. A.; Jotterand, N.;



- Carrico, I. S.; Imperiali, B. *J. Am. Chem. Soc.* **2001**, *123*, 5160.  
(e) Walkup, G. K.; Burdette, S. C.; Lippard, S. J.; Tsien, R. Y. *J. Am. Chem. Soc.* **2000**, *122*, 5644.
7. (a) Goldman, M.; Wehry, E. L. *Anal. Chem.* **1970**, *42*, 1178.  
(b) Bardez, E.; Devol, I.; Larrey, B.; Valeur, B. *J. Phys. Chem.* **1997**, *101*, 7786.
8. Prodi, L.; Montalti, M.; Zaccheroni, N.; Bradshaw, J. S.; Izatt, R. M.; Savage, P. B. *J. Incl. Phenom.* **2001**, *41*, 123–127.
9. Bordinov, A. V.; Bradshaw, J. S.; Zhang, X. X.; Dalley, N. K.; Kou, X.; Izatt, R. M. *Inorg. Chem.* **1996**, *35*, 7229.
10. Schulman, S. G. *Anal. Chem.* **1971**, *42*, 1178.
11. Phillips, J. P.; Fernando, Q. *J. Am. Chem. Soc.* **1953**, *75*, 3768.
12. Meech, S. R.; Phillips, D. *J. Photochem.* **1983**, *23*, 193.
13. Credi, A.; Prodi, L. *Spectrochim. Acta, Part A* **1998**, *54*, 159.
14. (a) Charbonnière, L. J.; Ziessel, R.; Montalti, M.; Prodi, L.; Zaccheroni, N.; Boehme, C.; Wipff, G. *J. Am. Chem. Soc.* **2002**, *124*, 7779. (b) Prodi, L.; Montalti, M.; Zaccheroni, N.; Pickaert, G.; Charbonnière, L.; Ziessel, R. *New J. Chem.* **2003**, *27*, 134.

# Selection of synthetic receptors capable of sensing the difference in binding of D-Ala-D-Ala or D-Ala-D-Lac ligands by screening of a combinatorial CTV-based library

Cristina Chamorro and Rob M. J. Liskamp\*

Department of Medicinal Chemistry, Utrecht Institute for Pharmaceutical Sciences, Utrecht University, P.O. Box 80082, 3508 TB Utrecht, The Netherlands

Received 23 January 2004; revised 24 June 2004; accepted 20 August 2004

Available online 7 October 2004

**Abstract**—Screening of a combinatorial CTV-based artificial, synthetic receptor library **1** {1-13, 1-13, 1-13} for binding of a variety D-Ala-D-Ala and D-Ala-D-Lac containing ligands (**6–11**) was carried out in phosphate buffer (0.1 N, pH=7.0). After screening and Edman sequencing, synthetic receptors were found containing amino acid sequences, which are either characteristic for binding dye labeled D-Ala-D-Ala or D-Ala-D-Lac containing ligands. For example, receptors capable of binding D-Ala-D-Ala containing ligands **6**, **7**, **9** and **11** contained—almost in all cases—at least one basic amino acid residue—predominantly Lys—in their arms. This was really a striking difference with the arms of the receptors capable of binding D-Ala-D-Lac containing ligands **8** and **10**, which usually contained a significant number of polar amino acids (Gln and Ser), especially in ligand **8**, but hardly any basic amino acids. Use of different (fluorescent) dye labels showed that the label has a profound, albeit not decisive, influence on the binding by the receptor. A hit from the screening of the CTV-library with FITC-peptidoglycan (**6**) was selected for resynthesis and validation.

© 2004 Elsevier Ltd. All rights reserved.

## 1. Introduction

The identification of artificial synthetic receptor molecules capable of binding specific peptide sequences has attracted considerable interest.<sup>1</sup> Many of these receptors have been designed, prepared and screened for their ability to bind resin attached peptides from combinatorial libraries.

Combinatorial solid phase synthesis offers an attractive strategy for the generation of libraries of synthetic receptor molecules capable of binding specific peptide sequences.<sup>2</sup>

**Keywords:** Synthetic receptors; CTV-based library; Screening; Fluorescent ligand; D-Ala-D-Ala-OH; D-Ala-D-Lac-OH.

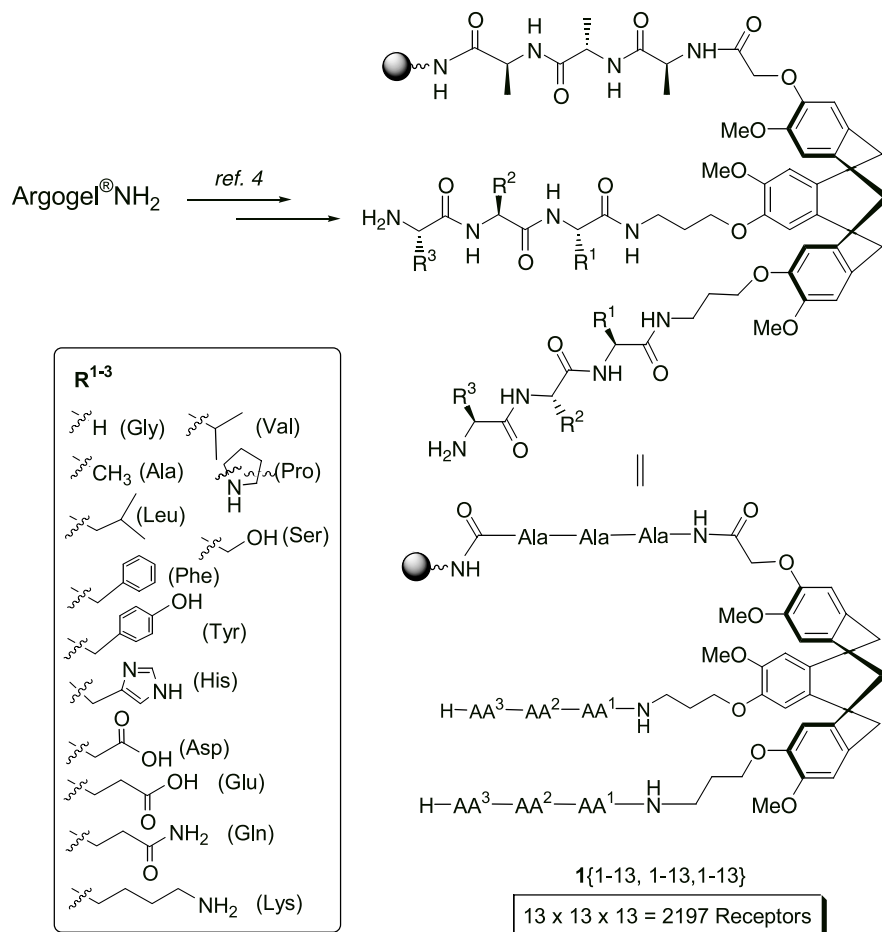
**Abbreviations:** Boc, *tert*-butoxycarbonyl; BOP, benzotriazol-tris-(dimethyl-amino)phosphonium hexafluoro-phosphate; <sup>t</sup>Bu, *tert*-butyl; Cbz, benzyl-oxycarbonyl; CTV, 2,7,12-trihydroxy-3,8,13-trimethoxy-10,15-dihydro-5H-tribenzof[a,d,g]cyclononene; DCM, dichloromethane; DIPEA, *N,N*-diisopropyl-*N*-ethylamine; DMF, dimethylformamide; Ds, Dansyl; ES-MS, electrospray ionization mass spectrometry; EtOAc, ethyl acetate; Et<sub>2</sub>O, diethyl ether; FITC, fluorescein isothiocyanate; Fmoc, *N*-fluoren-9-ylmethoxy-carbonyl; NBD, 7-nitrobenz-2-oxa-1,3-diazol; NMP, *N*-methyl-pyrrolidone; Rt, retention time; rt, room temperature; TEA, triethylamine; TFA, trifluoroacetic acid.

\* Corresponding author. Tel.: +31-30-2537396; fax: +31-30-2536655; e-mail: [r.m.j.liskamp@pharm.uu.nl](mailto:r.m.j.liskamp@pharm.uu.nl)

Recently, we have prepared a 2197-member split-mix<sup>3</sup> combinatorial library of artificial tripodal receptors **1**{1-13, 1-13, 1-13} on the solid phase,<sup>4</sup> using cyclotrimeratrylene (CTV)<sup>5</sup> as a scaffold (Scheme 1). Thus, every bead contains one unique CTV-based receptor with three peptide arms, one of them attached to the solid phase and different from the other two identical peptide arms. Selectivity and affinity for ligands might be enhanced, since the CTV-scaffold is clearly capable of aligning peptide arms.<sup>6</sup>

The CTV-based receptors were attached to Argogel<sup>®</sup>-NH<sub>2</sub> resin, therefore an 'on-bead screening assay'<sup>3c,7</sup> for binding of different peptide sequences by the CTV-based combinatorial library **1**{1-13, 1-13, 1-13} can be performed. Beads containing receptors capable of binding particular ligands are visually identified and removed for structural elucidation by Edman degradation.<sup>8</sup> In order to visualize the best CTV-receptor binders, fluorescence or staining of the library beads resulting from binding a specific peptide sequence or ligand in solution is an attractive approach. For this purpose labeling with a (fluorescent) dye of these peptides or ligands is required.

As a still very challenging example of screening for binding of specific peptide sequences by the CTV-based library **1**{1-13, 1-13, 1-13}, peptide sequences D-Ala-D-Ala and



**Scheme 1.** Combinatorial synthesis of a 2197-member library of CTV-based tripodal receptors **1**{1-13, 1-13, 1-13}.<sup>4</sup>

D-Ala-D-Lac were chosen. Vancomycin and other closely related glycopeptide antibiotics<sup>9</sup> bind to the D-Ala-D-Ala end of the Gram-positive bacterial peptidoglycan cell wall precursor thereby interfering with its cross-linking, resulting in an incomplete bacterial cell wall, leading to osmotic lysis and bacteria death.<sup>10</sup> Unfortunately, the terminal D-alanine is substituted by D-lactate in vancomycin-resistant bacterial strains, resulting in a 1000-fold decrease in affinity and essentially useless antibiotic activity of vancomycin.<sup>11</sup> Thus, identification of synthetic receptors capable of binding with high affinity to the above mentioned sequences could have a potential application for overcoming vancomycin resistance problems. This is nevertheless an extremely difficult problem to address, since the number of interactions of the small D-Ala-D-Ala and D-Ala-D-Lac ligands with either 'synthetic' or 'natural' receptors (viz. vancomycin) is very limited. Despite this, Nature managed to come up with the natural 'receptor' vancomycin having a high affinity for D-Ala-D-Ala ( $K_a \sim 10^6 \text{ M}^{-1}$ ).<sup>12</sup>

In this report a 2197-member library of CTV-based synthetic tripodal receptor **1**{1-13, 1-13, 1-13} attached to the solid phase was screened for binding of D-Ala-D-Ala and D-Ala-D-Lac containing ligands, in phosphate buffer (0.1 N, pH=7.0). So far there are not many examples of screening for binding properties by synthetic receptors in aqueous systems.<sup>2a-b,13</sup> However, this was deemed absolutely essential for moving ultimately to biologically relevant

systems and finding hits for these. We found that it is no longer difficult to find hits of synthetic receptors with good to excellent binding properties in organic solvents.<sup>1c,f,h,2b-c</sup> The challenge, however, is to discover molecules with good binding properties in an aqueous environment, since intermolecular interactions (hydrogen bond, electrostatic) between ligand and receptor are much weaker here than in apolar solvents.

Since D-Ala-D-Ala or D-Ala-D-Lac ligands are relatively small, the influence of the (fluorescent) dye was evaluated by varying it from fluorescein (FITC), dansyl (Ds), or 7-nitrobenz-2-oxa-1,3-diazol (NBD), to disperse red (DR). The best synthetic receptors were selected and subjected to Edman degradation<sup>8</sup> and the binding sequences were analyzed. Validation of 'hits' by resynthesis on the solid phase of the selected library member has been carried out. The resynthesized receptors have been tested in vitro against *Staphylococcus aureus* Newman.

One can philosophize how Nature did find such a good candidate for binding as vancomycin. However, it seems plausible that the 'natural' equivalent of combinatorial approaches, i.e. evolution led to the emergence of such a good binder for binding D-Ala-D-Ala. Similarly, we propose that ultimately combinatorial approaches will lead to new binders and possibly antibiotics. Here, we describe the screening of a CTV library as a step in this direction.

## 2. Results and discussion

In order to investigate the binding properties for D-Ala-D-Ala and D-Ala-D-Lac containing ligands by the fully deprotected recently described CTV-based receptor library 1{1-13, 1-13, 1-13}<sup>4</sup>, fluorescent FITC-peptidoglycan,<sup>14</sup> (6), NBD-(CH<sub>2</sub>)<sub>5</sub>-C(O)-Gly-D-Ala-D-Ala-OH (7), and Ds-Gly-D-Ala-D-Ala-OH (9), as well as red-colored ligand DR-C(O)-(CH<sub>2</sub>)<sub>2</sub>-C(O)-Gly-D-Ala-D-Ala-OH (11) were prepared corresponding to cell wall precursors of vancomycin sensitive bacteria. In addition, fluorescent NBD-(CH<sub>2</sub>)<sub>5</sub>-C(O)-Gly-D-Ala-D-Lac-OH (8), and Ds-Gly-D-Ala-D-Lac-OH (10) were synthesized as a small parts of cell wall precursors of vancomycin resistant bacteria. The (fluorescent) dye labels were chosen to study their possible influence on binding.

### 2.1. Synthesis of the (fluorescent) dye labeled D-Ala-D-Ala and D-Ala-D-Lac containing ligands (7–11)

The D-Ala-D-Ala containing ligands (7, 9 and 11) were prepared by attachment of the different fluorescent or dye labels to H-Gly-D-Ala-D-Ala-O<sup>t</sup>Bu (4) (Scheme 2). The common intermediate 4 was obtained by BOP coupling<sup>15</sup> of commercially available Cbz-D-Ala-OH and H-D-Ala-O<sup>t</sup>Bu and hydrogenolysis to the dipeptide H-D-Ala-D-Ala-O<sup>t</sup>Bu

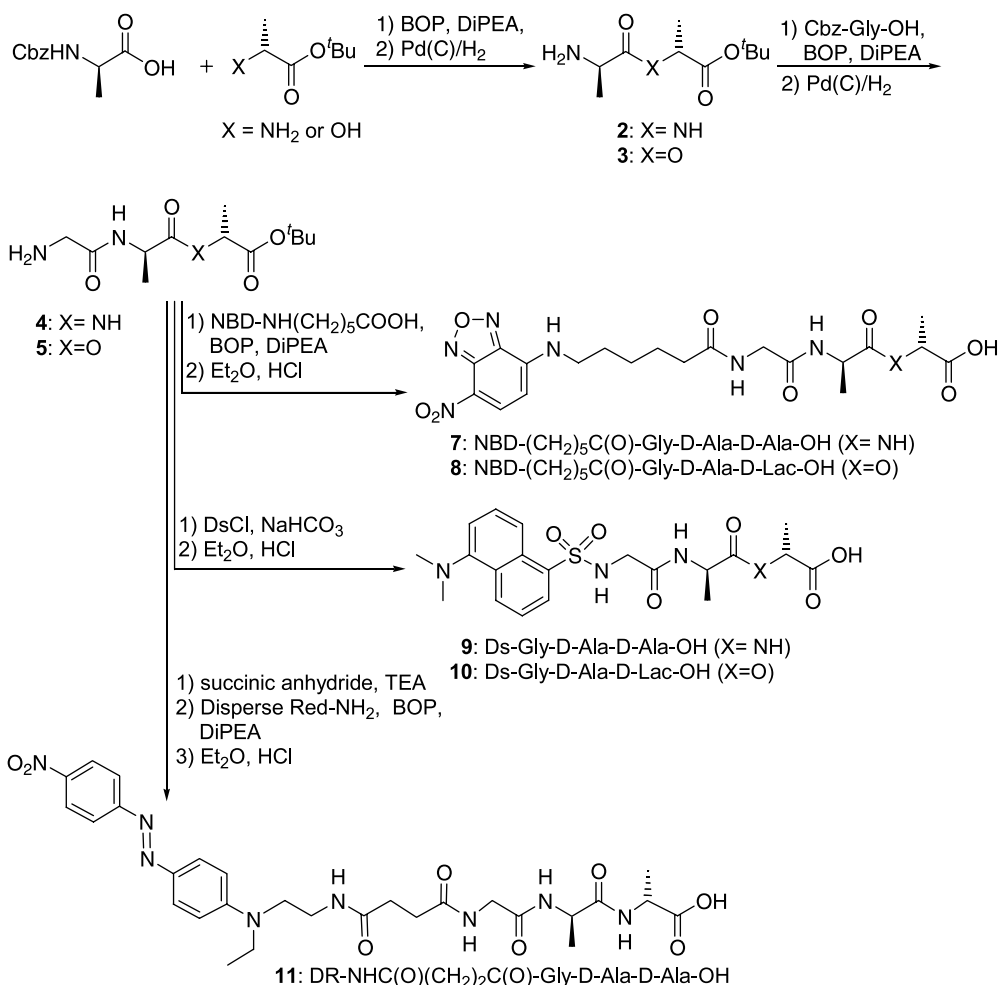
(2) (92%), followed by BOP coupling of Cbz-Gly-OH to 2, and again hydrogenolysis.

NBD-(CH<sub>2</sub>)<sub>5</sub>-C(O)-Gly-D-Ala-D-Ala-OH (7) was synthesized by BOP coupling of fluorescent 6-(7-NitroBenzo-2-oxa-1,3-Diazole) hexanoic acid to 4 and cleavage of the *t*-Bu-ester under acidic conditions. Treatment of 4 with a slight excess of dansyl chloride in the presence of NaHCO<sub>3</sub> and cleavage of the *t*-Bu-ester led to the dansylated D-Ala-D-Ala containing ligand (Ds-Gly-D-Ala-D-Ala-OH) 9. Similar approaches were used, for the preparation of the NBD and Ds-labeled D-Ala-D-Lac containing ligands 8 and 10. For these ligands H-Gly-D-Ala-D-Lac-O<sup>t</sup>Bu (5) was used as a precursor. This precursor was synthesized analogously to 4, but using H-D-Lac-O<sup>t</sup>Bu instead of H-D-Ala-O<sup>t</sup>Bu (Scheme 2).

Disperse red D-Ala-D-Ala containing ligand (11) was synthesized by treatment of 4 with succinic anhydride under basic conditions followed by BOP coupling of disperse red-NH<sub>2</sub><sup>16</sup> and final cleavage of *t*-Bu-ester.

### 2.2. Screening of library 1{1-13, 1-13, 1-13} for binding of D-Ala-D-Ala or D-Ala-D-Lac containing ligands

The fully deprotected CTV-based receptor library 1{1-13, 1-13, 1-13} was screened for binding of the dye containing



**Scheme 2.** Synthesis of the (fluorescent) dye labeled D-Ala-D-Ala and D-Ala-D-Lac containing ligands (7–11).

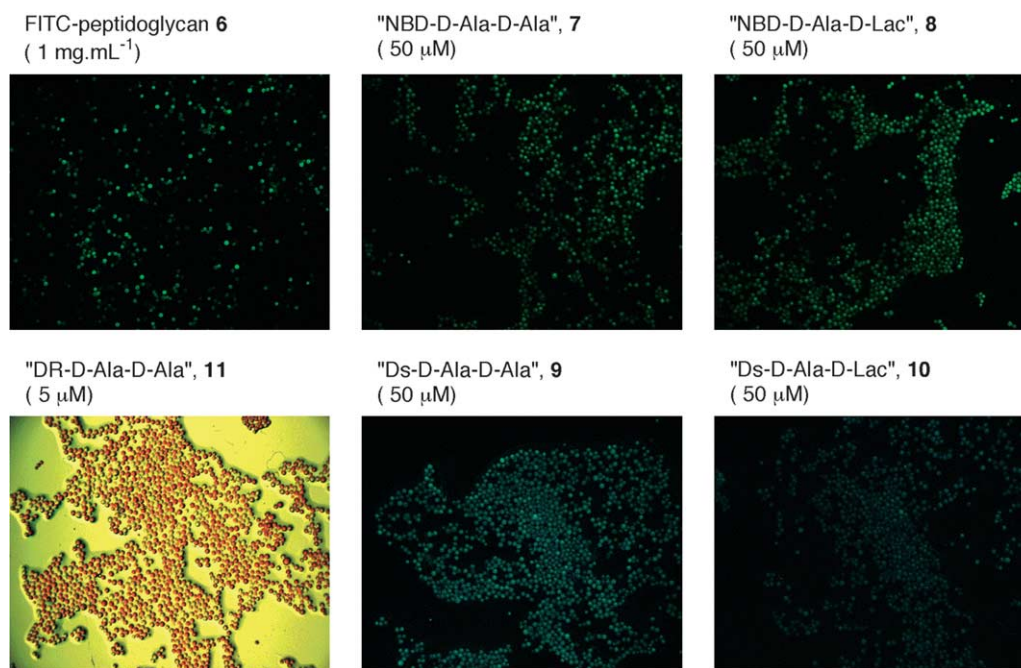


**Figure 1.** Screening for binding for D-Ala-D-Ala and D-Ala-D-Lac containing ligands (**6–11**) by the CTV-based receptor library **1**{1-13, 1-13, 1-13}.

D-Ala-D-Ala or D-Ala-D-Lac ligands (**6–11**) in phosphate buffer (0.1 N, pH = 7.0). Although this aqueous system is a biologically more meaningful environment, peptide recognition by the artificial receptors is more difficult than in the frequently used apolar organic systems due to the ability of water molecules to compete for hydrogen bonding by solvation and thus disruption of these non-covalent interactions between peptides and synthetic receptors. For the fluorescent dyes the overexposure mode of the Leica DC-100 digital camera system and image analysis was used for estimation of the relative fluorescence intensities in a semi-quantitative manner. Different ligand concentrations were used to determine the optimal selectivity, as judged by the number of highly fluorescent beads against either no or slightly fluorescent beads. For NBD- or Ds-labeled

ligands (**7–10**), no selectivity of binding at higher concentrations than 50  $\mu\text{M}$  was observed. At concentrations lower than 10  $\mu\text{M}$ , fluorescent beads were barely visible. Good discrimination between fluorescent and non-fluorescent beads was possible at 50  $\mu\text{M}$ , and therefore this concentration was used for screening experiments with fluorescent ligands (**7–10**). FITC-labeled peptidoglycan fragment ligand (**6**) was tested at concentrations of 10, 1 and 0.1  $\text{mg mL}^{-1}$ , leading to the best discrimination when a concentration of 1  $\text{mg mL}^{-1}$  was used. The best discrimination between red and colorless beads was obtained when 5  $\mu\text{M}$  of the disperse-red labeled ligand **11** was used. In general, the observed fluorescence intensity was slightly higher for D-Ala-D-Ala containing ligands than for D-Ala-D-Lac containing ligands. This might be

**Table 1.** Identity of the peptide arms as obtained by Edman degradation of the selected solid phase attached CTV-based receptors

	FITC-peptidoglycan <b>6</b>	"NBD-D-Ala-D-Ala" <b>7</b>	"NBD-D-Ala-D-Lac" <b>8</b>	"Ds-D-Ala-D-Ala" <b>9</b>	"Ds-D-Ala-D-Lac" <b>10</b>	"DR-D-Ala-D-Ala" <b>11</b>
Bead	AA <sup>3</sup> -AA <sup>2</sup> -AA <sup>1</sup>	AA <sup>3</sup> -AA <sup>2</sup> -AA <sup>1</sup>	AA <sup>3</sup> -AA <sup>2</sup> -AA <sup>1</sup>	AA <sup>3</sup> -AA <sup>2</sup> -AA <sup>1</sup>	AA <sup>3</sup> -AA <sup>2</sup> -AA <sup>1</sup>	AA <sup>3</sup> -AA <sup>2</sup> -AA <sup>1</sup>
1	Lys-Leu-Lys	Leu-Lys-Phe	Val-Phe-Phe	Ser-Lys-Ala	Ala-Leu-Val	Phe-Lys-His
2	Lys-Leu-Lys	Phe-Lys-Phe	Leu-Ala-Phe	Ser-Lys-Glu	Ala-Leu-Ala	Leu-Lys-Gly
3	Lys-Phe-Lys	Val-Lys-Phe	Phe-Ser-Phe	Ser-Lys-Gly	Val-Leu-Leu	Tyr-Lys-Ala
4	Lys-Lys-Lys	Leu-Val-Lys	Val-Gly-Phe	Gly-Lys-Ala	Val-Phe-Leu	Lys-Phe-Tyr
5	Ala-Ala-Lys	Leu-Phe-Lys	Phe-Phe-Gln	Gly-Lys-Val	Ala-Ala-Gln	Lys-Leu-Phe
6	Ala-Val-Lys	Phe-Val-Lys	Leu-Phe-Thr	Gly-Ala-Lys	Val-Ala-Gln	Gly-Gly-Lys
7	Phe-Val-Lys	Tyr-Leu-Lys	Gln-Phe-Val	Lys-Phe-Phe	Gly-Lys-Gly	Ala-Leu-His
8	Val-Pro-Lys	Lys-Phe-Leu	Gln-Ser-Leu	Lys-Leu-Leu	Leu-Phe-Gly	Val-Gly-Ala
9	Lys-Lys-Val	Leu-Gln-Phe	Ser-Leu-Gln	Ser-Ala-Gly	Lys-Phe-Val	Ala-Phe-Leu
10			Leu-Pro-Val	Ser-Gly-Ala	Leu-Lys-Gln	
NF	Ser-Ala-Glu	Gln-Asp-Glu	Pro-Asp-Glu	Phe-Val-Asp	Pro-His-Asp	Phe-Asp-Ser

NF, non-fluorescent bead.



a qualitative indication of stronger binding of the D-Ala-D-Ala sequence. A higher fluorescence intensity was generally observed when NBD-label ligands were used instead of the Ds-label. The best selectivity was found when FITC-peptidoglycan (**6**) was used as ligand (Fig. 1).

For every independent screening nine or ten of the most intensively fluorescent beads were selected and sequenced by Edman degradation.<sup>8</sup> Edman sequencing was carried out in all the cases for a fourth cycle, which always showed no amino acid for all the beads, thus confirming the *tripeptide*-identity of the library members. In addition, a non-fluorescent bead was selected and sequenced as a negative control.

Table 1 shows the identity of the peptide arms of the selected solid phase attached CTV-based receptors. In Figure 2, the relative abundance of amino acids at each residue position of the receptor is shown. The general trends are very clear and can be summarized as follows. First, the negative controls, i.e. the selected non-fluorescent or non-

colored beads, contained amino acids especially Glu and Asp in their receptors, which were not found in the fluorescent or colored beads. Second, the receptors capable of binding of D-Ala-D-Ala containing ligands **6**, **7**, **9** and **11** contained—almost in all cases—at least one basic amino acid residue (indicated in blue in Table 1)—predominantly Lys—in their arms. This was really a striking difference with the arms of the receptors capable of binding D-Ala-D-Lac containing ligands **8** and **10**, which usually contained a significant number of polar amino acids (Gln and Ser), especially in binding ligand **8**, but hardly any basic amino acids. Although there was a significant influence of the label (*vide infra*) on binding of the ligand to the synthetic receptors, fortunately, the labels did not conceal the differences in binding of D-Ala-D-Ala or D-Ala-D-Lac ligands, i.e. they did not obscure the selectivity of binding. The differences in the sequences of the receptors in binding of D-Ala-D-Ala or D-Ala-D-Lac remained manifest irrespective of the (fluorescent) dye label. Nevertheless, there were appreciable differences in sequences of receptors capable of binding the D-Ala-D-Ala with the various labels. For example, the synthetic receptors capable of binding

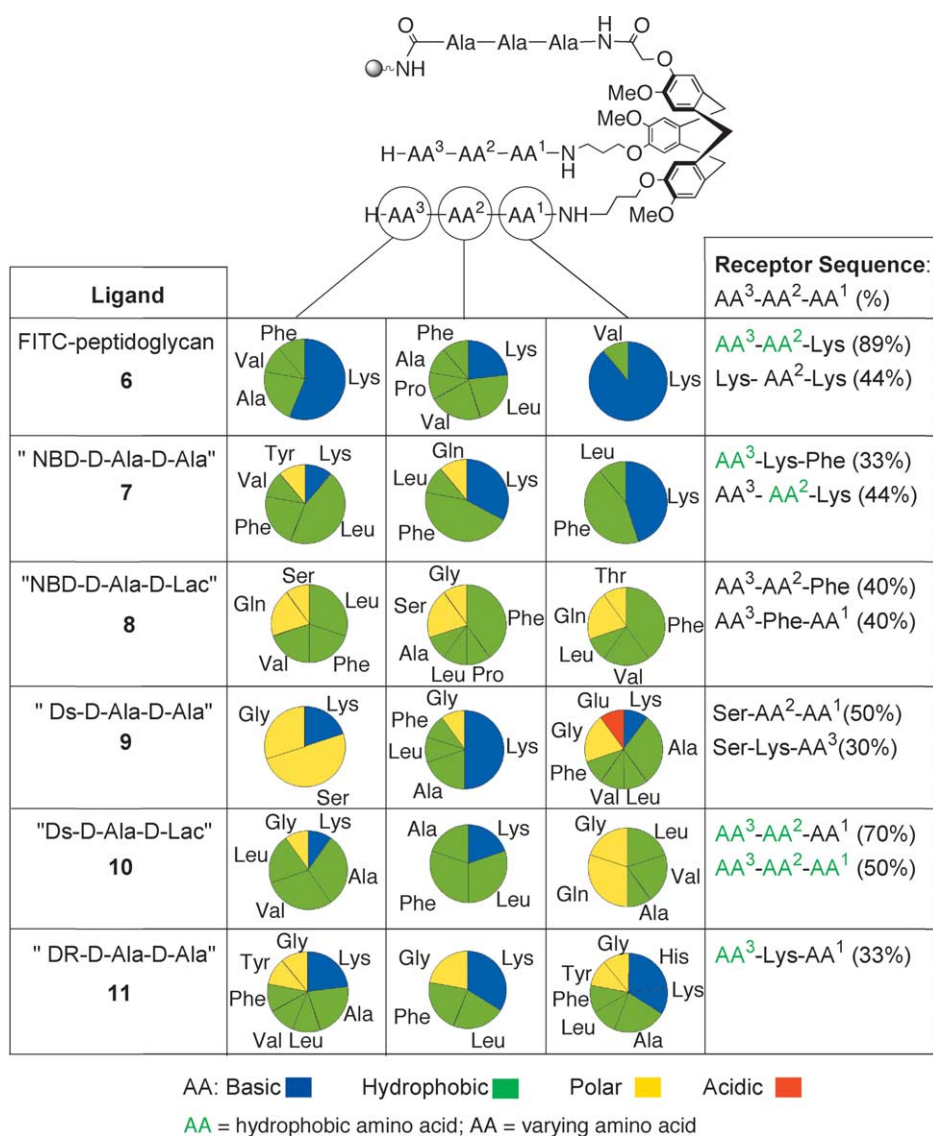


Figure 2. Relative abundance of amino acids at each residue position of the CTV-based receptor.

'NBD-D-Ala-D-Ala' (**7**) contained—in addition to Lys—virtually only hydrophobic amino acids (Leu, Phe, Val), whereas the synthetic receptors capable of binding 'Ds-D-Ala-D-Ala' (**9**) contained—in addition to Lys—a number of more polar Ser residues as well as the smaller hydrophobic amino acids such as Ala. The behavior of synthetic receptors, which bound 'DR-D-Ala-D-Ala' (**11**) was somewhat intermediate: Lys residues, large hydrophobic amino acids (Leu, Phe) but also the smaller hydrophobic amino acid Ala was found, but no polar amino acids like Ser. Thus, we found synthetic receptors selective for binding either the D-Ala-D-Ala or the D-Ala-D-Lac sequence. As such these compounds can be considered as 'sensors' for these particular peptide sequences and synthetic receptors acting as sensors for other peptide ligands might be accessible using this combinatorial approach. Possibly, by simply screening this library with another peptide ligand one might even uncover synthetic receptors acting as sensors for other peptides. The binding behavior of the synthetic receptors—as reflected in the amino acid sequences—was influenced by the character of the (fluorescent) dye label, but the selectivity remained.

In order to reduce the influence of the label, which is required for screening, different labels which have a minimal influence on binding, are called for. Alternatively, the relative influence of the label on binding by a particular synthetic receptor can be diminished by screening synthetic receptors capable of binding larger ligands as compared to the size of the label. The found selectivities for binding D-Ala-D-Ala vs. binding D-Ala-D-Lac are quite remarkable considering the fact that the only difference between these ligands is present in the linkage connecting the two residues: an amide 'N-H' in D-Ala-D-Ala and an ester '-O' in D-Ala-D-Lac.

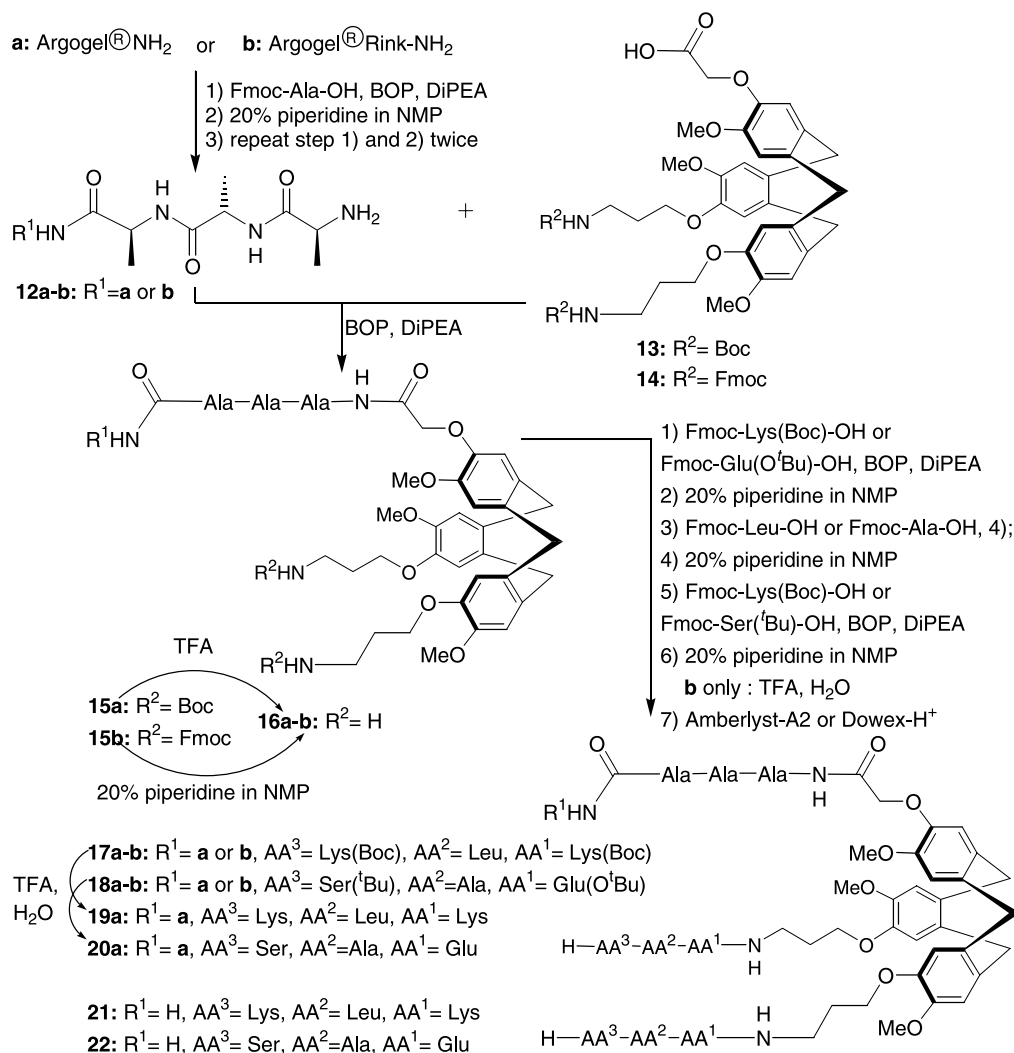
It is revealing to look at the relative abundance of the various amino acids at each residue position of the receptor shown in Figure 2. In 89% of the sequenced synthetic receptors capable of binding fluorescein labeled D-Ala-D-Ala (FITC-peptidoglycan, **6**), Lys is found at the first position (AA<sup>1</sup>), closest to the CTV-scaffold. Lys in this position is also found in 44% of the receptors capable of binding 'NBD-D-Ala-D-Ala' (**7**). Although in 44% of the receptors binding FITC-peptidoglycan (**6**), Lys is found at the third position (AA<sup>3</sup>), Lys can also be present at the second position (AA<sup>2</sup>) in 33% of the receptors binding 'NBD-D-Ala-D-Ala' (**7**), in 30% of the receptors binding 'Ds-D-Ala-D-Ala' (**9**) and in 33% of the receptors binding 'DR-D-Ala-D-Ala' (**11**). As was discussed above, the absence of Lys residues in synthetic receptors capable of binding D-Ala-D-Lac in ligands **8** and **10** is remarkable.

Likewise, the combination of the basic Lys residue with hydrophobic amino acids indicated in green in the receptor sequences, when a varying hydrophobic amino acid is found. Especially with the NBD-ligands **7** and **8**, Phe was found in 33% of the receptors binding D-Ala-D-Ala (in ligand **7**) and in 80% AA<sup>1</sup> and 40% AA<sup>2</sup> of the receptors binding D-Ala-D-Lac (in ligand **8**). The presence of this particular amino acid may point to a special contribution of the NBD label on binding, since this amino acid was not in majority present in the receptors binding the other ligands. Nevertheless the presence of

hydrophobic amino acids was very striking in the receptors capable of binding D-Ala-D-Lac, i.e. **8** and **10**. In the latter case even 50% of the sequenced receptors contained hydrophobic amino acids at each of the three amino acid positions and a good 70% had at least two hydrophobic amino acids, i.e. at the third (AA<sup>3</sup>) and second (AA<sup>2</sup>) position of the synthetic receptors. Finally, the presence of Ser in the third position in 50% of the synthetic receptors binding 'Ds-D-Ala-D-Ala' (**9**) was also surprising and in 30% of the receptors the consensus sequence Ser-Lys-AA<sup>1</sup> was found. This cannot be solely ascribed to an effect of the Ds-label, as the corresponding Ds-containing D-Ala-D-Lac ligand did not bind to receptors containing Ser residues.

### 2.3. Validation by resynthesis

Validation of 'hits' by resynthesis of the selected synthetic receptors and reproducing the properties for which the library (1{1-13, 1-13, 1-13}) was screened is essential in any combinatorial approach towards finding compounds with desired—in this case binding—properties. A hit from the screening of the CTV-library with FITC-peptidoglycan (**6**) was selected, which was found twice (Table 1, beads 1 and 2, screening with **6**), corresponding to the consensus sequence Lys-AA<sup>2</sup>-Lys found in 44% of the sequenced beads. In addition the 'negative control', i.e. a sequenced non-fluorescent bead giving the CTV-based synthetic receptor sequence Ser-Ala-Glu, (AA<sup>3</sup>-AA<sup>2</sup>-AA<sup>1</sup>) was synthesized on Argogel<sup>®</sup>-NH<sub>2</sub> resin (**a**) as well as on the Argogel<sup>®</sup>-Rink resin (**b**) (Scheme 3). Resynthesis of the CTV-based receptors **19a** and **20a**, covalently attached to Argogel<sup>®</sup>-NH<sub>2</sub> resin, and **17b** and **18b** on the Argogel<sup>®</sup>-Rink resin, was performed analogously to the preparation of the CTV-based receptor library 1{1-13, 1-13, 1-13}<sup>4</sup> except for the use of the compatible (Fmoc)<sub>2</sub>-CTV-OH scaffold **14** on the acid labile Argogel<sup>®</sup>-Rink resin, instead of the (Boc)<sub>2</sub>-CTV-OH scaffold **13**. The different peptide-binding arm was built up by three subsequent BOP couplings/Fmoc-deprotection of Fmoc-L-Ala-OH on both, Argogel<sup>®</sup>-NH<sub>2</sub> and Argogel<sup>®</sup>-Rink-NH<sub>2</sub> resin to obtain **12a** and **12b**, respectively (Scheme 3). Then, either the Boc-protected CTV-scaffold (**13**) or the Fmoc-protected CTV-scaffold (**14**) was coupled to the first peptide-binding arm to give **15a** or **15b**. Cleavage of the Boc groups under acidic conditions from **15a** led to **16a**, while Fmoc-cleavage under standard conditions from **15b** led to **16b**. The construction of the two identical peptide arms was performed as depicted in Scheme 3. After three coupling/Fmoc-deprotection cycles involving subsequently Fmoc-L-Lys(Boc)-OH, Fmoc-L-Leu-OH and Fmoc-L-Lys(Boc)-OH, resin bound synthetic receptors **17a** and **17b** were obtained. The same procedure involving the use of subsequently Fmoc-L-Glu(O<sup>t</sup>Bu)-OH, Fmoc-L-Ala-OH and Fmoc-L-Ser(O<sup>t</sup>Bu)-OH led to resin bound synthetic receptors **18a** and **18b**. Treatment of **17a** and **18a** with TFA led to the—still resin bound—deprotected synthetic receptors, **19a** and **20a**, respectively (Scheme 3). In contrast, treatment with TFA of **17b** or **18b** led to deprotection and cleavage of the receptors from the Argogel<sup>®</sup>-Rink-resin to afford the trifluoroacetate salts of [Lys-Leu-Lys]-containing or [Ser-Ala-Glu]-containing synthetic receptors **21** and **22**, respectively (Scheme 3). ES-MS showed the identity of the trifluoroacetate salts receptors **21** and **22**. The purity of them was 94% purity in both cases, as shown by HPLC. The



**Scheme 3.** Resynthesis of resin bound (**19a** and **20a**) and cleaved synthetic receptors (**21** and **22**).

overall yields (76 and 69%, respectively) were very good considering the eight steps performed for their solid-phase synthesis (corresponding to 97 and 95% average yield per step). Finally, desalting using either Amberlyst-A21 or

Dowex-H<sup>+</sup> ion exchange resins led to receptors **21** and **22**, respectively (Scheme 3).

Binding experiments of the resynthesized CTV-based

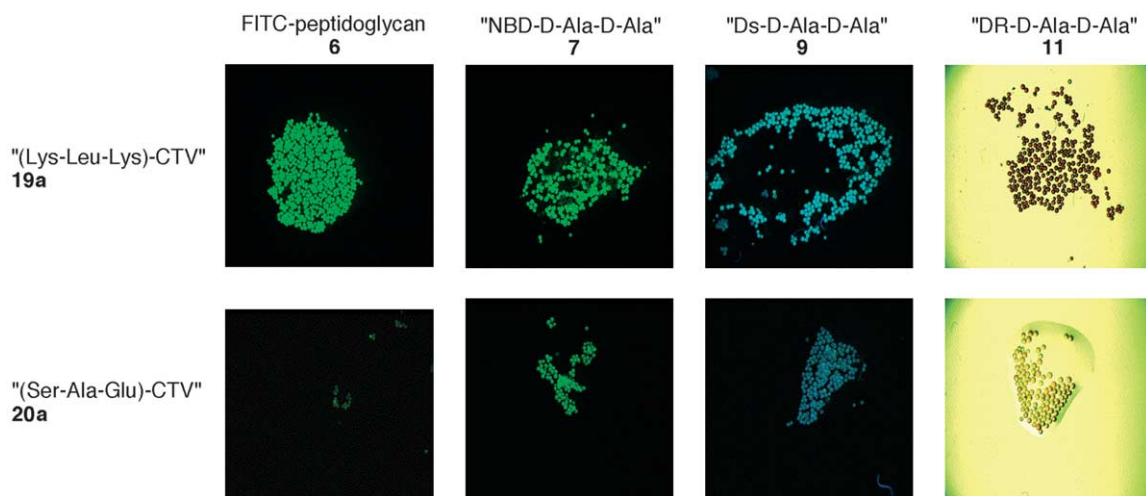


**Figure 3.** Screening for binding for D-Ala-D-Ala and D-Ala-D-Lac containing ligands (**6**, **7**, **9**, and **11**) by the resynthesized CTV-based receptor **19a** and **20a**.

receptors **19a** and **20a** was carried out by incubation with a 1 mg mL<sup>-1</sup> suspension of FITC-peptidoglycan (**6**). Homogeneous fluorescent beads were observed for receptor **19a**, clearly showing affinity for FITC-peptidoglycan while no fluorescence was observed for the control receptor **20a** (Fig. 3). These findings independently confirmed the identity of the receptors as obtained by the split-mix procedure.

In order to investigate whether the affinity of the resynthesized CTV-based receptor **19a** was due to either their interaction with D-Ala-D-Ala or with a different part from the FITC-peptidoglycan ligand (**6**), the binding of resin bound receptor **19a** for NBD, Dansyl- and disperse-red-D-Ala-D-Ala containing ligands **7**, **9**, and **11** was tested. For that purpose the [Lys-Leu-Lys]-containing CTV receptor **19a** and the 'control' [Ser-Ala-Glu]-containing CTV-based receptor **20a** were incubated with a 50 μM solution of ligands **7** or **9** or a 5 μM solution of ligand **11**. Homogeneous fluorescent beads were observed in all cases involving synthetic receptor **19a**, while no fluorescent beads were observed with control synthetic receptor **20a** (Fig. 3). Thus, binding is independent from the (fluorescent) dye label and really seems to involve recognition of the D-Ala-D-Ala sequence.

In view of these results, it was attempted to inhibit bacterial growth by the resynthesized [Lys-Leu-Lys]-containing CTV-receptor **21**. [Ser-Ala-Glu]-containing CTV-receptor **22** was also included in the experiments. A range of concentrations from 0 to 100 μM of **21** or **22** were used to determine a possible minimal inhibitory concentration (MIC) against *Staphylococcus aureus* Newman. Vancomycin was used as a positive control. Unfortunately, no inhibition of bacterial growth was observed for the CTV-based receptor **21** indicating no cell wall disruption and therefore no bacterial death. Negative control synthetic receptor **22** was also inactive. Although a possible explanation for the absence of antibacterial activity by synthetic receptor **21** might be too low a binding affinity for the D-Ala-D-Ala sequence, an alternative explanation is proteolytic degradation of the peptide arms of synthetic receptor **21**.

### 3. Conclusions

Thus by screening a CTV-based library containing tripeptide arms, one attached to the solid phase and two identical varying arms, we were able to find synthetic receptors containing amino acid sequences, which are either characteristic for binding dye labeled D-Ala-D-Ala or D-Ala-D-Lac containing ligands. This opens up possibilities for finding by combinatorial approaches synthetic receptors, which can act as 'sensors' for particular peptides. By attachment of fluorescent groups to these sensors or by immobilizing them to suitable surfaces one might be able to devise read-out systems for monitoring the extent of binding of peptide or other ligands. Selectivity of binding by synthetic receptors as sensors might be conveniently determined by exposing them to for example to a library of peptides, followed by measuring the relative binding affinity by mass spectrometry.

Use of different (fluorescent) dye labels showed that the label has a profound, albeit not decisive, influence on the binding by the receptor. In view of the facts that D-Ala-D-Ala as well as D-Ala-D-Lac are only small ligands, with very limited of interactions and that the only difference between these ligands is present in the linkage connecting the two residues: an amide 'N-H' in D-Ala-D-Ala and an ester '-O' in D-Ala-D-Lac, underlines the significance of the findings. Nevertheless, a resynthesized receptor based on the sequences found in the library screening was inactive against Gram-positive bacteria. If degradation of the synthetic receptor by proteases is largely responsible for this observation, then synthetic receptors containing D-amino acids might be more promising, which is under study now.

## 4. Experimental

### 4.1. General

All reagents were purchased from commercial sources and used without further purification. Argogel<sup>®</sup>-NH<sub>2</sub> (0.40 mmol g<sup>-1</sup>, average bead diameter 178 μm), Argogel<sup>®</sup>-Rink-NH-Fmoc (0.33 mmol g<sup>-1</sup>, average bead diameter 164 μm) resins were purchased from Argonaut Technologies, Inc., Amberlyst-A21 ion exchange resin (4.8 mmol g<sup>-1</sup>) from Aldrich, and Dowex 50×8 (H<sup>+</sup> form, 20–50 mesh) from Fluka. The Argogel<sup>®</sup>-NH<sub>2</sub> resin was dried over P<sub>2</sub>O<sub>5</sub>. The protected amino acids were purchased from Alexis Corporations (Läufelfingen, Switzerland) and Advanced Chemtech Europe (UK). All reactions on the solid phase were performed in standard glassware or poly(ethylene) glycol (PE) syringes with PE frits. Peptide grade solvents, dried on molecular sieves were used for reactions and resin washing. Kaiser and bromophenol blue (BPB) tests were used for detection of primary amines on the solid phase.<sup>17,18</sup> Analytical thin layer chromatography (TLC) was performed on Merck pre-coated silica gel 60 F<sub>254</sub> (0.25 mm) plates. Spots were visualised with UV light, ninhydrine, or Cl<sub>2</sub>-TDM.<sup>19</sup> Column chromatography was carried out using Merck Kieselgel 60 (40–63 μm). <sup>1</sup>H NMR and <sup>13</sup>C NMR were obtained on a Varian 300 MHz spectrometer. Chemical shifts are given in ppm with respect to internal TMS for <sup>1</sup>H NMR. <sup>13</sup>C NMR spectra were recorded using the attached proton test (APT) pulse sequence. ES-MS experiments were performed on a Shimadzu LCMS QP8000 system. HPLC analyses were performed on a Shimadzu-10Avp (Class VP) using PL-ELS-1000 detector and UV detector operating at 220 and 254 nm. An Adsorbosphere XL C18, 300 Å (4.6 mm×250 mm, 5 μm) was used; flow rate 1 mL min<sup>-1</sup>; two mobile phases (mobile phases A, 99.9% water, 0.1% TFA; mobile phase B, 5% water, 95% acetonitrile, 0.085% TFA) with a standard protocol, 0% B for 5 min to 100% B in 20 min, 100% B for 5 min to 0% B in 5 min and reequilibrated at 0% B for 5 min.

**4.1.1. H-D-Ala-D-Ala-O<sup>t</sup>Bu (2).** To a solution of Cbz-D-Ala-OH (1.16 g, 5 mmol) and HCl·H-D-Ala-O<sup>t</sup>Bu (0.91 g, 5 mmol) in DCM (30 mL), BOP (2.21 g, 5 mmol) and DiPEA (2.61 mL, 15 mmol) were added. After stirring at rt for 3 h, the reaction was evaporated to dryness in vacuo and



the residue was dissolved in EtOAc (60 mL). The solution was washed with Na<sub>2</sub>CO<sub>3</sub> (1 M), KHSO<sub>4</sub> (1 M), H<sub>2</sub>O, and brine. After drying (Na<sub>2</sub>SO<sub>4</sub>) and evaporating the solvent, Cbz-D-Ala-D-Ala-O<sup>t</sup>Bu (1.61 g, 92%) was obtained as white solid and used without further purification. *R*<sub>f</sub>=0.56 (DCM/methanol, 10:1). <sup>1</sup>H NMR (CDCl<sub>3</sub>, 300 MHz) δ: 7.33 (s, 5H, Ph), 6.42 (bs, 1H, NH(CO)), 5.29 (bs, 1H, NH(CO)O), 5.10 (s, 2H, CH<sub>2</sub>Ph), 4.40, 4.22 (2m, 2H, CHα), 1.44 (s, 9H, C(CH<sub>3</sub>)<sub>3</sub>), 1.37, 1.34 (2d, 6H, CH<sub>3</sub>β, *J*=6.9 Hz). <sup>13</sup>C NMR (CDCl<sub>3</sub>, 75 MHz) δ: 171.8, 171.5 (COO, NH(CO)), 155.8 (NH(CO)O), 136.2 (Ar-C), 128.5, 128.1, 128.0 (Ar-H), 82.1 (C(CH<sub>3</sub>)<sub>3</sub>), 66.9 (CH<sub>2</sub>Ph), 50.4, 48.6 (Cα), 27.9 (C(CH<sub>3</sub>)<sub>3</sub>), 18.4 (CH<sub>3</sub>β).

To a cooled solution (ice bath) of Cbz-D-Ala-D-Ala-O<sup>t</sup>Bu (1.40 g, 4 mmol) in methanol (200 mL), Pd on charcoal (10%) (20% w/w) was added and the suspension was stirred under H<sub>2</sub> pressure from a balloon at rt for 2 h. The reaction was filtered and the solvent was evaporated to give **2** (0.86 g, 99%) as a colorless syrup. *R*<sub>f</sub>=0.14 (DCM/methanol, 10:1). <sup>1</sup>H NMR (CDCl<sub>3</sub>, 300 MHz) δ: 7.67 (bs, 1H, NH(CO)), 4.40, 3.46 (2m, 2H, CHα), 1.43 (s, 11H, NH<sub>2</sub>, C(CH<sub>3</sub>)<sub>3</sub>), 1.34, 1.30 (2d, 6H, CH<sub>3</sub>β, *J*=6.9 Hz). <sup>13</sup>C NMR (CDCl<sub>3</sub>, 75 MHz) δ: 175.2, 172.4 (COO, NH(CO)), 81.7 (C(CH<sub>3</sub>)<sub>3</sub>), 50.6, 48.1 (Cα), 27.9 (C(CH<sub>3</sub>)<sub>3</sub>), 21.7, 18.4 (CH<sub>3</sub>β).

**4.1.2. H-D-Ala-D-Lac-O<sup>t</sup>Bu (3).** A solution of Cbz-D-Ala-OH (1.16 g, 5 mmol), H-D-Lac-O<sup>t</sup>Bu (0.73 g, 5 mmol) and BOP (2.21 g, 5 mmol) in DCM (30 mL) was cooled to -20 °C and DiPEA (2.61 mL, 15 mmol) was added. After stirring for 3 h, the reaction was evaporated to dryness in vacuo and the residue was dissolved in EtOAc (60 mL). The solution was washed with Na<sub>2</sub>CO<sub>3</sub> (1 M), KHSO<sub>4</sub> (1 M), H<sub>2</sub>O, and brine. After drying (Na<sub>2</sub>SO<sub>4</sub>) and evaporating the solvent, the crude **3** was purified by column chromatography using DCM/methanol, 30:1 to give Cbz-D-Ala-D-Lac-O<sup>t</sup>Bu (1.55 g, 88%) as a colorless syrup. *R*<sub>f</sub>=0.52 (DCM/methanol, 10:1). <sup>1</sup>H NMR (CDCl<sub>3</sub>, 300 MHz) δ: 7.34–7.29 (s, 5H, Ph), 5.26 (bs, 1H, NH(CO)O), 5.11 (d, 1H, CH<sub>2a</sub>Ph, *J*=12.2 Hz), 5.06 (d, 1H, CH<sub>2b</sub>Ph), 4.97 (m, 1H, CHα-Lac), 4.42 (m, 1H, CHα-Ala), 1.51, 1.45 (2d, 6H, CH<sub>3</sub>β, *J*=6.9 Hz), 1.43 (s, 9H, C(CH<sub>3</sub>)<sub>3</sub>). <sup>13</sup>C NMR (CDCl<sub>3</sub>, 75 MHz) δ: 172.5, 169.4 (2COO), 155.6 (NH(CO)O), 136.2 (Ar-C), 128.5, 128.1, 128.0 (Ar-H), 82.2 (C(CH<sub>3</sub>)<sub>3</sub>), 69.7 (Cα-Lac), 66.9 (CH<sub>2</sub>Ph), 49.4 (Cα-Ala), 27.9 (C(CH<sub>3</sub>)<sub>3</sub>), 18.6, 16.8 (CH<sub>3</sub>β). Hydrogenolysis of Cbz-D-Ala-D-Lac-O<sup>t</sup>Bu (1.40 g, 4 mmol) was performed following the same procedure as was used for Cbz-D-Ala-D-Ala-O<sup>t</sup>Bu. **3** (0.76 g, 87%) was obtained as a colorless syrup. *R*<sub>f</sub>=0.33 (DCM/methanol, 5:1). <sup>1</sup>H NMR (CDCl<sub>3</sub>, 300 MHz) δ: 4.94 (m, 1H, CHα-Lac), 4.11 (m, 1H, CHα-Ala), 2.30 (bs, 2H, NH<sub>2</sub>), 1.45 (d, 3H, CH<sub>3</sub>β-Lac, *J*=7.7 Hz), 1.43 (s, 9H, C(CH<sub>3</sub>)<sub>3</sub>), 1.34 (d, 3H, CH<sub>3</sub>β-Ala, *J*=6.9 Hz).

**4.1.3. H-Gly-D-Ala-D-Ala-O<sup>t</sup>Bu (4).** Coupling (see preparation of **2**) of Cbz-Gly-OH (0.79 g, 3.8 mmol) to **2** (0.82 g, 3.8 mmol) gave Cbz-Gly-D-Ala-D-Ala-O<sup>t</sup>Bu (1.38 g, 89%) as a white foam without further purification. *R*<sub>f</sub>=0.76 (DCM/methanol, 5:1). <sup>1</sup>H NMR (CDCl<sub>3</sub>, 300 MHz) δ: 7.32 (s, 5H, Ph), 6.82 (d, 1H, NH(CO), *J*=7.1 Hz), 6.73 (d, 1H, NH(CO), *J*=7.4 Hz), 5.60 (bs, 1H, NH(CO)O), 5.09 (s, 2H,

CH<sub>2</sub>Ph), 4.53, 4.38 (2m, 2H, CHα), 3.87 (d, 2H, CH<sub>2</sub>-Gly, *J*=5.2 Hz), 1.43 (s, 9H, C(CH<sub>3</sub>)<sub>3</sub>), 1.35, 1.33 (2d, 6H, CH<sub>3</sub>β, *J*=6.9 Hz). <sup>13</sup>C NMR (CDCl<sub>3</sub>, 75 MHz) δ: 171.8, 171.3, 168.6 (COO, 2NH(CO)), 156.6 (NH(CO)O), 136.1 (Ar-C), 128.5, 128.2, 128.1 (Ar-H), 82.1 (C(CH<sub>3</sub>)<sub>3</sub>), 67.2 (CH<sub>2</sub>Ph), 48.8 (Cα), 44.4 (Cα-Gly), 27.9 (C(CH<sub>3</sub>)<sub>3</sub>), 18.7, 18.3 (CH<sub>3</sub>β). ES-MS (*m/z*)=430.35 (100%, [M+Na]<sup>+</sup>), 408.30 (9%, [M+H]<sup>+</sup>), 352.25 (42%, [M-<sup>t</sup>Bu+H]<sup>+</sup>).

Hydrogenolysis of Cbz-Gly-D-Ala-D-Ala-O<sup>t</sup>Bu (1.30 g, 3.19 mmol) gave **4** (0.85 g, 98%) as a colorless syrup. *R*<sub>f</sub>=0.06 (DCM/methanol, 5:1). <sup>1</sup>H NMR (CDCl<sub>3</sub>, 300 MHz) δ: 7.71 (d, 1H, NH(CO), *J*=7.7 Hz), 7.04 (d, 1H, NH(CO), *J*=6.9 Hz), 4.51, 4.33 (2m, 2H, CHα), 3.29 (s, 2H, CH<sub>2</sub>-Gly), 1.39 (s, 11H, NH<sub>2</sub>, C(CH<sub>3</sub>)<sub>3</sub>), 1.33 (d, 3H, CH<sub>3</sub>β, *J*=6.9 Hz), 1.28 (d, 3H, CH<sub>3</sub>β, *J*=7.1 Hz). <sup>13</sup>C NMR (CDCl<sub>3</sub>, 75 MHz) δ: 172.7, 171.8, 171.7 (COO, 2NH(CO)), 81.7 (C(CH<sub>3</sub>)<sub>3</sub>), 48.6, 48.2 (Cα), 44.6 (Cα-Gly), 27.8 (C(CH<sub>3</sub>)<sub>3</sub>), 18.4, 18.1 (CH<sub>3</sub>β).

**4.1.4. H-Gly-D-Ala-D-Lac-O<sup>t</sup>Bu (5).** Overnight coupling (see preparation of **2**) of Cbz-Gly-OH (0.67 g, 3.2 mmol) to **3** (0.70 g, 3.2 mmol) gave Cbz-Gly-D-Ala-D-Lac-O<sup>t</sup>Bu (1.28 g, 98%) as a colorless syrup after column chromatography using a gradient DCM/methanol from 40:1 to 20:1. *R*<sub>f</sub>=0.77 (DCM/methanol, 10:1). <sup>1</sup>H NMR (CDCl<sub>3</sub>, 300 MHz) δ: 7.33 (s, 5H, Ph), 6.51 (d, 1H, NH(CO), *J*=7.4 Hz), 5.40 (bs, 1H, NH(CO)O), 5.12 (s, 1H, CH<sub>2</sub>Ph), 4.95, 4.62 (2m, 2H, CHα), 3.88 (s, 2H, CH<sub>2</sub>-Gly), 1.45, (2d, 6H, CH<sub>3</sub>β, *J*=7.1 Hz), 1.43 (s, 9H, C(CH<sub>3</sub>)<sub>3</sub>). <sup>13</sup>C NMR (CDCl<sub>3</sub>, 75 MHz) δ: 172.2, 169.3, 168.5 (2COO, NH(CO)), 156.6 (NH(CO)O), 136.1 (Ar-C), 128.5, 128.2, 128.1 (Ar-H), 82.3 (C(CH<sub>3</sub>)<sub>3</sub>), 69.8 (Cα-Lac), 67.2 (CH<sub>2</sub>Ph), 47.9 (Cα-Ala), 44.4 (Cα-Gly), 27.9 (C(CH<sub>3</sub>)<sub>3</sub>), 18.3, 16.8 (CH<sub>3</sub>β). Hydrogenolysis of Cbz-Gly-D-Ala-D-Lac-O<sup>t</sup>Bu (1.20 g, 2.94 mmol) gave **5** (0.52 g, 64%) as a colorless syrup. *R*<sub>f</sub>=0.16 (DCM/methanol, 10:1). <sup>1</sup>H NMR (CDCl<sub>3</sub> with a few drops of CD<sub>3</sub>OD, 300 MHz) δ: 4.88, 4.47 (2m, 2H, CHα), 3.97 (d, 1H, CH<sub>2a</sub>-Gly, *J*<sub>gem</sub>=14.0 Hz, *J*<sub>a,NH</sub>=6.9 Hz), 3.92 (d, 1H, CH<sub>2b</sub>-Gly, *J*<sub>b,NH</sub>=6.9 Hz), 1.39 (d, 6H, CH<sub>3</sub>β, *J*=7.1 Hz), 1.39 (s, 9H, C(CH<sub>3</sub>)<sub>3</sub>).

## 4.2. Synthesis of D-Ala-D-Ala and D-Ala-D-Lac containing ligands (7–11)

**4.2.1. NBD-(CH<sub>2</sub>)<sub>5</sub>-C(O)-Gly-D-Ala-D-Ala-OH (7).** To a suspension of **4** (0.27 g, 1 mmol), 6-(7-nitrobenzo-2-oxa-1,3-diazole)-hexanoic acid (0.29 g, 1 mmol) and BOP (0.44, 1 mmol) in DCM (6 mL), DiPEA (0.35 mL, 2 mmol) was added. After stirring the orange solution at rt for 3 h, the reaction mixture was evaporated to dryness in vacuo and the residue was dissolved in EtOAc (6 mL). The solution was washed with KHSO<sub>4</sub> (1 M), H<sub>2</sub>O, and brine. After drying (Na<sub>2</sub>SO<sub>4</sub>) and evaporating the solvent, the crude product was purified by column chromatography using a gradient of DCM/methanol from 30:1 to 10:1 and NBD-(CH<sub>2</sub>)<sub>5</sub>-C(O)-Gly-D-Ala-D-Ala-O<sup>t</sup>Bu (0.45 g, 82%) was obtained as an orange solid. *R*<sub>f</sub>=0.49 (DCM/methanol, 10:1). <sup>1</sup>H NMR (CDCl<sub>3</sub>, 300 MHz) δ: 8.45 (d, 1H, H-6-NBD, *J*=8.8 Hz), 7.22 (bs, 1H, NH), 6.93 (d, 1H, NH(CO)-Ala, *J*=7.1 Hz), 6.65 (d, 1H, NH(CO)-Ala, *J*=7.1 Hz), 6.43 (t, 1H, NH(CO)-Gly, *J*=5.1 Hz), 6.14 (d, 1H, H-5-NBD), 4.52, 4.40 (2m, 2H, CHα), 4.00 (dd, 1H, CH<sub>2a</sub>-Gly, *J*<sub>gem</sub>=



16.7 Hz,  $J_{\text{a,NH}}=5.5$  Hz), 3.92 (dd, 1H,  $\text{CH}_{2\text{b}}\text{-Gly}$ ,  $J_{\text{b,NH}}=5.5$  Hz), 3.52 (m, 2H,  $\text{CH}_2\text{NH-NBD}$ ), 2.29 (t, 2H,  $\text{CH}_2\text{C(O)-NBD}$ ,  $J=6.7$  Hz), 1.83–1.48 (m, 6H,  $\text{CH}_2\text{-NBD}$ ), 1.41 (s, 9H,  $\text{C}(\text{CH}_3)_3$ ), 1.38, 1.34 (2d, 6H,  $\text{CH}_3\beta$ ,  $J=6.9$  Hz).  $^{13}\text{C}$  NMR ( $\text{CDCl}_3$ , 75 MHz)  $\delta$ : 173.4, 171.7, 171.5, 168.5 (COO,  $\text{NH}(\text{CO})$ ), 144.3 (C-NBD), 136.7 (C-6, 5-NBD), 82.3 ( $\text{C}(\text{CH}_3)_3$ ), 53.4 (C $\alpha$ -Gly), 48.9 (C $\alpha$ -Ala), 43.0, 35.7 ( $\text{CH}_2\text{-NBD}$ ), 27.9 ( $\text{C}(\text{CH}_3)_3$ ), 27.9, 26.2, 24.6 ( $\text{CH}_2\text{-NBD}$ ), 18.8, 18.3 ( $\text{CH}_3\beta$ ). ES-MS ( $m/z$ )=572.40 (100%,  $[\text{M}+\text{Na}]^+$ ), 550.25 (45%,  $[\text{M}+\text{H}]^+$ ), 4.94.35 (96%,  $[\text{M}-^t\text{Bu}+\text{H}]^+$ ).

Treatment overnight of  $\text{NBD-(CH}_2)_5\text{-C(O)-Gly-D-Ala-D-Ala-O}^t\text{Bu}$  (0.30 g, 0.54 mmol) with DCM/saturated HCl(g) in ether (1:1) (20 mL) led to an orange precipitate. Filtration and washing of the precipitate with cold ether gave to **7** (0.19 g, 70%) as an orange solid.  $R_f=0.04$  (DCM/methanol, 5:1).  $^1\text{H}$  NMR (DMSO, 300 MHz)  $\delta$ : 8.51 (d, 1H, H-6-NBD,  $J=9.1$  Hz), 8.33 (d, 1H,  $\text{NH}(\text{CO})$ ,  $J=6.9$  Hz), 8.06 (t, 1H,  $\text{NH}$ ,  $J=6.0$  Hz), 7.98 (d, 1H,  $\text{NH}(\text{CO})$ ,  $J=7.4$  Hz), 6.42 (d, 1H, H-5-NBD), 4.34–4.19 (m, 2H,  $\text{CH}\alpha$ ), 3.67 (d, 2H,  $\text{CH}_2\text{-Gly}$ ,  $J=5.5$  Hz), 3.35 (bs, 2H,  $\text{CH}_2\text{NH-NBD}$ ), 2.14 (m, 2H,  $\text{CH}_2\text{C(O)-NBD}$ ), 1.66, 1.54, 1.35 (3m, 6H,  $\text{CH}_2\text{-NBD}$ ), 1.27, 1.19 (2d, 6H,  $\text{CH}_3\beta$ ,  $J=7.1$  Hz).  $^{13}\text{C}$  NMR ( $\text{CDCl}_3$ , 75 MHz)  $\delta$ : 174.4, 173.1, 172.4, 169.3 (COOH,  $\text{NH}(\text{CO})$ ), 144.2 (C-NBD), 137.0 (C-6,5-NBD), 58.0 (C $\alpha$ -Gly), 48.0, 47.9 (C $\alpha$ -Ala), 42.4, 35.3, 30.3, 26.0, 24.6 ( $\text{CH}_2\text{-NBD}$ ), 17.7, 16.9 ( $\text{CH}_3\beta$ ). ES-MS ( $m/z$ )=516.30 (40%,  $[\text{M}+\text{Na}]^+$ ), 494.15 (100%,  $[\text{M}+\text{H}]^+$ ). HPLC ( $R_t=17.75$  min, 99% purity).

**4.2.2. NBD-(CH<sub>2</sub>)<sub>5</sub>-C(O)-Gly-D-Ala-D-Lac-OH (8).** The same procedure as was used for the preparation of **7** was followed. **5** (0.14 g, 0.5 mmol) gave  $\text{NBD-(CH}_2)_5\text{-C(O)-Gly-D-Ala-D-Lac-O}^t\text{Bu}$  (0.22 g, 80%) as an orange solid.  $R_f=0.59$  (DCM/methanol, 10:1).  $^1\text{H}$  NMR ( $\text{CDCl}_3$ , 300 MHz)  $\delta$ : 8.46 (d, 1H, H-6-NBD,  $J=8.5$  Hz), 6.87, 6.60, 6.30 (3bs, 3H,  $\text{NH}$ ), 6.14 (d, 1H, H-5-NBD), 4.66–4.53 (m, 2H,  $\text{CH}\alpha$ ), 3.97 (s, 2H,  $\text{CH}_2\text{-Gly}$ ), 3.50 (m, 2H,  $\text{CH}_2\text{NH-NBD}$ ), 2.29 (t, 2H,  $\text{CH}_2\text{C(O)-NBD}$ ,  $J=6.9$  Hz), 1.86–1.70 (m, 4H,  $\text{CH}_2\text{-NBD}$ ), 1.56–1.49 (m, 2H,  $\text{CH}_2\text{NBD}$ ), 1.49, 1.46 (2d, 6H,  $\text{CH}_3\beta$ ,  $J=7.1$  Hz), 1.42 (s, 9H,  $\text{C}(\text{CH}_3)_3$ ). ES-MS ( $m/z$ )=573.35 (100%,  $[\text{M}+\text{Na}]^+$ ), 517.30 (45%,  $[\text{M}-^t\text{Bu}+\text{Na}]^+$ ), 495.13 (30%,  $[\text{M}-^t\text{Bu}+\text{H}]^+$ ).

Cleavage of the  $^t\text{Bu}$  ester of  $\text{NBD-(CH}_2)_5\text{-C(O)-Gly-D-Ala-D-Lac-O}^t\text{Bu}$  (0.18 g, 0.33 mmol) led to **8** (0.11 g, 65%) as an orange solid.  $R_f=0.03$  (DCM/methanol, 10:1).  $^1\text{H}$  NMR ( $\text{CD}_3\text{OD}$ , 300 MHz)  $\delta$ : 8.69 (d, 1H, H-6-NBD,  $J=8.8$  Hz), 6.53 (d, 1H, H-5-NBD), 5.12, 4.66 (2m, 2H,  $\text{CH}\alpha$ ), 4.09 (d, 2H,  $\text{CH}_{2\text{a}}\text{-Gly}$ ,  $J_{\text{gem}}=16.7$  Hz), 4.02 (d, 2H,  $\text{CH}_{2\text{b}}\text{-Gly}$ ), 3.72 (bs, 2H,  $\text{CH}_2\text{NH-NBD}$ ), 2.49 (t, 2H,  $\text{CH}_2\text{C(O)-NBD}$ ,  $J=7.3$  Hz), 1.98, 1.89, 1.66 (3m, 6H,  $\text{CH}_2\text{-NBD}$ ), 1.63, 1.62 (2d, 6H,  $\text{CH}_3\beta$ ,  $J=7.4$ , 7.1 Hz). ES-MS ( $m/z$ )=517.45 (100%,  $[\text{M}+\text{Na}]^+$ ), 495.19 (25%,  $[\text{M}+\text{H}]^+$ ). HPLC ( $R_t=18.98$  min, 94% purity).

**4.2.3. Ds-Gly-D-Ala-D-Ala-OH (9).** To a solution of **4** (0.27 g, 1 mmol) in 3%  $\text{NaHCO}_3$  (10 mL), a solution of dansyl chloride (0.30 mL, 1.1 mmol) in acetone (10 mL) was added. After stirring the fluorescent solution in the absence of light overnight, the reaction mixture was evaporated to dryness in vacuo and the residue was dissolved in EtOAc (10 mL). The solution was washed with  $\text{H}_2\text{O}$ , dried

( $\text{Na}_2\text{SO}_4$ ) and the solvent was evaporated. The crude product was purified by column chromatography using a gradient of DCM/methanol from 50:1 to 30:1 to give  $\text{Ds-Gly-D-Ala-D-Ala-O}^t\text{Bu}$  (0.41 g, 82%) as a light-green solid.  $R_f=0.48$  (DCM/methanol, 9:1).  $^1\text{H}$  NMR ( $\text{CDCl}_3$ , 300 MHz)  $\delta$ : 8.51, 8.30 (2d, 2H, Ar,  $J=8.5$  Hz), 8.21 (d, 1H, Ar,  $J=7.4$  Hz), 7.50, 7.47 (2d, 2H, Ar,  $J=16.0$  Hz), 7.36, 7.26 (2d, 2H,  $\text{NH}(\text{CO})$ ,  $J=7.7$  Hz), 7.13 (d, 1H, Ar), 6.92 (bs, 1H,  $\text{NHSO}_2$ ), 4.52, 4.36 (2m, 2H,  $\text{CH}\alpha$ ), 3.61 (s, 2H,  $\text{CH}_2\text{-Gly}$ ), 2.85 (s, 6H,  $\text{N}(\text{CH}_3)_2$ ), 1.44 (s, 9H,  $\text{C}(\text{CH}_3)_3$ ), 1.30, 1.13 (2d, 6H,  $\text{CH}_3\beta$ ,  $J=7.0$  Hz). ES-MS ( $m/z$ )=529.35 (16%,  $[\text{M}+\text{Na}]^+$ ), 451.35 (100%,  $[\text{M}-^t\text{Bu}+\text{Na}]^+$ ).

After the cleavage of the  $^t\text{Bu}$  ester of  $\text{Ds-Gly-D-Ala-D-Ala-O}^t\text{Bu}$  (0.17 g, 0.33 mmol), the reaction mixture was evaporated in vacuo and  $\text{KHSO}_4$  (1 M), was added. The pH of the aqueous layer was adjusted to 3–4 by addition of NaOH (1 N) and extracted with EtOAc (70 mL) three times. The combined organic layers were washed with brine, dried ( $\text{Na}_2\text{SO}_4$ ) and concentrated to afford **9** (0.11 g, 65%) as a light-green solid.  $R_f=0.52$  (methanol/chloroform/ $\text{NH}_4\text{OH}$ , 60:45:20).  $^1\text{H}$  NMR ( $\text{CD}_3\text{OD}$ , 300 MHz)  $\delta$ : 8.57, 8.34 (2d, 2H, Ar,  $J=8.5$ , 8.8 Hz), 8.21 (d, 1H, Ar,  $J=7.4$  Hz), 7.54–7.63 (m, 2H, Ar), 7.27 (d, 1H, Ar,  $J=7.7$  Hz), 4.93–4.22 (m, 2H,  $\text{CH}\alpha$ ), 3.54 (s, 2H,  $\text{CH}_2\text{-Gly}$ ), 2.86 (s, 6H,  $\text{N}(\text{CH}_3)_2$ ), 1.37, 1.17 (2d, 6H,  $\text{CH}_3\beta$ ,  $J=7.4$ , 7.1 Hz).  $^{13}\text{C}$  NMR ( $\text{CD}_3\text{OD}$ , 75 MHz)  $\delta$ : 177.3 (COOH), 174.1, 170.7 (2 $\text{NH}(\text{CO})$ ), 153.3, 135.98 (Ar-C), 131.6 (Ar-H), 131.2, 130.9 (Ar-C), 130.6, 129.6, 124.3, 120.2, 116.7 (Ar-H), 50.3 (C $\alpha$ -Ala), 46.4 (C $\alpha$ -Gly), 45.8 ( $\text{N}(\text{CH}_3)_2$ ), 18.0, 17.8 ( $\text{CH}_3\beta$ ). ES-MS ( $m/z$ )=451.35 (100%,  $[\text{M}+\text{H}]^+$ ). HPLC ( $R_t=15.93$  min, 99% purity).

**4.2.4. Ds-Gly-D-Ala-D-Lac-OH (10).** The same procedure as was used for **9** was followed for the preparation of **10**. **5** (0.14 g, 0.5 mmol) gave  $\text{Ds-Gly-D-Ala-D-Lac-O}^t\text{Bu}$  as a light-green solid. Cleavage of the  $^t\text{Bu}$  ester of  $\text{Ds-Gly-D-Ala-D-Lac-O}^t\text{Bu}$  led to **10** (0.17 g, 75% over 2 steps) as a light-green solid.  $R_f=0.63$  (methanol/chloroform/ $\text{NH}_4\text{OH}$ , 60:45:20).  $^1\text{H}$  NMR ( $\text{CDCl}_3$ , 300 MHz)  $\delta$ : 8.52 (2d, 2H, Ar,  $J=8.5$  Hz), 8.28 (d, 1H, Ar), 8.20 (1d, 1H, Ar,  $J=7.1$  Hz), 7.74–7.56 (m, 2H, Ar), 7.19 (1d, 1H, Ar,  $J=7.7$  Hz), 7.13 (d, 1H,  $\text{NH}(\text{CO})$ ,  $J=7.4$  Hz), 6.49 (bt, 1H,  $\text{NHSO}_2$ ), 5.92 (bs, 1H, COOH), 5.01 (1m, 1H,  $\text{CH}\alpha\text{-Lac}$ ), 4.45 (1m, 1H,  $\text{CH}\alpha\text{-Ala}$ ), 3.59 (bs, 2H,  $\text{CH}_2\text{-Gly}$ ), 2.88 (s, 6H,  $\text{N}(\text{CH}_3)_2$ ), 1.48, 1.21 (2d, 6H,  $\text{CH}_3\beta$ ,  $J=7.1$ , 7.4 Hz).  $^{13}\text{C}$  NMR ( $\text{CDCl}_3$ , 75 MHz)  $\delta$ : 173.6 (COOH), 172.2, 169.0 (2 $\text{NH}(\text{CO})$ ), 151.4, 133.6 (Ar-C), 130.7, 130.0 (Ar-H), 129.7, 129.4 (Ar-C), 128.8, 123.4, 118.8, 115.2 (Ar-H), 69.6 (C $\alpha$ -Lac), 48.0 (C $\alpha$ -Ala), 45.6 (C $\alpha$ -Gly), 45.4 ( $\text{N}(\text{CH}_3)_2$ ), 17.0, 16.6 ( $\text{CH}_3\beta$ ). ES-MS ( $m/z$ )=452.3 (100%,  $[\text{M}+\text{Na}]^+$ ). HPLC ( $R_t=15.90$  min, 99% purity).

**4.2.5. DR-C(O)-(CH<sub>2</sub>)<sub>2</sub>-C(O)-Gly-D-Ala-D-Ala-OH (11).** To solution of **4** (0.27 g, 1 mmol) in DCM (2 mL), succinic anhydride (0.1 g, 1 mmol) and TEA (0.15 mL, 1.1 mmol) were added. After stirring the mixture at rt for 2 h, the reaction mixture was evaporated in vacuo and the residue was dissolved in butanol (3 mL). The solution was washed with  $\text{KHSO}_4$  (1 M),  $\text{H}_2\text{O}$ , and brine. After drying ( $\text{Na}_2\text{SO}_4$ ) and evaporation of the solvent,  $\text{HOOC-(CH}_2)_2\text{-C(O)-Gly-D-Ala-D-Ala-O}^t\text{Bu}$  (0.32 g, 87%) was obtained as a white

solid.  $R_f=0.23$  (DCM/methanol, 10:1).  $^1\text{H}$  NMR (DMSO, 300 MHz)  $\delta$ : 12.16 (bs, 1H, COOH), 8.16 (d, 2H, 2 NH(CO),  $J=6.6$  Hz), 7.94 (d, 1H, NH(CO),  $J=7.7$  Hz), 4.30, 4.07 (2m, 2H, CH $\alpha$ ), 3.66 (d, 2H, CH $_2$ -Gly,  $J=5.7$  Hz), 2.41–2.35 (m, 4H, CH $_2$ ), 1.36 (s, 9H, C(CH $_3$ ) $_3$ ), 1.23, 1.19 (2d, 6H, CH $_3\beta$ ,  $J=7.4$ , 7.1 Hz).  $^{13}\text{C}$  NMR (DMSO, 75 MHz)  $\delta$ : 174.1, 172.1, 171.8, 171.8, 168.6 (COOH, COO, NH(CO)), 80.5 (C(CH $_3$ ) $_3$ ), 48.5, 47.78 (C $\alpha$ -Ala), 42.3 (C $\alpha$ -Gly), 30.0, 29.3 (CH $_2$ ), 27.8 (C(CH $_3$ ) $_3$ ), 18.5, 17.0 (CH $_3\beta$ ). ES-MS ( $m/z$ ) = 396.25 (100%, [M+Na] $^+$ ), 374.25 (7%, [M+H] $^+$ ), 318.10 (18%, [M- $t$ Bu+H] $^+$ ).

HOOC-(CH $_2$ ) $_2$ -C(O)-Gly-D-Ala-D-Ala-O $t$ Bu (0.31 g, 0.83 mmol), Disperse red-NH $_2$ <sup>16</sup> (0.26 g, 0.83 mmol), BOP (0.37 g, 0.83 mmol) and DiPEA (0.29 mL, 1.66 mmol) were dissolved in DCM (50 mL). After stirring the dark red solution at rt overnight, the solvent was evaporated in vacuo and the residue was dissolved in EtOAc (10 mL). This solution was washed with KHSO $_4$  (1 M), H $_2$ O, and brine. After drying (Na $_2$ SO $_4$ ) and evaporating the solvent, the crude product was purified by column chromatography using a gradient of DCM/methanol from 50:1 through 30:1 to 10:1 and DR-C(O)-(CH $_2$ ) $_2$ -C(O)-Gly-D-Ala-D-Ala-O $t$ Bu (0.28 g, 51%) was obtained as a dark red solid.  $R_f=0.58$  (DCM/methanol, 10:1).  $^1\text{H}$  NMR (CDCl $_3$  and a few drops of CD $_3$ OD, 300 MHz)  $\delta$ : 8.27, 7.87 (2d, 4H, Ar,  $J=9.1$  Hz), 7.84 (d, 2H, Ar,  $J=9.9$  Hz), 7.39 (bs, 2H, 2 NH(CO)), 7.09 (d, 1H, NH(CO),  $J=7.4$  Hz), 6.92 (bs, 1H, NH(CO)), 6.75 (d, 2H, Ar,  $J=9.3$  Hz), 4.42, 4.32 (2m, 2H, CH $\alpha$ ), 3.95, 3.76 (d, 2H, CH $_2$ -Gly,  $J=16.8$  Hz), 3.51–3.38 (m, 6H, CH $_2$ -N), 2.48 (s, 4H, CH $_2$ -C(O)), 1.40 (s, 9H, C(CH $_3$ ) $_3$ ), 1.35, 1.31 (2d, 6H, CH $_3\beta$ ,  $J=7.1$  Hz), 1.21 (t, 3H, CH $_3$ ,  $J=7.1$  Hz). ES-MS ( $m/z$ ) = 691.50 (70%, [M+Na] $^+$ ), 669.50 (100%, [M+H] $^+$ ).

Cleavage of the  $t$ Bu ester of DR-C(O)-(CH $_2$ ) $_2$ -C(O)-Gly-D-Ala-D-Ala-O $t$ Bu (0.20, 0.3 mmol), as was described above except for the use of dioxane instead of DCM, gave **11** (0.14 g, 75%) as a dark red solid.  $R_f=0.05$  (DCM/methanol, 10:1).  $^1\text{H}$  NMR (CDCl $_3$  and a few drops of CD $_3$ OD, 300 MHz)  $\delta$ : 8.06, 7.64 (2d, 4H, Ar,  $J=9.1$  Hz), 7.62 (d, 2H, Ar,  $J=9.3$  Hz), 6.57 (d, 2H, Ar,  $J=9.1$  Hz), 4.06, 3.90 (2m, 2H, CH $\alpha$ ), 3.66 (s, 2H, CH $_2$ -Gly,  $J=16.8$  Hz), 3.26–3.10 (m, 6H, CH $_2$ -N), 2.35–2.19 (m, 4H, CH $_2$ C(O)), 1.16, 1.09 (2d, 6H, CH $_3\beta$ ,  $J=7.1$  Hz), 0.97 (t, 3H, CH $_3$ ,  $J=7.1$  Hz).  $^{13}\text{C}$  NMR (CD $_3$ OD, 75 MHz)  $\delta$ : 179.3 (COOH), 175.5, 174.9, 173.7, 171.7 (COO, NH(CO)), 158.1, 153.0, 148.5, 144.7 (Ar-C), 127.2, 125.6, 123.4, 112.5 (Ar-H), 51.8, 50.6 (C $\alpha$ -Ala), 46.3, 43.6, 38.1, 32.0, 31.9, 30.6 (CH $_2$ N, CH $_2$ C(O), C $\alpha$ -Gly), 19.3, 17.9 (CH $_3\beta$ ), 12.5 (CH $_3$ ). ES-MS ( $m/z$ ) = 635.40 (15%, [M+Na] $^+$ ), 613.45 (100%, [M+H] $^+$ ). HPLC (Rt = 21.70 min, 99% purity).

### 4.3. General procedure for coupling Fmoc amino acids, (Boc) $_2$ -CTV-OH (**13**) or (Fmoc) $_2$ -CTV-OH (**14**) on the solid phase

The resin (1 equiv) was swollen in NMP (2 min) and, after draining the solvent, BOP (4 equiv), the desired Fmoc amino acid (4 equiv) and NMP (15 mL/mmol) were added. The mixture was shaken until complete dissolution and then DiPEA (8 equiv) was added. For coupling of **13** or **14**, 2 equiv of **13** or **14**, 2 equiv of BOP, and 4 equiv of DiPEA

were used and the reaction was shaken at rt overnight. After 3 h of shaking, the resin was washed with NMP (5  $\times$  15 mL/mmol, each 2 min) and DCM (5  $\times$  15 mL/mmol, each 2 min). Negative Kaiser and BPB tests indicated completion of the coupling. The loading of the resin was determined by Fmoc-spectrophotometric quantification, after drying the resin under vacuum overnight.

### 4.4. General procedure for N $^z$ -Fmoc deprotection

The N $^z$ -Fmoc-protected resin was swollen in NMP (2 min) and, after draining the solvent, the resin was shaken with 20% piperidine in NMP (3  $\times$  20 mL per mmol, each 10 min). The resin was washed with NMP (5  $\times$  10 mL per mmol, each 2 min) and DCM (5  $\times$  10 mL per mmol, each 2 min). Positive Kaiser and BPB tests indicated Fmoc-deprotection.

**4.4.1. Loading of Argogel $^{\text{®}}$ -NH $_2$  or Argogel $^{\text{®}}$ -Rink-NH $_2$  (**16a**, **16b**).** Fmoc-L-Ala-OH  $\cdot$  H $_2$ O (1.05 g, 3.2 mmol) was coupled to Argogel $^{\text{®}}$ -NH $_2$  resin (**a**) (2 g, 0.8 mmol) or to Fmoc-deprotected Argogel $^{\text{®}}$ -Rink-NH $_2$  (**b**) (2.42 g, 0.8 mmol). Then the N $^z$ -Fmoc group was cleaved, following the general procedure and coupling of Fmoc-L-Ala-OH  $\cdot$  H $_2$ O was repeated twice. Prior to the last N $^z$ -Fmoc deprotection step, the loading was determined to be 0.31 and 0.25 mmol g $^{-1}$ , respectively. After N $^z$ -Fmoc deprotection, **12a** was coupled to **13** to give **15a**, and **12b** was coupled to **14** to give **15b**. Treatment of **15a** with 50% TFA in DCM, (7 mL) for 45 min and additional washing of the resin with NMP (3  $\times$  7 mL, each 2 min), 25% DiPEA in NMP (4  $\times$  7 mL, each 2 min), NMP (5  $\times$  7 mL, each 2 min), and finally DCM (5  $\times$  7 mL, each 2 min) led to resin **16a**. Fmoc-deprotection of **15b** using the general procedure gave resin **16b**.

**4.4.2. Resynthesis of receptors 19a and 20a on Argogel $^{\text{TM}}$ -NH $_2$  resin and 17b and 18b on the Argogel $^{\text{®}}$ -Rink resin.** Resins **16a** and **16b** (each containing 0.051 mmol of amino groups) were dried overnight under vacuum and were separately swollen in NMP (for 2 min). After draining the solvent, three subsequent coupling/N $^z$ -Fmoc deprotection cycles were carried out of Fmoc-L-Lys(Boc)-OH, Fmoc-L-Leu-OH and Fmoc-L-Lys(Boc)-OH following the general procedures to give **17a** and **17b**. The same procedure was followed for the synthesis of **18a** and **18b**, except for the use of Fmoc-L-Glu(O $t$ Bu)-OH, Fmoc-L-Ala-OH, and Fmoc-L-Ser( $t$ Bu)-OH as amino acids. The Boc groups from **17a** and **18a** were cleaved using 95% TFA in H $_2$ O, 95:5. The resin was washed with NMP (3  $\times$  1.5 mL, each 2 min), 25% DiPEA in NMP: (4  $\times$  1.5 mL, each 2 min), NMP (5  $\times$  1.5 mL, each 2 min), DCM (5  $\times$  1.5 mL, each 2 min), dioxane (4  $\times$  1.5 mL, each 2 min), dioxane/H $_2$ O, 1:1 (4  $\times$  1.5 mL, each 2 min), H $_2$ O (4  $\times$  1.5 mL, each 2 min), and Et $_2$ O (5  $\times$  1.5 mL, each 2 min) to give the receptors **19a** and **20a**, respectively.

**4.4.3. Deprotection of the acid labile side-chains and cleavage of the receptors 17b and 18b from the Argogel $^{\text{®}}$ -Rink resin.** Receptors **17b** and **18b** on the Argogel $^{\text{®}}$ -Rink resin were swollen in DCM (2  $\times$  2 min) and the solvent was drained. After addition of 95% TFA in H $_2$ O (20 mL/mmol), resins were shaken at rt for 4 h, removed by

filtering and washed with TFA/H<sub>2</sub>O, 95:5. The filtrates were combined and Et<sub>2</sub>O was added to give suspensions of the cleaved synthetic receptors. After centrifugation (3500 ppm, 5 min) of the suspensions, the volatiles were removed and the white solids were dissolved in H<sub>2</sub>O followed by lyophilization to give trifluoroacetate salt of **21** (86 mg, 76%); HPLC: Rt=17.80 min, 94% purity, ES-MS (*m/z*)=766.95 (100%, [M+2H]<sup>2+</sup>), 511.50 (100%, [M+3H]<sup>3+</sup>), 383.75 (58%, [M+4H]<sup>4+</sup>), and trifluoroacetate salt of **22** (56 mg, 69%); HPLC: Rt=17.68 min, 94% purity; ES-MS (*m/z*)=1390.00 (25%, [M+Na]<sup>+</sup>), 1368.30 (100%, [M+H]<sup>+</sup>), 684.60 (60%, [M+2H]<sup>2+</sup>), respectively.

#### 4.5. Procedure for liberation of the amine from the TFA-salt

A solution of trifluoroacetate salt of **21** (6.6 μmol) in acetonitrile/H<sub>2</sub>O (1:1) (1.2 mL) was added to Amberlyst A21-ion exchange resin (264 μmol) and the resin was shaken for 45 min. After filtration, the solution was lyophilized to give quantitatively **21**. In case of the trifluoroacetate salt of **22**, Dowex 50×8 (H<sup>+</sup> form) ion exchange resin (1 g) was used. The resin was shaken for 4 h and the solvent was drained. 25% NH<sub>3</sub> in H<sub>2</sub>O was added to the resin and shaking was continued for 1 h. After filtration the solution was lyophilized to give **22**.

#### 4.6. Screening of library 1{1-13, 1-13, 1-13} with D-Ala-D-Ala and D-Ala-D-Lac containing ligands (6–11)

A 1 mg mL<sup>-1</sup> suspension of **6**, a 50 mM solution of **7–10**, and a 5 mM solution of **11** in phosphate buffer (0.1 N, pH=7.0) (1.3 mL) were added to different portions of library 1{1-13, 1-13, 1-13} (14 mg, ~11,000 beads, ~4 copies/receptor) and incubated at 20 °C for 72 h. The resin was drained and was washed with phosphate buffer (0.1 N, pH=7.0) (5×1.3 mL, each 2 min). Next, the resin was poured into a petri dish and spread into a monolayer. The beads were viewed under a fluorescence microscope. By use of a long needle, most fluorescent or colored beads were isolated (~100 beads). The fluorescence of the preselected beads was reevaluated using the overexposure mode of the Leica DC-100 digital camera system and image analysis to estimate the relative fluorescence intensities semi-quantitatively. Reevaluation of the red colored beads in the case of **11** was judged by eye. Only nine to ten best fluorescent or colored beads were selected and analysed by independent Edman degradation together with a non-fluorescent bead from each screening.

#### 4.7. Binding affinity for with D-Ala-D-Ala containing ligands (6, 7, 9 and 11 by 19a and 20a)

A 50 μM solution of **7** or **9** (1.45 mL) or a 5 μM solution of **11**, or a 1 mg mL<sup>-1</sup> (433 μL) suspension of **6** in phosphate buffer (0.1 N, pH=7.0) was added to the resynthesized receptors **19a** or **20a** (0.6 mg, ~480 beads) and incubated at 20 °C for 72 h. The resins were drained and washed with phosphate buffer (0.1 N, pH=7.0) (5×1.3 mL, each 2 min). The resin was poured into a petri dish and spread into a monolayer. The beads were viewed under a fluorescence microscope.

#### Acknowledgements

We thank Arwin Brouwer for the preparation of disperse red-NH<sub>2</sub>. Dr. Jos A.G. van Strijp and Erik Heezius of Eijkman Winkler Institute (Utrecht Medical Center, The Netherlands) are gratefully acknowledged for providing us with FITC-peptidoglycan and for testing the synthetic receptors **21** and **22**. This work was supported by the European Commission (Marie Curie Individual Fellowship, contract No. HPMFCT-2000-00704).

#### References and notes

- (a) Arienzo, R.; Kilburn, J. D. *Tetrahedron* **2002**, *58*, 711–719. (b) Henley, P. D.; Waymark, C. P.; Guillies, I.; Kilburn, J. D. *Chem. Soc. Perkin Trans. 1* **2000**, 1021–1031. (c) Van Wageningen, A. M. A.; Liskamp, R. M. J. *Tetrahedron Lett.* **1999**, *40*, 9347–9351. (d) Iorio, E. J.; Still, W. C. *Bioorg. Med. Chem. Lett.* **1999**, *9*, 2145–2150. (e) Ryan, K.; Still, W. C. *Bioorg. Med. Chem. Lett.* **1999**, *9*, 2673–2678. (f) Löwik, D. W. P. M.; Weingarten, M. D.; Broekema, M.; Brouwer, A. J.; Liskamp, R. M. J. *Angew. Chem. Int. Ed. Engl.* **1998**, *37*, 1846–1850. (g) Burger, M. T.; Still, W. C. *J. Org. Chem.* **1997**, *62*, 4785–4790. (h) Löwik, D. W. P. M.; Mulders, S. J. E.; Cheng, Y.; Shao, Y.; Liskamp, R. M. J. *Tetrahedron Lett.* **1996**, *37*, 8253–8256. (i) Pernía, G. J.; Kilburn, J. D.; Essex, J. W.; Mortishire-Smith, R. J.; Rowley, M. *J. Am. Chem. Soc.* **1996**, *118*, 10220–10227. (j) Shao, Y.; Still, W. C. *J. Org. Chem.* **1996**, *61*, 6086–6087. (k) Yoon, S. S.; Still, W. C. *Tetrahedron* **1995**, *51*, 567–578. (l) Zimmerman, S. C. *Top. Curr. Chem.* **1993**, *165*, 71–102.
- (a) Chamorro, C.; Hofman, J.-W.; Liskamp, R. M. J. *Tetrahedron* **2004**, *60*, 8691–8699. (b) Monnee, M. C. F.; Brouwer, A. J.; Liskamp, R. M. J. *QSAR and Combinatorial Science*, **2004**, *23*, in press. (c) Monnee, M. C. F.; Brouwer, A. J.; Verbeek, L. M.; Van Wageningen, A. M. A.; Liskamp, R. M. J. *Bioorg. Med. Chem. Lett.* **2001**, *11*, 1521–1525. (d) Braxmeier, T.; Demarcus, M.; Fessmann, T.; McAteer, S.; Kilburn, J. D. *Chem. Eur. J.* **2001**, *7*, 1889–1898. (e) Botana, E.; Ongerì, S.; Ariezo, R.; Demarcus, M.; Frey, J. G.; Piarulli, U.; Potenza, D.; Kilburn, J. D.; Gennari, C. *Eur. J. Org. Chem.* **2001**, 4625–4634. (f) Fressmann, T.; Kilburn, J. D. *Angew. Chem. Int. Ed.* **1999**, *38*, 1993–1996.
- (a) Houghten, R. A.; Pinilla, C.; Appel, J. R.; Blondelle, S. E.; Dooley, C. T.; Eichler, J.; Nefzi, A.; Ostresh, J. M. *J. Med. Chem.* **1999**, *42*, 3743–3778. (b) Furka, A.; Sebestyen, F.; Asgedom, M.; Dibo, G. *Int. J. Pept., Protein Res.* **1991**, *36*, 487–493. (c) Lam, K. S.; Salmon, S. E.; Hersh, E. M.; Hruby, V. J.; Kazmierski, W. M.; Knapp, R. J. *Nature* **1991**, *354*, 82–84. (d) Houghten, R. A.; Pinilla, C.; Blondelle, S. E.; Appel, J. R.; Dooley, C. T.; Cuervo, J. H. *Nature* **1991**, *354*, 84–86.
- Chamorro, C.; Liskamp, R. M. J. *J. Comb. Chem.* **2003**, *5*, 794–801.
- Colet, A. *Tetrahedron Lett.* **1987**, *43*, 5725–5759.
- Rump, E. T.; Rijkers, D. T. S.; Hilbers, H. W.; de Groot, P. G.; Liskamp, R. M. J. *Chem. Eur. J.* **2002**, *8*, 4613–4621.
- Rothman, J. H.; Still, W. C. *Bioorg. Med. Chem. Lett.* **1997**, *7*, 3159–3164.
- (a) Edman, P.; Begg, G. *Eur. J. Biochem.* **1967**, *1*, 80–91. (b) Edman, P. *Acta Chem. Scand.* **1950**, *4*, 283–293.

9. (a) Malabarba, A.; Nicas, T. I.; Thompson, R. S. *Med. Res. Rev.* **1997**, *17*, 69–137. (b) Reynolds, P. E. *Eur. J. Clin. Microbiol. Infect. Dis.* **1989**, *8*, 943–950.
10. (a) Reynolds, P. E.; Somner, E. A. *Drugs Exp. Clin. Res.* **1990**, *16*, 385–389. (b) Barna, J. C. J.; Williams, D. H. *Annu. Rev. Microbiol.* **1984**, *38*, 339–357.
11. Bugg, T. D. H.; Wright, G. D.; Dutka-Mallen, S.; Arthur, M.; Courvalin, P.; Walsh, C. T. *Biochemistry* **1991**, *30*, 10408–10415.
12. William, D. H.; Bardsley, B. *Angew. Chem. Int. Ed. Engl.* **1999**, *38*, 1172–1193.
13. (a) Jensen, K. B.; Braxmeier, T. M.; Demarcus, M.; Frey, J. G.; Kilburn, J. K. *Chem. Eur. J.* **2002**, *8*, 1300–1309. (b) Anslyn, E. V. *J. Am. Chem. Soc.* **2000**, *122*, 542–543. (c) Dong, D. L.; Ruiping, L.; Sherlock, R.; Wingler, M. H.; Nestler, H. P. *Chem. Biol.* **1999**, *6*, 133–141. (d) Xu, R.; Greiveldinger, G.; Marenus, L. E.; Cooper, A.; Ellman, J. A. *J. Am. Chem. Soc.* **1999**, *121*, 4898–4899. (e) Davies, M.; Bonnat, M.; Guillier, F.; Kilburn, J. D.; Bradley, M. *J. Org. Chem.* **1998**, *63*, 8696–8703. (f) Torneiro, M.; Still, W. C. *Tetrahedron* **1997**, *53*, 8739–8750.
14. Peptidoglycan was isolated from *S. aureus* according to a method described by C. Timmermans, ‘Chemilumescence of human polymorphonuclear leukocytes after stimulation with whole cells and cell wall components of *Staphylococcus epidermidis*’ (from the Thesis entitled: *Staphylococcus epidermidis* infections. C.P. Timmermans. 1991, Chapter 7). Peptidoglycan is labeled afterwards with 1 mg/mL FITC for 1 h and then dialysed against PBS at 4 °C for 24 h. Mattson, E.; Rollof, J.; Verhoef, J.; van Dijk, H.; Fleer, A. *Infect. Immun.* **1994**, *62*, 3837–3843.
15. Castro, B.; Dormoy, J. R.; Evin, G.; Selve, C. *Tetrahedron Lett.* **1975**, *14*, 1219–1222.
16. The Disperse red-NH<sub>2</sub> was obtained by Staudinger reaction of the Disperse red-N<sub>3</sub> derivative.
17. Kaiser, E.; Colescott, R. L.; Bossinger, C. D.; Cook, P. I. *Anal. Biochem.* **1970**, *34*, 595–598.
18. Krchnak, V.; Vagner, J.; Safar, P.; Lebl, M. *Collect. Czech. Chem. Commun.* **1988**, *53*, 2542–2548.
19. Arx, E.; von Faupel, M.; Bruggen, M. *J. Chromatogr.* **1976**, *120*, 224.

# Fluorescent detection of glutamate with a dicopper(II) polyamine cage

Marco Bonizzoni, Luigi Fabbrizzi,\* Giulio Piovani and Angelo Taglietti

*Dipartimento di Chimica Generale, Università di Pavia, via Taramelli 12, I-27100 Pavia, Italy*

Received 2 February 2004; revised 22 June 2004; accepted 26 August 2004

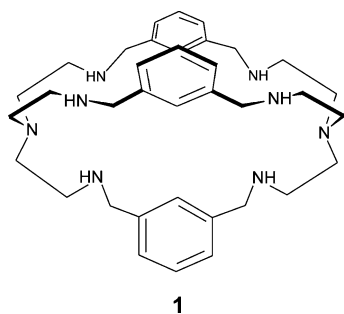
Available online 8 October 2004

**Abstract**—A dicopper(II) octamine cage includes selectively the L-glutamate ion in water at pH 7, establishing  $\text{Cu}^{2+}/\text{-COO}^-$  coordinative interactions. In particular, L-glutamate is able to displace the quenched rhodamine indicator from the cage, whose fluorescence is then fully restored. Other typical neurotransmitters (glycine, GABA) and some related amino acids are discriminated.  
© 2004 Elsevier Ltd. All rights reserved.

## 1. Introduction

There exists a broad interest on the development of methods for the detection of neurotransmitters in biological fluids (intra- and extra-cellular).<sup>1</sup> In this perspective, fluorescent molecular sensors are especially convenient since they allow real time and real space monitoring of the activity of the desired analyte with the use of a fluorescence microscope.<sup>2</sup> We describe here the design of a selective receptor suitable for the fluorescent detection of the L-glutamate ion. L-glutamate is a major excitatory transmitter in the central nervous system,<sup>3</sup> and its selective determination in presence of other neurotransmitters is strongly required by neurophysiologists.<sup>4</sup> Some biosensors based on enzyme immobilisation on an optical fiber have been developed in the past few years.<sup>5</sup> An artificial system based on a  $\text{Cu}^{\text{II}}$ -pyrene-cyclodextrin complex for the fluorescent detection of L-glutamate has been recently reported.<sup>6</sup> Anslyn et al. used a coordinatively unsaturated  $\text{Zn}^{\text{II}}$ -terpy complex for the optical sensing of L-glutamate and L-aspartate in a 1:1 water/methanol mixture.<sup>7</sup>

In the way of the rational design of a fluorescent sensor for L-glutamate in pure water, we considered that, at a physiological pH, L-glutamate exists as an anion of charge  $-1$  (two carboxylate groups plus one ammonium group). Synthetic receptors for anions are expected to provide a cavity of suitable shape and size, containing positively charged groups (e.g., ammonium, guanidinium, or pyridinium groups).<sup>8</sup> However, the electrostatic interactions which are established between the receptor and the substrate are rarely strong enough to compensate the endothermic dehydration terms, and recognition studies are often restricted to non-aqueous media (e.g., MeCN, DMSO). On the other hand, metal-ligand interactions are usually more intense and allow the occurrence of selective interactions with anions displaying coordinating tendencies in pure water. In this sense, cyclic and polycyclic amines containing transition metal centers may act as effective receptors for a variety of anions.<sup>9</sup> In particular, we have shown that the dicopper(II) complex of the bis-tren cage **1** is able to include ambidentate anions like  $\text{N}_3^-$  and  $\text{NCO}^-$ , which are recognized on the basis of their bite (i.e., the distance between terminal donor atoms).<sup>10</sup> Thus, we considered the opportunity to use as a receptor of the L-glutamate ion a dimetallic complex with a bis-tren cage displaying a cavity of suitable size for selective inclusion and recognition.



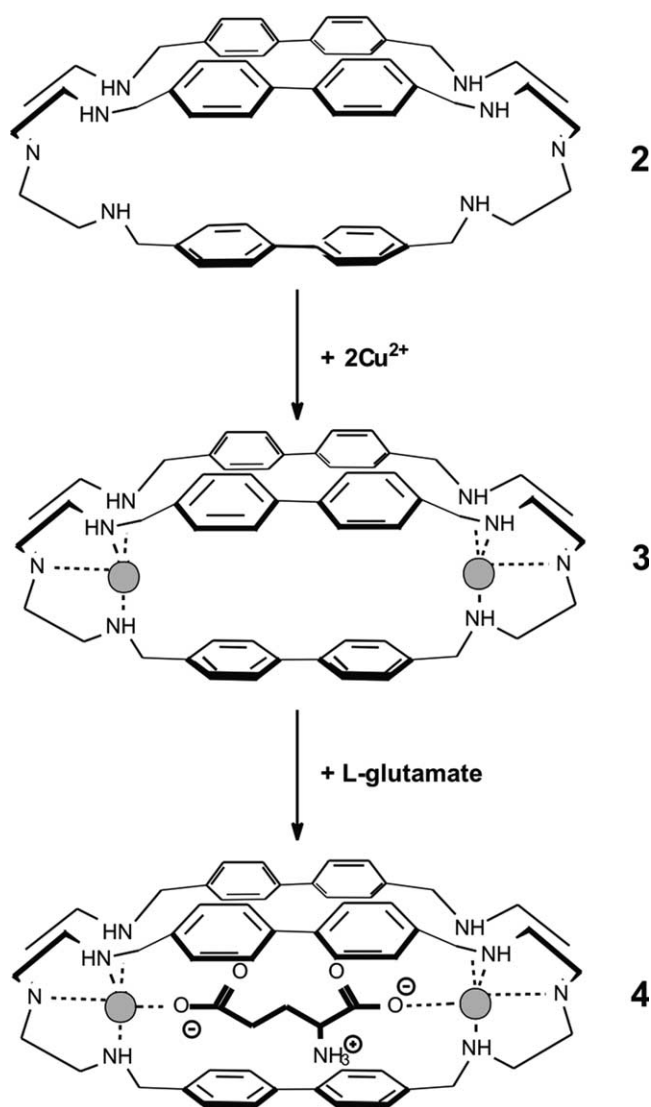
## 2. Results and discussion

On designing a dimetallic receptor for L-glutamate, we considered that the  $\text{-COO}^-$  group shows a good affinity for the  $\text{Cu}^{\text{II}}$  ion. Thus, we placed two copper(II) ions inside the octamine cage **2** (see Scheme 1), in which two tripodal tetramine subunits (tren) are linked by diphenyl spacers. Each tren compartment is expected to coordinate a metal center according to a trigonal bipyramidal geometry, in

**Keywords:** Glutamate; Copper cryptates; Fluorescent probes; Molecular recognition; Sensors.

\* Corresponding author. Tel.: +39 382 507 325; fax: +39 382 528 544; e-mail: [luigi.fabbrizzi@unipv.it](mailto:luigi.fabbrizzi@unipv.it)





**Scheme 1.** Cascade mechanism for the consecutive inclusion of two Cu<sup>II</sup> ions and a dicarboxylate ion (e.g., glutamate) within a bis-tren cage with diphenyl spacers.

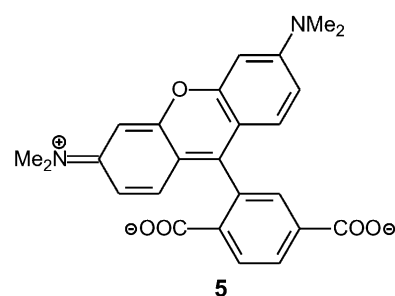
which one of the two axial positions is left available for the interaction with a further ligand (a solvent molecule, an anionic group). We guessed that a glutamate anion could place two oxygen atoms of the two carboxylate groups in the two available coordination sites, allowing inclusion within the octamine cage, according to the cascade mechanism illustrated in Scheme 1.

In order to sense glutamate inclusion and recognition, we chose the ‘chemosensing ensemble’ paradigm.<sup>11</sup> According to this approach, the receptor must include first a fluorescent indicator, whose emission is quenched due to the interaction of its excited state with the receptor. Then, the desired substrate is added, which displaces the indicator from the cavity. When released to the solution, the indicator displays its full fluorescence, thus signalling the recognition of the substrate.

As a fluorescent indicator, we chose 6-carboxy-tetramethyl-rhodamine, **5**, which, when excited at 528 nm (isosbestic point), emits at 571 nm (orange fluorescence). Compound **5**

contains two carboxylate groups, which can bridge the two Cu<sup>II</sup> centers of the dimetallic cage complex **3**. In order to verify the inclusion of **5** by **3**, an aqueous solution  $2.5 \times 10^{-7}$  M in the fluorescent indicator and buffered to pH 7 with HEPES was titrated with a standard solution of the dimetallic complex **3**. Addition of **3** made the fluorescence intensity of **5** decrease, until complete quenching. Least-squares non-linear fitting of the titration profile indicated the formation of a 1:1 adduct between the dimetallic cage **3** and the indicator **5**, whose association constant  $\log K_1$  is  $7.0 \pm 0.2$ . It is suggested that the carboxylate bound Cu<sup>II</sup> centers quench the indicator through either an electron transfer or an electronic energy transfer process.

Thus, we prepared the chemosensing ensemble solution, which contained the cage complex **3** ( $2.5 \times 10^{-6}$  M) and the indicator **5** ( $2.5 \times 10^{-7}$  M), whose fluorescence was completely quenched. Then, the solution, adjusted to pH 7 with HEPES, was titrated with a solution of L-glutamic acid. On titration, 6-carboxy-tetramethyl-rhodamine fluorescence was progressively restored. Figure 1 reports the family of emission spectra obtained in the course of the titration.



On non-linear least-squares treatment of the titration profile (inset of Fig. 1: fluorescence intensity,  $I_F$  vs molar concentration of L-glutamate),<sup>12</sup> using a reported algorithm,<sup>13</sup> a value of  $\log K_{\text{ass}} = 6.9 \pm 0.2$  (apparent association constant, at pH 7) was obtained for the adduct-formation equilibrium: **3** + glutamate  $\rightleftharpoons$  adduct. It is hypothesized that, in the adduct, the glutamate zwitterion is included within the cage and bridges the two Cu<sup>II</sup> centers with two negatively charged oxygen atoms of its carboxylate groups. Metal coordination of both  $-\text{COO}^-$  groups is corroborated by the behavior of the homologous, amine-free, glutarate ion:  $-\text{OOC}-(\text{CH}_2)_3-\text{COO}^-$ . In particular, the equilibrium: **3** + glutarate  $\rightleftharpoons$  adduct, studied through the described spectrofluorimetric procedure, is characterized by the same value of  $\log K_{\text{ass}}$  ( $7.0 \pm 0.2$ ), within the experimental uncertainty.

Notice that, on titration of the chemosensing ensemble solution with D-glutamic acid, the same spectrophotometric pattern and the same titration profile were obtained. This is the expected behavior in view of the achiral nature of the cage.

Then, chemosensing ensemble solution was titrated with a variety of neurotransmitters, which included glycine and  $\gamma$ -aminobutanoate, and with some related amino acids: L-alanine, L-aspartate;  $\delta$ -aminopentanoate. Corresponding titration profiles are reported in Figure 2 and compared to that obtained for L-glutamate. In particular, a distinct

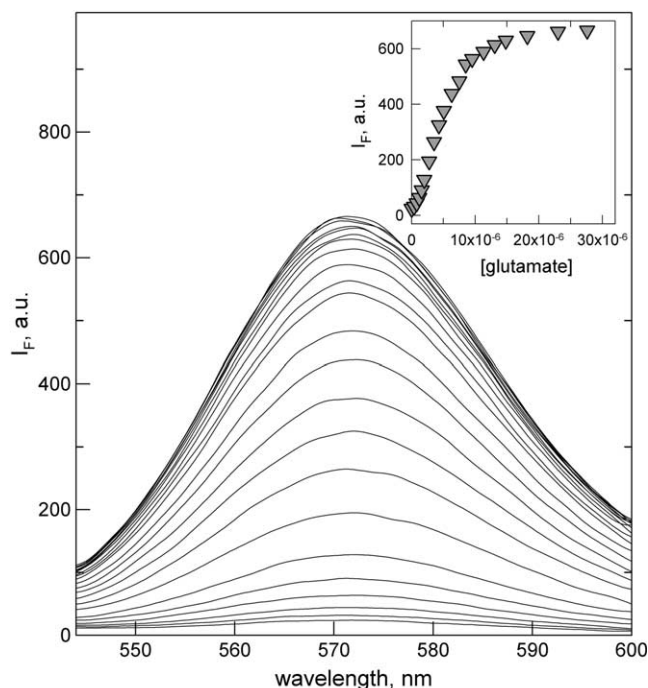


**Figure 1.** Emission spectra obtained during the titration with L-glutamic acid of a solution containing the cage complex **3** ( $2.5 \times 10^{-6}$  M) and the indicator **5** ( $2.5 \times 10^{-7}$  M). Inset: titration profile (fluorescence intensity,  $I_F$  vs molar concentration of glutamic acid).

selectivity in favor of L-glutamate is observed. Such a selectivity is ascribed to the fact that L-glutamate, like glutarate, has the right ‘length’ for positioning its donor oxygen atoms in each one of the positions required by the two  $\text{Cu}^{\text{II}}$  ions (the axial sites of a trigonal bipyramid), without inducing any endothermic rearrangement of the cage. The best competitor is L-aspartate, which, like L-glutamate, possesses two carboxylate groups for bridging the two  $\text{Cu}^{\text{II}}$  ions, but is too ‘short’ to encompass the intermetallic distance of the relaxed receptor. The two  $\gamma$ -aminobutanoic and  $\delta$ -aminopentanoic acids possess only one carboxylate group for  $\text{Cu}^{\text{II}}$  binding. Thus, coordination of the second metal ion, at pH 7, could occur with the primary amine group, but this process involves the endothermic deprotonation of the ammonium group of the zwitterion, which drastically reduces the affinity for the receptor. On the other hand, the relatively good affinity of glycine for **3** has to be ascribed to the fact that two molecules of the amino acid are included by the dimetallic cage, with the formation of two regular  $\text{Cu}^{\text{II}}$ -carboxylate coordinative bonds ( $\beta_2 = 7.7 \pm 0.2$ ).

In conclusion, it has been shown that the dicopper(II) cage complex **3** is a selective receptor for glutamate, even if it is not able to perform enantioselective recognition. Selectivity derives from the fact that glutamate possesses two negatively charged groups (i) which display a good affinity towards the two coordinatively unsaturated  $\text{Cu}^{\text{II}}$  centers and (ii) whose distance encompasses quite well the metal–metal distance within the cage. Such requirements are not met by other neurotransmitters and related amino acids, which possess only one carboxylate group or do not have the right length to match the  $\text{Cu}^{\text{II}}$ – $\text{Cu}^{\text{II}}$  distance. The use of a fluorescent indicator displaying coordinative affinity for the

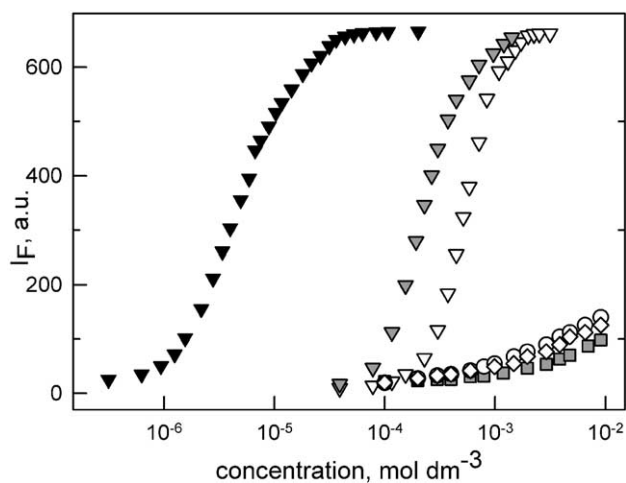


**Figure 2.** Fluorescence intensity,  $I_F$ , of the emission band of the rhodamine indicator ( $\lambda_{\text{max}} = 571$  nm), measured during the titration of an aqueous solution of the chemosensing ensemble (**3**,  $2.5 \times 10^{-6}$  M; **5**,  $2.5 \times 10^{-7}$  M; pH 7) with standard solutions of neurotransmitters and related amino acids. Black triangles: L-glutamate; grey triangles: L-aspartate; white triangles: L-glycine; circles:  $\delta$ -aminopentanoate; squares: L-alanine; diamonds:  $\gamma$ -aminobutanoate.

receptor (e.g., 6-carboxy-tetramethyl-rhodamine) comparable to that of the analyte provides a convenient sensing procedure (OFF–ON switching of fluorescence).

### 3. Experimental

#### 3.1. Data for compounds

The octamine cage **2** was prepared through a modification of a described procedure.<sup>14</sup> The dicopper(II) complex of **2** was prepared by dissolving 0.32 g (1.33 mmol) of  $\text{Cu}(\text{NO}_3)_2 \cdot 3\text{H}_2\text{O}$  in MeOH and adding this solution to a MeOH solution of 0.50 g (0.6 mmol) of **2**. The resulting solution was heated to reflux, and after a few minutes a complex salt of formula  $[\text{Cu}^{\text{II}}_2(\text{2})](\text{NO}_3)_4 \cdot 3\text{H}_2\text{O}$  (**3**) precipitated as a bright blue powder, which was collected by vacuum filtration. Yield: 75% (found: C, 51.57%; H, 5.82%; N, 13.42%, calcd for  $\text{C}_{54}\text{H}_{72}\text{Cu}_2\text{N}_{12}\text{O}_{15}$ : C, 51.63%; H, 5.78%; N, 13.38%).

Determination of apparent association constants between  $[\text{Cu}^{\text{II}}_2(\text{2})](\text{NO}_3)_4 \cdot 3\text{H}_2\text{O}$  and the indicator **5** was carried out in a degassed water solution buffered at pH 7 with HEPES 0.05 M; concentration of the indicator was  $2.5 \times 10^{-7}$  M. Aliquots of a fresh standard solution of  $\text{Cu}(\text{NO}_3)_2 \cdot 3\text{H}_2\text{O}$  were added, and emission spectra of the indicator were recorded ( $\lambda_{\text{em}} = 528$  nm, isosbestic point;  $\lambda_{\text{em}} = 571$  nm). The chemosensing ensemble solution for competition assays was prepared by adding  $\text{Cu}(\text{NO}_3)_2 \cdot 3\text{H}_2\text{O}$  to an aqueous solution, buffered at pH 7 with HEPES 0.05 M, containing the indicator **5**. The concentration of  $[\text{Cu}^{\text{II}}_2(\text{2})]^{4+}$  in the chemosensing ensemble solution was  $2.5 \times 10^{-6}$  M. The chemosensing ensemble solutions were titrated with standard solutions of amino acids. All spectrofluorimetric titration curves were fitted with the HYPERQUAD program,<sup>12</sup> to evaluate the apparent association constant between receptor and indicator, and between receptor and amino acids.

### Acknowledgements

The financial support of the European Union (RTN Contract HPRN-CT-2000-00029) and the Italian Ministry of University and Research (PRIN—Dispositivi Supramolecolari; FIRB—Project RBNE019H9K) is gratefully acknowledged.

### References and notes

1. Jane, D. E. In *Medicinal Chemistry into the Millennium*; Campbell, M. M., Blagbrough, I. S., Eds.; Royal Society of Chemistry: Cambridge, 2001; pp 67–84.
2. Czarnik, A. W. *Chem. Biol.* **1995**, *2*, 423.
3. Skerry, T. M.; Genever, P. G. *Trends Pharmacol. Sci.* **2001**, *22*, 174. Watkins, J. C. *Biochem. Soc. Trans.* **2000**, *28*, 297. Dingleline, R.; Borges, K.; Bowie, D.; Traynelis, S. F. *Pharmacol. Rev.* **1999**, *51*, 7.
4. Fletcher, E. J.; Loge, D. In *An Introduction to Neurotransmitters in Health and Disease*; Riederer, P., Kopp, N., Pearson, J., Eds.; Oxford University Press: New York, 1990; Chapter 7.
5. Issberner, J. P.; Schauer, C. L.; Trimmer, B. A.; Walt, D. R. *J. Neurosci. Methods* **2002**, *120*, 1–10. Bang, L.; Tan, W. *Anal. Chim. Acta* **1999**, *401*, 91–94. Cordek, J.; Wang, X.; Tan, W. *Anal. Chem.* **1999**, *71*, 1529–1533.
6. Santra, S.; Zhang, P.; Tan, W. *Chem. Commun.* **1999**, 1301–1302.
7. Ait-Haddou, H.; Wiskur, S. L.; Lynch, V. M.; Anslyn, E. V. *J. Am. Chem. Soc.* **2001**, *123*, 11296–11297.
8. (a) Bianchi, A.; Bowman-James, K.; García-España, E. *Supramolecular Chemistry of Anions*; Wiley-VCH: New York, 1997. (b) Schmidtchen, F. P.; Berger, M. **1997**, *Chem. Rev.* *97*, 1609. (c) Fabbrizzi, L.; Licchelli, M.; Rabaioli, G.; Taglietti, A. **2000**, *Coord. Chem. Rev.* *205*, 85. (d) Beer, P. D.; Gale, P. A. **2001**, *Angew. Chem., Int. Ed.* *40*, 487.
9. (a) Fabbrizzi, L.; Marcotte, N.; Stomeo, F.; Taglietti, A. *Angew. Chem., Int. Ed.* **2002**, *41*, 3811–3814. (b) Hortala, M. A.; Fabbrizzi, L.; Marcotte, N.; Stomeo, F.; Taglietti, A. *J. Am. Chem. Soc.* **2003**, *125*, 20–21. (c) Marcotte, N.; Taglietti, A. *Supramol. Chem.* **2003**, *15*, 617. (d) Amendola, V.; Bastianello, E.; Fabbrizzi, L.; Mangano, C.; Pallavicini, P.; Perotti, A.; Manotti Lanfredi, A.; Ugozzoli, F. *Angew. Chem., Int. Ed. Engl.* **2000**, *39*, 2917.
10. Fabbrizzi, L.; Leone, A.; Taglietti, A. *Angew. Chem., Int. Ed.* **2001**, *40*, 3066.
11. (a) Wiskur, S. L.; Ait-Haddou, H.; Lavigne, J. J.; Anslyn, E. V. *Acc. Chem. Res.* **2001**, *34*, 963. (b) Fabbrizzi, L.; Licchelli, M.; Taglietti, A. *Dalton Trans.* **2003**, 3471.
12. The Hyperquad<sup>®</sup> package was used: Gans, P.; Sabatini, A.; Vacca, A. *Talanta* **1996**, *43*, 1739.
13. Connors, K. A. *Binding Constants, the Measurements of Molecular Complex Stability*; Wiley: New York, 1987.
14. Baldes, R.; Schneider, H.-J. *Angew. Chem., Int. Ed. Engl.* **1995**, *34*, 321.

# Materials chemistry approach to anion-sensor design

Pavel Anzenbacher, Jr.,<sup>a,\*</sup> Karolina Jursikova,<sup>a</sup> Dmitry Aldakov,<sup>a</sup> Manuel Marquez<sup>b,c</sup>  
and Radek Pohl<sup>a,d</sup>

<sup>a</sup>Center for Photochemical Sciences, Bowling Green State University, Bowling Green, OH 43403, USA

<sup>b</sup>Los Alamos National Laboratory, Chemistry Division, Los Alamos, NM 87545, USA

<sup>c</sup>Kraft Foods, Inc., R&D, The Nanotechnology Lab, 801 Waukegan Road, Glenview, IL 60025, USA

<sup>d</sup>Institute of Organic Chemistry and Biochemistry, Academy of Sciences of the Czech Republic, Flemingovo nam. 2,  
166 10 Prague, Czech Republic

Received 8 February 2004; revised 26 June 2004; accepted 19 August 2004

Available online 28 September 2004

**Abstract**—A new approach to sensing of aqueous phosphate-related anions based on chromogenic conductive polymers is demonstrated. The anion-sensor affinity can be adjusted by externally applied voltage. Introduction of p-doping to the polymers results in augmented anion sensitivity, which is ascribed to the effect of synergy between low-level p-doping in a polythiophene polymer and hydrogen bonding. The chromogenic conductive polymer films display anion-specific changes in color, conductivity, and mass upon increasing concentration of anions.

© 2004 Elsevier Ltd. All rights reserved.

## 1. Introduction

The design of reliable optical sensors for inorganic anions remains a challenge even after more than a decade of efforts, and reliable and selective sensors that can potentially be applied in real-life applications are still relatively rare.<sup>1</sup> Very few optical sensors exist that display high selectivity and reliability, and function in aqueous media without interference from endogenous substrates. This is because, compared to isoelectric cations, anions often display high energy of hydration, tautomerism, and possess low surface-charge density, features that make the binding of anions less effective.<sup>2</sup> In order for a sensor to be able to compete for an anion in the presence of water, the corresponding receptors must display high substrate selectivity and affinity. The increase in the receptor–anion affinity may be achieved by incorporating a positive charge in the receptor moieties. Unfortunately, electrostatic interactions are nondirectional and, as a result, all anions present in the medium are attracted to the receptor. It is, therefore, desirable to include weak directional interactions such as hydrogen bonding to improve the selectivity in receptor–anion association.<sup>2b,3</sup> The synthesis of receptors that comprise both positive charges and hydrogen bond donors acting in a synergistic

manner is, by no means, a trivial task, and the few sensors of this type, despite their elegant design and structures, are difficult to synthesize and their practical use is limited.<sup>1</sup> This is because the focus on the supramolecular chemistry of receptors usually results in a high cost of synthesis, decrease in chemical stability, and a potential loss of the real-time response due to slow dissociation of the substrate–receptor complex.

The materials chemistry approach to the anion-sensor design offers numerous advantages over the classical supramolecular chemistry approaches, namely due to its focus on the collective properties of materials that allow harnessing the potential of materials for self-assembly, self-organization, self-replication, and inter-component communication. Additionally, the materials bulk properties offer support and spatial definition to the material components (e.g., preventing undesired receptor self-association). In terms of the optical sensor development, the above features are particularly useful in signal transduction because the changes in conformation<sup>4</sup> and inter-strand/component association<sup>5</sup> generate the optical output signal.

In the design of our sensor material, we decided to take the material concept even further. We reasoned that the sensor material could serve both as a receptor and signal transducer at the same time. Perhaps, a conductive polymer with incorporated receptors capable of hydrogen bonding, while being able to be injected with positive charge (undergo an

**Keywords:** Anion; Sensor; Receptor; Conductive polymer; Chromogenic material.

\* Corresponding author. Tel.: +1-4193722080; fax: +1-4193729809;  
e-mail: [pavel@bgnet.bgsu.edu](mailto:pavel@bgnet.bgsu.edu)

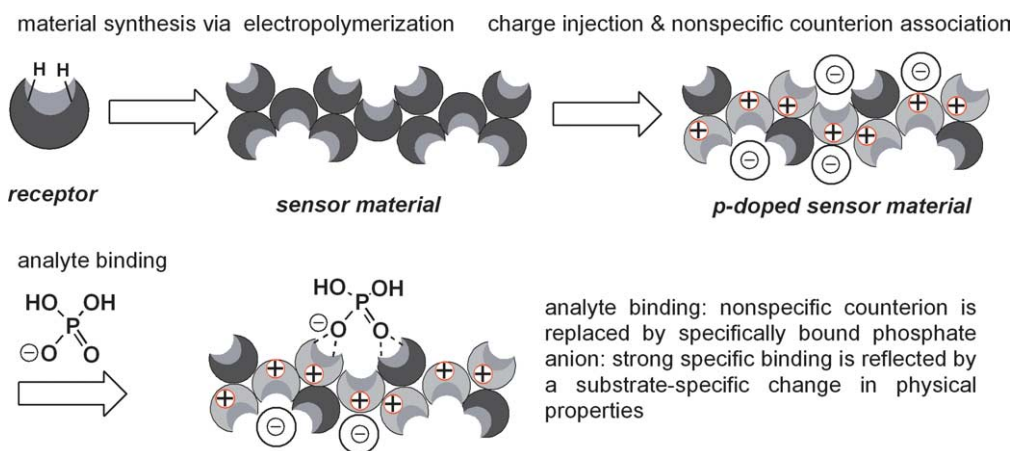


**Figure 1.** Schematic representation of the synergy between hydrogen-bonding and coulombic attraction in anion sensor materials based on a p-doped conductive polymer.

adjustable degree of p-doping), could provide an inexpensive alternative to the complex multi-feature sensors carrying a positive charge as well as hydrogen-bond donors (Fig. 1).

## 2. Results and discussion

In order to utilize the synergy between hydrogen bonding and coulombic interaction, we designed a conductive polymer that combines both properties: the monomers are hydrogen-bond donors and can bind anions, and the resulting polymer can be p-doped, thus possessing a positively charged backbone, which aids in anion binding. We decided to utilize the propensity of thiophenes<sup>6</sup> and quinoxalines<sup>7</sup> to yield conductive polymers. Additionally, quinoxaline modified with two pyrrole units (DPQ) is capable of binding anions via hydrogen bonding while more or less pronounced color change occurs.<sup>8</sup> Because DPQ alone does not polymerize to yield a stable conductive polymer, we modified it with two polymerizable ethylenedioxythiophene (EDOT)<sup>9</sup> units to obtain monomer **1**. Monomer **1** was polymerized to yield poly-**1**, a sensor material used in this study (see Fig. 2). In order to ensure that the pyrrole moieties of DPQ are not involved in the

polymerization process, we also synthesized monomer **1C** and poly-**1C** with chloro-substituents blocking the pyrrole alpha-positions.

The synthesis of monomers **1** and **1C** is shown in Figure 3. Treatment of 3,6-dibromo-1,2-benzenediamine (**2**)<sup>10</sup> with 1,2-di(pyrrole-2-yl)ethane-1,2-dione (**3**)<sup>8a</sup> in acetic acid yielded 5,8-dibromo-2,3-di(1*H*-2-pyrrolyl)quinoxaline (**4**). Compound **4** was then coupled with (2,3-dihydrothieno[3,4-*b*][1,4]dioxin-5-yl)tributylstannane (**6**)<sup>11</sup> to give monomer **1**. Monomer **1C** was prepared by treatment of **4** with sulfonyl chloride according to literature,<sup>12</sup> providing dichloro-dibromo intermediate **5**. The intermediate **5** was coupled with **6** using the same procedure for monomer **1**.

We have tested the monomers **1**<sup>13</sup> and **1C** affinity for anions in DMSO with various aqueous anions.<sup>14</sup> Monomer **1** and, even more so, **1C** show changes in color upon binding of pyrophosphate<sup>2-</sup> (PP), fluoride, and, to a lesser extent, dihydrogenphosphate, and cyanide anions. Analysis of anion-induced changes in the absorption spectra of **1** and **1C** allowed for determination of the respective binding constants that were found to be in the order of  $10^6 \text{ M}^{-1}$  for fluoride and pyrophosphate and less than  $10^2 \text{ M}^{-1}$  for chloride and sulfate. In the case of phosphate anion, the

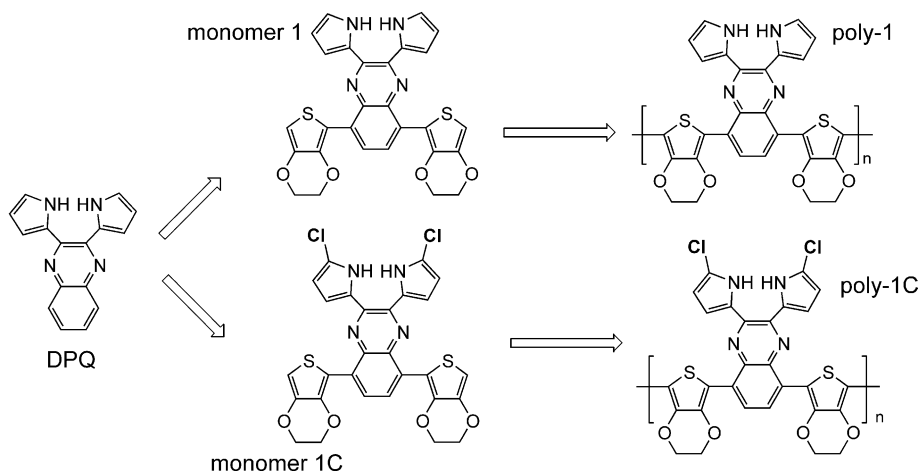


**Figure 2.** Schematic representation of the design of sensor materials poly-**1** and poly-**1C**.



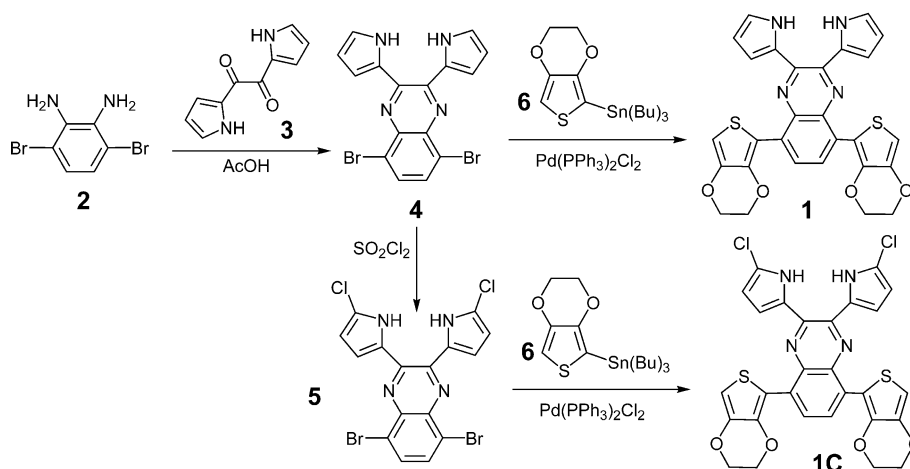


Figure 3. Synthetic sequence used to synthesize monomer receptor precursors **1** and **1C**.

binding constants calculated for **1** and **1C** were significantly different ( $< 10^2$  vs.  $10^6$ , respectively). Such an increase in the affinity for dihydrogenphosphate in receptors comprising halogenated pyrroles such as DPQ was previously described.<sup>15</sup>

Encouraged by the anion binding properties of **1** and **1C**, we decided to subject the monomers to oxidative electropolymerization to form a film of conductive poly-**1** or poly-**1C** deposited on an ITO-modified transparent electrode.<sup>14</sup> Poly-**1** or poly-**1C** were deposited as green-colored polymers on the ITO surface (Fig. 4). This poly-**1** or poly-**1C** modified transparent working electrode was rinsed and immersed in the spectroelectrochemistry cell equipped with a stirrer, a miniature Ag/Ag<sup>+</sup> reference electrode, and platinum wire auxiliary electrode. DMSO solution containing 0.1 M tetrabutylammonium perchlorate (TBAP) was used as a supporting electrolyte. Spectroelectrochemical analysis of the poly-**1** and poly-**1C** films allowed for investigation of the polymer electronic structure and determination of the polymer band gaps (Fig. 4). The band gaps for poly-**1** and poly-**1C** were determined as the onset of  $\pi$ - $\pi^*$  absorption peaks and were found to be 1.39 and 1.36 eV, respectively.

In order to test the anion sensing ability of the polymers, poly-**1** and poly-**1C** films were titrated at a constant potential of 0.0 V by anions added as tetrabutylammonium (TBA) salts (5.0 mM, pH  $\approx$  6.5) in water while vis-NIR spectra were recorded. As expected, the addition of fluoride, pyrophosphate, and, in the case of poly-**1C**, also phosphate anions into the cell containing the sensor films resulted in gradual changes in the absorption spectra (Fig. 5). The respective binding isotherms that show well-defined saturation were obtained, and apparent affinity constants were calculated.<sup>16</sup> The low-level p-doping (at 0.70 V) and a corresponding positive charge in the polymer resulted in a dramatic increase of the anion affinity. For example, the apparent affinity constant ( $\text{dm}^3/\text{mol}$ ) for poly-**1** and pyrophosphate recorded at 0.70 V was calculated as  $K_{\text{PP}}(0.7\text{ V}) = 260,000\text{ M}^{-1}$ , while the constant recorded at 0.00 V was  $K_{\text{PP}}(0.0\text{ V}) = 61,100\text{ M}^{-1}$ . The examples of such vis-NIR spectroscopic titrations are shown in Figure 5. The top panel shows poly-**1** titrated by aqueous pyrophosphate at 0.00 V ( $K_{\text{PP}} = 61,100\text{ M}^{-1}$ ) (Fig. 5A), the center panel shows poly-**1** titrated by aqueous pyrophosphate at 0.70 V ( $K_{\text{PP}} = 260,100\text{ M}^{-1}$ ) (Fig. 5B). The lower panel (Fig. 5C) shows the result of a control experiment, where poly-**1** was titrated by aqueous chloride. It is known that the

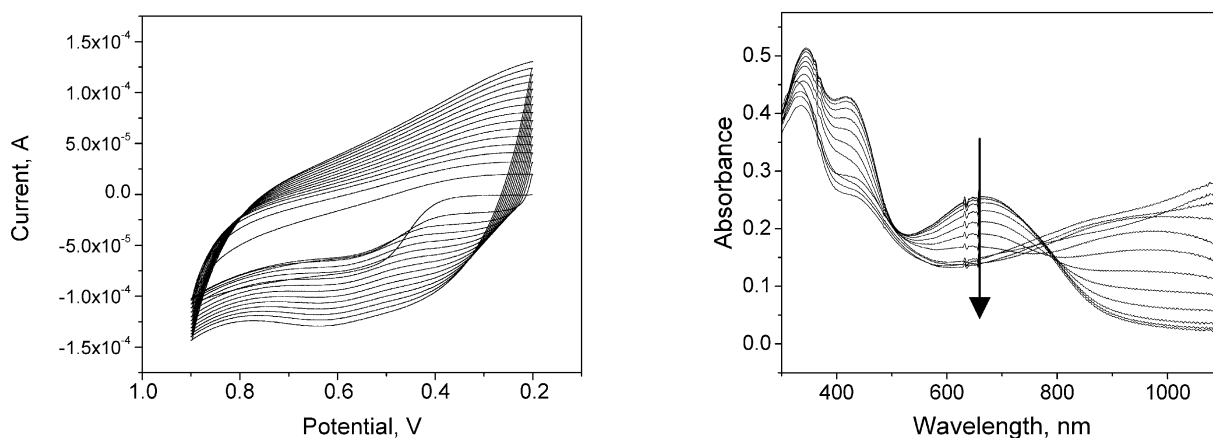
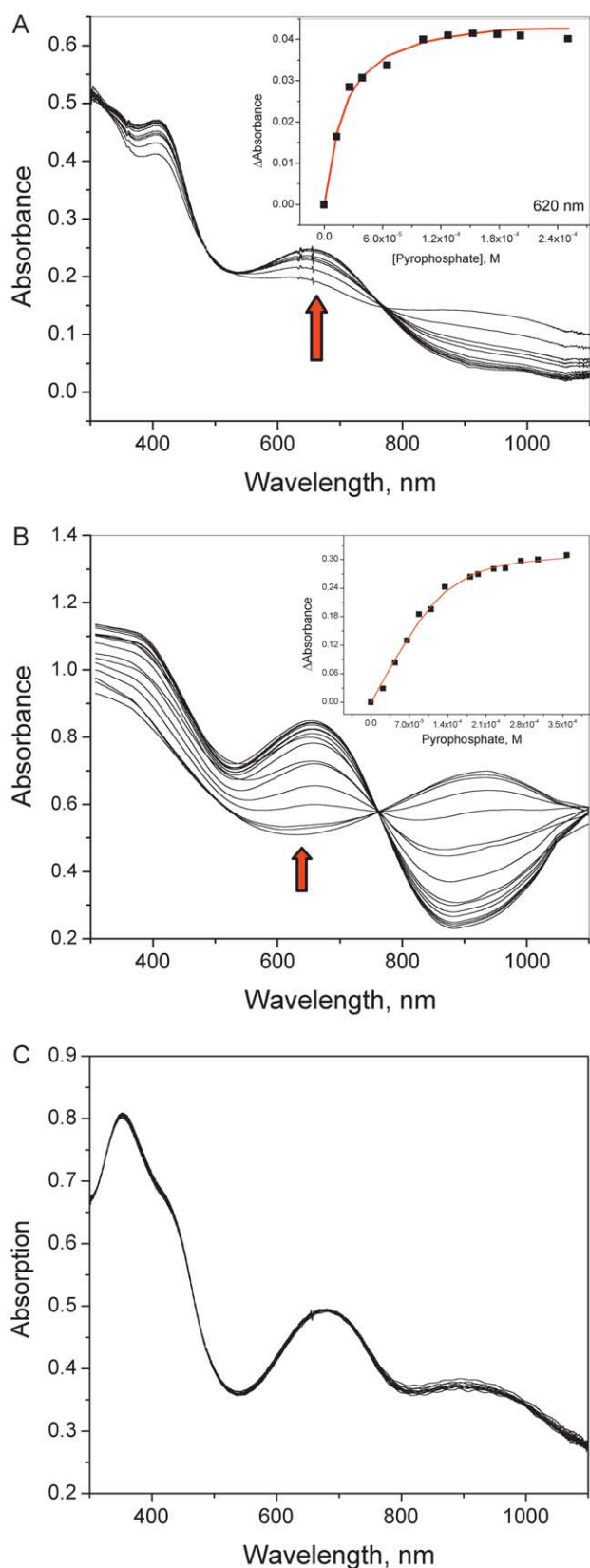


Figure 4. Left panel: Electrochemical polymerization of **1** in 0.1 M TBAP in ACN at 100 mV/s with Ag/Ag<sup>+</sup> used as a reference; Right panel: Optoelectrochemical analysis of poly-**1** at applied potentials (shown) varying with an increment of 0.1 V in ACN.



**Figure 5.** Panel A: Changes in vis-NIR spectra of poly-1 during titration with aqueous pyrophosphate (pH  $\sim$  6.0) at 0.00 V; Panel B: Titration of poly-1 by aqueous pyrophosphate at 0.70 V; Panel C: Titration of poly-1 by aqueous chloride at 0.70 V does not induce observable changes in vis-NIR spectra.

DPQ receptors do not bind chloride,<sup>8</sup> and, therefore, we were not surprised that poly-1 does not bind or respond to chloride regardless of the applied voltage (0.00–0.70 V). Poly-1C displays generally similar anion binding properties; however, stronger binding and higher affinity constants compared to poly-1 are observed, which is not unexpected given higher acidity of NH-bonds of the chlorinated pyrrole.

Additionally, to confirm that the changes in vis-NIR spectra are due to the anion binding to poly-1 and poly-1C, we used the electrochemical quartz crystal microbalance method (EQCM).<sup>17</sup> After the deposition of poly-1 on the EQCM probe, aqueous solutions of the anions were added. The addition of anions (pyrophosphate<sup>2-</sup>, fluoride, dihydrogenphosphate, but not chloride) caused a rapid increase in the mass of the deposited polymer. EQCM titration experiments resulted in a typical saturation profile, thus confirming that the changes in vis-NIR spectra are, indeed, a result of anion binding. In addition, EQCM provides an indispensable tool for the number of control experiments. The role of water in the anion sensing studies utilizing hydrogen bonding is generally considered to be a disruptive factor as it competes for the coordination with anionic analytes.<sup>18</sup> However, our control experiments show that the addition of water does change neither the mass of the deposited polymer nor its vis-NIR spectrum. Conversely, the addition of aqueous anion solutions leads to significant increase in sensor mass as well as anion-induced change in vis-NIR spectra. From these observations we conclude that the presence of water does not significantly affect the binding. We ascribe this to the effective synergy between the strong coulombic attraction and the hydrogen bonding. EQCM titrations offer a great potential for the quantitative characterization of anion binding process by monitoring the mass accumulation, and the corresponding studies are currently underway.

In summary, the electropolymerized anion receptors yielded uniform transparent thin films of conductive polymers potentially useful for optical sensing of aqueous phosphate-type anions. We demonstrated that the anion-sensor affinity may be adjusted by external voltage. We believe that this increase in anion-sensor affinity is a direct result of synergy between low-level p-doping in a polythiophene polymer and receptor–anion hydrogen bonding. The chromogenic conductive polymers poly-1 and poly-1C show anion-specific changes both in color and conductivity upon increasing concentration of anions, namely fluoride, pyrophosphate and, to a lesser extent, also dihydrogenphosphate.

### 3. Experimental

#### 3.1. General

<sup>1</sup>H and <sup>13</sup>C NMR spectra were recorded using a Varian Unity 400 (400 MHz) spectrometer. The chemical shifts ( $\delta$ , ppm) are referenced to a solvent. EI-DIP mass spectra were recorded using a Shimadzu QP5050A spectrometer. Absorption spectra were recorded using a Hitachi U-3010 and Hewlett Packard 8453 spectrophotometers. Optically dilute solutions used for all photophysical experiments were prepared in spectroscopic grade solvents.

Electrochemical measurements were performed in DMSO solutions containing 0.1 M recrystallized tetrabutylammonium perchlorate (TBAP) as a supporting electrolyte. TBAP was recrystallized from absolute ethanol. A BioAnalytical Systems Epsilon controller was used to perform the electropolymerization reaction and the electrochemistry experiments. A platinum wire auxiliary electrode and Ag/Ag<sup>+</sup> nonaqueous reference electrode were used for all measurements. A scan rate of 100 mV/s was typically employed. Under these experimental conditions the ferrocene/ferrocenium couple was determined to be +0.124 V versus Ag/Ag<sup>+</sup>.

Anion titrations were carried out in DMSO solutions (0.1 M tetrabutylammonium perchlorate) of the monomer by adding the aqueous solutions of the following anions as tetrabutylammonium salts 5.5 mM (for chloride sensing attempts 180 mM solution was used). Data fitting was performed using a quadratic equation for 1:1 binding model. Spectroelectrochemical measurements were carried out in a custom-built sealed stirred cell using indium–tin-oxide (ITO) coated glass slide (50×7×0.9 mm<sup>3</sup>,  $R_s \leq 100 \Omega$ ) as a working electrode. Electrochemical quartz crystal microbalance (EQCM) experiments were carried out on CHI-430 electrochemical workstation equipped with time-resolved EQCM from CH Instruments with AT-cut polished bound 100 A Cr+1000A gold-coated quartz crystals.

**3.1.1. 5,8-Dibromo-2,3-di(1*H*-2-pyrrolyl)quinoxaline (4).** 3,6-Dibromo-1,2-benzenediamine (326 mg, 1.0 mmol) and 1,2-di(1*H*-2-pyrrolyl)ethane-1,2-dione (188 mg, 1.0 mmol) were dissolved in glacial acetic acid (50 ml), and heated to reflux for 24 h shielded from ambient light. The volume of the reaction mixture was reduced to 10% in vacuum, dissolved in chloroform–methanol (9:1, 300 ml), washed with 1 M NaOH, brine, and dried over anhydrous Na<sub>2</sub>SO<sub>4</sub>. The residue after evaporation was subjected to column chromatography on silica gel using hexane–dichloromethane mixture (1:3, v/v). The product was obtained as yellow powder (210 mg, 50% yield). Mp 229–230 °C. <sup>1</sup>H NMR (DMSO-*d*<sub>6</sub>,  $\delta$ ): 6.19 (ddd, 2H,  $J=2.5, 3.7, 4.7$  Hz), 6.41 (ddd, 2H,  $J=1.5, 2.5, 3.7$  Hz), 7.09 (ddd, 2H,  $J=1.5, 2.5, 4.1$  Hz), 7.92 (s, 2H), 11.39 (br s, 2H). <sup>13</sup>C APT NMR (DMSO-*d*<sub>6</sub>,  $\delta$ ): 109.38 CH, 113.08 CH, 121.96 C, 122.98 CH, 127.75 C, 132.32 CH, 137.58 C, 145.79 C. EI/MS (70 eV): 418 (100) [M<sup>+</sup>], 336 (15), 256 (25). Anal. Calcd (%) for C<sub>16</sub>H<sub>10</sub>Br<sub>2</sub>N<sub>2</sub> (418.09): C, 45.96; H, 2.41; N, 13.40. Found: C, 45.86; H, 2.41; N, 13.22.

**3.1.2. 5,8-Dibromo-2,3-di(5-chloro-1*H*-2-pyrrolyl)quinoxaline (5).** 5,8-Dibromo-2,3-di(1*H*-2-pyrrolyl)quinoxaline (4) (100 mg, 0.239 mmol) was dissolved in chloroform (50 mL) and cooled down to 0 °C. SO<sub>2</sub>Cl<sub>2</sub> (20  $\mu$ L) was added to the reaction mixture in chloroform (15 mL). After 5 h the mixture was washed with a saturated aqueous solution of sodium hydrogencarbonate, the organic layer was collected, dried, and evaporated in vacuum. The residue was subjected to column chromatography on silica gel using hexane–dichloromethane mixture (1:3, v/v) as the eluent. The product was obtained as a yellow powder (48 mg, 41% yield). Mp >260 °C. <sup>1</sup>H NMR (CDCl<sub>3</sub>,  $\delta$ ): 6.14 (dd, 2H,  $J=1.0, 3.7$  Hz), 7.18 (dd, 2H,  $J=1.2, 3.7$  Hz), 7.70 (s, 2H), 9.65 (br s, 2H). <sup>13</sup>C APT NMR (DMSO-*d*<sub>6</sub>,  $\delta$ ): 108.40 CH,

114.13 CH, 118.71 C, 122.59 C, 128.12 C, 133.35 CH, 138.25 C, 145.45 C. EI/MS (70 eV): 451 (100) [M<sup>+</sup>], 486 (55), 416 (50).

**3.1.3. 5,8-Di(2,3-dihydrothieno[3,4-*b*][1,4]dioxin-5-yl)-2,3-di(1*H*-2-pyrrolyl)quinoxaline (1).** 5,8-Dibromo-2,3-di(1*H*-2-pyrrolyl)quinoxaline (50 mg, 0.12 mmol) and 2,3-dihydrothieno[3,4-*b*][1,4]dioxin-5-yltributylstannane<sup>11</sup> (258 mg, 0.6 mmol) were dissolved in dry THF (100 ml), the solution was purged with argon for 15 min, and PdCl<sub>2</sub>(PPh<sub>3</sub>)<sub>2</sub> (15 mg, 0.02 mmol) was added at room temperature under argon atmosphere. The mixture was stirred at 100 °C under argon atmosphere for 15 h, cooled, and concentrated on the rotary evaporator. The residue was purified by column chromatography (DCM–hexane 3:1) to afford an orange solid (31 mg, 48% yield). Mp >260 °C. <sup>1</sup>H NMR (CDCl<sub>3</sub>,  $\delta$ ): 4.28–4.41 (m, 8H, *ethylene*); 6.29 (ddd, 2H,  $J=2.6, 3.7, 5.4$  Hz); 6.57 (s, 2H, *EDOT*), 7.09 (ddd, 2H,  $J=1.3, 2.5, 3.7$  Hz); 7.26 (ddd, 2H,  $J=1.3, 2.6, 3.6$  Hz); 8.41 (s, 2H, *H6*); 10.03 (br s, 2H, *NH*). <sup>13</sup>C APT NMR (CDCl<sub>3</sub>,  $\delta$ ): 65.74 CH<sub>2</sub>, 65.29 CH<sub>2</sub>, 102.20, 110.21, 113.48, 113.67, 122.10, 127.49, 127.86, 129.91, 135.90, 140.57, 141.14, 142.05. EI/MS (70 eV):  $m/z$  540 (87) [M<sup>+</sup>], 269 (100), 267 (70). Anal. Calcd (%) for C<sub>28</sub>H<sub>20</sub>N<sub>4</sub>O<sub>4</sub>S<sub>2</sub>·0.5 H<sub>2</sub>O (549.1): C, 61.19; H, 3.85; N, 10.19; O, 13.10; S, 11.67. Found: C, 61.16; H, 3.71; N, 10.04.

**3.1.4. 5,8-Di(2,3-dihydrothieno[3,4-*b*][1,4]dioxin-5-yl)-2,3-di(5-chloro-1*H*-2-pyrrolyl)quinoxaline (1C).** The title compound was synthesized from 5,8-dibromo-2,3-di(5-chloro-1*H*-2-pyrrolyl)quinoxaline according to the procedure described above for **1**. The product was a red solid (256 mg, 33% yield). Mp >260 °C. <sup>1</sup>H NMR (CDCl<sub>3</sub>,  $\delta$ ): 4.28–4.41 (m, 8H, *ethylene*); 6.12 (dd, 2H,  $J=1.0, 3.7$  Hz); 6.59 (s, 2H, *EDOT*), 7.17 (dd, 2H,  $J=1.0, 3.7$  Hz); 8.36 (s, 2H, *H6*); 9.95 (br s, 2H, *NH*). <sup>13</sup>C APT NMR (DMSO-*d*<sub>6</sub>,  $\delta$ ): 64.43 CH<sub>2</sub>, 65.42 CH<sub>2</sub>, 103.78 CH, 108.24 CH, 112.21 C, 113.30 CH, 117.51 C, 127.51 CH, 128.13 C, 128.59 C, 135.97 C, 141.05 C, 141.81 C, 142.06 C. EI/MS (70 eV):  $m/z$  608 (100) [M<sup>+</sup>], 610 (78), 573 (86). HRMS (ESI) Calcd for C<sub>28</sub>H<sub>19</sub>Cl<sub>2</sub>N<sub>4</sub>O<sub>4</sub>S<sub>2</sub> (M + H<sup>+</sup>):  $m/z$  609.0225. Found:  $m/z$  609.0219.

**3.1.5. Poly-5,8-di(2,3-dihydrothieno[3,4-*b*][1,4]dioxin-5-yl)2,3-di(1*H*-2-pyrrolyl)quinoxaline (poly-1).** The title compound was prepared potentiodynamically from 0.5 mM solution of **1** in TBAP/ACN. Monomer oxidation potential (onset of polymerization current):  $E_m=0.40$  V. Polymer half-wave oxidation:  $E_{1/2,p}=0.70$  V. Band gap as determined from vis-NIR spectroelectrochemistry in the reduced form:  $E_g=1.39$  eV. Conductivity:  $\sigma=54$  S/cm.

**3.1.6. Poly-5,8-di(2,3-dihydrothieno[3,4-*b*][1,4]dioxin-5-yl)2,3-di(5-chloro-1*H*-2-pyrrolyl)quinoxaline (poly-1C).** The title compound was prepared potentiodynamically from 0.5 mM solution of **1C** in TBAP/ACN.  $E_m=0.48$  V.  $E_{1/2,p}=0.72$  V.  $E_g=1.36$  eV.  $\sigma=23$  S/cm.

#### Acknowledgements

This work was financially supported by Kraft Foods, Inc., NSF (NER Grant#0304320, SENSOR Grant# 0330267

to P. A.), BGSU (TIE and FRCRIG grants to P. A.), McMaster Endowment (McMaster Fellowship to D. A.), and ACS-PRF (Grant # 38110-G4 to P. A.).

### References and notes

1. Martinez-Manez, R.; Sancenon, F. *Chem. Rev.* **2003**, *103*, 4419–4476.
2. (a) Beer, P. D.; Gale, P. A. *Angew. Chem., Int. Ed.* **2001**, *40*, 487–516. (b) Atwood, J. L.; Steed, J. W. *Supramol. Chem. Anions* **1997**, 147–215.
3. (a) *Supramolecular Chemistry of Anions*; Bianchi, A., Bowman-James, K., Garcia-Espana, E., Eds.; Wiley-VCH: New York, 1997. (b) *Supramolecular Chemistry*; Atwood, J. L., Davies, J. E., MacNicol, D. D., Vögtle, F., Reinhoudt, D. N., Lehn, J.-M., Eds.; Pergamon-Elsevier: Oxford, 1996.
4. (a) Ho, H. A.; Leclerc, M. *J. Am. Chem. Soc.* **2003**, *125*, 4412–4413. (b) Takeuchi, M.; Shioya, T.; Swager, T. *Angew. Chem., Int. Ed.* **2000**, *40*, 3372–3376.
5. Kim, D.; McQuade, D. T.; McHugh, S. K.; Swager, T. M. *Angew. Chem., Int. Ed.* **2000**, *39*, 3868–3872.
6. *Handbook of Oligo- and Polythiophenes*; Fichou, D., Ed.; Wiley-VCH: New York, 1999.
7. Kanbara, T.; Yamamoto, T. *Macromolecules* **1993**, *26*, 3464–3466.
8. (a) Black, C. B.; Andrioletti, B.; Try, A. C.; Ruiperez, C.; Sessler, J. L. *J. Am. Chem. Soc.* **1999**, *121*, 10438–10439. (b) Anzenbacher, P.; Try, A. C.; Miyaji, H.; Jursikova, K.; Lynch, V. M.; Marquez, M.; Sessler, J. L. *J. Am. Chem. Soc.* **2000**, *122*, 10268–10272.
9. Groenendaal, L.; Jonas, F.; Freitag, D.; Pielartzik, H.; Reynolds, J. *Adv. Mater.* **2000**, *12*, 481–494.
10. Tsubata, Y.; Suzuki, T.; Miyashi, T.; Yamashita, Y. *J. Org. Chem.* **1992**, *57*, 6749–6755.
11. Zhu, S. S.; Swager, T. M. *J. Am. Chem. Soc.* **1997**, *119*, 12568–12577.
12. Cordell, G. A. *J. Org. Chem.* **1975**, *40*, 3161–3169.
13. Aldakov, D.; Anzenbacher, P. *Chem. Commun.* **2003**, 1394–1395.
14. Aldakov, D.; Anzenbacher, P. *J. Am. Chem. Soc.* **2004**, *126*, 4752–4753.
15. Anzenbacher, P.; Try, A. C.; Miyaji, H.; Jursikova, K.; Lynch, V. M.; Marquez, M.; Sessler, J. L. *J. Am. Chem. Soc.* **2000**, *122*, 10268–10272.
16. Apparent affinity constants were calculated using equation for 1:1 stoichiometry. The equation uses the concentration of added anion to be a sum of a free anion (unbound) and anion bound by the receptor. The latter is considered equal to the receptor concentration. Because the receptor concentration on the surface of the material is unknown, the affinity constant is designated as ‘apparent’, and the respective values are relative. In fact, judging from the dynamic range of the sensors, the affinity of poly-**1** and poly-**1C** for anions is equal or higher to affinity of the monomers **1** and **1C**.
17. (a) Zotti, G.; Zecchin, S.; Schiavon, G.; Berlin, A. *Chem. Mater.* **2002**, *14*, 3607–3614. (b) Baker, C. K.; Qiu, Y.-J.; Reynolds, J. R. *J. Phys. Chem.* **1991**, *95*, 4446–4452.
18. Bianchi, A.; Bowman-James, K.; Garcia-Espana, E. *Supramolecular Chemistry of Anions*; Wiley-VCH: New York, 1997.

# Functional polythiophenes as optical chemo- and biosensors

Maïté Béra-Abérem, Hoang-Anh Ho and Mario Leclerc\*

Département de Chimie, Université Laval, Vachon Building, Québec City, Que., Canada, G1K 7P4

Received 30 January 2004; revised 23 June 2004; accepted 19 August 2004

Available online 15 September 2004

**Abstract**—Synthesis of fluorescent, chromic and postfunctionalizable poly[3-(*N*-succinimido(tetraethoxy)oxy)-4-methylthiophene] is described. This polymer bears succinimidyl carbamate side-chains which are able to react with amine groups, affording new smart polythiophene derivatives. Detection of different analytes (affinitychromism) was realized by UV–Visible and fluorescence means. In order to develop biosensors, water-soluble cationic thiophene-based homopolymers and random copolymers were also investigated.  
 © 2004 Elsevier Ltd. All rights reserved.

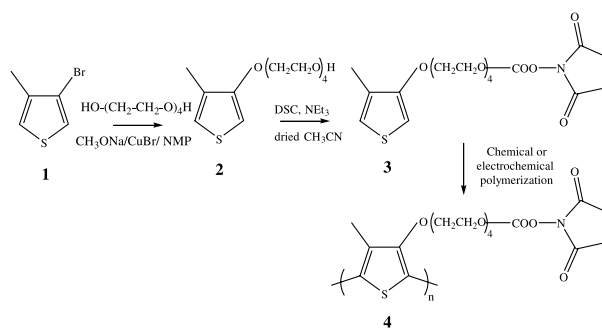
## 1. Introduction

Conjugated electroactive and/or photoactive polythiophenes can be successfully utilized for the specific detection of a large variety of analytes such as cations, anions, proteins, nucleic acids.<sup>1–3</sup> Recently, our group reported the synthesis of postfunctionalizable poly[3-(*N*-succinimido-*p*-phenyl-carboxylate(tetraethoxy)oxy)-4-methylthiophene]<sup>4</sup> for colorimetric detection of interactions between various combinations of ligands (covalently attached to the polymeric transducer) and targets. The color changes were related to a conformational transition of the polymer backbone, between a planar (highly conjugated) and a nonplanar (less conjugated) form, triggered by adequately functionalized and responsive side chains. However, this postfunctionalizable and chromic polymer, prepared by electrochemical means, was obtained in poor yields (less than 5%) and was insoluble in water. In order to improve the preparation of this type of functional polymers, we describe here the chemical synthesis of a new thiophene derivative and its corresponding functional homopolymer. To increase the solubility in water, a random postfunctionalizable copolymer bearing positive charges on its side chain was also designed and synthesized.

## 2. Results and discussion

### 2.1. Synthetic route

As shown in Scheme 1, monomer (3) was prepared in two



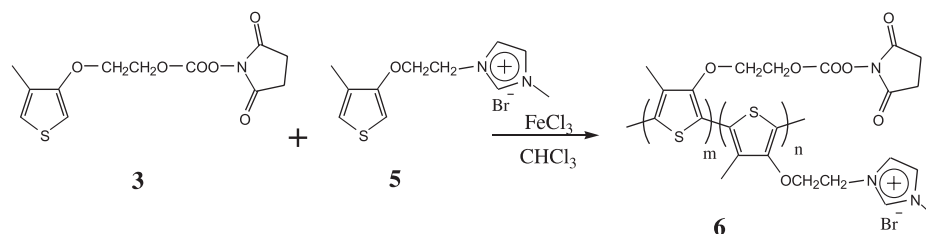
**Scheme 1.** Synthesis of polymer 4 from 3-bromo 4-methyl thiophene as starting material.

steps. The first one involves the nucleophilic substitution reaction between tetraethyleneglycol and 3-bromo-4-methyl thiophene (1), catalysed by CuBr to obtain 3-methyl-4-(tetraethoxy)oxythiophene (2).<sup>5</sup> The terminal hydroxy group was activated by *N,N'*-disuccinimidyl carbonate (DSC) to form an activated ester group (3). The corresponding homopolymer (4) was obtained by chemical polymerization using FeCl<sub>3</sub> as the oxidizing agent,<sup>6</sup> followed by a reduction step with zinc. It is important to note here that the neutral polythiophene can only be obtained after a reduction reaction, often performed with hydrazine.<sup>6</sup> This is totally inappropriate in this case because this reducing agent can react with the succinimidyl carbonate (SC) group. A comparative IR study between neutral polymer (4) prepared by chemical polymerization and that prepared by electrochemical polymerization was carried out. In both cases, the characteristic peaks associated to the succinimide function remain clearly visible (around 1740–1820 cm<sup>-1</sup>) after electrochemical or chemical reduction and are comparable to the fingerprints obtained with the starting monomer (3).

**Keywords:** Sensors; Polythiophenes; Affinitychromism.

\* Corresponding author. Tel.: +1-418-656-7916; fax: +1-418-656-7916;  
 e-mail: mario.leclerc@chm.ulaval.ca



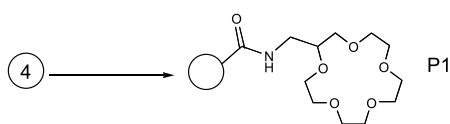


Scheme 2. Synthesis of water-soluble copolymers (6).

Water-soluble copolymers (6) were also synthesized following procedures described in Scheme 2. Monomer (5) was prepared, according to a previously published procedure.<sup>3a</sup> An oxidative reaction of the mixture of monomers (3) and (5) at the different proportions gave copolymers (6) which became soluble in water, only with a starting composition of more than 70 mol% of monomer (5).

## 2.2. Specific detection of alkali metal ions

Because of the succinimidyl carbonate (SC) group, homopolymer (4) can react with amines under very mild conditions to form the corresponding carbamate derivatives in high yields. In order to detect the alkali metal ions, 2-(aminomethyl)-15-crown-5 was added to a thin film of the chemically-prepared polythiophene (4), yielding polymer (P1) (see Scheme 3). The FTIR spectra<sup>7</sup> recorded before and after the binding show that all SC functions were replaced by the crown-ether group (Supporting Information). Figure 1 displays the UV–visible absorption spectra when P1 was tested with different alkali cations. The yellow solution of 15-crown-5 modified polymer (P1) exhibits a maximum of absorption at 429 nm in THF (Fig. 1, a). This absorption maximum at a relatively short wavelength should be related to a random-coil conformation of the polythiophene derivative, as any twisting of the conjugated backbone leads to a decrease of the effective conjugation length. The



Scheme 3. Synthesis of functionalized polythiophene, P1.

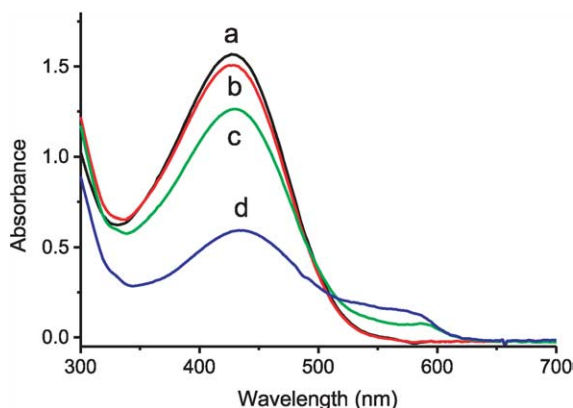


Figure 1. UV–Vis absorption spectra of polymer (P1) ( $4.6 \times 10^{-3}$  M based on monomeric units) in different THF solutions. (a) P1 alone; (b)  $1 \times 10^{-3}$  M  $\text{LiCF}_3\text{SO}_3$ ; (c)  $1 \times 10^{-3}$  M  $\text{NaCF}_3\text{SO}_3$ ; (d)  $1 \times 10^{-3}$  M  $\text{KCF}_3\text{SO}_3$ .

same UV–visible spectrum was observed upon addition of  $2 \times 10^{-6}$  mol of  $\text{LiCF}_3\text{SO}_3$  in 2 mL of THF (Fig. 1, b). Under identical conditions, addition of  $\text{NaCF}_3\text{SO}_3$  (Fig. 1, c) or  $\text{KCF}_3\text{SO}_3$  (Fig. 1, d) leads to a new absorption band around 580 nm which is the optical signature of a coplanar or aggregated structure of the polymer (P1). These results are essentially the same as those observed on polythiophene analogs:<sup>8</sup> the sodium salt showing the weakest effect and the potassium salt leading to the strongest ionochromic effect. These optical changes can be explained by the formation of a more stable complex between two 15-crown-5 ligands and one potassium ion,<sup>8,9</sup> which forces the aggregation of the conjugated backbone. Interestingly, a fluorometric detection of cation binding is also possible because the fluorescence of polymer (P1) is quenched in the planar or aggregated form. The yellow or random-coil form of P1 is fluorescent with a maximum emission at 543 nm when excited at 429 nm (Fig. 2, a). Upon addition of different alkali cations, the fluorescence intensity decreases in the following order:  $\text{K}^+ > \text{Na}^+ > \text{Li}^+$  (Fig. 2, b–d), which are in good agreement with the results obtained from UV–visible measurements.

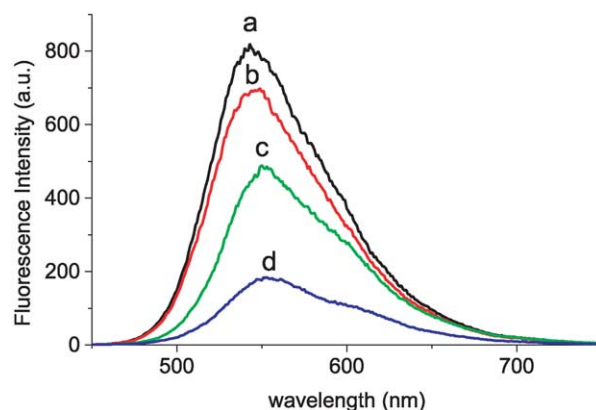
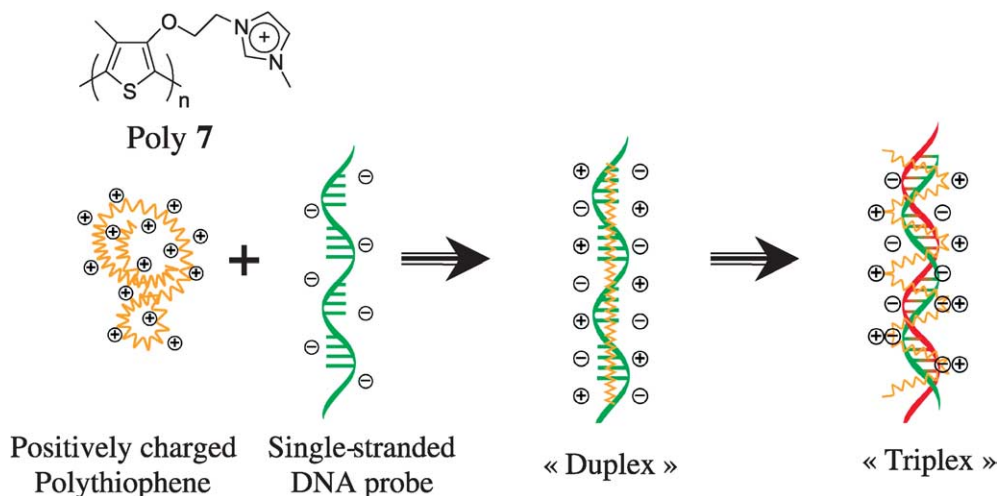


Figure 2. Fluorescence spectra of polymer (P1) ( $4.6 \times 10^{-3}$  M based on monomeric units) in different THF solutions. (a) P1 alone; (b)  $1 \times 10^{-3}$  M  $\text{LiCF}_3\text{SO}_3$ ; (c)  $1 \times 10^{-3}$  M  $\text{NaCF}_3\text{SO}_3$ ; (d)  $1 \times 10^{-3}$  M  $\text{KCF}_3\text{SO}_3$ .

## 2.3. Detection of nucleic acids

As a second example of the usefulness of functional polythiophenes as sensors, polymer 7 was selected for the detection of nucleic acids. Detection was carried out following our previously published procedures<sup>3a</sup> (Scheme 4). The novelty here is to find new hybridization conditions that allow the base-pairing reactions at room temperature. For this purpose, we report the use of formamide as denaturing agent to reduce reaction temperatures.<sup>10</sup>



**Scheme 4.** Schematic description of the formation polythiophene/single stranded nucleic acid duplex and polythiophene/hybridized nucleic acid triplex.

Temperature of the detection is a particularly important parameter for future technological applications using microfluidic devices. Figure 3 exhibits the UV–visible absorption experiments carried out with different oligonucleotides. For instance, at 25 °C, aqueous solution (20% v/v of formamide and 80 mM of EDTA) of the cationic polymer **7** is yellow ( $\lambda_{\max} = 405$  nm; Fig. 3, a). This absorption maximum at a short wavelength is again related to a random-coil conformation of the polythiophene. As any cationic polyelectrolytes, the polymer **7** is able to form a strong complex with negatively charged oligonucleotides. For example, upon addition of 1.0 equiv on a monomeric unit basis (the concentrations of the 20-mer oligonucleotides correspond therefore to the twentieth of those reported for the synthetic polydisperse polythiophene which are given per repeat unit) of capture oligonucleotide **X1** (5'-CAT-GATTGAACCATCCACCA-3'), the mixture becomes immediately red ( $\lambda_{\max} = 528$  nm) (Fig. 3, b). This behaviour

can be explained by the formation of a so-called duplex between the polythiophene and the oligonucleotide probe (see Scheme 4). After 5 min of mixing at room temperature in the presence of 1.0 equiv of the complementary oligonucleotide **Y1** (3'-GTACTAACTTGGTAGGTGGT-5'), the solution becomes yellow ( $\lambda_{\max} = 430$  nm) (Fig. 3, c); presumably due to the formation of a new complex termed triplex (Scheme 4), formed by complexation of the polymer with hybridized nucleic acids. To verify the specificity of this polymeric optical transducer in presence of imperfect or incomplete hybridization reactions, different oligonucleotides (20-mers differing by only one mismatch (**Y3**: 3'-GTACTAACTTCGTAGGTGGT-5') (Fig. 3, e) or 2 nucleotides (**Y2**: 3'-GTACTAACTTCGAAGGTGGT-5') (Fig. 3, d) were investigated. In both cases, the color change is partly inhibited. Therefore, it is possible to distinguish one or two mismatches from no mismatch in 5 min at 25 °C.

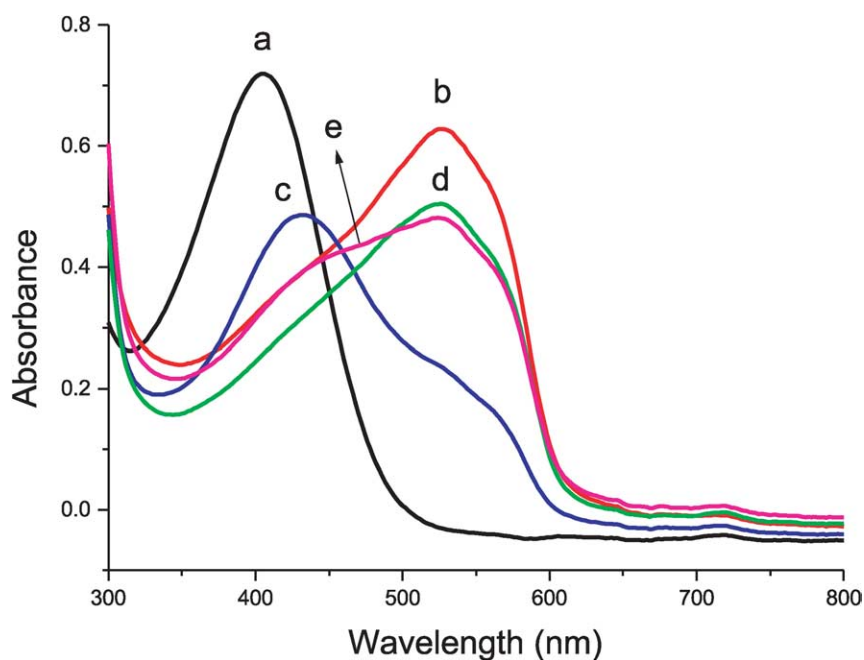
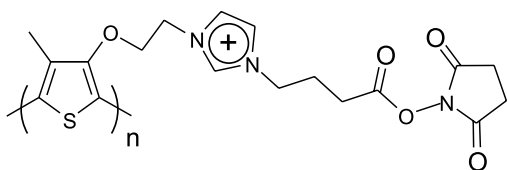


**Figure 3.** UV–visible absorption spectra of (a) polymer **7** alone, (b) polymer **7/X1** duplex, (c) polymer **7/X1/Y1** triplex (perfect match), (d) polymer **7/X1/Y2** mixture (two mismatches), and (e) polymer **7/X1/Y3** mixture (1 mismatch) after 5 min of mixing at 25 °C in 0.08 M EDTA and 20% (v/v) formamide.

To obtain a covalent attachment of the DNA probe on water-soluble polymer (combination of succinimidyl carbonate and positive charge as side chain), a set of new copolymers (**6**) (Scheme 2) at different concentrations of monomers (**3**) and (**5**) was prepared for tentative detections of nucleic acids. In order to determine the real percentage of monomer (**3**) incorporated in the resulting copolymer, a FTIR calibration curve was established. For example, a mixture of 80/20 (in mole) of monomers (**5**) and (**3**) respectively was chemically polymerized to afford a copolymer (**6**) with less than 5% of monomer (**3**). This water-soluble copolymer was used to graft an oligonucleotide ended with an amine group (5'-NH<sub>2</sub>-C<sub>6</sub>-CAT GAT TGA ACC ATC CAC CA-3') as capture probe and hybridized with its complementary strand **Y1**. Unfortunately, under similar conditions as those described above, the copolymer (**6**) functionalized with 20-mer oligonucleotide did not show any change in absorbance after hybridization with its complementary target. Further studies are in progress in our laboratory to synthesize a homopolymer having on each repeat unit, one positive charge and one succinimidyl carbonate group (Scheme 5). These new structures should yield highly water-soluble and highly functionalizable chromic polythiophenes.



**Scheme 5.** Example a polythiophene derivative bearing on each repeat unit, cationic and NHS groups.

### 3. Conclusion

This article has shown that some conjugated polythiophenes can detect and transduce chemical or biochemical information into an optical signal. Indeed, using appropriate side-chain ligands, these smart materials can provide new platforms for the optical transduction of molecular binding interactions, including molecules of biological importance. In particular, it has been demonstrated that versatile postfunctionalization or electrostatic approaches can easily lead to a large number of different responsive (chromic) polythiophene derivatives. It is firmly believed that these novel optical chemo- and biosensors should find applications in the areas of diagnostics, therapeutics, and drug screening.

## 4. Experimental

### 4.1. Materials

All chemical reagents were obtained commercially from Aldrich and were used without further purification unless otherwise noted. <sup>1</sup>H and <sup>13</sup>C NMR spectra were recorded using a Varian 300 MHz. UV–Vis absorption spectra were measured with a Hewlett–Packard spectrophotometer

(model HP 8452A). The fluorescence spectra were taken on a Carry Eclipse (Varian Inc.) spectrofluorometer. Molecular weights were evaluated by size exclusion chromatography (SEC) on PLGEL, KF804 columns in THF using a Waters instrument equipped with an absorbance detector (model 441). The calibration curve was obtained by using polystyrene standards. FTIR spectra were recorded using a Nicolet Magna 560 spectrometer with a resolution of 4 cm<sup>-1</sup> from KBr pellets or films cast from CHCl<sub>3</sub> or water solution on NaCl or BaF<sub>2</sub> disks.

**4.1.1. 3-Methyl 4-(tetraethoxy)thiophene (2).** The title compound was synthesized as previously described.<sup>5</sup>

**4.1.2. 3-[N-Succinimido(tetraethoxy)oxy]-4-methyl thiophene (3).** *N,N'*-Disuccinimidyl carbonate (DSC) (0.6 g, 2.4 mmol) and triethylamine (0.48 g, 4.8 mmol) were added to a stirred solution of 3-methyl 4-(tetraethoxy) thiophene (**2**) (0.47 g, 1.6 mmol) in acetonitrile (10 mL), under argon, at room temperature during 4 h. After evaporation of the solvent, the crude product was washed with an aqueous solution of NaHCO<sub>3</sub> (1 M) and extracted with ethyl acetate. The combined organic layers were dried over MgSO<sub>4</sub>, filtered and evaporated. The final product was purified by column chromatography on silica gel with ethyl acetate–hexane (9/1) as a yellow oil (0.6 g, 90%). IR: 3113; 2922; 2871; 1813; 1789; 1743; 1560; 1474; 1100 cm<sup>-1</sup>. <sup>1</sup>H NMR: (CDCl<sub>3</sub>, 300 MHz) δ 2.08 (s, 3H); 2.81 (s, 4H); 3.73 (m, 10H); 3.86 (t, 2H, *J*=9.8 Hz); 4.11 (t, 2H, *J*=9.8 Hz); 4.44 (t, H, *J*=9.3 Hz); 6.17 (d, 1H, *J*=3.3 Hz); 6.81 (d, 1H, *J*=2.8 Hz). <sup>13</sup>C: NMR (CDCl<sub>3</sub>, 75 MHz) δ 12.69; 25.43; 68.30; 69.65; 70.24; 70.59; 70.71; 70.84; 96.56; 119.91; 129.17; 151.64; 155.91; 168.68.

HRMS: Calcd for C<sub>18</sub>H<sub>25</sub>O<sub>9</sub>NS: 431.1250; exp.: 431.1255.

**Chemical polymerization of monomer (3).** A solution of monomer (**3**) (0.26 g, 0.6 mmol) in chloroform (10 mL) was added dropwise to a solution of iron trichloride (0.39 g, 2.4 mmol) in chloroform (10 mL) under argon. The mixture was stirred at room temperature for a period of 24 h. The resulting polymer was precipitated by addition of an excess of acetone, washed by Soxhlet extraction with acetone until the washing solvent was colorless. The oxidized polymer was then reduced in chloroform (250 mL) in the presence of zinc (100 mg) as reducing agent for 16 h with stirring. After filtration, the neutral polymer, soluble in chloroform was evaporated under reduced pressure to yield polymer (**4**) (0.08 g, 30%). IR: 2926; 2875; 1813; 1789; 1743; 1100 cm<sup>-1</sup>. <sup>1</sup>H NMR: (CDCl<sub>3</sub>, 300 MHz) δ 2.30 (s, 3H); 2.81 (s, 4H); 3.72 (m, 10H); 3.95 (s, 2H); 4.01 (s, 2H); 4.44 (s, 2H). GPC: *M*<sub>w</sub> = 30,000.

**Electropolymerization of monomer (3).** A three-electrode cell was employed. The working and counter electrodes were platinum plates and the reference electrode was the Ag/AgNO<sub>3</sub> (0.01 M in 0.1 M Bu<sub>4</sub>NBF<sub>4</sub>) in acetonitrile. The monomer (**3**) was electropolymerized at a concentration of 0.1 M in acetonitrile containing 0.1 M Bu<sub>4</sub>NBF<sub>4</sub> by successive scanning potential at 100 mV/s between -0.15 and 1 V. After the electropolymerization, the pellet polymer (**4**) was rinsed with fresh acetonitrile and acetone. IR: 2921; 2871; 1813; 1789; 1743; 1089 cm<sup>-1</sup>. Yields: <5%.

**4.1.3. Copolymer (6).** A solution of monomers (3) (0.086 g, 0.2 mmol) and (5) (0.24 g, 0.8 mmol) in chloroform (8 mL) was added dropwise to a solution of iron trichloride (0.65 g, 4 mmol) in chloroform (18 mL) under argon. The mixture was stirred at room temperature for a period of 24 h. The resulting polymer was precipitated by addition of an excess of diethyl ether, washed by Soxhlet extraction with diethyl ether (to remove low-molecular weight materials) until the washing solvent was uncolored. After drying, the final polymer (6) is neutral without reduction step as black powder (0.2 g, 61%).

#### 4.2. Procedure for detection of alkali cations

A film of polymer (4) ( $4.6 \times 10^{-6}$  mol based on monomeric units) was prepared by evaporation of the corresponding polymer solution (0.5 mL, 4 mg/mL). The resulting film was put in contact on solid state with an excess of 2-(aminomethyl)-15-crown-5 (0.1 M) in acetonitrile (HPLC grade) for an optimized time of 5 min, washed with  $\text{CH}_3\text{CN}$ , dried and dissolved in THF.

#### 4.3. General procedure for specific detection of nucleic acids

In a quartz cuvette with an optical pathlength of 1.0 cm, 13.4  $\mu\text{L}$  aliquot of a  $7.3 \times 10^{-4}$  M (on a repeat unit basis) aqueous solution of polymer 7 was added to 100  $\mu\text{L}$  of an aqueous solution of 20% (v/v) formamide containing 80 mM of EDTA. 2  $\mu\text{L}$  of a  $2.4 \times 10^{-4}$  M solution of the capture oligonucleotide X1 (20 nucleic acids) was added to the previous mixture, and the resulting red solution was kept at room temperature for 5 min. The appropriate oligonucleotide target (volume of 2  $\mu\text{L}$  at concentration of  $2.4 \times 10^{-4}$  M) was added to the duplex solution at room temperature over 5 min.

#### Acknowledgements

This work was supported by the Natural Sciences and Engineering Research Council of Canada (NSERC) and Infectio Diagnostic (IDI) Inc. The authors thank Dr. M. Boissinot, R. Peytavis and F. Raymond for useful discussions and help in the synthesis of some nucleic acids.

#### Supplementary data

Supplementary data associated with this article can be found in the online version, at doi:10.1016/j.tet.2004.08.053.

#### References and notes

- (a) McQuade, D. T.; Pullen, A. E.; Swager, T. M. *Chem. Rev.* **2000**, *100*, 2537–2574. (b) Leclerc, M.; Faid, K. *Adv. Mater.* **1997**, *9*, 1087–1094. (c) Leclerc, M. *Adv. Mater.* **1999**, *11*, 1491–1498. (d) McCullough, R. D. *Adv. Mater.* **1998**, *10*, 93–116.
- (a) Faid, K.; Leclerc, M. *J. Am. Chem. Soc.* **1998**, *120*, 5274–5278. (b) Kumpumbu-Kalemba, L.; Leclerc, M. *Chem. Commun.* **2000**, 1847–1848. (c) Ewbank, P. C.; Nuding, G.; Suenaga, H.; McCullough, R. D.; Shinkai, S. *Tetrahedron Lett.* **2001**, *42*, 155–157.
- (a) Ho, H.-A.; Boissinot, M.; Bergeron, M. G.; Corbeil, G.; Doré, K.; Boudreau, D.; Leclerc, M. *Angew. Chem., Int. Ed.* **2002**, *41*, 1548–1551. (b) Nilsson, K. P. R.; Inganäs, O. *Nat. Mater.* **2003**, *2*, 419–424. (c) Ho, H.-A.; Leclerc, M. *J. Am. Chem. Soc.* **2003**, *125*, 4412–4413. (d) Ho, H.-A.; Leclerc, M. *J. Am. Chem. Soc.* **2004**, *126*, 1384–1387.
- Bernier, S.; Garreau, S.; Béra-Abérem, M.; Gravel, C.; Leclerc, M. *J. Am. Chem. Soc.* **2002**, *124*, 12463–12468.
- Lévesque, I.; Leclerc, M. *Macromolecules* **1997**, *30*, 4347–4352.
- Daoust, G.; Leclerc, M. *Macromolecules* **1991**, *24*, 455–459.
- Schönherr, H.; Feng, C.; Shovskey, A. *Langmuir* **2003**, *19*, 10843–10851.
- Boldea, A.; Lévesque, I.; Leclerc, M. *J. Mater. Chem.* **1999**, *9*, 2133–2138.
- (a) Flink, S.; Boukamp, B. A.; Van der Berg, A.; Van Veggel, F. C. J. M.; Reinhoudt, D. N. *J. Am. Chem. Soc.* **1998**, *120*, 4652–4657. (b) Kim, J.; McQuade, D. T.; McHugh, S. K.; Swager, T. M. *Angew. Chem., Int. Ed.* **2000**, *39*, 3868–3872.
- Hames, B. D.; Higgins, S. J. *Nucleic Acid Hybridisation, a Practical Approach*; IRL: Oxford, Washington, DC, 1985; pp 64–65.



# Binary and ternary phenylboronic acid complexes with saccharides and Lewis bases

 L. I. Bosch,<sup>a</sup> T. M. Fyles<sup>b,\*</sup> and T. D. James<sup>a,\*</sup>
<sup>a</sup>Department of Chemistry, University of Bath, Bath BA2 7AY, UK

<sup>b</sup>Department of Chemistry, University of Victoria, Victoria, BC, Canada

Received 1 February 2004; revised 30 June 2004; accepted 19 August 2004

Available online 25 September 2004

**Abstract**—Cumulative formation constants for the association of three boronic acids (phenylboronic acid and its *ortho*-anilinomethyl and *ortho*-benzylaminomethyl derivatives) with four saccharides (fructose, glucose, mannitol, and sorbitol) were determined by potentiometric titration. Similarly, the constants for the formation binary complexes of the three boronic acids with (hydrogen) phosphate, (hydrogen) citrate, or imidazole were determined. Finally, the formation of ternary complexes of the boronic acids, phosphate, citrate or imidazole, and the saccharides were determined based on the determined values of the binary complexes. The previously unrecognized ternary complexes are significant in all systems investigated, and under some solution compositions, they can be the dominant species in solution over a wide pH range. A value of 15–25 kJ mol<sup>-1</sup> was determined for the energy of the B–N interaction in the benzylmethyl derivative based on the relative stabilities of the ternary phosphate complexes of the three boronic acids. The data are used to rationalize the medium dependence of stepwise formation constants and the apparent acidity constants of previous literature reports.

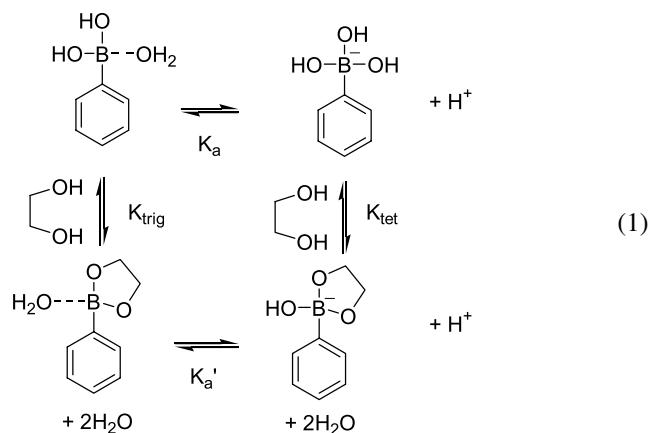
© 2004 Elsevier Ltd. All rights reserved.

## 1. Introduction

Recognition of saccharides by boronic acids has a unique place in supramolecular chemistry.<sup>1</sup> Not only is the pair-wise interaction energy large enough to allow single-point molecular recognition, the primary interaction involves the reversible formation of a pair of covalent bonds (rather than non-covalent attractive forces). This interaction has been very widely exploited,<sup>2</sup> with a particular recent emphasis on using the interaction in fluorescent and colorimetric sensors<sup>3,4</sup> and the sensing of saccharides and related species.<sup>5–12</sup> Despite a long history—the first structural and quantitative binding constant data were reported in the 1950s<sup>13–15</sup>—the structure of the boronic acid–saccharide complexes in aqueous solution continues to be discussed.<sup>16–18</sup> There is general agreement that boronic acids covalently react with 1,2 or 1,3 diols to form five or six membered cyclic esters. The adjacent rigid *cis*-diols of saccharides form stronger cyclic esters than simple acyclic diols such as ethylene glycol. With saccharides the choice of diol used in the formation of a

cyclic ester is complicated by the possibility of pyranose to furanose isomerization of the saccharide moiety. Lorand and Edwards first determined the selectivity of phenylboronic acid towards saccharides, and this selectivity order seems to be retained by all monoboronic acids.<sup>15</sup>

The equilibria involved in phenylboronate binding of a diol are conventionally summarized as a set of coupled equilibria (1):<sup>15,18–21</sup>



In aqueous solution, phenylboronic acid reacts with water to

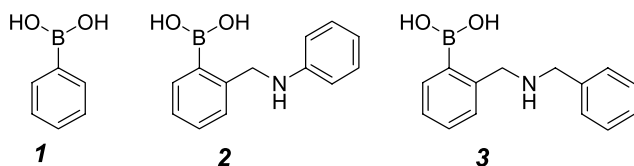
**Keywords:** Phenylboronic acids; Saccharides; Molecular recognition; Cumulative formation constants.

\* Corresponding authors. Tel.: +44-1225-383810; fax: +44-1225-386231 (T.D.J.); e-mail addresses: tmf@uvic.ca; t.d.james@bath.ac.uk



form the boronate anion plus a hydrated proton thereby defining an acidity constant  $K_a$ .<sup>†</sup> Values of about 8.8 have been reported for the  $pK_a$  of phenylboronic acid.<sup>23–25</sup> The formation of a diol boronate complex, defined by  $K_{tet}$  formally liberates 2 equiv of water, but this stoichiometric factor is usually ignored as a constant in dilute aqueous solution. The magnitude of  $\log K_{tet}$  varies with the diol, ranging from about 3.8 for fructose, to about 1.2 for simple diols such as ethylene glycol.<sup>15</sup> In a formal sense, phenylboronic acid could also bind diols to form a trigonal complex ( $K_{trig}$ ), and this species would itself act as an acid according to  $K'_a$ . The ‘acidification’ of solutions containing phenylboronic acid and diols is always discussed in terms of the trigonal complex being a stronger acid than the parent phenylboronic acid, that is,  $K'_a > K_a$ .<sup>3,4</sup> As a result,  $K_{tet} > K_{trig}$ . The system of four equilibria as illustrated in Eq. (1) is over-determined since any three of the constants will give a value of the fourth, for example  $K'_a = K_a K_{tet} / K_{trig}$ .

Much of the reported data for values of the equilibrium constants of Eq. 1 is in the form of apparent values determined spectrophotometrically at a defined pH and buffer composition. In addition, there is strong evidence of ‘medium dependence’<sup>21</sup> presumably due to the direct interaction of buffer components with the species of Eq. 1. Our long-range goal is the design of new fluorescence and membrane sensors for sugars. The purpose of this study is to determine values of formation constants for simple phenylboronic acid–saccharide interactions and to elucidate the role of the buffer components. Accordingly, we chose a range of simple compounds that would be indicative of the complexes of interest. The parent phenylboronic acid (**1**) has been studied by several authors<sup>15,21,24–26</sup> and will provide data for the simplest possible interaction. The *ortho*-substituted derivatives **2** and **3** contain the basic binding sites of reported colorimetric, fluorimetric, and electrochemical sensors for sugars.<sup>4</sup> Both systems offer the potential for a B–N interaction, a feature that dominates the solution chemistry of **3** as revealed by <sup>11</sup>B NMR and pH titration.<sup>27</sup> The extent of the B–N interaction in **2** is likely smaller than in **3** due to the lower basicity of an anilino nitrogen relative to a secondary amino nitrogen.



Since multi-component equilibria are involved, the formation constants were determined using the potentiometric titration technique.<sup>28</sup> This is a simple, sensitive and quantitative method for the determination of formation constants in complex equilibria which does not depend on

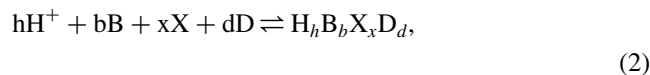
<sup>†</sup> Eq. 1 shows an explicit water molecule ‘coordinated’ to the trigonal boronic acids. There is undoubtedly water in rapid exchange on the Lewis acidic boron in the same way that hydrated Lewis acidic metal ions exchange bound water. A good analogy is  $Zn^{2+}$  (aq), which ionizes in water to give a  $pK_a = 8.8$ , that is,  $Zn-OH_2 \rightarrow Zn-OH + H^+$ .<sup>22</sup> Coordinated water is omitted in subsequent structures.

the spectroscopic properties of the species in solution. As noted above, the various literature reports lead us to expect additional associations of the boronic acids with buffer conjugate bases. Binary boronate–X complexes were found for several Lewis bases (X), together with ternary species (boronate–X–saccharide). In some cases, these previously unrecognized species persist into acidic solution and under some stoichiometric conditions they can be the dominant components of the solution. The data determined allow a rationalization of apparent and medium dependent constants previously reported and point to new directions in the development of sensors and signaling systems.

## 2. Results and discussion

### 2.1. Titration method

In a system containing one or more weak acids that undergo additional complex forming reactions, the existence of the complex species, and the magnitude of the association constants, can be determined from an acid–base titration of solutions of known total concentrations of the components.<sup>28</sup> The method is commonly used to study metal–ligand equilibria, but is equally applicable to the boronate–diol equilibria considered here. Consider the direct association of individual reactants (the conjugate base of a boronic acid B, a second conjugate base X, a diol D, and protons) to give a complex species of a particular stoichiometry ( $H_h B_b X_x D_d$ ). The direct equilibrium defines the cumulative formation constant  $\beta_{hbxd}$  for the complex according to Eq. 2:



$$\beta_{hbxd} = \frac{[H_h B_b X_x D_d]}{[H]^h [B]^b [X]^x [D]^d}$$

Note that  $\beta_{hbxd}$  is defined in terms of concentration rather than activity, since the required activity coefficients for the complex species are unknown. Note as well that the defining equilibrium is associative, thus the dissociative acidity constant of an individual protonated species (e.g.,  $K_a$  for the species HB) is the reciprocal of the formation constant ( $K_a = 1/\beta_{1100}$ ). The cumulative constants for a system are fundamental and fully describe the chemical speciation. They can be used to derive stepwise constants (such as  $K_{trig}$ ) and apparent constants such as those determined spectroscopically.

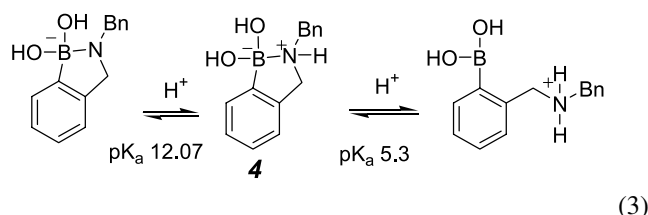
The procedure starts from the acid–base titration of simple systems containing only the protonated complexes of each reactant in turn, to determine the relevant acidity constants. Once these are known, the binary systems can be examined, using the previously determined acidity constants as fixed inputs to calculate the unknown  $\beta$ -values for the binary complexes. Once cumulative formation constants are known for binary systems, then ternary systems can be examined using all previously determined values as fixed inputs. A total of 63 systems (boronic acid, saccharide, buffer base, solvent) was examined over a range of three or

more concentrations and stoichiometric ratios. A subset of 12 systems was independently re-examined, starting from new solid reagents, to assess the overall precision. A total of 205 cumulative constants were determined (27 individual replicates). The overall precision of the values at the 95% confidence level for  $\log \beta$  is  $\pm 0.05$  for single component systems,  $\log \beta \pm 0.15$  for binary systems, and  $\log \beta \pm 0.2$  for ternary systems. The data in terms of  $\log \beta$  is given in Tables in the Experimental section. The subsequent discussion uses conventional stepwise constants derived directly from the cumulative formation constants.

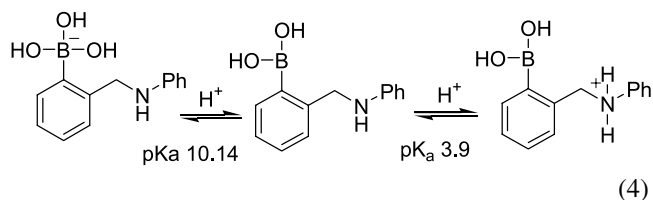
## 2.2. Protonation equilibria

The data are in good agreement with directly comparable literature values. Stepwise  $pK_a$  values are derived from the difference between successive  $\log \beta$  values. For example, the literature value for ionization of  $H_2PO_4^-$  ( $pK_2=6.57$  at  $I=0.5 M^{22}$ ) can be compared with  $\log \beta_{21} - \log \beta_{11} = 18.29 - 11.77 = 6.52$ . The  $pK_1$  value for **1** (8.70) can be compared with previously reported values of 8.92,<sup>25</sup> 8.86,<sup>23</sup> 8.83,<sup>24</sup> and 8.8<sup>21,29</sup> in water (without added NaCl).<sup>‡</sup> The data also show the expected shift to more basic  $pK_a$  as the solvent shifts from water to methanol–water (1:2 v/v). Thus the  $pK_a$  value of **1** in 1:2 methanol/water (9.04) shows a  $\Delta pK_a = 0.34$  due to change in solvent, in good agreement with a value of 0.32 interpolated from the data of Juillard.<sup>24</sup>

The first stepwise acidity constant of **2** determined from a fluorimetric titration is 10.21,<sup>30</sup> in good agreement the value of 10.14 determined here by direct titration. The acidity constants of **3** have been previously examined by Wulff,<sup>31</sup> and independently by Anslyn, Canary, and co-workers:<sup>27</sup> both report a value of 5.3 for the second stepwise protonation in water. Our value in methanol/water is fortuitously identical. More importantly, Anslyn et al. showed by <sup>11</sup>B NMR that the monoprotonated species (**4**) was tetrahedral at boron.<sup>27</sup> The equilibria can this be formulated as Eq. 3:

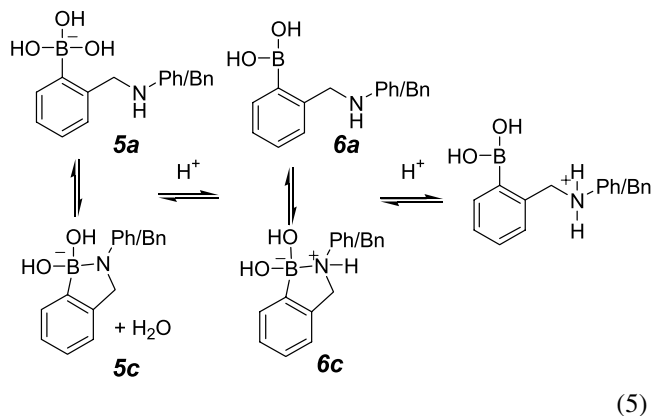


The extent of any B–N interaction in the closely related **2** system is unknown. At the limit of no interaction, the equilibria would be as shown in Eq. 4:



<sup>‡</sup> We also determined  $pK_a$  (**1**) =  $8.78 \pm 0.06$  ( $I=0.05 M$  NaCl) and  $8.79 \pm 0.05$  ( $I=0.1 M$  NaCl). If the free boronic acid binds chloride ion, the apparent 1:1 binding constant  $< 0.5 M^{-1}$  from these data. Any chloro complexes were ignored in the subsequent analysis.

To the extent that a B–N interaction occurs, it may be formulated as a dehydration equilibrium of the boronate, or a simple Lewis acid–Lewis base reaction of the boronic acid. The general case is illustrated in Eq. 5, where acyclic forms (**5a**, **6a**) are shown in equilibrium with cyclic forms (**5c**, **6c**). The potentiometric titration technique cannot distinguish between these pairs of structures, which have the same stoichiometry or which differ only by a molecule of water, since the water is taken to be at constant concentration by definition. In the most general sense, the **2** and **3** systems are similar, with experimental evidence favoring predominantly the cyclic forms over the acyclic forms for **3**.



## 2.3. Saccharide binding

The logarithm of the stepwise binding constants  $K_{tet}$  and  $K_{trig}$  (as defined in Eq. 1) for the three boronic acids can be derived from the  $\log \beta$  values to give the data in Table 1.<sup>§</sup> The derived data for **1** compare well with some literature values. For example,  $\log K_{tet}$  for **1** + fructose has been reported as 3.55,<sup>25</sup> 3.64,<sup>15</sup> and as a range of values up to 3.77.<sup>21</sup> Other values for **1** in water with the remaining diols are in good agreement with Lorand and Edwards' values,

**Table 1.** Logarithm of derived stepwise constants for saccharide binding<sup>a</sup>

Diol	<b>1</b> <sup>b</sup>	<b>1</b> <sup>c</sup>	<b>2</b> <sup>c</sup>	<b>3</b> <sup>c</sup>	
Fructose	$\log K_{tet}$	3.8	3.7	4.1	4.0
	$\log K_{trig}$	$< -1.4$	$-0.5$	1.1	2.0
Glucose	$\log K_{tet}$	2.3	2.2	2.4	2.1
	$\log K_{trig}$	$-0.3$	$-0.8$	0.3	1.0
Mannitol	$\log K_{tet}$	3.4	3.5	4.1	2.4
	$\log K_{trig}$	0.3	0.7	1.8	1.2
Sorbitol	$\log K_{tet}$	3.9	3.8	3.2	2.6
	$\log K_{trig}$	0.8	1.0	0.5	1.3

<sup>a</sup> At 25 °C;  $\log K \pm 0.2$ (fructose/glucose) or  $\pm 0.15$ (mannitol/sorbitol).

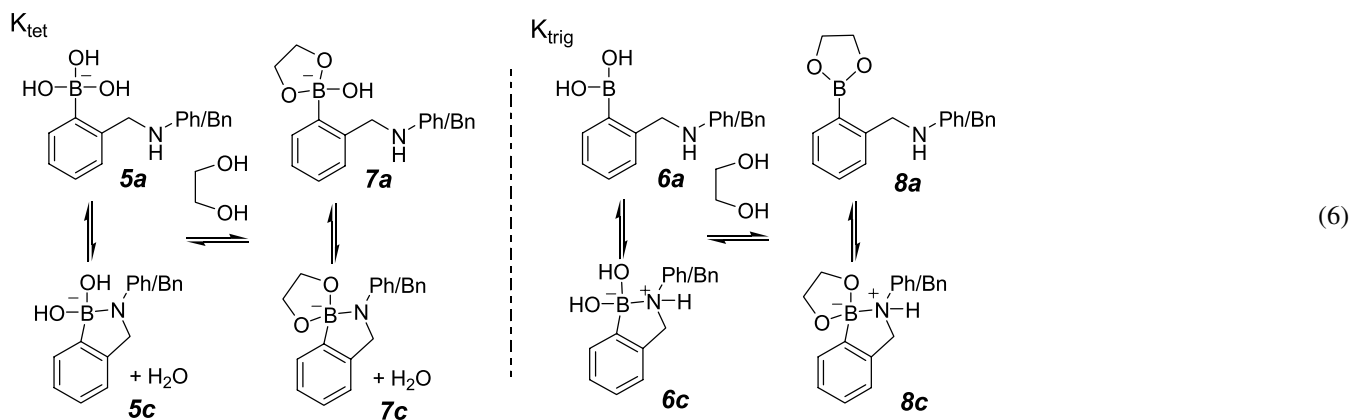
<sup>b</sup> 0.5 M NaCl in water.

<sup>c</sup> 0.1 M NaCl in methanol/water 1:2 (vol/vol).

<sup>§</sup> The mannitol and sorbitol systems have  $\log K_{tet} = \log \beta_{011}$  and  $\log K_{trig} = \log \beta_{111} - \log \beta_{110}$  (boronic acid  $pK_a$ ). Fructose and glucose are sufficiently acidic that their  $pK_a$  values must be considered, thus  $\log K_{tet}$  for **1** + fructose =  $\log \beta_{111}$  (**1** + fructose) –  $\log \beta_{101}$  (fructose  $pK_a$ ) =  $15.72 - 11.95 = 3.8$  (in water), and  $\log K_{trig}$  (**1** + fructose) =  $\log \beta_{211}$  (**1** + fructose) –  $\log \beta_{101}$  (fructose  $pK_a$ ) –  $\log \beta_{110}$  (**1**  $pK_a$ ) =  $19.3 - 11.95 - 8.70 = -1.4$  (in water). The glucose systems, and the complexes of **2** and **3** are calculated similarly.

as is the agreement with the value of 0.6 for  $\log K_{\text{trig}}$  for **1** + mannitol.<sup>15</sup> Our values lie within the ranges of  $\log K_{\text{trig}}$  reported for glucose and sorbitol, but our value for the **1** + fructose complex is more negative than the lowest value previously reported.<sup>21</sup> The shift to methanol/water solvent has very little effect on the values of  $\log K_{\text{tet}}$ , as previously assumed.<sup>32</sup> All four saccharides show significant stabilization of the trigonal complex for the shift to the less polar solvent, consistent with a shift to weaker acidity of the boronic acid as noted above.

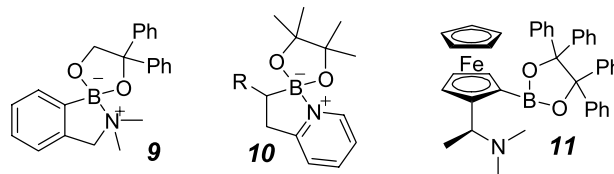
The substituted phenylboronic acids **2** and **3** offer two possible ways to formulate the  $K_{\text{tet}}$  and  $K_{\text{trig}}$  equilibria (Eq. 6), depending on the extent of the B–N interaction (no B–N interactions **7a**, **8a**; full B–N interaction **7c**, **8c**). As already noted, the potentiometric technique does not allow a distinction between species of the same stoichiometry (**8a,c**) or that simply differ in the number of water molecules (**7a,c**).



There are some significant differences in values in Table 1 in the two trend directions between the three boronic acids (rows) and four saccharides (columns). The mannitol and sorbitol values of  $\log K_{\text{tet}}$  are unexpectedly low for **3** relative to fructose and glucose or to **1** and **2**. At the same time, the values of  $\log K_{\text{trig}}$  for **3** with fructose and glucose appear to be unexpectedly high. There must be specific secondary structural effects beyond the simple diol–boronate interaction, presumably related to the extent of B–N interaction in the starting and final complexes. The similarities between **1** and **2** relative to **3** suggest that the B–N interaction is much less important in **2** than it is in **3**, that is, that the complexes of **2** are better formulated as **7a** and **8a**, while the complexes of **3** are better formulated as **7c** and **8c**.

The available structural evidence in related systems indicates that the extent of B–N interaction is a balance of steric and electronic factors. Compound **9** shows a B–N distance of 175.4 pm in the solid state,<sup>33</sup> and <sup>11</sup>B NMR indicates substantial B–N interaction in compound **10**.<sup>34</sup> Conversely, **11** shows no B–N interaction in the solid-state or in solution.<sup>20,35</sup> An analysis of 144 solid state and gas phase structures of coordinative B–N complexes concludes that steric interactions and/or ring strain can elongate the B–N bond with concomitant reduction in the tetrahedral character at boron.<sup>36</sup> Compound **9**, which involves the same

type of chelate ring as postulated in **8c**, shows a B–N distance near the long end of the range observed for boronate complexes.<sup>36</sup> Thus the increased steric bulk and the lower N basicity as benzyl is changed to phenyl between **3** and **2** could be sufficient to shift the complexes from **7c/8c** for **3** to **7a/8a** for **2**.



Species distribution diagrams calculated<sup>37</sup> for individual systems under comparable conditions illustrate the effects of the competing equilibria. Figure 1 shows the distribution of species formed at  $[B] = [D] = 0.05$  M as a function of pH for

the three boronates with fructose and mannitol. The conditions presented were chosen to bring out the weaker complexes, particularly the very minor trigonal fructose complex of **1** (species 211). The key feature evident in Figure 1 is the relative abundance of the monoprotonated saccharide complexes of **2** and **3** relative to the analogous species formed from **1**. Since the monoprotonated boronates in this pH region are tetrahedral,<sup>27</sup> is likely that the tetrahedral formulation persists into the diol complexes where the B is expected to be more Lewis acidic. The diprotonated species must be nominally trigonal at boron (monoprotonated for **1**), and these species only become significant in acidic solution. The combined effect of the boronic acid  $\text{p}K_{\text{a}}$  and the stabilization afforded by diol binding means that at pH 4, the fructose complexes of **1** are negligible, and amount to only 18% of the total **3** speciation, but amount to 40% of the total **2** speciation. In the mannitol + **2** system, complex 211 persists even at pH 2. Thus the adjacent basic site significantly alters the pairwise saccharide–boronic acid interaction despite the fact that this diprotonated complex must be trigonal at boron, that is, the anilino nitrogen is protonated and therefore not coordinated to B (**8a** plus a proton on N).

The diol complexes are stronger acids than the parent boronic acids. For a simple monoboronic acid such as **1** the apparent acidity constant of the complex is  $K'_{\text{a}}$  as

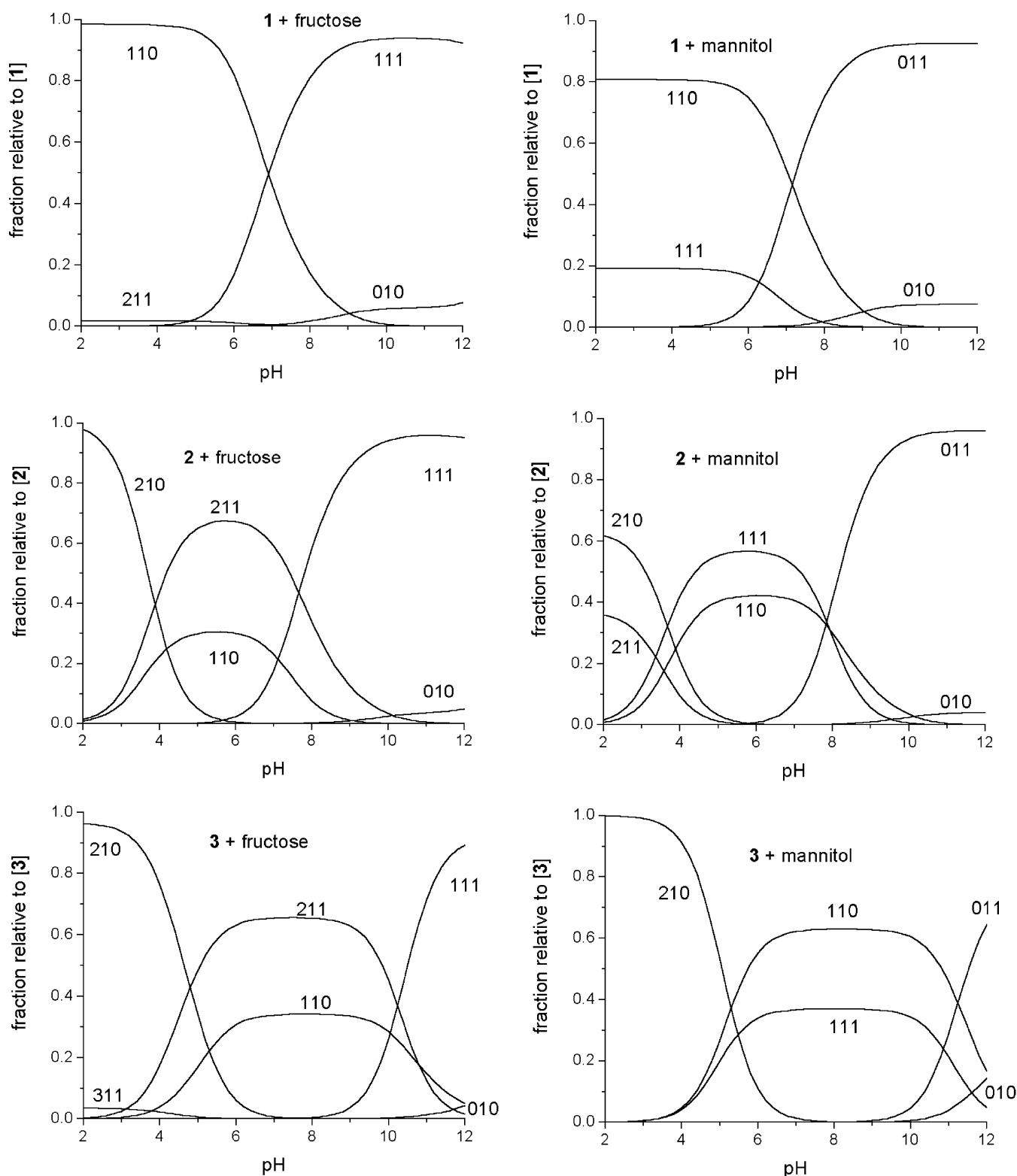


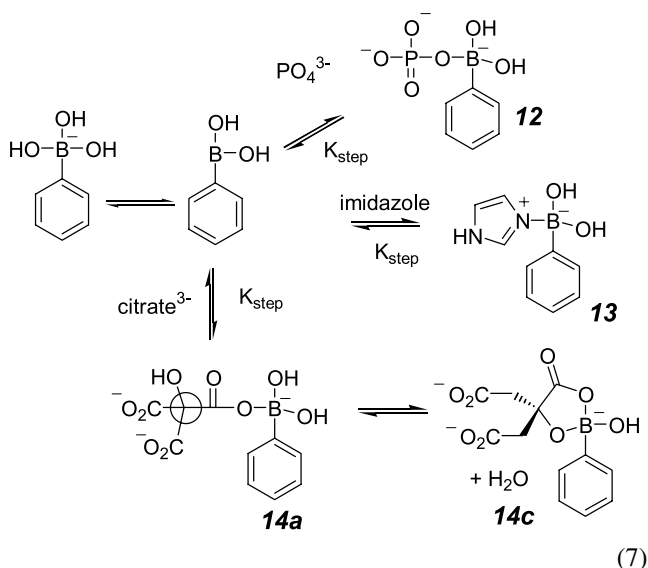
**Figure 1.** Species distribution diagrams calculated<sup>37</sup> for equimolar saccharide + boronate binary mixtures at a concentration of 0.05 M. Curve labels give the  $h+b+d$  stoichiometry of the species.

defined in Eq. 1, which is equal to  $K_a K_{tet} / K_{trig}$  (or  $pK'_a = pK_a + \log K_{trig} - \log K_{tet}$ ). For **1** with fructose  $pK'_a = 9.04 + (-0.5) - 3.7 = 5.2$ . More complex equilibria can be treated similarly, but it is more useful to consider the conditions where the free boronic acid has an equivalent concentration to the saccharide complex for a given boronate–saccharide mixture.

From **Figure 1** the **3** + fructose system gives a value of about pH 4.8 while the **2** + fructose system gives a value of pH 4.0, both for the crossing of the 210 (boronic acid) and 211 (complex) curves. Thus the fructose complexes of **2** can collectively be considered as stronger acids than the **3** + fructose complexes under comparable solution compositions.

## 2.4. Binary complexes of boronic acids with Lewis bases

Given the known medium dependence of boronate equilibria,<sup>21</sup> it was not surprising to be able to detect binary complexes of citrate, imidazole and phosphate with all three boronic acids. The majority of the complexes detected can be conceptually derived from a stepwise equilibrium of the ‘free’ boronic acid ( $h+b+x$  species 110) accepting a Lewis base according to Eq. 7 to produce a species with  $h+b+x=111$  stoichiometry. Over a range of pH in the titration, a series of phosphate and citrate conjugate bases is formed (phosphate, hydrogen phosphate, dihydrogen phosphate, etc) which produces protonated forms of the complexes illustrated. It is likely that these additional protonations would occur on the citrate and phosphate oxygens. The citrate complexes of Eq. 7 could be formulated as a single Lewis acid–base interaction with one of the three carboxylates as in **14a**, or as a chelate interaction of the central hydroxy acid as in **14c**. Although a bis-boronic acid is reported to show high affinity for some  $\alpha$ -hydroxy acids,<sup>38</sup> the cyclic formulation **14c** is incompatible with the ternary complexes discussed below. Values computed for the stepwise equilibria forming the various detected species are given in Table 2 ( $\log K_{\text{step}} = \log \beta_{n11} - \log \beta_{110} - \log \beta_{(n-1)01}$ ).



Additional species with  $h+b+x=011$  stoichiometry are also detected in a few cases. For the imidazole complexes these are simply derived by deprotonation of the 111 complex **13**. For phosphate and citrate there is no

**Table 2.** Logarithm of derived stepwise constants for addition of Lewis bases to neutral boronic acids<sup>a</sup>

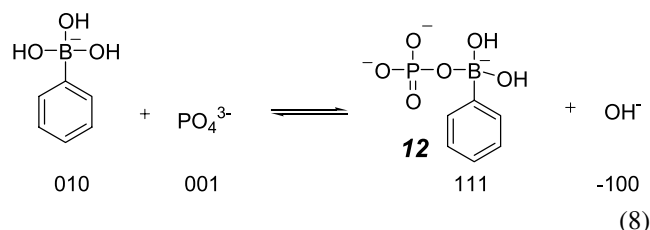
Lewis base	1 <sup>b</sup>	1 <sup>c</sup>	2 <sup>c</sup>	3 <sup>c</sup>
Citrate <sup>3-</sup>	1.5	nd	0.6	2.9
Hcitrate <sup>2-</sup>	1.8	1.6	2.0	4.2
H <sub>2</sub> citrate <sup>-</sup>	1.9	1.9	3.1	5.6
Imidazole	1.0	0.8	1.5	1.3
PO <sub>4</sub> <sup>3-</sup>	4.1	5.0	4.5	2.6
HPO <sub>4</sub> <sup>2-</sup>	1.3	2.0	2.5	1.9
H <sub>2</sub> PO <sub>4</sub> <sup>-</sup>	1.0	1.3	2.1	1.2

<sup>a</sup> At 25 °C;  $\log K \pm 0.2$ .

<sup>b</sup> 0.5 M NaCl in water.

<sup>c</sup> 0.1 M NaCl in methanol/water 1:2 (vol/vol).

dissociable proton in the 111 complexes (**12** and **14**), so these 011 complexes are best viewed as the product of a substitution reaction that generates the same product species as the above equilibrium ( $h+b+x=111$  stoichiometry) but produces a hydroxide ion as well (Eq. 8). Hydroxide ‘subtracts’ acidity from the solution so free hydroxide is the ‘-100’ species: that is, for the observed 011 species of phosphate with **1** the product is 111 + -100 (sum = 011 in the balanced equation). Other examples of this substitution reaction are discussed below.



From a structural perspective, the postulated B–O–phosphate interaction in **12** is the basic building block of borophosphate polyanions as found in the solid-state.<sup>39,40</sup> There is also a report of the role of phosphate as a catalyst for hydroxide exchange on fluorophenylboronic acids, presumably via the substitution process in Eq. 8.<sup>41</sup> Imidazolyl borate anions related to **13** are structurally characterized in the solid state.<sup>42–44</sup> Similarly, the B–O–carboxylate interaction of **14** is known from stable carboxylate esters of phenylboronic acids,<sup>27,45</sup> and the oxalate + **1** complex has been recently characterized by NMR.<sup>18</sup>

Species distribution diagrams for the phosphate and citrate systems with **1** and **3** are given in Figure 2. Some qualitative trends are evident. Firstly, the binary complexes are generally minor, except for the citrate complexes of **3** (and **2** not illustrated). High values for stepwise complexes involving PO<sub>4</sub><sup>3-</sup> are given in Table 2, but the species produced occur only at basic pH and in competition with hydroxide, so their overall contribution is small. Among the phosphate complexes, the stability increases as the charge on the incoming base, as expected for an increasing Lewis base strength along this series. Paradoxically, the opposite trend is observed for the citrate complexes, that is, the lower charged Lewis bases have the higher stepwise binding constants. The trend is statistically insignificant for **1**, but is well outside the expected experimental error for **2** and **3**. The species distribution diagrams show these complexes to be abundant into acidic solution. In fact, the free boronic acid is suppressed somewhat for **1** and virtually entirely for **2** and **3**. Complexes **12–14** are formulated as tetrahedral. The citrate anions thus allow the coordinated boronate form to persist to below pH 2. The phosphate anions are not as effective, even though the dihydrogenphosphate ion is abundant in the correct pH range. One possibility is that the cyclic form of the citrate complexes (**14c**) plays a significant stabilizing role. There also may be a complementary ‘matching’ of pK<sub>a</sub> with the boronate in which the citrate species pK<sub>a</sub>s (5.94, 4.58, 3.17) cover the range (2.3.9, 3.5.3) better than phosphate species (7.30, 2.34). Finally, the effect may relate to the hardness of the boronic acid relative to the various bases presented: base hardness increases in the order imidazole < dihydrogenphosphate < carboxylate implying



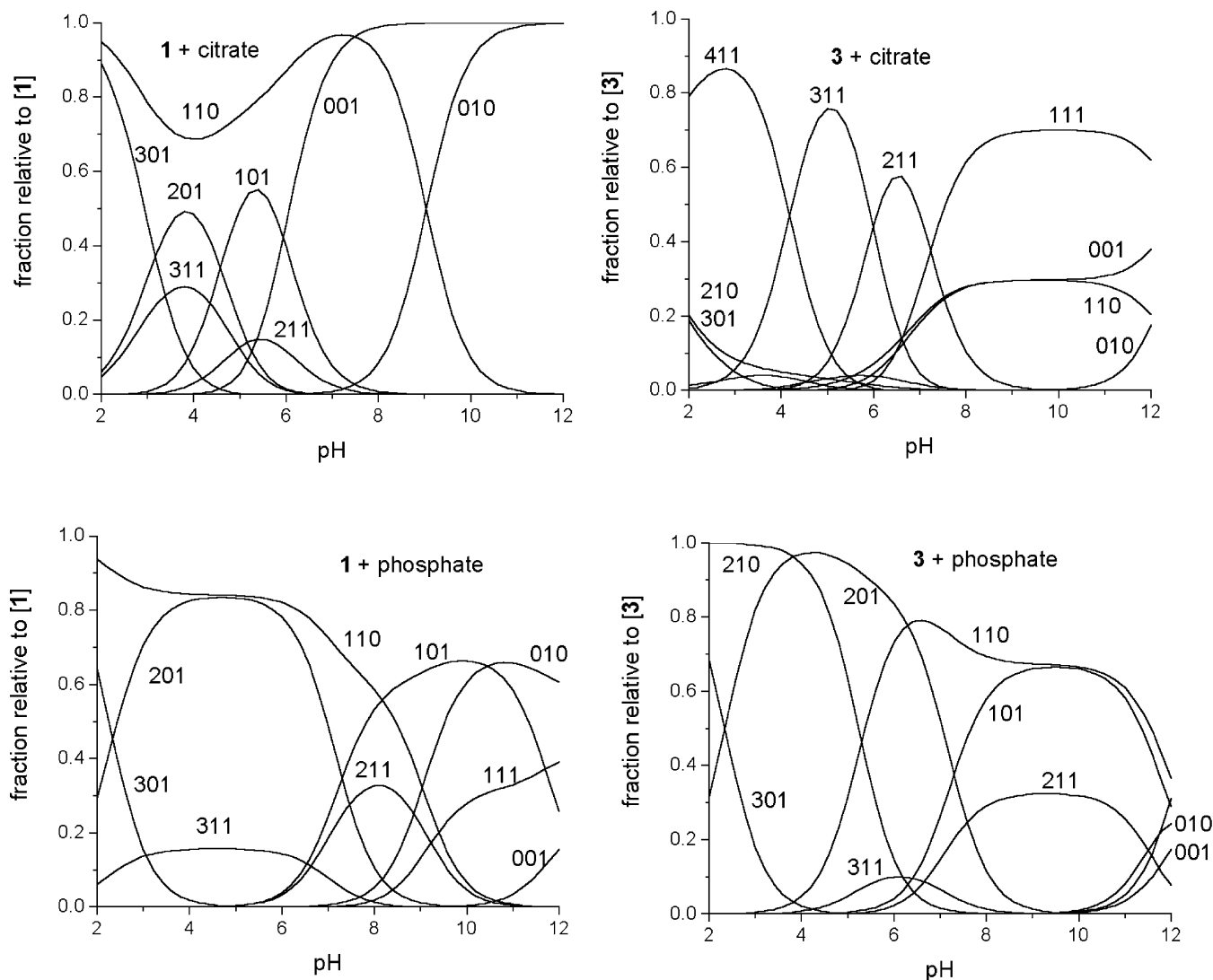
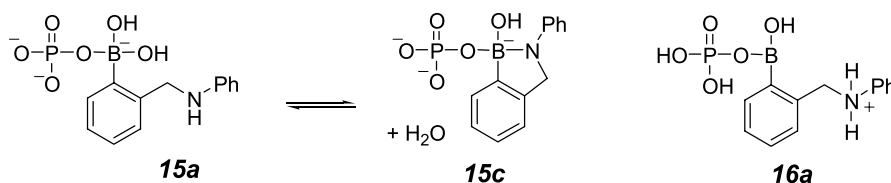


**Figure 2.** Species distribution diagrams calculated<sup>37</sup> for equimolar binary mixtures of boronates and citrate or phosphate at a concentration of 0.01 M. Curve labels give the  $h+b+x$  stoichiometry of the species.

that the boronic acid is a reasonably hard acid.<sup>46</sup> All these three factors act in the same sense and their relative importance cannot be resolved by the data determined here.

As with the other complexes of **2** and **3**, there is the potential for B–N interaction through hydration and Lewis acid–Lewis base equilibria. Some examples for the phosphate + **2** system are shown below. The  $h+b+x=111$  complex can occur as either an acyclic (**15a**) or cyclic form (**15c**). The fully protonated complex  $h+b+x=411$  complex **16a** must involve a protonated nitrogen, thus cannot involve B–N coordination (Scheme 1).



**Scheme 1.**

## 2.5. Ternary complexes of boronic acids, Lewis bases, and saccharides

Ternary complexes were detected for every combination of the three boronic acids, four saccharides, and additional Lewis bases. Under some conditions these complexes are very abundant and dominate the speciation in solution. These complexes can be rationalized as arising from the three processes already discussed namely a Lewis acid form of the diol complex adding a Lewis base, deprotonation of an imidazole complex, or a substitution of hydroxide by an incoming phosphate or citrate species. Equilibria that involve the ionization of the complexes formed in one of

**Table 3.** Logarithm of derived stepwise constants for addition of Lewis bases to trigonal saccharide complexes<sup>a</sup>

	Citrate <sup>3-</sup>	Hcitrate <sup>2-</sup>	H <sub>2</sub> citrate <sup>-</sup>	Imidazole	PO <sub>4</sub> <sup>3-</sup>	HPO <sub>4</sub> <sup>2-</sup>	H <sub>2</sub> PO <sub>4</sub> <sup>-</sup>
1+Fructose	2.9	2.8	2.7	3.1	9.6	4.1	nd
1+Glucose	2.4	2.5	nd	2.7	8.9	4	2.8
1+Mannitol	2	1.9	nd	1.9	8.3	3.1	1.8
1+Sorbitol	1.8	1.6	1.7	2.4	8.7	3.5	2.1
2+Fructose	1.5	1.2	1.5	2.4	7.4	2.9	1.6
2+Glucose	1.7	1.6	2.4	2.1	7.1	2.7	1.6
2+Mannitol	1.1	0.8	1.8	1.5	7	2.8	2.3
2+Sorbitol	3.5	3.5	3.5	2.3	7.8	3.3	2.6
3+Fructose	3.3	3.5	3.8	2.2	nd	2.4	1.3
3+Glucose	3.6	3.9	4.3	2	4.2	3.1	2.8
3+Mannitol	4.1	4.4	4.8	2.2	4.1	3.1	2.8
3+Sorbitol	4.3	4.5	nd	1.5	3.7	3.1	2.8

<sup>a</sup> At 25 °C; 0.1 M NaCl in methanol/water 1:2 (vol/vol); log  $K \pm 0.3$ ; nd=not detected, not needed for adequate fit.

the other processes can also be written, but like  $K'_a$ , these can be derived from the more fundamental complexation equilibria and the acidity of the reactants. **Table 3** gives values for the derived stepwise constants for addition of Lewis bases to the acid forms of the diol complexes ( $\log K_{\text{step}} = \log \beta_{n111} - \log \beta_{2101} - \log \beta_{(n-2)010}$  for fructose/glucose or  $\log K_{\text{step}} = \log \beta_{n111} - \log \beta_{1101} - \log \beta_{(n-1)010}$  for mannitol/sorbitol). **Table 4** gives values derived for the substitution reactions observed ( $\log K_{\text{step}} = \log \beta_{1111} - \log \beta_{1101}$  for fructose/glucose or  $\log K_{\text{sub}} = \log \beta_{0111} - \log \beta_{0101}$  for mannitol/sorbitol). Species distribution dia-

**Table 4.** Logarithm of derived stepwise constants for substitution reactions to form 0111 (or 011) complexes<sup>a</sup>

	Citrate <sup>3-</sup>	Imidazole	PO <sub>4</sub> <sup>3-</sup>
1+Fructose		0.0	3.0
1+Glucose	1.2	1.3	3.4
1+Mannitol		1.0	3.4
1+Sorbitol		1.0	3.7
2+Fructose		2.2	
2+Glucose		1.5	
2+Mannitol		0.7 <sup>b</sup>	3.6
2+Sorbitol	3.1	1.9	
3+Glucose	2.7		
3+Mannitol	4.0	2.2	3.7
3+Sorbitol	4.0	1.5	3.6
1			2.5
2	0.6	2.1	3.1

<sup>a</sup> At 25 °C; 0.1 M NaCl in methanol/water 1:2 (vol/vol); log  $K \pm 0.3$ ; values left blank are not detected, not needed for adequate fit.

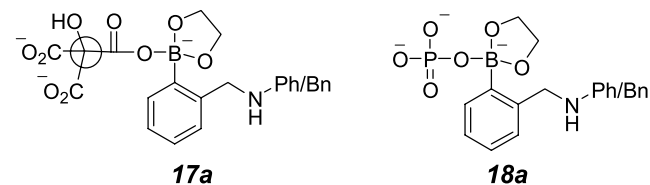
<sup>b</sup> log  $\beta \pm 0.4$ .

grams calculated for a subset of the systems investigated are given in **Figure 3**. A 1:1:3 ratio of boronate, phosphate, and saccharide was used since this ratio produced a reasonable separation of the curves across the six systems illustrated.

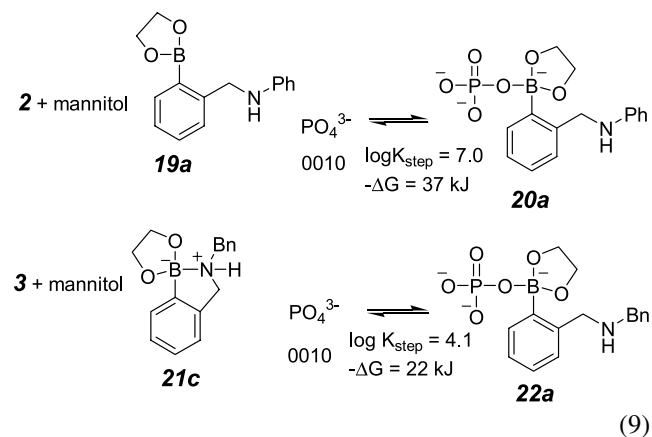
The trend noted for the binary complexes of citrate and phosphate is still prevalent: the stability of the phosphate complexes increases with the phosphate species charge, but decreases with the citrate species charge. This is presumed to be due to the factors discussed above, for example, a suitable  $pK_a$  matching with the available acids and bases leads to a stabilization of the boronate (tetrahedrally coordinated) forms into acidic solution. However, since the saccharide complexes are more acidic than the parent boronic acids, there is a better  $pK_a$  matching with phosphate, and ternary boronate–phosphate–diol complexes are significant in acidic solution, especially for the 3+

phosphate + mannitol system. The reverse is also true resulting in a poorer match with the citrate  $pK_a$ s. The net result of all the competing complexes is that the system tends to shift towards the ‘best possible’ boronate complex available from the species present at a given pH. This is seen in a comparison of the 3+phosphate versus 3+citrate complexes for the two saccharides. The binary 3+citrate complexes are well matched, thus the ternary 3+citrate + saccharide complexes are suppressed at acidic pH relative to the converse at basic pH. The comparable binary phosphate species are weak, thus the ternary 3+phosphate + saccharide species are prevalent in acidic solution. Note as well in **Figure 3** that under these conditions, the ternary complexes are the most significant species through a wide range of pH.

The ternary complexes must all be formulated without a B–N interaction in order to limit the coordination at boron to four as shown for a citrate complex **17a** and a phosphate complex **18a**. A chelate interaction of the  $\alpha$ -hydroxy acid in citrate is clearly not possible in **17a**.



Complexes **17a** and **18a** do form so the B–N stabilization energy cannot be crucial. The data allow an estimate of the energy of the interaction, through a comparison of the following equilibria (Eq. 9):



Consider the two limiting possibilities—no B–N interaction

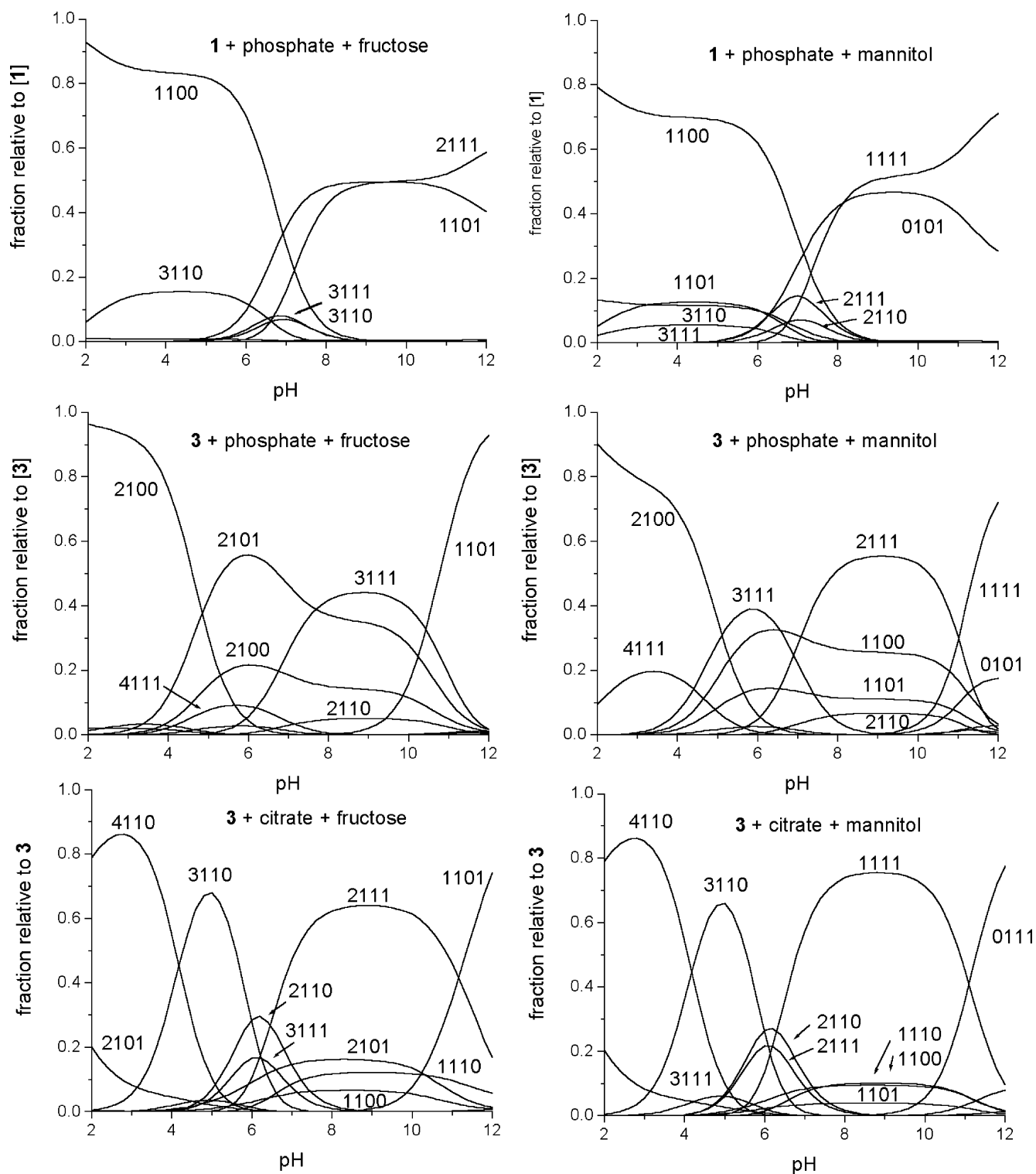


**Figure 3.** Species distribution diagrams calculated<sup>37</sup> for ternary mixtures of boronates, phosphate or citrate, and saccharides at concentrations of 0.01, 0.01, and 0.03 M, respectively. Curve labels give the  $h+b+x+d$  stoichiometry of the species.

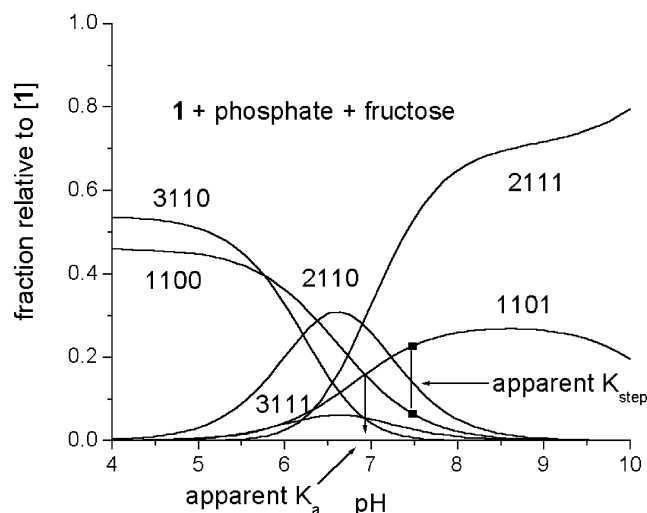
in the starting state versus a fully developed bond in the starting state. The data of Table 3 for phosphate binding suggests that **2** lies close to **1** where no B–N bond is possible. In contrast the data for the **3** + phosphate stepwise constants is significantly less than for **1** + phosphate for the three saccharides where both complexes are detected. If we take the **2** case as the value for the ‘no-bond’ condition (**19a**) and the **3** case as the value for the fully formed B–N bond

(**21c**), then the difference in  $\log K_{\text{step}}$  will be related to the extent that the B–N bond breakage (**21c** to **22a**) is unfavorable relative to **19a** to **20a** (15 kJ/mol in Eq. 9). There will be solvation differences between **2** and **3**, but these are likely to be minor as indicated by the constancy of the values for the substitution reactions that form the ternary boronate + phosphate + saccharide complexes in Table 4. Based on all possible **2**–**3** comparisons, the differences

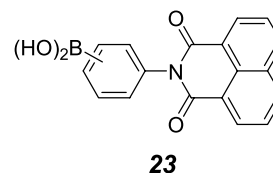
correspond to 15, 15, and 22 kJ/mol for the glucose, mannitol, and sorbitol complexes, respectively. Using **1** as the no-bond reference point gives values of 25, 22, and 26 kJ/mol for the three saccharides, respectively. Thus the B–N interaction cannot be greater than  $\sim 25$  kJ/mol, and to the extent that **21c** reflects the fully formed interaction,  $\sim 15$  kJ/mol must be about the lower bound. Thus, this interaction energy is of about the same order of magnitude as the other binding interactions observed throughout this system. A recent computational exploration of the extent of B–N interaction in a closely related system gave B–N distances within the expected range<sup>36</sup>, and estimated the interaction energy to be 13 kJ or less in the absence of solvent.<sup>47</sup> This is an important issue since the use of such B–N interactions is a basis for sensing applications of boronic acids. If this interaction were much weaker, then the internal base would not compete successfully with external bases and no signal would develop. On the other hand, if it were much stronger, binding could not disrupt the quenching, and no differential signal would develop.<sup>4</sup> This balance of energetics is essential to the sensor application, whatever the photophysical quenching mechanism might be.<sup>47</sup>

## 2.6. Comparisons with constants determined by other methods

As noted in various places above, the agreement between stepwise formation constants calculated from our data and comparable literature values is generally good. The latter are, however, a subset of the available data. Much more common are ‘apparent’ constants that depend upon the concentrations of the reactants, the medium, and the pH.<sup>7,8,10,21</sup> It is clear from the data presented that the medium dependence is related in part to the formation of additional Lewis base adducts beyond those envisaged by simple diol binding equilibria. As illustrated in the Figures, under some stoichiometric conditions these additional species can come to dominate the speciation in solution. If our data and analysis is correct, it should be possible to derive values for apparent constants from our values.



We illustrate the analysis using, as one example among many, the monoboronic acid naphthalimide derivatives **23** previously reported.<sup>11,48</sup> The formation constants (reciprocal of the reported dissociation constants) are about an order of magnitude weaker than those reported for  $K_{tet}$  for **1** in Table 1. The fluorescence titrations employed a 0.1 M phosphate buffer at pH 7.5<sup>11,48</sup> thus we expect the amount of free boronic acid available under these conditions to be diminished through the formation of phosphate complexes as well as through partial protonation of the boronate. The combined extent of these perturbations can be seen in the species distribution diagram, calculated using the concentrations reported for the titration (Fig. 4, left).



The fluorescence observed arises primarily from the free boronic acid (species 1100), while the simple boronate + fructose complex exhibits much weaker fluorescence due to quenching by the boronate.<sup>48</sup> It is reasonable to assume that the excited states of the binary and ternary boronate + phosphate complexes are at least as efficiently quenched as the simple boronate, that is, that a coordinated phosphate group is at least as effective as a hydroxyl group as a quencher. We also assume that the fluorescence lifetimes of the complexes are short relative to the complexation–decomplexation rates, thus any effect of a differential between ground and excited state binding constants would not be evident in these steady-state fluorescence experiments. The reported fluorescence lifetimes for **23** are in the nano- to pico-second range. If the complexes form at a diffusion controlled rate, the binding constants require complex lifetimes of hundreds of nanoseconds or greater. These assumptions can be collectively tested using the reported emission intensities as a function of added sugar. If

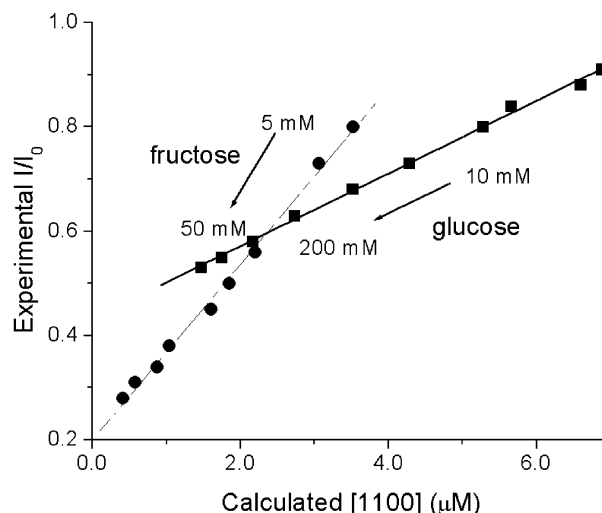


**Figure 4.** (Left) Species distribution diagram calculated<sup>37</sup> for the **1** + phosphate + fructose system under the concentrations of the fluorescence titration of meta-**23b**<sup>11</sup> ( $[1] = 3 \times 10^{-5}$  M; [phosphate] = 0.1 M; [fructose] = 0.01 M). Curve labels give the  $h+b+x+d$  stoichiometry of the species. (Right) Experimental<sup>11</sup> fluorescence intensity of meta-**23** versus the calculated<sup>37</sup> concentration of the 1100 species for a range of saccharide concentrations at pH 7.5.

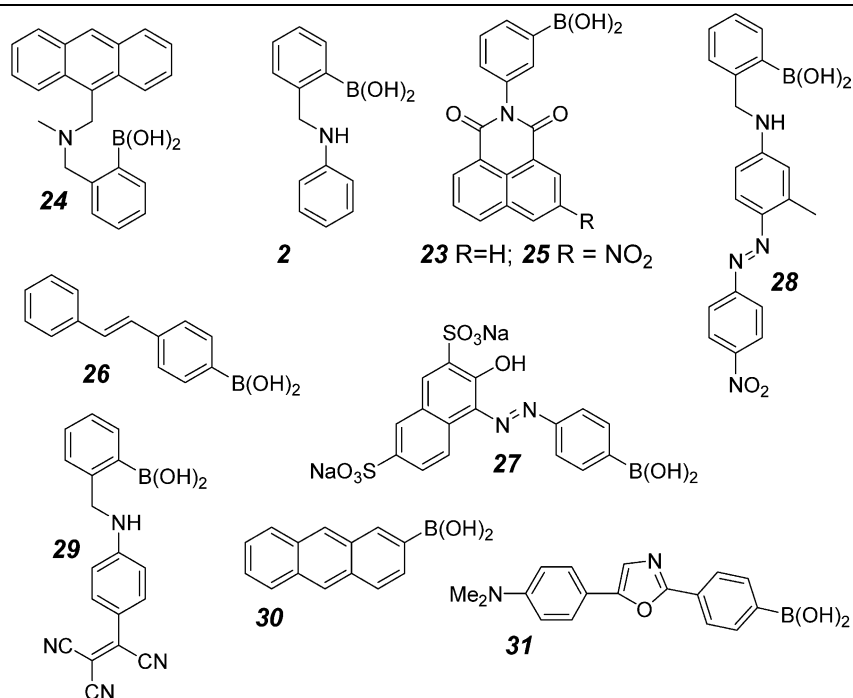
the assumptions are good, then there should be a linear relationship between the observed emission and the calculated concentration of the 1100 species (free boronic acid). If the assumptions are poor, and the phosphate species make a significant contribution to the observed fluorescence intensity or the excited state complex binding constants play a significant role, then a non-linear relationship of intensity with [1100] would be expected since these processes vary independently of [1100]. The right panel of Figure 4 shows the result for both fructose and glucose calculated assuming that **23** will behave the same way as **1**. The total fluorescence intensity is directly related to the calculated equilibrium concentration of the boronic acid alone. Thus, even though phosphate complexes dominate the solution speciation over the entire pH range, these are effectively 'invisible' by the fluorescence technique utilized.

At pH 7.5, the concentrations needed for the calculation of the apparent stepwise association constant are indicated by the points on Figure 4 (left): apparent  $K_{\text{step}} = [1101]/([1100][0001])$  where the free fructose concentration ([0001]) is essentially the stoichiometric concentration since it is present in a very large excess. The values calculated ( $\log K_{\text{step}} = 1.3$  for glucose, 2.8 for fructose) compare well with the experimental values reported for the *ortho* isomer of **23** ( $\log K_{\text{step}} = 1.24$  for glucose, 2.79 for fructose) or the *meta* isomer of **23** ( $\log K_{\text{step}} = 1.34$  for glucose, 2.88 for fructose).<sup>48</sup>

This methodology involving the inclusion of the phosphate complexes at a defined pH correctly reproduces the extent to which the apparent formation constant is lower than the values determined in Table 1 for a large number of similar studies where the buffer concentrations are reported (Table 5). For

**Table 5.** Comparison of experimental and calculated apparent saccharide binding constants for previously reported systems

Sensor	Saccharide	log $K$ expt	log $K$ calcd	Expt – calc	Reference compound
<b>24</b> <sup>19</sup>	Fructose	3	2.3	0.7	<b>3</b>
	Glucose	1.8	1.7	0.1	<b>3</b>
<b>2</b> <sup>30</sup>	Fructose	2	2.1	–0.1	<b>2</b>
	Glucose	1.3	1.6	–0.3	<b>2</b>
<b>23</b> <sup>48</sup>	Fructose	2.9	2.7	0.2	<b>1</b>
	Glucose	1.3	1.3	0	<b>1</b>
<b>25</b> <sup>11</sup>	Fructose	2.7	2.7	0	<b>1</b>
	Glucose	1.6	1.8	–0.2	<b>1</b>
<b>26</b> <sup>49</sup>	Fructose	3	3	0	<b>1</b>
	Glucose	2	1.8	0.2	<b>1</b>
<b>27</b> <sup>50</sup>	Fructose	2.2	2.1	0.1	<b>1</b>
	Glucose	0.4	0.4	0	<b>1</b>
<b>28</b> <sup>51</sup>	Fructose	2.5	2.2	0.3	<b>2</b>
	Glucose	1.5	1.6	–0.1	<b>2</b>
<b>29</b> <sup>52</sup>	Fructose	2.2	2.1	0.1	<b>2</b>
	Glucose	0.9	1.6	–0.7	<b>2</b>
<b>30</b> <sup>53</sup>	Fructose	2.4	2.5	–0.1	<b>1</b>
	Glucose	2.7	2.1	0.6	<b>1</b>
<b>31</b> <sup>54</sup>	Fructose	1.4	1.1	0.3	<b>1</b>





each system, a suitable model compound was chosen (**1**, **2**, **3**) and the equilibrium speciation was calculated for a range of saccharide concentrations.<sup>37</sup> The computed equilibrium concentration of the boronate complex, or of the free boronic acid over the range of saccharide concentrations was then fit to a 1:1 binding model to derive a value for the apparent  $K$ . This method is a bit more complex than the single point procedure indicated in the discussion of Figure 4 but avoids making any assumption about the free saccharide concentration. Table 5 shows a few large discrepancies between the experimental and the calculated values of the apparent constants but the average difference over the set is 0.05 with an average absolute deviation of 0.2. This is well within the precision of the input values. We conclude that the formation constants determined here adequately reproduce the apparent constants reported previously by a number of authors in a wide variety of systems. At the same time, we recognize that the photophysics of the individual systems might not support the assumptions made in the analysis, but there is too little photophysical data to evaluate this potential problem at this time.

Another experimental parameter that is frequently determined is the apparent  $pK_a$  at a given saccharide concentration. Returning to the example of **23**, the left panel of Figure 4 shows this  $pK_a$  value as equal to the pH where the free boronic acid concentration is equal to the boronate complex concentration, that is, where  $[1100]=[1101]$ . For the 0.01 M fructose concentration in the Figure, the apparent  $pK_a$  is predicted to be 6.9. The  $pK_a$  values reported for *ortho*-**23** are 6.0 at 0.05 M fructose and 7.2 for 0.2 M glucose.<sup>48</sup> Under directly comparable concentration conditions the calculated values based on **1** (6.2 for fructose and 7.1 for glucose) are in reasonable agreement with experiment. In principle we could determine these apparent  $pK_a$  values for a range of compounds, akin to the process that lead to Table 5. This is not particularly useful, as electronic effects on the  $pK_a$  of the boronic acid are significant, and our three model compounds are insufficient to cover the range of cases.

An extensive set of data, of apparent  $pK_a$  values of saccharide complexes of **1** as a function of saccharide concentration, has been reported.<sup>21</sup> The experiment utilized the change in absorbance at 268 nm due to a differential molar absorptivity between tetrahedral boronate complexes and trigonal free boronic acid to determine apparent  $pK_a$  values by UV titration. Making the same assumptions as above, that is, that the phosphate complexes behave similarly to the hydroxo complexes allows computation of a curve of apparent  $pK_a$  as a function of saccharide concentration using the appropriate cumulative constants. The theoretical<sup>37</sup> and experimental<sup>21</sup> values are compared in Figure 5 (left) which correctly reproduces the trends for the three compounds with an offset of about 0.3  $pK$  units. This reflects the weakness of the assumption that the phosphate and hydroxo complexes have similar molar absorptivities. Even with this caveat, this result further confirms that apparent values can be derived from the cumulative formation constants determined. We note as well that the apparent asymptote of these curves was used as a surrogate value for  $pK'_a$ .<sup>21</sup> This is not correct, as the asymptotic value depends on both the pH and the phosphate concentration, whereas  $pK'_a$  should be completely independent of any concentration term. As noted above,  $K'_a = K_a K_{trig}/K_{tet}$  thus  $pK'_a = 3.5, 5.6$  and  $6.1$  for fructose, sorbitol, and glucose, respectively. These must be compared with reported values of 4.6, 5.7 and 6.8 derived as in Figure 5, which are only apparent values in 0.1 M phosphate buffer.<sup>21</sup> The reasonable agreement in the sorbitol case is simply due to the contribution of the trigonal sorbitol complex (1101) that effectively suppresses competition from phosphate complexes in this system. This incorrect interpretation of the meaning of the asymptotic values means the derived values of  $K_{tet}$  and  $K_{trig}$  reported<sup>21</sup> are also incorrect by an unknown factor. These cannot be re-evaluated as was done in Table 8 without recourse to the original titration data (unpublished).<sup>21</sup>

The effect of phosphate complexation on an apparent formation constant (Fig. 5, right panel) has also been reported.<sup>21</sup> The diol in this case is Alizarin Red S (**32**), and the apparent constants were determined from a fluorescence

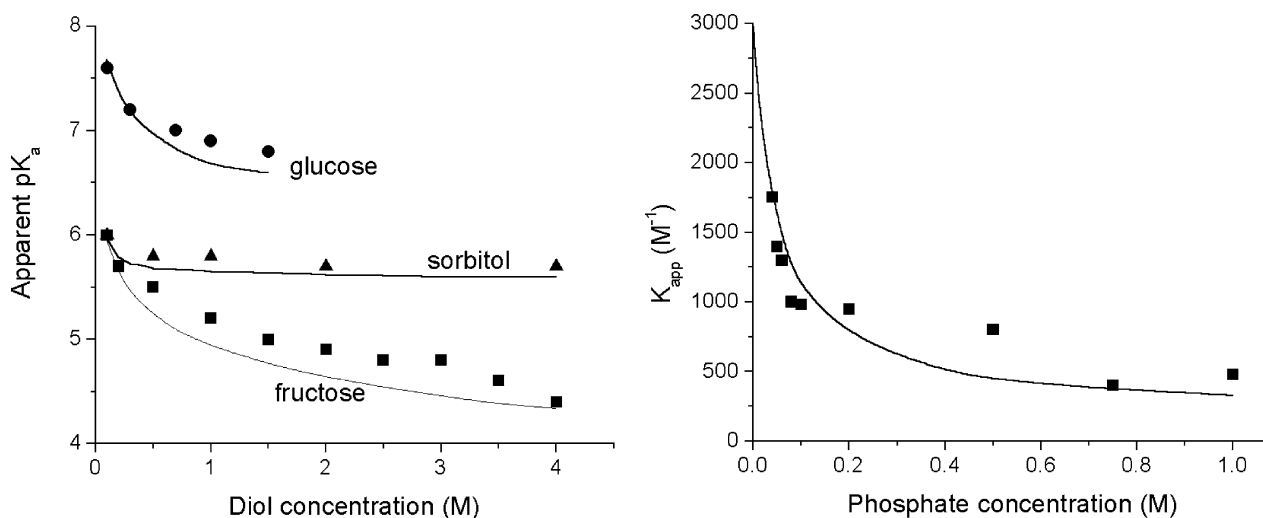
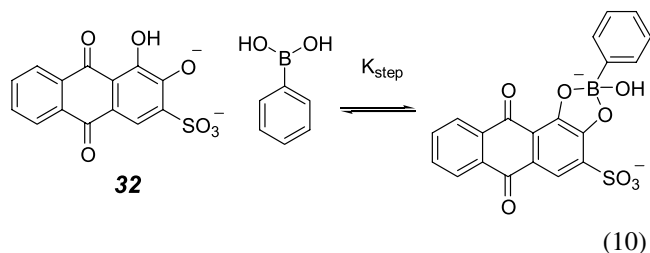


**Figure 5.** (Left) Apparent  $pK_a$  of **1** as a function of diol concentration. Data of reference;<sup>21</sup> lines calculated using cumulative formation constants determined here. (Right) Apparent association constant for **1** and Alizarin Red S as a function of total phosphate concentration. Data of reference;<sup>21</sup> line calculated as described in text based on cumulative formation constants determined here.

titration (data given in the reference). At the pH of the experiment, **32** is monoprotonated, so a minimum of three constants are required to calculate the required concentrations for comparison with experiment: two  $\text{pK}_{\text{a}}$ s given as 5.5 and 10.0<sup>21</sup> and a value for the formation constant in the absence of phosphate ( $\log \beta_{2101}$ ). The latter value was determined from the published titration data<sup>21</sup> by calculating the concentration of free boronic acid expected ( $[1100]$ ) at each concentration of total **1** in the titration experiment. The published intensity curve<sup>21</sup> as a function of calculated  $[1100]$  was then fit to a 1:1 binding isotherm to generate a value for the stepwise constant for the equilibrium (Eq. 10;  $K_{\text{step}}=2800 \text{ M}^{-1}$ ;  $\log K_{\text{step}}=3.45$ ). Thus  $\log \beta_{2101}=\log K_{\text{step}}+\log \beta_{1100}+\log \beta_{1001}=3.45+8.70+10.0=22.15$ . These three additional values were then used to determine the values of the apparent binding constants for the **1**+phosphate+**32** system where  $K_{\text{app}}=[2101]/([1001][1100])$ . This calculation makes the same assumption as discussed above with respect to Figure 4, namely that phosphate complexes are indistinguishable from the hydroxo complexes of the boronates and therefore are invisible. It also ignores any possible contribution by phosphate complexes of the **1**+**32** complex. Given the number of steps involved, the agreement between theory (line) and experiment (points) in Figure 5 is remarkably good. Certainly, the effect of competing phosphate complexes is correctly reproduced, thereby confirming their role in this system.



### 3. Conclusions

The species ‘detected’ in this study are not surprising as many structural analogs are known. What was unexpected was the extent to which competing ternary species complicate otherwise simple boronate–saccharide binding equilibria. We have shown that the cumulative formation constants determined allow many apparent or ‘conditional’ constants for the simple equilibria to be ‘back calculated’ for a wide variety of compounds. This confirms that the cumulative constants are consistent with much prior work, and at the same time establishes the basis for the medium dependence of such constants previously reported. Many authors argue that these apparent or conditional values are suitable for developing new applications and new sensor materials. We agree, providing that the competing equilibria do not so overwhelm the system that the changes of interest are masked. The general effect of the competing equilibria we determine here is to attenuate the response of the sensor—either fluorimetric or colorimetric—through a reduction in the concentrations of the key species needed for signal production. In the cases discussed, the competing species are invisible in the sense that they do not produce

unique signals of any sort. Their effect is indirect, but nonetheless attenuating.

It is possible to avoid many of these competing species and equilibria by avoiding buffers with significant concentrations of strongly Lewis basic components. The **1**+**32** complex stability is reported to be independent of the concentration of HEPES buffer.<sup>21</sup> Similar zwitterionic buffers (MOPS, MES, etc.) are presumably only weakly coordinating as well. Thus, it will be possible to work around these limitations in the initial laboratory stages of sensor development. At some point however, ‘real world’ samples will present inherently competing components from the sample matrix. It is reasonable to conclude that any boronic acid based sensor will potentially interact with Lewis bases from the sample, thus detection schemes where the signal is generated from the free boronic acid will be inherently disadvantaged relative to schemes in which the signal arises from a specific complex. Fluorimetric sensors generally have a potential additional complexity related to the quenching efficiency of the coordinated Lewis bases. Our results and analysis at this stage suggest that this might pose little practical difficulty since the competing species we examined appear to be closely similar to the hydroxo complexes of the boronic acid. If general, this is a very encouraging result.

## 4. Experimental

### 4.1. Materials

Phenylboronic acid (**1**, Lancaster) was azeotropically dried to the anhydride by successive removal of toluene in vacuo (3 times). The other two boronic acids were prepared by reductive amination of *ortho*-formylphenylboronic acid with the corresponding amines as follows.

**4.1.1. N-(2-Dihydroxyborylbenzyl)aniline (2).** 2-Formylphenylboronic acid (1.0 g, 6.7 mmol) was dissolved in a mixture of EtOH and toluene (90:10 vol:vol, 50 ml) then aniline (621.0 mg, 6.7 mmol) was added. A Dean–Stark trap was fixed to the reaction vessel and filled with 25 ml of the same solvent mixture. The reaction was stirred at reflux for 16 h. After cooling to 0 °C with an ice bath, sodium borohydride (1.25 g, 33.3 mmol) was added slowly to the mixture and stirred for 2.5 h at room temperature. The solvent was removed under reduced pressure. Water (100 ml) was added to the residue and the resulting solution was extracted with chloroform (3 × 100 ml). The organic phases were combined, washed with brine (150 ml) and dried over  $\text{MgSO}_4$ . The solvent was then removed in vacuo. Precipitation from chloroform/*n*-hexane afforded **2** (813 mg, 54%) as a cream-colored powder. Mp 125–129 °C;  $^1\text{H NMR}$  (300 MHz;  $\text{CD}_3\text{OD}$ ) 4.21 (2H, s,  $\text{CH}_2$ ), 6.6–6.7 (3H, m, ArH), 6.95–7.25 (6H, m, ArH);  $^{13}\text{C NMR}$  (75 MHz;  $\text{CD}_3\text{OD}$ ) 51.6, 117.4, 121.5, 126.9, 127.9, 129.8, 130.2, 132.7, 146.0, 149.1;  $m/z$  (FAB) 497.3 ( $[\text{M}+2(3-\text{HOCH}_2\text{C}_6\text{H}_4\text{NO}_2)-2\text{H}_2\text{O}]^+$ , 100%).  $\text{C}_{13}\text{H}_{14}\text{BNO}_2\cdot\text{H}_2\text{O}$  requires C, 74.72; H, 5.80; N, 6.70%; Found: C, 74.70; H, 5.97; N, 6.63.

**4.1.2. N-(2-Dihydroxyborylbenzyl)-N-benzylamine (3).**<sup>27</sup> 2-Formylphenylboronic acid (3.0 g, 20.0 mmol) was

dissolved in a mixture of EtOH and toluene (90: 10, v:v; 100 ml) then benzylamine (2.1 g, 20.0 mmol) was added. A Dean–Stark trap was fixed to the reaction vessel and filled with 25 ml of the same solvent mixture. The reaction was stirred at reflux for 10 h. After cooling, the solution was diluted with EtOH (50 ml) and cooled 0 °C with an ice bath. Sodium borohydride (3.8 g, 100.0 mmol) was then added slowly to the mixture and stirred while warming overnight to room temperature. The solvent was removed under reduced pressure. Water (100 ml) was added to the residue and the resulting solution was extracted with chloroform (3 × 100 ml). The organic phases were combined, washed with brine (150 ml) and dried over MgSO<sub>4</sub>. The solvent was then removed in vacuo. Precipitation from chloroform/*n*-hexane afforded sensor **3** (1.8 g, 37%) as a white powder. Mp 118–125 °C; <sup>1</sup>H NMR (300 MHz; CD<sub>3</sub>OD): 3.88 (2H, s, CH<sub>2</sub>–NH), 3.99 (2H, s, CH<sub>2</sub>–NH), 7.07–7.11 (1H, m, ArH), 7.21–7.23 (2H, m, ArH), 7.35–7.49 (6H, m, ArH); <sup>13</sup>C NMR (75 MHz; CD<sub>3</sub>OD) 52.6, 54.6, 124.7, 128.1, 128.7, 129.9, 130.3, 131.2, 132.1, 136.6, 142.7; FAB MS (*m*-NBA, *m/z*): 512.2 ([M + 2(3 – HOCH<sub>2</sub>C<sub>6</sub>H<sub>4</sub>NO<sub>2</sub>) – 2H<sub>2</sub>O]<sup>+</sup>, 34%); HRMS Found: [M + H + 2(3 – HOCH<sub>2</sub>C<sub>6</sub>H<sub>4</sub>NO<sub>2</sub>) – 2H<sub>2</sub>O]<sup>+</sup>, 512.1997, C<sub>28</sub>H<sub>27</sub>BN<sub>3</sub>O<sub>6</sub> requires *m/z* 512.1993.

## 4.2. Potentiometric titrations

Solutions were prepared volumetrically using degassed deionized and distilled water and HPLC grade methanol. Stock solutions of sodium chloride, sodium hydroxide, trisodium phosphate decahydrate, citric acid, fructose, glucose, mannitol and sorbitol were prepared from the solids obtained commercially in >99% purity. Hydrochloric acid titrant, diluted from concentrated HCl, was standardized bi-weekly versus sodium borate. Sodium hydroxide was prepared weekly and standardized against the primary standard, potassium hydrogen phthalate (phenolphthalein endpoint), and by direct titration with the secondary standard HCl as titrant.

The titrations were performed using a Mettler DL21 automatic titrimer with data collection to a custom macro running under Microsoft Excel. The macro controlled the functions of the titrimer via a serial port to the automatic titrimer. The titrations were performed in a closed jacketed cell at a temperature of 25.0 ± 0.2 °C under an atmosphere of nitrogen. The measurement circuit consider of: glass electrode |titration solution|glass frit|0.5 M NaCl in water or 0.1 M NaCl in 1:2 MeOH/water |glass frit| saturated KCl in water |AgCl/Ag. The system was designed to allow titration of 4.0 ml of solution. The electrode system was calibrated daily, according to the protocol outlined for the program GLEE<sup>55</sup> modified for the acid-into-base titration mode. Thus, electrolyte (0.5 M NaCl in water or 0.1 M NaCl in 2:1 M/W, 4.0 ml) and a known amount of sodium hydroxide was titrated with HCl, and the resultant strong acid–strong base curve of potential versus volume was converted via the standard concentrations to a curve of potential versus p[H<sup>+</sup>]. The required pK<sub>w</sub> value for 0.5 M NaCl in water was taken from Martell<sup>22</sup> (13.72). The pK<sub>w</sub> value in 0.1 M NaCl in 1:2 M/W (13.82) was determined by the procedure of Jameson and Wilson<sup>56</sup> using the pH meter calibrated using buffers prepared in 33.3 wt% methanol.<sup>57</sup> The curve of potential versus p[H<sup>+</sup>]

was linear between 2.4 < p[H<sup>+</sup>] < 11.4 in both solvent systems, and gave a slope of >99% of the Nernstian value and an intercept value for the electrode. Triplicate values of the slope and intercept were determined daily for use in calculation of the formation constants determined that day. The intercept value over time (weeks) was constant ± 1.6 mV, taken as the standard error. The standard error in the titer was determined from a series of gravimetric experiments to be 0.0002 ml for an aliquot volume of 0.01 ml, using the 1.0 ml buret on the titrimer.

Solutions for titration were prepared from stock solutions of the using microliter syringes and calibrated 5.0 ml volumetric flasks. Solutions in methanol water utilized methanolic stock solutions of the boronic acids, plus additional methanol as required, made to the final volume with water. All solutions included a sufficient volume of standard sodium hydroxide to fully deprotonate the boronic acid, plus the citric acid if present. A 4.0 ml sample was titrated within 2 h of solution preparation. Duplicate solutions prepared independently from the same stock solutions were routinely prepared. Each system involved at least two, and usually three different concentrations (relative stoichiometries) of the components. Concentrations and aliquot volumes were chosen to produce 30–70 significant data points from each titration to give 90–140 points per system including duplicates/triplicates.

The titrimer macro exported a formatted file for direct input to HYPERQUAD.<sup>58</sup> For each system, the individual titration curves were examined to explore the possible complexes to be considered, followed by a final computation involving one curve at each composition. The duplicate data were then computed using the same model. The refined parameters differed by less than the computed standard deviations in all cases of direct duplicates prepared from a common stock solution. HYPERQUAD produces a goodness-of-fit statistic (chi-squared) that indicates if the residuals (calculated-experimental) are normally distributed relative to a determined measurement precision.<sup>58</sup> The only species included in the input model were those required to generate a chi-squared value better than that expected for the 95% confidence level. On a practical level this means that the species usually must account for >20% of the total boronic acid concentration for some range of data in the titration curve. A preliminary survey allowed a choice of concentrations and stoichiometric ratios to ensure that the minor species fulfilled this requirement. The overall reliability of the data was determined by comparison of independently prepared replicates as discussed in the text.

At the high concentrations of saccharide required, a small but significant amount of deprotonation was noted for systems containing fructose and glucose (but not mannitol or sorbitol). Accordingly an apparent pK<sub>a</sub> was determined for these two sugars under conditions comparable to those of the other titrations where they occur in large excess relative to the other bases in the system. Sodium hydroxide, equivalent to the highest concentration of basic species expected (2 equiv for the boronate plus 3 equiv for the phosphate or citrate), was added to a variable amount of the sugar (in its protonated form). The extent of deprotonation varied up to about 35% for the lowest sugar concentration.

**Table 6.** Logarithm of cumulative association constants for protonation equilibria<sup>a</sup>

System	Species <i>hx</i>	Water <sup>b</sup>	M/W <sup>c</sup>
Citrate	11	5.36	5.94
	21	9.16	10.52
	31	11.25	13.69
Fructose	11	11.95	12.15
Glucose	11	11.98	12.16
Imidazole	11	7.16	6.71
Phosphate <sup>d</sup>	11	11.77	12.22
	21	18.29	19.52
	31	20.12	21.86
<b>1</b>	11	8.70	9.04
<b>2</b>	11	ns	10.14
	21	ns	14.03
<b>3</b>	11	ns	12.07
	21	ns	17.37

<sup>a</sup> At 25 °C; log  $\beta_{hx} \pm 0.05$ ; ns—not soluble at a concentration of 0.05 M.<sup>b</sup> 0.5 M NaCl; [X] range = 0.015–0.05 M except [fructose] and [glucose] 0.1–0.8 M.<sup>c</sup> 0.1 M NaCl in methanol/water 1:2 (v/v), [X] range = 0.012–0.025 M except [fructose] and [glucose] 0.2–0.4 M.<sup>d</sup> Includes 1:1 complex  $\text{Na}^+ + \text{PO}_4^{3-}$ ; log  $\beta = 0.6$  in water,<sup>22</sup> log  $\beta = 1.1$  in M/W.**Table 7.** Logarithm of cumulative association constants for binary systems<sup>a</sup>

System, X or D	Species, <i>hbx</i> or <i>hbd</i>	<b>1</b> <sup>b</sup>	<b>1</b> <sup>c</sup>	<b>2</b> <sup>c</sup>	<b>3</b> <sup>c</sup>
Fructose	111	15.72	15.88	16.29	16.03
	211	19.3 <sup>d</sup>	20.7 <sup>d</sup>	23.41	26.27
	311	na	na	nd	29.4 <sup>d</sup>
Glucose	111	14.32	14.39	14.98	14.23
	211	20.37	20.37	22.61	25.08
Mannitol	011	3.42	3.52	4.09	2.47
	111	8.91	9.81	11.94	13.34
	211	na	na	15.3 <sup>d</sup>	nd
Sorbitol	011	3.91	3.85	3.24	2.63
	111	9.49	10.0 <sup>d</sup>	10.62	13.33
Citrate	111	10.20	nd	10.70	14.97
	211	15.86	16.51	18.08	22.20
	311	19.75	21.49	23.76	28.19
	411	na	na	27.87	32.37
Imidazole	011	nd	nd	2.14	nd
	111	9.68	9.58	11.66	13.38
	211	na	na	18.24	20.04
Phosphate	011	nd	2.48	3.11	nd
	111	12.86	14.05	14.66	14.65
	211	21.85	23.28	24.83	26.15
	311	28.06	29.91	31.74	32.8
	411	nd	nd	35.58	nd

<sup>a</sup> At 25 °C; log  $\beta \pm 0.15$  except as noted; nd = not detected, not needed for adequate fit; na = complex of this stoichiometry not applicable.<sup>b</sup> 0.5 M NaCl in water; [B] range = 0.025–0.05 M; [B]/[X] = 0.5–1.1; [B]/[D] = 4–16.<sup>c</sup> 0.1 M NaCl in methanol/water 1:2 (v/v); [B] range = 0.012–0.018 M; [B]/[X] = 1–1.5; [B]/[D] = 15–50.<sup>d</sup> log  $\beta \pm 0.3$ .

Saccharide containing solutions were made basic and titrated within 2 h to minimize any base catalyzed decomposition. An additional complexity of phosphate containing systems is the presence of a weak sodium complex of  $\text{PO}_4^{3-}$ .<sup>22</sup> A value for the sodium-phosphate association constant was determined from titrations involving progressive substitution of tetramethyl ammonium chloride for NaCl to maintain the overall ionic strength ( $I = 0.5$  M in water;  $I = 0.1$  in 1:2 M/W), and was included

**Table 8.** Logarithm of cumulative association constants for ternary systems<sup>a</sup>

System	Species <i>hbdx</i>	<b>1</b> <sup>b</sup>	<b>1</b> <sup>c</sup>	<b>2</b> <sup>c</sup>	<b>3</b> <sup>c</sup>
Citrate + fructose	1111	17.3	nd	nd	nd
	2111	23.3	23.6	24.9	29.5
	3111	28.1	29.5	30.5	35.7
Citrate + glucose	4111	nd	34.0	35.4	40.6
	1111	15.9	15.6	nd	17.0
	2111	23.2	22.8	24.3	28.6
Citrate + mannitol	3111	28.1	28.8	30.2	34.9
	4111	nd	nd	35.6	39.9
	0111	5.7	nd	nd	6.4
Citrate + sorbitol	1111	11.7	11.7	13.0	17.5
	2111	16.7	17.7	18.7 <sup>d</sup>	23.7
	3111	nd	22.3	24.3	28.7
Imidazole + fructose	0111	5.7	nd	6.4	6.7
	1111	11.7	11.8	14.2	17.7
	2111	16.3	17.6	20.1	23.7
Imidazole + glucose	3111	nd	22.2	24.6	nd
	1111	nd	15.9 <sup>d</sup>	18.5	nd
	2111	23.5	23.8	25.9	28.5
Imidazole + mannitol	3111	na	na	32.2	34.8
	1111	nd	15.7	16.4	nd
	2111	21.7	23.1	24.7	27.1
Imidazole + sorbitol	3111	na	na	30.9	33.2
	0111	4.1	4.5	4.8 <sup>d</sup>	4.6
	1111	11.6	11.7	13.5	15.5
Phosphate + fructose	2111	na	na	19.7	22.1
	0111	4.3	4.9	5.1	4.2 <sup>d</sup>
	1111	12.1	12.0	12.9	15.4
Phosphate + glucose	2111	na	na	19.3	21.9
	1111	18.7	18.9	nd	nd
	2111	28.9	30.4	30.8	38.3
Phosphate + mannitol	3111	35.1	37.1	38.3	40.9
	4111	nd	nd	44.6	47.1
	5111	na	na	nd	51.2
Phosphate + sorbitol	1111	17.2	17.8 <sup>d</sup>	nd	nd
	2111	27.8	29.3	30.5	29.2 <sup>d</sup>
	3111	34.7	36.6	38.3	40.4
Phosphate + fructose	4111	nd	42.7 <sup>d</sup>	44.5	47.5
	5111	na	na	48.5	52.1
	0111	6.0	7.0	7.7	6.2
Phosphate + mannitol	1111	16.8	18.1	19.0	17.5
	2111	23.3	25.2	27.0	28.7
	3111	nd	31.1 <sup>d</sup>	33.7	35.6
Phosphate + sorbitol	4111	nd	nd	37.1	40.0
	0111	6.6	7.5	nd	6.2
	1111	17.3	18.7	18.5	17.1
Phosphate + glucose	2111	23.6	25.7	26.1	28.6
	3111	nd	31.6	32.7	35.6
	4111	nd	nd	36.0	39.9

<sup>a</sup> At 25 °C; log  $\beta \pm 0.2$  except as noted; nd = not detected, not needed for adequate fit; na = complex of this stoichiometry not applicable.<sup>b</sup> 0.5 M NaCl in water; [B] = [X] = 0.025 M; [B]/[D] = 8–16.<sup>c</sup> 0.1 M NaCl in methanol/water 1:2 (vol/vol); [B] = [X] = 0.012 M; [B]/[D] = 16–32.<sup>d</sup> log  $\beta \pm 0.3$ .

with the analytical sodium concentration in all systems containing phosphate

Values of the logarithm of cumulative association constants for protonation equilibria are given in Table 6, for binary systems in Table 7, and for ternary systems in Table 8.

### Acknowledgements

The support of this work by NSERC—Canada, the

University of Victoria, and the University of Bath is gratefully acknowledged. TF thanks the Chemistry Department at Bath for the stimulating environment that encouraged the development of these ideas.

### References and notes

1. Aoyama, Y. *Comprehensive Supramolecular Chemistry*; Vogtle, F., Ed.; Elsevier: Amsterdam, 1996; Vol. 2, pp 279–306.
2. Hartley, J. H.; James, T. D.; Ward, C. J. *J. Chem. Soc. Perkin Trans. 1* **2000**, 3155–3184.
3. de Silva, A. P.; Gunaratne, H. Q. N.; Huxley, A. J. M.; McCoy, C. P.; Rademacher, J. T.; Rice, T. E. *Chem. Rev.* **1997**, *97*, 1515.
4. James, T. D.; Shinkai, S. *Top. Curr. Chem.* **2002**, *218*, 159.
5. Eggert, H.; Fredericksen, J.; Morin, C.; Norrild, J. C. *J. Org. Chem.* **1999**, *64*, 3864.
6. Yang, W.; Dreuckhammer, D. G. *Angew. Chem. Int. Ed. Engl.* **2001**, *40*, 1714.
7. DiCesare, N.; Lakowicz, J. R. *Chem. Commun.* **2001**, 2022.
8. Tong, A.-J.; Yamauchi, A.; Hayashita, T.; Zhang, Z.-Y.; Smith, B. D. *Anal. Chem.* **2001**, *73*, 1530.
9. Vishnu Vardhan, K.; Xingming, G.; Shouhai, G.; Wenqian, Y.; Weijuan, N.; Sabapathy, S.; Wang, B. *Bioorg. Med. Chem.* **2002**, *12*, 3373.
10. Camara, J. N.; Suri, J. T.; Cappuccio, F. E. W.; R, A.; Singaram, B. *Tetrahedron Lett.* **2002**, *43*, 1139.
11. Cao, H.; Diaz, D. I.; DiCesare, N.; Lakowicz, J. R.; Heagy, M. D. *Org. Lett.* **2002**, *4*, 1503–1505.
12. Zhong, Z.; Anslyn, E. V. *J. Am. Chem. Soc.* **2002**, *124*, 9014.
13. Kuivala, H. G.; Keough, A. H.; Soboczenski, E. J. *J. Org. Chem.* **1954**, *19*, 780.
14. Roy, G. L.; Laferrriere, A. L.; Edwards, J. O. *J. Inorg. Nucl. Chem.* **1957**, *114*, 106.
15. Lorand, J.; Edwards, J. O. *J. Org. Chem.* **1959**, *24*, 769–774.
16. Norrild, J. C.; Eggert, H. *J. Am. Chem. Soc.* **1995**, *117*, 1479.
17. Norrild, J. C.; Eggert, H. *J. Chem. Soc. Perkin Trans. 1* **1996**, 2583.
18. Rohovec, J.; Maschmeyer, T.; Aime, S.; Peters, J. A. *Chem. Eur. J.* **2003**, *9*, 2193–2199.
19. James, T. D.; Sandanayake, K. R. A. S.; Iguchi, R.; Shinkai, S. *J. Am. Chem. Soc.* **1995**, *117*, 8982–8987.
20. Norrild, J. C.; Sotofte, I. *J. Chem. Soc. Perkin Trans. 2* **2001**, 727–732.
21. Springsteen, G.; Wang, B. *Tetrahedron* **2002**, *58*, 5291–5300.
22. Martell, A. E.; Smith, R. M. In *Critical Stability Constants*, Plenum: New York, 1976; Vol. 4.
23. Branch, G. E. K.; Yabroff, D. L.; Bettman, B. *J. Am. Chem. Soc.* **1934**, *56*, 937–941.
24. Juillard, J.; Gueguen, N. *Comp. Rend. Acad. Sci. C.* **1967**, *264*, 259–261.
25. Soundararajan, S.; Badawi, M.; Kohlrust, C. M.; Hageman, J. H. *Anal. Biochem.* **1989**, *178*, 125–134.
26. Sienkiewicz, P. A.; Roberts, D. C. *J. Inorg. Nucl. Chem.* **1980**, *42*, 1559–1575.
27. Wiskur, S. L.; Lavigne, J. J.; Ait-Haddou, H.; Lynch, V.; Chiu, Y. H.; Canary, J. W.; Anslyn, E. V. *Org. Lett.* **2001**, *3*, 1311–1314.
28. Martell, A. E.; Motekaitis, R. J. *Determination and Use of Stability Constants*; VCH: New York, 1992.
29. Yuchi, A.; Tatebe, A.; Kani, S.; James, T. D. *Bull. Chem. Soc. Jpn* **2001**, *74*, 509–510.
30. Arimori, S.; Bosch, L. I.; Ward, C. J.; James, T. D. *Tetrahedron Lett.* **2001**, *42*, 4553–4555.
31. Wulff, G. *Pure Appl. Chem.* **1982**, *54*, 2093–2102.
32. Hartley, J. H.; Phillips, M. D.; James, T. D. *New J. Chem.* **2002**, *26*, 1228–1237.
33. Toyota, S.; Oki, M. *Bull. Chem. Soc. Jpn* **1992**, *65*, 1832–1836.
34. Biedrzycki, M.; Scouten, W. H.; Biedrzycka, Z. *J. Organomet. Chem.* **1992**, *431*, 255–270.
35. Norrild, J. C. *J. Chem. Soc. Perkin Trans. 2* **2001**, 719–725.
36. Hopfl, H. *J. Organomet. Chem.* **1999**, *581*, 129–149.
37. Alderighi, L.; Gans, P.; Ienco, A.; Peters, D.; Sabatini, A.; Vacca, A. *Coord. Chem. Rev.* **1999**, *184*, 311–318.
38. Gray, C. W.; Houston, T. A. *J. Org. Chem.* **2002**, *67*, 5426–5428.
39. Zhao, Y.; Shi, Z.; Ding, S.; Bai, N.; Liu, W.; Zou, Y.; Zhu, G.; Zhang, P.; Mai, Z.; Pang, W. *Chem. Mater.* **2000**, *12*, 2550–2556.
40. Boy, I.; Stowasser, F.; Schafer, G.; Kneip, R. *Chem. Eur. J.* **2001**, *7*, 834–840.
41. London, R. E.; Gabel, S. A. *J. Am. Chem. Soc.* **1994**, *116*, 2562–2569.
42. Knop, O.; Bakshi, P. K. *Can. J. Chem.* **1995**, *73*, 151–160.
43. Effendy; Lobbia, G. G.; Pelli, M.; Pettinari, C.; Santini, C.; Skelton, B. W.; White, A. H. *J. Chem. Soc. Dalton Trans.* **2001**, 528–534.
44. Hamilton, B. H.; Kelly, K. A.; Wagler, T. A.; Espe, M. P.; Ziegler, C. J. *Inorg. Chem.* **2002**, *41*, 4984–4986.
45. Ishihara, K.; Ohara, S.; Yamamoto, H. *Org. Synth.* **2002**, *79*, 176–180.
46. Basolo, F.; Pearson, R. G. *Mechanisms of Inorganic Reactions: A Study of Metal Complexes in Solution*, 2nd ed.; Wiley: New York, 1967.
47. Franzen, S.; Ni, W.; Wang, B. *J. Phys. Chem. B* **2003**, *107*, 12942–12948.
48. DiCesare, N.; Adhikari, D. P.; Heynekamp, J. J.; Heagy, M. D.; Lakowicz, J. R. *J. Fluorescence* **2002**, *12*, 147–154.
49. DiCesare, N.; Lakowicz, J. R. *J. Phys. Chem. A* **2001**, *105*, 6834–6840.
50. DiCesare, N.; Lakowicz, J. R. *Org. Lett.* **2001**, *3*, 3891–3893.
51. Ward, C. J.; Patel, P.; James, T. D. *J. Chem. Soc. Perkin Trans. 1* **2002**, 462–470.
52. Ward, C. J.; Patel, P.; James, T. D. *Org. Lett.* **2002**, *4*, 477–479.
53. Yoon, J.; Czarnik, A. W. *J. Am. Chem. Soc.* **1992**, *114*, 5874–5875.
54. DiCesare, N.; Lakowicz, J. R. *Chem. Commun.* **2001**, 2022–2023.
55. Gans, P.; O’Sullivan, B. *Talanta* **2000**, *51*, 33–37.
56. Jameson, R. F.; Wilson, M. F. *J. Chem. Soc. Dalton* **1972**, 2607–2610.
57. Perrin, D. D.; Dempsey, B. *Buffers of pH and Metal Ion Control*; Chapman & Hall: London, 1974.
58. Sabatini, A.; Vacca, A.; Gans, P. *Talanta* **1996**, *43*, 53–65.



# Integrating chemosensors for amine-containing compounds into cross-linked dendritic hosts<sup>☆</sup>

Eric Mertz, Stephanie L. Elmer, Amy M. Balija and Steven C. Zimmerman\*

Department of Chemistry, University of Illinois, 600 S. Mathews Ave., Urbana, IL 61801, USA

Received 2 March 2004; revised 23 June 2004; accepted 19 August 2004

Available online 6 October 2004

**Abstract**—Trifluoroacetylazo dye **1**, a known chemosensor for amines, has been integrated into cross-linked dendrimer hosts. Thus, boronic acid **16** was linked to iododye **9** via a Suzuki coupling reaction. In situ deprotection and alkylation with dendrons **3** and **4**, containing 8 homoallyl or allyl ether groups, respectively, afforded dendrons **18** and **19** with chemosensor units at their focal point. Conversion of **18** (**19**) to the bis-imine of butane 1,4-diamine, extensive cross-linking via the ring closing metathesis reaction with Grubbs catalyst **25**, and hydrolysis produced dendrimer hosts **28** and **29**. Host-guest studies with a small library of amines and alcohols showed **28** and **29** to selectively signal certain diamines but not due to template mediated imprinting.  
 © 2004 Elsevier Ltd. All rights reserved.

## 1. Introduction

Developing sensors that complex ions and molecules with a distinct change in color or fluorescence (chemosensors) is a topic of considerable current interest and technological importance.<sup>2</sup> A common approach is to covalently link a recognition unit to a chromogenic reporter group.<sup>3</sup> Alternatively, the chromogenic group may complex to the recognition unit with the ligand of interest displacing it and producing the sensor's response.<sup>2c</sup> There are advantages and disadvantages to both approaches.

We recently reported a cross-linked dendritic host for diamines in which a chromogenic reporter group was covalently integrated into the dendrimer framework.<sup>4</sup> In this case, the advantage of covalently linking the chromophore within the binding unit was two-fold. First, the reporter group was designed to signal binding by covalently complexing the guest (vide infra), thus providing a direct connection between the binding and signaling events. Second, it was unclear what guests would bind making it difficult to design a priori an appropriate displacement assay. Herein we provide a full account of our efforts to integrate reporter groups into cross-linked dendritic hosts, including a comparison of two homologous dendritic frameworks.

<sup>☆</sup> See Ref. 1.

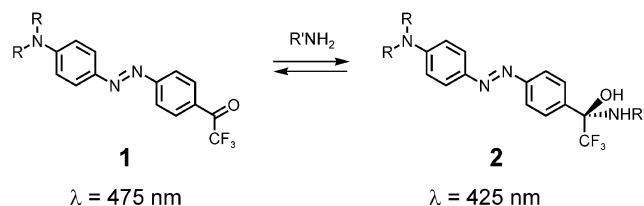
**Keywords:** Chemosensor; Dendrimer host; Diamines.

\* Corresponding author. Tel.: +1 217 333 6655; fax: +1 217 244 9919; e-mail: sczimmer@uiuc.edu

## 2. Results and discussion

### 2.1. Design of dendrons with focal point chromogenic recognition units

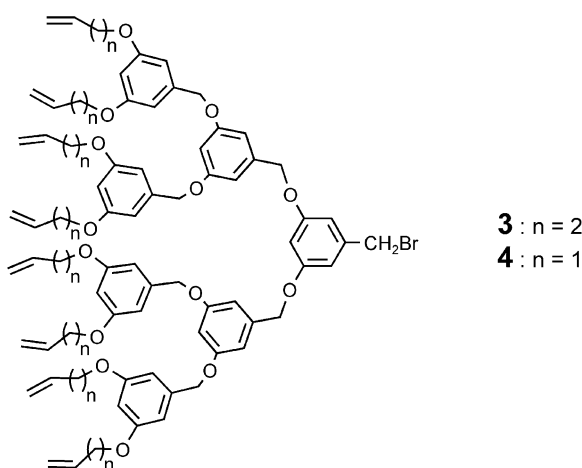
In an effort to improve the performance of molecularly imprinted polymers (MIPs)<sup>5</sup> we have taken a 'bottom-up' approach in which a single binding site is imprinted into the interior of a dendrimer (i.e., MID approach).<sup>6,7</sup> To extend this approach to new guests and integrate a chromogenic reporter group into the dendrimer, attention was turned to azo dye **1**. Building upon earlier work by Simon,<sup>8</sup> Mohr and co-workers have extensively developed **1** and its analogs as optical sensors for amines and alcohols.<sup>9</sup> Upon reversibly forming hemiaminal **2**, or the corresponding zwitterion, **1** undergoes a shift in  $\lambda_{\text{max}}$  of about 50 nm, corresponding to a visible color change from red-orange to yellow (Scheme 1). In the course of developing sensor applications, **1** has been covalently linked to several polymer matrices and imbedded in a thin layer of polyvinylchloride (PVC).<sup>9</sup>



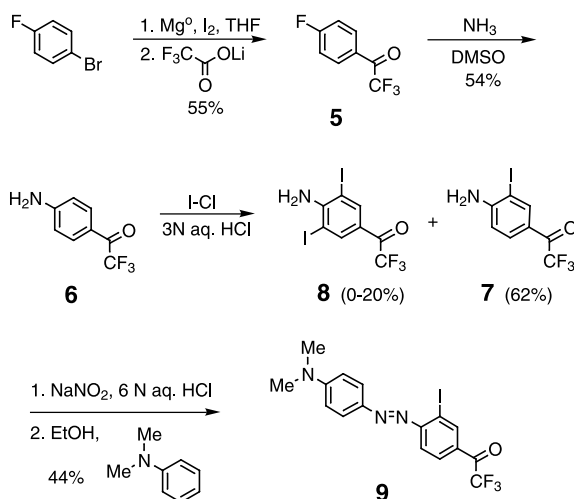
Scheme 1.

## 2.2. Synthesis of dendrons with focal point chromogenic recognition units

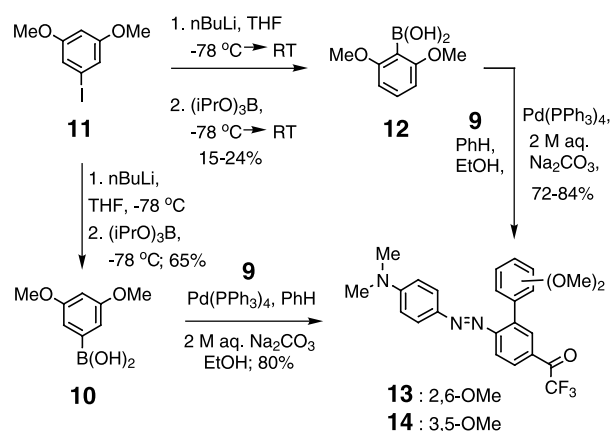
A number of dendrimers are known in which azobenzene units are present at the core, peripheral sites, and within the branching units.<sup>10</sup> In the present case, the first objective was to link azo dye **1** to dendrons **3** and **4**; **3** being the key compound used to synthesize cross-linked and cored dendrimers.<sup>11,12</sup> and to imprint porphyrins within dendrimers.<sup>6,7,13</sup> Because allyl ether-based dendron **4** is easier and less expensive to prepare<sup>14</sup> and might produce a more rigid imprint, there was interest in comparing its performance to that of **3**. To retain the planar conjugation of the donor and acceptor groups essential to the function of **1** it was decided to attach dendron **3** through an aryl substituent ortho to the azo-group. The aryl attachment was envisioned to occur through a Suzuki coupling<sup>15</sup> of iodide **9** and boronic acid **10**.



The synthesis of **9** is outlined in Scheme 2. Following the procedure of Burton,<sup>16</sup> 4-fluorobromobenzene was converted to the corresponding Grignard reagent which was subsequently added to the lithium salt of trifluoroacetic acid.<sup>17</sup> The resulting ketone **5** was treated with ammonia to afford amine **6**.<sup>16</sup> Iodination with iodine monochloride afforded **7** with variable amounts of diiodide **8** which were removed by chromatography. Diazotization and reaction with *N,N*-dimethylaniline gave key intermediate **9**.



Scheme 2.



Scheme 3.

The required boronic acid, **10**, was envisioned to arise from metal-halogen exchange of **11** followed by treatment with triisopropyl borate. In the event, a modest yield of the isomeric boronic acid **12** was obtained (Scheme 3).<sup>18</sup> As a model reaction **12** was coupled to **9** under Suzuki conditions affording **13**, whose X-ray structure analysis<sup>†</sup> (Fig. 1) confirmed the structural assignment of both **9** and **13**.

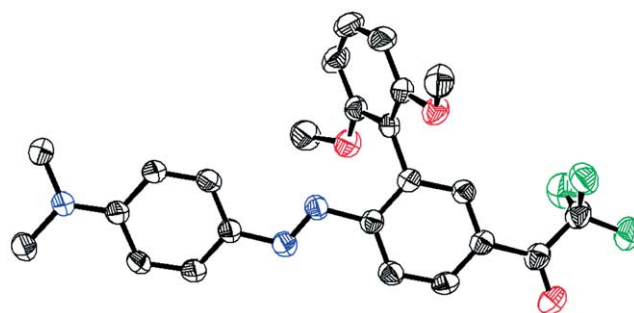
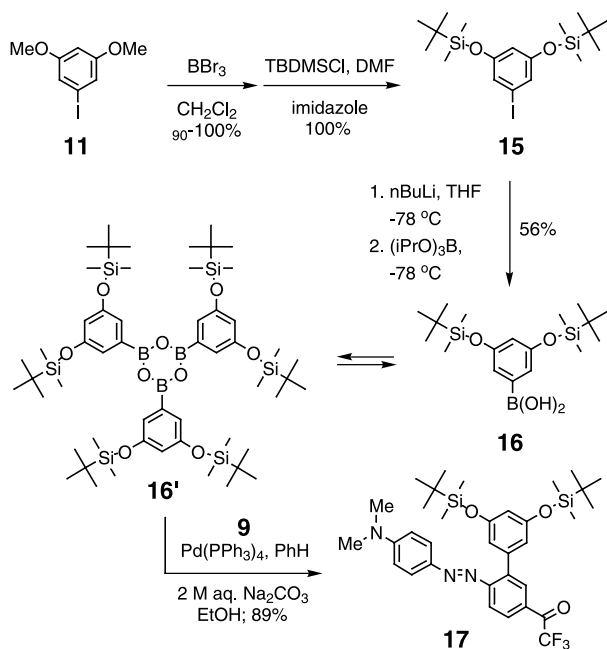


Figure 1. ORTEP diagram from X-ray analysis of **13**. Ellipsoids represent 50% probability and hydrogen atoms are removed for clarity.

Although dendrons **3** and **4** might be linked to **13** through the 2,6-dimethoxy functionality, the less sterically congested 3,5-isomer was preferred. By carefully maintaining the temperature of both the metal-halogen exchange and boronylation reactions at  $-78\text{ }^\circ\text{C}$ , the conversion of **11** to **10** was accomplished in 65% yield. Coupling of **9** and **10** under Suzuki conditions afforded **14** in 80% yield. However, attempts to demethylate the phenolic groups resulted in low yields of product and decomposition of the starting material.

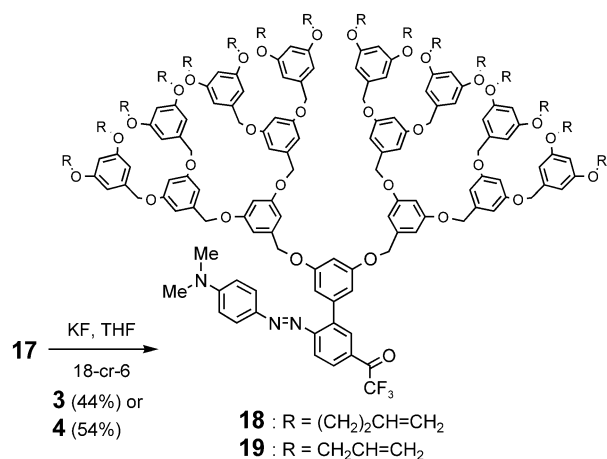
An alternative route used TBDMS protecting groups. Thus, **11** was deprotected with boron tribromide, protected with TBDMS-Cl, and boronylated to give **16** (Scheme 4).<sup>19</sup> The absence of signals corresponding to the boronic acid group in the <sup>1</sup>H NMR spectrum of **16** combined with the FD-MS spectrum showing an  $m/z = 1092$  ( $3 \times M - 3\text{H}_2\text{O}$ ) suggested that **16** trimerized to give cyclic boroxime structure **16'**. Cross-coupling of **16** with **9** gave **17**.

<sup>†</sup> CCDC 231899 contains the supplementary crystallographic data for this paper. These data can be obtained free of charge via [www.ccdc.cam.ac.uk/data\\_request/cif](http://www.ccdc.cam.ac.uk/data_request/cif) or by e-mailing [data\\_request@ccdc.com.ac.uk](mailto:data_request@ccdc.com.ac.uk).



Scheme 4.

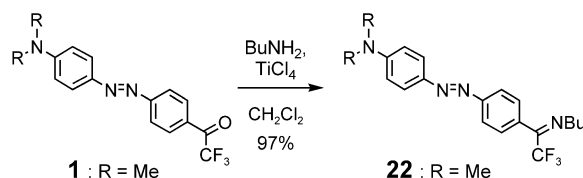
The TBDMS groups in **17** could be removed in 77% yield (TBAF, THF) and the resultant diol could be alkylated with **3** but in low yield despite exploring a range of conditions. Ultimately, a deprotection—in situ alkylation protocol was developed using KF and 18-crown-6 in THF (Scheme 5). By this method, dendrons **18** and **19** were obtained in 44 and 54% yield, respectively. Evidence that the dye unit withstood the conditions of the alkylation reaction came from the MALDI spectrum of **18**, which indicated the correct molecular weight (MW=3004), with Na<sup>+</sup> and K<sup>+</sup> adducts also present. Analytical size exclusion chromatography (SEC) also indicated a molecular weight that was consistent with alkylation product **18**. <sup>1</sup>H, <sup>13</sup>C, and <sup>19</sup>F NMR spectroscopy indicated that **18** was formed with the trifluoromethyl ketone group intact. Similarly, UV–Vis spectroscopy indicated λ<sub>max</sub> of **18** to be 480.0 nm, consistent with an unreacted trifluoromethyl ketone group.



Scheme 5.

### 2.3. Synthesis of didendrons using diamine templates

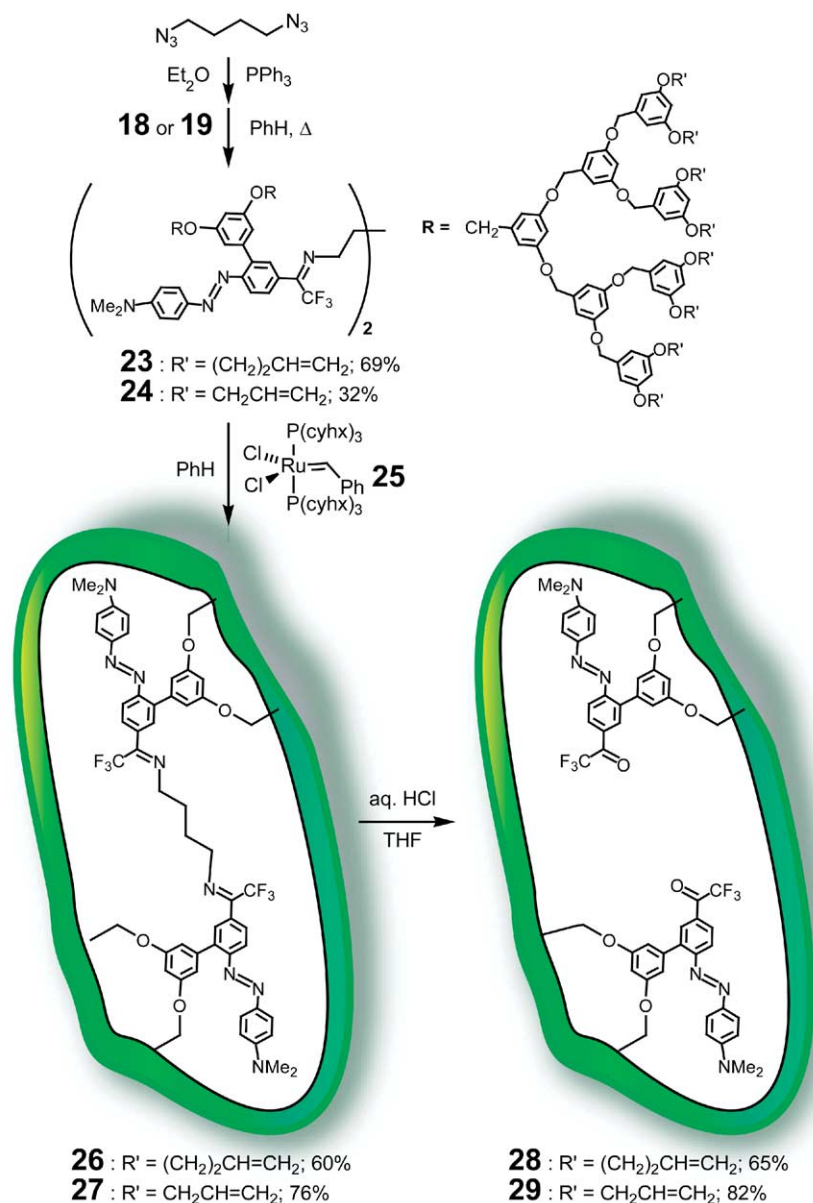
Two point covalent imprinting was examined by using 1,4-diaminobutane (**20**) as a template. Although **20** likely formed a 2:1 covalent complex with **18** (bis-carbinolamine, see **2**), it was not stable under the high-dilution conditions needed for the intramolecular cross-linking reaction. It was decided instead to link the two dendrons to the diamine core through the bis-imine.<sup>20</sup> A model study was undertaken to find conditions under which butylamine (**21**) would react with dye **1** (R=Me) to form imine **22**. The most suitable conditions found involved treating **1** with **21** and TiCl<sub>4</sub> in CH<sub>2</sub>Cl<sub>2</sub>,<sup>21</sup> the product imine (**22**) obtained in 97% yield (Scheme 6). Unfortunately, reaction of **18** with 1,3,5-tris(aminomethyl)benzene in the presence of TiCl<sub>4</sub> did not produce the corresponding tris-imine dendrimer, rather extensive degradation of **18** occurred.



Scheme 6.

In an attempt to find a more general way to attach templates to **18** (**19**), an aza-Wittig strategy was chosen because of its mild reaction conditions and compatibility with a variety of functional groups.<sup>22</sup> As shown in Scheme 7, this approach was applied to 1,4-diazidobutane. The resultant didendron, which would be imprinted with 1,4-diaminobutane, was favored over the corresponding tridendron from 1,3,5-tris(azidomethyl)benzene because of the known rearrangement of aza-Wittig products of benzylamines.<sup>23</sup> Furthermore, the smaller didendron would test the limits of the monomolecular imprinting approach, determining whether just two dendrons and two-point covalent binding are sufficient for imprinting.

The synthesis of the target didendron and its subsequent cross-linking is outlined in Scheme 7. Butane 1,4-diazide was treated with triphenylphosphine and the resultant bis(iminophosphorane) reacted immediately with either **18** or **19** to produce, respectively, bis-imines **23** and **24** in 69 and 32% yields. The didendrons were purified to homogeneity by first silica gel and then SEC. The ring closing metathesis (RCM) mediated cross-linking of **23** and **24** was performed at high dilution in benzene with Grubbs type I catalyst **25**. The cross-linked products, **26** and **27** were purified by SEC giving product in 60 and 76% yield, respectively. The extent of cross-linking in both **26** and **27** was examined by MALDI-MS. For **26** the highest peaks corresponded to 14 cross-links ( $m/z = 5242.6$ ,  $M - 14C_2H_4 + Na^+$ ) and 15 cross-links ( $m/z = 5214.5$ ,  $M - 15C_2H_4 + Na^+$ ). In the MALDI spectrum of **26**, lower intensity peaks were also evident at  $m/z$  values corresponding to 16 and 13 cross-links. The most intense peak in the MALDI spectrum of **27** corresponded to 15 cross-links, while somewhat smaller peaks for 16 and 14 cross-links were also seen.



Scheme 7.

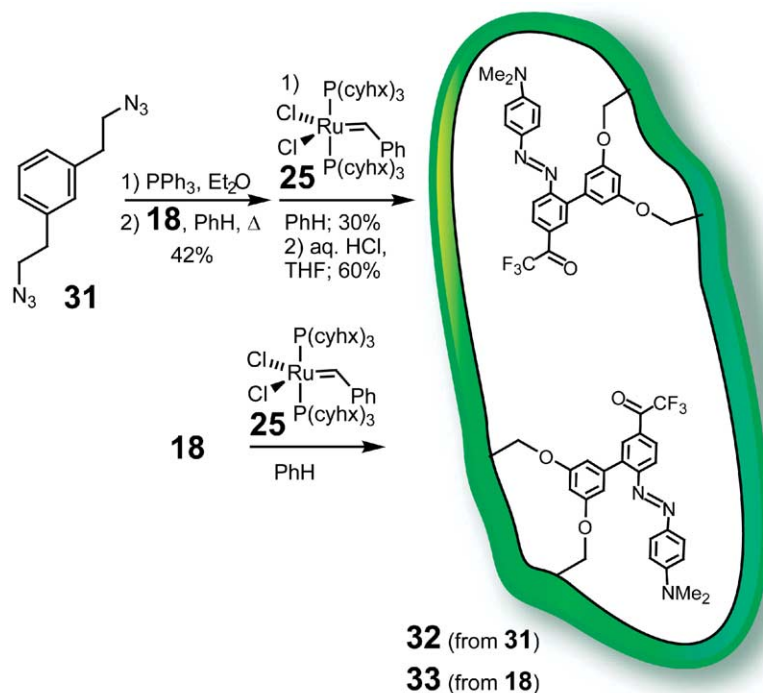
Consistent with previous investigations of cross-linked dendrimers,<sup>7,11</sup> the <sup>1</sup>H NMR spectrum of **26** and **27** showed significant broadening of signals due to the large number of isomers formed during alkene metathesis. A new, broadened signal in the  $\delta$  5.65–5.40 ppm range is particularly indicative of formation of the cross-links, as this peak corresponds to the alkene protons of newly cross-linked homoallyl ether groups. Similarly, the UV–Vis and <sup>19</sup>F NMR spectra of **23** (**24**) and **26** (**27**) indicated that alkene metathesis did not affect either the azobenzene chromophore or the imine linkages between the dendrimer core and the dendrons.

The 1,4-diaminobutane core in **26** (**27**) could be removed under mild hydrolytic conditions (Scheme 7). Stirring a solution of **26** (**27**) in THF with ~1% aqueous HCl at room temperature resulted in the hydrolyzed dendrimer **28** with two unbound ketone groups in its core. The MALDI mass

spectrum of **28** was consistent with hydrolytic removal of 1,4-diaminobutane from the core of **26**. MALDI also revealed some degradation of the dendrimer's cross-linked periphery during the hydrolysis reaction. A distribution of small peaks appeared below the molecular weight of fully cross-linked isomers of **28**. The molecular weight of these peaks matches the mass of **28** with missing homoallyl groups or their RCM counterparts. This impurity could not be removed by silica gel chromatography, and it remained in the sample of **28** used for complexation studies. In the case of **27** it was found that a very short treatment with the same aqueous acid fully removed the 1,4-diaminobutane core, but without any degradation in the cross-linked allyl ether periphery.

Two dendrimers were prepared as controls (Scheme 8). The first was synthesized identically to **28** except that 1,3-bis(amino-ethyl) benzene (**30**) was chosen as the template





Scheme 8.

because diazide **31** could be readily synthesized in two steps from commercially available 1,3-phenylenediacetic acid.<sup>4</sup> More importantly, the availability of **28** and **32** would allow application of a rigorous test of imprinting by comparing the cross-reactivities of two dendrimers derived from different templates, a method occasionally applied to MIPs.<sup>24</sup>

The second control dendrimer was prepared without a template. Thus, cross-linking of **18** at a concentration of  $10^{-3}$  M in benzene with catalyst **25** afforded a mixture of cross-linked **18**, cross-linked dimer **33**, and cross-linked trimer. Preparatory SEC readily separated the products, and the MALDI-TOF spectrum of **33** confirmed its dimeric structure and indicated 16 out of a possible 16 cross-links (intermolecular and intramolecular) were formed. The polystyrene-based molecular weight ( $MW_{\text{PS}}$ ) value of **33**,  $MW_{\text{PS}} = 3646$  is very close to that obtained for **28**,  $MW_{\text{PS}} = 3620$ , and they exhibit nearly identical NMR spectra.

#### 2.4. Complexation studies using small libraries of amine and alcohol guests

Before performing complexation studies on the cross-linked dendrimers, model titration experiments were carried out using **1** ( $R = \text{Me}$ ). Titration of a chloroform ( $\text{CHCl}_3$ ) solution of **1** ( $R = \text{Me}$ ) ( $15.6 \mu\text{M}$ ) with 10,400 equiv of butyl amine (**21**) in  $\text{CHCl}_3$  produced a 50 nm blue shift in the dye's absorbance spectrum. The overlaid spectra obtained showed only an approximate isosbestic point at 438 nm, suggesting the presence of more than two discrete species. The reactivity of **1** with **21** in  $\text{CHCl}_3$  appeared to be quite low, and, without insuring full equilibration, a very approximate 1:1 association constant ( $K_{\text{assoc}}$ ) of  $5 \text{ M}^{-1}$  was calculated in  $\text{CHCl}_3$ .

Mohr and co-workers performed titration studies of dye **1**

( $R = \text{C}_8\text{H}_{17}$ ) with primary amines in diethyl ether, and a similar binding affinity was found.<sup>9</sup> In our hands, titrations of **1** ( $R = \text{Me}$ ) in diethyl ether did not display clean isosbestic behavior, possibly due to evaporation of solvent. Ultimately THF was chosen for complexation studies because titrations of **1** ( $R = \text{Me}$ ) with butyl amine showed both clean isosbestic points and strongly enhanced covalent binding. Thus, addition of only 55 equiv of butyl amine to a THF solution of **1** ( $R = \text{Me}$ ) ( $29.6 \mu\text{M}$ ) resulted in a 31.5 nm blue shift in the absorbance spectrum of the dye. From titration studies monitoring the loss of absorbance at  $\lambda_{\text{max}} = 475 \text{ nm}$ , a  $K_{\text{assoc}} = 790 \pm 210 \text{ M}^{-1}$  was calculated. The change in  $\lambda_{\text{max}}$  and both  $^{19}\text{F}$  and  $^{13}\text{C}$  NMR spectra were consistent with the formation of a iminal **2** ( $R = \text{Me}$ ).

In examining the cross-linked dendrimers, a simple screening assay was devised in which THF solutions of **28** were prepared such that absorbance at 475 nm was ca. 0.4 ( $\sim 20 \mu\text{M}$ ). One equivalent of amine or alcohol guest was added to each dendrimer solution, and the solutions were mixed for 30 s. A UV-Vis spectrum was obtained for each solution, and the increase in absorbance at 425 nm ( $\Delta A_{425}$ ) was recorded. As seen in Figure 2, a remarkably high level of selectivity was observed for the simple alkyl diamine guests.

Qualitatively, the binding profile for **29** with the same guests and under the same conditions was very similar to that seen in Figure 2. This result suggests that the allyl ether-based dendrons, which are cheaper and easier to prepare,<sup>14</sup> serve as suitable substitutes for the homoallyl-based (Wendland-type<sup>11</sup>) dendrons, at least in the systems studied here.

Evidence for two point covalent, but reversible, complexation through formation of a bis-aminal came from several directions. First, a Job plot gave a maximum concentration



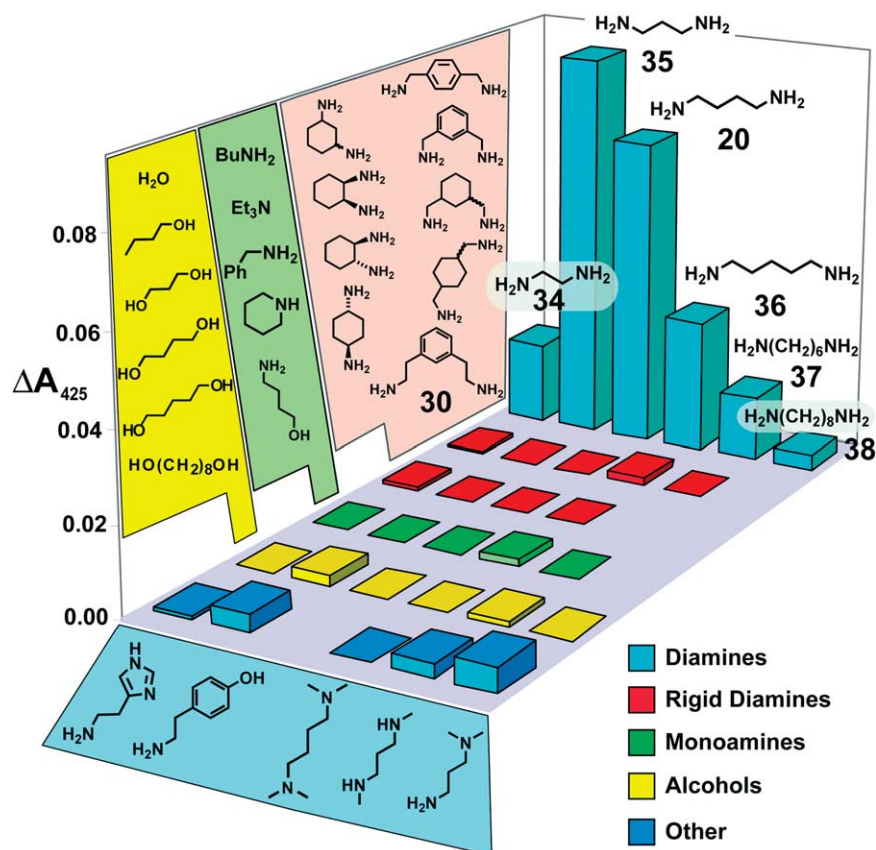
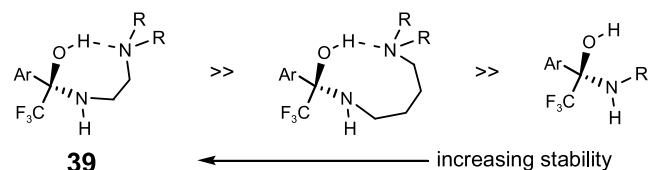


Figure 2. Guest binding selectivity profile for **28**. See text for details.

of complex with a 1:1 mixture of **20** and **28**, consistent with a 1:1 stoichiometry in the complex. A dilution study verified the reversible nature of the **28**·**20** complex. A THF solution of **28** (40.7  $\mu\text{M}$ ) and **35** (81.4  $\mu\text{M}$ ) gave  $\lambda_{\text{max}}$  of 440 nm, consistent with approximately 70% complexation. After the addition of several aliquots of THF such that the concentration of **28** was 5.1  $\mu\text{M}$  and the concentration of **20** was 10.2  $\mu\text{M}$ , the observed  $\lambda_{\text{max}}$  shifted to 473.5 nm, near to the  $\lambda_{\text{max}}$  of uncomplexed **28**. Finally, quantitative determination of the binding constants showed a significant increase in complex stability as a result of formation of the second aminal.

In comparing the various  $K_{\text{assoc}}$  in Table 1, several trends are apparent. First, **28** and **29** show very similar  $K_{\text{assoc}}$  values. Although butyl amine appears to bind slightly stronger to cross-linked dendritic host **29**, its very slow reaction rate with the dye chromophore (vide infra) meant that some

variability can be attributed to the equilibration time used in the binding titration. The enhanced stability of the **1**·**34** complex relative to **1**·**21** (butyl amine) was attributed to an intramolecular hydrogen bond as in **39** and it is not possible to rule out a 2:1 complex between **34** and **28** (**29**) given the magnitude of the  $K_{\text{assoc}}$  for these host-guest pairings (Scheme 9). On the other hand, the increased stability of **28**·**20** and **29**·**20** relative to **1**·**20** and **28**(**29**)·**34** is consistent with two-point binding by 1,4-diaminobutane.



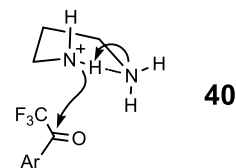
Scheme 9.

Table 1. Association constants ( $K_{\text{assoc}}$ ) for **1**, **28**, and **29** and amine guests<sup>a</sup>

Guest	$K_{\text{assoc}}$ ( $\text{M}^{-1}$ ) for hosts <b>1</b> (R=Me), <b>28</b> , <b>29</b>		
	<b>1</b>	<b>28</b>	<b>29</b>
BuNH <sub>2</sub> ( <b>21</b> )	790 ± 210	780 ± 200	2300 ± 1200
<b>34</b>	28,000 ± 6000	12,000 <sup>b</sup>	15,000 ± 3000
<b>35</b>	N.D.	N.D.	26,000 ± 3000
<b>20</b>	4200 ± 2600	27,000 <sup>b</sup>	33,000 ± 2500

<sup>a</sup> At 25 °C in THF, monitoring  $\lambda_{\text{max}} = 475$  nm with guest added to host and waiting until full equilibration. Values for **1** taken from Ref. 25. Values for BuNH<sub>2</sub> complex with **28** and **29** assumed two independent binding sites. N.D., not determined.

<sup>b</sup> Single determination.



Is the remarkable selectivity seen in Figure 2 a result of highly effective imprinting? As a first step toward answering this question the binding of the same small library of guests was examined with cross-linked dendrimer **32**, which was

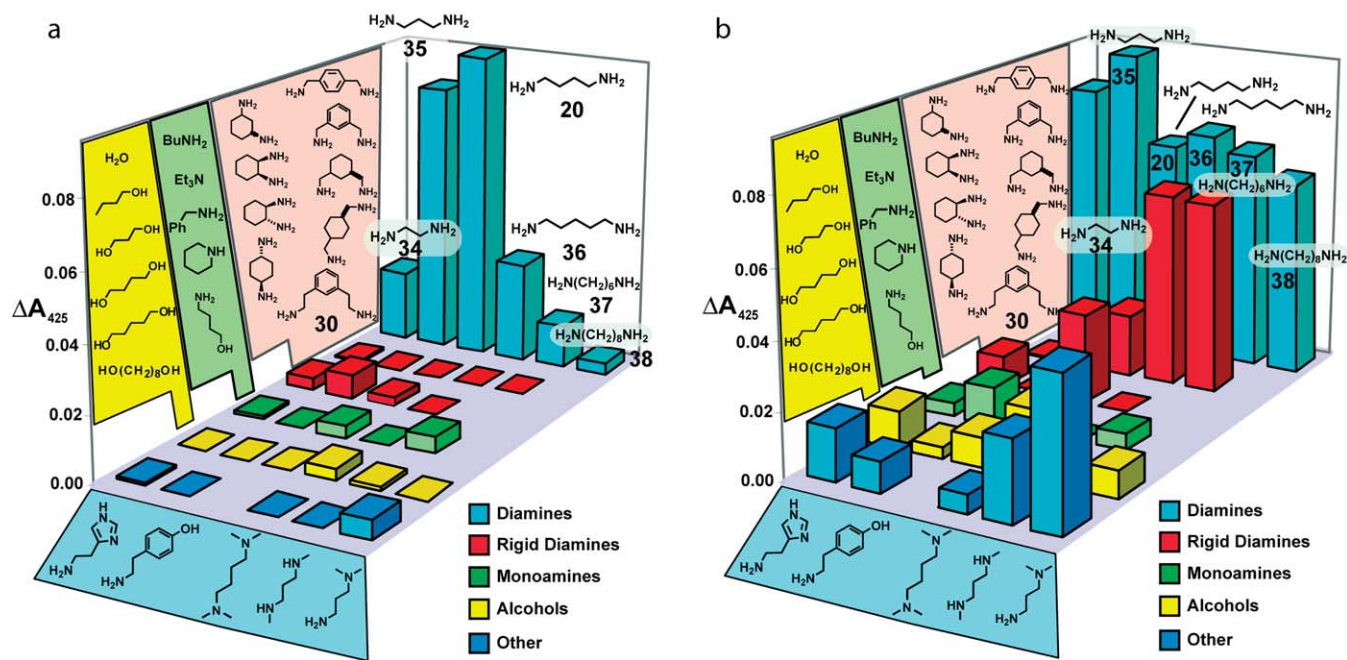


**Figure 3.** Guest binding selectivity profile using the same guests as in Figure 2 for (a) **32** after 30 s mixing (b) **28** after 12 h mixing. In (b) bar heights are only approximately correlated with  $K_{\text{assoc}}$  as a result of concentration and kinetic differences, etc. See text for additional details.

synthesized from template **31**. The imprinting of **32** with **31** would be expected to produce a very different selectivity profile and, in particular, a higher affinity for 1,3-bis(aminoethyl)benzene (**30**). In fact, the qualitative selectivity profile for **32** (Fig. 3a) was very similar to that observed for **28**. More striking was the fact that a similar selectivity trend (the entire library was not examined) was seen with **33**, whose preparation occurred without any template.

The possibility that the binding selectivity observed in Figures 2 and 3a was kinetic in origin was examined by allowing the solutions in Figure 2 to stand for 12 h prior to measuring the  $A_{425}$  value. As seen in Figure 3b many of the diamines give enhanced signal and even some of the monoamines and alcohols show binding. This result clearly implicates a kinetic effect in the binding ‘selectivity’ observed at short time periods. A careful kinetic analysis<sup>25</sup> confirmed this conclusion and further showed it to originate in an intramolecular general base catalyzed reaction similar to that reported by Jencks for the addition of alkane diamines to acetyl imidazole.<sup>26</sup> Thus, rigid diamines like **30** cannot enjoy the transition state stabilization optimized in **35** and illustrated in **40**.

Molecular modeling of **28** (**29**) is challenging because there are many isomers that may be produced in the RCM-mediated cross-linking reaction. Nonetheless, preliminary modeling of **28** suggests that the two dendrons may cross-link while leaving the dye moieties at the surface. Indeed, the fact that the azo-dye is linked to the dendron through a biphenyl linkage means that unless this rotation is hindered by the dendritic framework, the trifluoroacetyl groups can very significantly adjust their separation. Under these circumstances one would expect the relaxed selectivity observed qualitatively. Thus, future improvements on these systems may involve linking the dye unit more rigidly to the

dendrons or using larger (or more) dendrons to better imbed the reporter chromophore within the imprint.

### 3. Conclusions

Azo dye **1**, a useful chromogenic reporter group for amines,<sup>9</sup> was successfully linked to the focal point of dendrons **18** and **19**. Conversion to bis-imine dendrimers using an aza-Wittig protocol, followed by cross-linking of the peripheral alkenes and hydrolytic core removal created dendrimers capable of reporting amine and alcohol binding at the dendrimer core. The integration of chromogenic reporter groups represents a compelling advance in the monomolecular dendrimer imprinting approach,<sup>6,7</sup> although in this particular case the dendrimers were too small to produce imprinting. Another key finding is that the dendrimers containing allyl ether peripheral groups smoothly underwent RCM-mediated cross-linking and the resultant dendritic structures behaved analogous to their homoallyl ether derived analogs. The allyl ether based systems are cheaper and more readily prepared.<sup>14</sup>

Cross-linked dendrimer hosts containing the (trifluoroacetyl) azobenzene dye described herein have the potential to achieve selective guest binding based solely on molecular imprinting. For this to occur, it is necessary to develop a better understanding of the relationship between the dendrimer size and structure, including the number and placement of the cross-linking functionality, and the subsequent ‘memory’ of the template molecule.

Once the rules of monomolecular imprinting with dye-functionalized dendrimers are better understood, dendrimer-based cross-linked hosts may find applications as sensors for biologically significant amines such as amino acids, amino sugars and alkaloid natural products. The strategies and

synthetic pathways outlined in this report may be applied to dendrimers containing other dye molecules which are able to report on other functional groups. The goal of building cross-linked dendrimer hosts capable of selectively recognizing any guest molecule imaginable may indeed be within reach.<sup>6</sup>

## 4. Experimental

### 4.1. General

All reactions were performed under N<sub>2</sub> in glassware that was oven dried at 105 °C prior to use. The full details of the synthesis of **3** and **4** are described elsewhere.<sup>11,14</sup> Reagents and solvents used in reactions were obtained from commercial sources and were used without further purification except as follows: tetrahydrofuran (THF) was distilled from sodium-benzophenone; *N,N*-dimethylformamide (DMF) was dried over 4 Å molecular sieves; benzene, methylene chloride (CH<sub>2</sub>Cl<sub>2</sub>), chloroform (CHCl<sub>3</sub>) and triethylamine were distilled from CaH<sub>2</sub>, triisopropyl borate was distilled from sodium. All reactions were monitored by TLC using silica gel 60 F<sub>254</sub> plastic, aluminum, or glass plates (Merck). Flash chromatography was performed with 32–63 μm silica gel (Merck). Preparatory size-exclusion chromatography (SEC) was performed using a 2.25 ft × 50 mm column of Bio-Beads S-X1 200–400 mesh beads (Bio-Rad) with reagent grade toluene as the eluent.

<sup>1</sup>H NMR, <sup>13</sup>C NMR, and <sup>19</sup>F NMR data were obtained on either 400 or 500 MHz Varian U400, U500, and 500NB instruments. <sup>1</sup>H NMR spectra obtained in CDCl<sub>3</sub> were referenced to 7.26 ppm. <sup>13</sup>C NMR spectra obtained in CDCl<sub>3</sub> were referenced to 77.23 ppm. <sup>19</sup>F NMR data are either unreferenced or referenced to an external 1.0% solution of trifluoroacetic acid. Chemical shifts are reported in parts per million (ppm) and coupling constants are reported in Hertz (Hz). IR spectra were collected on a Mattson FTIR 5000 with major bands reported in cm<sup>-1</sup>. UV–Vis spectra were obtained using a Shimadzu UV-2501PC recording spectrophotometer. Analytical SEC, used to determine the purity of final dendrimer products, was performed using a 2 × styragel HR3, 1 × styragel HR4E column in THF with a 1.0 mL/min flow rate. Peak detection was achieved using a Viscotek triple array 300 refractive index detector, and SEC-derived molecular weights are based on calibration with linear polystyrene. FDMS, FABMS, EIMS data were collected by the mass spectrometry service at the University of Illinois, and MALDI-TOF spectra were obtained using an Applied Biosystems Voyager-DE STR mass spectrometer. The spectra of dendrimers were obtained in a 2-(4-hydroxyphenylazo)-benzoic acid (HABA) matrix. Elemental analysis was performed by the microanalytical laboratory at the University of Illinois. Melting points were measured with a Thomas Hoover melting point apparatus and are uncorrected.

Detailed procedures for the determination of *K*<sub>assoc</sub> values and for performing kinetic measurements can be found in Refs. 4 and 25.

### 4.2. Synthetic procedures

**4.2.1. 1-[4-(4-Dimethylaminophenylazo)phenyl]-2,2,2-trifluoroethanone (1, R=Me).** A suspension containing 120 mg (640 μmol) of **6** and 1 mL of 6 N aqueous HCl was prepared and cooled in an ice bath for 15 min. A solution of 42 mg (609 μmol) of sodium nitrite in 500 μL of distilled water was added slowly, dropwise to the cooled suspension. The suspension cleared to a slightly yellow solution which was stirred for 15 min in an ice bath. This diazonium mixture was added slowly, dropwise to an ice-cold solution of 810 μL (6.40 mmol) *N,N*-dimethylaniline in 3.5 mL of ethanol. The ethanol solution became a deep purple-red color. The mixture was stirred in an ice bath for 3 h. The mixture was warmed to room temperature and stirred for an additional 1 h. Solvent was removed under vacuum, and the red oily residue was partitioned between 100 mL of CH<sub>2</sub>Cl<sub>2</sub> and 100 mL of saturated aqueous Na<sub>2</sub>CO<sub>3</sub>. The organic layer was dried over Na<sub>2</sub>SO<sub>4</sub>, filtered, and evaporated to yield a purple oily solid which was dry-loaded onto silica gel. Flash chromatography (5% EtOAc–petroleum ether (PE) stepped to 25% EtOAc–PE) afforded 140 mg (69%) of **1** as a shiny, crystalline purple solid. Additional purification was accomplished by recrystallization from 20% EtOAc–hexane: mp 159–160 °C; <sup>1</sup>H NMR (400 MHz, CDCl<sub>3</sub>) δ 8.18 (d, 1.5H, *J*=7.8 Hz), 7.94 (apparent dt of AA'XX', 2H, *J*=8.6, 2.2 Hz), 7.92 (apparent dt of AA'XX', 2H, *J*=9.0, 2.2 Hz), 6.77 (apparent d of AA'XX', 2H, *J*=9.2 Hz), 3.14 (s, 6H); <sup>13</sup>C NMR (125 MHz, CDCl<sub>3</sub>) δ 157.6, 153.6, 144.1, 131.6, 129.6, 126.3, 122.8, 111.7, 40.5; <sup>19</sup>F NMR (400 MHz, CDCl<sub>3</sub>) δ -71.79; IR (film) 1700.4, 1610.7, 1595.2; UV–Vis (EtOAc) λ<sub>max</sub>=472; MS (EI) *m/z*=321.1 (M<sup>+</sup>); Anal. Calcd for C<sub>16</sub>H<sub>10</sub>F<sub>3</sub>N<sub>3</sub>O: C, 59.81; H, 4.39; N, 13.08. Found: C, 59.61; H, 4.19; N, 12.90.

**4.2.2. 1-(4-Amino-3-iodo-phenyl)-2,2,2-trifluoroethanone (7).** To a solution of 168 mg (890 μmol) 4-amino- $\alpha,\alpha,\alpha$ -trifluoroacetophenone **6** in 8 mL of 3 N aqueous HCl and 2 mL water was added 40 μL (800 μmol) of iodine monochloride. The resultant mixture was stirred at room temperature for 12 h, at which time TLC (1:4 EtOAc–PE) indicated nearly complete consumption of **6**. The reaction mixture was partitioned between 30 mL of EtOAc and 30 mL water, and saturated aqueous NaHCO<sub>3</sub> was added slowly to the suspension to neutralize. The organic layer was separated, and the remaining aqueous layer was extracted with 30 mL of EtOAc. The combined organic layers were dried over anhydrous MgSO<sub>4</sub>, and then dry loaded onto silica gel. Flash chromatography (15% EtOAc–PE stepped to 20% EtOAc–PE) was used to isolate 154 mg (62%) of **7** as a white solid. Further purification was accomplished by recrystallization from 10% EtOAc–PE: mp 114–116 °C; <sup>1</sup>H NMR (400 MHz, CDCl<sub>3</sub>) δ 8.37 (d, 1H, *J*=1.0 Hz), 7.85 (dq, 1H, *J*=8.6, 0.7 Hz), 6.74 (d, 1H, *J*=8.6 Hz), 4.96 (bs, 2H); <sup>13</sup>C NMR (125 MHz, CDCl<sub>3</sub>) δ 177.3 (q, *J*=34 Hz), 164.7, 153.1, 142.6, 132.5, 121.5, 117.1 (q, *J*=291 Hz), 113.2; MS (EI) *m/z*=315.0 (M<sup>+</sup>), 246.0 (M<sup>+</sup>–CF<sub>3</sub>); Anal. Calcd for C<sub>8</sub>H<sub>5</sub>F<sub>3</sub>NIO: C, 30.50; H, 1.60; N, 4.45. Found: C, 30.39; H, 1.44; N, 4.33.

1-(4-Amino-3,5-diiodo-phenyl)-2,2,2-trifluoroethanone (**8**) was isolated as a faster eluting side product during flash chromatography: <sup>1</sup>H NMR (400 MHz, CDCl<sub>3</sub>) δ 8.32 (d,



2H,  $J=0.7$  Hz), 5.40–5.50 (bs, 2H); MS (EI)  $m/z=440.9$  ( $M^+$ ), 371.9 ( $M^+ - CF_3$ ).

**4.2.3. 1-[4-(4-Dimethylaminophenylazo)-3-iodo-phenyl]-2,2,2-trifluoroethanone (9).** A solution of 50 mg (720  $\mu$ mol) of sodium nitrite in 5 mL of deionized water was added slowly, dropwise to 10 mL of an ice-cold solution of 235 mg (746  $\mu$ mol) of **7** in a 6 N aqueous solution of HCl. The resulting suspension was stirred at 0 °C until it cleared to a yellow solution. This solution was added slowly, dropwise to an ice-cold solution of 700  $\mu$ L (5.5 mmol) *N,N*-dimethylaniline in 25 mL of absolute ethanol. During the addition process, the reaction mixture became a deep red purple color. The mixture was warmed to room temperature and stirred for 12 h. The mixture was concentrated to a viscous dark red oil, which was partitioned between 50 mL of  $CH_2Cl_2$  and 50 mL of saturated aqueous  $NaHCO_3$ . The aqueous layer was extracted with two additional 50 mL portions of  $CH_2Cl_2$ . The combined organic layers were evaporated with silica (dry load). Flash chromatography (15% EtOAc–PE stepped to 25% EtOAc–PE) afforded 145 mg (44%) of **9** as a crystalline purple solid. Additional purification was accomplished by recrystallization from 30% EtOAc–PE to give purple needles: mp 142–143 °C;  $^1H$  NMR (400 MHz,  $CDCl_3$ )  $\delta$  8.63 (d, 1H,  $J=1.0$  Hz), 8.06 (d, 1H,  $J=1.0$  Hz), 7.97 (dt, 2H,  $J=9.3, 3.2$  Hz), 7.67 (d, 1H,  $J=8.6$  Hz), 6.77 (dt, 2H,  $J=9.3, 3.2$  Hz), 3.15 (s, 6H);  $^{13}C$  NMR (125 MHz,  $CDCl_3$ )  $\delta$  179.0 (q,  $J=35.9$  Hz), 156.3, 153.9, 144.2, 141.8, 131.5 (q,  $J=233$  Hz), 130.9, 130.9, 127.1, 117.6, 111.7, 101.0, 40.5; UV–Vis ( $CHCl_3$ )  $\lambda_{max}=495.5$ ; MS (EI)  $m/z=447.2$  ( $M^+$ ); Anal. Calcd for  $C_{16}H_{13}F_3N_3IO$ : C, 42.97; H, 2.93; N, 9.40. Found: C, 42.78; H, 2.90; N, 9.14.

**4.2.4. 1-[4-(4-Dimethylaminophenylazo)-3-(2,6-dimethoxyphenyl) phenyl]-2,2,2-trifluoroethanone (13).** To a solution of 150 mg (0.340 mmol) **9** in 16 mL of benzene was added 8.2 mL of a 2 M aqueous solution of  $Na_2CO_3$ . To the resultant emulsion was added 16 mg (14  $\mu$ mol) of  $Pd(PPh_3)_4$ . The reaction mixture was charged with nitrogen, and a solution of 125 mg (690  $\mu$ mol) **12** in 20 mL of ethanol was added via syringe. The reaction mixture was heated at 50–55 °C for 12 h. The reaction mixture was cooled to room temperature and stirred for 12 h. TLC (15% EtOAc–PE) indicated little formation of a new product. An additional 125 mg (690  $\mu$ mol) of **12** and an additional 16 mg (14  $\mu$ mol) of  $Pd(PPh_3)_4$  were added to the reaction mixture and stirring at 50 °C continued for 12 h. The reaction mixture was cooled to room temperature and 1 drop of 15% (v/v) aqueous  $H_2O_2$  was added. The mixture was stirred at room temperature for 1 h and partitioned between 50 mL of water and 50 mL of diethyl ether. The aqueous layer was extracted with 50 mL of EtOAc. The organic layer was dried over  $MgSO_4$  and evaporated. The product was dry loaded onto silica gel and flash chromatography (15% EtOAc–PE) afforded 130 mg (84%) of **13** as a purple solid. X-ray quality crystals were obtained by dissolving **13** in 20% EtOAc–PE and storing the resultant solution at 0 °C in a capped vial for approximately 1 month.  $^1H$  NMR (500 MHz,  $CDCl_3$ )  $\delta$  8.16 (s, 1H), 8.10 (dq,  $J=8.6, 1.1$  Hz, 1H), 7.79 (d, 1H,  $J=8.6$  Hz), 7.65 (AA 'XX', apparent dt,  $J=9.2, 3.2$  Hz, 2H), 7.35 (t,  $J=8.4$  Hz, 2H), 6.67 (d, 2H,  $J=10.0$  Hz), 6.65 (d, 2H,  $J=8.4$  Hz), 3.64 (s,

6H), 3.07 (s, 6H);  $^{13}C$  NMR (125 MHz,  $CDCl_3$ )  $\delta$  180.2 (q,  $J=34$  Hz), 158.1, 156.1, 153.0, 144.4, 135.5, 133.6, 130.0, 129.8, 129.2, 125.9, 117.8 (q,  $J=292$  Hz), 116.7, 111.5, 103.9, 56.0, 40.4; UV–Vis ( $CH_2Cl_2$ )  $\lambda_{max}=460.5$  nm; MS (FAB)  $m/z=458.2$  ( $M+H^+$ ).

**4.2.5. 1-[4-(4-Dimethylaminophenylazo)-3-(3,5-dimethoxyphenyl)phenyl]-2,2,2-trifluoroethanone (14).** To a solution of 100 mg (223  $\mu$ mol) **9** in 11 mL of benzene was added 5.5 mL of a 2 M aqueous solution of  $Na_2CO_3$ . To the resultant emulsion was added 21 mg (18  $\mu$ mol) of  $Pd(PPh_3)_4$ . The reaction mixture was charged with nitrogen, and a solution of 160 mg (880  $\mu$ mol) of **10** in 25 mL of ethanol was added via syringe. The reaction mixture was heated at 50–55 °C for 4 h at which time TLC ( $CH_2Cl_2$ ) indicated complete formation of product. The mixture was cooled to room temperature and 2 mL of a 15% (v/v) aqueous solution of  $H_2O_2$  was added. The mixture was stirred at room temperature for an additional 1 h, and then partitioned between 50 mL water and 50 mL  $CH_2Cl_2$ . The aqueous layer was extracted with 50 mL  $CH_2Cl_2$ . The combined organic layers were dried over  $Na_2SO_4$  and evaporated over silica gel (dry load). Flash chromatography with  $CH_2Cl_2$  elution afforded 82 mg (80%) of **14** as a red solid: mp 153–155 °C;  $^1H$  NMR (400 MHz,  $CDCl_3$ )  $\delta$  8.25 (s, 1H), 8.11 (dq, 1H,  $J=8.5, 0.7$  Hz), 7.79 (apparent dt of AA'XX', 2H,  $J=9.3, 3.2$  Hz), 7.79 (d, 1H,  $J=8.5$  Hz), 6.71 (apparent dq of AA'XX', 2H,  $J=9.5, 3.2$  Hz), 6.64 (d, 2H,  $J=2.4$  Hz), 6.54 (t, 2H,  $J=2.2$  Hz), 3.79 (s, 6H), 3.11 (s, 6H);  $^{13}C$  NMR (125 MHz,  $CDCl_3$ )  $\delta$  180.1 (q,  $J=180.1$  Hz), 160.4, 155.0, 153.4, 144.5, 140.0, 139.9, 133.0, 130.2, 129.4, 126.5, 117.4, 117.0 (q,  $J=29$  Hz), 109.1, 100.5, 55.6, 40.5; MS (FAB)  $m/z=458.2$  ( $M+H^+$ ).

**4.2.6. 1,3-Bis-(tert-butyl)dimethylsilyloxy-5-iodobenzene (15).** A solution of 2.05 g (8.70 mmol) 5-iodoresorcinol, 5.0 g (33 mmol) of *tert*-butyldimethylsilyl chloride, 2.0 g (29 mmol) of imidazole, and 25 mL of DMF was stirred at room temperature for 36 h. The reaction mixture was poured into 80 mL of 5 °C water and the resulting suspension was extracted twice with 80 mL portions of methylene chloride. The combined organic layers were dried over  $Na_2SO_4$ , filtered, and evaporated to yield an amber colored oil. Flash chromatography (5% EtOAc–PE) afforded 4.03 g (100%) of **15** as a clear, slightly yellow oil:  $^1H$  NMR (400 MHz,  $CDCl_3$ )  $\delta$  6.83 (d, 2H,  $J=2.2$  Hz), 6.27 (t, 1H,  $J=2.2$  Hz), 0.96 (s, 19H), 0.86 (s, 12H);  $^{13}C$  NMR (100 MHz,  $CDCl_3$ )  $\delta$  157.2, 123.1, 112.2, 93.7, 25.8, 18.4, –4.3; MS (EI)  $m/z=464.1$  ( $M^+$ ), 407 ( $M^+ - tert-butyl$ ).

**4.2.7. 1,3-Bis-(tert-butyl)dimethylsilyloxyphenylboronic acid (16).** To a solution of 3.1 g (6.7 mmol) of **15** in 40 mL of THF cooled to –78 °C was added dropwise 15 mL (10.5 mmol) of a 1.3 M solution of *n*-butyl lithium in hexane. The resulting solution was stirred at –78 °C for 30 min. The cold solution was added rapidly, dropwise via a canula to a –78 °C solution of 7 mL of triisopropyl borate in 4 mL of THF. Care was taken to avoid contamination of reagents with frost building up on the canula during the dropwise addition process. The mixture was stirred for 10 min at –78 °C and at room temperature overnight. The mixture was partitioned between 25 mL of a 1% (v/v) aqueous solution of HCl and 250 mL EtOAc. The organic

layer was separated and the aqueous layer was extracted with an additional 100 mL of EtOAc. The combined organic layers were dried over Na<sub>2</sub>SO<sub>4</sub>, filtered, and evaporated to yield an orange oily solid. The crude product was dry loaded onto silica and flash chromatography (15% EtOAc–PE stepped to 35% EtOAc–PE) afforded 1.44 g (56%) of **16** as a white powder. Additional purification was accomplished by precipitation from 1:1 EtOAc–PE: mp 234–240 °C; <sup>1</sup>H NMR (400 MHz, CDCl<sub>3</sub>) δ 7.29 (d, 2H, *J*=2.4 Hz), 6.59 (t, 1H, *J*=2.4 Hz), 1.03 (s, 18H), 0.26 (s, 12H); <sup>13</sup>C NMR (100 MHz, CDCl<sub>3</sub>) δ 156.7, 120.2, 117.0, 26.0, 18.5, –4.1; MS (FD) *m/z*=1092 (3×M–3×H<sub>2</sub>O); Anal. Calcd for C<sub>54</sub>H<sub>99</sub>B<sub>3</sub>O<sub>9</sub>Si<sub>6</sub>: C, 59.32; H, 9.13. Found: C, 58.36; H, 9.06.

**4.2.8. 1-[4-(4-Dimethylaminophenylazo)-3-(3,5-bis(*tert*-butyldimethylsilyloxy)phenyl)phenyl]-2,2,2-trifluoroethanone (17).** To a solution of 500 mg (1.12 mmol) of **9** in 65 mL of benzene was added 32 mL of a 2 M aqueous solution of Na<sub>2</sub>CO<sub>3</sub>. To the resultant emulsion was added 60 mg (52 μmol; 5 mol%) of Pd(PPh<sub>3</sub>)<sub>4</sub>. The reaction mixture was charged with nitrogen, and a solution of 490 mg (1.28 mmol) of **16** in 25 mL ethanol was added via syringe. The mixture was heated at 50–55 °C for 3 h. The mixture was cooled to room temperature and stirred for 12 h. TLC (20% EtOAc–PE) indicated that some **9** still remained so an additional 10 mg (8 μmol) of Pd(PPh<sub>3</sub>)<sub>4</sub> and 50 mg (130 μmol) of **16** was added. Heating at 50–55 °C resumed for 2 h. The reaction mixture was cooled to room temperature and 1 mL of a 15% (v/v) aqueous solution of H<sub>2</sub>O<sub>2</sub> was added. The mixture was stirred at room temperature for 1 h, and partitioned between 100 mL of brine and 100 mL of diethyl ether. The ether layer was washed with 100 mL water. The combined organic layer was dried over Na<sub>2</sub>SO<sub>4</sub>, filtered, and evaporated to a red film. The product was dry loaded onto silica and flash chromatography (20% EtOAc–PE stepped to 25% EtOAc–PE) afforded product which was further purified by precipitation from PE to afford 660 mg (89%) of **17** as a red powder: mp 100–102 °C; <sup>1</sup>H NMR (400 MHz, CDCl<sub>3</sub>) δ 8.18 (s, 1H), 8.09 (d, 1H, *J*=8.6 Hz), 7.78 (dt, 2H, *J*=3.2, 9.0 Hz), 7.74 (d, 1H, *J*=8.6 Hz), 6.69 (dt, 2H, *J*=3.2, 9.3 Hz), 6.58 (d, 2H, *J*=2.2 Hz), 6.39 (t, 1H, *J*=2.2 Hz), 3.10 (s, 6H), 0.96 (s, 18H), 0.18 (s, 11H); <sup>13</sup>C NMR (125 MHz, CDCl<sub>3</sub>) δ 180.2 (q, *J*=35.0 Hz), 156.2, 155.1, 153.3, 144.7, 139.9, 139.8, 133.1, 130.0, 129.4, 126.5, 117.4, 116.2, 117.0 (q, *J*=291.8 Hz), 116.2, 111.6, 40.5, 27.2, 25.9, 18.4, –4.2; UV–Vis (CHCl<sub>3</sub>) λ<sub>max</sub>=495.5; MS (FAB) *m/z*=658.3 (M+H<sup>+</sup>); Anal. Calcd for C<sub>34</sub>H<sub>46</sub>F<sub>3</sub>N<sub>3</sub>O<sub>3</sub>Si<sub>2</sub>: C, 62.07; H, 7.05; N, 6.39. Found: C, 62.02; H, 7.10; N, 6.45.

**4.2.9. 1-[4-(4-Dimethylaminophenylazo)-3-[[3,5-bis(3,5-bis(3-butene-1-oxy)benzyloxy)benzyloxy]benzyloxy]phenyl]-2,2,2-trifluoroethanone (18).** To a solution of 680 mg (500 μmol) of **3** in 35 mL of THF was added 32 mg (550 μmol) of potassium fluoride, 54 mg (200 μmol) of 18-crown-6, and 163 mg (248 mmol) of **17**. The resultant solution was stirred at 60 °C for 29 h. Twice over this period, additional portions of 32 mg (550 μmol) of potassium fluoride, and 54 mg (200 μmol) of 18-crown-6 were added to the mixture. With minimal heating, the mixture was evaporated over silica (dry-load). Flash

chromatography (PE stepped to 50% EtOAc–PE) afforded 660 mg (88%) of **18** as a viscous red oil. Additional purification was accomplished using preparative SEC (yield from prep. SEC was reduced to 44%): <sup>1</sup>H NMR (400 MHz, CDCl<sub>3</sub>) δ 8.25 (s, 1H), 8.08 (d, 1H, *J*=8.8 Hz), 7.79 (d, 2H, *J*=9.3 Hz), 7.76 (d, 1H, *J*=8.6 Hz), 6.76 (d, 2H, *J*=1.9 Hz), 6.71 (t, 1H, *J*=2.2 Hz), 6.65 (d, 8H, *J*=2.0 Hz), 6.65–6.68 (m, 4H), 6.64 (d, 2H, *J*=7.3 Hz), 6.55 (d, 19H, *J*=2.0 Hz), 6.52–6.55 (bt, 6H), 6.39 (t, 9H, *J*=2.2 Hz), 5.87 (ddt, 18H, *J*=17.1, 10.3, 6.6 Hz), 5.14 (ddt, 19H, *J*=17.1, 1.7, 1.2 Hz), 5.08 (dd, 19H, *J*=10.3, 1.7 Hz), 4.96 (s, 4H), 4.92 (s, 25H), 3.97 (t, 36H, *J*=6.8 Hz), 2.92 (s, 5H), 2.51 (q, 36H, *J*=6.6 Hz); <sup>13</sup>C NMR (126 MHz, CDCl<sub>3</sub>) δ 180.0 (d, *J*=35.0 Hz), 160.5, 160.3, 159.5, 155.0, 144.5, 139.9, 139.5, 139.4, 139.3, 134.6, 132.9, 129.4, 128.4, 126.5, 125.5, 117.3, 117.0 (d, *J*=209 Hz), 111.6, 106.7, 106.6, 106.5, 106.1, 102.0, 101.8, 101.7, 101.1, 70.4, 70.2, 67.4, 40.3, 33.8; <sup>19</sup>F NMR (400 MHz, CDCl<sub>3</sub>) δ –71.79; UV–Vis (CHCl<sub>3</sub>) λ<sub>max</sub>=480; MS (MALDI-TOF) *m/z*=3004.21 (M<sup>+</sup>); 3026.7 (M+Na<sup>+</sup>); 3043.8 (M+K<sup>+</sup>).

**4.2.10. 1-[4-(4-Dimethylaminophenylazo)-3-[[3,5-bis(3,5-bis(3,5-bis(2-propene-1-oxy)benzyloxy)benzyloxy]phenyl]-2,2,2-trifluoroethanone (19).** To 2.55 g (2.0 mmol) of **4** in 100 mL of THF was added 340 mg (5.9 mmol) of KF, 110 mg (410 μmol) of 18-crown-6, and 530 mg (810 μmol) of **17**. The mixture was heated to 60 °C for 16 h and an additional 178 mg (3.1 mmol) of KF and 54 mg (200 μmol) of 18-crown-6 were added. The mixture was stirred for an additional 24 h. The solvent was removed at reduced pressure and the resultant red oil was loaded onto a silica gel plug and eluted with 30% EtOAc–PE. The crude product was further purified by preparative SEC to afford 1.20 g (54%) of **19** as a red oil: <sup>1</sup>H NMR (400 MHz, CDCl<sub>3</sub>) δ: 8.25 (d, 1H, *J*=1.2 Hz), 8.09 (dd, 1H, *J*=9.6, 1.2 Hz), 7.80 (dt, 2H, *J*=9.6, 2.4 Hz), 7.78 (d, 1H, *J*=8.8 Hz), 6.77 (d, 2H, *J*=2.4 Hz), 6.66 (d, 8H, *J*=2.0 Hz), 6.58 (d, 18H, *J*=2.4 Hz), 6.58 (d, 1H, *J*=2.4 Hz), 6.44 (t, 8H, *J*=2.4 Hz), 6.03 (ddt, 16H, *J*=17.2, 10.4, 5.2 Hz), 5.34 (ddt, 16H, *J*=17.2, 1.6, 1.2 Hz), 5.27 (ddt, 16H, *J*=10.4, 1.6, 1.2 Hz), 4.94 (s, 24H), 4.50 (dt, 32H, *J*=5.2, 1.6 Hz), 2.94 (s, 6H); <sup>13</sup>C NMR (100 MHz, CDCl<sub>3</sub>) δ: 160.3, 160.2, 160.1, 159.5, 153.3, 144.5, 139.5, 139.2, 133.3, 129.4, 118.0, 111.7, 106.7, 106.6, 106.5, 106.4, 101.8, 101.7, 101.5, 70.4, 70.2, 69.1, 40.3; <sup>19</sup>F NMR (500 MHz, CDCl<sub>3</sub>) δ: –71.40; UV–Vis (THF) λ<sub>max</sub>=480.5; MS (MALDI-TOF) *m/z* 2782.0 (M<sup>+</sup>), 2805.0 (M+Na<sup>+</sup>), 2821.4 (M+K<sup>+</sup>); SEC (THF) calcd MW=3380. Additionally 207 mg (21%) of the monoalkylated product was obtained as a red oil: <sup>1</sup>H NMR δ 8.25 (d, 1H, *J*=1.2 Hz), 8.09 (dd, 1H, *J*=9.6, 1.2 Hz), 7.80 (dt, 2H, *J*=9.6, 2.4 Hz), 7.78 (d, 1H, *J*=8.8 Hz), 6.77 (d, 2H, *J*=2.4 Hz), 6.66 (d, 4H, *J*=2.0 Hz), 6.58 (d, 9H, *J*=2.4 Hz), 6.58 (d, 1H, *J*=2.4 Hz), 6.44 (t, 4H, *J*=2.4 Hz), 6.03 (ddt, 8H, *J*=17.2, 10.4, 5.2 Hz), 5.34 (ddt, 8H, *J*=17.2, 1.6, 1.2 Hz), 5.27 (ddt, 8H, *J*=10.4, 1.6, 1.2 Hz), 4.94 (s, 12H), 4.50 (dt, 16H, *J*=5.2, 1.6 Hz), 2.94 (s, 6H).

**4.2.11. {4-[4-(1-Butylimino-2,2,2-trifluoroethyl)phenyl-azo]phenyl}dimethylamine (22).** To a solution of 150 mg (467 μmol) of **1** in 8 mL of CH<sub>2</sub>Cl<sub>2</sub> was added 150 μL (1.52 mmol) of *n*-butyl amine. The resultant mixture was cooled over an ice bath, and 260 μL (260 μmol) of a 1.0 M



CH<sub>2</sub>Cl<sub>2</sub> solution of titanium tetrachloride was added slowly, dropwise. During the dropwise addition process, the solution became a lighter orange-red color and much vapor evolved. The mixture warmed to room temperature, and stirred for 12 h. An additional 100  $\mu$ L (1.00 mmol) of *n*-butyl amine and 240  $\mu$ L (0.240 mmol) of a 1.0 M titanium tetrachloride solution in CH<sub>2</sub>Cl<sub>2</sub> were added to the mixture which was stirred at room temperature for 2 h. The mixture was filtered through a celite plug, the solvent was evaporated, and the orange-red residue was re-dissolved in diethyl ether. The solution was passed through another celite plug, and solvent was evaporated to afford 171 mg (97%) of **22** as a waxy, semi-crystalline red solid: mp 73–74 °C; <sup>1</sup>H NMR (400 MHz, CDCl<sub>3</sub>)  $\delta$  7.91 (d, 2H, *J* = 8.1 Hz), 7.91 (d, 2H, *J* = 9.0 Hz), 7.35 (d, 2H, *J* = 8.3 Hz), 6.76 (apparent d of AA'XX', 2H, *J* = 9.0 Hz), 3.44 (td, 2H, *J* = 7.1, 1.7 Hz), 3.10 (s, 6H), 1.66 (quintet, 2H, *J* = 7.3 Hz), 1.31 (sextet, 2H, *J* = 7.8 Hz), 0.89 (t, 3H, *J* = 7.3 Hz); <sup>13</sup>C NMR (100 MHz, CDCl<sub>3</sub>)  $\delta$  157.9 (d, *J* = 34 Hz), 154.1, 153.0, 143.7, 130.9, 128.8, 125.6, 123.1 (q, *J* = 300 Hz), 122.5, 111.6, 53.4, 40.5, 32.5, 20.6, 14.0; IR (film) 1700.4, 1610.7, 1595.2; MS (EI) *m/z* = 376.3 (M<sup>+</sup>).

**4.2.12. *N,N'*-Bis-[1-[4-(4-dimethylaminophenylazo)-3-[[3,5-bis[3,5-bis(3,5-bis(3-buteneoxy)benzyloxy)benzyloxy]phenyl]-phenyl]-2,2,2-trifluoroethylidene]butane-1,4-diamine (23).** A solution of 19 mg (73  $\mu$ mol) of triphenylphosphine in 1 mL of diethyl ether was added in portions to a solution of 5 mg (40  $\mu$ mol) of 1,4-diazidobutane in 1 mL of diethyl ether. The resulting solution was stirred at 35 °C for 2.5 h. Ether was evaporated and the residue was immediately combined with a solution of 225 mg (75  $\mu$ mol) of **18** in 5 mL of benzene. The resultant mixture was refluxed for 17 h, cooled to room temperature, and the solvent removed to afford an orange oil which was partially purified on a silica plug eluting with a solvent mixture of 40% EtOAc–0.5% triethylamine-PE. The eluted orange-red material was further purified using preparative SEC. SEC fractions containing pure dendrimer were concentrated, and fractions containing impure dendrimer were subjected to additional preparative SEC runs. The combined purified fractions afforded 180 mg (69%) of **23** as an orange oil: <sup>1</sup>H NMR (400 MHz, CDCl<sub>3</sub>)  $\delta$  7.79 (d, 4H, *J* = 9.0 Hz), 7.73 (d, 2H, *J* = 8.3 Hz), 7.44 (s, 2H), 7.23 (dd, 2H, *J* = 6.8, 1.2 Hz), 6.76 (d, 4H, *J* = 2.2 Hz), 6.69 (bt, 2H, *J* = 1.8 Hz), 6.65 (d, 30H, *J* = 2.2 Hz), 6.64 (d, 4H, *J* = 10 Hz), 6.55 (d, 36H, *J* = 2.2 Hz), 6.54 (t, 12H, *J* = 2.4 Hz), 6.40 (t, 18H, *J* = 2.2 Hz), 5.87 (ddt, 32H, *J* = 17.1, 10.5, 6.6 Hz), 5.15 (ddt, 34H, *J* = 17.1, 1.7, 1.5 Hz), 5.09 (ddt, 34H, *J* = 10.3, 1.7, 1.2 Hz), 4.94 (s, 8H), 4.92 (s, 50H), 3.97 (t, 72H, *J* = 6.6 Hz), 3.49 (bt, 4H), 2.89 (s, 12H), 2.50 (q, 72H, *J* = 6.6 Hz), 1.72 (m, 4H); <sup>13</sup>C NMR (126 MHz, CDCl<sub>3</sub>)  $\delta$  160.5, 160.3, 159.5, 139.5, 139.3, 139.2, 134.6, 129.7, 125.9, 117.3, 111.6, 106.7, 106.1, 101.8, 101.6, 101.1, 70.4, 70.2, 67.4, 40.2, 33.8, 28.3; <sup>19</sup>F NMR (400 MHz, CDCl<sub>3</sub>)  $\delta$  -71.46; UV-Vis (CHCl<sub>3</sub>)  $\lambda_{\max}$  = 435.5; MS (MALDI-TOF) *m/z* = 6061.99 (M<sup>+</sup>); 6085.57 (M + Na<sup>+</sup>); 6100.91 (M + K<sup>+</sup>).

**4.2.13. *N,N'*-Bis-[1-[4-(4-dimethylaminophenylazo)-3-[[3,5-bis[3,5-bis(3,5-bis(2-propeneoxy)benzyloxy)benzyloxy]phenyl]-phenyl]-2,2,2-trifluoroethylidene]butane-1,4-diamine (24).** 1,4-Butanediamine, *N,N'*-

bis(triphenylphosphoranylidene) was prepared by dissolving 70 mg (500  $\mu$ mol) of 1,4-diazidobutane in 20 mL of diethyl ether and adding 260 mg (1.00 mmol) of triphenylphosphine. The mixture was heated to 30 °C for 5 h, cooled to room temperature, and evaporated to afford crude yellow crystals weighing 300 mg (100%): <sup>1</sup>H NMR  $\delta$  7.61 (m, 12H), 7.46 (m, 6H), 7.39 (m, 12H), 3.03 (dt, 4H, *J* = 18.5, 3.5 Hz), 1.58 (q, 4H, *J* = 3.5 Hz); MS (FD) *m/z* 609 (M<sup>+</sup>). To a solution of 300 mg (110  $\mu$ mol) of **19** in 10 mL of benzene was added 33 mg (54  $\mu$ mol) of the bis-phosphoranylidene. The mixture was heated at 65 °C for 24 h, cooled to room temperature, and the benzene evaporated. The crude product was subjected to a silica gel plug eluted with 50% EtOAc–PE. The crude product purified by preparative SEC to afford 97 mg (32%) of **24** as an orange oil: <sup>1</sup>H NMR (500 MHz, CDCl<sub>3</sub>)  $\delta$  7.76 (d, 4H, *J* = 9.0 Hz), 7.71 (d, 2H, *J* = 1.5 Hz), 7.41 (dd, 2H, *J* = 8.0, 1.5 Hz), 7.22 (dd, 2H, *J* = 8.0, 1.5 Hz), 6.74 (d, 4H, *J* = 2.0 Hz), 6.63 (d, 28H, *J* = 2.0 Hz), 6.55 (d, 32H, *J* = 2.0 Hz), 6.51 (t, 14H, *J* = 2.0 Hz), 6.41 (t, 16H, *J* = 2.0 Hz), 6.00 (ddt, 32H, *J* = 17.5, 10.5, 5.5 Hz), 5.36 (ddt, 32H, *J* = 17.5, 1.5, 1.5 Hz), 5.24 (ddt, 32H, *J* = 10.5, 1.5, 1.5 Hz), 4.91 (s, 48H), 4.99 (s, 8H), 4.47 (dt, 64H, *J* = 5.5, 1.5 Hz), 3.47 (m, 4H), 2.88 (s, 12H), 1.70 (m, 4H); <sup>13</sup>C NMR (100 MHz, CDCl<sub>3</sub>)  $\delta$  160.3, 160.2, 160.1, 159.5, 139.4, 139.3, 125.9, 106.7, 106.4, 101.9, 101.6, 70.2, 69.1, 69.0, 40.2; <sup>19</sup>F NMR (500 MHz, CDCl<sub>3</sub>)  $\delta$  -70.869; MS (MALDI-TOF) *m/z* 5615.6 (M<sup>+</sup>), 5638.4 (M + Na<sup>+</sup>), 5650.8 (M + K<sup>+</sup>); SEC (toluene) MW<sub>PS</sub> = 5616.

**4.2.14. Cross-linking of dendrimer 23 (26).** To a solution of 110 mg (18  $\mu$ mol) of **23** in 1.8 L of benzene was added 38 mg (46  $\mu$ mol, 8 mol% per alkene) of **25**. The resulting solution was stirred at room temperature for 24 h. The mixture was slowly poured through a silica gel plug with benzene. A dark black layer remained on the top of the silica plug. An orange band was eluted from this top layer with 500 mL of 5% EtOAc–CH<sub>2</sub>Cl<sub>2</sub>. The orange colored eluent was collected and evaporated to a thick brown oil. The crude product was redissolved in 250 mL of benzene and filtered through another silica gel plug using 5% EtOAc–CH<sub>2</sub>Cl<sub>2</sub> as the eluent. Concentration of the orange colored eluent afforded an orange oil. Two successive preparative SEC columns afforded 60 mg (60%) of **26** as a yellow-orange oil: <sup>1</sup>H NMR (400 MHz, CDCl<sub>3</sub>)  $\delta$  7.80–7.60 (bs, 8H), 6.70–6.20 (bd, 85H), 6.00–5.80 (bs, 8H), 5.70–5.40 (bs, 28H), 5.20–5.00 (bs, 13H), 5.00–4.40 (bs, 55H), 4.10–3.60 (s, 64H), 3.60–3.50 (bs, 12H), 2.90–2.60 (bs, 14H), 2.60–2.20 (bs, 61H); <sup>19</sup>F NMR (400 MHz, CDCl<sub>3</sub>)  $\delta$  -70.93, -71.40; UV-Vis (CHCl<sub>3</sub>)  $\lambda_{\max}$  = 436.5; MS (MALDI-TOF) *m/z* = 5640.0 (16 cross-links + Na<sup>+</sup>), 5667.0 (15 cross-links + Na<sup>+</sup>), 5694.3 (14 cross-links + Na<sup>+</sup>), 5706.6 (14 cross-links + K<sup>+</sup>).

**4.2.15. Cross-linking of dendrimer 24 (27).** To a solution of 140 mg (25  $\mu$ mol) of **24** in benzene was added 53 mg (64  $\mu$ mol, 8 mol% per alkene) of **25**. The reaction was stirred at room temperature for 24 h and slowly poured through a 3 cm  $\times$  3 in. silica gel plug equilibrated with benzene. The column was eluted with 1.0 L of 5% EtOAc–CH<sub>2</sub>Cl<sub>2</sub>. The brown colored eluent was collected and evaporated to an brown oil which was redissolved in 500 mL benzene and filtered through another silica gel plug

eluting with 5% EtOAc–CH<sub>2</sub>Cl<sub>2</sub>. The product was evaporated to an orange oil. Two successive preparative SEC columns afforded 98 mg (76%) of **27** as a yellow-orange oil: <sup>1</sup>H NMR (400 MHz, CDCl<sub>3</sub>) δ 7.80–7.60 (bs, 10H), 6.70–6.20 (bd, 94H), 6.00–5.60 (bs, 32H), 5.20–5.00 (bs, 56H), 5.00–4.40 (bs, 64H), 3.60–3.10 (bs, 4H), 2.90–2.60 (bs, 12H), 1.80–1.60 (bs, 4H); <sup>19</sup>F NMR (400 MHz, CDCl<sub>3</sub>) δ –70.88, –71.34; UV–Vis (THF) λ<sub>max</sub> = 443.5; MS (MALDI-TOF) *m/z* = 5186.4 (16 cross-links + Na<sup>+</sup>), 5214.5 (15 cross-links + Na<sup>+</sup>), 5230.6 (15 cross-links + K<sup>+</sup>), 5242.6 (14 cross-links + Na<sup>+</sup>); SEC (toluene) MW<sub>PS</sub> = 2460.

**4.2.16. Cross-linked dendrimeric host 28.** To a solution of 60 mg (11 μmol) of **26** in 20 mL of THF was added 10 mL of 1% (v/v) aqueous solution of HCl. The mixture quickly turned from orange-yellow to red and 1 mL of CHCl<sub>3</sub> was added to ensure homogeneity. The mixture was stirred at room temperature for 15 h. The mixture was poured into 25 mL of a 10% (v/v) aqueous solution of HCl. The resulting suspension was extracted three times with 20 mL of CHCl<sub>3</sub>. The combined organic layers were washed with a saturated aqueous solution of sodium bicarbonate. The organic layer was dried over anhydrous Na<sub>2</sub>SO<sub>4</sub>, filtered, and evaporated to 46 mg (65%) of **28** as a red film. Purification (with some loss in yield) was accomplished by silica gel flash chromatography using 10% EtOAc–CH<sub>2</sub>Cl<sub>2</sub> as the eluent: <sup>1</sup>H NMR (400 MHz, CDCl<sub>3</sub>) δ 8.30–7.90 (bd), 7.80–7.60 (bs, 1H), 6.80–6.00 (bd, 27H), 6.00–5.70 (bs, 2H), 5.70–5.10 (bs, 8H), 5.20–5.00 (bs, 3H), 5.00–4.40 (bs, 16H), 4.10–3.50 (s, 20H), 2.90–2.60 (bs, 2H), 2.60–2.20 (bs, 20H); <sup>19</sup>F NMR (400 MHz, CDCl<sub>3</sub>) δ –70.62, –71.44; UV–Vis (THF) λ<sub>max</sub> = 480.0, ε (475 nm) = 25,400 M<sup>-1</sup>; MS (MALDI-TOF) *m/z* = 5585.4 (16 cross-links + Na<sup>+</sup>), 5612.0 (15 cross-links + Na<sup>+</sup>), 5639.7 (14 cross-links + Na<sup>+</sup>), 5667.7 (13 cross-links + Na<sup>+</sup>).

**4.2.17. Cross-linked dendrimeric host 29.** To a solution of 17 mg (3 μmol) of **27** in 10 mL of THF was added 5 mL of a 1% (v/v) aqueous solution of HCl and 1 mL of CHCl<sub>3</sub>. The reaction mixture was stirred at room temperature for 5 min. The mixture was poured into 10 mL of a 10% (v/v) aqueous solution of HCl. The resultant residue was extracted three times with 10 mL of CHCl<sub>3</sub>. The combined organic layers were washed with a saturated aqueous solution of sodium bicarbonate, dried over sodium sulfate, filtered, and evaporated. The crude product was loaded onto a silica gel column (5 × 15 cm<sup>2</sup>) eluting with 1 L of 10% EtOAc–PE to afford 14 mg (82%) of **29** as a red oil: <sup>1</sup>H NMR (400 MHz, CDCl<sub>3</sub>) δ 7.80–7.20 (bs, 10H), 6.70–6.10 (bs, 94H), 6.10–5.70 (bs, 32H), 5.00–4.80 (bs, 56H), 4.80–4.40 (bs, 64H), 2.90–2.60 (s, 12H); <sup>19</sup>F NMR (400 MHz, CDCl<sub>3</sub>) δ –70.62; UV–Vis (THF) λ<sub>max</sub> = 477.0; MS (MALDI-TOF) *m/z* = 5135.2 (16 cross-links + Na<sup>+</sup>), 5162.2 (15 cross-links + Na<sup>+</sup>), 5178.2 (15 cross-links + K<sup>+</sup>); SEC (toluene) MW<sub>PS</sub> = 2920.

**4.2.18. 1,3-Bis(azidoethyl)benzene (31).** To a solution of 1.9 g (5.9 mmol) of 1,3-benzenediethanol dimethane-sulfonate in 15 mL of DMF was added 0.95 g (15 mmol) of sodium azide. The resultant mixture was stirred at 50 °C for 12 h, cooled to room temperature, and partitioned between 50 mL of ether and 100 mL of water. The aqueous layer was

extracted with 50 mL of ether, and the combined organic layers were washed with 50 mL of a saturated aqueous solution of sodium bicarbonate. The organic layers were dried over Na<sub>2</sub>SO<sub>4</sub>, filtered, and evaporated to yield a yellow oil. Flash chromatography using 25% EtOAc–PE as the eluent isolated 820 mg (63%) **31** as a clear oil: <sup>1</sup>H NMR (400 MHz, CDCl<sub>3</sub>) δ 7.28 (t, 1H, *J* = 7.6 Hz), 7.11 (dd, 2H, *J* = 7.6, 1.5 Hz), 7.08 (t, 1H, *J* = 1.5 Hz), 3.51 (t, 4H, *J* = 7.1 Hz), 2.89 (t, 4H, *J* = 7.1 Hz); MS (EI) *m/z* = 131.8 (M – 2N<sub>3</sub>).

**4.2.19. N,N'-Bis-{1-[4-(4-dimethylaminophenylazo)-3-[[3,5-bis(3,5-bis(3,5-bis(3-buteneoxy)benzyloxy)benzyloxy]benzyloxy]phenyl]-phenyl}-2,2,2-trifluoroethylidene}-1,3-bis(aminoethyl)benzene (32).** A solution of 25 mg (95 μmol) of triphenylphosphine in 2 mL of diethyl ether was added in portions to a solution of 10 mg (46 μmol) of **31** in 1 mL of diethyl ether. The resulting solution was stirred at 35 °C for 2.5 h. The solvent was evaporated and the residue was immediately combined with a solution of 410 mg (136 μmol) **18** in 10 mL of benzene. The mixture was refluxed for 24 h, cooled to room temperature and concentrated to an orange oil which was partially purified on a silica plug eluting with a solvent mixture of 30% EtOAc–0.1% triethylamine–PE. The eluted orange-red material was further purified using preparative SEC. SEC fractions containing pure dendrimer were concentrated, and fractions containing impure dendrimer were subjected to additional preparative SEC runs. Combined purified fractions from all SEC runs provided 120 mg (42%) of product as an orange oil: <sup>1</sup>H NMR (400 MHz, CDCl<sub>3</sub>) δ 7.75 (d, 4H, *J* = 9.0 Hz), 7.57 (d, 2H, *J* = 8.1 Hz), 7.20 (s, 2H), 7.08 (t, 1H, *J* = 7.4 Hz), 6.89 (d, 2H, *J* = 7.6 Hz), 6.84 (s, 1H), 6.76 (dd, 2H, *J* = 8.3, 1.5 Hz), 6.69 (d, 5H, *J* = 2.0 Hz), 6.66 (bt, 2H, *J* = 2.0 Hz), 6.63 (d, 27H, *J* = 2.2 Hz), 6.60 (d, 4H, *J* = 9.3 Hz), 6.53 (d, 35H, *J* = 2.2 Hz), 6.54 (m, 14H), 6.40 (t, 17H, *J* = 2.2 Hz), 5.85 (ddt, 32H, *J* = 17.1, 10.3, 6.6 Hz), 5.13 (ddt, 35H, *J* = 17.1, 1.9, 1.5 Hz), 5.06 (ddt, 35H, *J* = 10.3, 1.9, 1.2 Hz), 4.94 (s, 8H), 4.92 (s, 48H), 3.97 (t, 70H, *J* = 6.8 Hz), 3.67 (t, 2H, *J* = 6.9 Hz), 2.91 (t, 4H, *J* = 6.9 Hz), 2.87 (s, 10H), 2.51 (qt, 72H, *J* = 6.8, 1.4 Hz); <sup>13</sup>C NMR (126 MHz, CDCl<sub>3</sub>) 160.4, 160.3, 159.4, 152.8, 151.4, 144.2, 140.3, 139.5, 139.3, 139.2, 134.6, 130.5, 129.6, 128.8, 128.6, 127.3, 125.9, 117.3, 111.6, 110.6, 106.7, 106.1, 101.8, 101.6, 101.1, 70.3, 70.2, 67.4, 55.0, 40.2, 33.7, 27.2; <sup>19</sup>F NMR (400 MHz, CDCl<sub>3</sub>) δ –70.99; UV–Vis (CHCl<sub>3</sub>) λ<sub>max</sub> = 436.5; MS (MALDI-TOF) *m/z* = 6137.1 (M<sup>+</sup>); 6159.2 (M + Na<sup>+</sup>); 6174.1 (M + K<sup>+</sup>).

**4.2.20. Cross-linked dendrimeric host 32.** To a solution of 110 mg (18 μmol) of the dendrimer described in Section 4.2.19 in 1.7 L of benzene was added 38 mg (46 μmol, 8% per mol alkene) of **25**. The resulting solution was stirred at room temperature for 24 h and slowly poured through a 3 cm × 3 in. silica gel plug that was pre-equilibrated with benzene. A dark black layer remained on the top of the silica plug. An orange band was eluted from this top layer with 500 mL of 3% EtOAc–CH<sub>2</sub>Cl<sub>2</sub>. The orange colored eluent was collected and evaporated to a thick brown oil. Two successive preparative SEC columns afforded 31 mg (30%) of cross-linked dendrimer as a yellow-orange oil: <sup>1</sup>H NMR (400 MHz, CDCl<sub>3</sub>) δ 7.80–7.40 (bs), 6.90–6.00 (bd, 85H), 6.00–5.80 (bs, 1H), 5.70–5.40 (bs, 27H), 5.20–5.00 (bs, 3H),

5.00–4.30 (bs, 42H), 4.10–3.00 (s, 64H), 3.00–2.60 (bs, 5H), 2.60–2.00 (bs, 48H);  $^{19}\text{F}$  NMR (400 MHz,  $\text{CDCl}_3$ )  $\delta$  –70.93; UV–Vis ( $\text{CHCl}_3$ )  $\lambda_{\text{max}}=438.5$ ; MS (MALDI-TOF)  $m/z=5688.1$  (16 cross-links), 5713.0 (16 cross-links +  $\text{Na}^+$ ), 5739.0 (15 cross-links +  $\text{Na}^+$ ). To a solution of 30 mg (5.2  $\mu\text{mol}$ ) of the dendrimer prepared above in 10 mL of THF was added 5 mL of a 1% (v/v) aqueous solution of HCl. The mixture quickly turned from orange-yellow to red and 1 mL of  $\text{CHCl}_3$  was added to ensure homogeneity. The mixture was stirred at room temperature for 4 h and poured into 10 mL of a 10% (v/v) aqueous solution of HCl. The resulting suspension was extracted three times with 30 mL  $\text{CHCl}_3$ . The combined organic layers were washed with a saturated aqueous solution of sodium bicarbonate, dried over  $\text{Na}_2\text{SO}_4$ , filtered, and evaporated to a red oil. Flash chromatography (10%  $\text{EtOAc}-\text{CH}_2\text{Cl}_2$ ) afforded 17.4 mg (60%) of **32** as a red film:  $^1\text{H}$  NMR (400 MHz,  $\text{CDCl}_3$ )  $\delta$  8.40–7.80 (bd, 2H), 7.80–7.40 (bs, 5H), 6.80–6.00 (bd, 90H), 6.00–5.70 (bs, 3H), 5.70–5.10 (bs, 32H), 5.20–5.00 (bs, 4H), 5.00–4.40 (bs, 54H), 4.10–3.60 (s, 64H), 2.90–2.60 (bs, 8H), 2.60–2.20 (bs, 66H);  $^{19}\text{F}$  NMR (400 MHz,  $\text{CDCl}_3$ )  $\delta$  –70.62, –71.44; UV–Vis (THF)  $\lambda_{\text{max}}=480.0$ ,  $\epsilon$  (475 nm) = 25,400  $\text{M}^{-1}$ ; MS (MALDI-TOF)  $m/z=5585.4$  (16 cross-links +  $\text{Na}^+$ ), 5612.0 (15 cross-links +  $\text{Na}^+$ ), 5639.7 (14 cross-links +  $\text{Na}^+$ ), 5667.7 (13 cross-links +  $\text{Na}^+$ ).  $^{19}\text{F}$  NMR (400 MHz,  $\text{CDCl}_3$ )  $\delta$  –70.64, –71.28; UV–Vis (THF)  $\lambda_{\text{max}}=480.0$ ,  $\epsilon$  (475 nm) = 26,000  $\text{M}^{-1}$ ; MS (MALDI-TOF)  $m/z=5558.8$  (16 cross-links), 5582.9 (16 cross-links +  $\text{Na}^+$ ), 5599.6 (16 cross-links +  $\text{K}^+$ ), 5612.7 (15 cross-links +  $\text{Na}^+$ ), 5628.9 (15 cross-links +  $\text{K}^+$ ).

**4.2.21. Cross-linked dimeric dendron (33).** To a solution of 110 mg (36  $\mu\text{mol}$ ) **18** in 15 mL of benzene was added 38 mg (46  $\mu\text{mol}$ , 8 mol% per alkene) of **25**. The resulting solution was stirred under a reflux condenser at room temperature for 24 h. Every 5–6 h, dry nitrogen gas was bubbled into the reaction mixture for five to ten min. The mixture was slowly poured through a 3 cm  $\times$  3 in. silica gel plug that was pre-equilibrated with benzene. A dark red layer remained on the top of the silica plug. A red band was eluted from this top layer with 500 mL of 20%  $\text{EtOAc}-\text{CH}_2\text{Cl}_2$ . The red colored eluent was collected and evaporated to a red film. Preparative SEC afforded 10 mg of **33** as a red-oily film. Additional purification was achieved using flash chromatography with 20%  $\text{EtOAc}-\text{CH}_2\text{Cl}_2$ :  $^1\text{H}$  NMR (400 MHz,  $\text{CDCl}_3$ )  $\delta$  8.30–8.20 (bs, 1H), 8.15–8.00 (bs, 2H), 7.80–7.60 (bs, 4H), 6.80–6.00 (bd, 67H), 6.00–5.80 (bs, 3H), 5.70–5.40 (bs, 23H), 5.20–5.00 (bs, 3H), 5.00–4.30 (bs, 40H), 4.10–3.80 (s, 43H), 3.00–2.60 (bs, 12H), 2.60–2.20 (bs, 47H);  $^{19}\text{F}$  NMR (400 MHz,  $\text{CDCl}_3$ )  $\delta$  –71.33; UV–Vis ( $\text{CHCl}_3$ )  $\lambda_{\text{max}}=438.5$ ; MS (MALDI-TOF)  $m/z=5560.6$  (16 cross-links), 5584.9 (16 cross-links +  $\text{Na}^+$ ), 5600.9 (16 cross-links +  $\text{K}^+$ ), 5612.9 (15 cross-links +  $\text{Na}^+$ ), 5629.5 (15 cross-links +  $\text{K}^+$ ).

#### Acknowledgements

Funding of this work by the National Institutes of Health (GM61067) is gratefully acknowledged. The authors thank Melissa J. Witmer for early work on the X-ray analysis and

James B. Beil, Annabelle Benin, Brian G. Carter, and Denise M. Junge for assistance with preparative work.

#### References and notes

1. Taken in part from the Ph.D. Thesis of Eric Mertz, University of Illinois, 2002.
2. Selected reviews of chemosensors: (a) Czarnik, A. W.; Yoon, J. *Perspect. Supramol. Chem.* **1999**, *4*, 177–191. (b) Xue, G.; Savage, P. B.; Bradshaw, J. S.; Zhang, X. X.; Izatt, R. M. *Adv. Supramol. Chem.* **2000**, *7*, 99–137. (c) Wiskur, S. L.; Ait-Haddou, H.; Lavigne, J. J.; Anslyn, E. V. *Acc. Chem. Res.* **2001**, *34*, 963–972. (d) James, T. D.; Shinkai, S. *Top. Curr. Chem.* **2002**, *218*, 159–200. (e) Wang, W.; Gao, X.; Wang, B. *Curr. Org. Chem.* **2002**, *6*, 1285–1317.
3. *Fluorescent Chemosensors for Ion and Molecule Recognition*; Czarnik, A. W., Ed.; American Chemical Society: Washington, DC, 1993. Czarnik, A. W. *Acc. Chem. Res.* **1994**, *27*, 302–308.
4. Mertz, E.; Zimmerman, S. C. *J. Am. Chem. Soc.* **2003**, *125*, 3424–3425.
5. Wulff, G. *Chem. Rev.* **2002**, *102*, 1–27. Haupt, K.; Mosbach, K. *Chem. Rev.* **2000**, *100*, 2495–2504. Shea, K. J. *Trends Polym. Sci.* **1994**, *2*, 166–173.
6. Zimmerman, S. C.; Lemcoff, N. G. *Chem. Commun.* **2004**, 5–14.
7. Zimmerman, S. C.; Wendland, M. S.; Rakow, N. A.; Zharov, I.; Suslick, K. S. *Nature (London)* **2002**, *418*, 399–403. Zimmerman, S. C.; Zharov, I.; Wendland, M. S.; Rakow, N. A.; Suslick, K. S. *J. Am. Chem. Soc.* **2003**, *125*, 13504–13518.
8. Behringer, C.; Lehmann, B.; Simon, W. *Chimia* **1987**, *41*, 397–398.
9. (a) Mohr, G. J.; Tirelli, N.; Lohse, C.; Spichiger-Keller, U. E. *Adv. Mater.* **1998**, *10*, 1353–1357. (b) Mohr, G. J.; Demuth, C.; Spichiger-Keller, U. E. *Anal. Chem.* **1998**, *70*, 3868–3873. (c) Mohr, G. J.; Citterio, D.; Demuth, C.; Fehlmann, M.; Jenny, L.; Lohse, C.; Moradian, A.; Nezel, T.; Rothmaier, M.; Spichiger, U. E. *J. Mater. Chem.* **1999**, *9*, 2259–2264. (d) Mohr, G. J.; Nezel, T.; Spichiger-Keller, U. E. *Anal. Chim. Acta* **2000**, *414*, 181–187. For a related system for amine detection see: (e) Feuster, E. K.; Glass, T. E. *J. Am. Chem. Soc.* **2003**, *125*, 16174–16175.
10. Jiang, D.-L.; Aida, T. *Nature (London)* **1997**, *388*, 454–456. Archut, A.; Azzellini, G. C.; Balzani, V.; De Cola, L.; Vögtle, F. *J. Am. Chem. Soc.* **1998**, *120*, 12187–12191. Villavicencio, O.; McGrath, D. V. *Adv. Dendritic Macromol.* **2002**, *5*, 1–44.
11. Wendland, M. S.; Zimmerman, S. C. *J. Am. Chem. Soc.* **1999**, *121*, 1389–1390. Schultz, L. G.; Zhao, Y.; Zimmerman, S. C. *Angew. Chem., Int. Ed.* **2001**, *40*, 1962–1966. Kim, Y.; Mayer, M. F.; Zimmerman, S. C. *Angew. Chem., Int. Ed.* **2003**, *42*, 1121–1126. The same chemistry has been applied to star polymers: Beil, J. B.; Zimmerman, S. C. *Macromolecules* **2004**, *37*, 778–787.
12. For related work on cross-linked dendrimers see: Wang, J.; Jia, X.; Zhong, H.; Wu, H.; Li, Y.; Xu, X.; Li, M.; Wei, Y. *J. Polym. Sci. A—Polym. Chem.* **2000**, *38*, 4147–4153. Guo, W.; Li, J. J.; Wang, Y. A.; Peng, X. *J. Am. Chem. Soc.* **2003**, *125*, 3901–3909. Becker, J. J.; Gagne, M. R. *Organometallics* **2003**, *22*, 4984–4998.

13. Monographs on dendrimers: Fréchet, J. M.J.; Tomalia, D. A. *Dendrimers and Other Dendritic Polymers*; Wiley: New York, 2001. Newkome, G. R.; Moorefield, C. N.; Vögtle, F. *Dendrimers and Dendrons: Concepts, Syntheses, Applications*; VCH: Weinheim, 2001. Selected reviews on the supramolecular chemistry of dendrimers: Zeng, F.; Zimmerman, S. C. *Chem. Rev.* **1997**, *97*, 1681–1712. Newkome, G. R.; He, E.; Moorefield, C. N. *Chem. Rev.* **1999**, *99*, 1689–1746. Baars, M. W. P. L.; Meijer, E. W. *Top. Curr. Chem.* **2000**, *210*, 131–182. Smith, D. K.; Diederich, F. *Top. Curr. Chem.* **2000**, *210*, 183–227. Gorman, C. B.; Smith, J. C. *Acc. Chem. Res.* **2001**, *34*, 60–71. Zimmerman, S. C.; Lawless, L. J. *Top. Curr. Chem.* **2001**, *217*, 95–120.
14. Elmer, S. L.; Zimmerman, S. C. *J. Org. Chem.* **2004**, in press.
15. Miyaura, N.; Suzuki, A. *Chem. Rev.* **1995**, *95*, 2457–2483.
16. Klabunde, K. J.; Burton, D. J. *J. Org. Chem.* **1970**, *35*, 1711–1712.
17. Grignard addition of 4-fluoro-bromobenzene was reported by: Dishart, K. T.; Levine, R. *J. Am. Chem. Soc.* **1956**, *78*, 2268–2270.
18. Quan, D. Q.; Sournies, F. *Bull. Chem. Soc. Fr.* **1973**, 767–769.
19. Alternative synthesis of **16**: Bharathi, P.; Zhao, H.; Thayumanavan, S. *Org. Lett.* **2001**, *3*, 1961–1964.
20. MIPs using imines: Shea, K. J.; Stoddard, G. J.; Shavelle, D. M.; Wakui, F.; Choate, R. M. *Macromolecules* **1990**, *23*, 4497–4507. Wulff, G.; Heide, B.; Helfmeier, G. *J. Am. Chem. Soc.* **1986**, *108*, 1089–1091.
21. The use of TiCl<sub>4</sub> to make imine core dendrimers has been reported in: Higuchi, M.; Shiki, S.; Yamamoto, K. *Org. Lett.* **2000**, *2*, 3079–3082.
22. Gololobov, Y. G.; Zhmurova, I. N.; Kasukhin, L. F. *Tetrahedron* **1981**, *37*, 437–472. Note: the aza-Wittig reaction is related to the Staudinger reaction: Staudinger, H.; Meyer, J. *Helv. Chim. Acta* **1919**, *2*, 635–646.
23. Soloshonok, V. A.; Gerus, I. I.; Yagupol'skii, Y. L.; Kukhar, V. P. *Zh. Org. Kim.* **1988**, *24*, 293–297.
24. Ramström, O.; Ye, L.; Mosbach, K. *Chem. Biol.* **1996**, *3*, 471–477.
25. Mertz, E.; Beil, J. B.; Zimmerman, S. C. *Org. Lett.* **2003**, *5*, 3127–3130.
26. Page, M. I.; Jencks, W. P. *J. Am. Chem. Soc.* **1972**, *94*, 8818–8827.



# The relationship among $pK_a$ , pH, and binding constants in the interactions between boronic acids and diols—it is not as simple as it appears

Jun Yan, Greg Springsteen,<sup>†</sup> Susan Deeter and Binghe Wang<sup>\*,‡</sup>

Department of Chemistry, Georgia State University, 33 Gilmer St. S.E., Atlanta, GA 30303 USA

Received 15 January 2004; revised 15 July 2004; accepted 19 August 2004

Available online 16 September 2004

**Abstract**—In our continuing efforts into designing boronic acid-based sensors that recognize cell-surface carbohydrates, it has been necessary to examine various factors that affect the binding affinity between a boronic acid moiety and a diol. The current prevailing view is that the strongest boronic acid/diol complexes are generated by a combination of high solution pH and a low boronic acid  $pK_a$ . However, there has never been a systematic examination of the relationship among the binding constants, boronic acid  $pK_a$ , and the pH of the solution. Herein we report our findings with a series of 25 arylboronic acids with various substituents and their binding affinities with diols. We have found that (1) the relationship between the  $pK_a$  of monosubstituted phenylboronic acid and its substituents can be described using a Hammett plot; (2) the optimal pH for binding is not always above the  $pK_a$  of the boronic acid, and is affected by the  $pK_a$  values of the boronic acid and the diol, and other unknown factors; and (3) the general belief that boronic acids with lower  $pK_a$  values show greater binding affinities for diols is not always true.

© 2004 Elsevier Ltd. All rights reserved.

## 1. Introduction

The formation of a boronic ester from a boronic acid and a diol is likely the strongest single-pair reversible functional group interaction in an aqueous environment among organic compounds that can be readily used for the construction of molecular receptors. The binding of phenylboronic acid with catechol, for example, has an equilibrium constant of about  $800 \text{ M}^{-1}$ .<sup>1,2</sup> Consequently, boronic acids have been used as the recognition moiety in the construction of sensors for saccharides,<sup>3–13</sup> as nucleotide and carbohydrate transporters,<sup>14–21</sup> and as affinity ligands for the separation of carbohydrates and glycoproteins.<sup>22–29</sup> Appropriately designed boronic acid compounds also have shown potential as antibody mimics targeted on cell-surface carbohydrates.<sup>30–32</sup> Critical to furthering these efforts is an understanding of the effect of various factors on the relative stability of boronate esters.<sup>33</sup> We are able to accurately determine boronic acid/diol binding affinities through a

recently developed fluorescent method that is not limited by the requirement for a fluorescent boronic acid.<sup>1,2</sup> This was accomplished with the addition of a fluorescent reporter compound, Alizarin Red S. This three-component, competitive method allowed us to determine the binding constants for a series of diols with phenylboronic acid and corrected several literature mistakes regarding the strength of boronic acid–diol interactions.

In our efforts to design boronic acid-based fluorescent sensors that recognize cell-surface carbohydrates as biomarkers, we are interested in examining various factors that affect the binding affinity between a boronic acid and a diol. Such information will undoubtedly assist our efforts to optimize the binding affinity and specificity of potential fluorescent sensors.

It has been commonly believed that the higher the pH, the higher the binding constant between a boronic acid and a diol. It is also assumed that boronic acids with lower  $pK_a$  values have higher affinities. Although some of our earlier work has indicated that this is probably not true,<sup>1</sup> there has never been a systematic examination of the relationship among the binding constants, boronic acid and diol  $pK_a$  values, and the pH of the solution. Herein we report our findings with a series of 25 arylboronic acids with various substituents and selected binding affinities with a series of

**Keywords:** Boronic acids; Binding constants;  $pK_a$ ; pH.

\* Corresponding author. Tel.: +1-404-651-0289; fax: +1-404-6510289; e-mail: [wang@gsu.edu](mailto:wang@gsu.edu)

<sup>†</sup> Present address: Department of Chemistry, Scripps Research Institute, La Jolla, CA 92037, USA.

<sup>‡</sup> Major part of the experimental work was performed at North Carolina State University.



diols at varying pH values. We have found that: (1) the  $pK_a$  of monosubstituted boronic acids can be predicted based on the substituent effect using a Hammett plot; (2) the optimal pH for binding is not always above the  $pK_a$  of the boronic acid, instead it is related to both the  $pK_a$  values of the boronic acid and the diol, although in an imprecise manner that cannot be directly predicted; and (3) the common belief that boronic acids with lower  $pK_a$  values have greater binding affinities at neutral pH is not always true.

## 2. Experimental

### 2.1. General methods

Alizarin Red S and arylboronic acids were purchased from Acros, Asymchem, Frontier Scientific and Aldrich, and were used as received. Sugars, buffers, and diols were bought from Aldrich and Acros, and were used as received. Water used for the binding studies was doubly distilled and further purified with a Milli-Q filtration system.

A Shimadzu RF-5301PC fluorometer was used for all fluorescent studies. A Shimadzu UV-1601 UV–visible spectrophotometer was used for the  $pK_a$  determination. Quartz cuvettes were used in all studies.

### 2.2. $pK_a$ and binding constant determination

The method for the binding constant determination has been published before by our group.<sup>1</sup> To a solution of  $9.0 \times 10^{-6}$  M ARS, enough boronic acid was added to keep about 20% of the ARS in free form as measured by fluorescence<sup>1</sup> and the solution was brought to the correct pH in 0.10 M phosphate buffer (Solution A). Then sugar was added to a portion of solution A so that about 80% of the ARS was in free form (Solution B). Solution B was then titrated into solution A to make mixtures with a constant concentration of ARS and PBA and a range of concentrations of diol. In general, eight different concentrations were made in order to cover as much of the binding curve as possible. Each mixture was allowed to stand for at least 5 min. Then 3.5 mL of the mixture was transferred into a cuvette for fluorescence measurement.

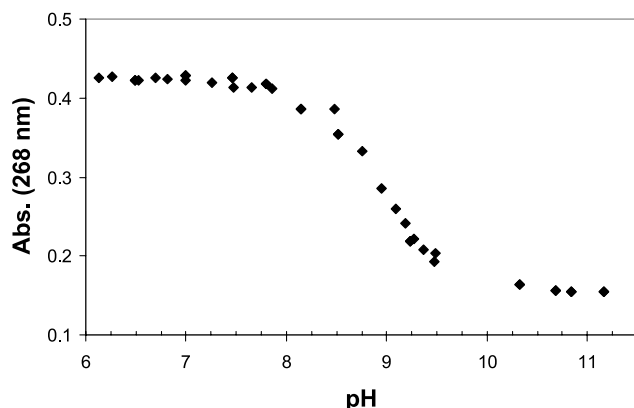


**Figure 1.** The  $pK_a$  of phenylboronic acid (PBA) can be determined by the absorbance change at 268 nm that occurs upon conversion from the trigonal form (low pH) to the tetrahedral form (high pH). ♦, PBA ( $1.0 \times 10^{-3}$  M) in 0.10 M phosphate buffer.

The apparent  $pK_a$  of each boronic acid was determined by observing the UV absorption changes that occur upon the hybridization change from the acidic trigonal form to the basic tetrahedral form (Fig. 1).<sup>34</sup>

## 3. Results and discussions

### 3.1. Effect of substituents on $pK_a$ of boronic acids

To determine the effect of different boronic acid acidities upon binding, we chose to examine a series of arylboronic acids with different substituents and two *N*-alkylated pyridinium boronic acids. At the extremes of this series were the electron rich 2-methoxyphenylboronic acid with the highest  $pK_a$  at 9.0, and the cationic *N*-benzylpyridinium boronic acid with the lowest  $pK_a$  at 4.2 (Table 1). With the  $pK_a$  values of these boronic acids spanning about 5  $pK_a$  units, its effect on the binding constants could be examined over a wide range. As expected, electron-withdrawing groups decreased the  $pK_a$  and electron-donating groups increased their  $pK_a$ . However, it does seem that the effect of electron donating groups is marginal compared with the electron withdrawing groups. For example, the  $pK_a$  of 2-methoxyphenyl boronic acid is only 0.2  $pK_a$  units higher than that of phenylboronic acid (8.8), while the  $pK_a$  of 3-nitrophenyl boronic acid is 1.7  $pK_a$  units lower than that of phenylboronic acid (Table 1). In an effort to gain a quantitative appreciation of the effect of different substituents, the Hammett values for different substituents<sup>35</sup> were plotted against the experimentally determined apparent  $pK_a$  values. A linear correlation was observed, and the measured slope of 2.1 is consistent with the formation of an anionic species as the final product (Fig. 2). Although the  $pK_a$  values of many boronic acids have been reported in the literature,<sup>12,36</sup> there has never been a systematic study examining such a large number of

**Table 1.** The  $pK_a$  values of a series of substituted phenylboronic acid compounds

Arylboronic acid	$pK_a$
2-Methoxyphenylboronic acid	9.0
3-Aminophenylboronic acid	8.9
Phenylboronic acid	8.8
4-Fluorophenylboronic acid	8.6
2,4-Dichlorophenylboronic acid	8.5
4-Bromophenylboronic acid	8.8
4-Aminomethylphenylboronic acid	8.3
3-Pyridinylboronic acid	8.1
4-Pyridinylboronic acid	8.0
4-Carboxyphenylboronic acid	8.0
3-Acetylphenylboronic acid	8.0
3-Chloro-4-fluorophenylboronic acid	7.8
3-Formylphenylboronic acid	7.8
4-Acetylphenylboronic acid	7.7
4-Formylphenylboronic acid	7.6
2,4-Difluorophenylboronic acid	7.6
3-Nitrophenylboronic acid	7.1
2,5-Difluorophenylboronic acid	7.0
3,4,5-Trifluorophenylboronic acid	6.8
2,3,4-Trifluorophenylboronic acid	6.8
2,4,5-Trifluorophenylboronic acid	6.7
2-Dimethylaminomethylphenylboronic acid	6.7
2-Fluoro-5-nitrophenylboronic acid	6.0
<i>N</i> -Methyl-3-pyridiniumboronic acid	4.4
<i>N</i> -Benzyl-3-pyridiniumboronic acid	4.2

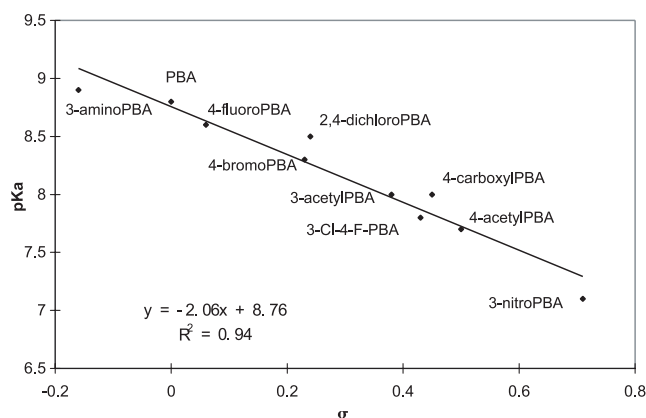
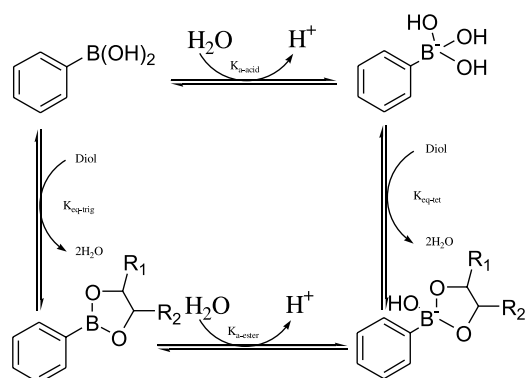


Figure 2.  $pK_a$  versus  $\sigma$  for substituted arylboronic acid compounds.

analogues. The availability of these  $pK_a$  data will serve as a baseline reference for the future design of boronic acid sensors with optimal affinity and specificity at physiological pH.

### 3.2. Binding affinities between arylboronic acids and sugars

As mentioned earlier, it has been generally believed that<sup>37–40</sup> (1) higher pH favors the binding between boronic acid and a diol, (2) the pH needs to be above the  $pK_a$  of the boronic acid to see meaningful binding, and (3) more acidic boronic acids bind more tightly with diols. However, in our earlier studies the pH binding profile of phenylboronic acid with Alizarin Red S showed an optimum at  $pH \sim 7$  (the binding constant is  $1500 M^{-1}$  at  $pH 7$ ,  $1100 M^{-1}$  at  $pH 7.5$ , and  $450 M^{-1}$  at  $pH 8.5$ ).<sup>1</sup> It is clear that at a pH above the  $pK_a$  of phenylboronic acid (8.8, Table 1), the binding constant is expected to be much lower than the optimal observed.<sup>1</sup> To further explore the theoretical basis for the pH dependence of the binding constants, we were interested in acquiring a further understanding of the relationship between proton concentration and the different equilibria involved. There are three acids in this mixture of boronic acid and diol. The first one is, of course, boronic acid itself (Scheme 1). The second one is the ester, which is often much more acidic than the acid, and the third is the diol. Although simple alcohols have  $pK_a$  values in the range of 16, vicinal diols are often much more acidic. For example,



Scheme 1. The relationships between phenylboronic acid and its diol ester.  $K_{eq-tert}$  and  $K_{eq-trig}$  are the equilibrium constants of tetrahedral and trigonal forms of the boronic acid.

the  $pK_a$  of glucose and fructose is about 12.<sup>41</sup> For catechol, the  $pK_a$  is about 9.3.<sup>41</sup> The lower  $pK_a$  of vicinal diols is presumably due to a combination of the hydrogen-bonding stabilization of the oxyanion in the deprotonated form by the neighboring hydroxyl group and the inductive electron-withdrawing effect of a neighboring oxygen. Based on these acid-based equilibria, two independent laboratories<sup>37–40</sup> have proposed that the optimal pH should be between the  $pK_a$  values of the boronic acid and diol (Eq. 1).

$$pH_{\text{optimal}} = (pK_{a-\text{acid}} + pK_{a-\text{diol}})/2 \quad (1)$$

The prediction from Eq. 1 for the optimal binding of Alizarin Red S. with phenylboronic acid (6.4, the  $pK_a$  of Alizarin Red S. is 4 and the  $pK_a$  of PBA is 8.8) is consistent with the experimental data which reaches a maximum at between  $pH 6.6$ – $7$ .<sup>1</sup> To further test this idea, the optimal pH for the binding of several boronic acids and Alizarin Red S. has been studied. The results shown in Table 2 demonstrate two points. First, the optimal pH does not necessarily need to be above the boronic acid  $pK_a$ . As a matter of fact, the optimal  $pK_a$  in the binding of all boronic acids tested with Alizarin Red S was below the  $pK_a$  of the boronic acids due to the low  $pK_a$  of Alizarin Red S. Second, Eq. 1 does not accurately predict the numerical values of the optimal pH. This is understandable since the equation does not take into consideration the effects of the solvent, buffer, and other intermolecular interactions such as sterics, hydrogen bonding, etc. Therefore, Eq. 1 can only be used as the basis to make an approximate estimation of the optimal pH. However, it is not suitable to be used for the quantitative prediction of the optimal pH.

In an effort to examine the relationship among  $pK_a$ , pH, and binding constants in a broader sense, the binding constants were determined for 6 substituted phenylboronic acids with glucose, fructose, and catechol at different pH values, and the results are summarized in Table 3. Figure 3 also shows a typical set of plots for the determination of the binding constants. These results show even more variation from the commonly believed situations stated above and that predicted by Eq. 1. First, the ranking of the binding constants among different boronic acids with a given diol at physiological pH does not always follow the trend of the boronic acid  $pK_a$ . For example, although 2,5-difluorophenylboronic acid has a higher apparent  $pK_a$  (7.6) than 3,4,5-trifluorophenylboronic acid (6.8), it also has a higher

Table 2. Optimal pH for binding between some phenylboronic acids and Alizarin Red S

Boronic acid	$pK_a$	Optimal pH	Predicted optimal pH
3,4,5-Trifluorophenylboronic acid	6.8	6	5.4
2-Fluoro-5-nitrophenylboronic acid	6	6	5.0
2-Methoxyphenylboronic acid	9	7.5	6.5
<i>N</i> -Benzyl-3-pyridiniumphenylboronic acid	4.2	4	4.1
<i>o</i> -Dimethylaminomethylphenylboronic acid	6.7	6	5.4
3-Chloro-4-fluorophenylboronic acid	7.8	6.5	5.9
4-Bromophenylboronic acid	8.3	6	6.2

**Table 3.** Binding constants<sup>a</sup> of boronic acids and sugars

Boronic acid (pK <sub>a</sub> )	PBA (8.8) <sup>b</sup>	4-Br-PBA (8.3)	3-Cl-4-F-PBA (7.8)	2,5-DifluoroPBA (7.6)	3,4,5-Trifluoro PBA (6.8)	2-F-5-NitroPBA (6.0)
Glucose (12.5) <sup>b</sup>						
pH 6.5	0.84	5.6	7.6	33	17	25
pH 7.5	4.6	20	26	47	41	47
pH 8.5	11	2.4 <sup>c</sup>	48	7.3 <sup>c</sup>	52	56
Predicted optimal pH	10.6	10.3	10.1	10.0	9.6	9.2
Fructose (12.3)						
pH 6.5	29	123	562	237	545	1398
pH 7.5	210	495	1003	2136	2523	2062
pH 8.5	560	1194	1853	120	4443	378 <sup>c</sup>
Predicted optimal pH	10.4	10.2	9.9	9.8	9.4	9.0
Catechol (9.2)						
pH 6.5	150	715	1646	8841	2137	3027
pH 7.5	830	1557	6100	4703	2896	4359
pH 8.5	3300	1966	7487	418 <sup>c</sup>	5376	3792
Predicted optimal pH	9.0	8.8	8.5	8.4	8.0	7.6

<sup>a</sup> Binding constants (M<sup>-1</sup>) were determined in 0.10 M phosphate buffer (see Section 2).

<sup>b</sup> The number in parenthesis is the pK<sub>a</sub> of the boronic acid or the diol.

<sup>c</sup> The experimental errors are in range of 20–40%, others are below 10%.

binding constant with glucose at pH 7.5, which goes against the conventional thinking. On the other hand, the ranking of the binding constants for these two boronic acids with fructose is reversed compared with binding with glucose. It is also interesting to note that the binding constants of 2,5-difluorophenylboronic acid and 3,4,5-trifluorophenylboronic acid with fructose at pH 7.5 are higher than that of 2-fluoro-5-nitrophenylboronic acid even though the latter has the lowest pK<sub>a</sub> among all six boronic acids tested.

Second, the ranking of the binding constants among different boronic acids with a given diol depends on the pH of the solution. For example, the binding constant between 2,5-difluorophenylboronic acid and fructose is higher than that of 3-chloro-4-fluorophenylboronic acid at

pH 7.5, but lower at pH 8.5. The binding of these two boronic acids with catechol also exhibits the same kind of pH-dependent reversal of ranking orders. Such results are partially attributable to the different optimal pH for these two boronic acids.

Therefore, when one discusses the relative binding constants of various boronic acids with a particular diol, one has to consider the specific conditions, particularly the pH of the solution under which the binding constants were determined.

Among the six boronic acids tested for their binding to various diols, 2,5-difluorophenylboronic acid and 2-fluoro-5-nitrophenylboronic acid showed especially large 'deviations' from that predicted by Eq. 1. For example, the predicted optimal pH for the binding between 2,5-difluorophenylboronic acid and glucose is 9.8. However, the highest binding constant was observed at pH 7.5. A similar situation with the binding to fructose was observed. In the latter case, the predicted optimal pH is 9.8 and the highest binding constant was observed at pH 7.5. Such results further indicate that the pK<sub>a</sub> values of the boronic acid and the sugars are not the only major determinants of the binding constants and optimal pH. Buffer<sup>1</sup> and steric factors<sup>42</sup> are all known to affect the binding constants. It is conceivable that conformational changes, interactions such as binding by a third hydroxyl,<sup>4,43</sup> and sterics are all idiosyncratic factors that affect binding.

#### 4. Conclusions

Understanding the factors that affect the binding affinity between boronic acid and diol moieties is important to the future design of boronic acid based sensors. The results reported indicate: (1) as expected, electron-withdrawing groups can significantly lower the pK<sub>a</sub> of boronic acids and a linear correlation can be used to predict the pK<sub>a</sub> of monosubstituted phenylboronic acids using the Hammett

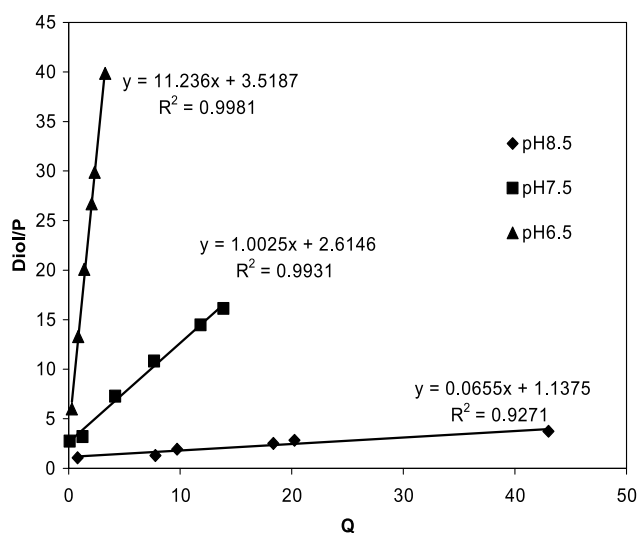


**Figure 3.** Binding constant determination for 3,4,5-trifluoroPBA with fructose at different pH values.  $P = [L_0] - 1/QK_{eq1} - [I_0]/(Q+1)$ ,  $Q = [I]/[IL]$ ; [diol]=total diol concentration, I=indicator (ARS),  $[I_0]$ =total indicator concentration, L=ligand (PBA),  $K_{eq1}$ =association constant of ARS–PBA complex. The  $K_{eq1}$  of boronic acid–diol complex can be calculated by dividing  $K_{eq1}$  by the slope of the plot.

values of the substituents; (2) the general belief that boronic acids with lower  $pK_a$  values show greater binding affinities is not always true and many other factors affect the binding constant; and (3) the optimal binding pH is not necessarily above the  $pK_a$  of the boronic acid.

### Acknowledgements

Financial support from the National Institutes of Health (CA88343, NO1-CO-27184, and DK55062), the North Carolina Biotechnology Center (2001ARG0016), the Georgia Cancer Coalition through a Distinguished Cancer Scientist Award (BW), and the Georgia Research Alliance through an Eminent Scholar endowment is greatly acknowledged.

### Supplementary data

Supplementary data associated with this article can be found, in the online version, at doi:10.1016/j.tet.2004.08.051

### References and notes

- Springsteen, G.; Wang, B. *Tetrahedron* **2002**, *58*, 5291–5300.
- Springsteen, G.; Wang, B. *Chem. Commun.* **2001**, 1608–1609.
- James, T. D.; Sandanayake, K. R. A. S.; Iguchi, R.; Shinkai, S. *J. Am. Chem. Soc.* **1995**, *117*, 8982–8987.
- Eggert, H.; Frederiksen, J.; Morin, C.; Norrild, J. C. *J. Org. Chem.* **1999**, *64*, 3846–3852.
- James, T. D.; Sandanayake, K. R. A. S.; Shinkai, S. *Angew. Chem. Int. Ed. Engl.* **1996**, *35*, 1910–1922.
- Wang, W.; Gao, S.; Wang, B. *Org. Lett.* **1999**, *1*, 1209–1212.
- Yoon, J.; Czarnik, A. W. *J. Am. Chem. Soc.* **1992**, *114*, 5874–5875.
- Adhikiri, D. P.; Heagy, M. D. *Tetrahedron Lett.* **1999**, *40*, 7893–7896.
- Arimori, S.; Bosch, L. I.; Ward, C. J.; James, T. D. *Tetrahedron Lett.* **2001**, *42*, 4553–4555.
- Cabell, L. A.; Monahan, M.-K.; Anslyn, E. V. *Tetrahedron Lett.* **1999**, *40*, 7753–7756.
- Yang, W.; He, H.; Drueckhammer, D. G. *Angew. Chem. Int. Ed.* **2001**, *40*, 1714–1718.
- Wang, W.; Gao, X.; Wang, B. *Curr. Org. Chem.* **2002**, *6*, 1285–1317.
- Yang, W.; Yan, J.; Springsteen, G.; Deeter, S.; Wang, B. *Bioorg. Med. Chem. Lett.* **2003**, *13*(6), 1019–1022.
- Draffin, S. P.; Duggan, P. J.; Duggan, S. A. M. *Org. Lett.* **2001**, *3*, 917–920.
- Gardiner, S.; Smith, B.; Duggan, P.; Karpa, M.; Griffin, G. *Tetrahedron* **1999**, *55*, 2857–2864.
- Karpa, M.; Duggan, P.; Griffin, G.; Freudigmann, S. *Tetrahedron* **1997**, *53*, 3669–3678.
- Mohler, L. K.; Czarnik, A. W. *J. Am. Chem. Soc.* **1993**, *115*, 2998–2999.
- Paugam, M.-F.; Bien, J. T.; Smith, B. D.; Chrisstoffels, L. A. J.; de Jong, F.; Reinhoudt, D. N. *J. Am. Chem. Soc.* **1996**, *118*, 9820–9825.
- Riggs, J. A.; Hossler, K. A.; Smith, B. D.; Karpa, M. J.; Griffin, G.; Duggan, P. J. *Tetrahedron Lett.* **1996**, *37*, 6303–6306.
- Smith, B. D.; Gardiner, S. J.; Munro, T. A.; Paugam, M. F.; Riggs, J. A. *J. Incl. Phenom. Mol. Recogn. Chem.* **1998**, *32*, 121–131.
- Westmark, P. R.; Gardiner, S. J.; Smith, B. J. *J. Am. Chem. Soc.* **1996**, *118*, 11093–11100.
- Adamek, V.; Liu, X.-C.; Zhang, Y. A.; Adamkova, K.; Scouten, W. H. *J. Chromatogr.* **1992**, *625*, 91–99.
- Bergold, A.; Scouten, W. H. *Chem. Anal. (NY)* **1983**, *66*, 149–187.
- Bouriotis, V.; Galpin, J.; Dean, P. D. G. *J. Chromatogr.* **1981**, *210*, 267–268.
- Liu, X.; Hubbard, J.; Scouten, W. J. *Organomet. Chem.* **1995**, *493*, 91–94.
- Psova, J.; Janiczek, O. *Chem. Listy* **1995**, *89*, 641–648.
- Seliger, H.; Genrich, V. *Experientia* **1974**, *30*, 1480–1481.
- Singhal, R.; DeSilva, S. Giddings, J., Grushka, E., Brown, P., Eds.; *Advanced Chromatography*; Marcel Dekker: New York, 1992; Vol. 31, pp 293–335.
- Westmark, P. R.; Valencia, L. S.; Smith, B. D. *J. Chromatogr. A* **1994**, *664*, 123–128.
- Sugasaki, A.; Sugiyasu, K.; Ikeda, M.; Takeuchi, M.; Shinkai, S. *J. Am. Chem. Soc.* **2001**, *123*, 10239–10244.
- Yang, W.; Gao, S.; Gao, X.; Karnati, V. R.; Ni, W.; Wang, B.; Hooks, W. B.; Carson, J.; Weston, B. *Bioorg. Med. Chem. Lett.* **2002**, *12*, 2175–2177.
- Yang, W.; Gao, X.; Wang, B. *Med. Res. Rev.* **2003**, *23*, 346–368.
- Mulla, H. R.; Agard, N. J.; Basu, A. *Bioorg. Med. Chem. Lett.* **2003**, *14*, 25–27.
- Soundararajan, S.; Badawi, M.; Kohlrust, C. M.; Hageman, J. H. *Anal. Biochem.* **1989**, *178*, 125–134.
- Corwin, H.; Leo, A.; Taft, R. W. *Chem. Rev.* **1991**, *91*, 165–195.
- James, T. D.; Linnane, P.; Shinkai, S. *Chem. Commun.* **1996**, 281–288.
- Van Duin, M.; Peters, J. A.; Kieboom, A. P. G.; Van Bekkum, H. *Tetrahedron* **1984**, *40*, 2901–2911.
- Liu, X.; Scouten, W. J. *J. Chromatogr. A* **1994**, *687*, 61–69.
- Singhal, R. P.; Ramamurthy, B.; Govindraj, N.; Sarwar, Y. *J. Chromatogr.* **1991**, *543*, 17–38.
- Sienkiewicz, P. A.; Roberts, D. C. J. *Inorg. Nucl. Chem.* **1980**, *42*(11), 1559–1575.
- Albert, A.; Serjeant, E. P. *The Determination of Ionization Constants*, 3rd ed.; London: Chapman and Hall, 1984.
- Mulla, H. R.; Agard, N. J.; Basu, A. *Bioorg. Med. Chem. Lett.* **2004**, *14*, 25–27.
- Bielecki, M.; Eggert, H.; Norrild, J. C. *J. Chem. Soc., Perkin Trans. 2* **1999**, *3*, 449–456.



# Mono- and oligosaccharide sensing by phenylboronic acid-appended 5,15-bis(diarylethynyl)porphyrin complexes

Osamu Hirata, Yohei Kubo, Masayuki Takeuchi\* and Seiji Shinkai\*

Department of Chemistry and Biochemistry, Graduate School of Engineering, Kyushu University, Hakozaki 6-10-1, Higashi-ku, Fukuoka 812-8581, Japan

Received 2 March 2004; revised 1 July 2004; accepted 20 August 2004

Available online 16 September 2004

**Abstract**—Porphyrin derivatives bearing a pair of boronic acid groups (**1**, **1·Zn**, and **1·Cu**) were designed and synthesized from **2** to construct a saccharide sensing system. Compounds **1**, **1·Zn**, and **1·Cu** have a diethynyl porphyrin rotational axis, which is expected to act as a saccharide-binding modulator. Saccharide binding studies were conducted by UV–vis, fluorescence, and circular dichroism (CD) spectroscopies. In a water–methanol 1:1 (v/v) mixed solvent, we have found that **1·Zn** can bind mono- and oligosaccharides including Lewis oligosaccharides to produce 1:1 host–saccharide complexes with the association constants of  $10^2$ – $10^3$  M<sup>-1</sup> range. This paper thus demonstrates a new principle to design a boronic acid-based saccharide receptor.

© 2004 Elsevier Ltd. All rights reserved.

## 1. Introduction

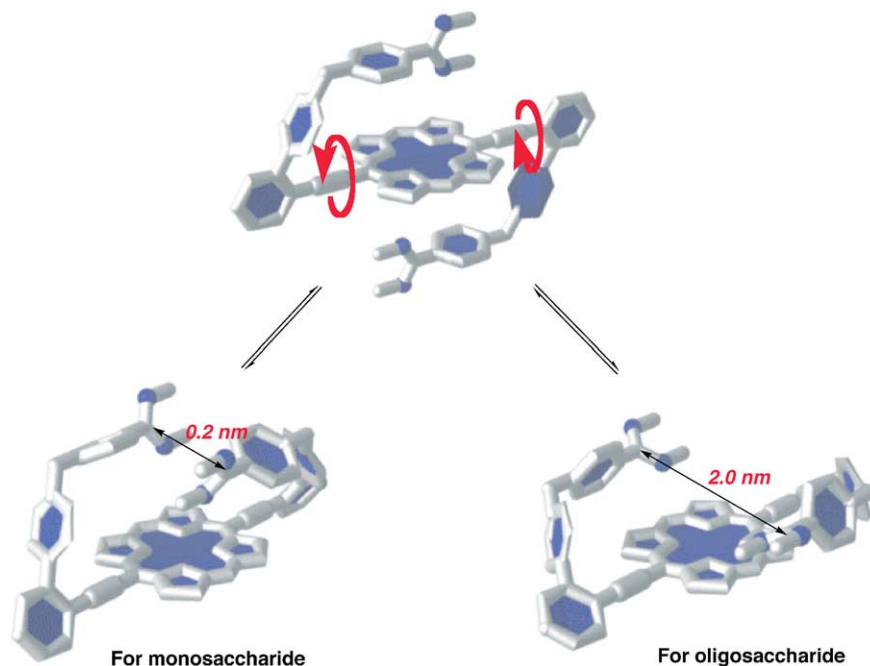
The recognition of biologically important molecular species by synthetic molecular receptors has gained momentum. Since the chemistry of saccharides plays a significant role in the metabolic pathways of living organisms, the detection of biologically important saccharides is necessary in a variety of medical and industrial contexts.<sup>1,2</sup> Although it is not so easy to ‘touch’ saccharides in water, it has been shown that boronic acid–saccharide covalent interactions, which readily and reversibly form in aqueous media, represent an important binding force in the recognition of saccharides and related molecular species.<sup>2,3</sup> Diboronic acid derivatives,<sup>2</sup> which can react with four of the five OH groups of a saccharide to form intramolecular 1:1 complexes, show a stability order different from monoboronic acid derivatives,<sup>4</sup> which is related to the specific spatial position of two boronic acid groups. This implies that the appropriate manipulation of two boronic acids in a same host molecule is of importance for sensing a specific oligosaccharide guest. In the course of our research goal to construct a highly sensitive and selective biologically important saccharide sensing system, this idea has been tested with a few diboronic acid systems bearing a long and rigid spacer:<sup>5,6</sup> e.g. diphenyl-3,3′-diboronic acid, stilbene-3,3′-diboronic acid, and *cis*-5,15-bis[2-(dihydroxyboronyl)phenyl]-10,20-

diphenylporphyrin. These diboronic acid derivatives show some selectivity for certain disaccharides but the selectivity and the affinity observed so far are not so high.<sup>5,6</sup> To improve the affinity and the selectivity toward oligosaccharides, we have planned to amalgamate two strategies, diboronic acid receptor<sup>2</sup> and positive homotropic allosterism<sup>7–9</sup> which can be utilized as a new concept to achieve both high guest selectivity and high guest affinity. With this design scheme in mind, we have reported allosteric mono- and oligosaccharide sensing by phenylboronic acids-appended bis[porphyrinato]cerium(IV) double decker porphyrin<sup>10</sup> and meso–meso porphyrin dimer.<sup>11</sup> Recently, we showed that a phenylboronic acids-appended 5,15-bis(triarylethynyl)porphyrin **3** acts as an allosteric monosaccharide receptor working in aqueous media.<sup>12</sup> Compound **3** has a diethynyl porphyrin rotational axis and two pairs of phenylboronic acids arranged around it. Through these studies, it occurred to us that a pair of phenylboronic acids arranged around the rigid rotational axis would bind oligosaccharides without the aid of allosterism when the distance between phenylboronic acids is adjustable to the distance between *cis*-1,2-diols and/or 1,3-diols in oligosaccharides. To test this working hypothesis, we designed and synthesized compound **1**. Compound **1** has a diethynyl porphyrin rotational axis and the distance between two phenylboronic acids can vary from 0.1 to 2.4 nm through the rotation of ethynyl axis (Scheme 1). Metallation of **1** induces a change in porphyrin plane geometry, which would influence the binding signal from host–saccharide complex. We describe here the saccharide binding properties of

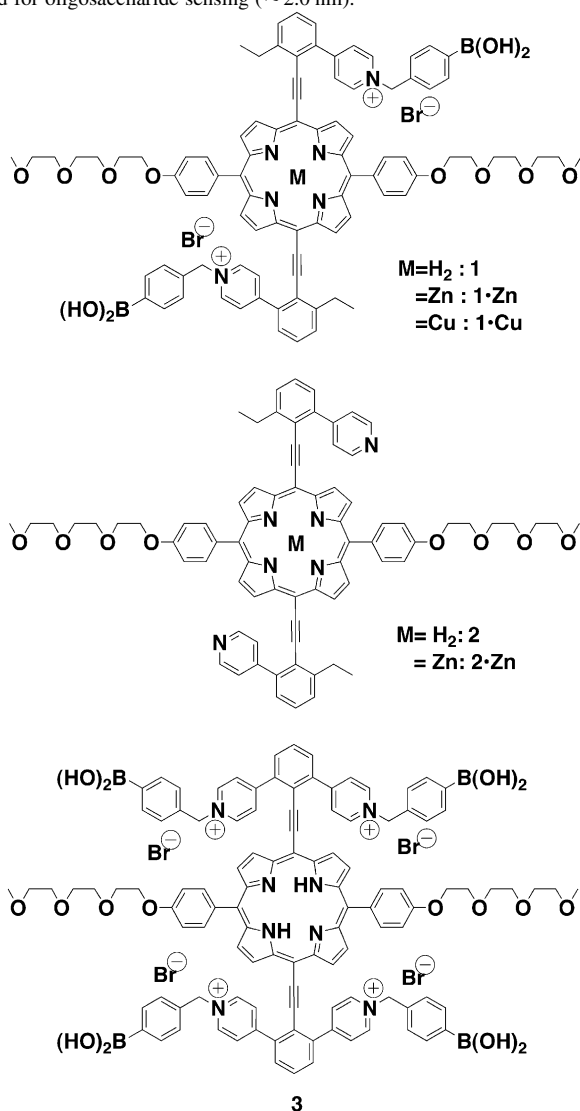
**Keywords:** Saccharide sensing.

\* Corresponding authors. Tel.: +81926423585; fax: +81926423611 (M.T.); e-mail addresses: [taketcm@mbox.nc.kyushu-u.ac.jp](mailto:taketcm@mbox.nc.kyushu-u.ac.jp); [seijitcm@mbox.nc.kyushu-u.ac.jp](mailto:seijitcm@mbox.nc.kyushu-u.ac.jp)





**Scheme 1.** Schematic illustration of **1** for mono- and oligosaccharide. The distance between boronic acids can vary for monosaccharide sensing (0.2–0.3 nm) and for oligosaccharide sensing ( $\sim 2.0$  nm).



porphyrin derivatives **1**, **1·Zn**, and **1·Cu** bearing a pairs of phenylboronic acids. From this new receptor molecule, we have found that **1·Zn** is a useful receptor for mono- and oligosaccharides.

## 2. Results and discussion

### 2.1. UV–vis and fluorescence spectroscopic studies

Compound **1** was previously synthesized by treatment of **2** with 2-(4-bromomethylphenyl)-1,3-dioxo-2-borinan in DMF.<sup>12</sup> Compounds **1·Zn** and **1·Cu** were synthesized from compounds **2·Zn** and **2**, respectively. These compounds were identified by <sup>1</sup>H NMR, MS spectral evidence, and elemental analyses.

Absorption spectra of **1**, **1·Zn**, and **1·Cu** were measured in water/MeOH mixed solvents at 25 °C. Recently, we found that the significant spectral change in **1** was induced in water–methanol mixed solvent above 30 vol% of water content.<sup>12</sup> A measurement condition was set to a water (pH 10.5 with 50 mM carbonate buffer)/MeOH = 1:1 (v/v) mixture into which **1**, **1·Zn**, and **1·Cu** were dissolved and boronate anion ( $-B(OH)_3^-$ ) showed the better saccharide affinity than those under the physiological conditions. The  $\lambda_{max}$  values of compounds **1**, **1·Zn**, and **1·Cu** appear at 442, 450, and 433 nm, respectively (Fig. 1(a)). Judging from the absorption bands appearing at around 300 nm assignable to the peripheral diaryl moieties, no characteristic band attributable to electronic transitions between mixed molecular levels of diaryl moieties and diethynyl porphyrin exist. The Soret bands and Q bands of **1**, **1·Zn**, and **1·Cu** were scarcely affected by saccharide addition, indicating that the saccharide binding does not induce any significant aggregation under these conditions. The fluorescence spectra of **1** and **1·Zn** were almost same as those in the

presence of saccharides. Thus, circular dichroism (CD) spectroscopy, which is known to be more sensitive to the saccharide binding event,<sup>2</sup> was applied for the present study.

## 2.2. CD spectroscopic studies in the presence of monosaccharides

In general, when a monosaccharide is bound to a boronic acid group in a host, the resultant complex becomes optically-active. It is already known that the complex can yield a strongly CD-active species only when the boronic acid groups form a macrocyclic structure with a saccharide intramolecularly.<sup>13</sup> Thus, we used CD spectroscopy to demonstrate the saccharide-sensing abilities of **1**, **1·Zn**, and **1·Cu**. First, we chose L-fucose as a guest monosaccharide because we recently found that **1** can bind L-fucose in 1:1 stoichiometry and the resultant complex yields a relatively large CD signal among monosaccharides tested.<sup>12</sup> Figure 1(b) shows CD spectra of the L-fucose complexes of **1**, **1·Zn** or **1·Cu**. Norrild et al.<sup>14</sup> reported that the rearrangement of the boronic acid–saccharide complex takes place in alkaline aqueous solution, which should influence the shape of CD spectra for host–saccharide complex. CD spectra observed for **1**·saccharide complexes were mostly unchanged in a day and gradually decreased in its intensity in a few days probably due to the slow decomposition of compound **1** under these conditions.<sup>15</sup> The results imply that base-promoted rearrangement of the boronic acid–saccharide complex does not take place in the present system. Addition of D-fucose to **1·Zn** gives the CD spectrum symmetrical to the corresponding L-isomer, showing that the spectral patterns are derived from the absolute structure inherent to each saccharide (Fig. 1(b)).

Since the shapes of CD spectra appearing at around 400 nm for **1** or **1·Cu**-L-fucose complex are similar to those of the absorption spectra of **1** or **1·Cu**, these spectra are regarded to be the ICD spectra induced by the bound saccharide. The

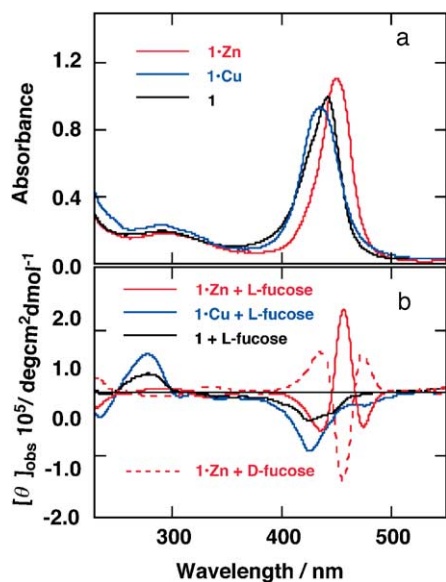
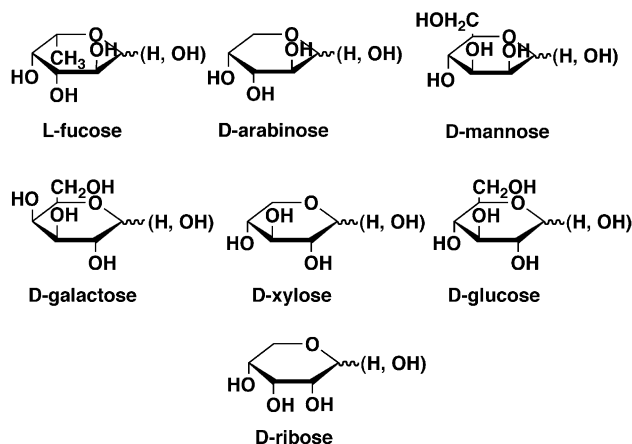


**Figure 1.** UV-vis (a) and CD spectra (b) of **1** (5.0  $\mu$ M), **1·Cu** (5.0  $\mu$ M) and **1·Zn** (6.15  $\mu$ M) in the presence of L-fucose (5.0 mM) in a water (pH 10.5 with 50 mM carbonate buffer)/MeOH=1:1 (v/v) mixture. Cell length=1.0 cm.

exciton-coupling type CD bands for **1·Cu**-L-fucose complexes were also observed at around 300 nm, indicating that the peripheral phenylboronic acid-appended biaryls in **1·Cu** can orientate in a chiral fashion. The rigid and square planer configuration of porphyrin-Cu complex in **1·Cu** would contribute to this exciton-coupling-type CD band appearance. In contrast to these complexes, **1·Zn**-L-fucose complex yields a split-type CD band at around 400 nm and an ICD band at around 300 nm. The  $[\theta]_{\text{obs}}$  value of **1·Zn**-L-fucose complex is larger than those of **1**- and **1·Cu**-L-fucose complexes, so that this band is suitable for monitoring the saccharide concentration.



Upon addition of monosaccharides (D-xylose, D-glucose, D-arabinose, D-mannose, D-galactose, and D-ribose) to **1**, **1·Zn**, or **1·Cu**, their characteristic CD spectra appeared (Fig. 2). These results indicate that two diol moieties in monosaccharides are used to bind two boronic acid groups, bridging two diarylmoieties. This view is further supported by the fact that 4,6-*O*-ethylidene- $\alpha$ -D-glucose which has only one useful diol moiety cannot yield the perceptible CD band. The CD spectroscopic data in Figure 2 are summarized in Table 1. The CD spectra of **1·Zn**-monosaccharide complexes feature the spectral pattern inherent to each monosaccharide, whereas **1**- and **1·Cu**-monosaccharide complexes show the almost same shape as that observed for L-fucose complex. Furthermore, **1·Zn** gave the largest  $[\theta]_{\text{obs}}$  among three host molecules and yielded the split type of CD spectra useful for sensing and discrimination of monosaccharides. Examination of Table 1 raises an intriguing coincidence between the CD sign of Soret band region and the absolute configuration of 2-OH: that is, when 2-OH has the (*S*)-configuration (D-glucose, D-galactose, D-xylose, and D-ribose), the **1·Zn** complex shows the plus–minus–plus CD signal at the Soret band region, whereas when 2-OH has the (*R*)-configuration (L-fucose, D-arabinose, and D-mannose), it tends to show the minus–plus–minus CD signal. Conceivably, the 2-OH group would regulate the twisting direction of the chromophoric porphyrin plane.

It is seen from Figure 2 and Table 1 that L-fucose, D-gulcose, D-arabinose, D-xylose, and D-galactose gave the strong  $[\theta]_{\text{obs}}$  values with **1·Zn** useful for the determination of their association constants, whereas the  $[\theta]_{\text{obs}}$  values with other host complexes are not so large enough to evaluate the binding process except for L-fucose complexes. Detailed

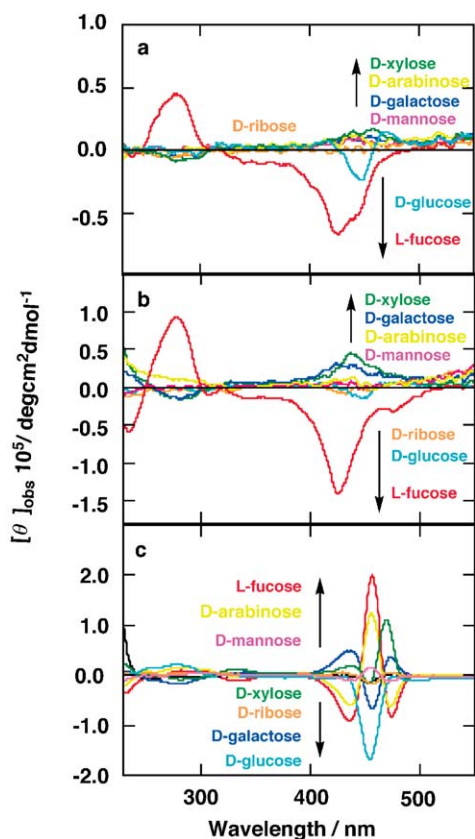


**Figure 2.** CD spectra of (a) **1** (5.0  $\mu\text{M}$ ), (b) **1**·**Cu** (5.0  $\mu\text{M}$ ), and (c) **1**·**Zn** (6.15  $\mu\text{M}$ ) in the presence of monosaccharides (5.0 mM) in a water (pH 10.5 with 50 mM carbonate buffer)/MeOH=1:1 (v/v) mixture. Cell length=1.0 cm.

spectral studies were carried out for **1**·**Zn**. The CD spectra measured as a function of monosaccharide concentration provided several isosbestic points maintaining the same shape, indicating that the reaction consists of only two species under one equilibrium (Fig. 3).

A plot of the  $[\theta]_{\text{obs}}$  versus the monosaccharide concentration gave a saturation curve (Fig. 4). The stoichiometry of the CD-active complexes was corroborated by a Job plot.<sup>16</sup> A plot of  $[\theta]_{\text{obs}}$  values at 456 nm against  $[\mathbf{1} \cdot \mathbf{Zn}] / ([\mathbf{1} \cdot \mathbf{Zn}] + [\text{monosaccharide}])$  has a maximum at 0.50. From analysis of the binding isotherm, the association constants ( $K$ ) for L-fucose, D-gulcose, D-arabinose, D-xylose, and D-galactose with **1**·**Zn** were evaluated to be 2100, 2800, 6100, 3800, and 3000  $\text{M}^{-1}$ , respectively. For **1**- and **1**·**Cu**-L-fucose com-

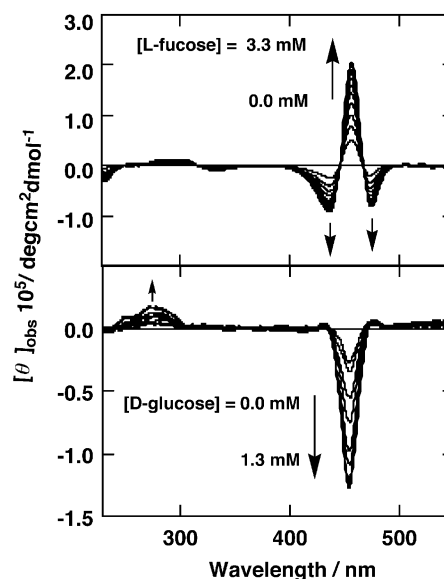


**Figure 3.** Change in the CD spectra of **1**·**Zn** (5.0  $\mu\text{M}$ ) by the addition of L-fucose (0–5.0 mM) or D-glucose (0–1.3 mM); 25 °C; water (pH 10.5 with 50 mM carbonate buffer)/MeOH=1:1 (v/v) mixture; cell length=1.0 cm.

plexes, the  $K$  values were determined to be 1500 and 1700  $\text{M}^{-1}$ , respectively. There is no large difference in the association constants for L-fucose among three host molecules tested herein and **1**·**Zn** showed the larger affinity toward monosaccharides. It is a surprise for us that a subtle structural change induced by metallation of porphyrin is so effective to change the pattern of CD signals and to enhance the  $[\theta]_{\text{obs}}$  value useful for sacharide sensing.

### 2.3. CD spectroscopic studies in the presence of oligosaccharides

Phenylboronic acid moieties in **1**, **1**·**Zn**, and **1**·**Cu** can adopt various angles with respect to the porphyrin plane through ethynylene rotation and the distance between them is adjustable from 0.1 nm to 2.4 nm, suggesting that these three host molecules could be suitable for sensing oligosaccharides (for example, the distance between two diol moieties of maltose is estimated to be ca.1.0 nm). To test this working hypothesis, we chose glucose dimers (maltose, isomaltose, laminalibiose, gentiobiose,  $\alpha,\alpha$ -trehalose, and cellobiose) as disaccharide guests. With **1** or **1**·**Cu**, the reproducible CD spectrum was obtained only from isomaltose (Fig. 5 and Table 2).

**Table 1.** CD spectral parameters for monosaccharides

	1-Saccharide complex		1·Cu-Saccharide complex		1·Zn-Saccharide complex		
	$[\theta]_{\text{obs}} 10^4 / \text{deg cm}^2 \text{ dmol}^{-1}$ ( $\lambda_{\text{max}}$ or $\lambda_{\text{min}}$ /nm)		$[\theta]_{\text{obs}} 10^4 / \text{deg cm}^2 \text{ dmol}^{-1}$ ( $\lambda_{\text{max}}$ or $\lambda_{\text{min}}$ /nm)		$[\theta]_{\text{obs}} 10^4 / \text{deg cm}^2 \text{ dmol}^{-1}$ ( $\lambda_{\text{max}}$ or $\lambda_{\text{min}}$ /nm)		
L-Fucose	4.45 (278.5)	−6.72 (426.5)	9.16 (278.0)	−14.1 (426.0)	−9.20 (436.0)	20.0 (456.5)	−8.26 (474.5)
D-Fucose					9.58 (435.0)	−21.0 (455.5)	9.06 (473.5)
D-Arabinose	(−) <sup>a</sup>	(−) <sup>a</sup>	(−) <sup>a</sup>	(−) <sup>a</sup>	−5.92 (437.0)	12.4 (456.0)	−6.29 (473)
D-Mannose	(−) <sup>a</sup>	(−) <sup>a</sup>	(−) <sup>a</sup>	(−) <sup>a</sup>	−0.925 (431.5)	1.59 (455.5)	−1.14 (473.5)
D-Glucose	(−)	−2.42 (448.0)	0.559 (299.5)	−1.60 (447.5)	−0.115 (430.0)	−16.9 (454.5)	−0.262 (475.5)
D-Galactose	−0.570 (282.0)		−1.73 (281.0)	3.08 (424.0)	4.88 (437.5)	−6.62 (457.0)	3.64 (473.5)
D-Ribose	(−) <sup>a</sup>	(−) <sup>a</sup>	(−) <sup>a</sup>	(−) <sup>a</sup>	0.641 (429.5)	−1.84 (457.0)	0.563 (472.0)
D-Xylose	−0.928 (279.0)	1.69 (457.0)	−1.63 (283.0)	4.57 (437.0)	1.87 (438.5)	−1.84 (454.0)	11.0 (469.5)

<sup>a</sup>  $[\theta]_{\text{obs}}$  is too small to obtain the correct value.

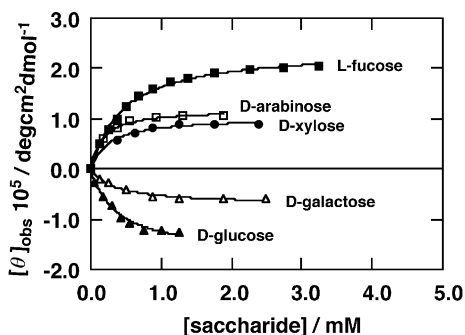


**Figure 4.** Plots of  $[\theta]_{\text{obs}}$  versus monosaccharide concentrations for  $1 \cdot \text{Zn}$ . 25 °C, water (pH 10.5 with 50 mM carbonate buffer)/MeOH=1:1 (v/v) mixture. Cell length=1.0 cm.

With  $1 \cdot \text{Zn}$ , the stronger CD bands were observable for 1–6 D-glucose dimers, isomaltose and gentiobiose (Fig. 6 and Table 2). The CD spectra for isomaltose and gentiobiose cross the  $[\theta]_{\text{obs}}=0$  line around the  $\lambda_{\text{max}}$  of the Soret band as

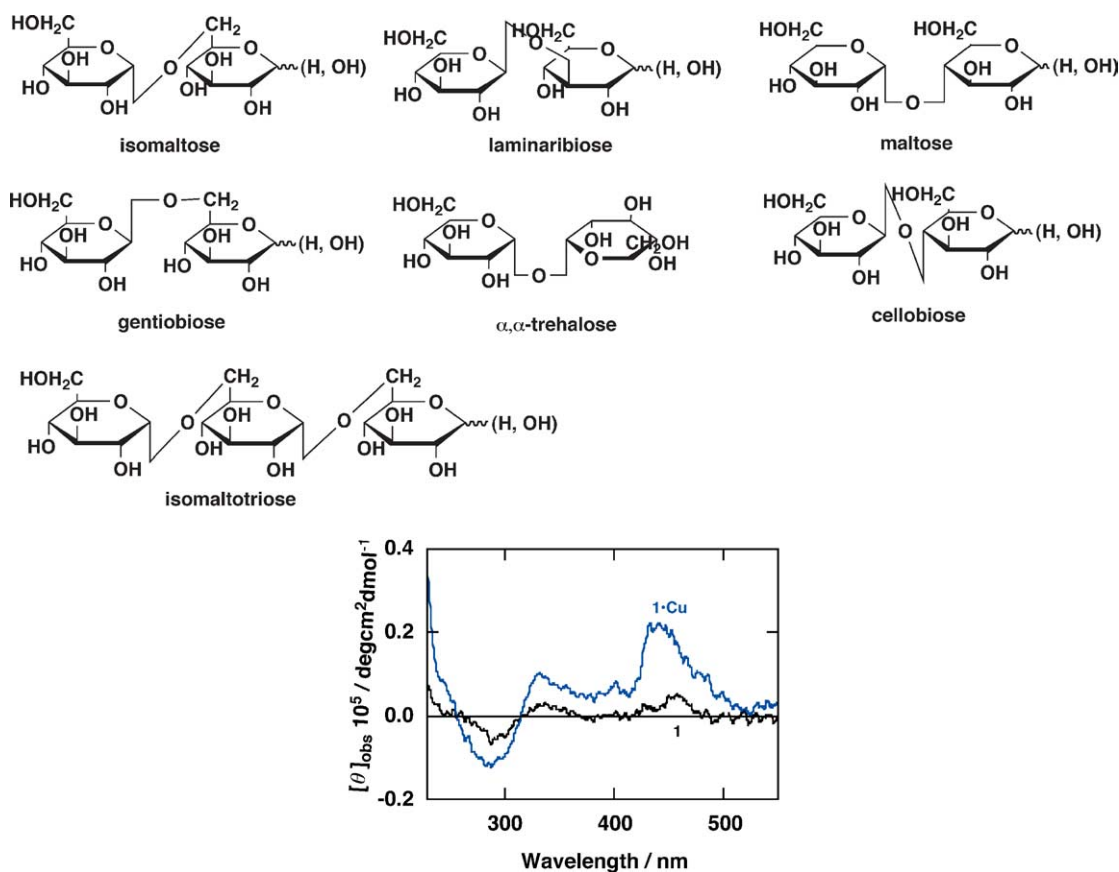


**Figure 5.** CD spectra of  $1$  and  $1 \cdot \text{Cu}$  (5.0  $\mu\text{M}$ ) in presence of isomaltose (5.0 mM) in a water (pH10.5 with carbonate buffer)/MeOH=1/1 (v/v) mixture. Cell length=1.0 cm.

**Table 2.** CD spectral parameters for oligosaccharides

	$1$ Saccharide complex		$1 \cdot \text{Cu}$ Saccharide complex		$1 \cdot \text{Zn}$ Saccharide complex		
	$[\theta]_{\text{obs}} 10^4 / \text{deg cm}^2 \text{ dmol}^{-1}$ ( $\lambda_{\text{max}}$ or $\text{min}/\text{nm}$ )	$[\theta]_{\text{obs}} 10^4 / \text{deg cm}^2 \text{ dmol}^{-1}$ ( $\lambda_{\text{max}}$ or $\text{min}/\text{nm}$ )	$[\theta]_{\text{obs}} 10^4 / \text{deg cm}^2 \text{ dmol}^{-1}$ ( $\lambda_{\text{max}}$ or $\text{min}/\text{nm}$ )	$[\theta]_{\text{obs}} 10^4 / \text{deg cm}^2 \text{ dmol}^{-1}$ ( $\lambda_{\text{max}}$ or $\text{min}/\text{nm}$ )	$[\theta]_{\text{obs}} 10^4 / \text{deg cm}^2 \text{ dmol}^{-1}$ ( $\lambda_{\text{max}}$ or $\text{min}/\text{nm}$ )		
Gentiobiose	(–) <sup>a</sup>	(–) <sup>a</sup>	(–) <sup>a</sup>	(–) <sup>a</sup>	3.96 (440.5)	–2.39 (458.0)	1.97 (474.0)
Isomaltose	–0.67 (288.5)	5.07 (456.5)	–1.22 (283.0)	2.24 (442.0)	1.98 (434.5)	–3.81 (456.0)	2.19 (474.0)
Isomaltotriose	(–) <sup>a</sup>	(–) <sup>a</sup>	(–) <sup>a</sup>	(–) <sup>a</sup>	1.90 (435.0)	–1.73 (456.0)	1.44 (472)
SLe <sup>x</sup>	3.02 (286.0)	–4.52 (428.5)	6.49 (281.0)	–8.55 (427.0)	–4.05 (436.5)	9.92 (456.5)	–3.46 (474.0)
Le <sup>x</sup>	3.58 (283.0)	–5.26 (426.0)	7.57 (282.0)	–10.7 (427.0)	–5.85 (436.5)	14.2 (456.5)	–5.29 (473.0)

<sup>a</sup>  $[\theta]_{\text{obs}}$  is too small to obtain the correct value.

already shown for monosaccharides. It is noteworthy that  $1 \cdot \text{Zn}$  can discriminate disaccharides having a 1–6 linkage among six disaccharides tested herein. The  $K$  value between  $1 \cdot \text{Zn}$  and isomaltose is calculated to be  $800 \text{ M}^{-1}$  (Fig. 7). In the titration of gentiobiose with  $1 \cdot \text{Zn}$ , the shape of the CD signal changed with the increase in the gentiobiose concentration, so that we could not evaluate the association constant precisely. Comparing the results for D-glucose with those for isomaltose, D-glucose showed the 3.5 times larger association constant and the 4.4 times larger  $[\theta]_{\text{obs}}$  values (Tables 1 and 2). Isomaltotriose, which is a trimer of D-glucose via  $\alpha$  1–6 linkage, shows the slightly smaller  $[\theta]_{\text{obs}}$  value than that of isomaltose (Table 2). These results suggest that the more flexible guest gives the smaller  $[\theta]_{\text{obs}}$  value and shows the smaller affinity with  $1 \cdot \text{Zn}$ . Since disaccharides are conformationally more flexible owing to the central glycoside linkage than monosaccharides, they seem to have a scarce ability to immobilize two boronic acids in host molecules.



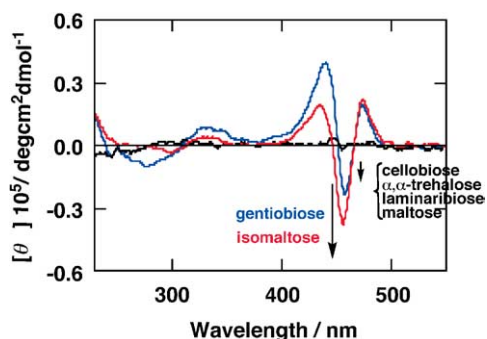


**Figure 6.** CD spectra of **1**·**Zn** (6.15  $\mu$ M) in presence of disaccharides (5.0 mM) in a water (pH 10.5 with 50 mM carbonate buffer)/MeOH=1:1 (v/v) mixture. Cell length=1.0 cm.

Next, we investigated Lewis oligosaccharide guests,<sup>10c,17</sup> such as Lewis<sup>X</sup> (Le<sup>X</sup>) and sialyl Lewis<sup>X</sup> (SLe<sup>X</sup>), which are involved in the adhesion of leukocytes and neutrophils to vesicular endothelial cells during normal and pathogenic inflammatory responses.<sup>18</sup> It is important to develop rationally designed artificial synthetic receptors for such oligosaccharides, which will lead to generation of small molecular antagonists and design of specific sensory systems. Undoubtedly, development of such artificial receptors is useful for the sensitive and convenient detection of these oligosaccharide antigens in the blood serum.<sup>19</sup>

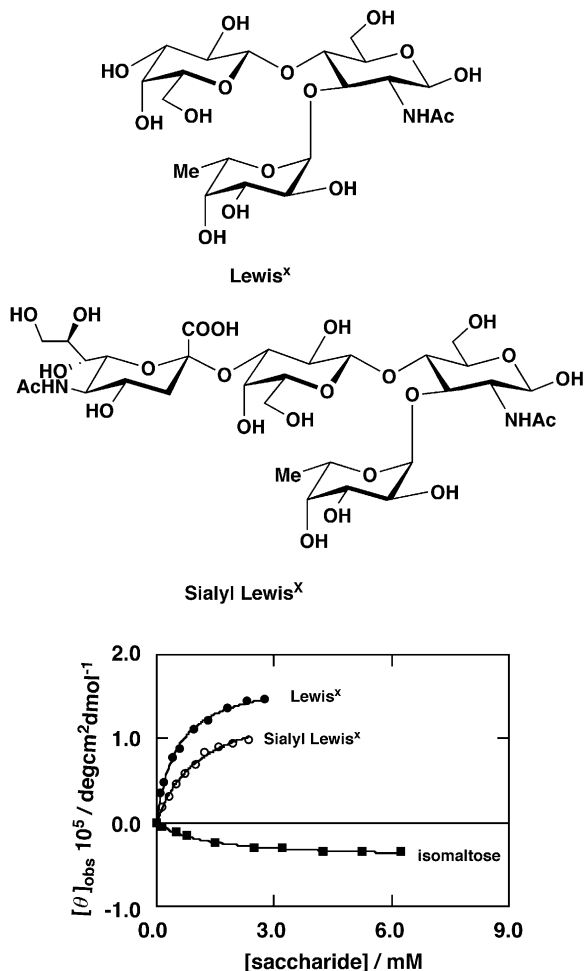


**Figure 7.** Plots of  $[\theta]_{\text{obs}}$  versus monosaccharide concentrations for **1**·**Zn**. 25 °C; water (pH 10.5 with 50 mM carbonate buffer)/MeOH=1:1 (v/v) mixture; cell length=1.0 cm.

Binding affinities of **1**, **1**·**Zn**, and **1**·**Cu** toward Lewis oligosaccharides were also evaluated by the CD spectroscopic method. Upon addition of Le<sup>X</sup> or SLe<sup>X</sup> to a solution of **1**, **1**·**Zn**, or **1**·**Cu**, ICD bands (for **1** and **1**·**Cu**) and the split-type CD bands (for **1**·**Zn**) were clearly observed (Fig. 8 and Table 2). Judging from the fact that the boronic acid group can interact only with the *cis*-1,2-diol or 1,3-diol moiety in saccharides,<sup>2</sup> it is undoubted that phenylboronic acid groups in **1**, **1**·**Zn**, and **1**·**Cu** interact with the 4,6-diol group of the galactose moiety and the 3,4-diol group of the fucose moiety in Le<sup>X</sup> and SLe<sup>X</sup> backbone. This is also supported by the fact that the CD band of **1**·**Zn**–Le<sup>X</sup> complex is very similar to that of **1**·**Zn**–SLe<sup>X</sup> complex. From the analysis of the binding isotherm (Fig. 7), the *K* values for Le<sup>X</sup> and SLe<sup>X</sup> with **1**·**Zn** were obtained to be 1900 and 890 M<sup>-1</sup>, respectively, which are almost in the same magnitude as those for monosaccharides. The large *K* value of Le<sup>X</sup> with respect to that of SLe<sup>X</sup> would be attributable to the bulkiness of sialic acid moiety in SLe<sup>X</sup>.

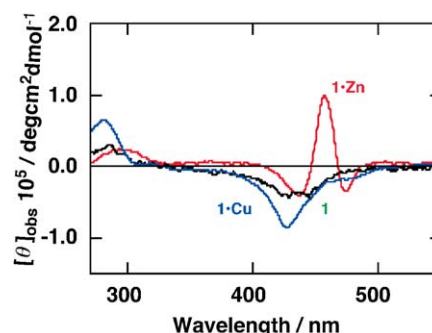


**Figure 8.** CD spectra of **1** and **1**·**Cu** (5.0  $\mu$ M) in the presence of SLe<sup>X</sup> (2.44 mM) and **1**·**Zn** (5.0  $\mu$ M) in the presence of SLe<sup>X</sup> (2.37 mM) in water (pH 10.5 with carbonate buffer)/MeOH=1/1 (v/v) mixture. Cell length=1.0 cm.

### 3. Conclusion

In conclusion, we have demonstrated that **1** is useful as a new scaffold for the design of a saccharide sensing system. The findings obtained here clearly show that the saccharide-binding subunits, which are arranged around the rigid rotational axis, can bind mono- and oligosaccharides. Moreover, a chromophore, porphyrin in the axis efficiently works as a reading-out functional moiety for the guest-binding information to give the CD spectra and the binding signal can be finely tuned by metallation of the porphyrin chromophore. Further studies are currently continued in this laboratory.

### 4. Experimental

#### 4.1. General

All starting materials and solvents were purchased from Aldrich, Tokyo Kasei Chemicals or Wako Chemicals and used as received. The <sup>1</sup>H NMR spectra were recorded either on a Bruker AC 250 (250 MHz) or Bruker DRX 600 (600 MHz) spectrometer. Chemical shifts are reported in ppm downfield from tetramethylsilane as the internal standard. MALDO-TOF and ESI mass spectral data were



obtained using a Perseptive Voyager RP MALDI TOF mass spectrometer and JEOL JMS-T100CS spectrometer, respectively. UV–vis, fluorescent, and CD spectra were recorded with a Shimadzu UV-2500 PC, Hitachi F-4500, and JASCO 720W spectrophotometer, respectively.

## 4.2. Synthesis

Synthesis of compounds **1**, **2**, and **2·Zn** was reported previously.<sup>12</sup>

**4.2.1. Compound 1·Zn.** Compound **2·Zn**<sup>12</sup> (15 mg, 0.012 mmol) and 2-(4-bromomethylphenyl)-1,3-dioxo-2-borinan<sup>20</sup> (30 mg, 0.12 mmol) were dissolved in dehydrated DMF (6 mL) and the mixture was heated at 50 °C for overnight. The progress of the quarternization reaction was monitored by a TLC method (alumina, acetone/methanol/trifluoroacetic acid=20:10:1 v/v/v). After confirming that the reaction was completed, the solution was cooled and evaporated to dryness, the solid residue being washed with ether to afford 11 mg of **1·Zn** as green powder. Yield 52%. Mp >300 °C. <sup>1</sup>H NMR (600 MHz, DMSO-*d*<sub>6</sub>, 27 °C, δ = ppm, *J*=Hz) 1.62 (t, *J*=7.5 Hz, 6H), 3.47–3.51 (m, 8H), 3.62 (t, *J*=4.6 Hz, 4H), 3.66 (d, *J*=4.9 Hz, 4H), 3.74 (d, *J*=4.9 Hz, 4H), 3.96 (s, 4H), 4.42 (s, 4H), 5.97 (s, 4H), 7.42 (d, *J*=8.2 Hz, 4H), 7.50 (d, *J*=7.7 Hz, 4H), 7.70–7.77 (m, 8H), 7.82 (d, *J*=7.82 Hz, 2H), 8.07 (s, 4H), 8.10 (d, *J*=7.9 Hz, 4H), 8.82–8.85 (m, 8H), 9.14 (d, *J*=4.4 Hz, 4H), 9.38 (d, *J*=6.3 Hz, 4H). Calcd for C<sub>90</sub>H<sub>86</sub>B<sub>2</sub>Br<sub>2</sub>ZnN<sub>6</sub>O<sub>12</sub>·4H<sub>2</sub>O: C, 61.33; H, 5.38; N, 4.77. Found: C, 61.40; H, 5.08; N, 4.80. UV–vis (water/MeOH=1:1 (v/v) mixture): λ<sub>max</sub> (log ε)=295 (4.48), 450 (5.26), 664 (4.65) nm. ESI-MS (CH<sub>3</sub>OH): calcd for [tetramethylester of **1·Zn**–2Br<sup>−</sup>]<sup>2+</sup> 792.32, found 792.28.

**4.2.2. Compound 2·Cu.** Copper acetate (250 mg, 1.25 mmol) in methanol (30 mL) was added to a solution of **2** (30 mg) in dichloromethane (20 mL). The resultant mixture was stirred for 12 h. After confirming that the reaction was completed by UV–vis spectroscopy, the organic layer was washed with 3% NH<sub>4</sub>Cl aq. (50 mL×3) and dried over anhydrous Na<sub>2</sub>SO<sub>4</sub>. After removal of the solvent, the green residue was chromatographed (silica gel, chloroform/methanol=10/–100/1 gradient) to give 25 mg of **2·Cu** as green powder (79%). Mp 171–173 °C. MALDI-TOF-MS (matrix: dithranol): calcd (found) [M]<sup>+</sup>: 1257.47 (1257.46). Calcd for C<sub>76</sub>H<sub>70</sub>CuN<sub>6</sub>O<sub>8</sub>·2H<sub>2</sub>O: C, 70.49; H, 5.76; N, 6.49. Found: C, 70.69; H, 5.64; N, 6.35.

**4.2.3. Compound 1·Cu.** **2·Cu** (20 mg, 0.016 mmol) and 2-(4-bromomethylphenyl)-1,3-dioxo-2-borinan<sup>20</sup> (41 mg, 0.16 mmol) were dissolved in dehydrated DMF (8 mL) and the mixture was heated at 60 °C for overnight. The progress of the quarternization reaction was monitored by a TLC method (alumina, acetone/methanol/trifluoroacetic acid=20:10:1 v/v/v). After confirming that the reaction was completed, the solution was cooled and evaporated to dryness, the solid residue being washed with ether to afford 24 mg of **1·Cu** as green powder. Yield 85%. Mp 220–222 °C. Calcd for C<sub>90</sub>H<sub>86</sub>B<sub>2</sub>Br<sub>2</sub>CuN<sub>6</sub>O<sub>12</sub>·4H<sub>2</sub>O: C, 61.39; H, 5.38; N, 4.77. Found: C, 61.53; H, 5.11; N, 4.77. UV–vis (water/MeOH=1:1 (v/v) mixture) λ<sub>max</sub> (log ε)=293 (4.67),

435 (5.27), 639 (4.59) nm. ESI-MS (CH<sub>3</sub>OH): calcd for [tetramethylester of **1·Cu**–2Br<sup>−</sup>]<sup>2+</sup> 791.83, found 791.77.

## Acknowledgements

We thank Ms. Hongyue Li at Kyushu University for <sup>1</sup>H NMR measurements. The present work is partially supported by a Grant-in-Aid for the 21st Century COE Program, 'Functional Innovation of Molecular Informatics' from the Ministry of Education, Culture, Science, Sports and Technology of Japan.

## References and notes

- Davis, A. P.; Wareham, R. S. *Angew. Chem. Int. Ed.* **1999**, *38*, 2978. (b) Wong, C.-H. *Acc. Chem. Res.* **1999**, *32*, 376.
- For recent comprehensive reviews see (a) James, T. D.; Linnane, P.; Shinkai, S. *J. Chem. Soc., Chem. Commun.* **1996**, 281. James, T. D.; Sandanayake, K. R. A. S.; Shinkai, S. *Angew. Chem. Int. Ed. Engl.* **1996**, *35*, 1911. (c) Takeuchi, M. *J. Syn. Org. Chem. Jpn* **1998**, *56*, 831. (d) Hartley, J. H.; James, T. D.; Ward, C. J. *J. Chem. Soc., Perkin Trans. 1* **2000**, 3155–3184. (e) James, T. D.; Shinkai, S. *Top. Curr. Chem.* **2002**, *218*, 159. (f) Yang, W.; Gao, X.; Wang, B. *Med. Res. Rev.* **2003**, *23*, 346.
- Recent saccharide sensing systems utilizing boronic acid–diol interactions, see: (a) Yang, H.; He, H.; Drucekhammer, D. G. *Angew. Chem. Int. Ed.* **2001**, *40*, 1714. DiCesareand, N.; Lakowicz, J. R. *J. Phys. Chem. A* **2001**, *105*, 6834. (c) Tong, A.-J.; Yamauchi, A.; Hayashita, T.; Zhang, Z.-Y.; Smith, B. D.; Teramae, N. *Anal. Chem.* **2001**, *73*, 1530. (d) Arimori, S.; Bell, M. L.; Oh, C. S.; Frimat, K. A.; James, T. D. *J. Chem. Soc., Perkin Trans. 1* **2002**, 803. (e) He, M.; Johnson, R. J.; Escobedo, J. O.; Beck, P. A.; Kim, K. K.; St Luce, N. N.; Davis, C. J.; Lewis, P. T.; Fronczek, F. R.; Melancon, B. J.; Mrse, A. A.; Treleaven, W. D.; Strongin, R. M. *J. Am. Chem. Soc.* **2002**, *124*, 5000. (f) Shoji, E.; Freund, M. S. *J. Am. Chem. Soc.* **2002**, *124*, 12486. (g) Otsuka, H.; Uchimura, E.; Koshino, H.; Okano, T.; Kataoka, K. *J. Am. Chem. Soc.* **2003**, *125*, 3493. (h) Suri, J. T.; Cordes, D. B.; Cappuccio, F. E.; Ritche, C.; Wessling, R. A.; Singaram, B. *Langmuir* **2003**, *19*, 5145. (i) Arimori, S.; Phillips, M. D.; James, T. D. *Tetrahedron Lett.* **2004**, *45*, 1539. (j) Nakata, E.; Nagase, T.; Shinkai, S.; Hamachi, I. *J. Am. Chem. Soc.* **2004**, *126*, 490. (k) Stones, D.; Manku, S.; Lu, X.; Hall, D. G. *Chem Eur. J.* **2004**, *10*, 92.
- Yoon, J.; Czarnik, A. W. *J. Am. Chem. Soc.* **1992**, *114*, 5874. (b) Mohler, L. K.; Czarnik, A. W. *J. Am. Chem. Soc.* **1993**, *115*, 2998. (c) Pagan, M. F.; Smith, B. D. *Tetrahedron Lett.* **1993**, *34*, 3723. (d) Nagai, Y.; Kobayashi, K.; Toi, H.; Aoyama, Y. *Bull. Chem. Soc. Jpn* **1993**, *66*, 2965. (e) Morin, G. T.; Hughes, M. P.; Pagan, M.-F.; Smith, B. D. *J. Am. Chem. Soc.* **1994**, *116*, 8895. (f) Westmark, P. R.; Smith, B. D. *J. Am. Chem. Soc.* **1994**, *116*, 9343.
- Sandanayake, K. R. A. S.; Nakashima, K.; Shinkai, S. *J. Chem. Soc., Chem. Commun.* **1994**, 1621.
- Kijima, H.; Takeuchi, M.; Shinkai, S. *Chem. Lett.* **1998**, 781.
- Rebek, J. *Acc. Chem. Res.* **1984**, *17*, 258. (b) Nabeshima, T. *Coord. Chem. Rev.* **1996**, *148*, 151. (c) Shinkai, S.; Sugasaki, A.; Ikeda, M.; Takeuchi, M. *Acc. Chem. Res.* **2001**, *34*, 494.

- (d) Takeuchi, M.; Sugasaki, A.; Ikeda, M.; Shinkai, S. *Acc. Chem. Res.* **2001**, *34*, 865. (e) Glass, T. E. *J. Am. Chem. Soc.* **2000**, *122*, 4522. (f) Raker, J.; Glass, T. E. *J. Org. Chem.* **2002**, *67*, 6113. (g) Raker, J.; Glass, T. E. *J. Org. Chem.* **2001**, *66*, 6505. (h) Raker, J.; Glass, T. E. *Tetrahedron* **2001**, *57*, 10233.
8. Tabushi, I.; Sasaki, T. *J. Am. Chem. Soc.* **1983**, *105*, 2901. (b) Tabushi, I. *Pure Appl. Chem.* **1988**, *60*, 581. (c) Rebek, J.; Costello, T.; Marshall, L.; Wattley, R.; Gadwood, R. C.; Onan, K. *J. Am. Chem. Soc.* **1985**, *107*, 7481–7487. (d) Traylor, T. G.; Mitchell, M. J.; Ciconene, J. P.; Nelson, S. *J. Am. Chem. Soc.* **1982**, *104*, 4986–4989. (e) Beer, P. D.; Rothin, A. S. *J. Chem. Soc., Chem. Commun.* **1988**, *52*. (f) Petter, R. C.; Salek, J. S.; Sikorski, C. T.; Kumaravel, G.; Lin, F.-T. *J. Am. Chem. Soc.* **1990**, *112*, 3860. (g) Schneider, H.-J.; Ref, D. *Angew. Chem. Int. Ed. Engl.* **1990**, *29*, 1159. (h) Sijbesma, R. P.; Nolte, R. J. *J. Am. Chem. Soc.* **1991**, *113*, 6695. (i) Kobuke, Y.; Satoh, Y. *J. Am. Chem. Soc.* **1992**, *114*, 789. (j) Kobayashi, K.; Asakawa, Y.; Kato, Y.; Aoyama, Y. *J. Am. Chem. Soc.* **1992**, *114*, 10307. (k) Pfeil, A.; Lehn, J.-M. *Chem. Commun.* **1992**, 838. (l) Blanc, S.; Yakirevitch, P.; Leize, E.; Meyer, M.; Libman, J.; Dorsselaer, A. V.; Albrecht-Gary, A.-M.; Shanzer, A. *J. Am. Chem. Soc.* **1997**, *119*, 4934. (m) Ishi-I, T.; Crego-Calama, M.; Timmerman, P.; Reinhoudt, D. N.; Shinkai, S. *Angew. Chem., Int. Ed.* **2002**, *41*, 1924.
9. Takeuchi, M.; Imada, T.; Shinkai, S. *Angew. Chem., Int. Ed.* **1998**, *37*, 2096. (b) Ikeda, M.; Takeuchi, M.; Sugasaki, A.; Robertson, A.; Imada, T.; Shinkai, S. *Supramol. Chem.* **2000**, *12*, 321. (c) Ikeda, M.; Tanida, T.; Takeuchi, M.; Shinkai, S. *Org. Lett.* **2000**, *2*, 1803. (d) Robertson, A.; Ikeda, M.; Takeuchi, M.; Shinkai, S. *Bull. Chem. Soc. Jpn* **2001**, *74*, 739. (e) Yamamoto, M.; Sugasaki, A.; Ikeda, M.; Takeuchi, M.; Frimat, K.; James, T. D.; Shinkai, S. *Chem. Lett.* **2001**, 520. (f) Kubo, Y.; Ikeda, M.; Sugasaki, A.; Takeuchi, M.; Shinkai, S. *Tetrahedron. Lett.* **2001**, *42*, 7435. (g) Kubo, Y.; Sugasaki, A.; Sugiyasu, K.; Ikeda, M.; Sonoda, K.; Ikeda, A.; Takeuchi, M.; Shinkai, S. *Org. Lett.* **2002**, *4*, 925. (h) Ayabe, M.; Ikeda, A.; Kubo, Y.; Takeuchi, M.; Shinkai, S. *Angew. Chem., Int. Ed.* **2002**, *41*, 2790. (i) Ikeda, M.; Takeuchi, M.; Shinkai, S.; Tani, F.; Naruta, Y.; Sakamoto, S.; Yamaguchi, K. *Chem. Eur. J.* **2002**, *8*, 5541.
10. Sugasaki, A.; Ikeda, M.; Takeuchi, M.; Koumoto, K.; Shinkai, S. *Tetrahedron* **2000**, *56*, 4717. (b) Sugasaki, A.; Ikeda, M.; Takeuchi, M.; Shinkai, S. *Angew. Chem., Int. Ed.* **2000**, *39*, 3839. (c) Sugasaki, A.; Sugiyasu, K.; Ikeda, M.; Takeuchi, M.; Shinkai, S. *J. Am. Chem. Soc.* **2001**, *123*, 10239.
11. Ikeda, M.; Shinkai, S.; Osuka, A. *Chem. Commun.* **2000**, 1047.
12. Hirata, O.; Yamamoto, M.; Sugiyasu, K.; Kubo, Y.; Ikeda, M.; Takeuchi, M.; Shinkai, S. *J. Supramol. Chem.* **2002**, *2*, 133.
13. Takeuchi, M.; Imada, T.; Shinkai, S. *J. Am. Chem. Soc.* **1996**, *118*, 10658. (b) Takeuchi, M.; Chin, Y.; Imada, T.; Shinkai, S. *Chem. Commun.* **1996**, 1867. (c) Takeuchi, M.; Kijima, H.; Hamachi, I.; Shinkai, S. *Bull. Chem. Soc. Jpn* **1997**, *70*, 699. (d) Shinmori, H.; Takeuchi, M.; Shinkai, S. *J. Chem. Soc., Perkin Trans. 2* **1998**, 847. (e) Takeuchi, M.; Mizuno, T.; Shinkai, S.; Shirakami, S.; Itoh, T. *Tetrahedron: Asymmetry* **2000**, *11*, 3311. (f) Yamamoto, M.; Takeuchi, M.; Shinkai, S.; Tani, F.; Naruta, Y. *J. Chem. Soc., Perkin Trans. 2* **2000**, *9*. (g) Mizuno, T.; Yamamoto, M.; Takeuchi, M.; Shinkai, S. *Tetrahedron* **2000**, *56*, 6193. (h) Yamamoto, M.; Takeuchi, M.; Shinkai, S. *Tetrahedron* **2002**, *58*, 7258.
14. Bielecki, M.; Eggart, H.; Norrild, J. C. *J. Chem. Soc. Perkin. 2* **1999**, 449.
15. Time course of the decomposition of **1**-saccharide complex was monitored by UV-vis spectroscopy under the measurement conditions. The Soret band scarcely changed and absorption band at around 300 nm assignable to the peripheral diaryl moieties changed gradually, indicating that peripheral boronic acid-appended diaryls would decompose.
16. Job, A. *Annales de Chimie (10th series)* **1928**, *9*, 113.
17. Yang, W.; Gao, X.; Gao, X.; Vardhan, V.; Karnati, R.; Ni, W.; Wang, B.; Hooks, W. B.; Carson, J.; Weston, B. *Bioorg. Med. Chem. Lett.* **2002**, *12*, 2175.
18. (a) Kobata, A. In *Biology of Carbohydrates*; Ginsburg, V., Robins, P. W., Eds.; John Wiley and Sons: New York, 1984; Vol. 2, p. 87. (b) Feizi, T. *Nature* **1985**, *314*, 53. (c) Hakomori, S. *Adv. Cancer Res.* **1989**, *52*, 257. (d) Schauer, R. *Adv. Carbohydr. Chem. Biochem.* **1982**, *40*, 131. (e) Looms, L. M.; Vemura, K.; Childs, R. A.; Paulson, J. C.; Rogers, G. N.; Scudder, P. R.; Michalski, J.; Hounsell, E. F.; Taylor-Robinson, D.; Feizi, T. *Nature* **1984**, *307*, 560. (f) Lorant, D. E.; Topham, M. K.; Whatley, R. E.; McEver, R. P.; McIntyre, T. M.; Prescott, S. M.; Zimmerman, G. A. *J. Clin. Invest.* **1993**, *92*, 559. (g) Lasky, L. A. *Science* **1992**, *258*, 964.
19. Monoclonal antibody has been used to determine the concentrations of SLe<sup>x</sup> antigen and sialyl Tn antigen by immunoradiometric assay and radioimmunoassay, respectively: see Springer, G. F. *Immunol. Ser.* **1990**, *53*, 587.
20. Shinmori, H.; Takeuchi, M.; Shinkai, S. *Tetrahedron* **1995**, *51*, 1893.

# Polymer-supported calix[4]arenes for sensing and conversion of NO<sub>2</sub>/N<sub>2</sub>O<sub>4</sub>

Yanlong Kang and Dmitry M. Rudkevich\*

Department of Chemistry and Biochemistry, University of Texas at Arlington, PO Box 19065, Arlington, TX 76019-0065, USA

Received 16 February 2004; revised 30 June 2004; accepted 20 August 2004

Available online 16 September 2004

**Abstract**—The use of simple calix[4]arenes **1a,b** for NO<sub>2</sub>/N<sub>2</sub>O<sub>4</sub> sensing and conversion is demonstrated, both in solution and in the solid state. Upon reacting with these gases, compounds **1a,b** encapsulate reactive NO<sup>+</sup> cations within their cavities with the formation of deeply colored ( $\lambda_{\text{max}} \sim 570$  nm) charge-transfer complexes **2a,b**. Further functionalization of the calix[4]arene platform is reported for attachment to solid supports. Polymer-supported calixarene material **3** was prepared, which reversibly traps NO<sub>2</sub>/N<sub>2</sub>O<sub>4</sub> with the formation of nitrosonium storing polymer **4**. Material **4** was effectively used for nitrosation of amides.

© 2004 Elsevier Ltd. All rights reserved.

## 1. Introduction

NO<sub>x</sub> gases are the sum of NO, NO<sub>2</sub>, N<sub>2</sub>O<sub>3</sub> (NO·NO<sub>2</sub>), N<sub>2</sub>O<sub>4</sub> (NO<sub>2</sub>·NO<sub>2</sub>), and N<sub>2</sub>O<sub>5</sub>.<sup>1</sup> These are atmospheric pollutants, originated in large quantities from fuel combustion and large-scale industrial processes. NO<sub>x</sub> are involved in the formation of ground-level ozone.

They form toxic chemicals and acid rains, and participate in global warming. NO<sub>x</sub> are also involved in various nitrosation processes with biomolecules, causing cancers and other diseases.<sup>2,3</sup> According to the US Environmental Protection Agency,<sup>1</sup> national emissions of NO<sub>x</sub> have increased over the past 30 years by ~10%. Extensive NO<sub>x</sub> circulation in the atmosphere, industry, and agriculture requires their systematic monitoring and also necessitates the development of improved methods for their conversion and utilization. We specifically target nitrogen dioxide (NO<sub>2</sub>). Current NO<sub>2</sub> sensors are mostly electrochemical and monitor changes of potential upon exposure metal surfaces to the gas.<sup>4</sup> In many cases, however, other vapors—H<sub>2</sub>O, O<sub>2</sub>, HCl, HBr, SO<sub>x</sub> and NH<sub>3</sub> significantly influence the detection selectivity and, therefore, sensitivity. Optical sensors, which are based on coloration reaction between NO<sub>2</sub> and certain organic compounds, are more selective as the reactions are specific.<sup>5</sup> At the same time, the reversibility is difficult to achieve.

**Keywords:** Calixarenes; Nitrogen oxides; Polymers; Sensors; Supramolecular chemistry.

\* Corresponding author. Tel.: +1-817-272-5245; fax: +1-817-272-3808; e-mail: [rudkevich@uta.edu](mailto:rudkevich@uta.edu)

We recently reported that simple calix[4]arenes such as **1a,b** reversibly interact with NO<sub>2</sub>/N<sub>2</sub>O<sub>4</sub> and entrap reactive nitrosonium cation (NO<sup>+</sup>) within their cavities (Fig. 1).<sup>6</sup> NO<sup>+</sup> is generated from N<sub>2</sub>O<sub>4</sub> upon its disproportionation. Deeply colored charge-transfer complexes **2a,b** formed. In this paper, we further explore our findings. We submit the solution studies of the NO<sub>2</sub>/N<sub>2</sub>O<sub>4</sub> entrapment by calixarenes for potential sensing applications, and also report on the synthesis of functionalized calix[4]arenes for attachment to polymeric supports. We further demonstrate the use of calixarene-based materials **3** (Fig. 1) for detection, entrapment and release of NO<sup>+</sup>. Finally, we show that polymeric nitrosating reagent **4** can be effectively used in syntheses of *N*-nitrosamides.

## 2. Results and discussion

### 2.1. Design and synthesis

NO<sub>2</sub> is a paramagnetic gas of a brown-orange color. It reversibly dimerizes into colorless dinitrogen tetroxide (N<sub>2</sub>O<sub>4</sub>).<sup>7</sup> The position of the equilibrium between NO<sub>2</sub> and N<sub>2</sub>O<sub>4</sub> varies with temperature. At the same time, N<sub>2</sub>O<sub>4</sub> may disproportionate to ionic NO<sup>+</sup>NO<sub>3</sub><sup>-</sup> upon reacting with aromatic compounds.<sup>7,8</sup>

Calix[4]arenes are popular building blocks in molecular recognition. They are widely used in the construction of various receptors, sensors and molecular containers.<sup>9</sup> Calix[4]arenes in a 1,3-alternate conformation (see for example, **1a,b**) are ideally preorganized to complex NO<sup>+</sup>,

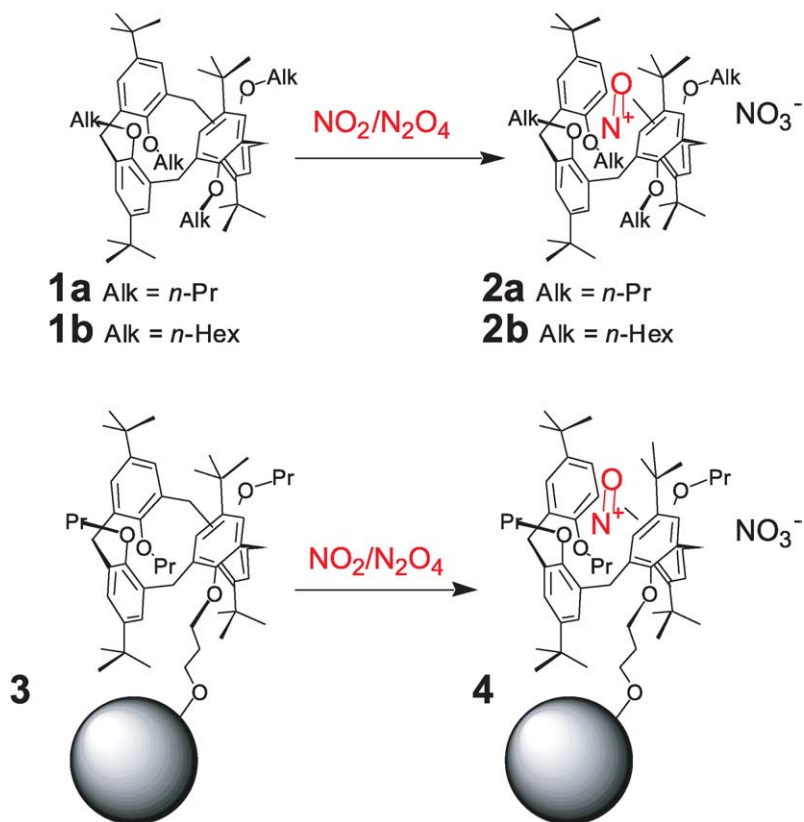


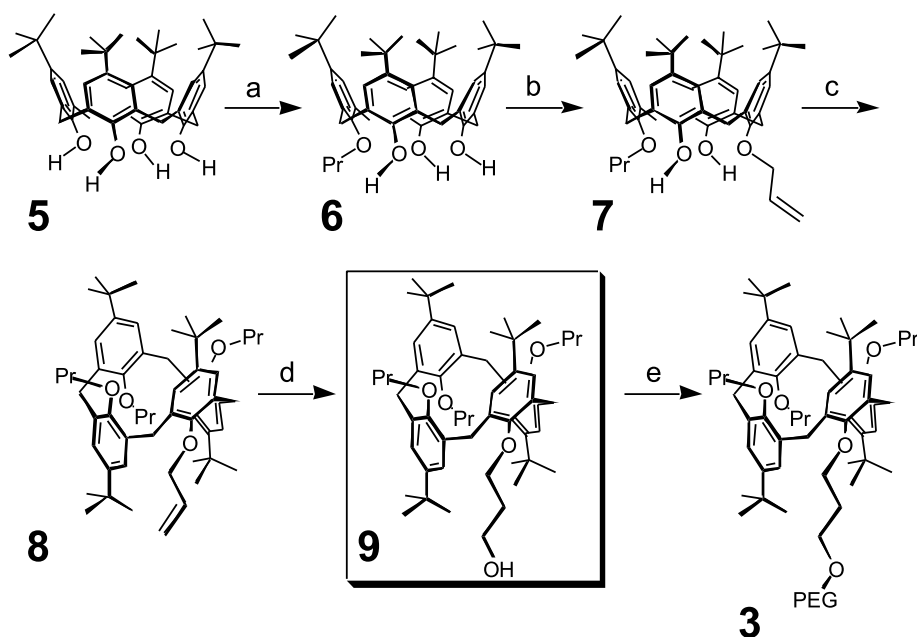
**Figure 1.** Chemical fixation of  $\text{NO}_2/\text{N}_2\text{O}_4$  by calix[4]arenes; formation of calixarene–nitrosonium complexes.

generated from  $\text{NO}_2/\text{N}_2\text{O}_4$ . They possess a cylindrical,  $\pi$ -electron rich inner tunnel, defined by two cofacial pairs of phenol rings, which are oriented orthogonal along the cavity axis (see **2a,b**, Fig. 1). According to numerous X-ray studies, this tunnel is  $\sim 5\text{--}6$  Å in diameter.<sup>10</sup>

For solution studies, 1,3-alternate tetrakis(*O*-alkyl)calix[4]arenes **1a,b** were resynthesized. Their preparation includes

the two-step alkylation of parent calix[4]arene **5** with either *n*-propyl or *n*-hexyl bromide, using successively  $\text{K}_2\text{CO}_3$  and then  $\text{Cs}_2\text{CO}_3$  in boiling MeCN.<sup>6,11</sup> The synthesis of terminally functionalized calixarenes starts with mono-alkylation of **5** with *n*-propyl bromide using  $\text{K}_2\text{CO}_3$  as a base in boiling MeCN (Scheme 1).

The resulting calixarene **6**<sup>12</sup> was further alkylated with allyl



**Scheme 1.** (a) *n*-PrBr,  $\text{K}_2\text{CO}_3$ , MeCN, reflux, 59%; (b) AllylBr,  $\text{K}_2\text{CO}_3$ , MeCN, reflux, 67%; (c) *n*-PrBr,  $\text{Cs}_2\text{CO}_3$ , MeCN, reflux, 70%; (d)  $\text{BH}_3 \cdot \text{THF}$ , THF, then NaOH,  $\text{H}_2\text{O}_2$ , 95%; (e)  $\text{MeOCH}_2(\text{CH}_2\text{OCH}_2\text{CH}_2)_n\text{OMs}$  (**10**), *t*-BuOK, THF,  $\sim 55\%$ .

bromide to afford diametrically substituted product **7** ( $\text{K}_2\text{CO}_3$ , MeCN, reflux, 67%). The next step includes formation of calixarene **8**, which is a  $\text{Cs}^+$ -templated alkylation of **7** with an excess *n*-propyl bromide ( $\text{Cs}_2\text{CO}_3$ , MeCN, reflux, 70%). This reaction proceeds with the conformation conversion from a cone to a 1,3-alternate. The allyl double bond in **8** was hydroxylated under the standard hydroboration conditions ( $\text{BH}_3 \cdot \text{THF}$ , THF, then aq NaOH,  $\text{H}_2\text{O}_2$ ) to afford calixarene **9** in 95% yield. Compound **9** is the key derivative for preparation of polymer-supported materials for  $\text{NO}_2/\text{N}_2\text{O}_4$  sensing and fixation. It has the structural features of typical 1,3-alternates and also possesses a terminal hydroxyl group for further functionalization.

## 2.2. Solution studies

When a stream of  $\text{NO}_2/\text{N}_2\text{O}_4$  was passed through the  $\text{CHCl}_3$  solution of calix[4]arenes **1a,b**, deeply colored, purple nitrosonium complexes **2a,b** formed within seconds (>95% yield, Fig. 1).<sup>6,13</sup>

The  $^1\text{H}$  NMR spectra of **2a,b** showed new sets of the calixarene signals, different from **1a,b** (Fig. 2). For example, aromatic CH protons of guest-free **1b** were seen as a singlet at 6.95 ppm. In nitrosonium complex **2b**, it was transformed into a singlet at 7.02 ppm. The methylene

bridge  $\text{CH}_2$  protons of **1b** were recorded as a singlet at 3.73 ppm. In complex **2b**, this was seen at 3.60 ppm. The methylene  $\text{OCH}_2$  triplet in **1b** is situated at 3.38 ( $J=7.5$  Hz), while it shifted to 3.77 ppm in complex **2b**. Spectral changes for **2a** are analogous. Independent structural evidence for **2a,b** came from the complexation experiments between calixarenes **1a,b** and commercially available  $\text{NO}^+\text{SbF}_6^-$  salt ( $\text{CDCl}_3$ , 295 K).<sup>14</sup> The corresponding complexation induced changes were in agreement with the data presented above for complex **2a,b** (Fig. 2), once again confirming the disproportionation of  $\text{N}_2\text{O}_4$  to  $\text{NO}^+\text{NO}_3^-$  by calixarenes. Addition of water destroys the nitrosonium complexes, quantitatively recovering empty calixarenes **1a,b**.

The UV–vis spectra of **2a,b** showed broad charge-transfer<sup>14,15</sup> band at  $\lambda_{\text{max}} \sim 560\text{--}580$  nm ( $\epsilon = 8 \times 10^3 \text{ M}^{-1} \text{ cm}^{-1}$ ) (Fig. 3). While neither calixarenes **1a,b** nor  $\text{NO}_2$  absorb in this region, addition of as little as  $\sim 1$  equiv  $\text{NO}_2$  ( $\sim 5 \times 10^{-5} \text{ M}$  in  $\text{CH}_2\text{Cl}_2$ ) to the solution of **1a** ( $6 \times 10^{-5} \text{ M}$  in  $\text{CH}_2\text{Cl}_2$ ) results in appearance of the charge-transfer band. Its absorbance grows upon addition of larger quantities of  $\text{NO}_2$  and reaches saturation when  $\sim 10$  equiv  $\text{NO}_2$  (e.g., 5 equiv  $\text{N}_2\text{O}_4$ ) is added. From the titration experiments, the apparent  $K_{\text{assoc}}$  value of  $\sim 10^4 \text{ M}^{-1}$  was estimated. Accordingly, calixarenes can detect  $\text{NO}_2$  already at micromolar concentrations.

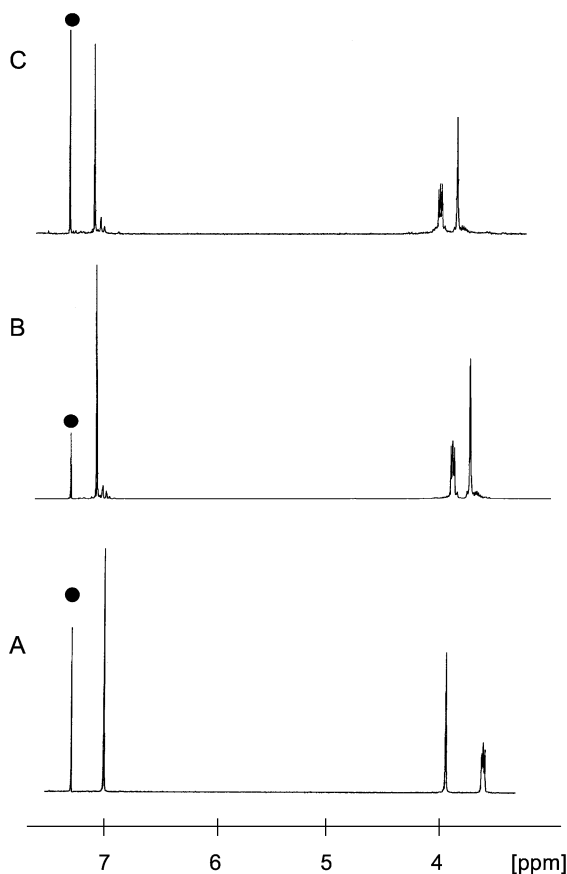


**Figure 2.** Portions of the  $^1\text{H}$  NMR spectra (500 MHz,  $\text{CDCl}_3$ ,  $295 \pm 1$  K) of: (A) calix[4]arene **1b**; (B) nitrosonium complex **2b** prepared from **1b** and  $\text{NO}_2/\text{N}_2\text{O}$ ; (C) nitrosonium complex, prepared upon addition of  $\text{NO}^+\text{SbF}_6^-$  to calixarene **1b**. The residual  $\text{CHCl}_3$  signals are marked '•'. Similar spectra were obtained for calixarene **1a** and complex **2a**.

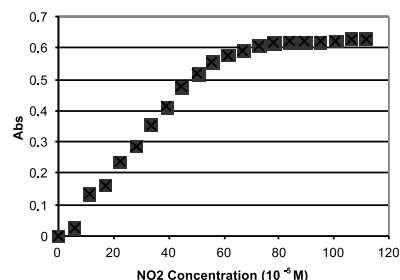


**Figure 3.** UV–vis spectroscopic titration experiments ( $\text{CH}_2\text{Cl}_2$ ,  $295 \pm 1$  K) with calix[4]arene **1a** and  $\text{NO}_2/\text{N}_2\text{O}$ . [**1a**] =  $6 \times 10^{-5} \text{ M}$ , [ $\text{NO}_2$ ] =  $0\text{--}1.2 \times 10^{-3} \text{ M}$ ;  $\lambda_{\text{max}} \sim 565$  nm.

Importantly for potential sensing, the calix[4]arene– $\text{NO}_2$  interactions (a) are reversible, (b) result in rapid and dramatic color changes and (c) are unique and specific for  $\text{NO}_2$ . This should guaranty its detection in the presence of such gases as  $\text{H}_2\text{O}$ ,  $\text{O}_2$ ,  $\text{HCl}$ ,  $\text{HBr}$ ,  $\text{SO}_x$ , and  $\text{NH}_3$ . Indeed, calixarenes are chemoselective for  $\text{NO}_2$ , and none of these vapors/gases undergoes such reactions with calixarenes. Neat nitric oxide ( $\text{NO}$ ) gas also does not react with calixarenes. In their excellent work on  $\text{NO}$  sensing,<sup>14</sup> Kochi, Rathore and co-workers showed that calixarenes had to be oxidized first, to form the corresponding cation-radicals, prior complexing  $\text{NO}$  within their interiors.

## 2.3. Toward polymer-supported calixarenes

For potential application in sensing technology, receptor molecules must be readily immobilizable on solid supports or surfaces. Although a wide variety of polymers is now commercially available,  $\text{NO}_2$  (and  $\text{NO}_x$  in general) react with many of them, causing destruction and aging.<sup>16</sup> As a



free radical  $\text{NO}_2$  readily attacks double bonds in polybutadienes, polyisoprenes and their copolymers, ester groups in poly(methyl)methacrylate, and also amide fragments in polyamides and polyurethanes. Furthermore,  $\text{NO}^+$ , generated from various  $\text{NO}_x$ , reacts with alkenes and other double bond containing structures.<sup>17</sup>

In these studies, the use of calixarene module **9** in the preparation of  $\text{NO}_2$ -sensitive and  $\text{NO}_2$ -trapping materials was demonstrated for polyethylene glycol (PEG) polymers. Specifically, commercial PEG 5'000 monomethyl ether ( $\sim 5000$  Da molecular weight; Fluka) quantitatively reacted with  $\text{MeSO}_2\text{Cl}$  in  $\text{CH}_2\text{Cl}_2$  to give the corresponding  $\alpha$ -methyl- $\omega$ -mesyl derivative **10**,<sup>18</sup> which was then coupled with **9** in THF using *t*-BuOK as a base to yield polymer **3** (Scheme 1). While the MALDI TOF spectra of **3** appeared to be rather complex, the presence of a calix[4]arene fragment was confirmed by the appearance of an intense  $\nu(\text{CH}_{\text{arom}})$  absorption band at  $\sim 2950\text{ cm}^{-1}$  in the FTIR spectrum (KBr disks). By integrating the calixarene aromatic signals vs the PEG OMe group in the  $^1\text{H NMR}$  spectrum of **3** in  $\text{CDCl}_3$ , the loading of  $\sim 55\%$  was estimated. Such rather modest number may be due to the steric bulkiness of the calixarene fragment.

Upon exposure to  $\text{NO}_2/\text{N}_2\text{O}_4$ , material **3** turns deep purple, both in apolar solution (chlorinated solvents, or even

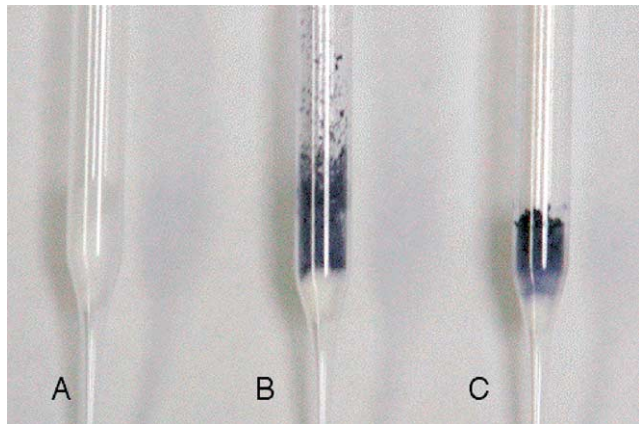


**Figure 4.**  $\text{NO}_2$  entrapment experiments. The columns were prepared as follows: (A) loaded with starting PEG monomethyl ether (Fluka); (B) loaded with dry polymer **3**; (C) loaded with **3** and flashed with hexanes. All three columns were then flashed with  $\text{NO}_2$  for 30 s.

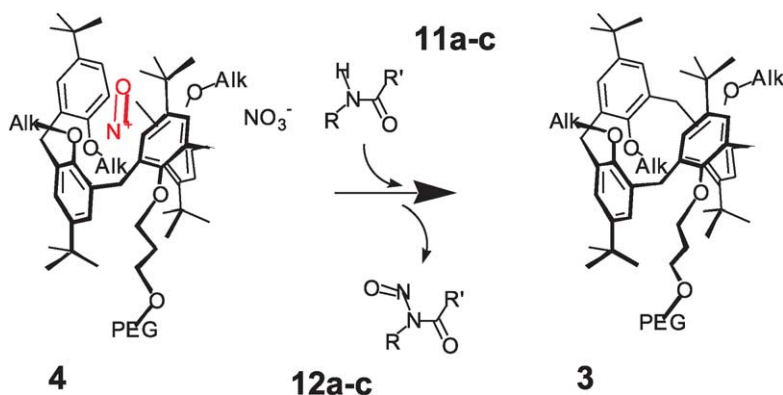


**Figure 5.** Nitrosation of amides **11a–c** with polymer **4**.

suspensions in hexanes) and in the solid state. Similar to monomeric calixarenes **1a,b**, the UV–vis spectrum of mixtures of polymer **3** and excess  $\text{NO}_2/\text{N}_2\text{O}_4$  in  $\text{CH}_2\text{Cl}_2$  showed broad charge-transfer band at  $\lambda_{\text{max}} \sim 575\text{ nm}$ , indicating the formation of calix–nitrosonium complex **4**. Starting PEG polymer does not exhibit any UV–vis spectral changes upon addition of  $\text{NO}_2/\text{N}_2\text{O}_4$ .

In the  $\text{NO}_2$  entrapment experiments, stream of the gas was passed through the Pasteur pipettes, loaded with starting PEG monomethyl ether and material **3** (Fig. 4). In one pipette, dry polymer **3** was loaded; the other pipette with **3** was preliminary flashed with hexanes. Both pipettes containing **3** instantly turned dark purple, indicating the  $\text{NO}^+$  complexation. The color of the wetted material appeared to be deeper and it stayed for hours. The dry material bleached faster. As expected, no coloration was observed for the pipette loaded with the starting PEG polymer. This once again emphasizes the role of calixarene cavities in the described processes and directly points at the use of polymer **3** for  $\text{NO}_2$  detection and separation of other nitrogen oxides, especially  $\text{NO}$ , from  $\text{NO}_2$ .

#### 2.4. Nitrosation

We previously reported, that calixarene–nitrosonium complexes **2a,b** may release  $\text{NO}^+$  and thus act as nitrosating agents for secondary amides.<sup>13</sup> Nitrosamides/amines are of great biomedical interest as potential  $\text{NO}$ -releasing drugs.<sup>19</sup> We are now exploring calixarene-containing polymer **3** for synthetic purposes.

Among the advantages of reagents immobilized on polymeric supports<sup>20</sup> are the ease of their separation from the reaction mixture, their recycling, and the simplification of handling toxic and odorous chemicals. Particularly useful are so-called soluble polymers, as they allow to overcome problems associated with the heterogeneous nature of the reaction conditions. At the same time, likewise with insoluble polymers, isolation of these polymers from the reaction mixture also includes precipitation.

Nitrosonium-storing polymer **4** (Fig. 5) was prepared upon bubbling  $\text{NO}_2/\text{N}_2\text{O}_4$  through the solution of **3** in  $\text{CH}_2\text{Cl}_2$  for 2–3 min, followed by flashing with  $\text{N}_2$  for 10 min to remove the remaining  $\text{NO}_2/\text{N}_2\text{O}_4$  gases. Deeply colored material formed (Fig. 4). When added to equimolar solutions of

amides  $\text{CH}_3(\text{CH}_2)_6\text{C}(\text{O})\text{NHR}$  **11a–c** (R = Me, Et, Pr, respectively) in  $\text{CH}_2\text{Cl}_2$ , it reacted quickly (2–3 h) at room temperature, yielding corresponding *N*-nitrosamides **12a–c** (Fig. 5). The solution's color discharged, thus visually indicating the reaction progress. Polymer **3** was subsequently recovered by precipitating with hexanes and filtered off. Yields of nitrosamides **12a–c** were determined by  $^1\text{H}$  NMR spectroscopy, integrating signals of the product vs the starting compounds. Signals for amides **11a–c** decrease, and characteristic signals for *N*-nitrosamides **12a–c** appear and grow. For example, a triplet at  $\sim 3.2$  ppm ( $\text{C}(\text{O})\text{CH}_2$ ) and a singlet at  $\sim 3.1$  ppm ( $\text{N}(\text{NO})\text{—CH}_3$ ) were clearly registered for nitrosoamide **12a**; these were identical to those obtained upon nitrosation of **11a** with neat  $\text{NO}_2/\text{N}_2\text{O}_4$  and different from the starting amide **11a** (Fig. 6).

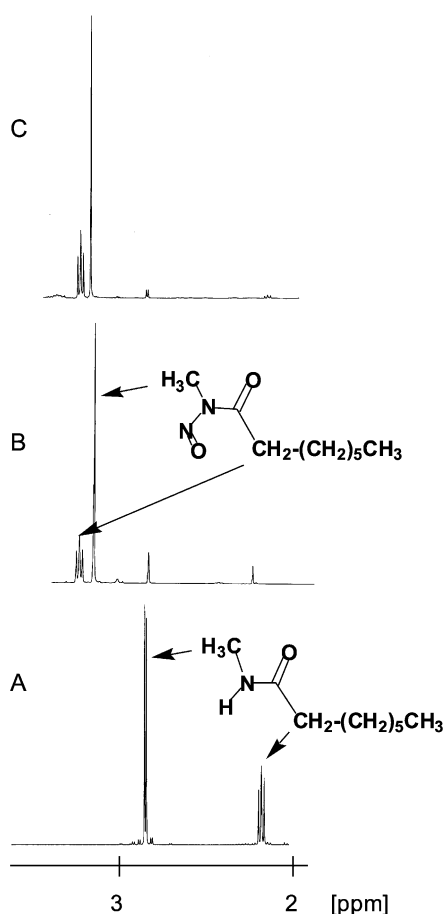


**Figure 6.** Fragments of the  $^1\text{H}$  NMR spectra (500 MHz,  $\text{CDCl}_3$ ,  $295 \pm 1$  K): (A) *N*-methylamide **11a**; (B) *N*-methyl-*N*-nitrosamide **12a** obtained from **11a** and  $\text{NO}_2/\text{N}_2\text{O}_4$ ;  $^{13}\text{C}$  (C) *N*-methyl-*N*-nitrosamide **12a** obtained from **11a** and polymer **4**.

After at least five runs, the averaged yields of **12** varied between 40% for **12c** to 60% for **12b** and 80% for **12a**, indicating the preference for less bulky substrates. At the same time, polymeric reagent **4** is obviously less size-shape selective, compared to monomeric species **2**, which showed exclusive selectivity for smaller *N*-Me derivative **11a**.<sup>13</sup> In control experiments, involving starting PEG polymer and amide **11a**, only trace amounts of **12a** were detected (<5%), again emphasizing the role of calixarene cavity in the described reaction.

### 3. Conclusions and outlook

Calix[4]arene derivatives can be effectively used for chemoselective colorimetric sensing of  $\text{NO}_2/\text{N}_2\text{O}_4$  gases both in solution and in the solid state. They also convert  $\text{NO}_2/\text{N}_2\text{O}_4$  into nitrosating reagents for organic synthesis. Immobilization of calixarenes on solid supports opens even wider opportunities for practical applications. We are currently preparing various calixarene-based polymers for  $\text{NO}_2/\text{N}_2\text{O}_4$  sensing and conversion and also exploring synthetic capabilities of the calixarene modules. Of particular interest are chiral calixarenes for stereoselective nitrosation and also calixarene-based nanotubes for  $\text{NO}_2/\text{N}_2\text{O}_4$  sensing and fixation. We are also looking at other  $\text{NO}_x$  gases.

### 4. Experimental

#### 4.1. General

$^1\text{H}$  and  $^{13}\text{C}$  NMR spectra were recorded in  $\text{CDCl}_3$  at  $295 \pm 1$  °C on a JEOL Eclipse 500 MHz spectrometer. Chemical shifts were measured relative to residual non-deuterated solvent resonances. FTIR spectra were recorded on a Bruker Vector 22 FTIR spectrometer. UV–vis spectra were measured on a Varian Cary-50 spectrophotometer. HRMS MALDI spectra were obtained on an Ion Spec Ultima FTMS. Elemental analysis was performed on a Perkin–Elmer 2400 CHN analyzer. All experiments with moisture- and/or air-sensitive compounds were run under a dried nitrogen atmosphere. For column chromatography, silica gel 60 Å was used (Sorbent Technologies, Inc.; 200–425 mesh). Tetrahydroxycalix[4]arene **5**<sup>21</sup> and 1,3-alternates **1a,b**<sup>6,11</sup> were prepared according to the published procedures. Amides **11a–c** and *N*-nitrosamides **12a–c** were synthesized as reported earlier.<sup>13</sup>  $\text{NO}_2/\text{N}_2\text{O}_4$  was generated from copper and concd  $\text{HNO}_3$ .

Caution 1:  $\text{NO}_2$  has an irritating odor and is very toxic!  
Caution 2: *N*-Nitrosoamides are carcinogens<sup>3</sup> and should be treated with extreme care!

**4.1.1. 5,11,17,23-Tetrakis(*t*-butyl)-25,26,27-trihydroxy-28-(*n*-propyloxy)calix[4]arene **6**.** In the modified procedure, to the solution of *t*-butyl calix[4]arene **5** (10.0 g, 15.41 mmol) in MeCN (300 mL),  $\text{K}_2\text{CO}_3$  (1.07 g, 7.71 mmol) was added. The mixture was refluxed for 15 min, and then *n*-propyl bromide (14 mL, 154.1 mmol) was added. The mixture was further refluxed for 24 h, and the solvent was evaporated under reduced pressure. The residue was taken up with  $\text{CH}_2\text{Cl}_2$  (200 mL), washed with 1 M HCl ( $2 \times 200$  mL) and  $\text{H}_2\text{O}$  (200 mL), and dried over  $\text{MgSO}_4$ . The solvent was evaporated, and the residual solid was recrystallized from  $\text{CHCl}_3/\text{CH}_3\text{OH}$  to afford product **6** as white crystals (59%). The spectral data are in agreement with the previously published.<sup>12</sup>  $^1\text{H}$  NMR:  $\delta = 10.20$  (s, 1H), 9.61 (s, 2H), 7.06 (m, 8H), 4.37 (d,  $J = 12.5$  Hz, 2H), 4.27 (d,  $J = 12.5$  Hz, 2H), 4.10 (t,  $J = 7.5$  Hz, 2H), 3.44 (d,  $J = 12.5$  Hz, 2H), 3.42 (d,  $J = 12.5$  Hz, 2H), 2.18 (m, 2H), 1.24 (t,  $J = 7.5$  Hz, 3H), 1.21 (s, 9H), 1.19 (s, 27H).

**4.1.2. 5,11,17,23-Tetrakis(*t*-butyl)-25-allyloxy-26,28-dihydroxy-27-(*n*-propyloxy)calix[4]-arene 7.** To the solution of calixarene **6** (4.0 g, 5.79 mmol) in MeCN (150 mL),  $K_2CO_3$  (3.2 g, 23.16 mmol) was added, and the mixture was refluxed under nitrogen for 15 min. Allyl bromide (9.5 mL, 10.58 mmol) was then added, and the mixture was further refluxed for 24 h. The solvent was evaporated under reduced pressure, the residue was redissolved in  $CH_2Cl_2$  (100 mL), washed with 1 M HCl ( $2 \times 50$  mL),  $H_2O$  (50 mL), and dried over  $MgSO_4$ . The solvent was evaporated, and the residual solid was recrystallized from  $CHCl_3/CH_3OH$  to afford **7** as white crystals in 67% yield; mp 187–190 °C;  $^1H$  NMR:  $\delta=7.64$  (s, 2H), 7.03 (s, 4H), 6.83 (s, 2H), 6.82 (s, 2H), 6.23 (m, 1H), 5.75 (d,  $J=15$  Hz, 1H), 5.36 (d,  $J=15$  Hz, 1H), 4.52 (d,  $J=2.0$  Hz, 2H), 4.28 (d,  $J=12.5$  Hz, 4H), 3.95 (t,  $J=7.5$  Hz, 3H), 3.29 (d,  $J=12.5$  Hz, 4H), 2.02 (m, 2H), 1.27 (s, 18H), 1.24 (t,  $J=7.5$  Hz, 3H), 0.98 (s, 18H);  $^{13}C$  NMR:  $\delta=150.8, 150.0, 149.9, 146.9, 146.8, 141.4, 133.2, 132.9, 127.9, 127.8, 125.6, 125.5, 125.1, 117.5, 33.9, 31.9, 31.8, 31.2, 23.5, 11.0$ ; FTIR (KBr,  $cm^{-1}$ ):  $\nu=3413, 2961, 2904, 1643, 1486, 1361, 1196$ . Anal. Calcd for  $C_{50}H_{66}O_4$ : C, 82.15; H, 9.10. Found: C 81.82, H 9.34; MALDI-FTMS,  $m/z$ : 753.4837 [(M+Na) $^+$ , calcd for  $C_{50}H_{66}O_4$  753.4853].

**4.1.3. 5,11,17,23-Tetrakis(*t*-butyl)-25-allyloxy-26,27,28-tris-(*n*-propyloxy)calix[4]arene, 1,3-alternate 8.** To the solution of calixarene **7** (5.0 g, 6.84 mmol) in MeCN (400 mL),  $Cs_2CO_3$  (17.83 g, 54.74 mmol) was added, and the mixture was refluxed under nitrogen for 15 min. *n*-Propyl bromide (6.2 mL, 68.4 mmol) was then added, and the mixture was further refluxed for 36 h. The solvent was evaporated under reduced pressure. The residue was redissolved in  $CH_2Cl_2$  (100 mL), washed with 1 M HCl ( $2 \times 50$  mL),  $H_2O$  (50 mL), and dried over  $MgSO_4$ . The solvent was evaporated to afford calixarene **8** as white crystals in 70% yield; mp 243–245 °C;  $^1H$  NMR:  $\delta=6.97$  (s, 2H), 6.95 (s, 2H), 6.94 (d,  $J=2.5$  Hz, 2H), 6.92 (d,  $J=2.5$  Hz, 2H), 5.38 (m, 1H), 4.76 (d,  $J=2$  Hz, 1H), 4.72 (s, 1H), 3.79 (s, 4H), 3.78 (s, 4H), 3.71 (m, 2H), 3.33 (m, 6H), 1.26 (s, 18H), 1.22 (s, 18H), 1.08 (m, 6H), 0.66 (t,  $J=7.5$  Hz, 9H);  $^{13}C$  NMR:  $\delta=154.9, 154.7, 154.5, 143.6, 143.5, 135.1, 133.5, 133.3, 133.2, 133.1, 126.3, 126.0, 125.7, 114.5, 72.0, 71.9, 71.6, 70.6, 39.3, 29.1, 34.0, 31.7, 22.7, 22.4, 22.35, 10.1$ ; FTIR (KBr,  $cm^{-1}$ ):  $\nu=2961, 2900, 2872, 1482, 1211$ . Anal. Calcd for  $C_{56}H_{78}O_4$ : C, 82.51; H, 9.64. Found: C 82.19, H 9.99; MALDI-FTMS,  $m/z$ : 837.5778 [(M+Na) $^+$ , calcd for  $C_{56}H_{78}O_4$  837.5792].

**4.1.4. 5,11,17,23-Tetrakis(*t*-butyl)-25-(3'-hydroxypropyloxy)-26,27,28-tris-(*n*-propyloxy)-calix[4]arene, 1,3-alternate 9.** Solution of  $BH_3 \cdot THF$  in THF (1.0 M, 36 mL) was added dropwise to a stirred solution of compound **8** (3.0 g, 3.68 mmol) in dry THF (200 mL) at  $-10$  °C under nitrogen. The reaction mixture was stirred for 1 h while warming to rt, then stirred for another 2.5 h. 1 M aq NaOH (20 mL) was added dropwise over 10 min, followed by  $H_2O_2$  (30%, 11 mL) and  $H_2O$  (2 mL). The mixture was stirred at rt for 1 h and then at 40 °C for 12 h. Brine was added, and the organic layer was separated. The aqueous layer was extracted with THF ( $2 \times 20$  mL), and the combined organic solution was washed with brine ( $3 \times 30$  mL) and dried over  $MgSO_4$ . The solvent was evaporated, and the residue was crystallized from  $CHCl_3/CH_3OH$  to afford product **9** as

white crystals (95%); mp  $>275$  °C;  $^1H$  NMR:  $\delta=7.00$  (d,  $J=2.5$  Hz, 2H), 6.98 (m, 4H), 6.95 (s, 2H), 3.82 (m, 8H), 3.32 (m, 10H), 1.39 (m, 2H), 1.26 (s, 18H), 1.24 (s, 18H), 1.03 (m, 2H), 0.92 (m, 4H), 0.61 (m, 9H);  $^{13}C$  NMR:  $\delta=154.9, 154.6, 143.9, 143.8, 133.5, 133.3, 132.9, 126.1, 126.0, 125.8, 125.5, 72.0, 71.8, 68.6, 60.9, 39.4, 39.2, 34.0, 33.97, 33.95, 32.5, 31.7, 22.6, 22.1, 10.2, 10.0$ ; FTIR (KBr,  $cm^{-1}$ ):  $\nu=3468, 2955, 2935, 2923, 2863, 1594, 1475, 1199, 1012$ . Anal. Calcd for  $C_{56}H_{80}O_5 \cdot 0.5H_2O$ : C, 79.86; H, 9.69. Found: C 79.70, H 10.01; MALDI-FTMS,  $m/z$ : 855.5886 [(M+Na) $^+$ , calcd for  $C_{56}H_{82}O_5$  855.5903].

**4.1.5. Polymer 3.** PEG monomethyl ether (10.0 g, 2 mmol) was dissolved in dry  $CH_2Cl_2$  (100 mL). The solution was cooled to 0 °C, and then  $Et_3N$  (0.54 mL, 4 mmol) and methanesulfonyl chloride (0.5 mL, 4 mmol) were consequently added. The reaction mixture was stirred at 0–5 °C for 2 h, washed with water ( $2 \times 40$  mL) and treated with brine (40 mL). The organic layer was separated and dried with  $MgSO_4$ , and the solvent was evaporated in vacuo. The residue was washed with hexanes to afford product **10** (98%).  $^1H$  NMR:  $\delta=3.65$  (m, 513H), 3.36 (s, 3H), 3.07 (s, 3H). To the solution of calixarene **9** (1.0 g, 1.2 mmol) in dry THF (100 mL) potassium *tert*-butoxide (0.81 g, 7.2 mmol) was added under nitrogen, and the resulting mixture was stirred at 50 °C for 20 min. After cooling to rt, polymer **10** (3.0 g, 0.59 mmol) in dry THF (100 mL) was added dropwise, and the mixture was stirred at 50 °C for 60 h. The solvent was evaporated; the residue was redissolved in  $CH_2Cl_2$  (50 mL), washed with water ( $2 \times 20$  mL), brine (20 mL), and dried over  $MgSO_4$ . The solvent was evaporated under reduced pressure, and the residual solid was washed thoroughly with diethyl ether to remove unreacted calixarene (TLC control). The resulted product **3** was air dried and then dried in vacuo for 12 h.  $^1H$  NMR:  $\delta=6.96$  (m, 4.39H), 3.36 (s, 3H), 1.24 (m, 21.7H), 0.97 (m), 0.59 (m); Calcd loading is 55%. FTIR (KBr,  $cm^{-1}$ ):  $\nu=2948, 2885, 2741, 2695, 2238, 1967, 1468, 1414, 1360, 1343, 1281, 1242, 1149, 1110, 1060, 962, 947, 842, 529$ .

**4.1.6. Nitrosation.**  $NO_2/N_2O_4$  was bubbled through the solution of polymer **3** (1 g, 0.17 mmol calixarene) in dry  $CH_2Cl_2$  (10 mL) for 2–3 min, after which  $N_2$  was bubbled through the solution for 10–15 min. The resulting dark solution was divided into three equal parts. *N*-methyl octanamide **11a** (5.4 mg, 0.034 mmol), *N*-ethyl octanamide **11b** (5.9 mg, 0.034 mmol), and *N*-propyl octanamide **11c** (6.3 mg, 0.034 mmol) were separately added to each solution, and the reaction mixtures were kept at rt for 2–3 h. The solvent was evaporated at rt under reduced pressure. Hexanes (10 mL) were added, and the mixture was stirred for 10 min, followed by filtration of the recovered polymer **3**. The solvent was evaporated at rt under reduced pressure, and the residue was dried for 3 h in vacuo. The product yield was determined by  $^1H$  NMR spectroscopy, using previously reported spectral data.<sup>13</sup> Selected data: *N*-methyloctanoylamide (**11a**).  $^1H$  NMR  $\delta=6.13$  (bs, 1H, NH), 2.73 (d, 3H,  $J=5$  Hz,  $NCH_3$ ), 2.12 (t, 2H,  $J=7.5$  Hz,  $CH_2$ ), 1.53–1.58 (m, 2H,  $CH_2$ ), 1.22–1.28 (m, 8H,  $4 \times CH_2$ ), 0.83 (t, 3H,  $J=7.5$  Hz,  $CH_3$ ). *N*-Ethyloctanoylamide (**11b**).  $^1H$  NMR  $\delta=5.41$  (bs, 1H, NH), 3.24–3.32 (m, 2H,  $CH_2$ ), 2.13 (t, 2H,  $J=7.5$  Hz,  $CH_2$ ), 1.52–1.64 (m, 2H,  $CH_2$ ), 1.20–1.34 (m, 8H,  $CH_2$ ), 1.12 (t, 3H,  $J=7.5$  Hz,  $CH_3$ ), 0.68



(t, 3H,  $J=7.5$  Hz, CH<sub>3</sub>). *N*-Propyloctanoylamide (**11c**). <sup>1</sup>H NMR  $\delta=5.24$  (bs, 1H, NH), 3.17–3.23 (m, 2H, CH<sub>2</sub>), 2.14 (t, 2H,  $J=7.5$  Hz, CH<sub>2</sub>), 1.63 (m, 2H, CH<sub>2</sub>), 1.47–1.56 (m, 2H, CH<sub>2</sub>), 1.20–1.34 (m, 8H, CH<sub>2</sub>), 0.93 (t, 3H,  $J=7.5$  Hz, CH<sub>3</sub>), 0.84 (t, 3H,  $J=7.5$  Hz, CH<sub>3</sub>). *N*-Methyl-*N*-nitrosooctanoylamide (**12a**). <sup>1</sup>H NMR  $\delta=3.19$  (t, 2H,  $J=7.5$  Hz, CH<sub>2</sub>C(O)), 3.12 (s, 3H, N(NO)CH<sub>3</sub>), 1.72–1.81 (m, 2H, CH<sub>2</sub>), 1.26–1.41 (m, 8H, (CH<sub>2</sub>)<sub>4</sub>), 0.86 (t, 3H,  $J=7.5$  Hz, CH<sub>3</sub>). *N*-Ethyl-*N*-nitrosooctanoylamide (**12b**). <sup>1</sup>H NMR  $\delta=3.80$  (q, 2H,  $J=7.5$  Hz, N(NO)CH<sub>2</sub>), 3.12 (t, 2H,  $J=7.5$  Hz, CH<sub>2</sub>C(O)), 1.75–1.82 (m, 2H, CH<sub>2</sub>), 1.26–1.41 (m, 8H, CH<sub>2</sub>), 0.96 (t, 3H,  $J=7.5$  Hz, CH<sub>3</sub>), 0.87 (t, 3H,  $J=7.5$  Hz, CH<sub>3</sub>). *N*-Propyl-*N*-nitrosooctanoylamide (**12c**). <sup>1</sup>H NMR  $\delta=3.72$  (t, 2H,  $J=7.5$  Hz, N(NO)CH<sub>2</sub>), 3.13 (t, 2H,  $J=7.5$  Hz, CH<sub>2</sub>C(O)), 1.75–1.82 (m, 2H, CH<sub>2</sub>), 1.36–1.42 (m, 2H, CH<sub>2</sub>), 1.26–1.41 (m, 8H, CH<sub>2</sub>), 0.87 (t, 3H,  $J=7.5$  Hz, CH<sub>3</sub>), 0.81 (t, 3H,  $J=7.5$  Hz, CH<sub>3</sub>).

#### 4.2. UV–vis spectroscopy measurements

The measurements with compounds **1–4** were performed at  $295 \pm 1$  K in CH<sub>2</sub>Cl<sub>2</sub>. In the titration studies, the UV–vis spectra were recorded at  $6 \times 10^{-5}$  M concentration of calixarene **1a** and concentration of NO<sub>2</sub> varied within  $\sim 5 \times 10^{-5}$ – $1.2 \times 10^{-3}$  M range. The apparent association constant was estimated from the changes in the absorbance at  $\lambda_{\max} = 565$  nm (charge-transfer band in complex **2a**). All measurements were performed at least in duplicate.

#### Acknowledgements

Financial support was kindly provided by the American Cancer Society Institutional Research Grant to the University of North Texas Health Science Center and the Texas Higher Education Coordinating Board—Advanced Technology Program (003656-0146-2003).

#### References and notes

- US EPA publications: <http://www.epa.gov/air/urbanair/nox/index.html>.
- (a) Lerdau, M. T.; Munger, J. W.; Jacob, D. J. *Science* **2000**, *5488*, 2291–2293. (b) Kirsch, M.; Korth, H.-G.; Sustmann, R.; de Groot, H. *Biol. Chem.* **2002**, *383*, 389–399.
- (a) Mirvish, S. S. *Cancer Lett.* **1995**, *93*, 17–48. (b) Hoffman, D.; Hoffman, I.; El-Bayoumy, K. *Chem. Res. Toxicol.* **2001**, *14*, 767–790. (c) Pfeiffer, S.; Mayer, B.; Hemmens, B. *Angew. Chem., Int. Ed.* **1999**, *38*, 1714–1731. (d) Butler, A. R.; Williams, D. L. H. *Chem. Soc. Rev.* **1993**, 233–241. (e) Tamir, S.; Burney, S.; Tannenbaum, S. R. *Chem. Res. Toxicol.* **1996**, *9*, 821–827.
- (a) Filippini, D.; Rösch, M.; Aragón, R.; Weimar, U. *Sens. Actuators, B* **2001**, *81*, 83–87. (b) Steffes, H.; Imawan, C.; Solzbacher, F.; Obermeier, E. *Sens. Actuators, B* **2001**, *78*, 106–112. (c) Pijolat, C.; Pupier, C.; Sauvan, M.; Tournier, G.; Lalauze, R. *Sens. Actuators, B* **1999**, *59*, 195–202. (d) Law, M.; Kind, H.; Messer, B.; Kim, F.; Yang, P. *Angew. Chem., Int. Ed.* **2002**, *41*, 2405–2408.
- (a) Bradford, A.; Drake, P. L.; Worsfold, O.; Peterson, I. R.; Walton, D. J.; Price, G. J. *Phys. Chem. Chem. Phys.* **2001**, *3*, 1750–1754. (b) Dooling, C. M.; Worsfold, O.; Richardson, T. H.; Tregonning, R.; Vysotsky, M. O.; Hunter, C. A.; Kato, K.; Shinbo, K.; Kaneko, F. *J. Mater. Chem.* **2001**, *11*, 392–398. (c) Baldini, F.; Capobianchi, A.; Falai, A.; Mencaglia, A. A.; Pennesi, G. *Sens. Actuators, B* **2001**, *74*, 12–17. (d) Nezel, T.; Fakler, A.; Zhylyak, G.; Mohr, G. J.; Spichiger-Keller, U. E. *Sens. Actuators, B* **2000**, *70*, 165–169. (e) Capone, S.; Mongelli, S.; Rella, R.; Siciliano, P.; Valli, L. *Langmuir* **1999**, *15*, 1748–1753. (f) Tanaka, T.; Ohshima, T.; Maruo, Y. Y.; Hayashi, T. *Sens. Actuators, B* **1998**, *47*, 65–69. (g) Hu, W. P.; Liu, Y. Q.; Liu, S. G.; Zhou, S. Q.; Zhu, D. B. *Supramol. Sci.* **1998**, *5*, 507–510.
- (a) Zyryanov, G. V.; Kang, Y.; Stamp, S. P.; Rudkevich, D. M. *Chem. Commun.* **2002**, 2792–2793. (b) Zyryanov, G. V.; Kang, Y.; Rudkevich, D. M. *J. Am. Chem. Soc.* **2003**, *125*, 2997–3007.
- Addison, C. C. *Chem. Rev.* **1980**, *80*, 21–39.
- (a) Bosch, E.; Kochi, J. K. *J. Org. Chem.* **1994**, *59*, 3314–3325. (b) Rathore, R.; Bosch, E.; Kochi, J. K. *Tetrahedron* **1994**, *50*, 6727–6758 and references therein.
- (a) Rudkevich, D. M. *Bull. Chem. Soc. Jpn* **2002**, *75*, 393–413. (b) *Calixarene 2001*; Asfari, Z., Böhmer, V., Harrowfield, J., Vicens, J., Eds.; Kluwer Academic: Dordrecht, 2001. (c) Gutsche, C. D. *Calixarenes Revisited*; Royal Society of Chemistry: Cambridge, 1998.
- (a) Iwamoto, K.; Shinkai, S. *J. Org. Chem.* **1992**, *57*, 7066–7073. (b) Beer, P. D.; Drew, M. G. B.; Gale, P. A.; Leeson, P. B.; Ogden, M. I. *J. Chem. Soc., Dalton Trans.* **1994**, 3479–3485. (c) Perez-Adelmar, J.-A.; Abraham, H.; Sanchez, C.; Rissanen, K.; Prados, P.; de Mendoza, J. *Angew. Chem., Int. Ed. Engl.* **1996**, *35*, 1009–1011. (d) de Mendoza, J.; Cuevas, F.; Prados, P.; Meadows, E. S.; Gokel, G. W. *Angew. Chem., Int. Ed.* **1998**, *37*, 1534–1537.
- Casnati, A.; Pochini, A.; Ungaro, R.; Ugozzoli, F.; Arnaud, F.; Fanni, S.; Schwing, M.-J.; Egberink, R. J. M.; de Jong, F.; Reinhoudt, D. N. *J. Am. Chem. Soc.* **1995**, *117*, 2767–2777.
- Iwamoto, K.; Araki, K.; Shinkai, S. *Tetrahedron* **1991**, *47*, 4325–4342.
- Zyryanov, G. V.; Rudkevich, D. M. *Org. Lett.* **2003**, *5*, 1253–1256.
- Kochi and co-workers obtained similar calix[4]arene–NO<sup>+</sup> complexes from either NO<sup>+</sup>SbCl<sub>6</sub><sup>-</sup> and free calixarene or NO gas and the calixarene cation-radical, see: Rathore, R.; Lindeman, S. V.; Rao, K. S. S.; Sun, D.; Kochi, J. K. *Angew., Chem. Int. Ed.* **2000**, *39*, 2123–2127.
- Review on arene–nitrosonium complexes: Borodkin, G. I.; Shubin, V. G. *Russ. Chem. Rev.* **2001**, *70*, 211–230.
- Pariiskii, G. B.; Gaponova, I. S.; Davydov, E. Ya. *Russ. Chem. Rev.* **2000**, *69*, 985–999.
- Stepanov, A. V.; Veselovsky, V. V. *Russ. Chem. Rev. (Russ. Ed.)* **2003**, *72*, 363–378.
- Kosior, M.; Malinowska, M.; Jozwik, J.; Caille, J.; Jurczak, J. *Tetrahedron: Asymmetry* **2003**, *14*, 239.
- (a) Wang, P. G.; Xian, M.; Tang, X.; Wu, X.; Wen, Z.; Cai, T.; Janczuk, A. J. *Chem. Rev.* **2002**, *102*, 1091–1134. (b) Megson, I. I.; Webb, D. J. *Expert Opin. Investig. Drugs* **2002**, *11*, 587–601. (c) Granik, V. G.; Grigor'ev, N. B. *Russ. Chem. Bull., Int. Ed.* **2002**, *51*, 1375–1422.
- (a) McNamara, C. A.; Dixon, M. J.; Bradley, M. *Chem. Rev.* **2002**, *102*, 3275–3300. (b) Dickerson, T. J.; Reed, N. N.; Janda, K. D. *Chem. Rev.* **2002**, *102*, 3325–3344. (c) Bergbreiter, D. E. *Chem. Rev.* **2002**, *102*, 3345–3384.
- (a) Gutsche, C. D.; Iqbal, M. *Org. Synth.* **1990**, *68*, 234–237. (b) Gutsche, C. D.; Levine, J. A.; Sujeeth, P. K. *J. Org. Chem.* **1985**, *50*, 5802–5806.

# Heterodinuclear ruthenium(II) bipyridyl-transition metal dithiocarbamate macrocycles for anion recognition and sensing

Michelle D. Pratt and Paul D. Beer\*

Department of Chemistry, Inorganic Chemistry Laboratory, University of Oxford, Oxford OX1 3QR, UK

Received 22 January 2004; revised 23 June 2004; accepted 19 August 2004

Available online 23 September 2004

**Abstract**—New heterodinuclear ruthenium(II) bipyridyl-transition metal dithiocarbamate macrocycles have been prepared in good yields via metal directed self-assembly and shown to recognise anions. <sup>1</sup>H NMR anion titration studies reveal the nature of the bipyridyl amide metal dithiocarbamate spacer unit in the respective dinuclear metal macrocycle influences significantly the strength of chloride and bromide complexation in DMSO solutions. Luminescence spectroscopy was used to sense anions in polar organic solutions via notable emission enhancement and quenching of the respective ruthenium(II) bipyridyl groups in the receptors.

© 2004 Elsevier Ltd. All rights reserved.

## 1. Introduction

Anionic species are well known to play numerous fundamental roles in biology and chemical processes and their detrimental effects as environmental pollutants is of growing concern.<sup>1</sup> In view of this, there is intense current interest being shown in the design and syntheses of receptors that are proficient at detecting anions in solution.<sup>1,2</sup> By incorporating redox- and photo-active transition metal inorganic signalling probes into various acyclic, macrocyclic and calixarene ligand frameworks, we have produced a series of selective spectral and electrochemical responsive reagents for anions.<sup>2a,3</sup> In an effort to construct new types of luminescent responsive receptors for anion recognition, we report here the synthesis of heterodinuclear ruthenium(II) bipyridyl-transition metal dithiocarbamate macrocycles using metal directed self-assembly.

## 2. Synthesis

We have exploited the positively charged ruthenium(II) bipyridyl moiety in the construction of a variety of acyclic and macrocyclic receptors for anion sensing.<sup>2a,3</sup> The preparation of these latter macrocyclic systems can be problematic as their synthesis requires high dilution conditions and often yields are moderate. These synthetic problems may be overcome by applying metal directed self-

assembly<sup>4</sup> in producing novel heterodinuclear ruthenium(II) bipyridyl-transition metal dithiocarbamate macrocyclic receptors.

Recently, the dithiocarbamate (dtc) moiety has proven to be a useful structural motif lending itself to the metal directed assembly of a range of structures including nano-sized resorcarene-based assemblies,<sup>5</sup> catenanes,<sup>6</sup> assorted macrocycles<sup>7</sup> and cryptands.<sup>8</sup> The dithiocarbamate ligand is simple to prepare via reaction of carbon disulfide with a secondary amine in the presence of base. Consequently, bipyridyl ligands were functionalised initially with secondary amines, and after chelation to the ruthenium(II) bis(bipyridyl) moiety, transition metal directed self-assembly using the dithiocarbamate ligand produced the target heterodinuclear macrocycles.

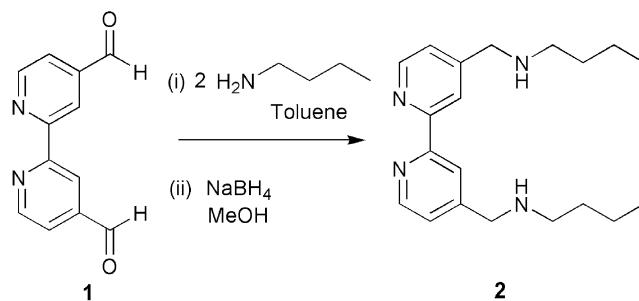
Reductive amination of 4,4'-diformyl-2,2'-bipyridyl **1** with butylamine afforded the bis amine **2** in 92% yield (Scheme 1). Condensation of 4,4'-bis(chlorocarbonyl)-2,2'-bipyridine **3** with 2 equiv of *N*-butyl-ethane-1,2-diamine **4** produced the bis-amide-amine bipyridyl derivative **5** in quantitative yield (Scheme 2). Amide-amine bipyridyl compound **9** was similarly prepared by condensation of 4,4'-bis(chlorocarboxyl)-2,2'-bipyridine **3** with 2 equiv of a Boc-protected diamine (Scheme 3), which was obtained from 4-nitrobenzaldehyde (see Section 6).

Refluxing the appropriate bipyridyl amine derivative with *cis*-Ru(bpy)<sub>2</sub>Cl<sub>2</sub> in aqueous ethanol solution followed by Sephadex column chromatography eluting with acetonitrile/methanol (95:5) and addition of excess NH<sub>4</sub>PF<sub>6</sub> produced

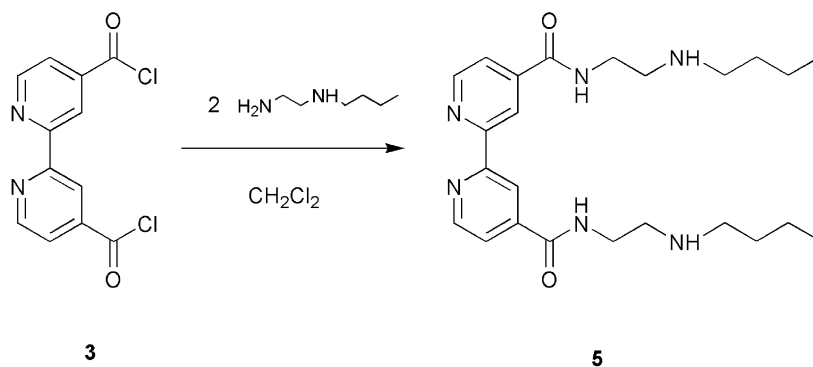
**Keywords:** Anion sensing; Ruthenium; bpy; Macrocycle; Luminescence; Metal directed self-assembly.

\* Corresponding author. Tel.: +44-1865285142; fax: +44-1865272690; e-mail: [paul.beer@chem.ox.ac.uk](mailto:paul.beer@chem.ox.ac.uk)

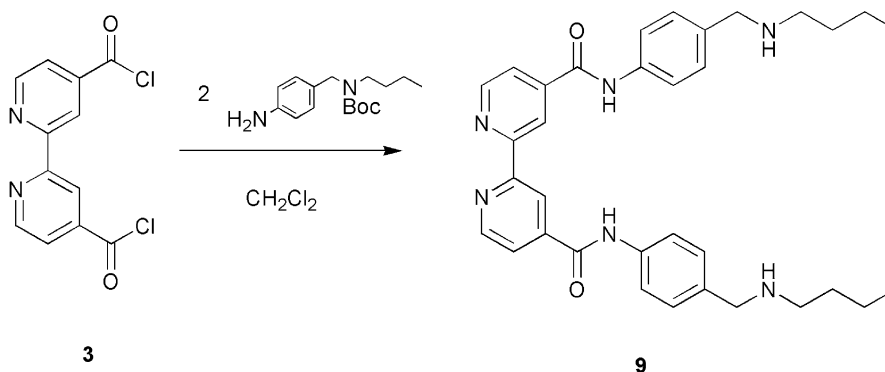




Scheme 1.



Scheme 2.



Scheme 3.

the respective ruthenium(II) complexes **10–12** in good yields (69–80%, Scheme 4).

One-pot macrocyclisation with 2 equiv of carbon disulfide, KOH and transition metal acetate salt in acetonitrile/water (9:1) or THF/water (9:1) solutions gave the target heterodinuclear receptors **13–21** in good yields (48–95%, Scheme 5). These macrocyclic systems were characterised by  $^1\text{H}$  NMR spectroscopy (for diamagnetic derivatives), electrospray mass spectrometry (ESMS) and elemental analysis (see Section 6). No evidence from ESMS was seen for dimeric or higher oligomeric structures.

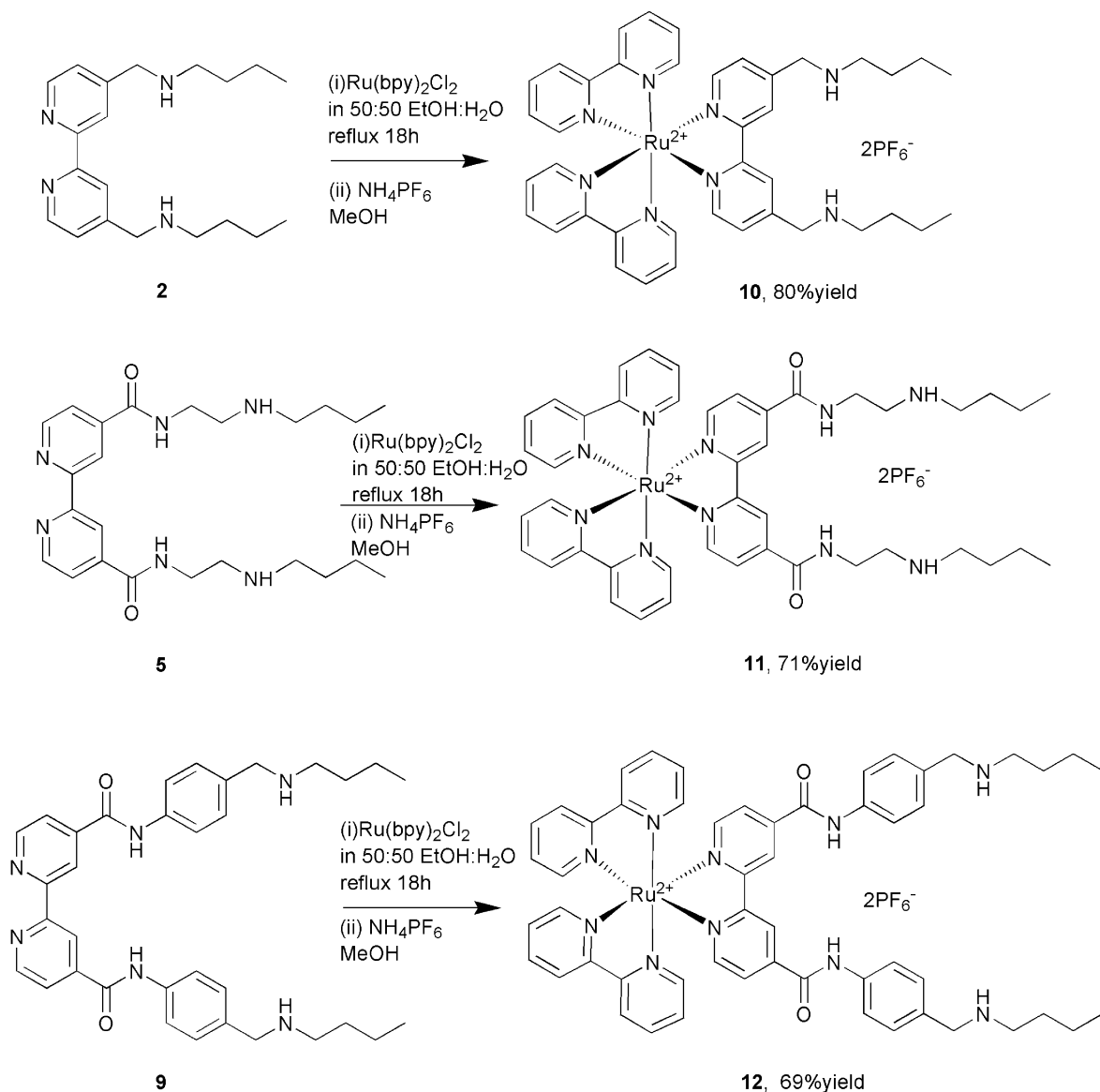
### 3. Anion coordination studies

The interactions of anions with acyclic ruthenium(II) bipyridyl receptors **11** and **12** and their corresponding

macrocycles **16–21** were investigated by a variety of spectroscopic techniques.

#### 3.1. NMR titrations

Solubility problems at NMR concentrations dictated that all titration experiments were undertaken in  $d_6$ -DMSO. The addition of tetrabutylammonium anion salts to  $d_6$ -DMSO solutions of diamagnetic transition metal containing receptors, in general, resulted in significant downfield perturbations of the respective bipyridyl  $\text{H}_3$  and amide receptor protons. EQNMR<sup>9</sup> analysis of the resulting titration curves suggested 1:1 receptor/anion stoichiometry in the majority of cases and the calculated stability constant values are shown in Table 1. Unfortunately with dihydrogen phosphate and acetate anions, precipitation problems during the titration experiment thwarted quantitative binding analysis for the majority of the receptors.



Scheme 4.

Table 1 shows that all three receptors containing ethyl spacer units connecting the ruthenium(II) bipyridyl amide unit to the respective secondary amine or transition metal dithiocarbamate complex **11**, **16** and **18** display the selectivity preference  $\text{Cl}^- > \text{Br}^- > \text{I}^-$ , which suggests the chloride anion is of complementary size to the receptors' cavity. These halide binding results contrast those of **19** and **21** where weak binding of all three halide anions is observed. Presumably, the aryl group containing macrocyclic cavity sterically hinders halide complexation. Acyclic receptor **12** complexes  $\text{Br}^-$  with similar strength to **11**, **16** and **18**. However, the stability of the  $\text{Cl}^-$  complex is significantly reduced in comparison.

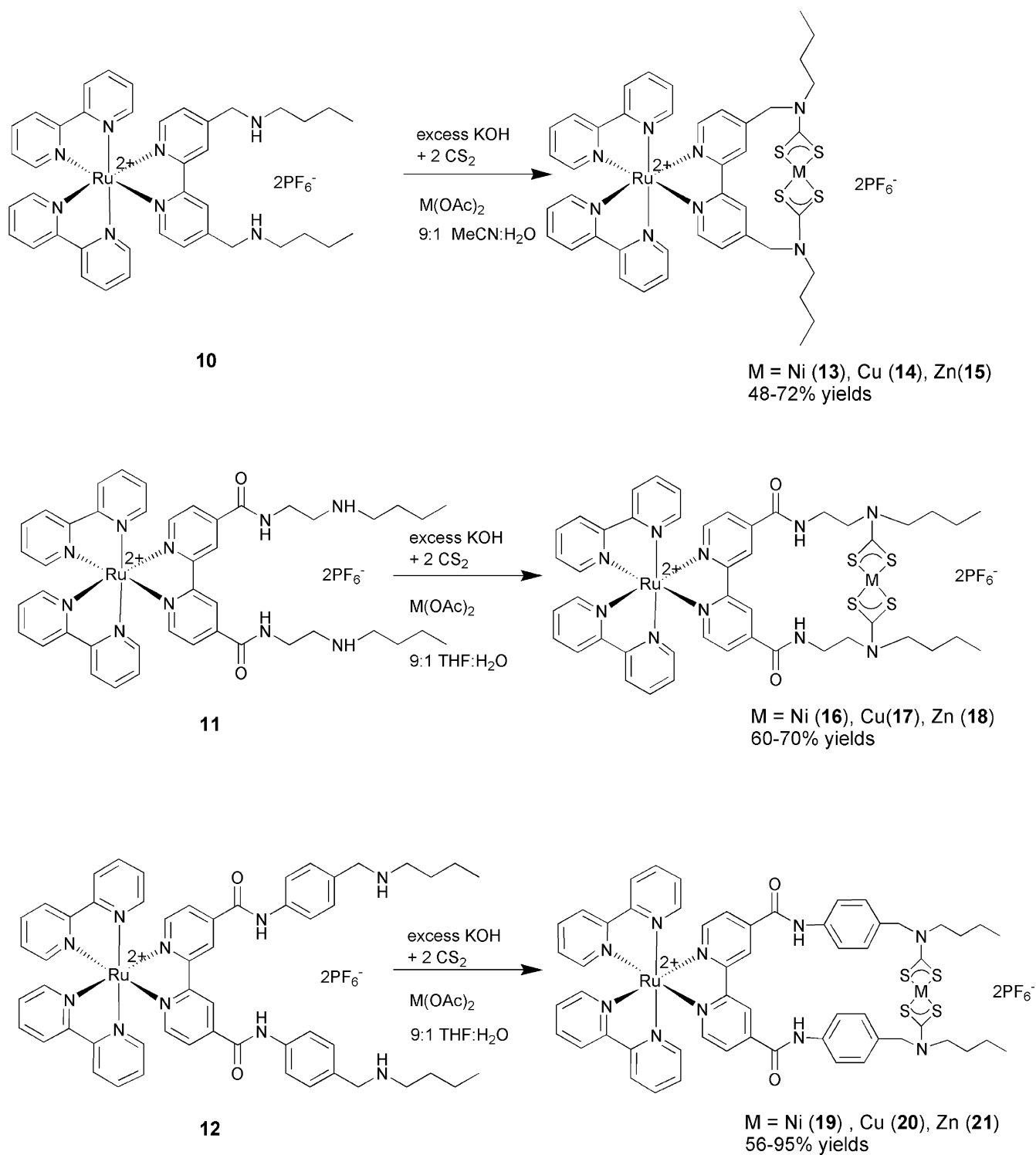
### 3.2. UV-visible

The electronic spectral characteristics of the receptors are shown in Table 2, where as noted previously,<sup>2a</sup> the electron withdrawing characteristics of the amide groups causes a lower energy MLCT transition compared to the MLCT

transition observed with  $[\text{Ru}(\text{bpy})_3]^{2+}$ . The majority of the electronic transitions associated with the transition metal dithiocarbamate complexes are hidden beneath the ruthenium(II) bipyridyl absorptions. The addition of anions to acetonitrile solutions of the respective receptors resulted in small perturbations of the electronic spectrum. In some cases isosbestic points were observed (Fig. 1). However, attempts to determine quantitative binding data using Spectfit<sup>10</sup> proved problematic.

### 3.3. Luminescence spectroscopy

The ability of  $[\text{Ru}(\text{bpy})_3]^{2+}$  to act as a luminescent receptor unit is well established.<sup>2</sup> The emission spectra of all receptors displayed a single broad emission maximum which is red-shifted relative to  $\text{Ru}(\text{bpy})_3 \text{PF}_6$  (Table 3). Again the amide substituents on the bipyridyl motif can explain the energy decrease of the MLCT excited state. It is interesting to note that the relative emission intensities of the heterodinuclear macrocycles vary greatly depending



Scheme 5.

upon the nature of the transition metal dtc complex. The presence of redox-active transition metals nickel(II) **16** and copper(II) **17**, causes luminescence quenching of the  $\text{Ru}(\text{bpy})_3^{2+}$  units. Figure 2 shows that the emission intensity for zinc(II) dtc containing macrocycle **18** is much larger than that of acyclic ruthenium(II) bipyridyl receptor **11** and that emission quenching is clearly observed with **16** and **17** relative to **11**. The effects of addition of anions in the luminescence spectra of the receptors were investigated in

acetonitrile for **11**, **16–18** and in DMSO for **12**, **19–21** due to solubility differences.

#### 3.4. Emission binding studies in acetonitrile

The effect of anion addition on the emission spectra depended on the receptor in question. For **11** there was typically a marked increase in the intensity of the emission upon addition of chloride, bromide, iodide, and acetate with

**Table 1.** Anion stability constant values  $K$  ( $M^{-1}$ ) in DMSO- $d_6$ 

	$M(dtc)_2$ $M=$	$H_2PO_4^-$	$AcO^-$	$Cl^-$	$Br^-$	$I^-$
<b>11</b>	—	1000	<sup>a</sup>	900	120	20
<b>12</b>	—	<sup>b</sup>	<sup>a</sup>	245	180	<10
<b>16</b>	Ni	<sup>b</sup>	990	1000	190	0
<b>18</b>	Zn	<sup>a</sup>	<sup>b</sup>	920	140	0
<b>19</b>	Ni	<sup>b</sup>	<sup>b</sup>	<10	<10	<10
<b>21</b>	Zn	<sup>b</sup>	<sup>b</sup>	<10	<10	<10

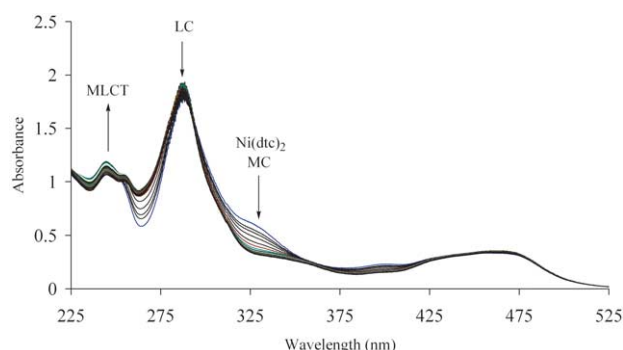
Errors estimated to be  $\leq 10\%$ , temp = 298 K.

<sup>a</sup> EQNMR<sup>8</sup> could not fit data.

<sup>b</sup> Precipitation occurred.

**Table 2.** UV–visible characterisation data in  $CH_3CN$  at  $1.25 \times 10^{-5}$  M

Compound	MLCT		LC		MLCT	
	Wavelength (nm)	$\epsilon/10^3 M^{-1} cm^{-1}$	Wavelength (nm)	$\epsilon/10^3 M^{-1} cm^{-1}$	Wavelength (nm)	$\epsilon/10^3 M^{-1} cm^{-1}$
$[Ru(bpy)_3]^{2+}$	244	27.2	287	79.8	450	14.3
<b>10</b>	245	180.0	287	75.6	454	75.2
<b>11</b>	246	20.6	288	46.8	451	8.2
<b>13</b>	245	45.9	288	72.9	454	14.0
<b>14</b>	245	24.2	287	53.3	454	11.0
<b>15</b>	245	41.6	288	89.6	454	17.5
<b>16</b>	246	49.7	288	79.5	456	12.6
<b>17</b>	244	28.7	287	55.2	445	10.5
<b>18</b>	254	41.0	286	75.8	455	12.6

**Figure 1.** UV–visible titration of **16** and  $AcO^-$  in  $CH_3CN$ .

a concomitant hypsochromic shift in the emission  $\lambda_{max}$  (Table 4). For example, the addition of excess chloride to **11** caused a 47% increase in intensity and a 4.5 nm blue shift in the emission maximum (Fig. 3). The hypsochromic shift indicates that the MLCT state moves to higher energy in the

**Table 3.** Emission data in  $CH_3CN$  except for compounds marked ‘\*’ were in DMSO,  $1.25 \times 10^{-5}$  M,  $\lambda_{excit}$  at maxima of MLCT

Receptor	$M(dtc)_2$ $M=$	Wavelength (nm)	Intensity (arbitrary units)
$[Ru(bpy)_3]$		597	56
$[PF_6]_2$			
<b>20</b>	—	603	214
<b>21</b>	—	631	87
<b>22*</b>	—	639	202
<b>23</b>	Ni	604	10
<b>24</b>	Cu	623	24
<b>25</b>	Zn	625	220
<b>26</b>	Ni	625	3
<b>27</b>	Cu	630	13
<b>29</b>	Zn	630	214
<b>30*</b>	Cu	635	119
<b>31*</b>	Zn	638	206

presence of an anion. The MLCT  $d\pi^*$  state has the electron formally residing on the bipyridine ligand, and this configuration is presumably less favourable when a negatively charged guest binds to the amide bipyridine group. The emission enhancement is probably due to the binding of an anion causing the receptor molecule to become more structurally rigid, by restricting its vibrational and rotational modes. This limits the pathways for radiationless decay, and hence increases the observed emission intensity.<sup>11</sup>

In contrast, macrocycle **18** displayed significant decreases in emission intensity on addition of anions. The luminescence quenching observed upon anion addition to the macrocyclic receptor is more difficult to explain. One possible cause of luminescence quenching is if the symmetry of the molecule is altered upon complexation, destabilising the <sup>3</sup>MLCT excited state. Thus the emission would be quenched, and an intensity decrease would be observed. This effect might also cause a change in the energy levels involved, which would be observed as a shift in the wavelength of the emission maximum.<sup>12</sup> Disappointingly, only small increases in

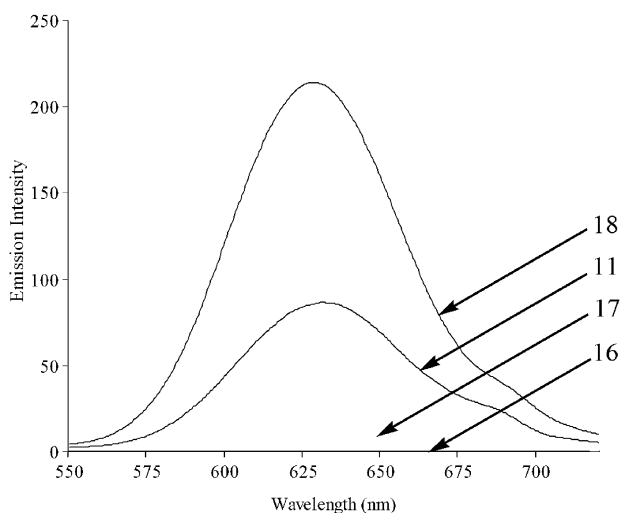


**Figure 2.** Emission spectra of **11** and **16–18** in  $\text{CH}_3\text{CN}$ ,  $1.25 \times 10^{-5}$  M.

**Table 4.** Percentage change in emission maxima intensity in  $\text{CH}_3\text{CN}$  and change in wavelength maxima upon addition of excess anions

Anion	$\text{AcO}^-$	$\text{H}_2\text{PO}_4^-$	$\text{Cl}^-$	$\text{Br}^-$	$\text{I}^-$
( <b>11</b> )	+64%	+39%	+47%	+38%	+7%
$\Delta\lambda_{\text{max}}$ (nm)	-12.5	-2.5	-4.5	-3.0	-3.0
( <b>18</b> )	-65%	-88%	-45%	-30%	-30%
$\Delta\lambda_{\text{max}}$ (nm)	-12.0	-2.0	-5.5	-4.5	-3.5

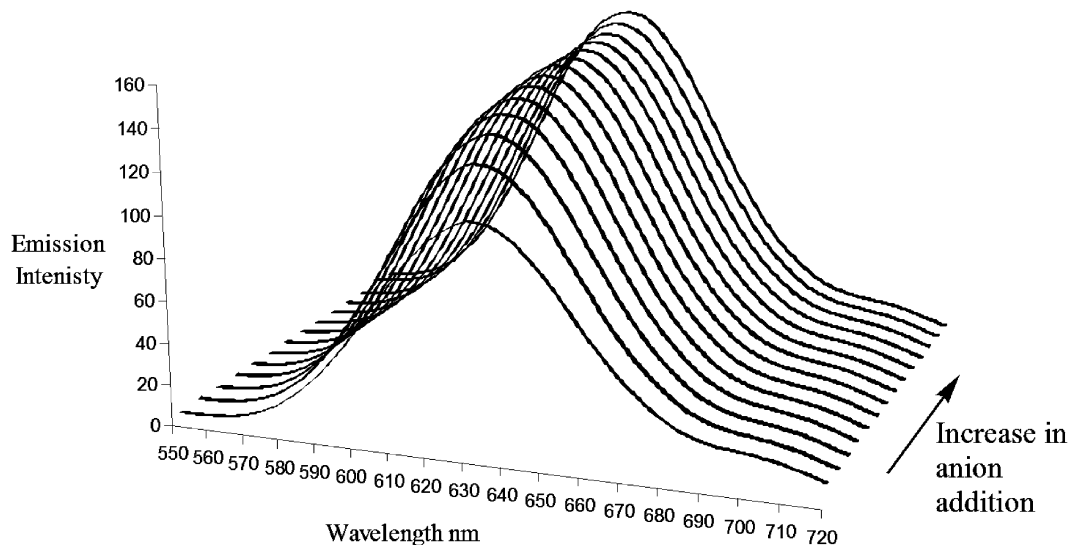


**Figure 3.** Luminescence titration of **11** with  $\text{Cl}^-$  in  $\text{CH}_3\text{CN}$ ,  $1.25 \times 10^{-5}$  M.

emission intensity upon addition of anions to macrocycles **16** and **17** were observed.

Specfit<sup>10</sup> analysis of the titration data enabled stability constants to be determined (Table 5). The stability constants in acetonitrile for receptor **11** are all very high in this solvent and are quoted as  $\log \beta_1 > 6$ , which is approaching the upper limit for  $\log \beta_1$  values by Specfit.<sup>10</sup> The halide anions (chloride, bromide and iodide) were all bound by receptor **11** with similarly large stability constants, whereas macrocycle **18** showed a selectivity trend  $\text{Cl}^- > \text{Br}^- > \text{I}^-$ , as seen in the <sup>1</sup>H NMR titration experiments. Stability constants for

receptors **11** and **18** with dihydrogen phosphate could not be determined due to the complexity of the emission responses, and acetate was bound strongly by both receptors.

### 3.5. Emission binding studies in DMSO

The anion emission titration studies for receptors **12** and **19–21** were conducted in DMSO, due to their poor solubility in acetonitrile. Addition of anions to the ruthenium(II) receptor **12** in DMSO resulted in small increases in the emission intensity and slight hypsochromic shifts. However, the changes in the emission intensity in



**Table 5.** Stability constants determined by Specfit<sup>10</sup> in CH<sub>3</sub>CN at receptor concentrations of 1.25 × 10<sup>-5</sup> M (Temp = 298 K)

	log β <sub>1</sub> <b>11</b>	log β <sub>1</sub> <b>18</b>
AcO <sup>-</sup>	>6	>6
H <sub>2</sub> PO <sub>4</sub> <sup>-</sup>	<sup>a</sup>	<sup>a</sup>
Cl <sup>-</sup>	>6	5.72 ± 0.07
Br <sup>-</sup>	>6	5.04 ± 0.04
I <sup>-</sup>	>6	4.76 ± 0.06

<sup>a</sup> Specfit<sup>10</sup> could not fit data.

DMSO were much less than those observed in CH<sub>3</sub>CN for compound **11**. This is to be expected due to the competitive nature of DMSO.<sup>13</sup> Addition of anions to the macrocycles **19–21** caused only small decreases in emission intensity.

The only anion to cause significant changes in the emission spectra was dihydrogen phosphate. For this anion stability constants could be determined with a 1:1 stoichiometry and are given in Table 6. The zinc(II) macrocycle **21** displayed an enhanced binding affinity for dihydrogen phosphate compared to its acyclic analogue **12**.

**Table 6.** Stability constants determined by Specfit<sup>10</sup>, in DMSO at receptor concentrations of 1.25 × 10<sup>-5</sup> M (Temp = 298 K)

	log β <sub>1</sub> <b>12</b>	log β <sub>1</sub> <b>21</b>
H <sub>2</sub> PO <sub>4</sub> <sup>-</sup>	4.2 ± 0.1	5.28 ± 0.06

#### 4. Electrochemical investigations

The electrochemical properties of **10**, **11** and copper(II) dtc containing receptors **14** and **17** were investigated using cyclic and square wave voltammetry with tetrabutylammonium tetrafluoroborate as supporting electrolyte. As expected the electrochemical data for **10** and **11** are similar to Ru(bpy)<sub>3</sub><sup>2+</sup>, displaying four redox waves assigned to a metal centred Ru(II)/(III) oxidation and three ligand centred bipyridyl reduction processes (Table 7). The electrochemical properties of copper(II) dithiocarbamate complexes are well-documented undergoing reversible one-electron oxidation and reduction redox processes.<sup>14–16</sup>

The copper(II/III) couple in macrocycles **14** and **17** is compared to the copper(II/III) couple in the model compound, copper(II) diethyl dithiocarbamate (Cu(Et<sub>2</sub>dte)<sub>2</sub>). The electrochemical investigations of **14** and **17** were limited to an electrochemical window of +1.25–0 V, in order to avoid decomposition of the macrocycles. Under more reducing conditions precipitation was observed and irreproducible results were noted. Thus assignment and

study of the 2,2'-bpy reductions was rendered impossible (Table 7).

For all receptors the ruthenium(II/III) redox wave was observed at ~1.0 V. For **11** the first bipyridyl ligand centred reduction is assigned to the 4,4'-amide-substituted bipyridyl. The electron withdrawing amide group means that this bipyridyl group is easier to reduce than its neighbouring ones. The anodic shifts in the copper(II/III) couple for the ruthenium macrocycles **14** and **17** compared to Cu(Et<sub>2</sub>dte)<sub>2</sub> may be a result of the close proximity of the positively charged ruthenium(II) centre. All four systems investigated displayed quasi-reversible behaviour for both the ruthenium (II/III) couple and the copper(II/III) redox couples (for receptors **14** and **17**).

The addition of dihydrogen phosphate to receptor **10** caused a small cathodic shift for the first bipyridyl reduction wave (10 mV), but addition of acetate, chloride, bromide, and iodide caused little change (<5 mV). Addition of anions to **11** also caused modest cathodic shifts of ~10 mV for the first bipyridyl wave. The shift was approximately the same for addition of all anions, and little discrimination was shown. For both receptors **10** and **11**, no shifts were observed for the ruthenium(II/III) couple or the second and third bipyridyl reduction couples on the addition of anions. Electrochemical studies on [Ru(bpy)<sub>3</sub>][(PF<sub>6</sub>)<sub>2</sub>] showed no perturbations upon addition of anions to either the ruthenium(II/III) oxidation wave, or the bipyridyl reduction waves.

Cathodic shifts occur because the complexation of anions increases the negative charge density adjacent to the binding site.<sup>17</sup> This in turn inhibits the reduction of the redox centre and so a greater formal reduction potential is required to add more electrons. As noted in previous systems, the fact that no shifts were observed for the second or third bipyridyl reduction couples or for the ruthenium(II/III) couple lends support to the hypothesis that the binding of anionic guests is centred in the vicinity of the substituted bipyridyl groups in solution.

Electrochemical investigations of the macrocycles **14** and **17** and Cu(Et<sub>2</sub>dte)<sub>2</sub> upon addition of anions revealed no perturbations of the ruthenium(II/III) redox wave. However, significant cathodic shifts were observed in the copper(II/III) redox wave (Table 8). The addition of dihydrogen phosphate to macrocycle **14** resulted in a shift of 40 mV. This shift was considerably larger than the shift observed for Cu(Et<sub>2</sub>dte)<sub>2</sub> (<10 mV). Receptor **14** showed little interaction with acetate. However, the large cathodic shift in the copper(II/III) redox potential of Cu(Et<sub>2</sub>dte)<sub>2</sub> upon addition

**Table 7.** Electrochemical data for **10**, **11**, **14**, **17** in CH<sub>3</sub>CN/0.1 M TBABF<sub>4</sub>, Ag/AgNO<sub>3</sub> reference electrode

Complex	Ru(II/III) couple E <sub>1/2</sub> /V	First 2,2'-bpy reduction E <sub>1/2</sub> /V	Second 2,2'-bpy reduction E <sub>1/2</sub> /V	Third 2,2'-bpy reduction E <sub>1/2</sub> /V	Cu(II/III) couple E <sub>1/2</sub> /V
[Ru(bpy) <sub>3</sub> ] <sup>2+</sup>	+1.03	-1.61	-1.82	-2.12	—
<b>10</b>	+1.02	-1.60	-1.83	-2.12	—
<b>11</b>	+1.03	-1.51	-1.80	-2.10	—
<b>14</b>	+1.00	—	—	—	+0.29
<b>17</b>	+1.02	—	—	—	+0.20
Cu(Et <sub>2</sub> dte) <sub>2</sub>	—	—	—	—	+0.19

$$E_{1/2} = (E_{pa} + E_{pc})/2.$$

**Table 8.** Cathodic shifts in Cu(II/III) redox wave upon addition of 5 equiv of anion in CH<sub>3</sub>CN/0.1 M TBABF<sub>4</sub>

Cu(II/III) couple $\Delta E$ (mV)	Cu(Et <sub>2</sub> dtc) <sub>2</sub>	<b>14</b>	<b>17</b>
H <sub>2</sub> PO <sub>4</sub> <sup>-</sup>	<10	40	<sup>a</sup>
AcO <sup>-</sup>	60	<10	<sup>a</sup>

<sup>a</sup> Precipitation occurred.

of acetate anions may imply there is a coordinative interaction between the copper(II) centre and the anion.

Unfortunately, no significant changes in oxidation potentials were observed on addition of bromide or iodide to **14** or **17**. At the concentrations used for the electrochemical experiments, addition of dihydrogen phosphate and acetate anions to receptor **17** caused precipitation, hindering further investigation.

## 5. Conclusions

A series of new 4,4'-amide-secondary amine substituted ruthenium(II) bipyridyl derivatives were prepared initially, which on applying metal directed self-assembly, using the dithiocarbamate ligand, produced novel heterodinuclear ruthenium(II) bipyridyl-transition metal dithiocarbamate macrocycles in good yields. A variety of spectroscopic and electrochemical techniques were employed to investigate their anion recognition and sensing capabilities. It is noteworthy that the nature of the spacer unit in the respective dinuclear metal macrocycles crucially dictates the strength of chloride and bromide binding in DMSO solutions with ethyl spacer containing macrocyclic receptors **16** and **18** forming much stronger complexes than the corresponding aryl linked systems **19** and **21**. Although UV-visible absorption spectroscopy proved largely insensitive to anion complexation, the luminescence spectra of the receptors were significantly perturbed on anion binding. Both anion complexation induced emission enhancement and quenching effects were noted, respectively, with **11** and **18**.

Voltammetric studies revealed modest anion induced cathodic shifts of the respective first bipyridyl reduction redox couple of acyclic receptors **10** and **11**, whereas a significant cathodic perturbation of the copper(II)/(III) dtc redox couple of **14** was noted with dihydrogen phosphate anion addition.

## 6. Experimental

### 6.1. General

NMR spectra were recorded on a Varian Mercury 300 or a Varian Unity Plus machine 500. FAB Mass spectrometry was carried out by the EPSRC mass spectrometry service, Swansea. Elemental analyses were performed by the Inorganic Chemistry Laboratory Microanalysis Service and electrospray mass spectrometry (ESMS) were performed on a Micromass ESI-TOF in the Inorganic Chemistry Department, University of Oxford. Fluorescence

spectra were recorded on a Perkin Elmer Lambda 6 UV-visible Spectrometer. Measurements were conducted at 25 °C using a 1×1 cm rectangular quartz cuvette. UV-visible spectra were recorded on a PE Lambda 6 spectrometer. Electrochemical studies were performed on a Princeton Applied Research potentiostat/galvanostat model 273 using a glassy carbon working electrode, a platinum counter electrode and an Ag/AgNO<sub>3</sub> reference electrode (0.33 V ± 10 mV vs SCE). Kemet diamond sprays (1 μm and 0.25 μm) were used to polish the working electrode.

4,4'-Diformyl-2,2'-bipyridine **1**,<sup>18</sup> 4,4'-bis(carboxy)-2,2'-bipyridine **3**,<sup>19</sup> and 4,4'-bis(chlorocarbonyl)-2,2'-bipyridine **4**,<sup>18</sup> were prepared according to literature procedures.

**6.1.1. 4,4'-Bis(butylaminomethyl)-2,2'-bipyridine, 2.** 4,4'-Diformyl-2,2'-bipyridine (0.20 g, 0.9 mmol) and *n*-butylamine (0.13 g, 1.8 mmol) were dissolved in toluene (100 ml). The mixture was refluxed under nitrogen for 45 min using Dean-Stark apparatus and then the solvent was removed to yield an orange oil. This was dissolved in MeOH (100 ml) and a fivefold excess of NaBH<sub>4</sub> was cautiously added and stirred for 1 h under nitrogen. HCl (aq) (2 M) was added carefully until pH = 1. The mixture was made basic (pH = 11) by the addition of KOH (aq) (2 M). The product was extracted into CH<sub>2</sub>Cl<sub>2</sub> (4×50 ml) and dried over K<sub>2</sub>CO<sub>3</sub>. Solvent removal and drying in vacuo yielded a yellow oil (0.27 g, 92%).

<sup>1</sup>H NMR in CDCl<sub>3</sub> (δ/ppm): 0.85 (t, 6H, <sup>3</sup>J = 7.2 Hz, CH<sub>3</sub>), 1.30 (m, 4H, <sup>3</sup>J = 7.2 Hz, CH<sub>2</sub>CH<sub>3</sub>), 1.45 (m, 4H, <sup>3</sup>J = 7.2 Hz, CH<sub>2</sub>CH<sub>2</sub>CH<sub>3</sub>), 2.58 (t, 4H, <sup>3</sup>J = 7.2 Hz, NCH<sub>2</sub>CH<sub>2</sub>), 3.83 (s, 4H, bpyCH<sub>2</sub>NH), 7.27 (d, 2H, <sup>3</sup>J = 4.8 Hz, bpy-H5,5'), 8.27 (s, 2H, bpy-H3,3'), 8.56 (d, 2H, <sup>3</sup>J = 4.8 Hz, bpy-H6,6').

<sup>13</sup>C NMR in CDCl<sub>3</sub> (δ/ppm): 14.67 (CH<sub>3</sub>), 23.50 (CH<sub>2</sub>), 32.23 (CH<sub>2</sub>), 50.03 (CH<sub>2</sub>NH), 53.43 (bpyCH<sub>2</sub>), 120.71 (bpy-C), 123.27 (bpy-C), 139.01 (bpy-C), 149.34 (bpy-C), 150.77 (bpy-C).

ESMS: *m/z* 327.3 [M + H]<sup>+</sup>.

**6.1.2. 4,4'- Bis-[(2-butylamino-ethyl-carbamoyl)] 2,2'-bipyridine, 5.** *N*-Butyl-ethane-1,2-diamine (0.2 g, 1.7 mmol) was dissolved in CH<sub>2</sub>Cl<sub>2</sub> (30 ml) under a nitrogen atmosphere. To this rapidly stirred solution, a solution of 4,4'-di(chlorocarbonyl)-2,2'-bipyridine **4** (0.24 g, 0.8 mmol) dissolved in CH<sub>2</sub>Cl<sub>2</sub> (30 ml) was added dropwise. A white precipitate formed immediately, but the solution was stirred for a further 15 min to ensure completion of the reaction. The product was filtered, washed with H<sub>2</sub>O (2×15 ml), Et<sub>2</sub>O (2×15 ml) and dried in vacuo to give a highly insoluble white solid in quantitative yield (0.38 g).

<sup>1</sup>H NMR in DMSO-*d*<sub>6</sub> (δ/ppm): 0.82 (t, 6H, <sup>3</sup>J = 3.9 Hz, CH<sub>3</sub>), 1.28 (m, 4H, CH<sub>2</sub>CH<sub>3</sub>), 1.52 (m, 4H, CH<sub>2</sub>CH<sub>2</sub>CH<sub>3</sub>), 2.65 (m, 4H, NHCH<sub>2</sub>CH<sub>2</sub>CH<sub>2</sub>CH<sub>3</sub>), 2.81 (m, 4H, CH<sub>2</sub>NH), 3.54 (m, 4H, CH<sub>2</sub>NHCO), 7.88 (m, 2H, bpy-H5,5'), 8.76 (s, 2H, bpy-H3,3'), 8.83 (m, 2H, bpy-H6,6'), 9.14 (m, 2H, CONH).

ESMS: *m/z* 441.6 [M + H]<sup>+</sup>, 463.6 [M + Na]<sup>+</sup>.

**6.1.3. Butyl-(4-nitro-benzyl)-amine, 6.** 4-Nitrobenzaldehyde (2 g, 13 mmol) and *n*-butylamine (0.96 g, 13 mmol) were dissolved in toluene (100 ml). The mixture was refluxed under nitrogen for 45 min using Dean–Stark apparatus and the solvent was removed to yield an orange oil. This was dissolved in MeOH (100 ml) and a five-fold excess of NaBH<sub>4</sub> was added cautiously and stirred for 1 h under nitrogen. HCl (aq) (2 M) was added carefully until pH=1 and then NaOH (aq) (2 M) until pH=11. The product was extracted into CH<sub>2</sub>Cl<sub>2</sub> (4×50 ml) and dried over K<sub>2</sub>CO<sub>3</sub>. Solvent removal and drying *in vacuo* yielded a yellow oil (1.76 g, 65% yield).

<sup>1</sup>H NMR in CDCl<sub>3</sub> (δ/ppm): 0.81 (t, 3H, <sup>3</sup>J=7.2 Hz, CH<sub>3</sub>), 1.19 (m, 2H, <sup>3</sup>J=7.2 Hz, CH<sub>2</sub>CH<sub>3</sub>), 1.40 (m, 2H, <sup>3</sup>J=7.2 Hz, CH<sub>2</sub>CH<sub>2</sub>CH<sub>3</sub>), 3.11 (m, 2H, NHCH<sub>2</sub>CH<sub>2</sub>), 4.43 (s, 2H, ArCH<sub>2</sub>), 7.30 (d, 2H, <sup>3</sup>J=7.8 Hz, Ar-H), 8.10 (d, 2H, <sup>3</sup>J=7.8 Hz, Ar-H).

ESMS: *m/z* 209.1 [M+H]<sup>+</sup>.

**6.1.4. Butyl-(4-nitro-benzyl)-carbamic acid *tert*-butyl ester, 7.** Bis-(*tert*-butoxycarbonyl)anhydride (0.27, 1.2 mmol) was dissolved in 30 ml of dioxane. This was added, over 2 1/2 h, to butyl-(4-nitro-benzyl)-amine (0.2 g, 1.1 mmol) (which was dissolved in 30 ml of dioxane). The solution was stirred for 30 min, after which time the solvent was removed *in vacuo* giving a white semi-solid. H<sub>2</sub>O (50 ml) was added and the product was extracted into CH<sub>2</sub>Cl<sub>2</sub> (3×50 ml), dried with MgSO<sub>4</sub>, filtered and reduced *in vacuo* leaving a clear, viscous oil (0.25 g, 74% yield).

<sup>1</sup>H NMR in CDCl<sub>3</sub> (δ/ppm): 0.85 (t, 3H, <sup>3</sup>J=7.8 Hz, CH<sub>2</sub>CH<sub>3</sub>), 1.23 (m, 4H, <sup>3</sup>J=6.6 Hz, CH<sub>2</sub>CH<sub>2</sub>CH<sub>3</sub>), 1.44 (s, 9H, C(CH<sub>3</sub>)<sub>3</sub>), 3.14 (m, 2H, NBocCH<sub>2</sub>CH<sub>2</sub>), 4.46 (s, 2H, ArCH<sub>2</sub>), 7.34 (d, 2H, <sup>3</sup>J=8.4 Hz, Ar-H), 8.13 (d, 2H, <sup>3</sup>J=8.1 Hz, Ar-H).

<sup>13</sup>C NMR in CDCl<sub>3</sub> (δ/ppm): 13.95 (CH<sub>3</sub>), 20.14 (CH<sub>2</sub>), 28.52 ((CH<sub>3</sub>)<sub>3</sub>C), 30.5 (CH<sub>2</sub>), 47.34 (CH<sub>2</sub>), 67.24 (ArCH<sub>2</sub>N), 80.24 ((CH<sub>3</sub>)<sub>3</sub>C), 123.88 (Ar-C), 128.22 (Ar-C), 128.26 (Ar-C), 147.32 (Ar-C).

ESMS: *m/z* 331.2 [M+Na]<sup>+</sup>.

**6.1.5. (4-Amino-benzyl)- butyl-carbamic acid *tert*-butyl ester, 8.** The nitro compound **7** (6.20 g, 0.018 mol) was reduced using Raney Nickel, 10 atm, 50 °C, 1 h in EtOH. The solvent was removed and the product purified by column chromatography on silica eluting with CH<sub>2</sub>Cl<sub>2</sub> to give the amine (3.62 g, 72% yield).

<sup>1</sup>H NMR in CDCl<sub>3</sub> (δ/ppm): 0.80 (t, 3H, <sup>3</sup>J=6.9 Hz, CH<sub>3</sub>), 1.11 (m, 4H, <sup>3</sup>J=6.6 Hz, CH<sub>2</sub>CH<sub>2</sub>CH<sub>3</sub>), 1.39 (s, 9H, CCH<sub>3</sub>), 3.03 (br s, 2H, NH<sub>2</sub>), 3.68 (m, 2H, NBocCH<sub>2</sub>CH<sub>2</sub>), 4.21 (s, 2H, ArCH<sub>2</sub>), 7.15 (d, 2H, <sup>3</sup>J=8.1 Hz, Ar-H), 7.26 (d, 2H, <sup>3</sup>J=7.8 Hz, Ar-H).

<sup>13</sup>C NMR in CDCl<sub>3</sub> (δ/ppm): 13.98 (CH<sub>3</sub>), 20.16 (CH<sub>2</sub>), 28.61 ((CH<sub>3</sub>)<sub>3</sub>C), 30.21 (CH<sub>2</sub>), 45.85 (CH<sub>2</sub>), 67.15 (ArCH<sub>2</sub>N), 79.27 ((CH<sub>3</sub>)<sub>3</sub>C), 115.08 (Ar-C), 128.10 (Ar-C), 129.33 (Ar-C), 146.14 (Ar-C).

ESMS: *m/z* 301.2 [M+Na]<sup>+</sup>.

**6.1.6. 4,4'' Bis-[(4-butylaminomethyl-phenyl)-carbonyl]-2,2'-bipyridine, 9.** (4-Amino-benzyl)- butyl-carbamic acid *tert*-butyl ester **8** (4.88 g, 1.7 mmol) was dissolved in CH<sub>2</sub>Cl<sub>2</sub> (30 ml) under a nitrogen atmosphere. To this a solution of 4,4'-di(chlorocarbonyl)-2,2'-bipyridine (2.03 g, 8.0 mmol) dissolved in CH<sub>2</sub>Cl<sub>2</sub> (30 ml) was added dropwise. An orange precipitate formed immediately, but the solution was stirred for a further 15 min to ensure completion of the reaction. The product was filtered, washed with H<sub>2</sub>O (2×15 ml), Et<sub>2</sub>O (2×15 ml) and dried *in vacuo* to give an orange solid (5.88 g, 96% yield). Interestingly during this reaction the amine protecting group (Boc) was removed to yield the free amine.

<sup>1</sup>H NMR in DMSO-*d*<sub>6</sub> (δ/ppm): 0.93 (t, 6H, CH<sub>3</sub>), 1.22 (m, 4H, CH<sub>2</sub>CH<sub>3</sub>), 1.43 (m, 4H, CH<sub>2</sub>CH<sub>2</sub>CH<sub>3</sub>), 3.15 (m, 4H, NHCH<sub>2</sub>CH<sub>2</sub>), 4.37 (s, 4H, ArCH<sub>2</sub>), 7.20 (d, 4H, <sup>3</sup>J=7.8 Hz, Ar-H), 7.75 (d, 4H, Ar-H), 8.03 (d, 4H, <sup>3</sup>J=7.2 Hz, bpy-H5,5'), 8.94 (m, 4H, bpy-H6,6' and CONH), 10.86 (s, 2H, bpy-H3,3').

ESMS: *m/z* 565.7 [M+H]<sup>+</sup>.

**6.1.7. Ruthenium(II) (4,4'-bis(butylaminomethyl)-2,2'-bipyridine)bis(2,2'-bipyridine)-bis(hexafluorophosphate), 10.** *cis*-Dichlorobis(2,2'-bipyridine)ruthenium(II) (0.12 g, 0.2 mmol) and 4,4'-bis-(butylaminomethyl)-2,2'-bipyridine **2** (0.09 g, 0.2 mmol) were dissolved in EtOH/H<sub>2</sub>O (50:50) (50 ml) and refluxed for 18 h. The solvent was removed *in vacuo* leaving a shiny deep purple solid. The crude product was purified by column chromatography on Sephadex<sup>®</sup> LH-20, eluting with MeCN to remove excess [Ru(bpy)<sub>2</sub>Cl<sub>2</sub>] and then 5% MeOH in MeCN to obtain the product. Solvent removal gave a deep purple shiny, flaky solid. It was noted that for this and all subsequent ruthenium compounds that there was a thin green band, between the purple of the *cis*-dichlorobis(2,2'-bipyridine)ruthenium(II) and the red of the product, attributed to a ruthenium(III) complex. The chloride counteranion was exchanged for hexafluorophosphate by dissolving the chloride salt in the minimum amount of MeOH and adding a saturated solution of NH<sub>4</sub>PF<sub>6</sub> (aq). This gives the hexafluorophosphate salt as a precipitate, which can be removed by filtration, washed with H<sub>2</sub>O, then Et<sub>2</sub>O and dried under vacuum to yield a red solid (typically 90–94% conversion from the chloride salt). The red solid was isolated and dried under vacuum (0.16 g, 80% yield).

<sup>1</sup>H NMR in CD<sub>3</sub>CN (δ/ppm): 0.94 (t, 6H, <sup>3</sup>J=7.0 Hz, CH<sub>3</sub>), 1.40 (m, 4H, <sup>3</sup>J=7.5 Hz, CH<sub>2</sub>CH<sub>3</sub>), 1.63 (m, 4H, <sup>3</sup>J=7.5 Hz, CH<sub>2</sub>CH<sub>2</sub>CH<sub>3</sub>), 2.96 (m, 4H, <sup>3</sup>J=7 Hz, NCH<sub>2</sub>CH<sub>2</sub>), 4.22 (s, 4H, bpyCH<sub>2</sub>NH), 7.44 (m, 6H, bpy-H<sub>6</sub> and bpy-H5,5'), 7.75 (m, 6H, bpy-H6,6' and bpy-H<sub>7</sub>), 8.09 (t, 4H, <sup>3</sup>J=7.8 Hz, bpy-H<sub>4</sub>), 8.52 (d, 6H, <sup>3</sup>J=7.8 Hz, bpy-H<sub>6</sub>), 8.59 (s, 2H, bpy-H3,3').

<sup>13</sup>C NMR in CD<sub>3</sub>CN (δ/ppm): 13.44 (CH<sub>3</sub>), 20.04 (CH<sub>2</sub>), 30.27 (CH<sub>2</sub>), 48.83 (CH<sub>2</sub>NH), 50.59 (bpyCH<sub>2</sub>), 124.56 (bpy-C), 125.01 (bpy-C), 127.87 (bpy-C), 127.92 (bpy-C), 138.19 (bpy-C), 151.76 (bpy-C), 151.85 (bpy-C), 152.03 (bpy-C), 157.07 (bpy-C), 157.17 (bpy-C).

Elemental analysis: found: C 44.7%, H 4.8%, N 10.4%.

Calculated (C<sub>40</sub>H<sub>46</sub>N<sub>8</sub>RuP<sub>2</sub>F<sub>12</sub>·2H<sub>2</sub>O): C 45.0%, H 4.7%, N 10.5%.

ESMS: *m/z* 739.9 [M–2PF<sub>6</sub>]<sup>+</sup>, 884.9 [M–PF<sub>6</sub>]<sup>+</sup>, 1029.9 [M]<sup>+</sup>.

**6.1.8. Ruthenium(II) 4,4'-bis-[(2-butylamino-ethyl-carbamoyl) 2,2'-bipyridine bis(2,2'-bipyridine)-bis(hexafluorophosphate), 11.** Procedure as for receptor **10**, using *cis*-dichlorobis(2,2'-bipyridine)ruthenium(II) (0.19 g, 0.36 mmol) and 4,4'-bis-[(2-butylamino-ethyl-carbamoyl) 2,2'-bipyridine **5** (0.16 g, 0.36 mmol) The hexafluorophosphate salt was then isolated (0.29 g, 71% yield).

<sup>1</sup>H NMR in CD<sub>3</sub>CN (δ/ppm): 0.96 (t, 6H, <sup>3</sup>J=7.2 Hz, CH<sub>3</sub>), 1.42 (m, 4H, <sup>3</sup>J=7.5 Hz, CH<sub>2</sub>CH<sub>3</sub>), 1.66 (m, 4H, <sup>3</sup>J=7.0 Hz, CH<sub>2</sub>CH<sub>2</sub>CH<sub>3</sub>), 3.07 (t, 4H, <sup>3</sup>J=8.0 Hz, NHCH<sub>2</sub>CH<sub>2</sub>CH<sub>2</sub>CH<sub>3</sub>), 3.28 (t, 4H, <sup>3</sup>J=5.1 Hz, CH<sub>2</sub>NHCH<sub>2</sub>CH<sub>2</sub>CH<sub>2</sub>), 3.71 (m, 4H, <sup>3</sup>J=7.0 Hz, CONHCH<sub>2</sub>), 7.44 (m, 4H, <sup>3</sup>J=5.7 Hz, bpy-H<sub>e</sub>), 7.73 (m, 6H, bpy-H<sub>5,5'</sub> and bpy-H<sub>f</sub>), 7.96 (d, 2H, <sup>3</sup>J=6.0 Hz, bpy-H<sub>6,6'</sub>), 8.10 (m, 4H, <sup>3</sup>J=6.0 Hz, bpy-H<sub>d</sub>), 8.55 (m, 6H, bpy-H<sub>c</sub> and 2CONH), 9.04 (s, 2H, bpy-H<sub>3,3'</sub>).

<sup>13</sup>C NMR in CD<sub>3</sub>CN (δ/ppm): 13.24 (CH<sub>3</sub>), 19.74 (CH<sub>2</sub>), 28.15 (CH<sub>2</sub>), 37.41 (CH<sub>2</sub>), 48.57 (CH<sub>2</sub>), 48.92 (CH<sub>2</sub>), 124.97 (bpy-C), 125.66 (bpy-C), 126.20 (bpy-C), 128.33 (bpy-C), 138.80 (bpy-C), 141.97 (bpy-C), 152.28 (bpy-C), 153.30 (bpy-C), 157.21 (bpy-C), 157.34 (bpy-C), 158.10 (bpy-C), 165.76 (CO).

Elemental analysis: found: C 43.2%, H 5.0%, N 11.1%.

Calculated (C<sub>44</sub>H<sub>52</sub>N<sub>10</sub>RuO<sub>2</sub>P<sub>2</sub>F<sub>12</sub>·4H<sub>2</sub>O): C 43.5%, H 5.0%, N 11.5%.

ESMS: *m/z* 427.2 [M–2PF<sub>6</sub>]<sup>2+</sup>, 500.2 [M–PF<sub>6</sub>]<sup>2+</sup>, 573.2 [M]<sup>2+</sup>.

**6.1.9. Ruthenium(II) (4,4'-bis-[(4-butylaminomethyl-phenyl)-carbamoyl]-2,2'-bipyridine) bis(2,2'-bipyridine)-bis(hexafluorophosphate), 12.** Procedure as for receptor **10** using *cis*-dichlorobis(2,2'-bipyridine)ruthenium(II) (0.85 g, 1.6 mmol) and 4,4'-bis-[(4-butylaminomethyl-phenyl)-carbamoyl]-2,2'-bipyridine **9** (1.25 g, 1.6 mmol) The product was isolated as a deep purple shiny, flaky solid. (1.40 g, 69% yield).

<sup>1</sup>H NMR in CD<sub>3</sub>CN (δ/ppm): 0.94 (t, 6H, <sup>3</sup>J=5 Hz, CH<sub>3</sub>), 1.39 (m, 4H, CH<sub>2</sub>CH<sub>3</sub>), 1.46 (m, 4H, CH<sub>2</sub>CH<sub>2</sub>CH<sub>3</sub>), 3.05 (t, 4H, <sup>3</sup>J=7.8 Hz, NHCH<sub>2</sub>CH<sub>2</sub>), 4.17 (s, 4H, ArCH<sub>2</sub>NH), 7.32 (d, 2H, bpy-H<sub>5,5'</sub>), 7.56 (m, 4H, <sup>3</sup>J=5.4 Hz, bpy-H<sub>e</sub>), 7.77 (d, 2H, <sup>3</sup>J=5.4 Hz, bpy-H<sub>6,6'</sub>), 7.88 (m, 4H, bpy-H<sub>f</sub>), 7.96 (m, 4H, bpy-H<sub>d</sub>), 8.19 (m, 8H, bpy-H<sub>c</sub> and ArH), 8.91 (m, 2H, bpy-H<sub>3,3'</sub> and ArH), 10.09 (br s, 1H, NHCO), 10.44 (br s, 1H, NHCO).

Elemental analysis: found: C 39.7%, H 4.1%, N 10.5%.

Calculated (C<sub>54</sub>H<sub>56</sub>F<sub>12</sub>N<sub>10</sub>O<sub>2</sub>P<sub>2</sub>Ru·3H<sub>2</sub>O): C 49.0%, H 4.7%, N 10.6%.

MALDI: *m/z* 978.2 [M–2PF<sub>6</sub>]<sup>+</sup>, 1122.8 [M–PF<sub>6</sub>]<sup>+</sup>.

## 6.2. General method for synthesis of macrocycles, 13–15

The macrocyclic receptors were synthesised in a one pot reaction. To a stirred solution of the respective ruthenium (II) receptor **10** in 10 ml MeCN/H<sub>2</sub>O mixture (9:1) was added an excess of KOH(aq) (1 M). Two equivalents of carbon disulphide were dropped into the solution and the mixture stirred for 10 min allowing formation of the potassium dithiocarbamate salt. This salt was not isolated but reacted *in situ* by the addition of 1 equiv of nickel, copper, or zinc (II) acetate. The mixture was stirred overnight. Addition of water precipitated the product. The mixture was stirred for a further 2 h before it was filtered and dried to give the macrocycles.

**6.2.1. Nickel(II) macrocycle, 13.** Procedure outlined above using receptor **10** (0.12 g, 0.1 mmol) and 1 equiv of nickel(II) acetate tetrahydrate. Red/brown solid (0.06 g, 48%).

<sup>1</sup>H NMR in CD<sub>3</sub>CN (δ/ppm): 0.87 (br m, 6H, CH<sub>3</sub>), 1.32 (m, 4H, CH<sub>2</sub>CH<sub>3</sub>), 1.62 (br m, 4H, <sup>3</sup>J=7.5 Hz, CH<sub>2</sub>CH<sub>2</sub>CH<sub>3</sub>), (obscured by solvent, NCH<sub>2</sub>CH<sub>2</sub>), 5.69 (dd, 4H, <sup>3</sup>J=6.3 Hz, <sup>4</sup>J=1.5 Hz, bpyCH<sub>2</sub>N), 7.43 (m, 6H, bpy-H<sub>6,6'</sub> and bpy-H<sub>e</sub>), 7.73 (t, 2H, <sup>3</sup>J=7.5 Hz, bpy-H<sub>f</sub>), 8.09 (m, 6H, bpy-H<sub>5,5'</sub> and bpy-H<sub>d</sub>), 8.55 (d, 4H, <sup>3</sup>J=7.5 Hz, bpy-H<sub>c</sub>), 8.99 (s, 2H, bpy-H<sub>3,3'</sub>).

Elemental analysis: found: C 39.9%, H 3.7%, N 8.8%.

Calculated (C<sub>42</sub>H<sub>42</sub>N<sub>8</sub>RuS<sub>4</sub>NiP<sub>2</sub>F<sub>12</sub>·2H<sub>2</sub>O): C 39.6%, H 3.6%, N 8.8%.

ESMS: *m/z* 474.2 [M–2PF<sub>6</sub>]<sup>2+</sup>.

**6.2.2. Copper(II) macrocycle, 14.** Procedure outlined above using receptor **10** (0.12 g, 0.1 mmol) and 1 equiv of copper(II) acetate monohydrate. Brown solid (0.077 g, 62%).

NMR broad, paramagnetic.

Elemental analysis: found: C 38.3%, H 3.4%, N 8.6%.

Calculated (C<sub>42</sub>H<sub>42</sub>N<sub>8</sub>RuS<sub>4</sub>CuP<sub>2</sub>F<sub>12</sub>·2H<sub>2</sub>O): C 39.6%, H 3.4%, N 8.8%.

ESMS: *m/z* 476.5 [M–2PF<sub>6</sub>]<sup>2+</sup>.

**6.2.3. Zinc(II) macrocycle, 15.** Procedure outlined above using receptor **10** (0.12 g, 0.1 mmol) and 1 equiv of zinc(II) acetate dihydrate. Red/brown solid (0.09 g, 72%).

<sup>1</sup>H NMR in CD<sub>3</sub>CN (δ/ppm): 0.85 (br m, 6H, CH<sub>3</sub>), 1.25 (m, 4H, CH<sub>2</sub>CH<sub>3</sub>), 1.65 (br m, 4H, <sup>3</sup>J=7.5 Hz, CH<sub>2</sub>CH<sub>2</sub>CH<sub>3</sub>), 3.97 (m, 4H, <sup>3</sup>J=6.3 Hz, NCH<sub>2</sub>CH<sub>2</sub>), 5.69 (dd, 4H, <sup>3</sup>J=6.3 Hz, <sup>4</sup>J=1.5 Hz, bpyCH<sub>2</sub>N), 7.31 (d, 2H, <sup>3</sup>J=4.2 Hz, bpy-H<sub>6,6'</sub>), 7.40 (m, 4H, <sup>3</sup>J=5.5 Hz, bpy-H<sub>e</sub>), 7.61 (t, 2H, <sup>3</sup>J=5.1 Hz, bpy-H<sub>f</sub>), 7.76 (dd, 4H, <sup>3</sup>J=20.0 Hz, <sup>4</sup>J=4.5 Hz, bpy-H<sub>5,5'</sub>), 8.05 (m, 4H, bpy-H<sub>d</sub>), 8.50 (d, 4H, <sup>3</sup>J=7.5 Hz, bpy-H<sub>c</sub>), 8.69 (s, 2H, bpy-H<sub>3,3'</sub>).

Elemental analysis: found: C 43.5%, H 3.9%, N 8.8%.

(C<sub>42</sub>H<sub>42</sub>N<sub>8</sub>RuS<sub>4</sub>ZnP<sub>2</sub>F<sub>12</sub>): C 42.0%, H 3.8%, N 8.5%.

ESMS: *m/z* 440.1 [M – CS<sub>2</sub> – 2PF<sub>6</sub>]<sup>2+</sup>, 478.0 [M – 2PF<sub>6</sub>]<sup>2+</sup>, 955.2 [M – 2PF<sub>6</sub>]<sup>+</sup>.

**6.2.4. Macrocycles, 16–21.** General procedure the same as for macrocycles **13–15**, but in a THF/H<sub>2</sub>O (9:1) mix.

**6.2.5. Nickel(II) macrocycle, 16.** Procedure given above, using ruthenium receptor **11** (0.08 g, 0.08 mmol) and 1 equiv of nickel(II) acetate tetrahydrate. The product was isolated as red/brown coloured solid (0.03 g, 62% yield).

<sup>1</sup>H NMR in DMSO-*d*<sub>6</sub> (δ/ppm): 0.90 (t, 6H, <sup>3</sup>*J* = 7.5 Hz, CH<sub>3</sub>), 1.29 (m, 4H, CH<sub>2</sub>CH<sub>3</sub>), 1.53 (m, 4H, CH<sub>2</sub>CH<sub>2</sub>CH<sub>3</sub>), 2.94 (br m, 4H, NHCH<sub>2</sub>CH<sub>2</sub>CH<sub>2</sub>CH<sub>3</sub>), 3.10 (br m, 4H, CH<sub>2</sub>NHCH<sub>2</sub>CH<sub>2</sub>CH<sub>2</sub>), 3.60 (m, 4H, CONHCH<sub>2</sub>), 7.74 (m, 4H, <sup>3</sup>*J* = 4.5 Hz, bpy-*H<sub>e</sub>*), 7.84 (d, 4H, <sup>3</sup>*J* = 4.5 Hz, bpy-*H<sub>f</sub>*), 7.84 (d, <sup>3</sup>*J* = 5.4 Hz, 2H, bpy *H5,5'*), 7.97 (d, 2H, <sup>3</sup>*J* = 5.4 Hz, bpy-*H6,6'*), 8.20 (m, 4H, <sup>3</sup>*J* = 6.3 Hz, bpy-*H<sub>d</sub>*), 8.86 (d, 4H, <sup>3</sup>*J* = 6.3 Hz, bpy *H<sub>c</sub>*), 9.15 (s, 2H, bpy-*H3,3'*), 9.25 (s, 2H, CONH).

Elemental analysis: found: C 40.4%, H 4.4%, N 9.8%.

Calculated (C<sub>46</sub>H<sub>50</sub>F<sub>12</sub>N<sub>10</sub>O<sub>2</sub>P<sub>2</sub>RuNi·H<sub>2</sub>O): C 40.3%, H 3.8%, N 10.2%.

ESMS: *m/z* 531.2 [M – 2PF<sub>6</sub>]<sup>2+</sup>, 1207.1 [M – PF<sub>6</sub>]<sup>+</sup>.

**6.2.6. Copper(II) macrocycle, 27.** Procedure given above, using ruthenium receptor **21** (0.2 g, 0.18 mmol) and 1 equiv of copper (II) acetate monohydrate. The product was isolated as brown solid (0.14 g, 59% yield).

NMR broad, paramagnetic.

Elemental analysis: found: C 38.2%, H 4.1%, N 9.3%.

Calculated (C<sub>46</sub>H<sub>50</sub>F<sub>12</sub>N<sub>10</sub>O<sub>2</sub>P<sub>2</sub>RuCu·3H<sub>2</sub>O): C 39.1%, H 4.0%, N 9.9%.

ESMS: *m/z* 533.6 [M – 2PF<sub>6</sub>]<sup>2+</sup>.

**6.2.7. Zinc(II) macrocycle, 18.** Procedure given above, using ruthenium receptor **11** (0.2 g, 0.18 mmol) and 1 equiv of zinc (II) acetate dihydrate. The product was isolated as red/brown coloured solid (0.13 g, 55% yield).

<sup>1</sup>H NMR in DMSO-*d*<sub>6</sub> (δ/ppm): 0.85 (t, 6H, <sup>3</sup>*J* = 7.5 Hz, CH<sub>3</sub>), 1.24 (m, 4H, CH<sub>2</sub>CH<sub>3</sub>), 1.65 (m, 4H, CH<sub>2</sub>CH<sub>2</sub>CH<sub>3</sub>), 3.70 (br m, 4H, NHCH<sub>2</sub>CH<sub>2</sub>CH<sub>2</sub>CH<sub>3</sub>), 3.79 (br m, 4H, CH<sub>2</sub>NHCH<sub>2</sub>CH<sub>2</sub>CH<sub>2</sub>), 3.97 (m, 4H, CONHCH<sub>2</sub>), 7.50 (br m, 4H, bpy-*H<sub>e</sub>*), 7.72 (d, 4H, <sup>3</sup>*J* = 4.5 Hz, bpy-*H<sub>f</sub>*), 7.82 (d, 2H, bpy *H5,5'*), 7.95 (d, 2H, <sup>3</sup>*J* = 5.7 Hz, bpy-*H6,6'*), 8.18 (m, 4H, <sup>3</sup>*J* = 7.5 Hz, bpy-*H<sub>d</sub>*), 8.84 (m, 4H, <sup>3</sup>*J* = 6.3 Hz, bpy *H<sub>c</sub>*), 9.12 (s, 2H, bpy-*H3,3'*), 9.32 (s, 2H, CONH).

Elemental analysis: found: C 39.7%, H 4.1%, N 9.3%.

Calculated (C<sub>46</sub>H<sub>50</sub>F<sub>12</sub>N<sub>10</sub>O<sub>2</sub>P<sub>2</sub>RuZn·<sup>3</sup>/<sub>2</sub>H<sub>2</sub>O): C 40.1%, H 3.8%, N 10.2%.

ESMS: *m/z* 535.2 [M – 2PF<sub>6</sub>]<sup>2+</sup>.

**6.2.8. Nickel(II) macrocycle, 19.** Procedure given above, using ruthenium receptor **12** (0.1 g, 0.07 mmol) and 1 equiv of nickel(II) acetate tetrahydrate. The product was isolated as red/brown coloured solid (0.095 g, 95% yield).

<sup>1</sup>H NMR in DMSO-*d*<sub>6</sub> (δ/ppm): 0.82 (t, 6H, <sup>3</sup>*J* = 7.5 Hz, CH<sub>3</sub>), 1.20 (m, 4H, CH<sub>2</sub>CH<sub>3</sub>), 1.49 (m, 4H, CH<sub>2</sub>CH<sub>2</sub>CH<sub>3</sub>), 3.29 (m, 4H, NBocCH<sub>2</sub>CH<sub>2</sub>), 4.77 (s, 4H, bpyCH<sub>2</sub>), 7.30 (d, 2H, bpy-*H5,5'*), 7.55 (br m, 2H, bpy-*H<sub>d</sub>*) 7.78 (m, 10H, Ar and bpy-*H<sub>c</sub>*), 7.97 (br m, 2H, bpy-*H6,6'*), 8.19 (br m, 2H, bpy-*H<sub>e</sub>*), 8.87 (br m, 2H, bpy-*H<sub>f</sub>*), 9.38 (br s, 2H, CONH).

Elemental analysis: found: C 44.0%, H 4.1%, N 9.4%.

Calculated (C<sub>56</sub>H<sub>54</sub>N<sub>10</sub>O<sub>2</sub>NiRuS<sub>4</sub>P<sub>2</sub>F<sub>12</sub>·3H<sub>2</sub>O): C 43.9%, H 4.0%, N 9.2%.

MALDI: *m/z* for PF<sub>6</sub> salt, 1186.2 [M – 2PF<sub>6</sub>]<sup>+</sup>, 1331.6 [M – PF<sub>6</sub>]<sup>+</sup>.

**6.2.9. Copper(II) macrocycle, 20.** Procedure given above, using ruthenium receptor **12** (0.1 g, 0.07 mmol) and 1 equiv of copper(II) acetate monohydrate. The product was isolated as brown solid (0.09 g, 91% yield).

NMR broad, paramagnetic.

Elemental analysis: found: C 43.7%, H 4.0%, N 8.8%.

Calculated (C<sub>56</sub>H<sub>54</sub>N<sub>10</sub>O<sub>2</sub>CuRuS<sub>4</sub>P<sub>2</sub>F<sub>12</sub>·3H<sub>2</sub>O): C 43.8%, H 3.9%, N 9.1%.

MALDI: *m/z* for PF<sub>6</sub> salt, 595.3 [M – 2PF<sub>6</sub>]<sup>2+</sup>, 1191.6 [M – 2PF<sub>6</sub>]<sup>+</sup>.

**6.2.10. Zinc(II) macrocycle, 21.** Procedure given above, using ruthenium receptor **12** (0.1 g, 0.07 mmol) and 1 equiv of zinc (II) acetate dihydrate. The product was isolated as red/brown coloured solid (0.058 g, 56%).

<sup>1</sup>H NMR in DMSO-*d*<sub>6</sub> (δ/ppm): 0.84 (t, 6H, CH<sub>3</sub>), 1.26 (m, 4H, CH<sub>2</sub>CH<sub>3</sub>), 1.66 (m, 4H, CH<sub>2</sub>CH<sub>2</sub>CH<sub>3</sub>), 3.29 (m, 4H, NHCH<sub>2</sub>CH<sub>2</sub>), 5.01 (s, 4H, bpyCH<sub>2</sub>), 7.33 (br m, 2H, bpy-*H5,5'*), 7.51 (br m, 2H, bpy-*H<sub>d</sub>*) 7.74 (m, 10H, Ar and bpy-*H<sub>c</sub>*), 7.89 (br m, 2H, bpy-*H6,6'*), 8.15 (m, 2H, bpy-*H<sub>e</sub>*), 8.83 (m, 2H, bpy-*H<sub>f</sub>*), 9.29 (br s, 2H, bpy-*H3,3'*), 10.75 (br s, 2H, NHCO).

Elemental analysis: found: C 43.6%, H 3.9%, N 9.0%.

Calculated (C<sub>56</sub>H<sub>54</sub>N<sub>10</sub>O<sub>2</sub>ZnRuS<sub>4</sub>P<sub>2</sub>F<sub>12</sub>·3H<sub>2</sub>O): C 43.7%, H 3.9%, N 9.1%.

MALDI: *m/z* for PF<sub>6</sub> salt, 607.2 [M – 2PF<sub>6</sub> + H<sub>2</sub>O]<sup>2+</sup>, 1193.4 [M – 2PF<sub>6</sub>]<sup>+</sup>.



## 7. Protocol for $^1\text{H}$ NMR titrations

A solution of the receptor (500  $\mu\text{l}$ ) was prepared at a concentration typically of the order of  $0.01 \text{ mol dm}^{-3}$  in deuterated dimethyl sulfoxide. The initial  $^1\text{H}$  NMR spectrum was recorded and aliquots of anion were added by gas-tight syringe from a solution made such that 1 mol equiv was added in 20  $\mu\text{l}$ . After each addition and mixing, the spectrum was recorded again and changes in the chemical shift of certain protons were noted. The result of the experiment was a plot of the displacement in chemical shift as a function of the amount of added anion, which was subjected to analysis by curve-fitting since the shape is indicative of the stability constant for the complex. The computer program EQMNR<sup>9</sup> was used which requires the concentration of each component and the observed chemical shift (or its displacement) for each data point. Typically these titrations experiments were repeated three times with at least fifteen data points in each experiment.

## Acknowledgements

We thank EPSRC for a studentship (MDP).

## References and notes

- (a) Beer, P. D.; Gale, P. A. *Angew. Chem. Int., Ed. Engl.* **2001**, *40*(3), 486. (b) Gale, P. A. *Coord. Chem. Rev.* **2003**, *240*, 191. (c) Schmidtchen, P.; Berger, M. *Chem. Rev.* **1997**, *97*, 1609. (d) Beer, P. D.; Smith, D. K. *Prog. Inorg. Chem.* **1997**, *46*, 1. (e) Atwood, J. L.; Holman, K. T.; Steed, J. W. *Chem. Commun.* **1996**, 1401. (f) *Supramolecular Chemistry of Anions*; Bianchi, A., Bowman-James, K., García-España, E., Eds.; Wiley-VCH: New York, 1997.
- (a) Beer, P. D. *Acc. Chem. Res.* **1998**, *31*, 71. (b) de Silva, A. P.; Guarantee, H. Q. N.; Gunnlaugsson, T.; Huxley, A. J.; McCoy, C. P.; Rademacher, J. T.; Rice, T. R. *Chem. Rev.* **1997**, *97*, 1515.
- (a) Beer, P. D. *Chem. Commun.* **1996**, 689. (b) Beer, P. D.; Cadman, J. *New J. Chem.* **1999**, *23*, 347. (c) Beer, P. D.; Hayes, E. J. *Coord. Chem. Rev.* **2003**, *240*, 167.
- (a) Saalfrank, R. W.; Bernt, I. *Curr. Opin. Solid State Mater. Sci.* **1998**, *3*, 407. (b) Fujita, M. *Chem. Soc. Rev.* **1998**, *27*, 417. (c) Leininger, S.; Olenyuk, B.; Stang, P. J. *Chem. Rev.* **2000**, *100*, 853.
- Fox, O. D.; Drew, M. G. B.; Beer, P. D. *Angew. Chem. Int., Ed. Engl.* **2000**, *39*, 136.
- Padilla-Tosta, M. E.; Fox, O. D.; Drew, M. G. B.; Beer, P. D. *Angew. Chem. Int., Ed. Engl.* **2001**, *40*, 4235.
- (a) Beer, P. D.; Berry, N.; Drew, M. G. B.; Fox, O. D.; Padilla-Tosta, M. E.; Patell, S. *Chem. Commun.* **2001**, 199. (b) Berry, N. G.; Pratt, M. D.; Fox, O. D.; Beer, P. D. *Supramol. Chem.* **2001**, *13*, 677.
- (a) Beer, P. D.; Cheetham, A. G.; Drew, M. G. B.; Fox, O. D.; Hayes, E. J.; Rolls, T. D. *Dalton Trans.* **2003**, *4*, 603. (b) Beer, P. D.; Berry, N. G.; Cowley, A. R.; Hayes, E. J.; Oates, E. C.; Wong, W. W. H. *Chem. Commun.* **2003**, *19*, 2408.
- Hynes, M. J. *J. Chem. Soc. Dalton Trans.* **1993**, 311–312.
- Binstead, R.A.; Zuberbühler, A.D. Specfit Global Analysis, version 2.90X; Binstead, R.A. Specfit, 32, 2000.
- Beer, P. D.; Szemes, F.; Balzani, V.; Sala, C. M.; Drew, M. G. B.; Dent, S. W.; Maestri, M. *J. Am. Chem. Soc.* **1997**, *119*(49), 11864.
- Wilson, R. DPhil Thesis, Oxford University; 1999.
- (a) Mayer, U.; Gutmann, V.; Gerger, W. *Monatsch. Chem.* **1975**, *106*, 1235. (b) Mayer, U. *Coord. Chem.* **1976**, *21*, 159.
- Bond, A. M.; Martin, R. L. *Coord. Chem. Rev.* **1984**, *54*, 23.
- Hendrickson, A. R.; Martin, R. L.; Rhode, N. M. *Inorg. Chem.* **1976**, *15*, 2115.
- Hendrickson, A. R.; Martin, R. L.; Rhode, N. M. *Inorg. Chem.* **1975**, *14*, 2980.
- Szemes, F.; Heseck, D.; Chen, Z.; Dent, S. W.; Drew, M. G. B.; Goulden, A. J.; Groydon, A. R.; Grieve, A.; Mortimer, R. J.; Wear, T.; Weightman, J. S.; Beer, P. D. *Inorg. Chem.* **1996**, *35*, 5868.
- Procedure adapted from Dupau, P.; Renouard, T.; Le Bozec, H. *Tetrahedron Lett.* **1996**, *37*, 7503.
- Garelli, N.; Vierling, P. *J. Org. Chem.* **1992**, *57*, 3042.
- Whittle, C. P. *J. Heterocycl. Chem.* **1997**, *14*, 191.

# Highly selective fluorescent chemosensors for cadmium in water

Thorfinnur Gunnlaugsson,<sup>a,\*</sup> T. Clive Lee<sup>b</sup> and Raman Parkesh<sup>a</sup>

<sup>a</sup>Department of Chemistry, Trinity College Dublin, Dublin 2, Ireland

<sup>b</sup>Department of Anatomy, Royal College of Surgeons in Ireland, St. Stephen's Green, Dublin 2, Ireland

Received 1 February 2004; revised 5 August 2004; accepted 19 August 2004

Available online 1 October 2004

**Abstract**—The design, synthesis and photophysical evaluation of two new chemosensors **1** and **2** is described for the selective detection of Cd(II) in water at pH 7.4. Both are based on the use of aromatic iminodiacetate receptors that connected to an anthracene fluorophore by covalent methyl spacers. These are highly water-soluble sensors where the fluorescence is ‘switched off’ between pH 3–11, due to photoinduced electron transfer (PET) quenching of the anthracene excited state by the receptor. Upon protonation of the receptor, the emission was however, ‘switched on’. From these changes pK<sub>a</sub>s of 1.8 and 2.5 were determined for **1** and **2** respectively. Both showed good selectivity for Cd(II) over competitive ions such as group II and Zn(II), Cu(II), Co(II). For **1**, having a single receptor, only a weak monomer anthracene emission was observed for the free sensor at pH 7.4 (HEPES buffer, 135 mM NaCl). Upon Zn(II) titration, a broad red shifted emission occurred, centred at 468 nm. In the presence of Cd(II), a similar red shifted emission was also observed, however, this time centred at 506 nm. In contrast to these results, the fluorescence of **2** in the presence of Zn(II) gave rise to typical monomeric anthracene emission, due to suppression of PET, that is, the anthracene emission was ‘switched on’. Nevertheless, in the presence of Cd(II) a broad emission centred at 500 nm was observed, similar to that seen for **1**. These ion induced long wavelength emission bands were assigned to the formation of charge-transfer complexes (exciplexes) between the anthracene moieties and the ion-receptor complexes. Importantly, for both **1** and **2**, a selective detection of Cd(II) was possible, even in the presence of Zn(II).

© 2004 Elsevier Ltd. All rights reserved.

## 1. Introduction

The development of luminescent sensors lies at the heart of supramolecular chemistry.<sup>1</sup> Several research groups have recently reviewed work in this area.<sup>1–3</sup> We have developed various types of luminescent devices, some of which have been developed as sensors for ions and molecules. These include fluorescent<sup>4</sup> and colorimetric<sup>5</sup> sensors as well as lanthanide luminescent<sup>6</sup> chemosensors for cations such as Li<sup>+</sup>, Na<sup>+</sup>, K<sup>+</sup>, Cu(II) and Zn(II) and anions such as F<sup>−</sup>, AcO<sup>−</sup>, H<sub>2</sub>PO<sub>4</sub><sup>−</sup>, pyrophosphate, carboxylates, and aromatic carboxylates such as salicylic acid. The main driving force for this work has been the increased use of chemosensors for medical diagnostics,<sup>7</sup> and in particular for critical care analysis.<sup>8</sup> During the course of our research we initiated an investigation into developing luminescent sensors for metal ions such as Cd(II), but only a few examples of sensors for Cd(II) have been reported.<sup>9</sup> Furthermore, those reported to date for Cd(II) detection suffer from several drawbacks such as low aqueous solubility, poor sensitivity and selectivity, as well as unsuitability for use in the physiological pH range. The need for developing ideal chemosensors for Cd(II), that

satisfy the aforementioned criteria is thus currently of great importance. In this paper we describe the design, synthesis and the photophysical evaluation of two novel fluorescent sensors, **1** and **2** for the selective sensing of Cd(II) under physiological pH conditions.<sup>10</sup>

Cadmium, an ion that poses an increasing environmental and health risk, has a naturally low abundance in nature (0.1–0.5 ppm).<sup>11</sup> However, cadmium levels as high as 500 ppm have recently been reported to accumulate in sedimentary rocks and marine phosphates and phosphorites.<sup>12</sup> One of the reasons for this is that Cd(II) is used in Ni–Cd batteries, as well as in fertilisers.<sup>13</sup> In the former, Cd(OH)<sub>2</sub> is used as one of the two principal electrode materials.<sup>14</sup> Even though Li<sup>+</sup> based batteries are now becoming more common, the disposal of unused Ni–Cd batteries is, and will be, a major environmental problem, particularly since cadmium has profound biological effects such as inducing renal dysfunction, reduced lung capacity and emphysema.<sup>15</sup> The tendency of this toxic ion to accumulate in organs such as the kidneys, hippocampus, thyroid and spleen, results in severe physiological effects.<sup>16</sup> Although only about 0.4% of the total amount of ingested cadmium is retained in the human body, recent studies indicate that high toxic levels of Cd(II) in the kidney and thyroid glands can occur, particularly in miners.<sup>17</sup>

**Keywords:** Chemosensors; Fluorescent; PET; Supramolecular chemistry.

\* Corresponding author. Tel.: +35316083459; fax: +35316712628; e-mail: [gunnlaut@tcd.ie](mailto:gunnlaut@tcd.ie)

Furthermore, it has recently been suggested that Cd(II) affects bone demineralisation by activating the osteoclast bone cells.<sup>18</sup> Moreover, cadmium is also thought to be a potential carcinogen.<sup>19</sup> All of these factors make the detection and quantification of Cd(II) a vital area of research. With this in mind we set out to develop the two chemosensors **1** and **2**. We designed these sensors on the fluorophore-spacer-receptor and the receptor-spacer-fluorophore-spacer-receptor models developed by de Silva et al. for PET sensors.<sup>20</sup> Here we give a full account of our effort.<sup>10</sup>

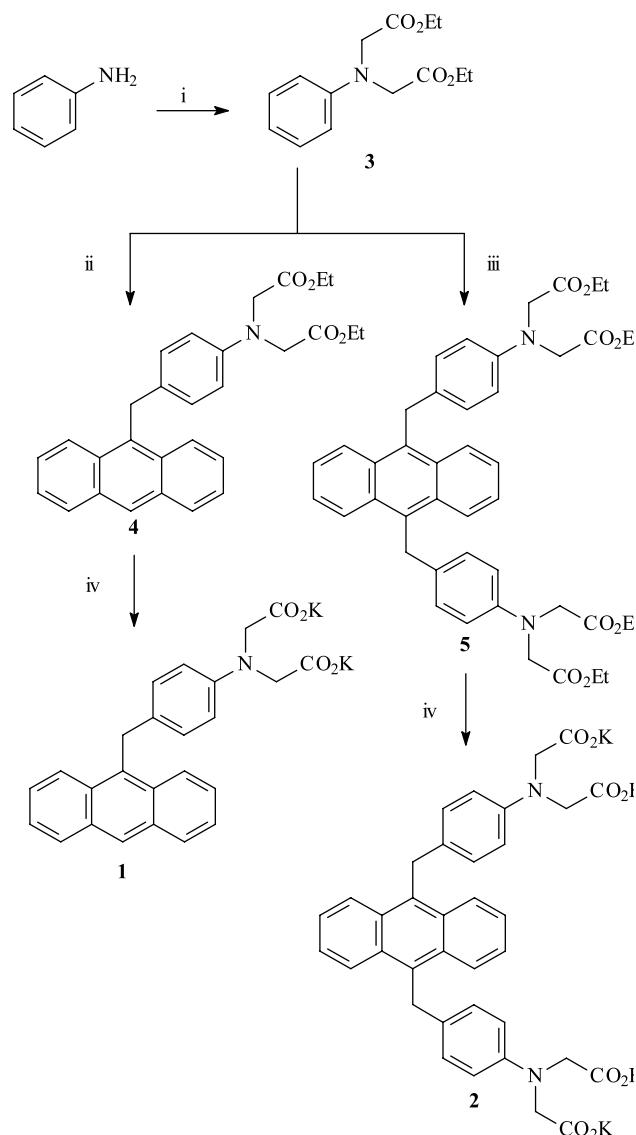
## 2. Results and discussion

### 2.1. Synthesis and characterisation of **1** and **2**

For the two chemosensors **1** and **2**, we selected anthracene as a fluorophore, and a simple aromatic iminodiacetate as the receptor. The reasons for this were twofold. First, the photophysical properties of anthracene in PET sensors is well established.<sup>3,20</sup> Secondly, the aniline based receptor could be used under physiological pH conditions as the nitrogen receptor moiety would only protonate under highly acidic conditions.<sup>21</sup> Moreover, this simple design would overcome any competitive binding of any other physiologically important cations such as Mg<sup>2+</sup> and Ca<sup>2+</sup>.<sup>21</sup> The use of potassium salts of the carboxylates would impart high water solubility to **1** and **2**. In the case of **2**, we predicted that the presence of two receptor units would statistically increase any PET rate quenching from the receptor to the excited singlet state of the anthracene, resulting in effective luminescent switching, where the emission would only be switched on in the presence of Cd(II).

The synthesis of **1** and **2** is shown in Scheme 1. It began with the synthesis of the iminodiester receptor **3**, by reacting aniline with ethyl bromoacetate, using potassium dihydrogen phosphate as a base in CH<sub>3</sub>CN in 89% yield. The two sensors were made in two steps from this intermediate. For **1**, this was achieved by Friedel–Crafts alkylation of **3** with 9-chloromethylanthracene (which was made in two steps from 9-anthraldehyde by reduction followed by chlorination). This alkylation was very successful, giving the desired product **4** in 70% yield using AlCl<sub>3</sub> in CH<sub>3</sub>CN, whereas using ZnBr<sub>2</sub> as catalyst resulted in a low yield of only 15%. The final product was purified using silica flash column chromatography using ethyl acetate:hexane (2:3) as eluant. In an analogous way, **2** was made by reacting 2 equiv of **3** with 9,10-bischloromethylanthracene (made by chloromethylation of anthracene in a single step),<sup>24</sup> yielding the tetraester **5**, in 72% yield, after purification by flash column chromatography using ethyl acetate:hexane (2:3) as eluant. The final products were obtained by alkaline ester hydrolysis of **4** and **5** using aqueous KOH in refluxing MeOH solution, yielding **1** and **2** in 92 and 90% yields respectively after precipitation from the cold solution.

The structures of **1**–**4** were confirmed by the usual spectroscopic methods (see the Section 4). In the <sup>1</sup>H NMR of **4**, a singlet at 8.4 ppm and two multiplets at 8.21–8.24 and 8.02–8.05 ppm, respectively were attributed to the anthracene protons, whereas two doublets at 6.98 and



**Scheme 1.** The synthesis of **1** and **2** from aniline. (i) CH<sub>3</sub>CN, KI, K<sub>2</sub>HPO<sub>4</sub>, BrCH<sub>2</sub>CO<sub>2</sub>Et, reflux; (ii) 9-chloromethylanthracene, AlCl<sub>3</sub>, CHCl<sub>3</sub>, reflux; (iii) 9,10-bischloromethylanthracene, KOH, H<sub>2</sub>O, MeOH, reflux.

6.47 ppm were observed for the phenyl protons. In comparison, the <sup>1</sup>H NMR of **1** showed two doublets for the phenyl protons at 6.20 and 6.82 ppm, respectively. The electrospray mass spectrum (ESMS) showed a peak at 476 mass units for M+H<sup>+</sup> (100%). In the <sup>1</sup>H NMR of **5**, the phenyl protons appeared as doublets at 6.50 and 7.01 ppm and a singlet was observed at 4.95 ppm for the two methyl spacers. The symmetrical nature of the molecule was further supported by the <sup>13</sup>C NMR in which only 13 carbon resonances were observed. Furthermore, the ESMS spectrum gave a peak at 733 mass units for M+H<sup>+</sup>. After alkaline hydrolysis of **5** the <sup>1</sup>H NMR spectrum of **2** (Fig. 1) showed two double–doublet resonances for the anthracene protons at 8.31–8.29 ppm and at 7.45–7.42 ppm whereas the phenyl protons were observed as two doublets at 6.91 and 6.28 ppm. The two methyl spacers appeared as a singlet at 4.86 ppm and the two methyl iminodiester spacers as a singlet at 4.86 ppm. The <sup>13</sup>C NMR gave, as expected, rise to only 11 resonances.

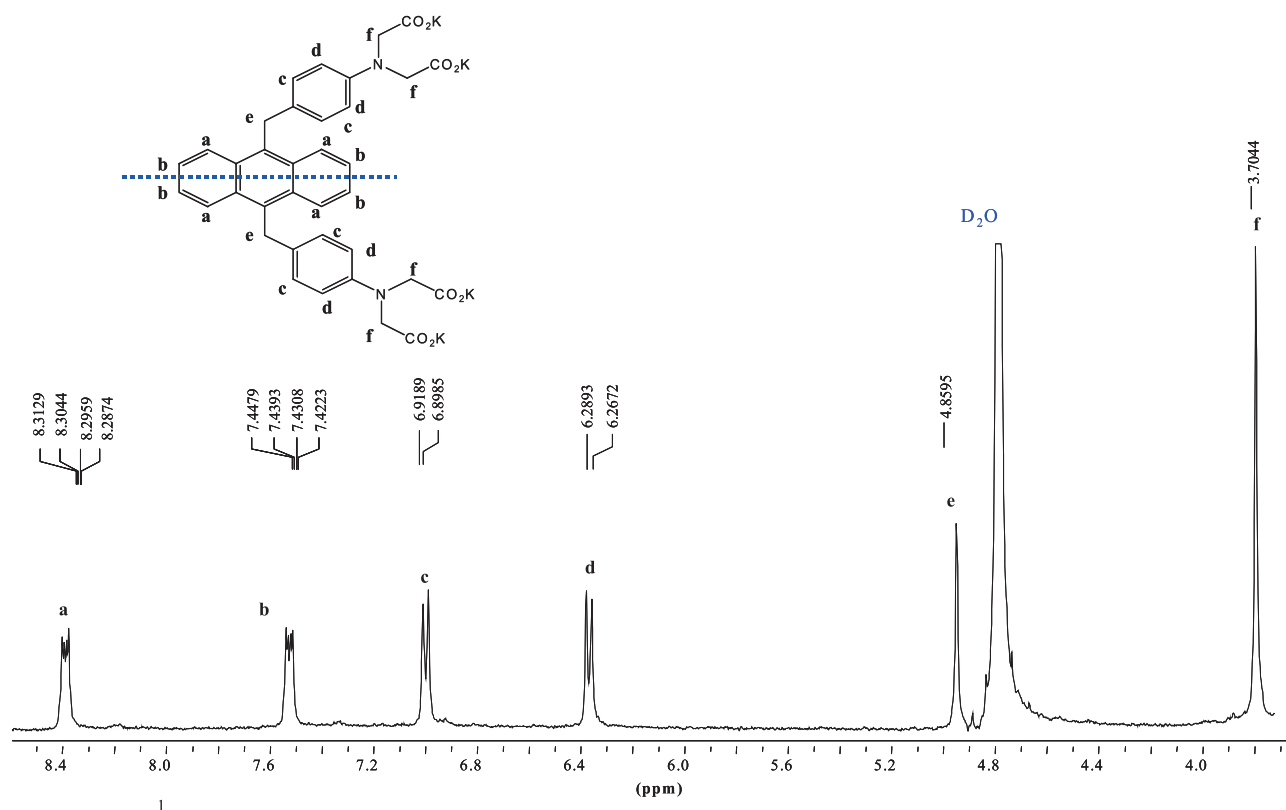


Figure 1. The  $^1\text{H}$  NMR of **2** ( $\text{D}_2\text{O}$ , 400 MHz). The appropriate resonances have been assigned as a–f.

## 2.2. Ground and excited state evaluation of **1** and **2**

The photophysical properties of the two chemosensors **1**, and **2** were evaluated in water and in pH 7.4 HEPES buffered solution in the presence of 0.135 M of NaCl to maintain constant ionic strength.

## 2.3. The effect of pH

We first evaluated the pH response of **1** and **2** in water. The absorption spectra of **1** exhibited five main absorption bands centred at 314, 337, 365, 385 and 402 nm ( $\epsilon = 17.1 \times 10^3 \text{ M}^{-1} \text{ cm}^{-1}$ ). The absorption spectra of **1** as a function of pH is shown in Figure 2. When an alkaline solution of **1** was titrated with acid, no absorption shifts were seen in the positions of the above mentioned bands. However, a small decrease in the absorption intensity (<5%) was observed. This was most likely due to the electronic effect observed between the anthracene fluorophore and positively charged aniline moiety upon protonation (through space). These small effects are well known and signify that no significant ground state interactions occur between the fluorophore and the receptor, due to the presence of the covalent spacer. The absorption spectra of **2** as a function of pH were recorded in a similar manner. The absorption spectra of **2** showed four absorption bands at 343, 362, 381 and 402 nm ( $\epsilon = 18.6 \times 10^3 \text{ M}^{-1} \text{ cm}^{-1}$ ) respectively. The absorption spectra generated during the pH titration showed only a negligible decrease in the intensity similar to that seen for **1** in Figure 2. This shows that under these conditions only minor ground state interactions take place between the receptors and the anthracene moiety, confirming the insulating role of the two methylene spacers.

In contrast to the above changes the fluorescence emission of **1** and **2** was substantially changed upon protonation of the amino moiety of the receptors ( $\lambda_{\text{ex}} = 381 \text{ nm}$ ). For **1** in basic solution (pH  $\sim 12$ ), the fluorescence was so minor that it can be said that the emission was switched off. This is due to PET quenching from the receptor to the excited state of the fluorophore. However, upon titration with acid, a gradual increase was observed for the anthracene emission, which had three characteristic bands centred at 392, 415 and 439 nm and a weak shoulder at 466 nm respectively. This fluorescence enhancement was approximately 60 fold. The increase in fluorescence is due to the protonation of the tertiary nitrogen atom of the receptor moiety, resulting in a decrease in the reduction potential of the receptor, which is typical PET behaviour. This prevents electron transfer from the receptor to the excited state of the anthracene, thus switching the emission on. Similar results were observed for **2** ( $\lambda_{\text{ex}} = 385 \text{ nm}$ ), as seen in Figure 3. In basic solution, the fluorescence of **2** was quenched, and in the pH range of pH = 3.5–12 virtually no emission was observed. However, at around pH 3.4, a broad band centered at 470 nm appeared with an increase in the emission intensity (Fig. 3, insert). Upon further acidification, between pH  $\sim 3.3$ –1.0, the normal anthracene emission with four main emission bands at 405, 428, 454 and 480 nm, respectively was observed with concomitant increase in the fluorescence intensity of ca. 600 fold.

We investigated these changes in some detail for **2**. Our studies revealed that from pH 12–3.5, the fluorescence of the anthracene moiety is efficiently quenched via a PET process from the receptors to the excited singlet state of the anthracene. However, as the pH is decreased protonation of

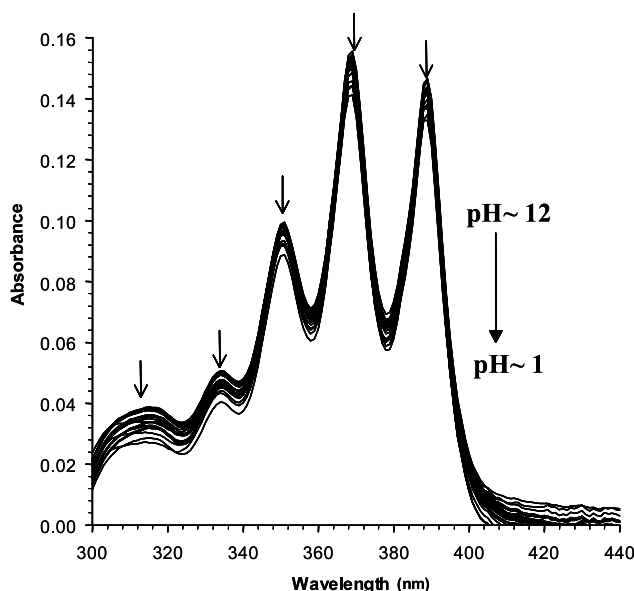


**Figure 2.** The changes in the absorption spectrum of **1** upon titration an alkaline solution of **1** with diluted acid.

the tertiary nitrogen of one receptor takes place, which causes a weak charge transfer (CT)<sup>23</sup> interaction between the protonated receptor and the anthracene fluorophore. This resulted in a charge transfer band at 470 nm. When the pH is decreased further, both receptors become protonated. These results in a repulsive interaction (RI), and to minimise it the receptors move as far apart as possible in space. Consequently, typical anthracene emission is observed in the pH range of 3.3–1. We were unable to determine more than one  $pK_a$  from the changes, Figure 4. The reason for this is most likely due to the fact that the changes in fluorescence emission correspond to the protonation of only one of the two receptors. Lippard et al. have reported similar observations in the case of fluorescein based sensors for Zn(II) ions, where the sensor also had two receptor moieties that could be protonated.<sup>22</sup>

Plotting the changes in the fluorescence emission as a function of pH resulted in a sigmoidal curve that changes over two pH units for both sensors. This pH dependent fluorescence behaviour is a typical ‘on-off’ PET sensor characteristic, indicating a simple acid-base equilibrium and one to one binding. The fluorescence intensity changes at 415 nm versus pH are shown for **2** in Figure 4. These, and the changes at any other wavelength, can be used to determine the  $pK_a$  of the protonation of the nitrogen moiety. Data fitting analysis of the emission intensity changes at 404, 428 and 454 nm respectively resulted in  $pK_a$  values of 2.4, 2.3 and 2.8 providing an average  $pK_a$  value of  $2.5 \pm 0.1$  for **2**. Similarly for **1**, the changes at 392, 415 and 439 nm gave  $pK_a$  values of 1.75, 1.74 and 2.0 ( $\pm 0.1$ ), providing an average  $pK_a$  of  $1.83 \pm 0.1$  for the protonation of the aniline receptor in **1**. This makes both **1** and **2** particularly attractive chemosensors for both physiological and environmental monitoring of Cd(II), for instance in highly acidic soils

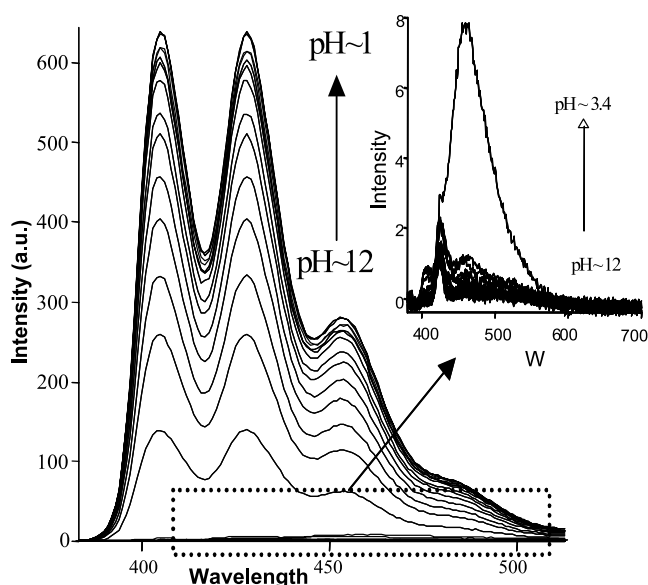


**Figure 3.** The changes in the fluorescence emission spectra of **2** upon acidification. Inserted are the changes observed between pH 3.4 and 12.

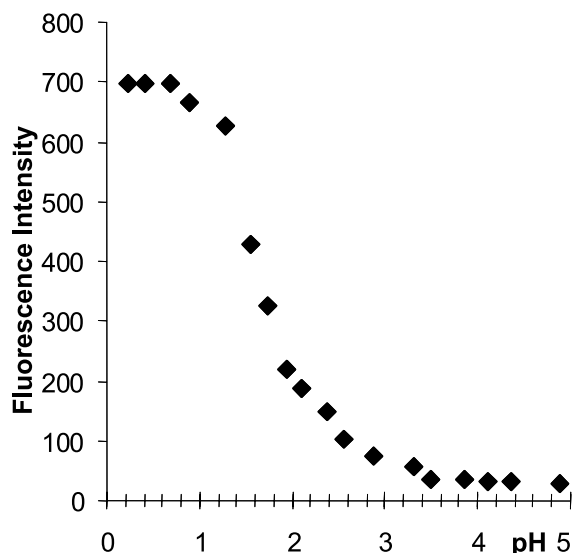


**Figure 4.** The plot of fluorescence intensity versus pH for **1** at 415 nm. Fitting of these data points using non-linear regression gave the  $pK_a$ .



where the pH 3–4 can be reached. Similarly, the pH titrations of the two esters **4** and **5** switched the fluorescence on for both of these molecules upon protonation of the aniline amine.

#### 2.4. The effect of group II and transition metal ions

The ability of **1** and **2** to recognise group II and various transition metal ions was investigated at pH 7.4 in buffered HEPES solution in the presence of 0.135 M of NaCl. We first evaluated the ability of **1** and **2** to recognise group II cations. The changes in the fluorescence emission spectra of **1** are shown in Figure 5 for titration with  $\text{Ca}^{2+}$ . As can be seen from this titration, the emission is very low in comparison to the changes seen in the pH titration (Fig. 3). The fluorescence is only minor and can be considered as being switched off (identical experimental settings were used for both measurements). Furthermore, no significant changes occurred upon titration of **1** with  $\text{Ca}^{2+}$ . In fact, even at high concentrations (0.01 M) of  $\text{Mg}^{2+}$  or  $\text{Ca}^{2+}$ , no significant spectral changes were observed in either the absorption or the fluorescence emission of the two sensors. This indicates that the receptors in these sensors were not coordinating significantly to these ions to prevent quenching by the receptors.<sup>21</sup>

We next evaluated the response of **1** and **2** towards various transition metal ions such as Co(II), Ni(II), Cu(II), Zn(II), Cd(II) and Hg(II) (as their  $\text{Cl}^-$ ,  $\text{NO}_3^-$  or  $\text{ClO}_4^-$  salts). Of these, only Zn(II) and Cd(II) gave rise to any significant changes in the fluorescence emission spectra and the absorption spectra. For **1**, the changes in the fluorescence spectra ( $\lambda_{\text{ex}}=370$  nm) upon titration with Zn(II) are shown in Figure 6. We foresaw that the coordination of the receptor (via the nitrogen lone pair and the two carboxylates) would, in a similar way to the protonation of the amino moiety, increase the oxidation potential of the receptor and prevent PET quenching. However, as can be seen from Figure 6, the monomeric anthracene emission was not switched on in an analogous way as previously shown for the pH titration in

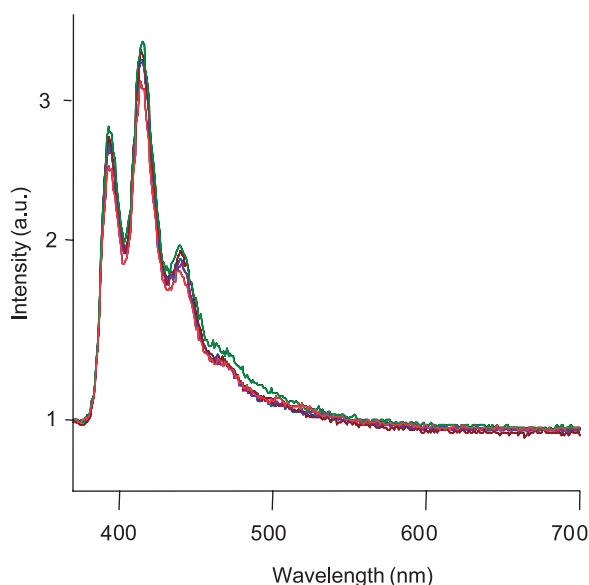


**Figure 5.** The changes in the fluorescence emission of **1** at pH 7.4, in 0.135 M NaCl, upon titration with  $\text{Ca}^{2+}$ ,  $[\text{Ca}^{2+}] = 0 \rightarrow 0.01$  M.

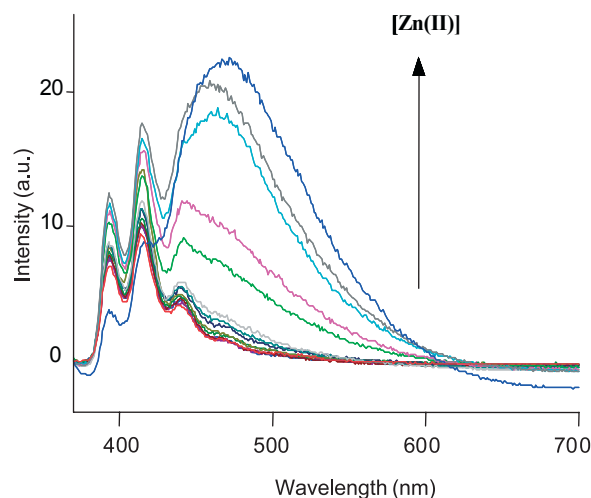


**Figure 6.** The changes in the fluorescence emission spectra of **1** upon titration with Zn(II).

Figure 3. Here, however, the monomeric anthracene emission was only slightly enhanced upon ion recognition, with the concomitant formation of a new red shifted broad emission band centred at 468 nm. Unlike that seen for the protonation previously, the fluorescent enhancement was much smaller for these changes. The affiliated changes in the absorption spectra were also interesting, as at low and medium concentration of Zn(II) the classical anthracene absorption bands were observed at 335, 350, 365 and 389 nm. Furthermore, these were only slightly reduced in intensity upon Zn(II) titration. Hence the classical PET behaviour was observed. However, at higher Zn(II) concentrations ( $\sim 2$  mM) dramatic shifts ( $\Delta\lambda=14$  nm) were observed in the absorption bands, which now became centred at 360, 376 and 404 nm, respectively. In conjunction with the changes in the fluorescence emission spectra (Fig. 6), one can deduce that these changes are due the formation of an intramolecular charge-transfer complex<sup>23</sup> (intramolecular exciplex) between the cation-bound acceptor and anthracene donor (see later) (Fig. 7).<sup>24</sup>

In comparison to these results we carried out an identical titration using **2**. The changes in the absorption spectra of **2** at low and high concentrations of Zn(II) are shown in Figure 8. Here it is clear that no major changes took place upon titration of **2** with Zn(II), with the three absorption bands being shifted by only 2–3 nm. Hence, one can conclude that in comparison to **1**, there are no major ground state interactions occurring between the fluorophore and the receptor. The corresponding changes in the fluorescence emission spectra are shown in Figure 9. They clearly demonstrate that the monomeric emission of the anthracene fluorophore is switched on, similar to that seen earlier for the pH titration. This indicates that the Zn(II) ion was able to coordinate to the carboxylates, as well as the aniline nitrogen and hence increase the oxidation potential of the receptors in a usual PET fashion. For these changes a fluorescence enhancement factor of several hundreds was observed. Most importantly, the Zn(II) recognition does not lead to any charge transfer interactions as seen previously for **1**. Hence, **2** is behaving as a typical PET sensor for Zn(II). A likely reason for this difference could be that the

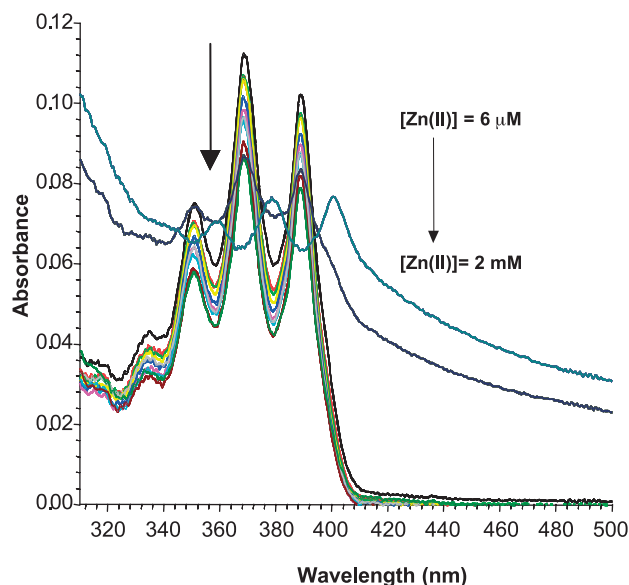


**Figure 7.** The changes in the absorption spectra of **1** upon titration with Zn(II).

Zn(II) binding forces the receptor to further away from the anthracene fluorophore possibly due to steric effects. However, we have not been able to obtain reliable experimental proof for this.

We were able to evaluate the affinity of both **1** and **2** for Zn(II) by plotting the relative intensity changes at 468 and 415 nm for **1** and **2** respectively, as a function of pZn ( $\text{pZn} = -\log [\text{Zn(II)}]$ ). For both, a sigmoidal curve was observed, which switched on over two logarithmic units between  $\text{pZn} \sim 5-3$ . This can be seen in Figure 10 for **2**. Hence, these binding interactions can be determined to be due to 1:1 binding between the two receptors of **2**, and Zn(II). This was indeed confirmed by using the Job plot method. From these changes a binding constant  $\log \beta$  of  $3.8 (\pm 0.1)$  was determined. Similarly, for **1**, a  $\log \beta$  of  $3.8 (\pm 0.1)$  was determined. Hence, both sensors have the same

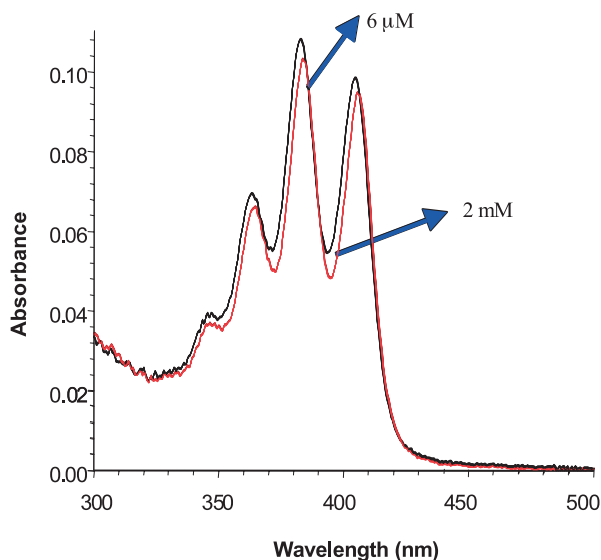


**Figure 8.** The changes in the absorption spectra of **2** at low and high concentration of Zn(II).

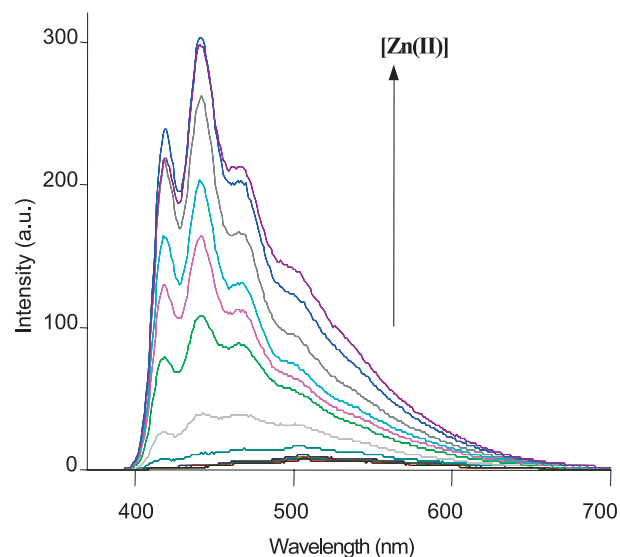


**Figure 9.** The changes in the fluorescence emission spectra of **2** upon titration with Zn(II).

affinity for Zn(II). We were unable to obtain a reliable binding constant from the absorption spectrum of **1**, as these changes were too small to give accurate binding.

In a similar manner we evaluated the affinity of **1** and **2** for Cd(II). The absorption response of **1** to Cd(II) was quite similar to that observed in the Zn(II) titration. Here, three anthracene absorption bands were observed at 350, 365 and 389 nm, and a small decrease in the absorption intensity was observed upon addition of Cd(II). However, at higher concentrations of Cd(II), the absorption spectra was gradually shifted to longer wavelengths with absorption maxima at 360, 376 and 406 nm, with the formation of isosbestic points at 370, 382 and 395 nm, respectively. As explained earlier, these latter changes are probably due to the charge transfer interaction occurring between the anthracene and receptor-Cd(II) complex. From these changes we were able to determine  $\log \beta$  of  $4.0 (\pm 0.1)$ .

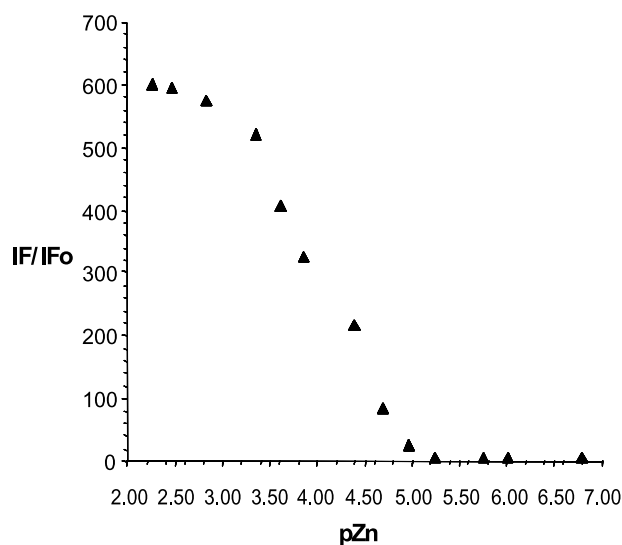


**Figure 10.** The relative changes in the fluorescence emission of **2** at 415 nm as a function of pZn.

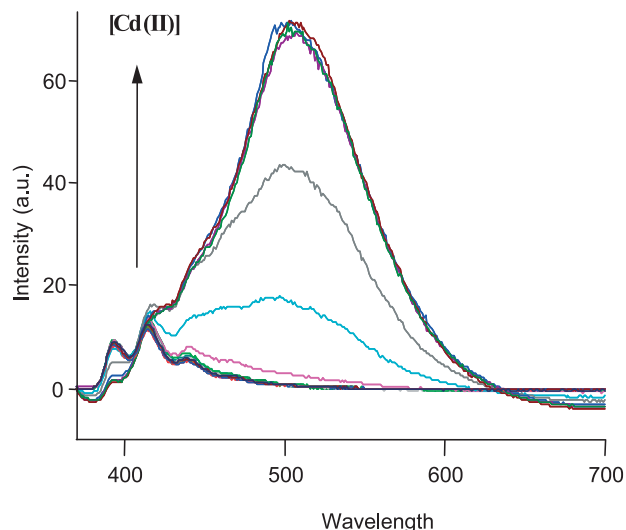


**Figure 11.** The changes in the fluorescence emission spectra of **1** upon titration with Cd(II).

The corresponding fluorescence emission changes for **1** can be seen in Figure 11. From these changes it is evident that the fluorescence emission is shifted to the red upon Cd(II) recognition, and that the monomeric emission is reduced. Furthermore, in contrast to the changes seen for the Zn(II) titration the emission is substantially more shifted, now centred at 506 nm. Moreover, the fluorescence enhancements are substantially greater than seen for the Zn(II) titration. Again, we suggest that these changes are due to the formation of a charge transfer complex between the anthracene moiety and the bound receptors, in a similar manner to that seen for the Zn(II) titration. As previously demonstrated it was possible to evaluate the binding affinity of **1** towards Cd(II), by plotting the changes at 506 nm as a function of pCd which gave rise to a sigmoidal curve that changed over two pCd units. Fitting these fluorescence

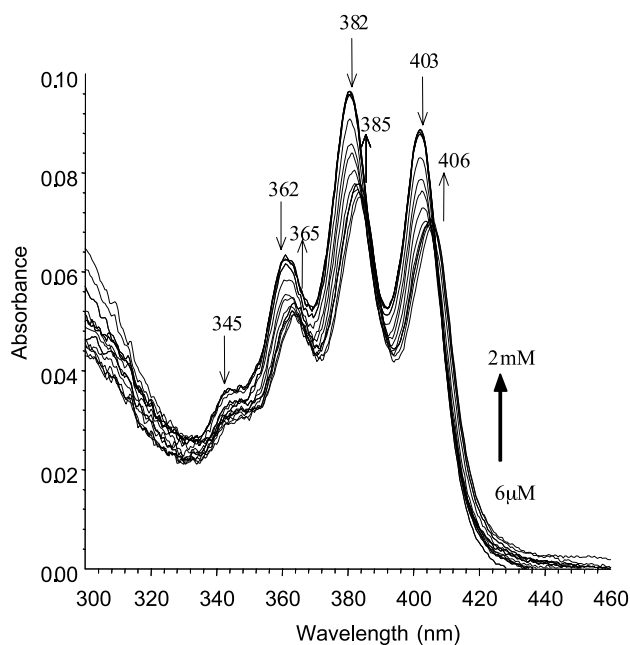


**Figure 12.** The changes in the UV-Vis spectra of **2**, upon titration with Cd(II).

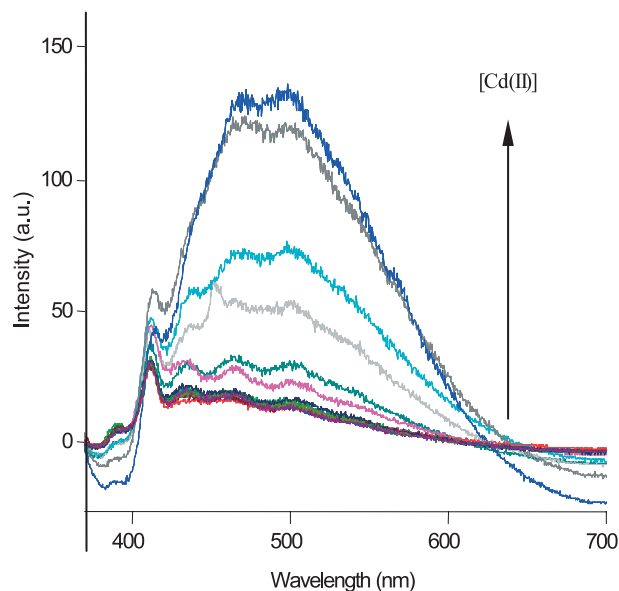


**Figure 13.** The changes in the fluorescence emission of **2** upon titration with Cd(II).

changes gave a  $\log \beta$  of  $4.2 (\pm 0.1)$ , indicating that selective detection of Cd(II) over Zn(II) should be feasible. Same results were observed when exciting at the isosbestic point.

The fluorescence response of **2** towards Cd(II) was similar to that observed for **1**. However, the absorption spectra were somewhat different to that seen for the Zn(II) titration, as seen in Figure 12. Here the recognition of the ion caused a red shift of ca. 3 nm, with clear isosbestic points being observed at 385 and 405 nm, respectively. From these changes, we were able to determine a binding constant  $\log \beta$  of  $4.1 (\pm 0.2)$ . In contrast to these results the fluorescence emission was red shifted, as shown in Figure 13, with the formation of a broad structure less red shifted band, centred at ca. 500 nm. As explained before, we believe that this is due to the anthracene-Cd(II) charge transfer interaction, in a similar manner to that seen for **1**. The same trends and spectral changes were observed upon excitation at the isosbestic points.

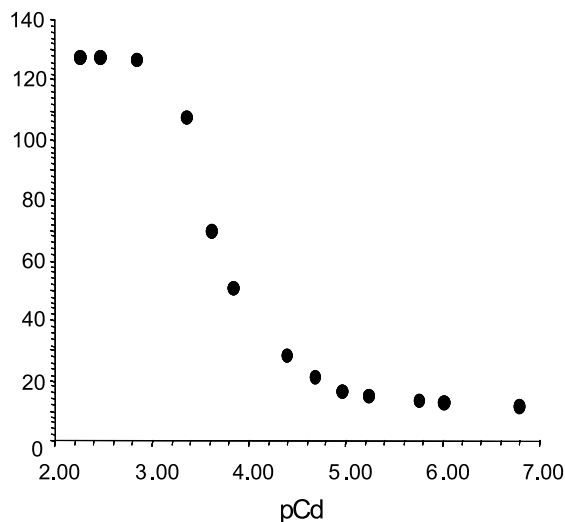


**Figure 14.** The changes in the fluorescence at 500 nm as a function of pCd.

A plot of fluorescence changes at 500 nm for **2** against pCd(II) resulted in a sigmoidal curve with two logarithmic unit changes, indicating a simple 1:1 equilibrium, Figure 14. From these changes a binding constant  $\log \beta$  of  $3.9 (\pm 0.1)$  was determined. These results demonstrate that both **1** and **2** can be considered as fluorescence chemosensors for Cd(II), as both have a marginally better selectivity for Cd(II) over that of Zn(II). The binding results are summarised in Table 1.

**Table 1**

Parameters	1	2
pK <sub>a</sub>	1.83 ( $\pm 0.1$ )	2.5 ( $\pm 0.1$ )
Log $\beta$ Zn(II) <sub>abs</sub>	—	—
Log $\beta$ Zn(II) <sub>nu</sub>	3.8 ( $\pm 0.1$ )	3.8 ( $\pm 0.1$ )
Log $\beta$ Cd(II) <sub>abs</sub>	4.0 ( $\pm 0.1$ )	4.1 ( $\pm 0.1$ )
Log $\beta$ Cd(II) <sub>nu</sub>	4.2 ( $\pm 0.1$ )	3.9 ( $\pm 0.1$ )

In summary, we have demonstrated efficient fluorescent sensing of Cd(II). For **1**, the sensing of both Zn(II) and Cd(II) gives rise to red shifts in the fluorescence spectra, with relatively little changes in the monomeric emission. However, there is a significant difference between these red shifts, for example, 468 versus 506 nm for Zn(II) and Cd(II) respectively. However, the largest contrast is seen for **2**, where the Zn(II) gives rise to large enhancements in the monomeric anthracene emission, but Cd(II) gives rise to the formation of the charge transfer band at long wavelengths. Consequently, **2** is a particularly attractive chemosensor for Cd(II) as it gives rise to a very different spectral response to different competitive ions. Furthermore, this difference was clearly visible under UV-light ( $\lambda_{\text{ex}} = 366$  nm) as at pH 7.4 the emission is switched off, whereas in the presence of Zn(II) and Cd(II) the sensors emits in the blue and green part of the electronic spectrum respectively. When these titrations were repeated using the two esters **4** and **5**, no fluorescence enhancement, or red shift emission was observed, indicating that these molecules were unable to coordinate to these ions. But what gives rise the large red shifted emission upon ion recognition? As we have indicated previously we believe that these are due to charge-transfer interactions between the metal bound receptor and the anthracene moiety. Similar results have recently been reported by Yoon et al.<sup>9c</sup> and Czarnik et al.<sup>9h</sup> utilising the anthracene fluorophore and aliphatic Cd(II) based receptors. Both researchers suggested that their anthracene–Cd(II) interactions were initially due to  $\pi$ -complex formation, which then gave rise to the formation of a  $\sigma$ -complex. However, for both of these examples the fluorescence emission was centred on 446 nm. This is a significantly smaller red shift than observed for either **1** and **2** upon recognition of Cd(II). Although, we do not predict that such  $\sigma$ -complex interaction can occur for either **1** or **2**, solely due to steric effects, as we, unlike Yoon et al. and Czarnik et al.<sup>9h</sup> use aromatic based receptors, the formation of the long emitting emission bands for both **1** and **2** strongly suggest the formation of  $\pi$ -complex interactions. Moreover, as the concentration of the sensor used in the titration studies is very low (1  $\mu$ M), intermolecular exciplex, excimer and mixed excimer formation can be effectively ruled out. To the best of our knowledge, **1** and **2** are the first examples of highly

selective fluorescent chemosensors for Cd(II), that can operate under physiological pH conditions.

## 2.5. Competitive Cd(II) measurements of **1** and **2**

To confirm the selectivity of **2** towards Cd(II) over Zn(II), we performed a Cd(II) titration in the presence of excess Zn(II). These results are summarised in Figure 15. A 1  $\mu$ M solution of **2** was prepared in HEPES buffer at pH 7.4. Under this condition the emission can be said to be switched off. This solution was adjusted to contain 3 mM of Zn(II), which caused normal fluorescence emission to be switched on. This Zn(II)-**2** solution was then titrated with Cd(II) in the same manner as described above. As predicted the addition of Cd(II) induced a shift to longer wavelength with the appearance of a new broad band at 500 nm, demonstrating that **2** is capable of selectively signalling the presence of Cd(II) over Zn(II). Similar effects were seen for **1**, where the emission further red shifted upon addition of Cd(II) to a solution of Zn(II). These results clearly show the high selectivity that these sensors have for Cd(II), even in the presence of highly competitive ions such as Zn(II). Its possible that as the binding constants for the two ions is so similar that this selectivity is due to the formation of a more kinetically stable complex in the case of Cd(II).

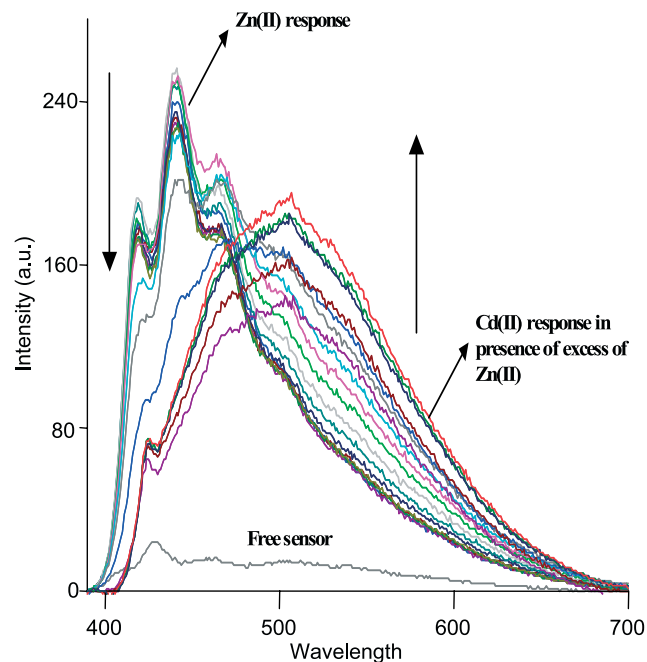


**Figure 15.** The titration of **2** with Cd(II) ([Cd(II)] 6 mM  $\rightarrow$  2.0 mM) in the presence of 2.0 mM of Zn(II) at pH 7.4.

## 3. Conclusion

Herein we have presented the results of two novel anthracene based fluorescent chemosensors **1** and **2** for the selective recognition of Cd(II). These were designed on the PET principle, using an anthracene fluorophore, connected to either one or two iminodiacetate receptors via a methylene spacer. These sensors were easily synthesized in two steps from the receptor **3** in a good yield.

The sensors exhibited high pH stability and aqueous solubility, where the fluorescence was switched off above pH ~3, enabling the use of these sensors in competitive pH media such as in physiological pH. The evaluation of the ground and excited state responses of these sensors demonstrated their capability to detect Zn(II) and Cd(II) and to discriminate these ions from group 2 and other transition metal ions. Whereas the recognition of Cd(II) at pH 7.4, gave rise to the formation of charge transfer complexes ( $\sigma$ -complexes) for both sensors ( $\lambda_{\max}$  ca. 506 and 500 nm for **1** and **2** respectively), the recognition of Zn(II) only switched on the (monomeric) anthracene emission of **2**, while for **1** it was red shifted ( $\lambda_{\max}$  = 468 nm). A discrimination test performed to evaluate the selectivity for Cd(II) in the presence of Zn(II) proved very successful, as the monomeric anthracene emission was red shifted upon detection of Cd(II). These results strongly support the possible application of these chemosensors as Cd(II) sensors in physiological samples. This is particularly the case for **2** which exhibits the unique feature of emitting in the blue upon detection of Zn(II), whereas upon the detection of Cd(II) it emits in the green. In this context further evaluation of **2** is required to determine the degree of toxicity, cell permeability and real time response. To the best of our knowledge these are the first examples of such highly selective Cd(II) fluorescent chemosensors.

## 4. Experimental

### 4.1. General

Starting materials were obtained from Sigma Aldrich, Strem Chemicals and Fluka. Columns were run using silica gel 60 (230–400 mesh ASTM) or aluminum oxide (activated, Neutral, Brockmann I STD grade 150 mesh). Solvents were used at GPR grade unless otherwise stated. Infrared spectra were recorded on a Mattson Genesis II FTIR spectrophotometer equipped with a Gateway 2000 4DX2-66 workstation. Oils were analysed using NaCl plates, solid samples were dispersed in KBr and recorded as clear pressed discs.  $^1\text{H}$  NMR spectra were recorded at 400 MHz using a Bruker Spectrospin DPX-400 instrument. Tetramethylsilane (TMS) was used as an internal reference standard, with chemical shifts expressed in parts per million (ppm or  $\delta$ ) downfield from the standard.  $^{13}\text{C}$  NMR were recorded at 100 MHz using a Bruker Spectrospin DPX-400 instrument. Mass spectroscopy was carried out using HPLC grade solvents. Mass spectra were determined by detection using Electrospray on a Micromass LCT spectrometer, using a Shimadzu HPLC or Water's 9360 to pump solvent. The whole system was controlled by MassLynx 3.5 on a Compaq Deskpro workstation.

**4.1.1. [(4-Anthracen-9-ylmethyl-phenyl)-ethoxycarbonyl-methyl-amino]-acetic acid ethyl ester (4).** 9-Chloromethylantracene (1.5 g, 6.64 mmol) and phenyliminodiacetic acid diethyl ester (**3**) (1.76 g, 6.64 mmol) and  $\text{AlCl}_3$  (0.91 g, 6.64 mmol) were dissolved in dry  $\text{CHCl}_3$  (50 mL) at  $-5^\circ\text{C}$ . The solution was refluxed overnight. After the reaction was complete (monitoring by TLC) the solution was cooled and washed with three 100 mL portions of water. The organic portion was dried over  $\text{MgSO}_4$ . After

evaporation of the solvent, crude product was subjected to column chromatography using ethyl acetate/hexane (2:3) as eluant to yield pure **4** (1.89 g, 70%) as light yellow thick liquid. Mp = 140–142  $^\circ\text{C}$ . MS ( $\text{ES}^+$ )  $m/z$  = 456 ( $\text{MH}^+$ ). Anal. Calcd for  $\text{C}_{29}\text{H}_{29}\text{NO}_4$ : C, 76.46; H, 6.42; N, 3.07. Found: C, 76.18; H, 6.28; N, 3.07.  $^1\text{H}$  NMR (400 MHz,  $\text{CDCl}_3$ ):  $\delta$ , 1.25 (t, 6H,  $J$  = 7.0 Hz,  $\text{NH}_2\text{CH}_2\text{CO}_2\text{CH}_2\text{CH}_3$ ), 4.07 (s, 4H,  $\text{NCH}_2\text{CO}_2\text{CH}_2\text{CH}_3$ ), 4.18 (q, 4H,  $J$  = 7.0 Hz,  $\text{NCH}_2\text{CO}_2\text{CH}_2\text{CH}_3$ ), 4.92 (s, 2H,  $\text{CH}_2$ ), 6.47 (d, 2H  $J$  = 8.5 Hz, Ar-H), 6.98 (d, 2H,  $J$  = 8.5 Hz, Ar-H), 7.45–7.48 (m, 4H, Ar-H), 8.03–8.05 (m, 2H, Ar-H), 8.22–8.25 (m, 2H, Ar-H), 8.43 (s, 1H, Ar-H).  $^{13}\text{C}$  NMR (100 MHz,  $\text{CDCl}_3$ ):  $\delta$ , 170.50, 145.68, 132.03, 130.12, 130.04, 131.24, 128.57, 128.45, 125.82, 125.26, 124.54, 124.40, 112.26, 60.53, 53.06, 32.02, 13.72. IR ( $\nu_{\max}$ , NaCl,  $\text{cm}^{-1}$ ): 3345, 2977, 1895, 1931, 1854, 1765, 1676, 1615, 1568, 1521, 1480, 1447, 1386, 1355, 1334, 1274, 1177, 1065, 970, 879, 820, 786, 728, 691, 650, 635, 602, 570, 538, 517.

**4.1.2. [(4-Anthracen-9-ylmethyl-phenyl)-ethoxycarbonyl-methyl-amino]-acetic acid potassium salt (1).** [(4-Anthracen-9-ylmethyl-phenyl)-ethoxycarbonylmethyl-amino]-acetic acid ethyl ester (**4**) (1 g, 2.19 mmol) was dissolved in methanol (20 mL) while stirring. To this was added aqueous KOH (1 mL, 3 M). The mixture was refluxed for 2 h. After cooling to room temperature, the reaction mixture was kept in the fridge, where the potassium salt precipitated. The resulting solution was filtered and the precipitate dried in vacuum to afford **1** as a pale yellow solid (0.96 g, 95%). Mp = 340  $^\circ\text{C}$  (decomp.). MS ( $\text{ES}^+$ )  $m/z$  = 476 ( $\text{MH}^+$ ). Anal. Calcd for  $\text{C}_{25}\text{H}_{19}\text{K}_2\text{NO}_4 \cdot 2\text{H}_2\text{O}$ : C, 58.69; H, 4.53; N, 2.74. Found: 57.80; H, 4.33; N, 2.56.  $^1\text{H}$  NMR (400 MHz,  $\text{D}_2\text{O}$ ):  $\delta$ , 3.67 (s, 4H,  $\text{NCH}_2\text{CO}_2\text{K}$ ), 4.65 (s, 2H,  $\text{CH}_2$ ), 6.20 (d, 2H,  $J$  = 8.5 Hz, Ar-H), 6.82 (d, 2H,  $J$  = 8.5 Hz, Ar-H), 7.36–7.38 (m, 4H, Ar-H), 7.91 (d, 2H,  $J$  = 5.5 Hz, Ar-H), 8.12 (d, 2H,  $J$  = 6.0 Hz, Ar-H), 8.30 (s, 1H, Ar-H).  $^{13}\text{C}$  NMR (100 MHz,  $\text{D}_2\text{O}$ ):  $\delta$ , 177.61, 144.74, 131.10, 129.26, 127.61, 126.89, 126.68, 126.55, 124.06, 123.95, 123.20, 122.57, 109.48, 53.54, 29.22. IR ( $\nu_{\max}$ , KBr,  $\text{cm}^{-1}$ ): 3400, 2877, 2844, 1964, 1915, 1723, 1660, 1500, 1445, 1336, 1256, 1186, 519, 535, 564, 601, 618, 656, 697, 758, 790, 819, 852, 1158, 1100, 987, 955, 903, 884.

**4.1.3. [(4-{10-[4-(Bis-ethoxycarbonylmethyl-amino)-benzyl]-anthracen-9-ylmethyl}-phenyl)-ethoxycarbonyl-methyl-amino]-acetic acid ethyl ester (5).** 9,10-Bischloromethyl anthracene (1.0 g, 3.63 mmol), phenyliminodiacetic acid diethyl ester (**3**) (1.93 g, 7.26 mmol) and  $\text{AlCl}_3$  (0.96 g, 7.26 mmol) were dissolved in dry  $\text{CHCl}_3$  (50 mL) at  $-5^\circ\text{C}$ . The solution was refluxed under stirring overnight (12 h). After the reaction was complete, (monitored by TLC) the solution was cooled and washed with three 100 mL portions of water. The organic portion was dried over  $\text{MgSO}_4$ . After evaporation of the solvent, the crude product was subjected to column chromatography and yielded pure **5** (1.56 g, 58%) as light yellow solid. Mp = 120–122  $^\circ\text{C}$ . MS ( $\text{ES}^+$ )  $m/z$  = 733 ( $\text{MH}^+$ ). Anal. Calcd for  $\text{C}_{44}\text{H}_{48}\text{N}_2\text{O}_8$ : C, 72.11; H, 6.60; N, 3.82. Found: C, 72.26; H, 6.45; N, 3.69.  $^1\text{H}$  NMR (400 MHz,  $\text{CDCl}_3$ ):  $\delta$  1.27 (t, 12H,  $J$  = 7.6 Hz,  $\text{NCH}_2\text{CO}_2\text{CH}_2\text{CH}_3$ ), 4.09 (s, 8H,  $\text{NCH}_2\text{CO}_2\text{CH}_2\text{CH}_3$ ), 4.19 (q, 8H,  $J$  = 7.0 Hz,  $\text{NCH}_2\text{CO}_2\text{CH}_2\text{CH}_3$ ), 4.95 (s, 4H,  $\text{CH}_2$ ), 6.50 (d, 4H,  $J$  = 9.0 Hz, Ar-H), 7.01 (d, 4H,  $J$  = 9.0 Hz, Ar-H), 7.44 (m, 4H, Ar-H), 8.27



(m, 4H, Ar-H).  $^{13}\text{C}$  NMR (100 MHz,  $\text{CDCl}_3$ , ppm):  $\delta$ , 170.52, 145.68, 131.35, 130.25, 130.00, 128.49, 125.19, 124.79, 112.29, 60.54, 53.07, 32.30, 13.74. IR ( $\nu_{\text{max}}$ , KBr,  $\text{cm}^{-1}$ ): 3450, 2979, 1895, 1931, 1859, 1734, 1616, 1568, 1524, 1448, 1371, 1030, 969, 865, 812, 781, 763, 655, 601, 573, 543, 506.

**4.1.4. [(4-{10-[4-(Bis-ethoxycarbonylmethyl-amino)-benzyl]-anthracen-9-ylmethyl}-phenyl)-ethoxycarbonylmethyl-amino]-acetic acid potassium salt (2).** [(4-{10-[4-(Bis-ethoxycarbonylmethyl-amino)-benzyl]-anthracen-9-ylmethyl}-phenyl)-ethoxycarbonylmethyl-amino]-acetic acid ethyl ester (**5**) (1 g, 1.36 mmol) was dissolved in methanol (20 mL) while stirring. To this aqueous KOH (2 mL, 3 M) was added. The mixture was refluxed for 2 h. After cooling to room temperature the mixture was kept in the fridge, where the potassium salt precipitated out. The resulting solution was filtered and the precipitate dried in vacuum to afford **2** as a pale yellow solid (0.95 g, 90%). Mp = 320 °C (decomp.). MS( $\text{ES}^+$ )  $m/z = 773$  ( $\text{M} + \text{H}$ ) $^+$ . Anal. Calcd for  $\text{C}_{36}\text{H}_{28}\text{K}_4\text{N}_2\text{O}_8 \cdot 3\text{H}_2\text{O}$ : C, 52.28; H, 4.14; N, 3.39. Found: C, 52.46; H, 4.02; N, 3.23.  $^1\text{H}$  NMR (400 MHz,  $\text{D}_2\text{O}$ ):  $\delta$ , 3.70 (s, 8H,  $\text{NCH}_2\text{CO}_2\text{K}$ ), 4.86 (s, 4H,  $\text{CH}_2$ ), 6.28 (d, 4H,  $J = 6.1$  Hz, Ar-H), 6.91 (d, 4H,  $J = 6.1$  Hz, Ar-H), 7.42–7.45 (m, 4H, Ar-H), 8.29–8.31 (m, 4H, Ar-H).  $^{13}\text{C}$  NMR (100 MHz,  $\text{D}_2\text{O}$ ):  $\delta$ , 179.22, 146.34, 129.27, 128.41, 128.15, 125.23, 124.95, 111.11, 55.11, 45.30, 31.13. IR ( $\nu_{\text{max}}$ , KBr,  $\text{cm}^{-1}$ ): 3450, 3006, 2005, 1851, 1660, 1574, 1515, 1446, 1404, 1320, 1209, 1043, 1029, 976, 913, 820, 790, 746, 706, 601.

### Acknowledgements

We would like to thank TCD, RCSI and HRB for financial support. We also thank Dr. Hazel M. Moncrieff and Dr. John E. O'Brien for their help and discussion. We especially thank Lisa J. Gillespie for her assistance in the preparation of this manuscript.

### References and notes

- Rurack, K.; Resch-Genger, U. *Chem. Soc. Rev.* **2002**, *31*, 116. Rurack, K. *Spectrochem. Acta A* **2001**, *57*, 2161. Lavigne, J. J.; Anslyn, E. V. *Angew. Chem., Int. Ed.* **2001**, *40*, 3119. Beer, P. D.; Gale, P. A. *Angew. Chem., Int. Ed.* **2001**, *40*, 486. deSilva, A. P.; Fox, D. B.; Huxley, A. J. M.; Moody, T. S. *Coord. Chem. Rev.* **2000**, *205*, 41. Fabbri, L.; Licchelli, M.; Rabaioli, G.; Taglietti, A. F. *Coord. Chem. Rev.* **2000**, *205*, 85. Czarnik, A. W. *Acc. Chem. Res.* **1994**, *27*, 302.
- Martínez-Mañez, R.; Sancenón, F. *Chem. Rev.* **2003**, *103*, 4419. de Silva, A. P.; Gunaratne, H. Q. N.; Gunnlaugsson, T.; Huxley, A. J. M.; McCoy, C. P.; Rademacher, J. T.; Rice, T. E. *Chem. Rev.* **1997**, *97*, 1515. Czarnik, A. W. *Acc. Chem. Res.* **1994**, *27*, 302. *Fluorescent Chemosensors for Ion and Molecular Recognition*; Czarnik, A. W., Ed.; ACS Books: Washington, 1993. Bissell, R. A.; de Silva, A. P.; Gunaratne, H. Q. N.; Lynch, P. L. M.; Maguire, G. E. M.; McCoy, C. P.; Sandanayake, K. R. A. S. *Top. Curr. Chem.* **1993**, *168*, 223.
- Luminescent devices including employing ion and molecular recognition include: de Silva, A. P.; McCaughan, B.; McKinney, B. O. F.; Querol, M. *Dalton Trans.* **2003**, 1902. Balzani, V. *Photochem. Photobiol. Sci.* **2003**, *2*, 459. Balzani, V.; Credi, A.; Venturi, M. *Pure Appl. Chem.* **2003**, *75*, 541. Raymo, F. M. *Adv. Mater.* **2002**, *14*, 401. Raymo, F. M.; Giordani, S. *J. Am. Chem. Soc.* **2004**, *2002*, 124. Brown, G. J.; de Silva, A. P.; Pagliari, S. *Chem. Commun.* **2002**, 2461. Ballardini, R.; Balzani, V.; Credi, A.; Gandolf, M. T.; Venturi, M. *Acc. Chem. Res.* **2001**, *36*, 445.
- Gunnlaugsson, T.; Lee, C. T.; Parkesh, R. *Org. Biomol. Chem.* **2003**, *1*, 3265. Gunnlaugsson, T.; Kruger, P. E.; Lee, T. C.; Parkesh, R.; Pfeffer, F. M.; Hussey, M. G. *Tetrahedron Lett.* **2003**, *44*, 6575. Gunnlaugsson, T.; Nieuwenhuyzen, M.; Richard, L.; Thoss, V. *J. Chem. Soc., Perkin Trans. 2* **2002**, 141. Gunnlaugsson, T.; Davis, A. P.; Glynn, M. *Org. Lett.* **2002**, *4*, 2449. Gunnlaugsson, T.; Bichell, B.; Nolan, C. *Tetrahedron Lett.* **2002**, *43*, 4989. Gunnlaugsson, T.; Davis, A. P.; Glynn, M. *Chem. Commun.* **2001**, 2556.
- Gunnlaugsson, T.; Kruger, P. E.; Jensen, P.; Pfeffer, F. M.; Hussey, M. G. *Tetrahedron Lett.* **2003**, *44*, 8909. Gunnlaugsson, T.; Kelly, J. M.; Nieuwenhuyzen, M.; O'Brien, A. M. K. *Tetrahedron Lett.* **2003**, *44*, 8571. Gunnlaugsson, T.; Leonard, J. P. *J. Chem. Soc., Perkin Trans. 2* **2002**, 1980. Gunnlaugsson, T.; Nieuwenhuyzen, M.; Richard, L.; Thoss, V. *Tetrahedron Lett.* **2001**, *42*, 4725.
- Gunnlaugsson, T.; Harte, A. J.; Leonard, J. P.; Senechal, K. *J. Am. Chem. Soc.* **2003**, *125*, 12062. Gunnlaugsson, T.; Leonard, J. P. *Chem. Commun.* **2003**, 2424. Gunnlaugsson, T.; Harte, A. J.; Leonard, J. P.; Nieuwenhuyzen, M. *Supramol. Chem.* **2003**, *15*, 505. Gunnlaugsson, T.; Harte, A. J.; Leonard, J. P.; Nieuwenhuyzen, M. *Chem. Commun.* **2002**, 2134. Gunnlaugsson, T.; Mac Dónaill, D. A.; Parker, D. *J. Am. Chem. Soc.* **2001**, *123*, 12866. Gunnlaugsson, T.; Mac Dónaill, D. A.; Parker, D. *Chem. Commun.* **2000**, 93. Gunnlaugsson, T. *Tetrahedron Lett.* **2001**, *42*, 8901.
- Chemical Sensors and Biosensors for Medical and Biological Applications*; Spichiger-Keller, U. C., Ed.; Wiley-VCH: Weinheim, Germany, 1998. *Chemosensors of Ion and Molecular Recognition*; Desvergne, J. P., Czarnik, A. W., Eds.; Kluwer Academic: Dordrecht, Netherland, 1997.
- He, H.; Mortellaro, M. A.; Leiner, M. J. P.; Fraatz, R. J.; Tusa, J. K. *J. Am. Chem. Soc.* **2003**, *125*, 1468. He, H.; Mortellaro, M. A.; Leiner, M. J. P.; Young, S. T.; Fraatz, R. J.; Tusa, J. K. *Anal. Chem.* **2003**, *75*, 549.
- (a) Costero, A. M.; Andreu, R.; Monrabal, E.; Martínez-Manez, R.; Sancenón, F.; Soto, J. *J. Chem. Soc., Dalton Trans.* **2002**, 1769. (b) Prodi, L.; Montalti, M.; Zaccaroni, N.; Bradshaw, J. S.; Izatt, R. M.; Savage, P. B. *Tetrahedron Lett.* **2001**, *42*, 2941. (c) Choi, M.; Kim, M.; Lee, K. D.; Han, K. N.; Yoon, I. A.; Chung, H. J.; Yoon, J. *Org. Lett.* **2001**, *3*, 3455. (d) Charles, S.; Yunus, S.; Dubois, F.; Vander Donckt, E. *Anal. Chim. Acta* **2001**, *440*, 37. (e) Ertas, N.; Akkaya, E. U.; Ataman, O. Y. *Talanta* **2000**, *51*, 693. (f) Prodi, L.; Bolletta, F.; Montalti, M.; Zaccaroni, N. *Eur. J. Inorg. Chem.* **1999**, *3*, 455. (g) Lu, J. Z.; Zhang, Z. *J. Analyst* **1995**, *120*, 453. (h) Huston, M. E.; Engleman, C.; Czarnik, A. W. *J. Am. Chem. Soc.* **1990**, *112*, 7054.
- Some of our preliminary work was recently published: Gunnlaugsson, T.; Lee, C. T.; Parkesh, R. *Org. Lett.* **2003**, *5*, 4065.
- Cadmium and Compounds*, US Environmental Protection Agency, 2001.
- Frausto da Silva, J. J. R.; Williams, R. J. In *The Biological*

- Chemistry of the Elements: The Inorganic Chemistry of Life*, 2nd ed.; Oxford University Press: Oxford, 2001. *CRC Handbook of Chemistry and Physics*, 77th ed., CRC: Boca Raton, Florida, 1996. Carr, D. S. Cadmium and Cadmium Alloys, 4th ed. In *Kirk-Othmer Encyclopaedia of Chemical Technology*, Vol. 4; Wiley: New York, 1992.
13. Dobson, S. *Cadmium-Environmental Aspects*; World Health Organisation: Geneva, 1992. Jackson, T.; MacGillivray, A. In *Accounting for Cadmium*; Stockholm Environment Institute: London, 1993. Jones, R.; Lapp, T.; Wallace, D. In *Locating and Estimating Air Emissions from Sources of Cadmium and Cadmium Compounds*, Institute for the US Environment Protection Agency, Office of Air and Radiation, Report EPA-453/R-93-040, **1993**.
  14. Rydh, C. J.; Svärd, B. *Sci. Total Environ.* **2003**, 302, 167.
  15. Benjamin, M. W.; Honeyman, B. D. In *Global Biogeochemical Cycles*; Butcher, S. S., Charlson, R. J., Orians, G. H., Wolfe, G. V., Eds.; Academic: London, 1992; p 317.
  16. Nordberg, G. F.; Nordberg, M. In *Biological Monitoring of Trace Metals*; Clarkson, T. W., Friberg, L., Nordberg, G. F., Sager, P. R., Eds.; Plenum: New York, 1998; Vol. 151.
  17. Falnoga, I.; Tusek-Znidaric, M.; Horvat, M.; Stegnar, P. J. *Environ. Pathol. Toxicol. Oncol.* **2000**, 19, 201.
  18. Regunathan, A.; Glesne, D. A.; Wilson, A. K.; Song, J.; Nicolae, D.; Flores, T.; Bhattacharyya, M. H. *Toxicol. Appl. Pharmacol.* **2003**, 191, 272.
  19. Nakadaira, H.; Nishi, S. *Sci. Total Environ.* **2003**, 309, 48.
  20. de Silva, A. P.; Sandanayake, K. R. A. S. *Angew. Chem., Int. Ed.* **1990**, 29, 1173. de Silva, A. P.; de Silva, S. A. *J. Chem. Soc., Chem. Commun.* **1986**, 1709.
  21. Structurally similar receptors have been used for the detection of  $Mg^{2+}$ : de Silva, A. P.; Gunaratne, H. Q. N.; Maguire, G. E. M. *J. Chem. Soc., Chem. Commun.* **1994**, 1213; and for Zn(II): Reany, O.; Gunnlaugsson, T.; Parker, D. *J. Chem. Soc., Perkin Trans. 2* **2000**, 1819.
  22. Burdette, S. C.; Walkup, G. K.; Spingler, B.; Tsien, R. Y.; Lippard J. *Am. Chem. Soc.* **2001**, 123, 7831.
  23. Bhattacharyya, K.; Chowdhury, M. *Chem. Rev.* **1993**, 93, 507.
  24. Cloninger, M. J.; Whitlock, H. W. *J. Org. Chem.* **1998**, 63, 6153.

# Rationally designed chromogenic chemosensor that detects cysteine in aqueous solution with remarkable selectivity

Min Su Han and Dong H. Kim\*

Department of Chemistry, Center for Integrated Molecular Systems, Division of Molecular and Life Sciences, Pohang University of Science and Technology, San 31 Hyojadong, Pohang 790-784, South Korea

Received 28 January 2004; revised 29 June 2004; accepted 19 August 2004

Available online 20 October 2004

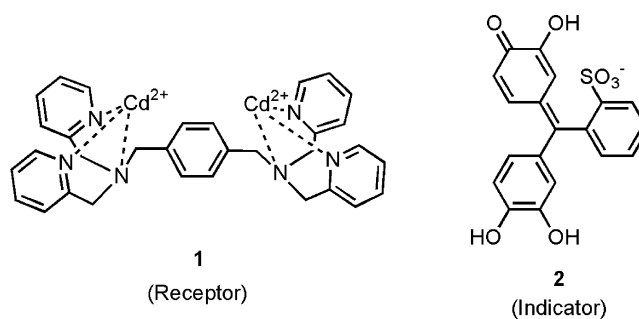
**Abstract**—A sensing ensemble for cysteine was assembled conveniently by simply mixing *N,N,N',N'*-tetra-(2-pyridylmethyl)-*p*-xylylenediamine (TPXD), cadmium perchlorate, and pyrocatechol violet in an 1:2:1 molar ratio in water of neutral pH. In the ensemble,  $[\text{Cd}_2(\text{TPXD})]^{4+}$  formed from TPXD and cadmium perchlorate serves as the receptor, and pyrocatechol violet functions as the indicator in sensing the analyte. The detection can be made either spectroscopically from the decrease of the UV–visible absorbance at 665 nm or visually from the color change to yellow upon addition of an aqueous solution of the analyte to the solution of the ensemble. The association constant ( $K_{\text{ass}}$ ) for the binding of the indicator to the receptor was determined with an isothermal titration calorimeter to be  $(2.77 \pm 0.98) \times 10^5 \text{ M}^{-1}$  and that for the binding of cysteine to the receptor was obtained to have  $(1.62 \pm 0.97) \times 10^7 \text{ M}^{-1}$  by the non-linear regression analysis of the titration curve obtained by titration of the solution of the ensemble with cysteine solution. The chemosensor showed excellent selectivity for cysteine over other amino acids including homocysteine.

© 2004 Elsevier Ltd. All rights reserved.

## 1. Introduction

Molecular recognition and selective detection of an amino acid of interest have been the subjects of intensive researches over several decades and remain to be challenging tasks.<sup>1</sup> Of twenty amino acids that are being used as building blocks for proteins, only a few amino acids can be probed by chemosensors. These include histidine<sup>2</sup> aspartic acid,<sup>3</sup> and lysine,<sup>4</sup> which bear in common an additional functional moiety such as imidazole or carboxylate besides the functionalities to be used for peptide bond formation. Very recently, Rusin et al. reported a chromogenic as well as fluorogenic detecting device for cysteine in an aqueous solution of pH 9.5, but it failed to differentiate cysteine from homocysteine.<sup>5</sup> We report herein design of a chemosensor that can detect free cysteine in aqueous solution of neutral pH with a remarkable selectivity. Cysteine is an essential amino acid for important biological motifs such as zinc-fingers,<sup>6</sup> cysteine-switch that is involved in the activation of matrix metalloproteases,<sup>7</sup> coenzyme A,<sup>8</sup> and glutathione.<sup>9</sup> The reversible oxidation–reduction reactions of the thiol group of cysteine are essential process in many biological

systems.<sup>10</sup> Furthermore, cysteine is the amino acid that plays a major role in determining three dimensional structure of proteins. Accordingly, detection of cysteine in the biological systems is of considerable importance.



The design of the present cysteine probe is based on the strategy developed by Anslyn, in which an analyte competes for a receptor with a chromogenic indicator.<sup>11</sup> The successful displacement of the receptor-bound indicator by the analyte results in to display an altered spectral feature that can be communicated spectroscopically. Hence, in designing chemosensors of this type, the following requirements should be satisfied: (i) the receptor can bind both the

**Keywords:** Chemosensor; Sensing ensemble; Cysteine; Homocysteine; Isothermal titration calorimeter; Amino acids.

\* Corresponding author. Tel.: +82-54-279-2101; fax: +82-54-279-5877; e-mail: dhkim@postech.ac.kr

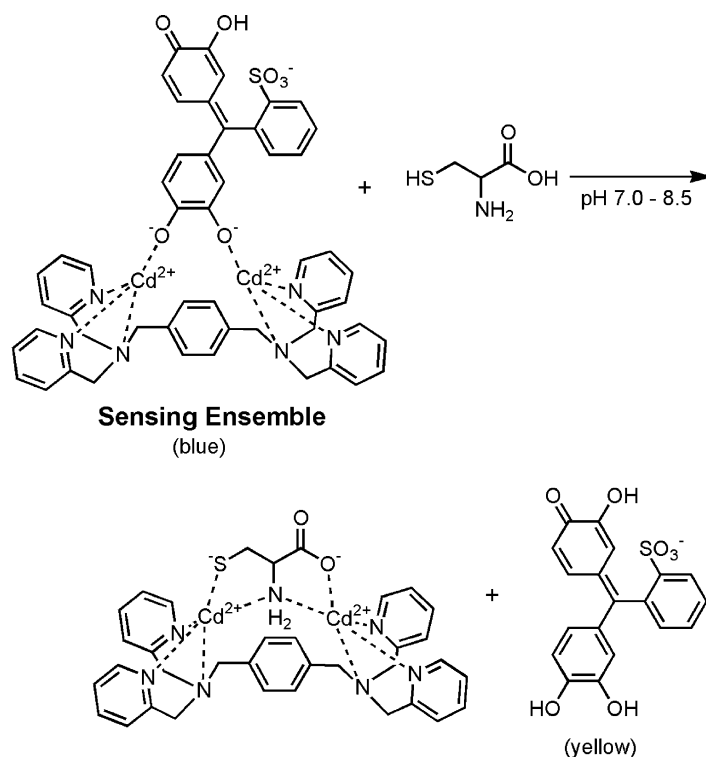


**Figure 1.** The schematic representation of the rationale used for designing a cysteine chemosensor. Cysteine displaces the indicator (1) that is bound to receptor (2), whereby the UV–visible absorbance at 665 nm decreases and there develops yellow color. (For interpretation of the references to colour in this figure legend, the reader is referred to the web version of this article.)

indicator and analyte, (ii) the binding affinity of the analyte towards the receptor is greater than the indicator, and (iii) the absorption spectrum of the indicator differs considerably from that of the indicator·receptor complex. We take

advantage of the strong metal–ligand interactions as the binding forces in designing the probe.<sup>12</sup> Such interactions are known to be strong enough to overcome the solvation of water molecules on the receptor metal ions, thus to enable

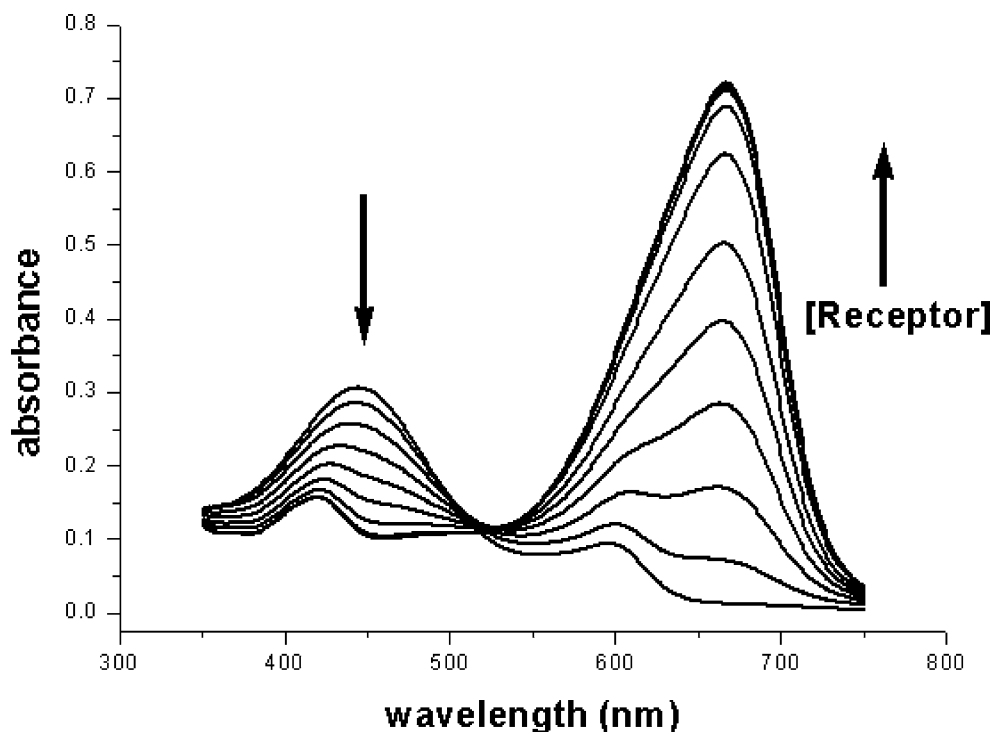


**Figure 2.** UV–visible spectra obtained upon addition of receptor solutions (final concentrations: 0, 5, 10, 15, 20, 25, 30, 35, 40, 45, and 50  $\mu\text{M}$ ) to the pH 7.0 aqueous buffer (HEPES, 10 mM) containing pyrocatechol violet (25  $\mu\text{M}$ ).

the detection of cysteine in an aqueous medium. Cysteine bears three functional groups, i.e. carboxylate, sulfhydryl, and amino groups. These groups can form a complex with a receptor having two metal ions that are separated from each other appropriately so that both the metal ions undergo coordinative bond formations with the functional groups in cysteine. With this in mind, we chose to use the metal complex of *N,N,N',N'*-tetra-(2-pyridylmethyl)-*p*-xylylenediamine<sup>13</sup> (TPXD) as receptor and pyrocatechol violet (**2**), a commercially available phenolic dye as the indicator for the present sensing ensemble. Pyrocatechol violet is chosen on the ground that its two *ortho*-positioned hydroxyls are expected to bind the metal ions in the receptor. As to the metal ions, Cd<sup>2+</sup> ion was found to be most satisfactory.<sup>12</sup> According to the hard–soft acid–base theory,<sup>14</sup> the soft-base mercapto group is expected to form a strong bond with Cd<sup>2+</sup> (soft-acid), but the interactions between the hard-base phenolic hydroxyl groups in **2** and Cd<sup>2+</sup> ion are comparatively weak, and thus the receptor-bound indicator would be displaced by the analyte, which is expectedly communicated by a change in the UV–visible absorbance. The design concept is illustrated schematically in Figure 1.

## 2. Results and discussion

Firstly, The molecular ensemble generated from **1** and **2** was evaluated. Figure 2 shows changes in the UV–visible absorption when the aqueous solution of **1** was titrated into the aqueous buffer containing **2** (25  $\mu$ M).

While the absorbance at 444 nm decreases, the absorbance at 665 nm increases as the indicator binds to the Cd<sup>2+</sup> ions in the receptor to form the sensing complex. The association constant of  $(2.77 \pm 0.98) \times 10^5 \text{ M}^{-1}$  for the binding of **2** to **1**

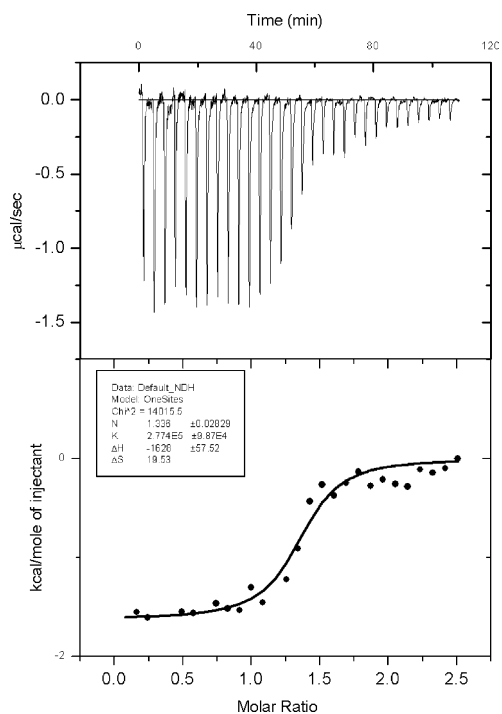


**Figure 3.** ITC plot for the titration of the receptor solution with indicator **2** in aqueous buffer (HEPES) pH 7.0 at 30 °C.

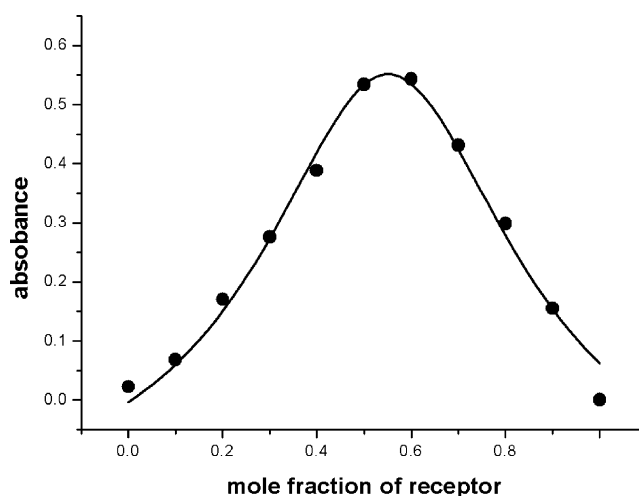


**Figure 4.** Job plot for binding of pyrocatechol violet (**2**) with the receptor (**1**) in a pH 7.0 (HEPES 10 mM) buffer solution. Aqueous solutions of the receptor (50  $\mu$ M) and pyrocatechol violet (50  $\mu$ M) were mixed in varying ratios and the changes of absorbance at 665 nm were measured.

was determined by isothermal titration calorimetry (ITC) (Fig. 3).<sup>15</sup> From the ITC experiment the thermodynamic parameters associated with the binding of **2** to **1** in the aqueous solution of pH 7.0 were also obtained as the following:  $\Delta H = -(1.63 \pm 0.01) \text{ kcal mol}^{-1}$  and  $\Delta S = +1.95 \text{ eu}$ , indicating that the binding is enthalpically driven. The stoichiometric coefficient value (*n*) was determined to be 1.33, but the 1:1 binding mode in the complex formation is evident from the Job's plot (Fig. 4).

Changes in the UV–visible absorption spectra upon additions of cysteine to the solution of the ensemble are shown in Figure 5: the absorbance at 665 nm decreases progressively, while the peak at 444 nm increases. These changes in absorbance of the solution demonstrates that the cysteine displaces successfully the receptor-bound indicator and binds to the Cd<sup>2+</sup> centers of **1** in line with the design rationale. As expected from the design rationale, complexes of TPXD formed with Fe<sup>2+</sup>, Cu<sup>2+</sup>, or Co<sup>2+</sup> failed to serve as a receptor for the present sensor. The association constant for the binding of cysteine to the receptor was determined to be  $(1.62 \pm 0.97) \times 10^7 \text{ M}^{-1}$  by the non-linear regression analysis of the titration curve in Figure 5 using the software Dynafit. The high affinity of cysteine shown to the receptor is supportive for the proposition that all the three functional groups in cysteine are involved in its coordination to the metal ions in **1** to form a tightly bound ternary complex having a pseudosymmetrical structure.

The effect of pH of the aqueous solution in the sensing of cysteine was studied to find that the UV–visible absorbance changes described above are in effect in the pH range of 7.0–8.5 as shown in Figure 6: both the binding affinities of the indicator and analyte to the receptor increase in a parallel fashion in that pH range. The present ensemble exhibits remarkable selectivity towards cysteine over other amino acids including serine, glutamic acid, and histidine as can be seen in Figure 7. Sensors that can detect analyte of interest by the naked eyes are of particular interest because of the convenience in its use. As shown in Figure 8, cysteine



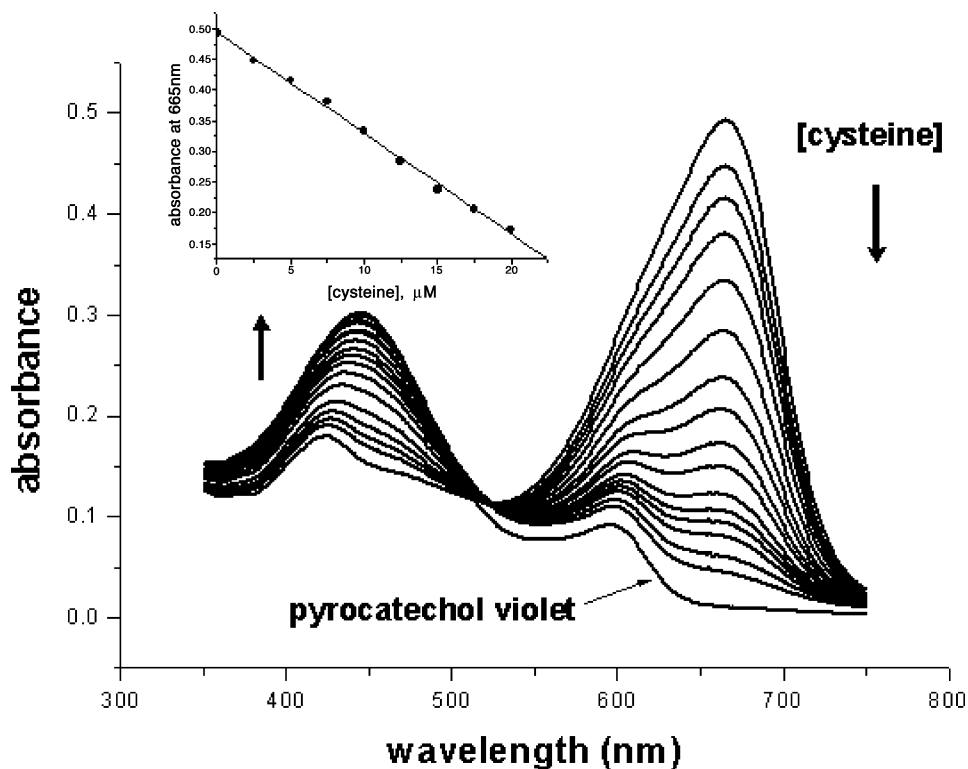


**Figure 5.** UV–visible spectra obtained by additions of cysteine solutions (final concentrations: 0, 2.5, 5, 7.5, 10, 12.5, 15, 17.5, 20, 22.5, 25, 27.5, 30, 32.5, 37.5, and 50  $\mu\text{M}$ ) to the pH 7.0 aqueous buffer (HEPES, 10 mM) containing the sensing ensemble,  $[\text{Cd}_2(\text{TPXD})(\text{pyrocatechol violet})]^{2+}$  (25  $\mu\text{M}$ ), and UV–visible spectrum of **2** (25  $\mu\text{M}$ ). Inset: plot of absorbance at 665 nm against concentration of cysteine.

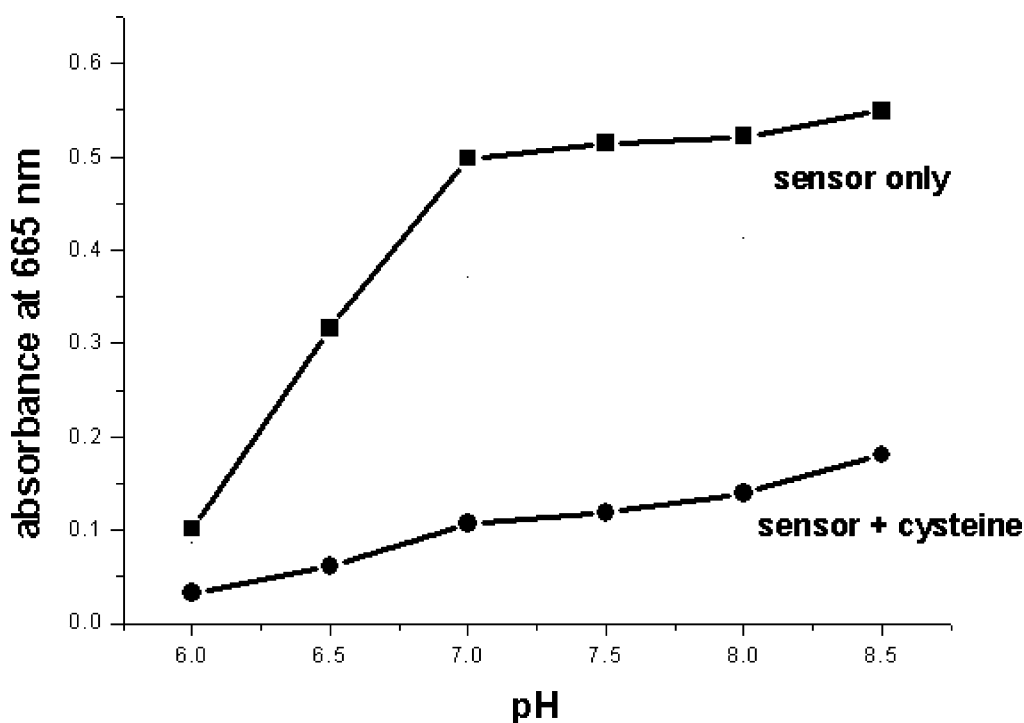


**Figure 6.** UV–visible absorbances of the aqueous solution of **1** (25  $\mu\text{M}$ ) and **1** with cysteine (25  $\mu\text{M}$ ) at various pHs. Compositions of the buffer solutions are as the following: pH 6.0 (MES 10 mM), pH 6.5 (MES 10 mM), pH 7.0 (HEPES 10 mM), pH 7.5 (HEPES, 10 mM), pH 8.0 (HEPES 10 mM), and pH 8.5 (CHES 10 mM).

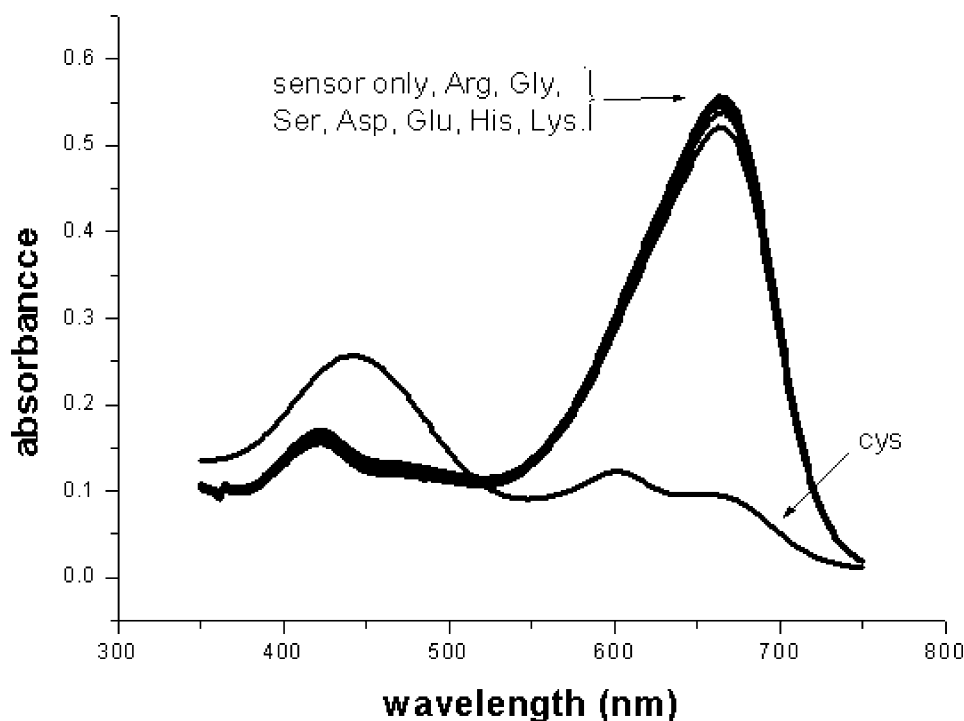


**Figure 7.** UV-visible spectra of the sensing ensemble (25  $\mu\text{M}$ ) in the presence of a variety of amino acids (25  $\mu\text{M}$ ) in pH 7.0 aqueous buffer (HEPES) solution.



**Figure 8.** Color of the sensing ensemble (25  $\mu\text{M}$ ) in the absence and presence of amino acids (25  $\mu\text{M}$ ): from left to right; the sensor only, and the sensor with Cys, Glu, Asp, His, Lys, Arg, Gly, Val and Ser.

is readily detected visually with the sensing ensemble: The color change of blue to yellow occurs only when the ensemble is added to a solution containing cysteine.

In order to shed light on the binding nature of cysteine to the receptor, we have examined the effects caused by homocysteine and derivatives of cysteine on the absorbance of the sensing ensemble. As can be seen in Figure 9, homocysteine lowered the absorbance intensity at 665 nm but in a much less extent (about 30% of the decrease caused by cysteine) compared with that brought about by cysteine, demonstrating the remarkable selectivity of the probe for cysteine. This is a feature of considerable importance since the concentration of homocysteine in human plasma is known to be in the range of  $\mu\text{M}$ .<sup>16</sup> As described earlier, the chemosensor developed by Rusin et al.<sup>5</sup> fails to differentiate cysteine from homocysteine. It is worth noting that methionine in which the mercapto group in cysteine is

converted into a methythio moiety failed to cause any change in the absorbance. Cysteine methyl ester brings about a much profound decrease in the absorbance than *N*-acetylcysteine. These observations together suggest also that all three functional groups in cysteine are involved in the binding interactions of cysteine with **1** to form a receptor-analyte complex as discussed in the design rationale.

In summary, we have rationally designed and assembled a sensing ensemble that can efficiently detect cysteine with excellent selectivity in the aqueous medium of physiological pH. The chemosensor probes the analyte from the decrease of the absorbance at 665 nm or with naked eyes by the color change from blue to yellow. The sensing ensemble can be prepared easily by simply mixing TPXD, cadmium perchlorate, and pyrocatechol violet in an 1:2:1 molar ratio in water of neutral pH.

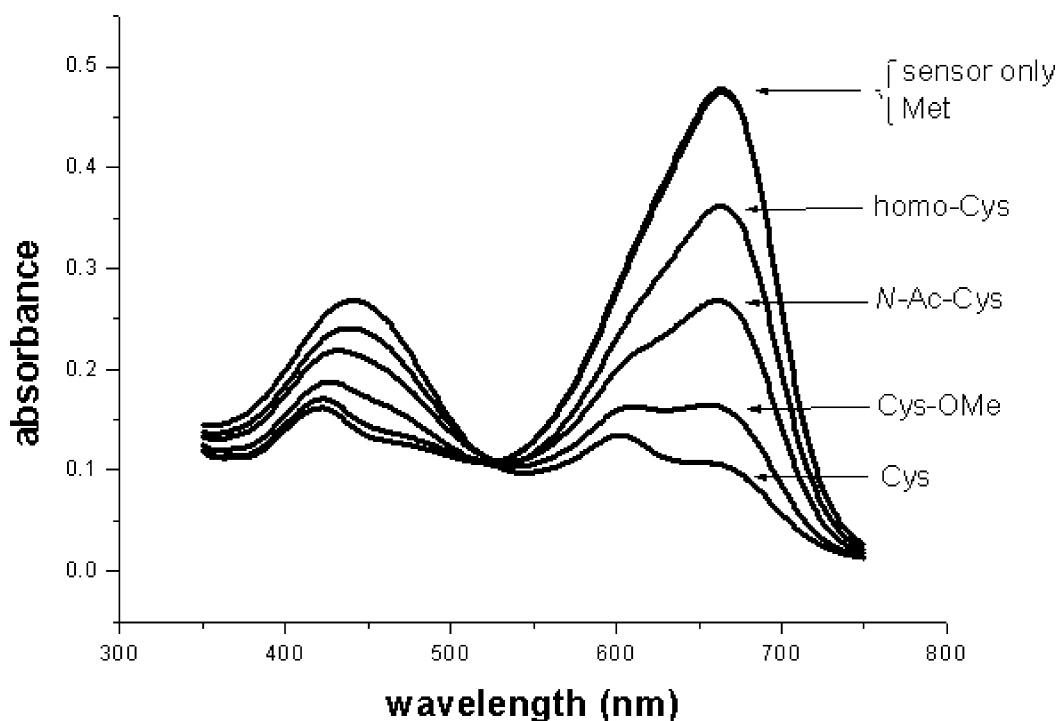


**Figure 9.** UV–visible spectral changes upon additions of cysteine, homocysteine and derivatives of cysteine (final concentration: 25  $\mu\text{M}$ ) to a pH 7.0 (HEPES 10 mM) buffer solution of the sensing ensemble (final concentration: 25  $\mu\text{M}$ ).

### 3. Experimental

#### 3.1. Reagents

All reagents used in this work were purchased from Sigma-Aldrich Chemical Co. and were used without further purification. Compound TPXD was prepared as described in the literature.<sup>13</sup>

#### 3.2. UV–visible spectrometric study

Buffer solutions were prepared with deionized water. UV–visible spectra were obtained with a Hewlett-Packard 8453 diode array spectrophotometer.

**3.2.1. Determination of the  $K_{\text{ass}}$  value for the binding of cysteine to **1**.** A 3.0 mL solution containing **1** (25  $\mu\text{M}$ ) in pH 7.0 buffer (HEPES, 10 mM) was prepared, and its UV–visible absorption was measured. Aliquots of cysteine solution in pH 7.0 buffer (HEPES, 10 mM) were titrated into solutions of **1** (25  $\mu\text{M}$ ) to give final concentrations of 2.5–32.5 (by 2.5  $\mu\text{M}$  increments), 37.5 and 50  $\mu\text{M}$ , and the absorption spectra were recorded. The  $K_{\text{ass}}$  value for the binding of cysteine to **1** was determined by non-linear regression analysis of the titration data (Fig. 5) using the software Dynafit.

**3.2.2. Determination of the stoichiometry for binding of **2** to **1** to form the sensing ensemble.** Aqueous solutions of **1** (50  $\mu\text{M}$ ) and **2** (50  $\mu\text{M}$ ) in pH 7.0 buffer (HEPES, 10 mM) were mixed in varying ratios and the changes of absorbance at 665 nm were measured. The stoichiometry was obtained from the titration plot (Job's plot) of the absorbance at 665 nm (Fig. 3).

**3.2.3. pH dependence of the sensing.** Aqueous buffer solutions (pH 6.0–8.5) containing **1** (25  $\mu\text{M}$ ) and **1** (25  $\mu\text{M}$ ) with cysteine (25  $\mu\text{M}$ ) were prepared, and their UV–visible absorbance at 665 nm was measured (Fig. 6) and plotted the absorbance against pH to obtain Figure 6. The compositions for the buffer solutions are as follows: pH 6.0 (MES 10 mM), pH 6.5 (MES 10 mM), pH 7.0 (HEPES 10 mM), pH 7.5 (HEPES, 10 mM), pH 8.0 (HEPES 10 mM), and pH 8.5 (CHES 10 mM).

#### 3.3. Determination of the thermodynamic parameters for the binding of **2** to **1** with an isothermal titration calorimeter

An aqueous solution (1.5 mL, pH 7.0, HEPES 10 mM) of **1** (0.2 mM) was added to the sample cell of an isothermal titration calorimeter and aqueous buffer solution (1.7 mL, pH 7.0, HEPES 10 mM) was added to the reference cell. Into the solution in the sample cell was injected 7  $\mu\text{L}$  portions of aqueous solution of **2** (3.3 mM) in 30 times with 200 s interval. Each mixture was continuously stirred at 300 rpm and kept at an operating temperature of 30  $^{\circ}\text{C}$ . After each addition of the aqueous solution of **2**, the heat ( $\mu\text{cal s}^{-1}$ ) released in the sample cell was measured with respect to a reference cell. The data were analyzed using the software Origin to give Figure 4.

#### Acknowledgements

The authors express their sincere thanks to Korea Science and Engineering Foundation and Korea Research Foundation (KRF-2000-015-DS0025) for financial support of this work.

## References and notes

1. Fabbrizzi, L.; Licchelli, M.; Rabaioli, G.; Taglietti, A. *Coord. Chem. Rev.* **2000**, *205*, 85–108.
2. Hortala, M. A.; Fabbrizzi, L.; Marcotte, N.; Stomeo, F.; Taglietti, A. *J. Am. Chem. Soc.* **2003**, *125*, 20–21.
3. Ait-Haddou, H.; Wiskur, S. L.; Lynch, V. M.; Anslyn, E. V. *J. Am. Chem. Soc.* **2001**, *123*, 11296–11297.
4. Sasaki, S.; Hashizume, A.; Citterio, D.; Fujii, E.; Suzuki, K. *Tetrahedron Lett.* **2002**, *43*, 7243–7245.
5. Rusin, O.; St. Luce, N. N.; Agbaria, R. A.; Escobedo, J. O.; Jiang, S.; Warner, I. M.; Dawan, F. B.; Lian, K.; Strongin, R. M. *J. Am. Chem. Soc.* **2004**, *126*, 483–489.
6. Klug, A.; Schwabe, J. W. R. *FASEB J.* **1995**, *9*, 597–604.
7. Van Wart, H. E.; Birkedal-Hassen, H. *Proc. Natl. Acad. Sci. U.S.A.* **1990**, *87*, 5578–5582.
8. Zubay, G. L.; Parson, W. W.; Vance, D. E. *Principles of Biochemistry*; Wm. C. Brown Publishers: Oxford, 1995; pp 210–212.
9. Sies, H. *Free Radical Biol. Med.* **1999**, *27*, 916–921.
10. For example: Wood, Z. A.; Schröder, E.; Harris, J. R.; Poole, L. B. *Trends Biochem. Sci.* **2003**, *28*, 32–40.
11. (a) Wiskur, S. L.; Ait-Haddou, H.; Lavigne, J. J.; Anslyn, E. V. *Acc. Chem. Res.* **2001**, *34*, 963–972. (b) Ait-Haddou, H.; Wiskur, S. L.; Lynch, V. M.; Anslyn, E. V. *J. Am. Chem. Soc.* **2001**, *123*, 11296–11297. (c) Wiskur, S. L.; Anslyn, E. V. *J. Am. Chem. Soc.* **2001**, *123*, 10109–10110. (d) Metzger, A.; Anslyn, E. V. *Angew. Chem., Int. Ed.* **1998**, *37*, 649–652. (e) Niikura, K.; Metzger, A.; Anslyn, E. V. *J. Am. Chem. Soc.* **1998**, *120*, 8533–8534.
12. (a) Fabbrizzi, L.; Leone, A.; Taglietti, A. *Angew. Chem., Int. Ed.* **2001**, *40*, 3066–3069. (b) Han, M. S.; Kim, D. H. *Angew. Chem., Int. Ed.* **2002**, *41*, 3089–3811. (c) Fabbrizzi, L.; Marcotte, N.; Stomeo, F.; Taglietti, A. *Angew. Chem., Int. Ed.* **2002**, *41*, 3811–3814. (d) Amendola, V.; Fabbrizzi, L.; Mangano, C.; Pallavicini, P.; Poggi, A.; Taglietti, A. *Coord. Chem. Rev.* **2001**, *219–221*, 821–837.
13. Kawahara, S.; Uchimaru, T. *Eur. J. Inorg. Chem.* **2001**, 2437–2442.
14. Lippard, S. J.; Berg, J. M. *Principles of Bioorganic Chemistry*; University Science Books: Mill Valley, 1994; p 22.
15. Jelesarov, I.; Bosshard, H. R. *J. Mol. Recog.* **1999**, *12*, 3–18.
16. Rauh, M.; Verwied, S.; Knerr, I.; Dörr, H. G.; Sönnichsen, A.; Koletzko, B. *Amino Acids* **2001**, *20*, 409–418.

# DNA hybridization-enhanced porous silicon corrosion: mechanistic investigations and prospect for optical interferometric biosensing

Claudia Steinem,<sup>†,||</sup> Andreas Janshoff,<sup>‡,||</sup> Victor S.-Y. Lin,<sup>§</sup> Nicolas H. Völcker<sup>¶</sup>  
and M. Reza Ghadiri\*

*Departments of Chemistry and Molecular Biology and The Skaggs Institute for Chemical Biology, The Scripps Research Institute, La Jolla, CA 92037, USA*

Received 10 February 2004; accepted 22 June 2004

Available online 23 August 2004

**Abstract**—Hybridization of DNA oligonucleotides in neutral aqueous solutions with complementary sequences immobilized on highly doped *p*-type porous silicon matrix is shown to result in an unexpectedly large shift in the Fabry–Perot interference pattern to lower wavelengths implying a decrease in effective optical thickness of the porous matrix. We have determined that the observed optical effects are due to enhanced corrosion (oxidation–hydrolysis) of the porous silicon layer triggered by the formation of complementary DNA duplexes. Scanning force microscopy and reflectance spectroscopy were employed at various stages of the signal evolution process to monitor and establish the material changes induced by the DNA binding events. We postulate that the slow background corrosion process initiated at the exposed Si–H<sub>x</sub> groups is dramatically enhanced as a result of the change in carrier charge density of the porous silicon layer in response to the local increase in the electrostatic field generated by the nucleic acid hybridization. The proposed mechanism is consistent with the experimental observations that the characteristics of the porous silicon matrix and the charge density of the hybridized DNA complexes can both influence the corrosion process. Functionalized porous silicon matrices prepared from highly doped silicon wafers (resistivity 1 mΩ·cm) produce large corrosion rates and improved signal to noise ratios. Moreover, the enhanced decrease in the effective optical thickness could be prevented by either shielding the negative charges of the DNA duplex in the presence of Mg<sup>2+</sup> ions, or by using backbone charge neutral peptide nucleic acids (PNA) in the DNA hybridization experiments. The observed phenomenon is thus an example of an active sensor matrix in which the molecular recognition signal is transduced and amplified by a profound change in the chemical reactivity and physical property of the solid support itself. With the signal amplification mechanism described, binding of unlabeled complementary DNA oligonucleotides of approximately 0.1 amol/mm<sup>2</sup> has been detected suggesting the potential utility of this new approach in DNA sensing. © 2004 Elsevier Ltd. All rights reserved.

## 1. Introduction

The signal from the initial binding of a ligand to its cellular receptor is typically amplified through signal transduction pathways involving a cascade of subsequent biochemical

steps. Typically very low ligand concentrations can induce significant cellular responses, often much larger than expected from a simple one to one binding event. Biological ligand–receptor pairs, such as antibody–antigen, DNA/DNA, and streptavidin–biotin, are usually used as the central element in biosensor designs because of their high specificity and association constants. However, in contrast to living cells, biosensor devices seldom employ built-in signal amplification mechanisms.<sup>1</sup> Enzyme coupled systems are the most commonly used approach to amplify the signal caused by an analyte binding in solution.<sup>2</sup> Other examples include gold-nanoparticle capture,<sup>3</sup> ligand-induced enzyme activation,<sup>4</sup> enzymatic recycling of the substrate,<sup>5</sup> and the use of transmembrane ion channels and pore structures<sup>6</sup> to transduce and amplify ligand binding interactions. Here, we present a ligand-induced signal amplification mechanism based on DNA-enhanced alteration of porous silicon morphology and optical properties.

**Keywords:** Biosensor; Porous silicon; DNA.

\* Corresponding author. Tel.: +1 858 784 2700; fax: +1 858 784 2798.; e-mail: [ghadiri@scripps.edu](mailto:ghadiri@scripps.edu)

<sup>†</sup> Present address: Institut fuer Analytische Chemie, Chemo- und Biosensorik, Universitaet Regensburg, 93040 Regensburg, Germany.

<sup>‡</sup> Present address: Institut fuer Physikalische Chemie, Johannes Gutenberg Universitaet, Jakob-Welder-Weg 11, 55128 Main, Germany.

<sup>§</sup> Present address: 1710 Gilman Hall, Department of Chemistry, Iowa State University, Ames, IA 50011-3111, USA.

<sup>¶</sup> Present address: Flinders University of South Australia, School of Chemistry, Physics and Earth Sciences, GPO Box 2100, Bedford Park, South Australia, 5042, Australia.

<sup>||</sup> These authors have contributed equally to this work.



Porous silicon is a high surface area material that can be prepared to have a large variety of pore morphologies by chemical or electrochemical etching processes.<sup>7</sup> The hydride terminated freshly etched porous silicon surface can be modified by a number of methods, such as oxidation, halogenation, nucleophilic substitution, and hydrosilylation.<sup>8</sup> Once oxidized the porous silicon surface can be further functionalized using common silane chemistry. Because of its unique electrical and optical properties, porous silicon has been used as the matrix and signal transducer in a variety of biosensing applications.<sup>9</sup> Recently, we reported that pore morphology of *p*-type porous silicon could be tuned to meet the requirements for biocompatibility by carefully choosing the etching conditions and the silicon dopant concentration.<sup>10a</sup> By immobilizing biotin on a porous silicon surface we were able to detect the binding of streptavidin inside the pores by interference spectroscopy. The induced red-shift in the Fabry–Perot fringe pattern caused by an increase in the refractive index of the medium upon molecular recognition of the protein by its ligand was explained by the effective medium approximations.<sup>11</sup> Furthermore, in an earlier study we described the observation that DNA hybridization to complementary sequences immobilized on a *p*-type porous silicon matrix resulted in an unexpected large decrease in the effective optical thickness (blue-shift of the interference spectrum).<sup>12</sup> However, the observed effects were subsequently attributed to simple background rates of porous silicon corrosion in aqueous medium,<sup>10</sup> thus effectively retracting the earlier claims<sup>12</sup> and the validity of the sensing scheme. Here we show that in fact hybridization of DNA oligonucleotides in neutral aqueous solutions to complementary sequences immobilized on highly doped *p*-type porous silicon matrix can result in a large shift in the Fabry–Perot interference pattern to lower wavelengths caused by the enhanced corrosion (oxidation–hydrolysis) of the porous silicon layer accelerated by the formation of complementary DNA duplexes. Furthermore, we propose a plausible mechanistic underpinning for this process and suggest the potential scope and current limitations of this approach in DNA sensing.

## 2. Results and discussions

### 2.1. Characterization of porous silicon layers

Porous silicon layers obtained from *p*<sup>+</sup> and *p*<sup>++</sup>-type silicon were characterized by means of scanning force/scanning electron microscopy, reflectance spectroscopy, nitrogen adsorption (BET) isotherms, and profilometry. Fabry–Perot layers differing in pore morphology and dopant concentration were investigated. The etching conditions of the two types of silicon wafers differing in resistivity were adjusted in a way that crucial properties such as porosity, pore radius, thickness and surface area are similar despite different dopant concentrations (Table 1). *p*<sup>++</sup> porous silicon with larger pores were obtained as described previously.<sup>10a</sup>

Scanning force microscopy (SFM) images of the porous layers etched at low current densities revealed the same predominant hillock structure for both the *p*<sup>+</sup> and *p*<sup>++</sup>

**Table 1.** Properties of three different porous silicon films

	<i>p</i> <sup>+</sup>	<i>p</i> <sup>++</sup> (A)	<i>p</i> <sup>++</sup> (B)
Current density	50–70 mA/cm <sup>2</sup>	100–150 mA/cm <sup>2</sup>	400–600 mA/cm <sup>2</sup>
HF-Concentration	25%	37.5%	37.5%
Porosity	65–75%	65–75%	80–90%
Pore radius	2–3 nm	2–5 nm	100–200 nm
Surface area	0.4 m <sup>2</sup>	0.4 m <sup>2</sup>	0.005 m <sup>2</sup>
Thickness	2–3 μm	2–3 μm	2–3 μm
Pore shape	Filamentous network	Filamentous network	Cylindrical pores

Porosity was determined by reflectance spectroscopy measurements. The average pore radii were obtained from the BJH pore size distribution and in the case of *p*<sup>++</sup>(B) from SFM measurements. Five point BET analysis provided the surface area in the case of *p*<sup>+</sup> and *p*<sup>++</sup>(A). The surface area for *p*<sup>++</sup>(B) samples was estimated from thickness, porosity, pore radii and pore shape. Thickness of the layers was obtained from SEM images and profilometer measurements. Cross-section analysis performed by SEM and SFM provides information about pore shape.

sample.<sup>13</sup> Pores were barely visible by SFM, and the surface roughness was low (root mean square: 0.2–0.5 nm). In order to determine the pore radii of these two kinds of etched samples BET isotherms were recorded revealing pore radii of 2–5 nm (Table 1) and an appearance typical for mesoporous materials (type IV hysteresis between adsorption and desorption branch).<sup>14</sup> SFM images of *p*<sup>++</sup> samples etched at higher current densities displayed large pore diameters of about 200 nm and consequently smaller surface areas. The layer thickness was adjusted by altering the etching time and determined by profilometer measurements. Porosities of the Fabry–Perot layers were obtained by reflectance spectroscopy in conjunction with applying an appropriate effective medium approximation.<sup>15</sup> For this purpose alteration of the effective refractive index was achieved by filling the porous material with various organic solvents differing in refractive index.<sup>10a</sup>

### 2.2. Functionalization of porous silicon

Diffuse reflectance FT-IR spectroscopy was used to monitor the functionalization steps of the porous silicon support. Bromine/air oxidized porous silicon samples display the most prominent broad band of an oxidized porous silicon layer at around 1110 cm<sup>-1</sup> (Si–O–Si vibrational band) and a large vibrational band diagnostic for Si–OH bonds (876 cm<sup>-1</sup>). Moreover, bands at 2256 and 2110 cm<sup>-1</sup> characteristic for O–Si–H and Si–H vibrational bands, respectively indicate the existence of silicon hydride bonds. Because of the large amount of Si–OH bonds due to bromine/air oxidation in contrast to thermal oxidation this surface can be easily functionalized with trimethoxysilanes. After derivatization with trimethoxy-3-bromoacetamidopropylsilane the FT-IR spectrum displays additional bands characteristic of the linker molecule (the amide A band at 3295 cm<sup>-1</sup>, the amide I band at 1656 cm<sup>-1</sup>, and the amide II band at 1546 cm<sup>-1</sup>).

### 2.3. Stability of porous silicon layers in aqueous solution

Freshly etched, hydride-terminated porous silicon hydrolyzes and oxidizes readily upon exposure to aqueous solution accompanied by generation of H<sub>2</sub> and a tremendous decrease in effective optical thickness,  $EOT = 2nl$ , with *n*,

the effective refractive index and  $l$  the thickness of the porous layer.<sup>10a</sup> The porous silicon samples prepared according to the procedure described in the experimental section exhibit a greenish color which changed to blue after prolonged exposure to an aqueous environment. The color change is indicative of oxide formation as comparative studies with thermal oxidation to porous silica revealed. The decrease in EOT and formation of hydrogen might be explained by conversion of silicon to silica leading to a decrease in the effective refractive index of the porous silicon layer ( $n_{\text{Si}} \approx 3.4$ ;  $n_{\text{SiO}_2} \approx 2.2$ ). For instance, the effective optical thickness would decrease by 600 nm employing the effective medium approximation of Looyenga<sup>15</sup> and assuming a change in the refractive index of silicon from  $n_{\text{Si}} = 3.4$  to  $n_{\text{Si}} = 3.0$ ,  $n_{\text{water}} = 1.33$  and a layer thickness of 2500 nm. Additionally, dissolution of the porous layer can result in a thickness decrease of the layer or an increase in porosity causing both a decrease in the effective optical thickness. As shown previously, oxidation and subsequent functionalization of porous silicon can suppress considerably the oxidation and subsequent dissolution in aqueous solution.<sup>10</sup> Besides freshly etched chips we investigated the stability of bromine oxidized and derivatized porous silicon layers. The stability toward corrosion in an aqueous environment decreases in the following order: monomethoxysilane linker modified  $\gg$  trimethoxysilane linker modified  $\gg$  bromine oxidized  $>$  freshly etched porous silicon sample. FT-IR-spectra of bromine oxidized silicon chips still display Si–H<sub>x</sub> and Si–OH bonds, which are both susceptible to oxidation and dissolution giving rise to a significant shift in EOT to smaller values. However, the high stability of surfaces modified with monomethoxysilane linker might be due to a higher surface coverage capping all oxidation sensitive sites on the porous silicon surface. Protection provided by the trimethoxysilane linker is less effective, which is presumably due to insufficient coverage of the surface.

#### 2.4. Quantitative determination of hybridized DNA

The amount of single-stranded DNA that could be captured by surface-immobilized DNA was determined by the fluorescence decay occurring after hybridization of a complementary, fluorescein-labeled DNA strand (Fig. 1).

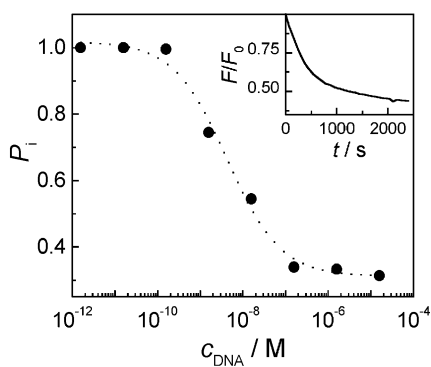


**Figure 1.** Relative decrease in fluorescence intensity  $P_i$  versus concentration of fluorescein labeled DNA (DNA-A') in solution. The inset shows a typical time course of the fluorescence intensity after addition of complementary DNA (DNA-A). The DNA-derivatized porous silicon chip was placed at the bottom of a cuvette and the fluorescence intensity was measured over time after each addition of complementary DNA.

The amount of bound DNA was calculated from Eq. 1:

$$n = V \times \sum_i^n P_i C_i. \quad (1)$$

$n$  denotes the mole number of bound DNA,  $V$  the volume of fluorescein-labeled DNA, and  $P_i$  the ratio of the fluorescence decrease over the initial fluorescence intensity of the  $i$ -th addition which is equivalent to  $dC_i/C_i$ , with  $C_i$ , the initial fluorescein-labeled DNA concentration. The maximum amount of DNA binding to a  $p^+$ -type porous silicon sample derivatized with a complementary DNA strand was estimated to be  $2 \times 10^{-8}$  mol/cm<sup>2</sup>. This number is at least two orders of magnitude higher than that of a monolayer on a flat surface. However, compared to the actual surface area of a porous silicon chip, which is increased by a factor of 4000 (Table 1) the surface coverage of bound DNA is only approx 2% of the whole surface area of the porous silicon layer. It remains to be elucidated if the low DNA surface coverage is due to insufficient linker coverage or due to restricted access of the molecules to the nanoporous material. It should be mentioned that adsorption of DNA in the porous matrix is diffusion-limited. This explains why even at sufficiently high DNA-concentrations ( $10^{-7}$ – $10^{-5}$  M) binding is not yet completed due to the slow mass transport within the porous network. The pore size is only about 2–5 nm in diameter thus retarding the DNA molecules.

#### 2.5. DNA Hybridization

The change in EOT upon hybridization of single-stranded DNA with the complementary DNA linked to a trimethoxy-3-bromoacetamidopropylsilane functionalized  $p^{++}$  porous silicon was monitored by continuously recording interference reflectance spectra vs. time and subsequently performing Fourier transformation (FFT) to extract the EOT data from each spectrum. Independent of the chosen DNA sequences (DNA-A/A', DNA-B/B', DNA-C/C'), the EOT-course (slow rate of background corrosion) does not alter after addition of non-complementary DNA up to a concentration of  $10^{-7}$  M. However, adding the complementary DNA to the derivatized porous silicon layer leads to a considerable decrease in the effective optical thickness (Fig. 2). The binding process is accompanied by an immediate generation of H<sub>2</sub> (bubble formation) and a slow change in color (green to blue) upon addition of the complementary DNA. The decrease in the effective optical thickness does not continue as strongly after rinsing with buffer, which can be explained in terms of diffusion controlled adsorption of DNA in the porous network. Mass transport of DNA molecules is very slow within the chosen concentration regime; the system is far from thermal equilibrium, so that rinsing with buffer removes DNA from solution preventing continued corrosion induced by further DNA-hybridization.

In order to rule out that the buffer composition does not influence the response of the porous silicon chip, we investigated the change in EOT under a variety of different buffer conditions. The control experiments were performed in 1 M NaCl<sub>(aq)</sub>, and in 100 mM phosphate buffer, pH 7.0 with and without 1 mM EDTA indicating that varying the

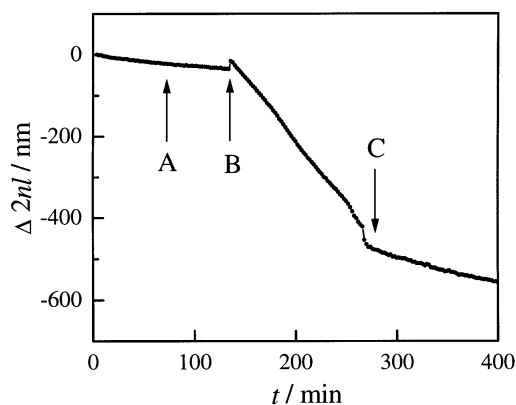


**Figure 2.** Time plot of the change in effective optical thickness ( $\Delta 2nl$ ) of a DNA derivatized porous silicon chip. (A) Addition of  $10^{-7}$  M non-complementary DNA (DNA-A'); (B) addition of  $10^{-7}$  M complementary DNA (DNA-B'); (C) washing with buffer. The measurement was carried out on a  $p^{++}$  porous silicon layer in 100 mM phosphate buffer, pH 7.0 functionalized with trimethoxy-3-bromoacetamidopropylsilane and DNA-B. The arrows indicate when each sample was introduced.

buffer composition does not influence the response of the silicon chips.

## 2.6. Scanning force microscopy

Since the enhanced decrease in effective optical thickness might be due to dissolution of silicon induced by hybridization of DNA resulting in a decreased effective refractive index and a decreased layer thickness, we performed SFM in order to garner information about morphological changes of the surface. Figure 3 shows a sequence of SFM images of a derivatized  $p^{++}$  chip etched at  $500 \text{ mA/cm}^2$  with pore radii of 100–200 nm. The chip was functionalized with DNA receptors (DNA-A) linked to the trimethoxysilane linker. The porous silicon surface was imaged before (Fig. 3(a)), after 30 min, after 1 h (Fig. 3(b)) and after 2 h (Fig. 3(c)) incubation with a  $10^{-7}$  M solution of the complementary DNA-strand (DNA-A'). Exposure of the chip to complementary DNA for 30 min did not result in any detectable mesoscopic changes in topography, although the effective optical thickness decreased by 200 nm. However, after 1 h incubation channel-like structures appeared on the porous surface concomitant with a change in effective optical thickness of 400 nm. The channels can be interpreted in terms of fused pores due to loss of complete pore walls. After 2 h incubation the reflectance spectrum of the sample did not display fringes anymore and the surface appeared matte. Furthermore, the pore size increased tremendously showing clefts or pores with lateral dimensions larger than  $4 \mu\text{m}$ . Eventually the porous layer dissolved completely leaving a polished surface behind. In the case of a  $p^+$  sample etched at  $50 \text{ mA/cm}^2$  (25% ethanolic HF) DNA hybridization on the surface caused similar structural changes leaving larger holes of sometimes regular structures behind. The results of the reflectance spectroscopy together with the SFM images demonstrate that the specific binding of DNA to the porous silicon surface led to a dramatic corrosion acceleration. We postulate that the corrosion initiates presumably at spots characterized by incomplete linker coverage and the presence of Si–H<sub>x</sub> groups.

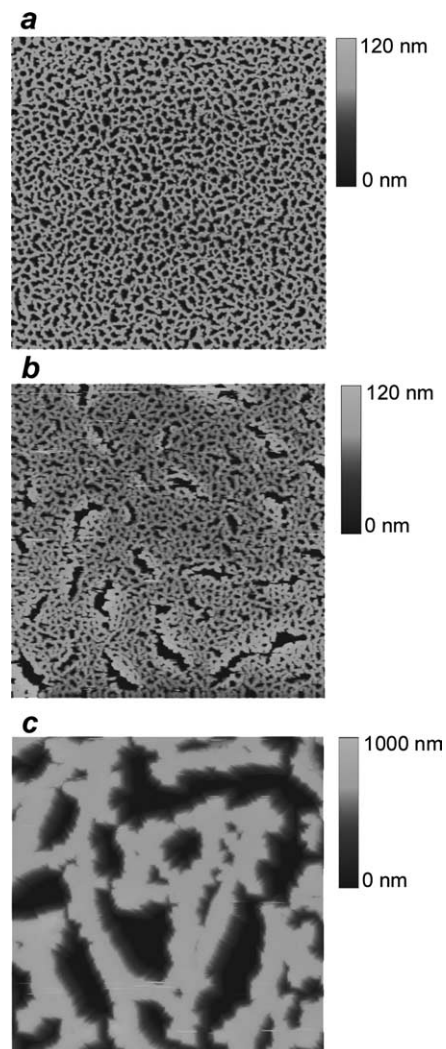


**Figure 3.** SFM images (TappingMode) before and after exposure of the surface to complementary DNA. Porous silicon samples ( $p^{++}$ ) were anodized at  $500 \text{ mA/cm}^2$  in order to obtain larger pores which were easier to image because of the larger surface features. The surface was derivatized with trimethoxy-3-bromoacetamidopropylsilane and DNA-A. (a) Image of the functionalized porous silicon layer before incubation with complementary DNA-A. (b) Porous silicon layer after 1 h incubation with DNA-A ( $10^{-7}$  M). The effective optical thickness decreased by app. 400 nm. (c) Porous silicon layer after 2 h incubation. No fringes could be observed after the incubation time; the surface appeared to be matte. All images were  $14 \times 14 \mu\text{m}^2$  in size.

## 2.7. Influence of charges

One parameter influencing the rate of oxidation and dissolution induced by DNA hybridization might be the dopant concentration (boron) in the silicon wafers—the carrier charge influence. We investigated the change in effective optical thickness upon binding of complementary DNA on two different types of silicon wafers:  $p^+$  (3–6  $\Omega \text{ cm}$ ) and  $p^{++}$  (0.6–1.0  $\text{m}\Omega \text{ cm}$ ) (Fig. 4). Reflectance spectroscopy could not be performed on  $n$ -type silicon since the roughness of the top and bottom surface were too high to obtain fringe patterns. In order to provide similar pore diameters and surface areas for the two wafer types, we have chosen appropriate etching conditions as reported previously (Table 1).<sup>10a</sup> In the case of the  $p^+$ -silicon chip, the



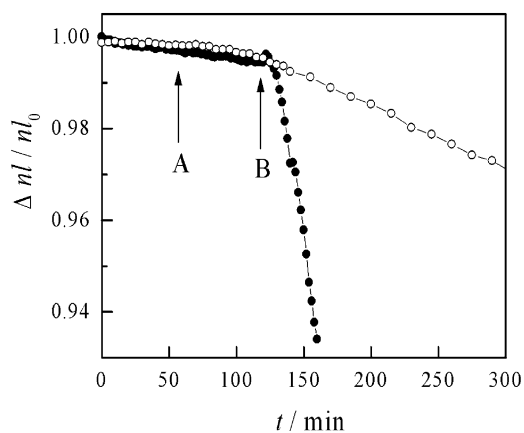


**Figure 4.** Change in effective optical thickness of a functionalized silicon chip (DNA-B) upon addition of non-complementary (DNA-A') and complementary DNA (DNA-B') in 100 mM phosphate buffer, pH 7.0. (●)  $p^+$  chip; (○)  $p^{++}$ (A) chip. (A) addition of non-complementary DNA-A' ( $10^{-7}$  M); (B) addition of complementary DNA-B' ( $10^{-7}$  M).

slope of the initial change in EOT before addition of complementary DNA was  $-0.17$  nm/min. The negative slope increased by a factor of 3.5 ( $-0.6$  nm/min) upon addition of complementary DNA. However, performing the same experiment on a  $p^{++}$ (A) chip, the negative slope was increased by a factor of 15 ( $-3.1$  nm/min), although the initial slope ( $-0.21$  nm/min) was similar to that of the  $p^+$  chip.

Since the dopant concentration of the silicon wafer alters the response of the chip upon binding of complementary DNA considerably, we hypothesized that accumulation of surface charges might be the key event. Given the fact that DNA is a polyanionic molecule, a significant quantity of charges are immobilized on the porous silicon surface upon hybridization. In order to establish whether charge accumulation indeed induces a higher surface oxidation rate, we conducted hybridization experiments on porous silicon surfaces using complementary PNA (peptide nucleic acid, PNA-C') instead of DNA, which carries no backbone phosphate charges and binds even stronger to the immobilized DNA (DNA-C).  $p^{++}$ (A) silicon wafers were chosen to attain the highest possible signal to noise ratio. In contrast to the formation of the DNA duplex, the oxidation rate did not alter upon addition of complementary PNA up to a concentration of  $10^{-7}$  M (Fig. 5).<sup>16</sup> In order to confirm that PNA was bound to the complementary DNA on the surface and saturated all available DNA binding sites, we added DNA-C after PNA hybridization to the chip. Again, no change in EOT could be observed indicating that the immobilized DNA binding sites were engaged in the PNA-DNA assembly and thus were not available for further hybridization with the DNA-C.

Further evidence for the hypothesis that immobilized negative charges on the surface are the reason for the observed acceleration of corrosion of the porous layer was given by a DNA hybridization experiment performed in the presence of 5 mM  $MgCl_2$  showing no significant decrease in EOT upon binding. Since  $Mg^{2+}$  ions bind to the DNA duplex and neutralize the negative charges of the phosphate groups, the shielding of negative charge accumulation at the

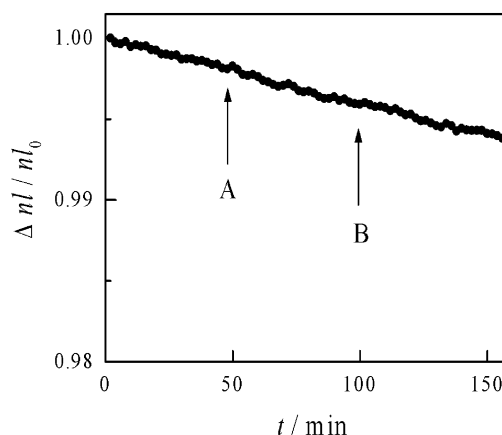


**Figure 5.** Change in effective optical thickness of a functionalized  $p^{++}$ (A)-silicon chip (DNA-C) upon addition of (A)  $10^{-7}$  M PNA-C' and (B)  $10^{-7}$  M DNA-C' in 100 mM phosphate buffer, pH 7.0. The arrow indicates the time when the sample was introduced.

porous silicon surface prevents an increase in oxidation/dissolution rate upon addition of complementary DNA. Moreover, removing the  $Mg^{2+}$  ions from the DNA duplex by rinsing the silicon chip with an EDTA containing buffer reactivated the charge-induced acceleration of surface oxidation/dissolution.

## 2.8. Outlook for biosensor applications

The discovery of these fairly dramatic structural and consequently optical changes of the porous silicon layers induced by molecular recognition of small DNA strands led us to question, whether this mechanism has potential utility in analytical applications. Reflectance spectroscopy is typically not useful for the detection of small molecules such as oligonucleotides, since such molecular interactions cause only very small changes in the refractive index of a thin layer. On the other hand, the corrosion enhanced by DNA recognition amplifies the binding signal and thus increases significantly the sensitivity for small molecule detection by reflectance spectroscopy. For instance, the expected increase in EOT for DNA binding with regard to effective medium approximations is less than 0.1 nm, in contrast to a decrease in EOT of about 200–400 nm in the present case. In our studies, the first notable change in the optical thickness of the porous film could be observed at concentrations of about  $10^{-11}$  M of complementary DNA using a derivatized  $p^{++}$ (A) silicon wafer (Fig. 6). The negative slope of the EOT versus time course increases by a factor of 6 in the presence of  $10^{-10}$  M DNA compared to background corrosion. Further increasing the DNA concentration in solution enhances the corrosion rate even more. Compared to the initial oxidation rate of  $-0.18$  nm/min, the rate is enhanced by a factor of 20 at a DNA concentration of  $10^{-7}$  M in solution. At first sight, a detection limit of 0.1 nM does not seem to be remarkably sensitive. But considering the fact that the absolute surface area is about  $0.4$  m<sup>2</sup> the number of molecules necessary for a complete coverage exceeds by far the number of molecules available in solution ( $6 \times 10^{10}$  molecules at a concentration of  $10^{-10}$  M with a volume of 1 ml). Assuming a homogeneous distribution of all molecules on the surface, this would result in a coverage of about  $10^6$  mol/mm<sup>2</sup>. From this point

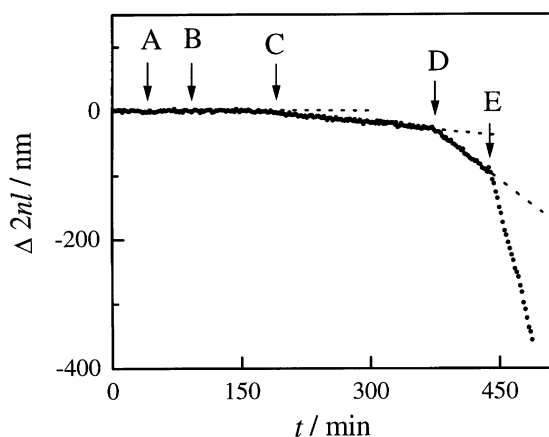


**Figure 6.** Change in effective optical thickness of a functionalized  $p^{++}$ -silicon chip (DNA-C) upon addition of increasing concentrations of complementary DNA-C' in 100 mM phosphate, pH 7.0. (A) DNA-B; (B)  $10^{-12}$  M DNA-C; (C)  $10^{-11}$  M DNA-C; (D)  $10^{-10}$  M DNA-C and (E)  $10^{-7}$  M DNA-C. The arrow indicates the time when the sample was introduced.

of view 0.1 amol of DNA seems to have been detected on  $1 \text{ mm}^2$  porous silicon chip.<sup>17</sup> Even though our results suggest that the corrosion-enhanced signal amplification can provide a highly sensitive process for unlabeled DNA detection, several practical limitations need to be overcome before practical utility of this new sensing technology can be fully realized. Although using the methods described here, a skilled personnel can often minimize the batch-to-batch materials differences that can cause significant variations in DNA-enhanced porous silicon corrosion rates and detection responses, we believe that the etching and surface chemical modification methods are the two critical areas that need to be further improved before reproducible porous silicon sensor elements could be routinely fabricated for use in biosensing applications.

### 2.9. Postulated mechanism of DNA-enhanced porous silicon dissolution

The experiments described above show that the large decrease in EOT are attributed to the corrosion of the porous silicon layer accelerated by the binding of negatively charged molecules. Moreover, our studies strongly suggest that exposed Si-H bonds are required in this process. Allongue et al. proposed a chemical reaction mechanism to explain the dissolution of hydride terminated porous silicon surfaces (Fig. 7).<sup>18</sup> According to this formalism a water molecule hydrolyses a Si-H<sub>2</sub> group producing H<sub>2</sub>. This is followed by the breakage of a Si-Si bond and generation of a new Si-H bond by attack of a second water molecule. Dissolution of the primary product HSi(OH)<sub>3</sub> involves attack of another water molecule. A second molecule of H<sub>2</sub> is produced by decomposition of HSi(OH)<sub>3</sub> in aqueous solution. The most remarkable feature of this reaction pathway is that the surface stays hydride terminated, which opens the way for further chemical dissolution without passivation. This mechanism is consistent with our observed results of hydrogen evolution and the persistence of surface Si-H<sub>x</sub> FT-IR bands during the course of the corrosion process. According to Allongue et al. a positive polarization of the Si atom which has already bound an OH-group

facilitates the attack of the second water molecule to break the Si-Si bond. We propose that the phenomena of DNA induced dissolution of porous silicon can be explained on this basis. Accumulation of negative charges on the silicon surface due to DNA hybridization can enhance the polarization of the silicon surface, for instance by the attracting positive charges in the vicinity of the binding event. The increase of majority carriers (depletion layer) at the surface could facilitate the nucleophilic attack by water molecules. This mechanistic model is also consistent with the observed higher susceptibility of  $p^{++}$  type porous silicon since more carriers are available to support the nucleophilic attack in an aqueous environment.

It is known that hydroxide ions also serve as a catalyst for the above described corrosion process of porous silicon. In order to compare the surface morphology of the porous silicon surface after DNA treatment with those treated with aqueous NaOH (pH 11), we investigated the porous silicon surfaces by SMF. The study revealed similar morphological changes for both the DNA treated chips and the sodium hydroxide treated samples involving the formation of channels.

### 2.10. Conclusion

Our studies show that hybridization of DNA oligonucleotides in neutral aqueous solutions with complementary sequences immobilized on highly doped  $p$ -type porous silicon matrix can result in a large decrease in effective optical thickness due to enhanced corrosion (oxidation-hydrolysis) of the porous silicon layer. The observed phenomenon is an example of an active sensor matrix in which the molecular recognition signal is transduced and amplified by a profound change in the chemical reactivity and physical property of the solid support itself. The detection of unlabeled DNA oligonucleotides down to concentrations below 0.1 nM by simple interferometric measurements suggests potential applications of this method in biosensing. Future advances in reproducible etching and surface chemical functionalization methods are needed before practical device applications can be realized.

## 3. Experimental

### 3.1. Etching procedure

Two different types of  $p$ -type silicon wafers (boron-doped, orientation (100)) with resistivities in the range of 3–6  $\Omega \text{ cm}$  ( $p^+$ ) and 0.6–1.0  $\text{m}\Omega \text{ cm}$  ( $p^{++}$ ), respectively were used to fabricate porous silicon by an anodic etch in ethanolic HF solution. Prior to the etching procedure the silicon wafers were rinsed thoroughly with ethanol and dried under a stream of nitrogen. As reported previously,<sup>10a</sup> silicon wafers with an exposed area of  $1.5 \text{ cm}^2$  were contacted on the backside with a strip of aluminum foil and mounted in a Teflon etching cell. A platinum mesh served as counter electrode in order to provide a homogeneous electrical field.  $P^+$  wafers were etched in HF/ethanol 1:1 (v/v), and  $p^{++}$  wafers in HF/ethanol 3:1 (v/v), prepared from 48% aqueous HF. Galvanostatic anodization was performed in the dark with current densities around 50–70  $\text{mA/cm}^2$  ( $p^+$ ) and



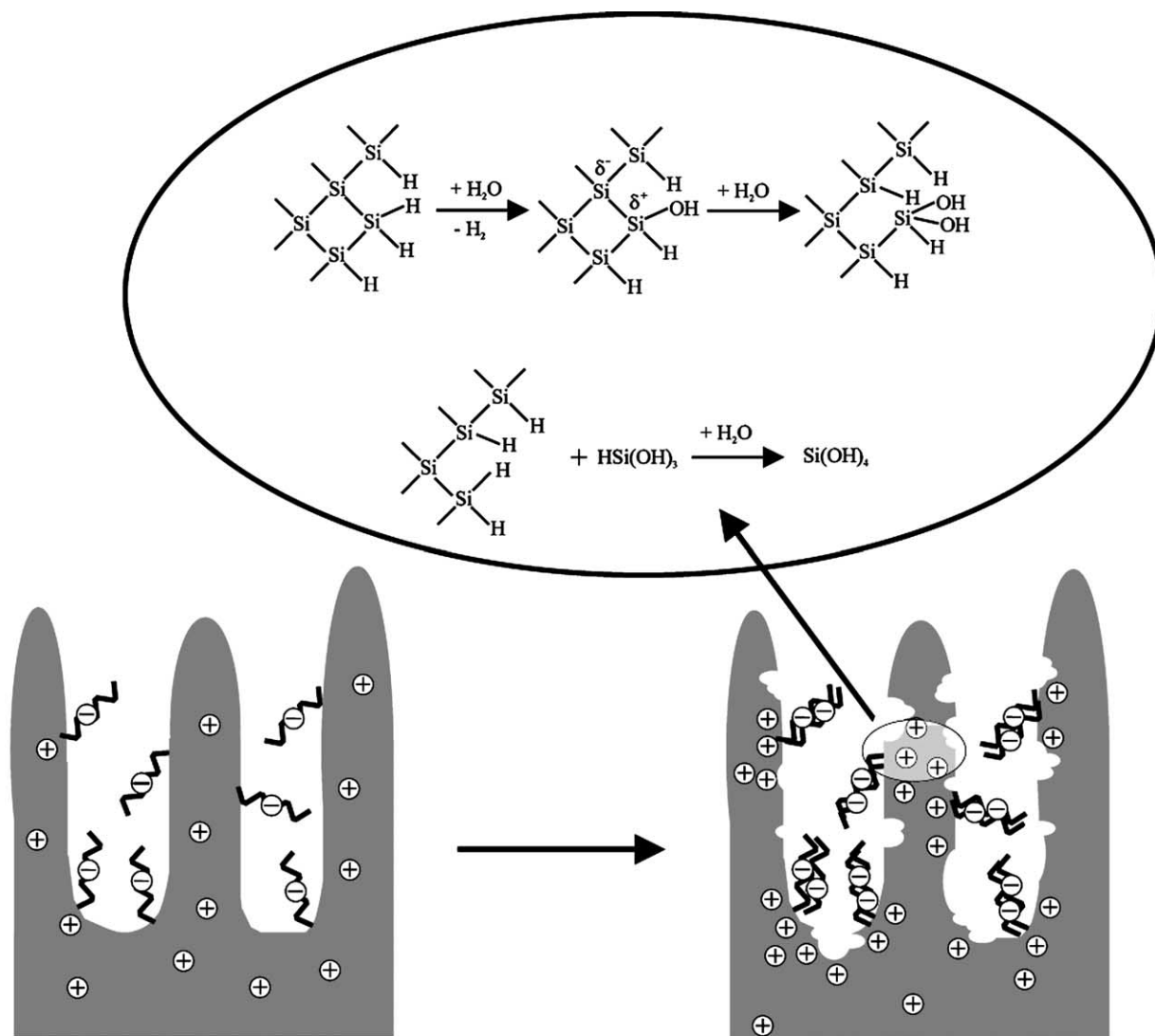


**Figure 7.** The proposed mechanism for the corrosion enhancement by DNA hybridization on *p*-type porous silicon surfaces. The reaction pathway describing the dissolution of silicon in an aqueous environment was first proposed by Allongue et al.<sup>18</sup> The binding of DNA is postulated to result in the accumulation of majority carriers in the vicinity of the molecular recognition event thus enhancing the polarization of the Si–H bonds and facilitating the nucleophilic attack by water molecules.

150–600 mA/cm<sup>2</sup> ( $p^{++}$ ), while the etching time was adjusted in order to obtain the approximate same layer thickness. After etching the samples were rinsed thoroughly with ethanol and methylene chloride, then dried under a stream of nitrogen.

### 3.2. Oxidation procedure

After anodization, the silicon surface is predominately hydride-terminated. This surface is sensitive to oxidation and dissolution upon exposure to aqueous solution. To increase the surface stability, and further functionalize the sample by silane chemistry the porous layers were exposed to  $\text{Br}_2$  vapor for 1 h followed by air oxidation for 30 min. The oxidized samples were rigorously rinsed with methylene chloride, acetone, and methanol and then dried under a stream of nitrogen. These hydroxy terminated porous silicon surfaces were stable under ambient conditions in air for several days.

### 3.3. Functionalization of oxidized porous silicon

Functionalization of the bromine oxidized porous silicon chips with a trimethoxysilane linker was performed by placing the samples in 50 mM trimethoxy-3-bromoacetamidopropylsilane dissolved in toluene for 10 min. Afterwards, the samples were rinsed first with toluene, then ethanol, water and finally acetone and subsequently dried under a stream of nitrogen. The porous silicon samples were then immersed in an aqueous solution of the desired 5'-thiophosphate oligonucleotide (DNA) in water/dimethyl formamide/5%  $\text{NaHCO}_3$  (1/1/0.5) for 1 h to immobilize the single-stranded DNA. After the reaction, the chips were washed 5× with 2 ml DMF, DMF/water (1:1), and water.

### 3.4. DNA Sequences

All DNA sequences were purchased from Operon Technologies, Inc. and HPLC purified. For hybridization

experiments, three 5'-thiophosphate terminated DNAs (DNA-A sequence: 5'-pGC CAG AAC CCA GTA GT-3', DNA-B sequence: 5'-pCC GGA CAG AAG CAG AA-3', DNA-C sequence: 5'-pTAG TTG TGA CGT ACA) and their corresponding complementary strands (DNA-A', DNA-B', and DNA-C') were chosen so that no hairpin loop formation or self-dimerization can occur. For PNA-DNA hybridization experiments, a purified PNA (PNA-C': H-TGT ACG TCA CAA CTA-NH<sub>2</sub>, a gift from Prof. P. Nielsen, University of Copenhagen, Denmark) complementary to DNA-C was used as received.

### 3.5. Fluorescence spectroscopy

Independent proof for DNA hybridization was obtained from recording the fluorescence decay of a fluorescein-labeled complementary DNA strand in solution due to duplex formation on a porous silicon chip mounted at the bottom of a regular fluorescence cuvette. The  $p^+$ -type silicon chip was etched at 50 mA/cm<sup>2</sup> for 2 min. The fluorescence of the fluorescein-labeled DNA in solution was monitored on an Aminco/Bowman luminescence spectrometer with 4 nm bandwidth equipped with a water-jacketed sample chamber thermostatted at 25 °C. Fluorescence was excited with 490 nm and the emission was read at 520 nm.

### 3.6. FT-IR Spectroscopy

FT-IR spectra were acquired with a Nicolet Model 550 Magna Series II FT-IR instrument in diffused reflectance mode (Spectra-Tech diffuse reflectance attachment). Diffuse reflectance absorption spectra are reported in Kubelka-Munk units. The FT-IR sample compartment was purged with nitrogen.

### 3.7. Interferometric reflectance spectra

Interferometric reflectance spectra of porous silicon were recorded by using an Ocean Optics spectrometer S 1000 fitted with a bifurcated fiber optic probe. A tungsten light source was focused via one of the fibers onto the center of a porous silicon surface with a spot size of approximately 1–2 mm. Spectra were recorded with a CCD-detector in the wavelength range of 400–1200 nm. The illumination of the surface as well as the detection of the reflected light was performed along an axis coincident with the surface normal. The effective optical thickness was obtained using Fast Fourier Transformation (FFT) of the spectra. The hybridization experiments were performed in a plexiglass fluid cell and the DNA was injected by a syringe.

### 3.8. Scanning force microscopy

SFM images were obtained under ambient conditions using a Nanoscope IIIa Multimode scanning probe microscope (Digital Instruments, Santa Barbara, CA) operating in TappingMode™ and contact mode. For TappingMode™ silicon NanoProbe™ tips (TESP, Digital Instruments) were used as purchased. Several tips were used to assure reproducible results. Contact mode was performed using microfabricated oxide sharpened V-shaped silicon nitride tips with a nominal tip radius of about 5–20 nm and a

nominal spring constant of 0.06 N/m (NP-S, Digital Instruments). The applied force was as low as possible.

### Acknowledgements

We thank Professor M. Sailor for helpful and stimulating discussions and Professor P. Nielsen for the kind gift of PNA. This work was supported by grants from the Office of Naval Research (N00014981073) and (N000149511293) through the Multidisciplinary University Research Initiative (MURI-95) of the Department of Defense. C.S. and N.H.V. thank the Deutsche Forschungsgemeinschaft (DFG) and A.J. the Fonds der Chemischen Industrie for postdoctoral Fellowships.

### References and notes

- For a review and comparison of techniques combining nucleic acid amplification and detection see: Schweitzer, B.; Kingsmore, S. *Curr. Opin. Biotechnol.* **2001**, *12*, 21–27.
- (a) Player, A. N.; Shen, L. P.; Kenny, D.; Antao, V. P.; Kolberg, J. A. *J. Histochem. Cytochem.* **2001**, *49*, 603–611. (b) Stojanovic, M. N.; De Prada, P.; Landry, D. W. *ChemBioChem* **2001**, *2*, 411–415. (c) Umek, R. M.; Lin, S. W.; Vielmetter, J.; Terbruegge, R. H.; Irvine, B.; Yu, C. J.; Kayyem, J. F.; Yowanto, H.; Blackburn, G. F.; Farkas, D. H.; Chen, Y.-P. *J. Mol. Diagn.* **2001**, *3*, 74–84.
- (a) Elghanian, R.; Storhoff, J. J.; Mucic, R. C.; Letsinger, R. L.; Mirkin, C. A. *Science* **1997**, *277*, 1078–1081. (b) Taton, T. A.; Mirkin, C. A.; Letsinger, R. L. *Science* **2000**, *289*, 1757–1760.
- Saghatelian, A.; Guckian, K. M.; Thayer, D. A.; Ghadiri, M. R. *J. Am. Chem. Soc.* **2003**, *125*, 344–345.
- Wollenberger, U.; Lisdat, F.; Scheller, F. W. *EXS* **1997**, *81*, 45.
- (a) Minami, H.; Sugawara, M.; Odashima, K.; Umezawa, Y.; Uto, M.; Michaelis, E. K.; Kuwana, T. *Anal. Chem.* **1991**, *63*, 2787. (b) Cornell, B. A.; Braach-Maksvytis, V. L. B.; King, L. G.; Osman, P. D. J.; Raguse, B.; Wiczorek, L.; Pace, R. J. *Nature* **1997**, *387*, 580. (c) Kasianowicz, J. J.; Brandin, E.; Branton, D.; Deamer, D. W. *Proc. Natl. Acad. Sci. U.S.A.* **1996**, *93*, 13770. (d) Schalkhammer, T.; Weiss-Wichert, C.; Smetazko, M.; Valina-Saba, M. *Proc. SPIE-Int. Soc. Opt. Eng.* **1997**, *2976*, 117. (e) Gu, L.-Q.; Braha, O.; Conlan, S.; Cheley, S.; Bayley, H. *Nature* **1999**, *398*, 686. (f) Bayley, H.; Martin, C. R. *Chem. Rev.* **2000**, *100*, 2575. (g) Sánchez-Quesada, J.; Ghadiri, M. R.; Bayley, H.; Braha, O. *J. Am. Chem. Soc.* **2000**, *122*, 11756. (h) Gu, L.-Q.; Cheley, S.; Bayley, H. *Science* **2001**, *291*, 636. (i) Vercootere, W.; Winters-Hilt, S.; Olsen, H.; Deamer, D.; Haussler, D.; Akesson, M. *Nat. Biotechnol.* **2001**, *19*, 248. (j) Howorka, S.; Cheley, S.; Bayley, H. *Nat. Biotechnol.* **2001**, *19*, 636. (k) Cornell, B. A. *Opt. Biosens.* **2002**, 457.
- (a) Beale, M. I. J.; Benjamin, J. D.; Uren, M. J.; Chew, N. G.; Cullis, A. G. *J. Cryst. Growth* **1985**, *73*, 622. (b) Canham, L. T. *Appl. Phys. Lett.* **1990**, *57*, 1046. (c) Smith, R. L.; Collins, S. D. *J. Appl. Phys.* **1992**, *71*, R1. (d) Searson, P. C. *Advances in Electrochemical Sciences and Engineering*. 1994 VCH: Mannheim.
- (a) Kim, N. Y.; Laibinis, P. E. *J. Am. Chem. Soc.* **1998**, *120*, 4516. (b) Song, J. H.; Sailor, M. J. *J. Am. Chem. Soc.* **1998**,

- 120, 2376. (c) Buriak, J. M.; Allen, M. J. *J. Am. Chem. Soc.* **1998**, *120*, 1339. (d) Gurtner, C.; Wun, A. W.; Sailor, M. J. *Angew. Chem., Int. Ed.* **1999**, *38*, 1966. (e) Buriak, J. M.; Stewart, M. P.; Geders, T. W.; Allen, M. J.; Choi, H. C.; Smith, J.; Raftery, D.; Canham, L. T. *J. Am. Chem. Soc.* **1999**, *121*, 11491. (f) Saghatelian, A.; Buriak, J. M.; Ghadiri, M. R. *Tetrahedron* **2001**, *57*, 5131–5136. (g) Buriak, J. M. *Chem. Rev.* **2002**, *102*, 1271.
9. (a) Beattie, K. L.; Beattie, W. G.; Meng, L.; Turner, S. L.; Coral-Vazquez, R.; Smith, D. D.; McIntyre, P. M.; Dao, D. D. *Clin. Chem.* **1995**, *41*, 700. (b) Starodub, N. F.; Fedorenko, L. L.; Starodub, V. M.; Dikij, S. P. *NATO ASI Ser., Ser. 3* **1997**, *42*, 91. (c) Schoning, M. J.; Ronkel, F.; Crott, M.; Thust, M.; Schultze, J. W.; Kordos, P.; Luth, H. *Electrochim. Acta* **1997**, *42*, 3185. (d) Canham, L. T. *EMIS Datarev. Ser.* **1997**, *18*, 371. (e) Noort, D. V.; Welin-Klintstrom, S.; Arwin, H.; Zangoie, S.; Lundstrom, I.; Mandenius, C.-F. *Biosens. Bioelectron.* **1998**, *13*, 439. (f) Thust, M.; Schoning, M. J.; Schroth, P.; Malkoc, U.; Dicker, C. I.; Steffen, A.; Kordos, P.; Luth, H. *J. Mol. Catal. B: Enzym.* **1999**, *7*, 77. (g) Starodub, V. M.; Fedorenko, L. L.; Sisetskiy, A. P.; Starodub, N. F. *Sens. Actuators, B: Chem.* **1999**, *B58*, 409. (h) Knott, M. *New Sci.* **1997**, *153*, 36. (i) Desai, T. A.; Hansford, D. J.; Leoni, L.; Essenpreis, M.; Ferrari, M. *Biosens. Bioelectron.* **2000**, *15*, 453. (j) Schoning, M. J.; Kurowski, A.; Thust, M.; Kordos, P.; Schultze, J. W.; Luth, H. *Sens. Actuators, B* **2000**, *B64*, 59. (k) Chan, S.; Fauchet, P. M.; Li, Y.; Rothberg, L. J.; Miller, B. L. *Phys. Status Solidi A* **2000**, *182*, 541. (l) Zairi, S.; Martelet, C.; Jaffrezic-Renault, N.; M'Gaieth, R.; Maaref, H.; Lamartine, R. *Thin Solid Films* **2001**, *383*, 325. (m) Chan, S.; Horner, S. R.; Fauchet, P. H.; Miller, B. L. *J. Am. Chem. Soc.* **2001**, *123*, 11797–11798. (n) Jenison, R.; Yang, S.; Haeberli, A.; Polisky, B. *Nat. Biotechnol.* **2001**, *19*, 62–65. (o) Starodub, V. M. *NATO Sci. Ser., II: Math., Phys. Chem.* **2002**, *57*, 383. (p) Xiao, C.; Boukherroub, R.; Wojtyk, J. T. C.; Wayner, D. D. M.; Luong, J. H. T. *Langmuir* **2002**, *18*, 4165. (q) Schmedake, T. A.; Cunin, F.; Link, J. R.; Sailor, M. J. *Adv. Mater.* **2002**, *14*, 1270.
10. (a) Janshoff, A.; Dancil, K.-P. S.; Steinem, C.; Greiner, D. P.; Lin, V. S.-Y.; Gurtner, C.; Motesharei, K.; Sailor, M. J.; Ghadiri, M. R. *J. Am. Chem. Soc.* **1998**, *120*, 12108. (b) Dancil, K.-P. S.; Greiner, D. P.; Sailor, M. J. *J. Am. Chem. Soc.* **1999**, *121*, 7925.
11. Theiss, W. *Surf. Sci. Rep.* **1997**, *29*, 91.
12. Lin, V. S.-Y.; Motesharei, K.; Dancil, K.-P. S.; Sailor, M. J.; Ghadiri, M. R. *Science* **1997**, *278*, 840.
13. Campbell, S. D.; Jones, L. A.; Nakamichi, E.; Wei, F.-X.; Zaijchowski, L. D.; Thomas, D. F. *J. Vac. Sci. Technol., B* **1995**, *13*, 1184.
14. Gregg, S. J.; Sing, K. S. W. *Adsorption, Surface Area, and Porosity*. 2nd ed.; Academic: New York, 1982.
15. Looyenga, H. *Physica* **1965**, *31*, 401.
16. Egholm, M.; Buchardt, O.; Christensen, L.; Behrens, C.; Freier, S. M.; Driver, D. A.; Berg, R. H.; Kim, S. K.; Norden, B.; Nielsen, P. E. *Nature* **1993**, *365*, 566.
17. Since this calculation does not take into account that only part of the molecules will be bound to the surface in the observed time period based on the formed diffusion layer in front of the surface and the equilibrium constant, the amount of bound DNA molecules is most likely even lower than the calculated one.
18. Allongue, P.; Costa-Kieling, V.; Gerischer, H. *J. Electrochem. Soc.* **1993**, *140*, 1018.

# Regioregular poly(thiophene-3-alkanoic acid)s: water soluble conducting polymers suitable for chromatic chemosensing in solution and solid state

Paul C. Ewbank, Robert S. Loewe, Lei Zhai, Jerry Reddinger, Geneviève Sauvé and Richard D. McCullough\*

Department of Chemistry, Carnegie Mellon University, 4400 Fifth Ave., Pittsburgh, PA 15213, USA

Received 26 March 2004; revised 2 July 2004; accepted 20 August 2004

Available online 23 September 2004

**Abstract**—Regioregular polythiophenes with pendant carboxylic acid functionality, poly(thiophene-3-propionic acid) (PTPA, **3**) and poly(thiophene-3-octanoic acid) (PTOA, **4**), were prepared as water soluble conducting polymers and their chemosensory response was studied. Treatment with aqueous base generated intensely colored water soluble conducting polymer salts, with the color varying both as a function of counter ion size and length of the carboxyalkyl substituent. PTPA showed a different colorimetric response to each of the alkali earth metals whereas the longer chain PTOA was only sensitive to ions larger than  $\text{Et}_4\text{N}^+$ . Distinct color changes were also noted in studies of divalent cations known to selectively bind carboxylates, such as  $\text{Zn}^{2+}$ ,  $\text{Mn}^{2+}$ , and  $\text{Cd}^{2+}$ . Cast films of PTPA have been found to act as sensors to acid vapor ( $\Delta\lambda_{\text{max}}$  of up to 132 nm). IR shows that the polymer self-assembles upon HCl vapor exposure, and that the process is completely reversible, leading to a good solid-state sensor for acids. This work demonstrates that regioregular polythiophenes containing acid side-chains have tremendous potential in the development of new sensors.

© 2004 Elsevier Ltd. All rights reserved.

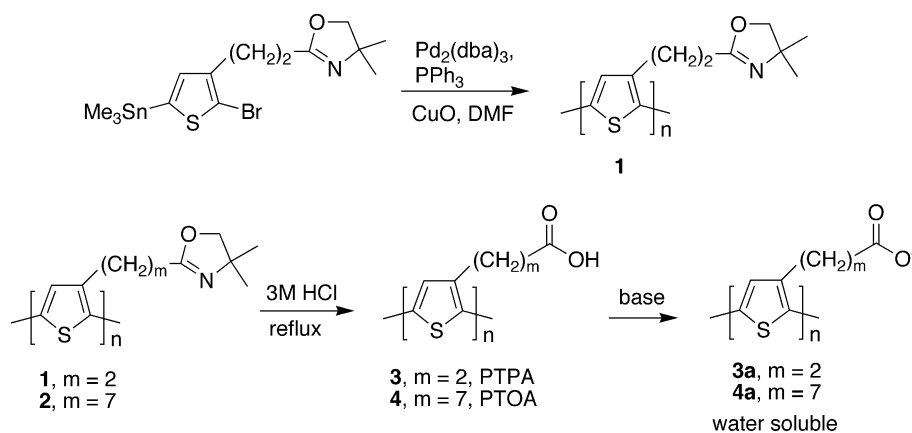
## 1. Introduction

Due to their excellent electrical properties, regioregular poly(3-alkylthiophene)s are rapidly being developed into new products with applications such as field effect transistors, sensors, solar cells and new electrostatic dissipative coatings and materials.<sup>1–8</sup> Their high conductivities and low band gaps are a consequence of their ability to self-assemble into  $\pi$ -stacked, planar aggregates.<sup>9–11</sup> Previous work in our lab has shown that both conformational order and solid state organization in regioregular polythiophene derivatives are remarkably sensitive to the placement and nature of the substituent chains.<sup>12,13</sup> This sensitivity provides the opportunity to design new conducting polymers in which self-assembly (and hence the color) is controlled by environmental factors. Changes in conformation of conjugated systems are readily detected not only by conductivity changes, but also by optical absorption changes. Various polythiophene derivatives are known to show striking chromatic responses, such as piezochromism (changes in pressure),<sup>6,14,15</sup> photochromism (changes in light),<sup>6,16,17</sup> electrochromism (changes in

electrical potential),<sup>18–20</sup> thermochromism (changes in temperature),<sup>6,21–25</sup> ionochromism (changes in chemical moieties),<sup>12,26–30</sup> biochromism,<sup>6,31–35</sup> and affinity chromism.<sup>36</sup> Chromatic responses are particularly useful since discernable changes are generally apparent to the human eye, obviating the need for expensive instrumentation and really represent an opportunity for chemists to develop new sensors.<sup>6,37,38</sup> We are particularly interested in developing sensors based on head-to-tail regioregular polythiophenes (rr-PTs).<sup>10</sup> These polymers do not have coupling defects, have a tendency to form elongated supermolecular structures with optimal orbital overlap and small HOMO–LUMO gaps,<sup>39–41</sup> and should exhibit a very wide response range between the minimally and maximally perturbed states, providing for excellent sensitivity. Of rr-PTs, the water soluble salts of carboxylic acid functionalized regioregular polythiophenes demonstrate one of the largest optical shifts in response to ions.<sup>26</sup> Here, we study the ionochromism of these polymers with the intent to understand the underlying mechanism of chromatic changes. Two representative polymers with differing substituent lengths were selected: head-to-tail coupled poly(thiophene-3-propionic acid) (PTPA) and head-to-tail coupled poly(thiophene-3-octanoic acid) (PTOA). The synthesis, characterization, and studies of ion binding by UV–vis and IR spectroscopy are reported.

**Keywords:** Conducting polymers; Polythiophenes; Sensors.

\* Corresponding author. Tel.: +1-4122685124; fax: +1-4122686897; e-mail: [rm5g@andrew.cmu.edu](mailto:rm5g@andrew.cmu.edu)



**Scheme 1.** Synthesis of the water soluble regioregular polythiophenes.

**Table 1.** UV/vis  $\lambda_{\text{max}}$  (nm) of PTPA and PTOA in water with 1 equiv of base ( $\text{R}^+\text{OH}^-$ ) per carboxylic acid residue

Polymer	$\text{NH}_4^+$	$\text{Me}_4\text{N}^+$	$\text{Et}_4\text{N}^+$	$\text{Pr}_4\text{N}^+$	$\text{Bu}_4\text{N}^+$	$\text{Li}^+$	$\text{Na}^+$	$\text{K}^+$	$\text{Cs}^+$
PTPA ( <b>3</b> )	550	486	476	446	426	546	532	512	506
PTOA ( <b>4</b> )	—	556	554	534	513	556	554	554	—

## 2. Results and discussion

### 2.1. Synthesis

Regioregular (rr) head-to-tail (HT) poly(thiophene-3-propionic acid) (PTPA, **3**) was synthesized by Stille/CuO polymerization of an oxazoline protected monomer followed by acid hydrolysis to afford a violet solid in yield of greater than 80%.<sup>26</sup> Regioregular head-to-tail poly(thiophene-3-octanoic acid) (PTOA, **4**), was prepared as previously described.<sup>42</sup> Although the polymers were not very soluble in common organic solvents, they were both soluble in aqueous base (species **3a** and **4a**) (Scheme 1).

### 2.2. Spectroscopic behavior in solution

Intensely colored solutions were formed when PTPA (**3**) or PTOA (**4**) reacted with 1 equiv alkali metal hydroxide or tetraalkylammonium hydroxide per carboxylic acid group, with colors ranging from violet to yellow depending on the size of the counter ion (Table 1). For PTPA, the observed  $\lambda_{\text{max}}$  varied over a range of  $\sim 124$  nm when the size of the ammonium counterion increased from  $\text{NH}_4^+$  to  $\text{Bu}_4\text{N}^+$ , and over a range of  $\sim 40$  nm when the alkali metal size increased from  $\text{Li}^+$  to  $\text{Cs}^+$ . For PTOA, on the other hand, the observed  $\lambda_{\text{max}}$  did not deviate much from 556 nm (violet color) until the ion size exceeded  $\text{Et}_4\text{N}^+$ . Even with the larger  $\text{Bu}_4\text{N}^+$ , the  $\lambda_{\text{max}}$  blue shifted by only 43 nm.

These results are explained as follows. Varying the size of the counterion in the carboxylate polymer changes the effective steric bulk of the substituent. Small cations favor a planar,  $\pi$ -stacked purple phase while large cations can prevent planarity and self-assembly to give a twisted, isolated yellow phase (Fig. 1). When a longer alkyl side chain was used, such as in PTOA, the chemoselectivity was limited to the larger cations ( $\text{Pr}_4\text{N}^+$  and  $\text{Bu}_4\text{N}^+$ ) because

longer chains can more easily accommodate the steric bulk of the substituent without compromising the  $\pi$ -stacked structure of the polymer.

The following results further support the role of steric bulk in the observed ionochromism. (1) All the solutions (in Table 1) became yellow when treated with a vast excess of base. (2) In a separate experiment, the yellow phase was also obtained by titrating a solution of PTPA and 1 equiv KOH (per carboxylic acid residue) with 18-Crown-6. This effectively changes the steric bulk of the cation (by complexation) without changing the ionic strength of the solution. A twisted, yellow phase became more pronounced as the concentration of crown ether increased, while the absorption at longer wavelength decreased. A clear isosbestic point was observed around 420 nm.

All the solutions described in Table 1 were stable, except for  $\text{NH}_4^+$ . For solutions of PTPA with 1 equiv of  $\text{NH}_4\text{OH}$ , the polymer tended to precipitate when the solutions were left undisturbed for several hours. This indicates that the polymer forms large aggregates. We believe that the

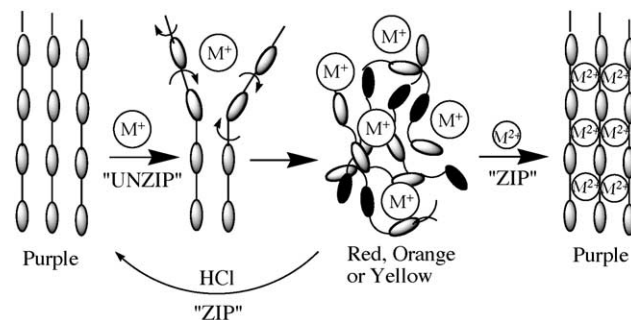


**Figure 1.** Polythiophene zipper sensors: analyte driven disassembly and self-assembly.



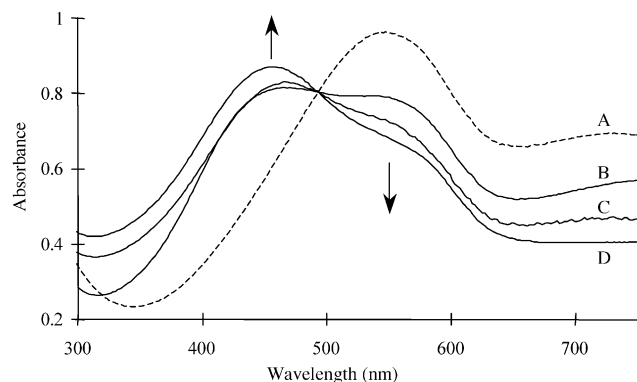


**Figure 2.** UV-vis of PTPA in water as a function of added  $\text{NH}_4\text{OH}$ . (A) 1 equiv; (B) 10 equiv; (C) 15 equiv; (D) 25 equiv of base per carboxylate group.

**Table 2.** Summary of results obtained when we added divalent metals to a red solution of PTPA and  $\text{Et}_4\text{NOH}$

Divalent metal added	Observations
$\text{Mn}^{2+}$ , $\text{Mg}^{2+}$ , $\text{Fe}^{2+}$	Solutions turned purple, formation of a purple precipitate
$\text{Cd}^{2+}$ , $\text{Cu}^{2+}$ , $\text{Zn}^{2+}$ , $\text{Hg}^{2+}$ , $\text{Co}^{2+}$ , $\text{Ni}^{2+}$	Solutions were red to purple, formation of magenta to brown solids

ammonium cation is involved in the assembly of this ordered, aggregated phase, for example, by hydrogen bonding or salt pairing, as indicated by IR experiments (discussed later). One could argue that the  $\text{NH}_4^+$  cation is not large enough to disrupt the ordered phase. However, solutions of PTPA with  $\text{Li}^+$ , a smaller cation than  $\text{NH}_4^+$ , are quite stable.

The aggregates of PTPA with  $\text{NH}_4^+$  can disassemble when large excess of base are added to the solution. For example, solutions that contain a large excess of  $\text{NH}_4\text{OH}$  ( $\sim 10$  equiv or greater) did not precipitate and solutions remained homogeneous indefinitely. This suggests that at higher concentrations of  $\text{NH}_4\text{OH}$ , steric or ionic repulsive interactions overcame some of the attractive inter-chain interactions and allowed for the rapid solvation in water. This is quite similar to deaggregation of proteins in water. Figure 2 shows the titration of an aqueous solution of PTPA with  $\text{NH}_4\text{OH}$ . Upon addition of excess ammonium hydroxide, the ordered purple phase is depleted and a higher energy non-aggregated and/or twisted (coiled) phase is produced. The conformational change from planar to twisted appears to occur via a cooperative mechanism, as shown by the presence of a clear isosbestic point. The UV-vis spectra of PTPA with  $\text{NH}_4\text{OH}$  also showed a significant absorption past 800 nm, which slowly decreased with increasing  $\text{NH}_4\text{OH}$  concentration. The origin of this absorption band was not studied, but suggests the presence of self-doping in the aggregated phase.

We found that divalent metal cations can ‘zip up’ the disordered solvated polymers back into an ordered phase (Fig. 1). When divalent cations were added to an aqueous basic solution of PTPA (or PTOA), a precipitate was formed, indicating aggregation (Table 2). Divalent metal cations can form coordination complexes with the polymers by binding to two carboxylate groups either intra- or inter-molecularly, and the latter is expected to drive self-assembly. The inter-chain attractive force is therefore

quite strong and could be used as a qualitative sensor to detect the presence of divalent cations.

In an effort to better understand the self-assembly by divalent cations, we attempted to get X-ray spectra of the filtered solids (for the samples in Table 2). While the X-ray study revealed several peaks in all cases, we could not easily discern structural order in any of the powder samples. Alternatively, we also tried to study the aggregation by UV-vis in solution, but this tended to be difficult due to the formation and precipitation of coordination polymers at very low cation concentrations. We were able to titrate a solution of PTOA in DMF with small quantities of aqueous  $\text{CdCl}_2$  without precipitation (up to 0.4 equiv). The UV-vis spectra are shown in Figure 3. Aggregation was promoted, as indicated by the increasing absorption at 610 nm, while

the proportion of disordered phase decreased. Polymer PTOA could therefore be a potential candidate for semiquantitative sensing of, for example, dangerous divalent cations in drinking water.

### 2.3. Spectroscopic behavior in the solid state

Thin films of PTPA and PTOA with ammonium hydroxide and with tetraalkylammonium hydroxide were prepared on quartz and the UV-vis spectra were examined (Table 3). Colors were similar to the parent solution, with larger ions yielding a larger hypsochromic shift. We can therefore conclude that the polymer structure in the films is similar to that in solution.

In order to gain more information about the polymer structure and the nature of chromatic changes discussed earlier, we analyzed films of PTPA with the ammonium salts by IR spectroscopy. In the case of tetraalkylammonium salts of PTPA, the IR spectra (Fig. 4) showed the presence of a carboxylate anion ( $1575\text{ cm}^{-1}$ ) and the absence of

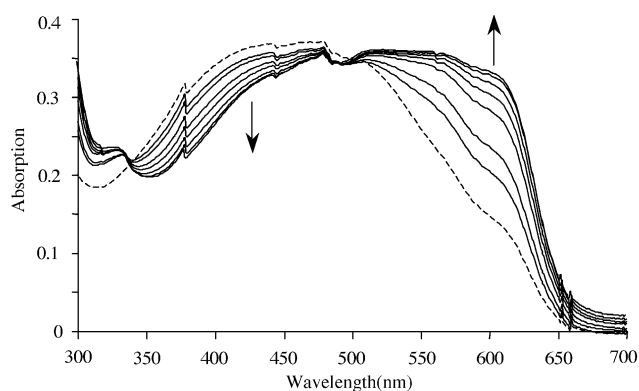


**Figure 3.** Titration of a  $10\ \mu\text{M}$  solution of PTOA in DMF with a  $0.5\ \mu\text{M}$  aqueous solution of  $\text{CdCl}_2$ . The amounts of added  $\text{Cd}_2\text{Cl}_2$  went from 0.05 (---) to 0.4 equiv of  $\text{Cd}_2\text{Cl}_2$ . At 0.45 equiv of  $\text{Cd}_2\text{Cl}_2$ , a precipitate was formed.

**Table 3.** UV/vis  $\lambda_{\max}$  (nm) of PTPA and PTOA thin films<sup>a</sup>

Polymer	H <sub>4</sub> N <sup>+</sup>	Me <sub>4</sub> N <sup>+</sup>	Et <sub>4</sub> N <sup>+</sup>	Pr <sub>4</sub> N <sup>+</sup>	Bu <sub>4</sub> N <sup>+</sup>
PTPA (3)	531	504	489	450	428
PTOA (4)	<sup>b</sup>	550	550	530	499

<sup>a</sup> Cast from solutions in water with 1 equiv of base (R<sup>+</sup>OH<sup>-</sup>) per carboxylic acid group.

<sup>b</sup> Not measured. We expect a value around 550 nm.

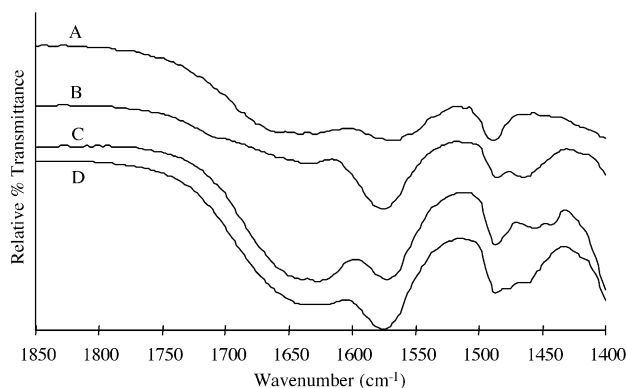


**Figure 4.** IR spectra of films of PTPA with 1 equiv of (A) Me<sub>4</sub>NOH; (B) Et<sub>4</sub>NOH; (C) Bu<sub>4</sub>NOH; and (D) Pr<sub>4</sub>NOH.

hydrogen bonded carboxylic acid (1710 cm<sup>-1</sup>). These results indicate that these films are completely deprotonated and that hydrogen bonding does not play a significant role in the structure.

We then exposed these disordered films to HCl vapor to see if carboxylic acid groups would form hydrogen bonds and cause the polymers to self-assemble. To our amazement, all four films quickly changed from red, orange or yellow (depending on the cation) to purple upon exposure to HCl vapor, even though the polymers were in the solid state (Fig. 5). Furthermore, IR showed that the carboxylate stretch (1565 cm<sup>-1</sup>) disappeared and that the hydrogen-bonded carbonyl stretch (~1725 cm<sup>-1</sup>) appeared upon exposure to HCl (Fig. 6). Protonation of the carboxylate groups therefore allowed the polymer chains to relax from a twisted conformation to a violet  $\pi$ -stacked conformation with H-bonding, essentially zipping the polymer up into an ordered phase (Fig. 1). When the films were left in air, they reverted back to their original color and IR characteristics due to HCl desorption. Films could be cycled several times

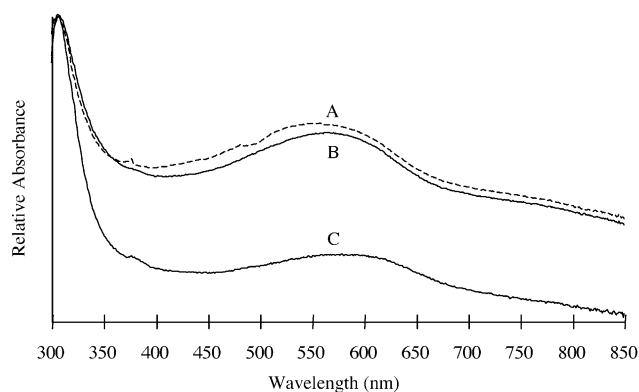


**Figure 5.** UV-vis spectra of films of alkylammonium hydroxides after exposure to HCl vapor. (A) Bu<sub>4</sub>NOH; (B) Pr<sub>4</sub>NOH; (C) Et<sub>4</sub>NOH.

through this color change ( $\Delta\lambda_{\max}$  up to 130 nm) without noticeable degradation of the spectrum. This reversible self-assembly and disassembly could provide a reliable, cheap method for optical detection of acidic vapors.

In contrast, films made from a solution of PTPA with 1 equiv NH<sub>4</sub>OH were purple (ordered phase). Analysis of the IR spectra revealed the presence of both hydrogen bonded carboxylic acid (1709 cm<sup>-1</sup>) and carboxylate anion (1550 cm<sup>-1</sup>) (Fig. 7A). Significant hydrogen bonding is therefore present at equilibrium and influences the molecular ordering.

To see if we could disassemble the ordered state with excess base, dried films cast from the 1:1 solution of PTPA/NH<sub>4</sub>OH were exposed to ammonia vapor. Exposing the films to NH<sub>3</sub> vapor essentially temporarily adds more NH<sub>4</sub><sup>+</sup> into the film. The IR spectra obtained showed that the carboxylate stretch at 1550 cm<sup>-1</sup> intensified while the carbonyl stretch at 1709 cm<sup>-1</sup> was suppressed (Fig. 7B). These films reverted

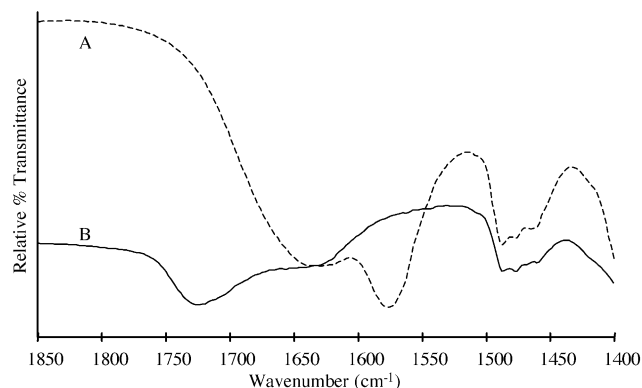


**Figure 6.** IR spectra of 3 with Bu<sub>4</sub>NOH (A) before and (B) after exposure to HCl.

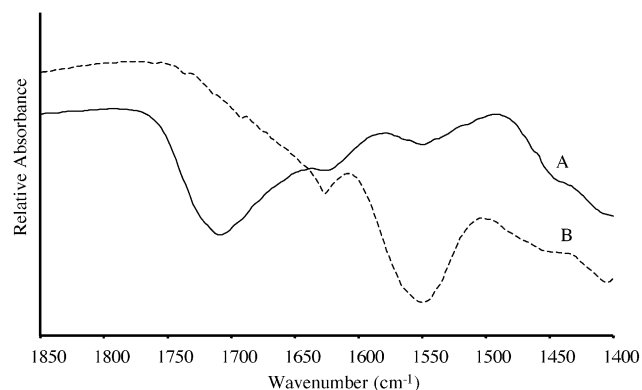


**Figure 7.** IR spectra of PTPA with NH<sub>4</sub>OH (A) before and (B) after exposure to NH<sub>3</sub>.

to their original IR characteristics upon standing, due to  $\text{NH}_3$  desorption. Exposure to ammonia therefore removed the H-bonds. However, the film color did not change, suggesting that the ordered phase was not affected. We surmise that salt-pairing through the ammonium cation might play a role in the ordered phase. The absence of a chromatic change in this experiment is quite unlike the behavior of aqueous solutions treated with excess  $\text{NH}_4\text{OH}$  (Fig. 2). This suggests that a change in solvation of the polymer system is important in the disassembly process in solution.

#### 2.4. X-ray of PTPA and PTOA

Bao and Lovinger have previously reported PTPA to be amorphous, though slight crystallinity could be obtained by slow evaporation of a DMSO solution.<sup>43</sup> They observed a weak peak at 11.5 Å, attributed to the lateral separation of polymer chains by substituents. We have found that crystalline X-ray can be observed upon careful preparation of the films, however most samples do not form good films as the acid polymer. The X-ray spectra of a thin film of PTOA (4) drop cast from DMF is shown in Figure 8. Three peaks were observed in the  $2\theta$  scan of the polymer. The broad reflection, corresponding to 3.7 Å distance, is assigned to the  $\pi$ - $\pi$  stacking distance between the polythiophene chains. Although this is smaller than the 3.8 Å reported for HT-PAT,<sup>44</sup> the resolution is too poor to draw any definitive conclusions. The two sharp reflections correspond to the lamellar interlayer spacing of the polymer chains. The observed distance of  $20.5 \pm 0.2$  Å compares favorably with 20.8 Å previously reported for HT-poly(3-octylthiophene).<sup>44</sup>

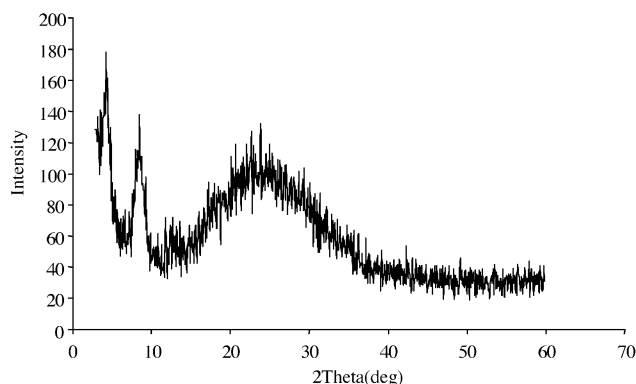


Figure 8. X-ray spectrum of PTOA drop cast from DMF.

### 3. Conclusions

In this work, we have explored the sensing properties of PTPA and PTOA in both basic solutions and thin films. In addition to ionochromism in basic solution with monovalent cations, these polymers are also quite sensitive to the presence of divalent metal cations. Furthermore, films cast from a solution of PTPA and 1 equiv  $\text{Bu}_4\text{NOH}$  underwent a dramatic visual color change from yellow to purple upon HCl vapor exposure. We expect that other detection methods such as fluorescence, conductivity and FET sensing could be used with these materials. Regioregular

polythiophene containing acid side-chains therefore show tremendous potential for the development of new sensors.

## 4. Experimental

### 4.1. General

All reactions were performed under prepurified nitrogen, using dry glassware. Glassware was either dried in an oven overnight or flame dried and then cooled under a stream of nitrogen. Tetrahydrofuran was dried over Na benzophenone ketyl radical and freshly distilled prior to use. Diisopropylamine was dried over  $\text{CaH}_2$  and distilled prior to use.

All UV-vis spectra were recorded using a Perkin-Elmer Lambda 900 UV/vis/near-IR spectrometer. NMR spectra were recorded on an IBM Bruker FT300 spectrometer. Infrared spectra were obtained using a Nicolet 7199 FTIR. The thin films of PTPA salts (3a) were prepared by casting a solution of PTPA with 1 equiv of  $\text{NH}_4\text{OH}$  per carboxylic acid group onto 3M Teflon IR cards and dried overnight in air. The GPC measurements were carried out on a Waters 2690 separation module with two 5  $\mu\text{m}$  Phenogel columns connected in series (guard, 1000 and 100 Å), and a Waters 2487 dual  $\lambda$  absorbance UV detector. Analyses were performed at 30 °C using chloroform as the eluent and the flow rate was 1.0  $\mu\text{L}/\text{min}$ . The calibration was based on polystyrene standards (Polymer Standards Service). GC-MS analysis was performed on a Hewlett-Packard 59970 GC-MS workstation with a HP fused silica capillary column cross-linked with 5% phenyl-methylsilicone as the stationary phase. The X-ray diffraction spectra were obtained with a Rigaku  $\theta/\theta$  X-ray diffractometer utilizing Cu K $\alpha$  source operating at 35 kV and 25 mA, a curved graphite diffracted beam monochromator and a NaI scintillation detector. Data was gathered from 3 to 60°, with steps of 0.05° and 2 s. Elemental Analysis was performed by Midwest Microlab, Indianapolis, IN.

### 4.2. Synthesis

The synthesis of HT-poly(3-(7-(4,5-dihydro-4,4-dimethyl-2-oxazolyl)heptyl)thiophene) (1), and HT-poly(thiophene-3-octanoic acid) (3) are reported in the literature.<sup>42</sup>

**4.2.1. 2-Bromo-3-(bromomethyl)thiophene. Caution! Repugnant, lachrymatory compound.** This compound has been described previously.<sup>45</sup> This procedure has been adapted to utilize benzene rather than  $\text{CCl}_4$  as the solvent. NBS (75.85 g, 427 mmol) was suspended in anhydrous benzene (250 mL) and heated to reflux. 2-Bromo-3-methylthiophene (75.0 g, 424 mmol) and AIBN (0.97 g, 5.9 mmol) were added, and the suspension was heated to reflux for 45 min. The crude reaction mixture was cooled to  $-40$  °C to precipitate some of the succinimide, and this was filtered off. The solvent was removed from the filtrate, causing more succinimide to precipitate. This crude oil was redissolved in excess hexanes and filtered through a pad of silica using hexanes as the eluent to remove remaining succinimide. The solvent was removed and the crude oil was distilled (64 °C, 0.5 T) to recover the product in 80% yield (86.8 g, 339 mmol).  $^1\text{H}$  NMR (300 MHz,  $\text{CDCl}_3$ ):  $\delta$  4.46

(s, 2H), 7.00 (d, 1H) 7.26 (d, 1H).  $^{13}\text{C}$  NMR (75 MHz,  $\text{CDCl}_3$ ):  $\delta$  25.7, 113.0, 126.4, 128.2, 136.9.

#### 4.2.2. 2-(2-(2-Bromothiophen-3-yl)ethyl)-4,5-dihydro-4,4-dimethyloxazole.

2,4,4-Trimethyl-2-oxazoline (7.0 mL, 54.7 mmol) was dissolved in THF (50 mL) and cooled to  $-70^\circ\text{C}$ . Butyllithium (2.62 M, 20 mL, 52.4 mmol) was added dropwise over a 10 min period while maintaining a temperature below  $-50^\circ\text{C}$ . After the mixture was stirred for 15 min, 2-bromo-3-(bromomethyl)thiophene (14.37 g, 56.11 mmol) was added precipitously. The reaction was extremely exothermic, heating to  $25^\circ\text{C}$  despite the cooling bath. The color varied from red to yellow. The cooling bath was removed and the reaction mixture was stirred for 20 min. The reaction was quenched with  $\text{H}_2\text{O}$  and the solvent was removed. The crude oil was poured into hexanes, the precipitated solids were filtered off, and the filtrate was filtered through silica using hexanes as the eluent. When TLC indicated no further elution of precursor 2-bromo-3-(bromomethyl)thiophene, the column was flushed with EtOAc to recover the product. (Note: unreacted 2-bromo-3-(bromomethyl)thiophene catalyses ring opening of the oxazoline upon heating.) The solvent was removed and the remaining oil was distilled ( $80^\circ\text{C}$ , 0.01 T) to recover the product in 77% yield (12.15 g, 42.20 mmol).  $^1\text{H}$  NMR (300 MHz,  $\text{CDCl}_3$ ):  $\delta$  1.24 (s, 6H), 2.52 (t, 2H,  $J=8.2$  Hz), 2.89 (t, 2H,  $J=8.1$  Hz), 3.91 (s, 2H), 6.84 (d, 1H,  $J_{4,5}=5.6$  Hz), 7.19 (d, 1H,  $J_{4,5}=5.6$  Hz).  $^{13}\text{C}$  NMR (75 MHz,  $\text{CDCl}_3$ ):  $\delta$  25.9, 28.1, 28.3, 66.9, 79.0, 109.6, 125.4, 128.1, 139.7, 164.5. Anal. Calcd: C, 45.83; H, 4.86; N, 4.86. Found: C, 45.80; H, 4.84; N, 4.79.

#### 4.2.3. 2-(2-(2-Bromo-5-(trimethylstannyl)thiophen-3-yl)ethyl)-4,5-dihydro-4,4-dimethyloxazole.

2-(2-(2-Bromothiophen-3-yl)ethyl)-4,5-dihydro-4,4-dimethyloxazole (4.885 g, 16.96 mmol) was dissolved in THF (40 mL) and cooled to  $-70^\circ\text{C}$ . LDA was prepared in a separate flask from diisopropylamine (2.50 mL, 17.8 mmol) and butyllithium (2.79 M, 6.10 mL, 17.0 mmol) in THF (10 mL). This was added while maintaining a solution temperature below  $-60^\circ\text{C}$ , and the reaction mixture was stirred at  $-70^\circ\text{C}$  for 1 h. Trimethylstannyl chloride (1.0 M, 26.74 mL, 26.7 mmol) was added dropwise, maintaining the temperature below  $-62^\circ\text{C}$ . The solution was stirred for 1 h, poured into 75 mL of aqueous KF and stirred for 20 min, then was partitioned between  $\text{H}_2\text{O}$  and ether. The organic layer was dried over  $\text{MgSO}_4$  and the solvent was removed. The remaining oil was distilled ( $110$ – $118^\circ\text{C}$ , 0.04 T) to recover the product (5.952 g, 13.20 mmol) in 78% yield.  $^1\text{H}$  NMR (300 MHz,  $\text{CDCl}_3$ ):  $\delta$  0.32 (t, 9H,  $J_{\text{Sn}}=28.5$  Hz), 1.23 (s, 6H), 2.51 (t, 2H,  $J=8.2$  Hz), 2.90 (t, 2H,  $J=8.8$  Hz), 3.89 (s, 2H), 6.89 (t, 1H,  $J=13.6$  Hz);  $^{13}\text{C}$  NMR (75 MHz,  $\text{CDCl}_3$ ):  $\delta$   $-8.4$ , 25.7, 28.2, 28.3, 67.0, 79.1, 114.2, 136.2 (t,  $J_{\text{Sn}}=52.1$  Hz), 138.3, 140.9, 164.8. Anal. Calcd: C, 37.28; H, 4.92; N, 3.11. Found: C, 37.32; H, 4.95; N, 3.23.

**4.2.4. HT-2,5-poly(3-(2-(4,5-dihydro-4,4-dimethyl-2-oxazolyl)ethyl)thiophene) (1).** Polymerization was done using Gronowitz conditions for the formation of dimers.<sup>46</sup> 2-(2-(2-Bromo-5-(trimethylstannyl)thiophen-3-yl)ethyl)-4,5-dihydro-4,4-dimethyloxazole (3.09 g, 6.86 mmol) was dissolved in DMF (80 mL). Tris(dibenzylidene

acetone)dipalladium(0) (336 mg, 0.05 equiv) was added, followed quickly by copper(II)oxide (367 mg, 1.0 equiv), and triphenylphosphine (570 mg, 0.20 equiv). The solution was warmed to  $100^\circ\text{C}$  and allowed to stir for 2 days. The reaction was quenched by pouring into methanol. The resulting solid was filtered and transferred into a Soxhlet thimble. The sample was extracted with methanol until the eluent was colorless, then was recovered by extraction with chloroform. The solvent was removed and the resulting purple solid was dried under vacuum overnight to recover the polymer (1.075 g, 5.19 mmol) in 76% yield.  $^1\text{H}$  NMR (300 MHz,  $\text{CDCl}_3$ ):  $\delta$  1.31 (s, 6H), 2.75 (t, 2H), 3.19 (t, 2H), 3.94 (s, 2H), 7.11 (s, 1H).  $^{13}\text{C}$  NMR (75 MHz,  $\text{CDCl}_3$ ):  $\delta$  26.4; 29.2; 29.6; 68.0; 80.0; 129.8; 132.4; 134.4; 138.4; 166.7.  $M_n=8\text{K}$ , PDI=1.2 (by GPC).

#### 4.2.5. HT-2,5-poly(thiophene-3-propionic acid) (3).

A sample of **1** (404.4 mg) was dissolved in 3 N HCl (90 mL) and heated to reflux for 12 h. The solution consisted of a dark purple suspension at this point. The solid was filtered, rinsed with  $\text{H}_2\text{O}$ , and dried to recover the product in 82% yield (248.4 mg). As prepared, most polymer samples submitted for elemental analysis contained large amounts of ash (10–15%). This suggests the presence of copper (II) salts and other impurities, though this has not been confirmed. A drastic reduction in the ash content was achieved by dissolving polymer PTPA (**3**) in aqueous base, re-precipitating it upon acidification, and recovering it by filtration. Re-precipitating two to three times eliminated the ash, giving elemental analysis results in reasonable agreement with the theoretical composition of this polymer.  $^1\text{H}$  NMR (300 MHz,  $\text{CD}_3\text{OD}$ ) (characterized as its cesium salt by adding CsOH):  $\delta$  7.05 (s, 1H); 3.92 (t, 2H); 2.35 (t, 2H). Anal. Calcd: C, 54.54; H, 4.08. Found: C, 52.64; H, 4.08.

### Acknowledgements

We are grateful to the NSF (CHE-0107178) for support. We thank Jason Wolf of CMU for doing the X-ray measurement of PTOA.

### References and notes

1. Skotheim, T. A.; Elsenbaumer, R. L.; Reynolds, J. R. *Handbook of Conducting Polymers*; Marcel Dekker: New York, 1998; p 1097.
2. Sirringhaus, H.; Tessler, N.; Friend, R. H. *Science (Washington, DC)* **1998**, *280*, 1741–1744.
3. Bao, Z.; Dodabalapur, A.; Lovinger, A. J. *Appl. Phys. Lett.* **1996**, *69*, 4108–4110.
4. Sirringhaus, H.; Brown, P. J.; Friend, R. H.; Nielsen, M. M.; Bechgaard, K.; Langeveld-Voss, B. M. W.; Spiering, A. J. H.; Janssen, R. A. J.; Meijer, E. W.; Herwig, P.; de Leeuw, D. M. *Nature (London)* **1999**, *401*, 685–688.
5. Kline, J. R.; McGehee, M. D.; Kadnikova, E. N.; Liu, J.; Frechet, J. M. J. *Adv. Mater.* **2003**, *15*, 1519–1522.
6. Leclerc, M. *Adv. Mater.* **1999**, *11*, 1491–1498.
7. Huynh, W. U.; Dittmer, J. J.; Alivisatos, A. P. *Science (Washington, DC)* **2002**, *295*, 2425–2427.

8. McQuade, D. T.; Pullen, A. E.; Swager, T. M. *Chem. Rev.* **2000**, *100*, 2537–2574.
9. McCullough, R. D. *Adv. Mater.* **1998**, *10*, 93–116.
10. McCullough, R. D.; Ewbank, P. C. *Handbook of Conducting Polymers*; Skotheim, T. A., Elsenbaumer, R. L., Reynolds, J. R., Eds.; Marcel Dekker: New York, 1998; pp 225–258.
11. McCullough, R. D.; Tristram-Nagle, S.; Williams, S. P.; Lowe, R. D.; Jayaraman, M. *J. Am. Chem. Soc.* **1993**, *115*, 4910–4911.
12. McCullough, R. D.; Williams, S. P. *J. Am. Chem. Soc.* **1993**, *115*, 11608–11609.
13. McCullough, R. D.; Lowe, R. D.; Jayaraman, M.; Anderson, D. L. *J. Org. Chem.* **1993**, *58*, 904–912.
14. Yoshino, K.; Nakao, K.; Onoda, M.; Sugimoto, R. *Solid State Commun.* **1988**, *68*, 513–516.
15. Yoshino, K.; Nakajima, S.; Onoda, M.; Sugimoto, R. *Synth. Met.* **1989**, *28*, C349–C357.
16. Mochizuki, H.; Nabeshima, Y.; Kitsunai, T.; Kanazawa, A.; Shiono, T.; Ikeda, T.; Hiyama, T.; Maruyama, T.; Yamamoto, T.; Koide, N. *J. Mater. Chem.* **1999**, *9*, 2215–2219.
17. Levesque, I.; Leclerc, M. *Macromolecules* **1997**, *30*, 4347–4352.
18. Hotta, S.; Soga, M.; Sonoda, N. *Synth. Met.* **1988**, *26*, 267–279.
19. Faid, K.; Cloutier, R.; Leclerc, M. *Macromolecules* **1993**, *26*, 2501–2507.
20. Heywang, G.; Jonas, F. *Adv. Mater.* **1992**, *4*, 116–118.
21. Inganäs, O.; Salaneck, W. R.; Österholm, J.-E.; Laakso, J. *Synth. Met.* **1988**, *22*, 395–406.
22. Tashiro, K.; Ono, K.; Minagawa, Y.; Kobayashi, M.; Kawai, T.; Yoshino, K. *J. Polym. Sci. Part B: Polym. Phys.* **1991**, *29*, 1223–1234.
23. Zerbi, G.; Chierichetti, B.; Inganäs, O. *J. Chem. Phys.* **1991**, *94*, 4646–4658.
24. Roux, C.; Leclerc, M. *Macromolecules* **1992**, *25*, 2141–2144.
25. Faid, K.; Frechette, M.; Ranger, M.; Mazerolle, L.; Levesque, I.; Leclerc, M.; Chen, T.-A.; Rieke, R. D. *Chem. Mater.* **1995**, *7*, 1390–1396.
26. McCullough, R. D.; Ewbank, P. C.; Loewe, R. S. *J. Am. Chem. Soc.* **1997**, *119*, 633–634.
27. Marsella, M. J.; Swager, T. M. *J. Am. Chem. Soc.* **1993**, *115*, 12214–12215.
28. Levesque, I.; Leclerc, M. *Chem. Mater.* **1996**, *8*, 2843–2849.
29. Wang, B.; Wasielewski, M. R. *J. Am. Chem. Soc.* **1997**, *119*, 12–21.
30. Boldea, A.; Levesque, I.; Leclerc, M. *J. Mater. Chem.* **1999**, *9*, 2133–2138.
31. Ewbank, P. C.; Nuding, G.; Suenaga, H.; McCullough, R. D.; Shinkai, S. *Polym. Prepr.* **1999**, *40*, 855.
32. Ewbank, P. C.; Nuding, G.; Suenaga, H.; McCullough, R. D.; Shinkai, S. *Tetrahedron Lett.* **2001**, *42*, 155–157.
33. Peter, K.; Nilsson, R.; Inganaes, O. *Nature Mater.* **2003**, *2*, 419–424.
34. Ho, H.-A.; Boissinot, M.; Bergeron, M. G.; Corbeil, G.; Dore, K.; Boudreau, D.; Leclerc, M. *Angew. Chem., Int. Ed. Engl.* **2002**, *41*, 1548–1551.
35. Yamamoto, T.; Shimizu, T.; Kurokawa, E. *React. Funct. Polym.* **2000**, *43*, 79–84.
36. Faid, K.; Leclerc, M. *J. Am. Chem. Soc.* **1998**, *120*, 5274–5278.
37. Lavigne, J. J.; Anslyn, E. V. *Angew. Chem.* **1999**, *38*, 3666–3669.
38. Rakow, N. A.; Suslick, K. S. *Nature (London)* **2000**, *406*, 710–713.
39. Yue, S.; Berry, G. C.; McCullough, R. D. *Macromolecules* **1996**, *29*, 933–939.
40. Brédas, J. L.; Street, G. B.; Thémans, B.; André, J. M. *J. Chem. Phys.* **1985**, *83*, 1323–1329.
41. Baughman, R. H.; Chance, R. R. *J. Appl. Phys.* **1976**, *47*, 4295–4300.
42. Zhai, L.; McCullough, R. D. *Adv. Mater.* **2002**, *14*, 901–905.
43. Bao, Z.; Lovinger, A. J. *Chem. Mater.* **1999**, *11*, 2607–2612.
44. Prosa, T. J.; Winokur, M. J.; McCullough, R. D. *Macromolecules* **1996**, *29*, 3654–3656.
45. Campagne, E.; Le Seur, W. M. *J. Am. Chem. Soc.* **1949**, *71*, 333–335.
46. Gronowitz, S.; Bjork, P.; Malm, J.; Hornfeldt, A. B. *J. Organomet. Chem.* **1993**, *460*, 127.



# Enantioselective fluorescent recognition of chiral acids by 3- and 3,3'-aminomethyl substituted BINOLs

Jing Lin, Amaresh R. Rajaram and Lin Pu\*

Department of Chemistry, University of Virginia, Charlottesville, VA 22904-4319, USA

Received 27 January 2004; revised 30 June 2004; accepted 19 August 2004

Available online 21 September 2004

**Abstract**—Benzylaminomethyl groups are introduced to the 3,3'-positions of BINOL. The resulting compounds can be used to conduct the enantioselective fluorescent recognition of mandelic acid and *N*-benzyloxycarbonylphenylglycine. In the presence of (*S*)-mandelic acid, compound (*R*)-2 showed over 30-fold fluorescence enhancement with the ef [ef= enantiomeric fluorescence difference ratio =  $(I_S - I_0)/(I_R - I_0)$ ] up to 4.2. In the presence of *D*-*N*-benzyloxycarbonylphenylglycine, compound (*RR*)-4 showed up to 15-fold fluorescence enhancement with the ef up to 5.0. These high fluorescence sensitivity and enantioselectivity make compounds (*R*)-2 and (*RR*)-4 practically useful sensors for the recognition of the chiral acids in apolar solvents.

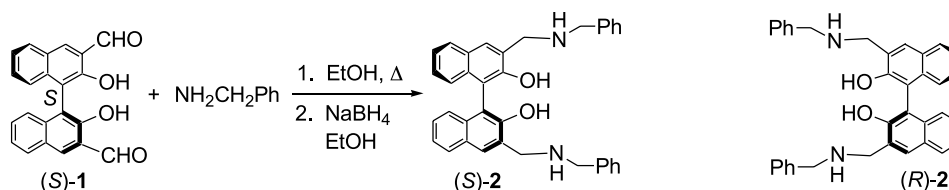
© 2004 Elsevier Ltd. All rights reserved.

## 1. Introduction

1,1'-Bi-2-naphthol (BINOL) and its derivatives have been extensively used in asymmetric synthesis and chiral recognition, and have exhibited outstanding chiral induction in many processes.<sup>1–3</sup> Recently, our laboratory has been interested in developing BINOL-based enantioselective fluorescent sensors for molecular recognition.<sup>4</sup> These sensors are potentially useful for real time assay of chiral molecules.<sup>5</sup> We have reported that both cyclic and acyclic *bis*(BINOL) compounds could be used to carry out the enantioselective recognition of  $\alpha$ -hydroxycarboxylic acids and  $\alpha$ -amino acid derivatives.<sup>4</sup> In this paper, we report our new finding that even monomeric BINOL molecules could also show high sensitivity and high enantioselectivity in the fluorescent recognition of the chiral acids.

## 2. Results and discussion

The binaphthyl dialdehyde compound (*S*)-1 was readily prepared from (*S*)-BINOL.<sup>6</sup> Condensation of (*S*)-1 with benzylamine followed by reduction gave the 3,3'-benzylaminomethyl substituted BINOL (*S*)-2 (Scheme 1). These amino methyl groups were introduced to quench the fluorescence of the BINOL unit through the photo-induced-electron-transfer (PET) as demonstrated previously in the analogous compounds.<sup>4,7</sup> The specific optical rotation of (*S*)-2 was  $[\alpha]_D = -70.4$  ( $C_6H_6$ ,  $c=0.215$ ). The UV–vis spectrum of (*S*)-2 ( $2.0 \times 10^{-5}$  M in benzene) gave absorptions at  $\lambda_{max}$  ( $\epsilon$ ) = 282 (10,300), 294 (sh, 8600), 330 (sh, 7000), 342 (9000) nm. Its fluorescence spectrum ( $1.0 \times 10^{-4}$  M in benzene containing 2% DME) gave an emission peak at 360 nm while excited at 320 nm.



**Scheme 1.** Synthesis of the 3,3'-benzylaminomethyl substituted BINOL (*S*)- and (*R*)-2.

**Keywords:** Enantioselective; Fluorescent sensors; Mandelic acid; Amino acids; BINOL.

\* Corresponding author. Tel.: +1-4349246953; fax: +1-4349243710; e-mail: lp6n@virginia.edu

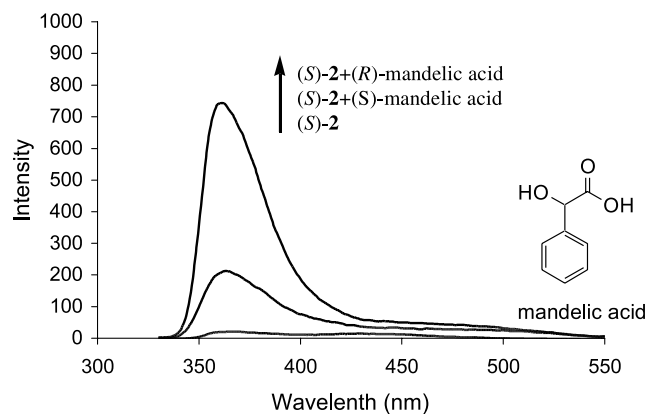


**Figure 1.** Fluorescence spectra of *(S)*-2 ( $1.0 \times 10^{-4}$  M in benzene containing 2% DME) with/without *(R)*- and *(S)*-mandelic acid ( $2.0 \times 10^{-2}$  M) ( $\lambda_{\text{exc}} = 320$  nm).

When *(S)*-2 was treated with *(R)*-mandelic acid, an  $\alpha$ -hydroxycarboxylic acid, a large fluorescence enhancement was observed. As shown in Figure 1, the fluorescence enhancement of *(S)*-2 in the presence of *(R)*-mandelic acid was over 30-fold. This fluorescence enhancement was about 10 times greater than the previously reported fluorescence responses of the *bis*binaphthyl sensors to mandelic acid.<sup>4</sup> It demonstrates that this 3,3'-diaminomethyl substituted

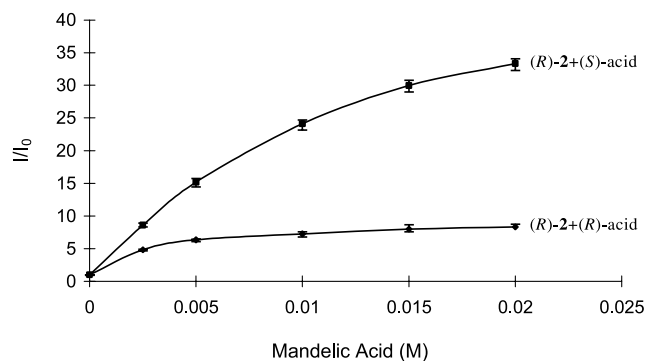


**Figure 2.** Fluorescence enhancement of *(R)*-2 ( $1.0 \times 10^{-4}$  M in benzene/2% DME) versus concentration of *(R)*- and *(S)*-mandelic acid ( $2.5 \times 10^{-3}$ – $2.0 \times 10^{-2}$  M) ( $\lambda_{\text{exc}} = 320$  nm).

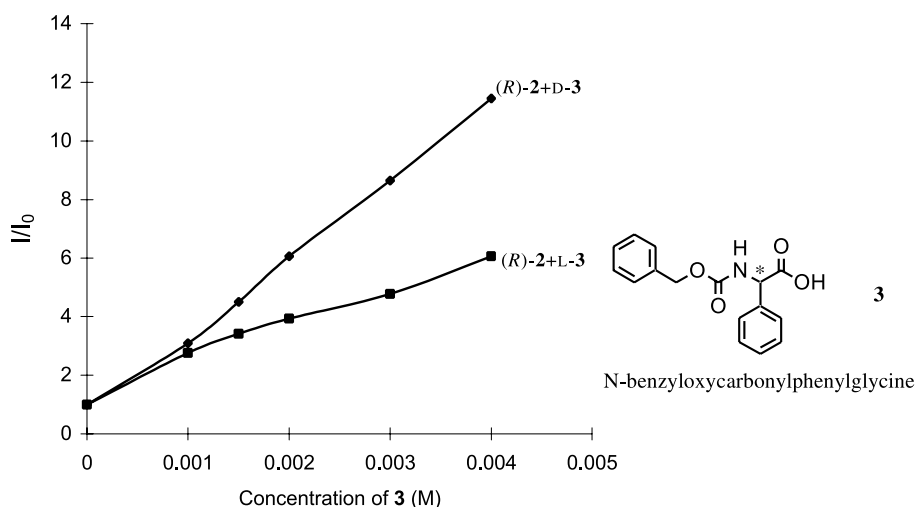


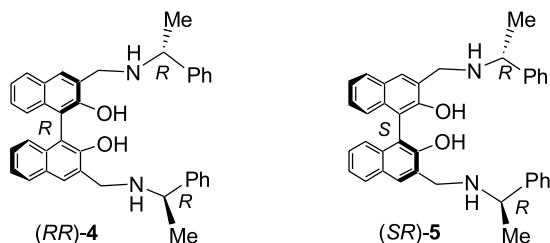
**Figure 3.** Fluorescence enhancement of *(R)*-2 ( $1.0 \times 10^{-4}$  M in benzene/2% DME) versus concentration of D/L-3 ( $\lambda_{\text{exc}} = 320$  nm).

monomeric BINOL molecule is a much more sensitive fluorescent sensor than those containing two binaphthyl units. *(S)*-2 also showed high enantioselectivity in the fluorescent recognition. When *(S)*-2 was treated with *(S)*-mandelic acid, the fluorescence enhancement was much smaller (Fig. 1).

We also prepared *(R)*-2, the enantiomer of *(S)*-2, by starting from *(R)*-BINOL. This compound showed large fluorescence enhancement in the presence of *(S)*-mandelic acid and much smaller one in the presence of *(R)*-mandelic acid. Thus, a mirror image relationship was established between *(S)*-2 and *(R)*-2 which confirmed the observed chiral recognition. Figure 2 shows the fluorescence enhancement of *(R)*-2 in the presence of various concentrations of *(R)*- and *(S)*-mandelic acid. In the plot, the error bars were obtained by four independent measurements. It showed that as the concentration of *(S)*-mandelic acid increased, the fluorescence intensity of *(R)*-2 could increase over 30 times, but *(R)*-mandelic acid could only lead to much smaller fluorescence enhancement. The enantiomeric fluorescence difference ratio (ef) [ $\text{ef} = (I_S - I_0)/(I_R - I_0)$ ] was 4.2 when the concentration of the acid was  $2.0 \times 10^{-2}$  M.

*(R)*-2 was used to interact with *N*-benzyloxycarbonyl-phenylglycine (D/L-3). As shown in Figure 3, D-3 enhanced the fluorescence of *(R)*-2 greater than L-3 did. At  $4.0 \times 10^{-3}$  M of D-3, the fluorescence intensity of *(R)*-2 increased over 11.5 fold in the presence of D-3 and only 6.1 fold by L-3. Thus, the ef (D/L) was 2.0.

In order to study how the chirality of the amine groups in *(R)*- or *(S)*-2 influenced the enantioselective fluorescent recognition, we synthesized two diastereomeric compounds (*RR*)-4 and (*SR*)-5 from the reactions of *(R)*- and *(S)*-1 with *(R)*- $\alpha$ -methylbenzylamine followed by reduction, respectively. The specific optical rotation of (*RR*)-4 was  $[\alpha]_D = +19.3$  ( $\text{C}_6\text{H}_6$ ,  $c = 0.19$ ) and that of (*SR*)-5 was  $[\alpha]_D = -18.5$  ( $\text{C}_6\text{H}_6$ ,  $c = 0.205$ ). Thus, the optical rotations of these compounds were determined by the chirality of the BINOL unit. Both of the compounds showed the same emission peak at 365 nm when excited at 320 nm in benzene containing 2% DME.



Compound  $(RR)$ -**4** ( $1.0 \times 10^{-4}$  M in benzene/2% DME) was interacted with the enantiomers of mandelic acid in the concentration range of  $2.5 \times 10^{-3}$ – $2.0 \times 10^{-2}$  M. At 0.02 M of  $(R)$ -mandelic acid, the fluorescent intensity of  $(RR)$ -**4** was enhanced by 4.8 fold. Under the same condition,  $(S)$ -mandelic acid enhanced the fluorescence of  $(RR)$ -**4** by 3.0 fold. The ef was 1.9. Both the fluorescence enhancement and enantioselectivity of  $(RR)$ -**4** decreased significantly in comparison with  $(R)$ -**2**. The greatly decreased fluorescence enhancement was probably due to the increased steric hindrance at the nitrogen atoms of  $(RR)$ -**4** which reduced their binding with mandelic acid. It also inverted the enantioselectivity of the sensor.

Compound  $(RR)$ -**4** showed much greater enantioselectivity in the fluorescent recognition of  $D/L$ -**3** with an ef up to 5.1 (Fig. 4). At  $4.0 \times 10^{-3}$  M of  $D$ -**3**, the fluorescence enhancement of  $(RR)$ -**4** was about 14.8 fold. This fluorescence

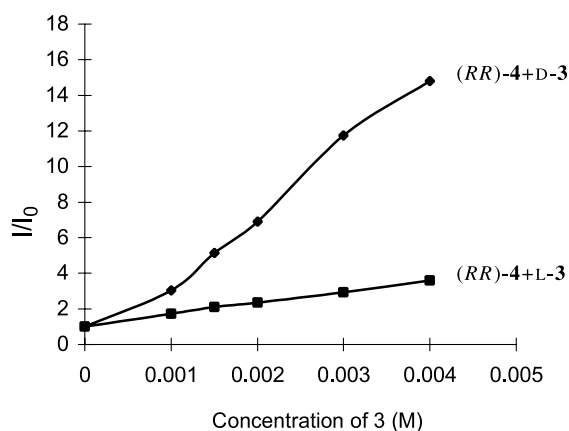


**Figure 4.** Fluorescence enhancement of  $(RR)$ -**4** ( $1.0 \times 10^{-4}$  M in benzene/2% DME) versus concentration of  $D/L$ -**3** ( $\lambda_{exc} = 320$  nm).

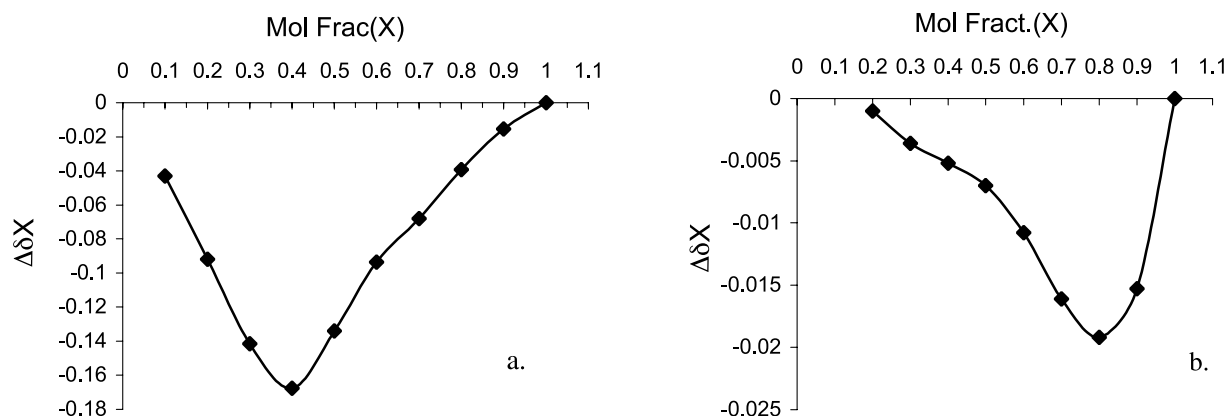
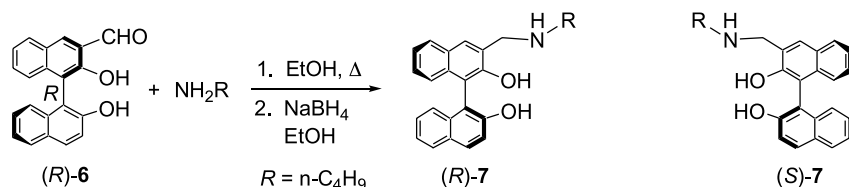


**Figure 5.** The Job plots of  $(R)$ -**2** (a) with  $(S)$ -mandelic acid, (b) with  $D$ -**3** ( $4.0 \times 10^{-3}$  M total concentration in  $C_6D_6$  containing 2% DME).

enhancement was close to that of  $(R)$ -**2** by  $D$ -**3**. Under the same condition,  $L$ -**3** led to 3.6 fold fluorescence enhancement for  $(RR)$ -**4**.

The fluorescence study of  $(R)$ -**2** and  $(RR)$ -**4** with mandelic acid and **3** indicated that the  $\alpha$ -hydroxycarboxylic acid responded differently to the steric hindrance at the amine substituents of the sensors than the  $N$ -protected amino acid. Increasing the steric hindrance from  $(R)$ -**2** to  $(RR)$ -**4** led to reduced as well as inverted enantioselectivity for the interaction with mandelic acid, but it increased the enantioselectivity for the interaction with **3**. This is consistent with the Job plots of  $(R)$ -**2** in the presence of mandelic acid and **3** (Fig. 5) as measured by using  $^1H$  NMR spectroscopy.<sup>8</sup> At a constant total concentration of  $4.0 \times 10^{-3}$  M, the  $^1H$  NMR spectra of  $(R)$ -**2** with  $(S)$ -mandelic acid or  $D$ -**3** in a variety of ratios in benzene- $d_6$  containing 2% DME were taken. It was found that the methine proton signal of  $(S)$ -mandelic acid at  $\delta$  4.20 and that of  $D$ -**3** at  $\delta$  4.96 underwent an upfield shift upon treatment with  $(R)$ -**2**. Plotting  $\Delta\delta X$  versus  $X$  ( $X$ : mole fraction of the acid.  $\Delta\delta$ : chemical shift change of the acid methine proton.) led to the Job plots as shown in Figure 5. Both of them exhibited multiple binding modes, but these two acids interacted with  $(R)$ -**2** in a very different fashion. In addition,  $(R)$ -**2** responded to the chiral configurations of the two acids in the opposite directions. While the  $S$  enantiomer of mandelic acid enhanced the fluorescence of  $(R)$ -**2** much greater than the  $R$  enantiomer, the  $D$  ( $R$ ) enantiomer of **3** enhanced much more than the  $L$  ( $S$ ) enantiomer.

Compound  $(SR)$ -**5** was interacted with both mandelic acid and the amino acid **3**. This diastereomeric isomer showed much lower enantioselectivity than that of  $(RR)$ -**4**. When  $(SR)$ -**5** ( $1.0 \times 10^{-4}$  M in benzene/2% DME) was treated with  $(R)$ - and  $(S)$ -mandelic acid ( $2.5 \times 10^{-3}$ – $2.0 \times 10^{-2}$  M), the fluorescence intensity of  $(SR)$ -**5** was linearly increased with the concentration of mandelic acid.  $(S)$ -Mandelic acid caused 3-fold fluorescence enhancement, which was higher than  $(R)$ -mandelic acid with an observed ef of up to 1.4. Similarly, the amino acid **3** increased the fluorescence of  $(SR)$ -**5** up to 4.8-fold as the concentration increased from  $1.0 \times 10^{-3}$  to  $4.0 \times 10^{-3}$  M and the ef ( $L/D$ ) was up to 1.9. The much lower enantioselectivity as well as lower fluorescence enhancement observed for  $(SR)$ -**5** than



**Scheme 2.** Synthesis of the 3-alkylaminomethyl substituted BINOL (*R*)- and (*S*)-7.

(*RR*)-4 indicated a mismatched chirality between the chiral amine centers and the chiral BINOL unit.

Compounds (*R*)- and (*S*)-7 that contained only one 3-alkylaminomethyl substituent were prepared from the reaction of the monoaldehyde (*R*)- or (*S*)-6<sup>9</sup> with butylamine followed by reduction (Scheme 2). When (*R*)- or (*S*)-7 ( $1.0 \times 10^{-4}$  M in benzene containing 1.25% DME) was used to interact with mandelic acid ( $2.5 \times 10^{-3}$ – $2.0 \times 10^{-2}$  M), over 10 fold fluorescence enhancement at  $\lambda_{\text{emi}} = 363$  nm ( $\lambda_{\text{exc}} = 336$  nm) was observed. However, the enantioselectivity was low with ef less than 1.4. Thus the  $C_2$  symmetric sensors (*R*)- and (*S*)-2 were much better than the  $C_1$  symmetric (*R*)- and (*S*)-7 in the fluorescent recognition.

In summary, amino methyl substituted BINOLs have been synthesized and their use in the fluorescent recognition of chiral acids has been examined. We found that compound (*S*)- or (*R*)-2 showed over 30 fold fluorescence enhancement in the presence of mandelic acid with ef up to 4.2, and compound (*RR*)-4 showed up to 15 fold fluorescence enhancement in the presence of *N*-benzyloxycarbonyl-phenylglycine with ef up to 5.0. These high fluorescence sensitivity and enantioselectivity make these compounds practically useful sensors for the recognition of the chiral acids in apolar solvents.

### 3. Experimental

#### 3.1. General

**3.1.1. Preparation and characterization of (*S*)- and (*R*)-2.** The aldehyde (*R*)- or (*S*)-1 (200 mg, 0.58 mmol) and benzylamine (248 mg, 2.32 mmol) were dissolved in absolute ethanol (25 mL). The mixture was degassed with nitrogen and then heated under reflux for one day. After cooled to room temperature, the precipitate was separated and washed with ethanol (ice cold) to afford the crude Schiff base. The Schiff base was combined with  $\text{NaBH}_4$  (88 mg, 2.32 mmol) and ethanol (25 mL). The resulting reaction mixture was degassed with nitrogen and heated at reflux for 4 h. The solvent was then removed, and methylene chloride (30 mL) and HCl (0.2 N, aq, 30 mL) were added. After stirred for 1 h, the organic layer was separated and washed with 0.5 N NaOH aqueous solution, water, brine, and dried over  $\text{MgSO}_4$ . After removal of the solvent, the residue was passed through a short silica gel column, and eluted with hexanes/ethylacetate (2:3) to afford the product (*S*)- or (*R*)-2:  $^1\text{H NMR}$  ( $\text{CDCl}_3$ , 300 MHz)  $\delta$  2.06 (s, 4H), 4.27 (dd, 4H), 7.20–7.29 (m, 16H), 7.67 (s, 2H), 7.80 (d,  $J = 7.5$  Hz, 2H).  $^{13}\text{C NMR}$  ( $\text{CDCl}_3$ , 75 MHz)  $\delta$  52.39, 52.73, 116.68, 123.0, 124.83, 126.09, 127.56, 127.7, 127.96, 128.23, 128.57, 128.63, 133.88, 153.73. Mp 197–199 °C.

$[\alpha]_{\text{D}} = -70.4$  ( $\text{C}_6\text{H}_6$ ,  $c = 0.215$ ). MS (EI) ( $m/z$ ) 525 ( $\text{M} + \text{H}$ )<sup>+</sup>. Anal. calcd for  $\text{C}_{36}\text{H}_{32}\text{N}_2\text{O}_2$ : C, 82.41; H, 6.15; N, 5.3. Found: C, 82.68; H, 6.08; N, 5.26. For (*R*)-2:  $[\alpha]_{\text{D}} = +73.4$  ( $\text{C}_6\text{H}_6$ ,  $c = 0.215$ ).

**3.1.2. Preparation and characterization of (*RR*)-4 and (*SR*)-5.** The procedures to prepare (*RR*)-4 and (*SR*)-5 were the same as that for (*S*)- and (*R*)-2, but the Schiff base intermediates were not isolated.  $\text{NaBH}_4$  was added directly after the formation of the Schiff base to give the product. (*RR*)-4:  $^1\text{H NMR}$  ( $\text{CDCl}_3$ , 300 MHz)  $\delta$  1.46 (d,  $J = 3.9$  Hz, 3H), 3.93 (q,  $J = 4.2$  Hz, 2H), 4.1 (dd, 4H), 7.15–7.32 (m, 16H), 7.58 (s, 2H), 7.75 (d,  $J = 4.8$  Hz, 2H).  $^{13}\text{C NMR}$  ( $\text{CDCl}_3$ , 75 MHz)  $\delta$  23.12, 51.21, 57.78, 116.67, 122.88, 124.92, 125.35, 125.94, 126.57, 127.53, 127.65, 128.21, 128.78, 133.82, 153.79. Mp 166–168 °C.  $[\alpha]_{\text{D}} = +19.3$  ( $\text{C}_6\text{H}_6$ ,  $c = 0.19$ ). MS (EI) ( $m/z$ ) 552 ( $\text{M} + \text{H}$ )<sup>+</sup>. Anal. calcd for  $\text{C}_{38}\text{H}_{36}\text{N}_2\text{O}_2$ : C, 82.58; H, 6.57; N, 5.07. Found: C, 82.57; H, 6.44; N, 5.25. (*SR*)-5:  $^1\text{H NMR}$  ( $\text{CDCl}_3$ , 300 MHz)  $\delta$  1.43 (d,  $J = 4.5$  Hz, 3H), 3.89–4.18 (m, 6H), 7.21–7.40 (m, 16H), 7.57 (s, 2H), 7.76 (d,  $J = 7.8$  Hz, 2H).  $^{13}\text{C NMR}$  ( $\text{CDCl}_3$ , 75 MHz)  $\delta$  23.15, 51.02, 57.60, 116.63, 122.94, 124.77, 126.01, 126.60, 127.57, 127.68, 127.78, 128.25, 128.81, 133.81, 153.73. Mp 170–175 °C.  $[\alpha]_{\text{D}} = -18.5$  ( $\text{C}_6\text{H}_6$ ,  $c = 0.205$ ). MS (EI) ( $m/z$ ) 552 ( $\text{M} + \text{H}$ )<sup>+</sup>. Anal. calcd for  $\text{C}_{38}\text{H}_{36}\text{N}_2\text{O}_2$ : C, 82.58; H, 6.57; N, 5.07. Found: C, 82.50; H, 6.49; N, 5.17.

#### 3.1.3. Preparation and characterization of (*R*)- and (*S*)-7.

Under nitrogen a mixture of the monoaldehyde (*R*)- or (*S*)-6 (0.314 g, 1.0 mmol) and butylamine (0.095 g, 1.3 mmol) in absolute ethanol (25 mL) was heated at reflux for 12–16 h. After removal of the solvent, the resulting Schiff base was redissolved in ethanol (16 mL) and combined with  $\text{NaBH}_4$  (0.0699 g, 3.0 mmol). The mixture was stirred for 4–5 h and the solvent was evaporated. The residue was dissolved in methylene chloride which was followed by the addition of HCl (1 N) to adjust the pH to 3–4. The organic layer was separated. A saturated  $\text{NaHCO}_3$  solution was added to make the aqueous layer basic, which was further extracted with methylene chloride. The combined organic layer was washed with water and brine, and dried over  $\text{Na}_2\text{SO}_4$ . After removal of the solvent, the residue was purified by column chromatography on silica gel eluted with 9:1 methylene chloride/acetone to afford (*R*)- or (*S*)-7 as a white solid. (*R*)-7: 63% yield. Mp 83–84 °C.  $^1\text{H NMR}$  ( $\text{CDCl}_3$ , 300 MHz)  $\delta$  7.77 (m, 2H), 7.68 (d,  $J = 7.8$  Hz, 2H), 7.56 (s, 1H), 7.27 (d,  $J = 7.8$  Hz, 1H), 7.19 (t,  $J = 7.2$  Hz, 2H), 7.11 (t,  $J = 7.2$  Hz, 2H), 7.04 (d,  $J = 8.4$  Hz, 2H), 5.89 (bs, 1H), 4.10 (s, 2H), 2.56 (t,  $J = 6.9$  Hz, 2H), 1.35 (m, 2H), 1.19 (m, 2H), 0.75 (t,  $J = 7.2$  Hz, 3H).  $^{13}\text{C NMR}$  ( $\text{CDCl}_3$ , 75 MHz)  $\delta$  155.52, 151.47, 133.74, 133.65, 129.71, 129.21, 128.67, 128.29, 128.15, 127.72, 126.70, 126.29, 125.17, 124.96, 124.53, 123.43, 123.12, 117.68, 115.19, 112.91,

52.94, 48.36, 31.27, 20.17, 13.77. MS  $m/z$  (relative intensity) 371 ( $M^+$ , 24), 370 (100).  $[\alpha]_D = -2.7$  ( $CH_2Cl_2$ ,  $c=0.95$ ). Anal. calcd for  $C_{25}H_{26}NO_2$ : C, 80.83; H, 6.78; N, 3.77. Found: C, 81.55; H, 6.99; N, 3.29. (*S*)-**7**: 52% yield. Mp 86 °C (dec). MS  $m/z$  (relative intensity) 371 ( $M^+$ , 22), 370 (100).  $[\alpha]_D = +2.5$  ( $CH_2Cl_2$ ,  $c=0.95$ ). Anal. calcd for  $C_{25}H_{26}NO_2$ : C, 80.83; H, 6.78; N, 3.77. Found: C, 80.99; H, 6.55; N, 3.81.

### 3.2. Preparation of samples for fluorescence measurement

**Materials.** Sensors were purified by column chromatography and then stored in refrigerator. The enantiomers of mandelic acid were purchased from Aldrich and recrystallized from methanol. They were then passed through a short column of silica gel (eluted with diethyl ether) and dried under vacuum. The enantiomers of protected amino acids were purchased from Advanced ChemTech and used without further purification. All the solvents were HPLC grade. All the stock solutions were freshly prepared for each measurement. A 0.1 M stock solution of mandelic acid was prepared using benzene containing 10% (V) DME. A 0.01 M stock solution of *N*-protected amino acid was prepared using benzene containing 5% (V) DME. DME was added to improve the solubility of the acid in benzene.

For the fluorescence study: A sensor solution was mixed with an acid solution at room temperature in a 5 mL volumetric flask, and DME was added to maintain the concentration. After diluted to the desired concentration, the solution was allowed to stand at room temperature for 4 h before the fluorescence measurements.

### 3.3. Experimental procedure for the job plots

The solutions ( $4.0 \times 10^{-3}$  M) of (*R*)-**2**, (*S*)-mandelic acid and **D-3** in 2% DME/ $C_6D_6$  were freshly prepared. The sensor

and acid solutions were added to NMR tubes in ratios of 10:0, 9:1, 8:2... to 0:10, respectively. The resulting mixture solutions were allowed to stand at room temperature for 4 h before the  $^1H$  NMR measurements.

### Acknowledgements

The support of this work from the National Institute of Health (R01EB002037) is gratefully acknowledged.

### References and notes

1. Pu, L. *Chem. Rev.* **1998**, *98*, 2405–2494.
2. Chen, Y.; Yekta, S.; Yudin, A. K. *Chem. Rev.* **2003**, *103*, 3155–3211.
3. Kočovský, P.; Vyskočil, S.; Smrčina, M. *Chem. Rev.* **2003**, *103*, 3213–3245.
4. (a) Lin, J.; Hu, Q. S.; Xu, M. H.; Pu, L. *J. Am. Chem. Soc.* **2002**, *124*, 2088–2089. (b) Xu, M.-H.; Lin, J.; Hu, Q.-S.; Pu, L. *J. Am. Chem. Soc.* **2002**, *124*, 14239–14246. (c) Lin, J.; Zhang, H.-C.; Pu, L. *Org. Lett.* **2002**, *4*, 3297–3300. (d) Lin, J.; Li, Z.-B.; Zhang, H.-C.; Pu, L. *Tetrahedron Lett.* **2004**, *45*, 103–106.
5. For a review on the enantioselective fluorescent recognition of chiral organic molecules, see: Pu, L. *Chem. Rev.* **2004**, *104*, 1687–1716.
6. Brunner, H.; Goldbrunner, J. *Chem. Ber.* **1989**, *122*, 2005–2010.
7. James, T. D.; Sandanayake, K. R. A. S.; Shinkai, S. *Nature* **1995**, *374*, 345–347.
8. (a) Blanda, M. T.; Horner, J. H.; Newcomb, M. J. *Org. Chem.* **1989**, *54*, 4626–4636. (b) Connors, K. A. *Binding Constants, The Measurement of Molecular Complex Stability*; Wiley-Interscience: New York, 1987; pp 24–28.
9. DiMauro, E. F.; Kozlowski, M. C. *Org. Lett.* **2001**, *3*, 1641–1644.



# A new terpyrrolic analogue of dipyrrolylquinoxalines: an efficient optical-based sensor for anions in organic media

Sergiy V. Shevchuk, Vincent M. Lynch and Jonathan L. Sessler\*

Department of Chemistry and Biochemistry, Institute for Cellular and Molecular Biology, 1 University Station-A5300, The University of Texas at Austin, Austin, TX 78712-0165, USA

Received 22 November 2003; revised 23 July 2004; accepted 19 August 2004

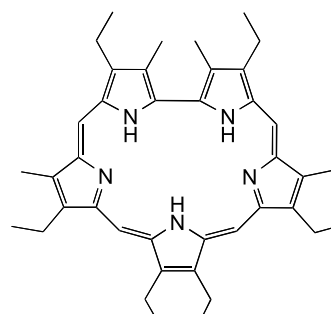
Available online 11 September 2004

**Abstract**—The synthesis and X-ray structural characterization of a new terpyrrolic analog of dipyrrolylquinoxaline (DPQ) is described that contains two pyrrole anion recognition groups bridged by a central 1,2-linked pyrrole. Relative to the ‘parent’ DPQ system, this new terpyrrolic scaffold acts as an improved colorimetric and fluorescent sensor for halide and dihydrogen phosphate anions in organic media. This enhancement is particularly dramatic in the case of  $\text{H}_2\text{PO}_4^-$  (studied as its tetrabutylammonium salt); in  $\text{CH}_2\text{Cl}_2$  it is bound with an affinity constant,  $K$ , of  $17,500 \text{ M}^{-1}$  by the terpyrrole of this report vs.  $80 \text{ M}^{-1}$  in the case of DPQ. The present findings thus support the emerging notion that a range of pyrrole-based anion recognition and sensing systems may be produced by replacing the central quinoxaline spacer in DPQs by other bridging subunits and that these new receptors may have properties that differ dramatically from their DPQ ‘parents’.

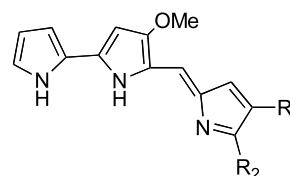
© 2004 Elsevier Ltd. All rights reserved.

## 1. Introduction

In recent years, increasing attention within the supramolecular community has been devoted to the development of neutral anion recognition systems.<sup>1–13</sup> Interest in such receptors is stimulated in part by the fact that anions play critical roles in biology,<sup>14–22</sup> medicine,<sup>23</sup> catalysis,<sup>24,25</sup> and the environment,<sup>26,27</sup> as well as the recent finding that the so-called chloride ion channel (CIC) contains no charged groups in its interior.<sup>28</sup> Currently, a wide range of uncharged synthetic anion receptors are known, with many of these relying on hydrogen bonding interactions to effect the critical anion recognition process.<sup>2–7,10–13,29–37</sup> Here, systems based on pyrrole are particularly noteworthy.<sup>10</sup> Originally suggested as an explanation for the fluoride anion binding of sapphyrin (e.g. **1**),<sup>38</sup> a pentapyrrolic ‘expanded porphyrin’ species that binds anions in both its mono- and diprotonated states,<sup>8</sup> pyrrole–anion interactions have recently been invoked to explain the mode of action of prodigiosin, tripyrrolic natural products (e.g. **2**) with promising anticancer and immunosuppressive characteristics.<sup>39–41</sup>



**1**



**2a**  $\text{R}_1 = \text{n-pentyl}; \text{R}_2 = \text{Me}$  (prodigiosin)

**2b**  $\text{R}_1 = \text{H}; \text{R}_2 = \text{n-dodecyl}$  (prodigiosin 25-C)

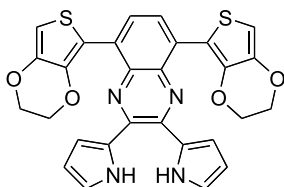
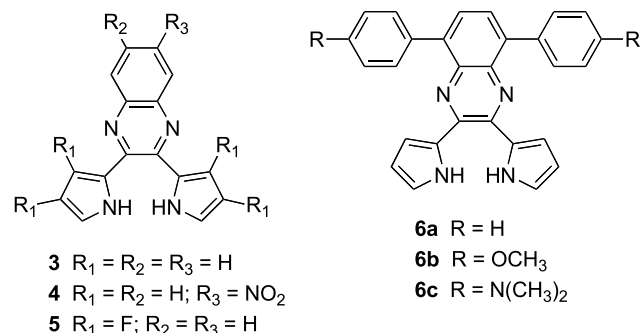
One of the reasons that pyrroles are attractive as anion binding motifs is that the pyrrolic NH groups are good hydrogen bond donors that are able to interact with Lewis basic anions. Also, in marked contrast to many other motifs, such as amides and related functional groups, pyrroles are free of a built-in hydrogen bond acceptors (e.g. carbonyls)

**Keywords:** Anion sensors; Pyrroles; Molecular recognition.

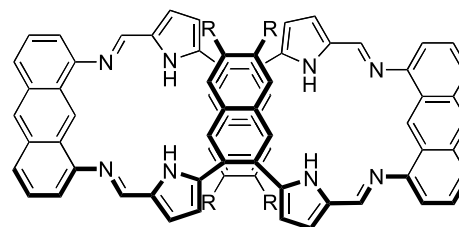
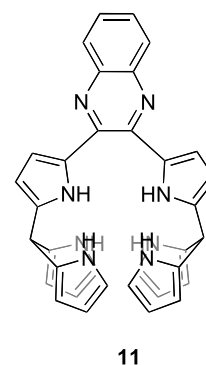
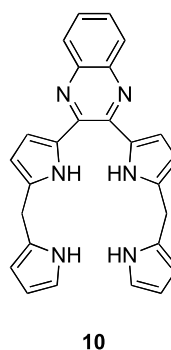
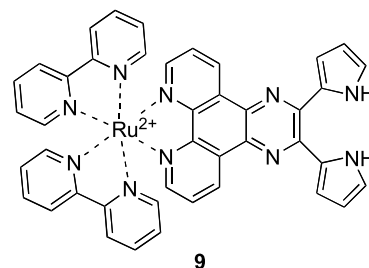
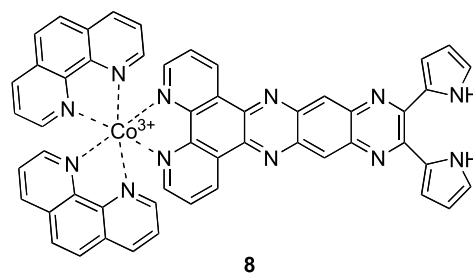
\* Corresponding author. Tel.: +1-512-471-5009; fax: +1-512-471-7550; e-mail: [ssessler@mail.utexas.edu](mailto:ssessler@mail.utexas.edu)

and this less prone to plagued by self-assembly or other ‘narcissistic’ interactions.<sup>42</sup> Furthermore, the pyrrole skeleton itself is relatively easy to functionalize, allowing pyrroles to be incorporated into more elaborate structures or combined with ion–dipole interactions to produce neutral or minimally charged receptors that display high affinities for anions.<sup>10</sup> Not surprisingly, therefore, over the past few years, we<sup>5,8,10,43–59</sup> and others<sup>10,44,60–67</sup> have exploited these features to generate a range of pyrrole-based anion receptors, including several categories of neutral anion binding systems, such as the calix[*n*]pyrroles,<sup>5–10,43–50,60–62</sup> calix[*n*]phyrins,<sup>51,52</sup> dipyrrolylquinoxalines,<sup>45,53–58,63–65</sup> and pyrrole amides.<sup>10,66,67</sup> Depending on the conditions, solvent, counter cation, substitution pattern, etc. these systems show a varying range of affinities and selectivities towards simple anions such as fluoride and dihydrogen phosphate.

Among the various neutral, pyrrole-based anion receptors produced to date, the dipyrrolylquinoxalines (DPQs) (e.g. **3–5**) have received particular attention.<sup>45,53–59,63,64</sup> This is because this simple class of anion binding agent allows for the facile detection of fluoride ions in dichloromethane and DMSO solution under both so-called naked-eye (i.e. direct visual) and fluorescence emission conditions. It has also been demonstrated that the colorimetric response of DPQs can be modified by appending substituents onto the receptor backbone, to give systems such as **4**,<sup>53</sup> **5**,<sup>45</sup> **6**,<sup>64</sup> and **7**,<sup>64</sup> or by ‘fusing’ them covalently to cation complexing agents (to give metal-containing species such as **8**<sup>54</sup> and **9**<sup>63</sup>). Likewise, it was found that the inherent selectivities could be modulated and the affinities increased by attaching ‘extra’ pyrrole recognition motifs to the  $\alpha$ -pyrrolic positions of **3** (to give, for instance, **10** and **11**)<sup>56</sup> or by generating macrocyclic structures (e.g. **12**).<sup>58</sup>



7



**12a**  $R = H$   
**12b**  $R = OCH_3$   
**12c**  $R = OCH_2CH_3$

While at present the exact mechanism of the colorimetric response remains to be elucidated, and could involve a range of factors, including charge transfer effects, changes in pyrrole NH bond polarization, and in the limit partial or complete deprotonation of the pyrrolic subunit, the conformational flexibility of the DPQ skeleton has led us to suggest that much of the effect is due to changes in geometry; specifically, it is proposed that anion binding leads to a rigidification of the system and a modulation of the pyrrole–quinoxaline–pyrrole orbital overlap that is directly manifest in terms of differences in the light absorbing and emitting properties of the chromophore as whole (cf. Fig. 1).<sup>53</sup> To the extent this mechanistic rationale proves true, it leads to the consideration that the basic DPQ-like approach to anion sensing could be generalized by replacing the pyrrole-bridging quinoxaline motif, shown as a box in Figure 1, with some other bridging chromophore.

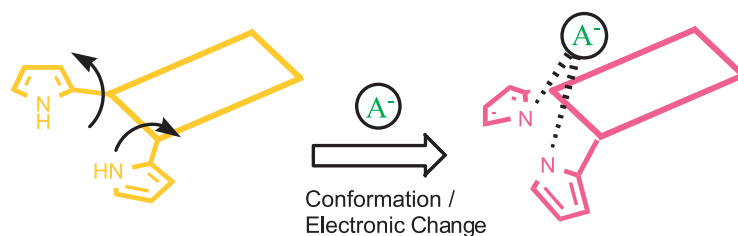
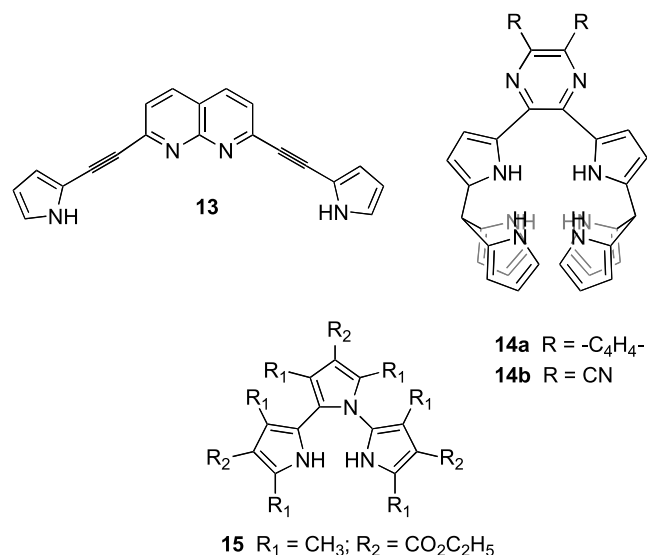


**Figure 1.** Schematic representation of the DPQ-based approach to anion recognition and sensing. Here, it is proposed that the orbital overlap between the pyrroles and the appended chromophore, quinoxaline in the original embodiment, but potentially a large range of chromophores, is perturbed as the result of anion binding. This figure originally appeared in Ref. 53 and is reproduced with permission. Copyright 1999, American Chemical Society.



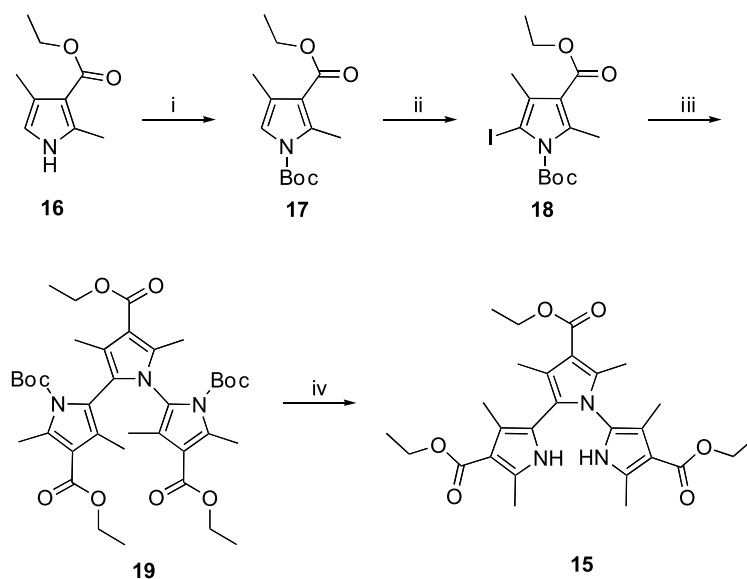
Recently, such a strategy has been realized by Fang and colleagues, wherein a bis-alkyne substituted naphthyridine subunit was used to replace the quinoxaline bridge (cf. structure **13**),<sup>65</sup> and by our own group by using pyrazine instead of quinoxaline as the critical pyrrole–pyrrole tethering element (e.g. **14**).<sup>57</sup> However, as implied by Figure 1, a much greater range of bridging chromophores can be anticipated. Towards this end, we report here the synthesis, X-ray structure, and anion binding properties of a

new terpyrrolic analogue (**15**) of DPQ that relies on a fused pyrrole bridging element. We also show that relative to the ‘parent’ DPQ system (**3**), compound **15** acts as an improved anion receptor and fluorescent anion sensor in organic media.

## 2. Results and discussion

Compound **15** was initially obtained in low yield (ca. 5%) as a by-product when compound **16** was subject to iodination. Appreciating its potential use as an anion receptor led us to prepare it via a more rational route, as summarized in Scheme 1. Briefly, pyrrole **16**, obtained in accord with a literature procedure,<sup>68</sup> was reacted with di-*tert*-butyl dicarbonate under conditions of basic catalysis to produce the BOC-protected pyrrole **17** in nearly quantitative yield (cf. Section 3). Direct iodination of pyrrole **17** with NaI and I<sub>2</sub> gave the iodopyrrole **18** in excellent yield. Two equivalents of this pyrrole were then coupled with 1 equiv of **16** to form terpyrrole **19** in ca. 70% yield. Acid-induced cleavage of the BOC groups then gave the target compound **15** in almost quantitative yield.

Proton NMR analysis of **15** revealed the NH signal as a broad singlet at 8.50 ppm that is shifted upfield by ca. 1 ppm as compared to the corresponding resonance in **3** ( $\delta = 9.54$ ).<sup>53</sup> In **15**, the methyl protons of ethyl esters were found to resonate as a set of multiplets between 1.31–1.41 ppm,



Scheme 1.

whereas six different singlets, corresponding to the  $CH_3$  protons, were observed in the spectrum between 1.62 and 2.57 ppm. Presumably, this large number of signals reflects the non-symmetric nature of terpyrrole **15**, wherein the two flanking pyrroles are connected to the central pyrrole via direct  $\alpha$ -carbon-to- $\alpha$ -carbon and  $\alpha$ -carbon-to-nitrogen linkages, respectively. On the other hand, the chemically distinct methylene groups present in **15** were found to resonate at the same frequency, appearing as a quartet at 4.25 ppm that integrates to the expected 6H. Similar  $^1H$  NMR spectral features were seen for precursor **19**. While, fewer signals were observed in the  $^{13}C$  NMR spectra of both

terpyrroles **15** and **19** than were expected based on their presumed structures, follow-up  $^1H$ - $^{13}C$  NMR correlation experiments confirmed that this was simply due to a coincident overlapping of signals.

A single crystal X-ray diffraction analysis of compound **15** served to confirm its expected structure. It also revealed that **15** forms aggregates in the solid state that are characterized by intermolecular hydrogen-bonding interactions between two pyrrole NH donor groups of a single terpyrrole and the carbonyl substituents of two neighboring molecules (cf. Fig. 2). Presumably, as the result of these interactions, the

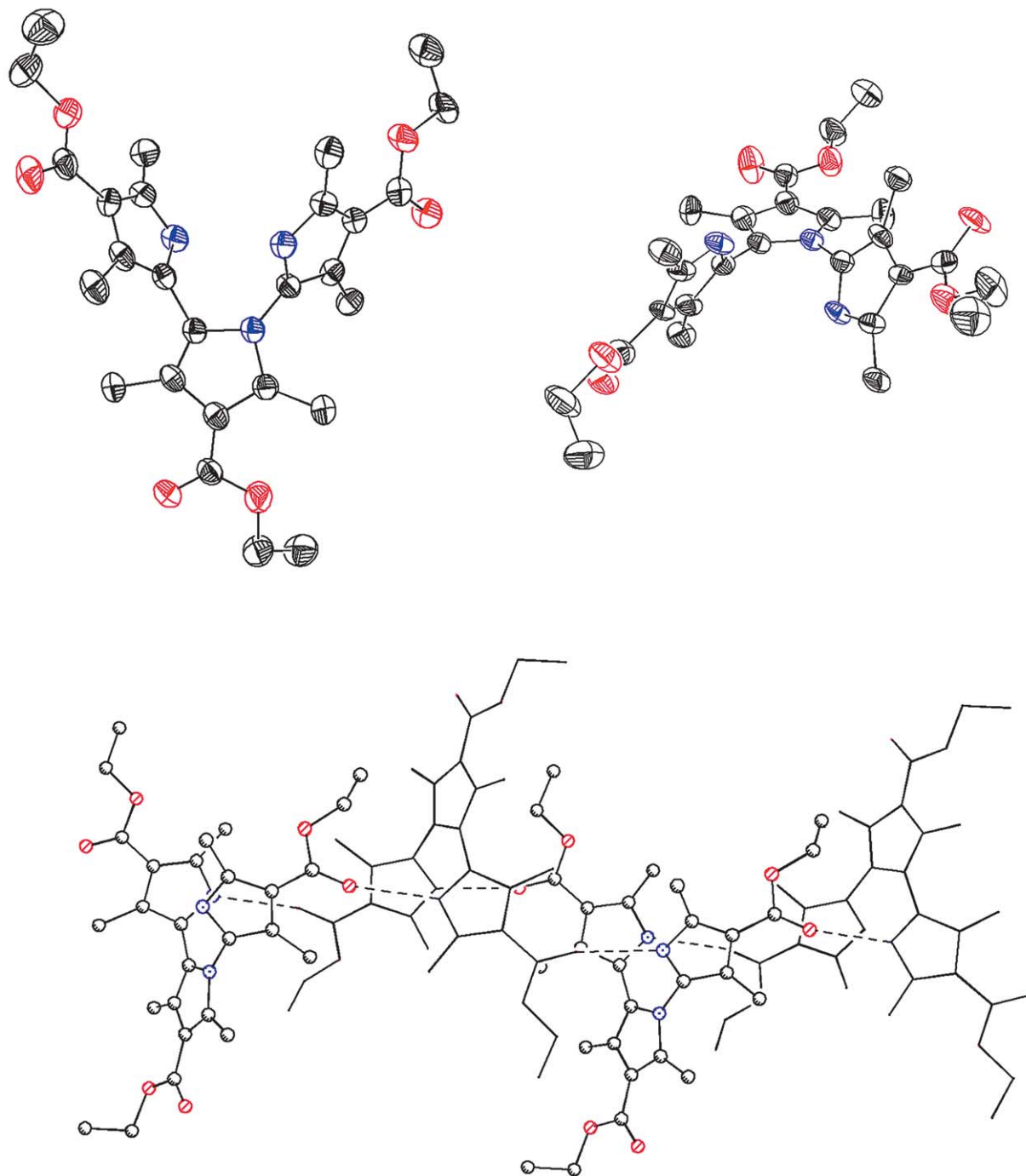


**Figure 2.** Top: two views of the solid state crystal structure of **15** (thermal ellipsoids are scaled to the 50% probability level). Bottom: unit cell packing diagram for **15** showing the hydrogen bonding interactions between two adjacent molecules.

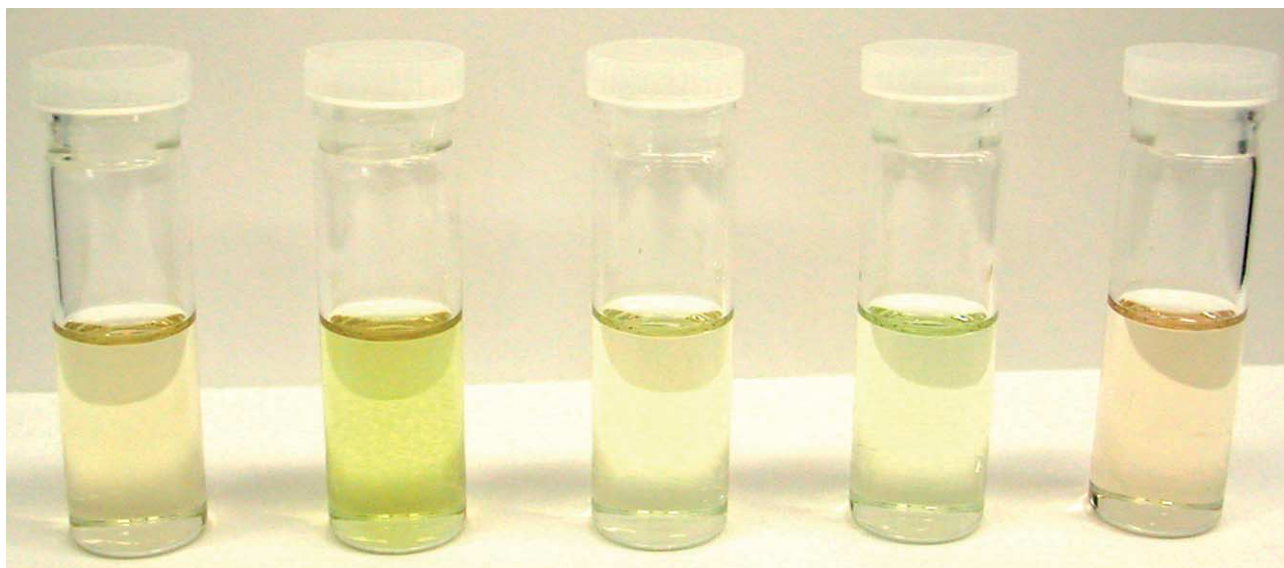


**Figure 3.** Color changes induced by the addition of anions (1.5 mequiv) in the form of their tetrabutylammonium salts to dichloromethane solution of receptor **15** (concentration = 1 mM). From left to right: **15**; **15** + F<sup>-</sup>; **15** + Cl<sup>-</sup>; **15** + Br<sup>-</sup>; **15** + H<sub>2</sub>PO<sub>4</sub><sup>-</sup>.

two NH groups of individual molecules of **15** are oriented in opposite directions relatively to one another.

Based on the binding site analogy between DPQs **3–5** and system **15**, this latter terpyrrole system was expected to act as a receptor for halide and phosphate anions in organic media, displaying, as does DPQ itself, the highest relative affinity for fluoride anion. Consistent with this supposition, compound **15** when made up as a dilute dichloromethane solution was found to undergo a visible color change when treated with the tetrabutylammonium salts of fluoride, chloride and dihydrogen phosphate, as illustrated in **Figure 3**. Similar color changes were also seen in DMSO, although only in the presence of a large excess of anionic substrate.

The fluorescence intensity of **15** was also found to be quenched when organic solutions containing it were titrated

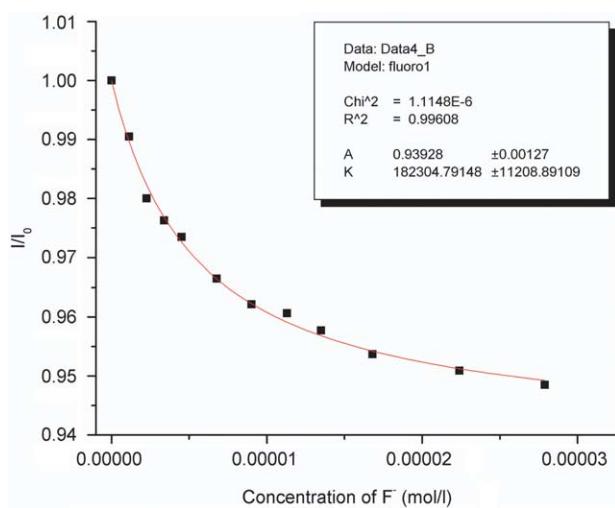


**Figure 4.** Binding isotherm produced when receptor **15** ( $1 \times 10^{-6}$  M) is titrated with increasing quantities of fluoride in dichloromethane at 22 °C. The points represent experimental values, while the line represents a least squares fit to these points assuming a 1:1 binding stoichiometry.

with increasing quantities of the targeted anions (again, in the form of their respective tetrabutylammonium salts). The use of a Scatchard analysis, in accord with Eq. (1),<sup>69</sup> then allowed quantification of the results.

$$F/F_0 = (1 + (k_f/k_s)K[L]) / (1 + K[L]) \quad (1)$$

Here,  $F$  and  $F_0$  refer to the fluorescence intensity,  $k_f$  and  $k_s$  are proportionality constants for the bound complex and the receptor, respectively, and  $K$  is the anion binding constant. An example of the plot produced when receptor **15** is titrated with fluoride in dichloromethane is presented on **Figure 4**. Data and curve fits consistent with 1:1 binding processes were obtained in all cases, with this stoichiometry being independently confirmed by Job plot analysis (cf. **Fig. 5**). The  $K$  values resulting from this combination of experimental study and data analysis are given in **Table 1**.

### 3. Conclusions

Compared to that reported earlier for analogue **3**, the

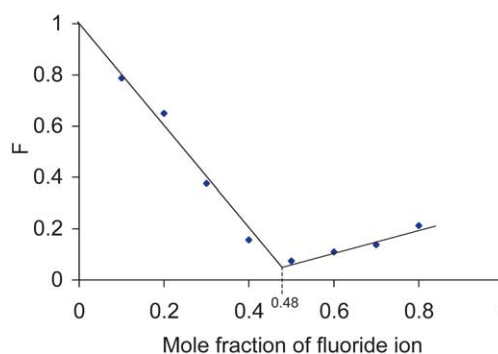


**Figure 5.** Job-plot analysis for a fluorescent titration experiment in chloroform involving the interaction of receptor **15** with fluoride ion (studied in the form of its commercially available tetrabutylammonium salt). In this experiment, fluorescence ( $F$ ) is measured as a function of the mole fraction of fluoride anion. The observation of maximum fluorescence when the mole fraction is 0.48 supports the proposed 1:1 binding stoichiometry.



**Table 1.** Anion binding constants ( $K$ ) for compounds **3**<sup>53</sup> and **15** in dichloromethane<sup>a</sup>

	<b>3</b> ( $M^{-1}$ )	<b>15</b> ( $M^{-1}$ )
F <sup>-</sup>	18,200	182,000
Cl <sup>-</sup>	65	160
Br <sup>-</sup>	—	60
H <sub>2</sub> PO <sub>4</sub> <sup>-</sup>	80	17,500

<sup>a</sup> Values obtained by fluorescent titration as detailed in the text; all errors were <10%.

fluoride anion affinity of receptor **15** is roughly an order of magnitude higher for studies carried out under identical conditions. While this increase can be ascribed to the presence of three electron-withdrawing ester substituents appended directly to the pyrrolic moieties of **15**, the fact that a dramatically increased affinity for dihydrogen phosphate is displayed by **15** relative to **3** leads to the suggestion that this new system could have a role to play as a selective anion sensor. On a more fundamental level, the present work serves to illustrate the potential versatility of the generalized DPQ paradigm. By selecting different aromatic, and perhaps non-aromatic, chromophores and using them to bridge the pyrrolic recognition subunits, a range of new receptors may be potentially obtained. It is to be anticipated that changing the pyrrole-linking spacers in this way will not only allow the inherent anion recognition selectivities of DPQ-type systems to be modified, but also produce systems wherein the nature of the optical signal used to monitor the anion binding event is further optimized (e.g. from anion-induced fluorescence quenching to anion-induced fluorescence enhancement). Accordingly, work on new DPQ receptor systems containing alternative, non-quinoxaline bridging elements is ongoing in our laboratory.

## 4. Experimental

### 4.1. General data

All chemicals (obtained from Aldrich Chemical Co.) and solvent (purchased from EM Science) were of reagent grade quality and used without further purification unless otherwise stated. Spectroscopic grade dichloromethane used for anion binding experiments was passed quickly through activated aluminium oxide prior sample preparation. All NMR solvents were purchased from Cambridge Isotope Laboratories, Inc. SAI silica gel 60 (230–400 mesh) and Aldrich aluminium oxide (activated, neutral, Brockmann I standard grade, 150 mesh, 58 Å) were used for column chromatography. Thin layer chromatography was performed on silica gel 60 Å, 200 µm plates purchased from Scientific Adsorbents, Inc. Electronic absorption spectra were recorded on a Beckman DU-7 spectrophotometer, using 1 cm quartz cells. Fluorescence excitation and emission spectra were recorded using a Fluorog 3 (Jobin Yvon-Spex) fluorimeter. Proton and <sup>13</sup>C NMR spectra were obtained on either Varian UNITY + 300 or Varian 500 MHz spectrometers. All NMR spectra were referenced to solvent. Mass spectra were measured with either a Finnigan-MAT 4023, Bell and Howell 21-491 or VG Analytical ZAB E/SE instrument. Elemental analyses were performed by Atlantic Microlab, Inc.

### 4.2. Techniques and materials

**4.2.1. 2,4-Dimethylpyrrole-1,3-dicarboxylic acid 1-tert-butyl ester 3-ethyl ester (17).** A mixture of 2,4-dimethyl-1H-pyrrole-3-carboxylic acid ethyl ester **16** (0.8361 g, 5 mmol),<sup>68</sup> di-tert-butyl dicarbonate (1.0913 g, 5 mmol) and 4-dimethylaminopyridine (0.0061 g, 0.05 mmol) in 30 ml of dichloromethane was stirred at room temperature under argon atmosphere for 2 h. The solution was concentrated in vacuo to give **17** as an oil (1.2960 g, 97%) which gradually solidified and used without further purification. <sup>1</sup>NMR (CDCl<sub>3</sub>), δ, ppm: 1.29 (t, 3H, CH<sub>2</sub>CH<sub>3</sub>), 1.53 (s, 9H, tert-butyl), 2.10 (s, 3H, CH<sub>3</sub>), 2.69 (s, 3H, CH<sub>3</sub>), 4.22 (q, 2H, CH<sub>2</sub>CH<sub>3</sub>), 6.85 (s, 1H, CH); <sup>13</sup>C NMR (CDCl<sub>3</sub>), δ, ppm: 12.3, 13.6, 14.1, 27.5, 59.3, 83.8, 116.3, 118.1, 121.2, 138.6, 148.8, 165.3; CI-MS (M<sup>+</sup>): 268.

**4.2.2. 5-Iodo-2,4-dimethylpyrrole-1,3-dicarboxylic acid 1-tert-butyl ester 3-ethyl ester (18).** Sodium bicarbonate (1.008 g, 12 mmol) and water (20 ml) were combined in a 250 ml round-bottom flask equipped with a reflux condenser. The solution was stirred and heated to 50 °C. To this was added 70 ml of 1,2-dichloroethane followed by 2,4-dimethylpyrrole-1,3-dicarboxylic acid 1-tert-butyl ester 3-ethyl ester (**17**, 1.07 g, 4 mmol). At this point, iodine (0.6731 g, 5.3 mmol) and sodium iodide (1.5 g, 10 mmol) dissolved in water (25 ml) were added over 20 min. The resulting dark solution was then heated at reflux for 3 h. The mixture was then cooled to room temperature and crystalline Na<sub>2</sub>S<sub>2</sub>O<sub>3</sub> added to discharge excess iodine. The mixture was then transferred to a separatory funnel, and the aqueous phase washed with CHCl<sub>3</sub> (3×30 ml). The combined organic layers were washed with a 5% solution of Na<sub>2</sub>S<sub>2</sub>O<sub>3</sub> (3×30 ml), a 5% solution of NaHCO<sub>3</sub> (3×30 ml), and then dried over Na<sub>2</sub>SO<sub>4</sub> before the solvent was removed on a rotary evaporator to leave an off-white solid which recrystallized from CH<sub>2</sub>Cl<sub>2</sub>/hexanes to give (1.573 g, 72%) of **18**. <sup>1</sup>NMR (CDCl<sub>3</sub>), δ, ppm: 1.37 (t, 3H, CH<sub>2</sub>CH<sub>3</sub>), 1.58 (s, 9H, tert-butyl), 1.97 (s, 3H, CH<sub>3</sub>), 2.15 (s, 3H, CH<sub>3</sub>), 4.35 (q, 2H, CH<sub>2</sub>CH<sub>3</sub>); <sup>13</sup>C NMR (CDCl<sub>3</sub>), δ, ppm: 10.7, 14.1, 24.7, 28.2, 61.5, 84.4, 89.7, 141.8, 143.3, 150.0, 162.5, 166.3; CI-MS (M<sup>+</sup>): 394.

**4.2.3. 3,5,3',5',3'',5''-Hexamethyl-[2,1',2',2'']terpyrrole-1,4,4',1'',4''-pentacarboxylic acid 1,1''-di-tert-butyl ester 4,4',4''-triethyl ester (19).** 2,4-Dimethylpyrrole-1,3-dicarboxylic acid 1-tert-butyl ester 3-ethyl ester (**17**, 0.317 g, 1.9 mmol) and NaHCO<sub>3</sub> (1.008 g, 12 mmol) were dissolved in 30 ml of acetonitrile. A solution of 5-iodo-2,4-dimethylpyrrole-1,3-dicarboxylic acid 1-tert-butyl ester 3-ethyl ester (**18**, 1.49 g, 3.8 mmol) in acetonitrile (15 ml) was added. The resulting mixture was put under reflux for 12 h. The solvent was then removed under reduced pressure and the residue was redissolved in dichloromethane, filtrated and washed with 1 M solution of HCl (3×50 ml), water (3×50 ml) and dried over Na<sub>2</sub>SO<sub>4</sub>, concentrated in vacuo to give oil. Column chromatography (silica gel, ethyl acetate/hexanes/ 30:70, R<sub>f</sub>=0.65) gave compound **19** (0.9347 g, 70.5%). <sup>1</sup>NMR (CDCl<sub>3</sub>), δ, ppm: 1.26 (br.s., 18H, tert-butyl); 1.35 (m, 9H, CH<sub>2</sub>CH<sub>3</sub>); 1.53 (s, 3H, CH<sub>3</sub>); 1.92 (s, 6H, CH<sub>3</sub>); 2.75 (s, 6H, CH<sub>3</sub>); 3.09 (s, 3H, CH<sub>3</sub>); 4.28 (q, 6H, CH<sub>2</sub>CH<sub>3</sub>); <sup>13</sup>C NMR (CDCl<sub>3</sub>), δ, ppm: 11.5, 14.1, 14.3,

27.4, 27.9, 59.6, 83.7, 115.2, 121.7, 123.5, 139.3, 149.3, 165.7; CI-MS ( $M^+$ ): 698.

#### 4.2.4. 3,5,3',5',3'',5''-Hexamethyl-1H,1''H-[2,1,2',2'']-terpyrrole-4,4',4''-tricarboxylic acid triethyl ester (**15**).

TFA (1.98 g, 17.4 mmol) in 15 ml of dichloromethane was added to 3,5,3',5',3'',5''-hexamethyl-[2,1,2',2'']terpyrrole-1,4,4',1'',4''-pentacarboxylic acid 1,1''-di-*tert*-butyl ester 4,4',4''-triethyl ester (**19**, 0.9 g, 1.3 mmol) in a single addition and the solution was stirred at room temperature for 16 h. The solution was concentrated in vacuo, redissolved in dichloromethane and washed with a 10% solution of  $Na_2CO_3$  (3 × 40 ml). The organic extract was dried over  $Na_2SO_4$  and concentrated on rotary evaporator. The product (0.62 g, 96%) was obtained after purification by column chromatography (silica gel, dichloromethane,  $R_f = 0.71$ ).  $^1NMR$  ( $CDCl_3$ ),  $\delta$ , ppm: 1.31–1.41 (m, 9H,  $CH_2CH_3$ ); 1.62 (s, 3H,  $CH_3$ ); 1.87 (s, 3H,  $CH_3$ ); 2.10 (s, 3H,  $CH_3$ ); 2.50 (s, 3H,  $CH_3$ ); 2.52 (s, 3H,  $CH_3$ ); 2.57 (s, 3H,  $CH_3$ ); 4.27 (q, 6H,  $CH_2CH_3$ ); 8.50 (br.s., 2H, NH);  $^{13}C$  NMR ( $CDCl_3$ ),  $\delta$ , ppm: 12.5, 14.0, 14.1, 14.2, 14.5, 14.7, 21.2, 59.2, 62.8, 89.0, 112.1, 118.7, 122.9, 138.1, 138.5, 141.3, 150.3, 165.7, 169.9; CI-MS ( $M^+$ ): 498. Anal. calcd. for  $C_{27}H_{35}N_3O_6$ , %: C, 65.17; H, 7.09; N, 8.44; Found, %: C, 65.30; H, 7.11; N, 8.42.

#### 4.3. Fluorescence titration studies

Fluorescence quenching experiments were performed as described previously.<sup>70</sup> Briefly, the procedure was as follows: Solutions of receptor **15** in dichloromethane were titrated with increasing quantities of concentrated solutions of the anions (as the corresponding tetrabutylammonium salts). The need to compensate for dilution effects was obviated by preparing and using stock anion solutions containing receptor **15** at its initial concentration. To provide further confirmation of the proposed 1:1 binding stoichiometry, separate titration studies were carried out at two different concentrations of receptor **15**, namely  $[15] = 1 \times 10^{-6}$  and  $[15] = 1 \times 10^{-5}$  M, respectively, with concordant results being obtained in both cases. Separate Job plot analyses were also carried out in some instances (cf. Fig. 5). Emission spectra were recorded between 350 and 600 nm, with excitation at  $\lambda_{ex} = 335$  nm. All titration

experiments were performed in triplicate and the results of individual determinations were found not to differ from one another by more than 15%.

#### 4.4. Crystal structure determination

Suitable single crystals of **15** were obtained in the form of pale yellow needles by slow vacuum sublimation. The data crystal was cut from a long needle and had approximate dimensions;  $0.24 \times 0.10 \times 0.06$  mm<sup>3</sup>. The data were collected on a Nonius Kappa CCD diffractometer using a graphite monochromator with Mo  $K\alpha$  radiation ( $\lambda = 0.71073$  Å). A total of 223 frames of data were collected using  $\omega$ -scans with a scan range of  $1^\circ$  and a counting time of 319 s per frame. The data were collected at 153 K using an Oxford Cryostream low temperature device. Details of structure refinement, data collection, and crystallographic data (excluding structure factors) for the structure reported in this paper have been deposited with the Cambridge Crystallographic Data Centre as supplementary publication number CCDC 223924. Copies of the data can be obtained, free of charge, on application to CCDC, 12 Union Road, Cambridge, CB2 1EZ, UK [fax: +44(0)-1223-336033 or e-mail: [deposit@ccdc.cam.ac.uk](mailto:deposit@ccdc.cam.ac.uk)]. A summary of the X-ray experimental parameters is also given in Table 2.

#### Acknowledgements

This work was supported by the National Institutes of Health (grant GM 58907 to J.L.S.).

#### References and notes

1. *Supramolecular Chemistry of Anions*; Bianchi, A., Bowman-James, K., Garcia-España, E., Eds.; Wiley-VCH: New York, 1997.
2. Antonisse, M. M. G.; Reinhoudt, D. N. *Chem. Commun.* **1998**, 443–448.
3. Snowden, T. S.; Anslyn, E. V. *Curr. Opin., Chem. Biol.* **1999**, 3, 740–746.
4. Beer, P. D.; Cadman, J. *Coord. Chem. Rev.* **2000**, 205, 131–155.
5. Gale, P. A.; Anzenbacher, P.; Sessler, J. L. *Coord. Chem. Rev.* **2000**, 222, 57–102.
6. Gale, P. A. *Coord. Chem. Rev.* **2001**, 213, 79–128.
7. Beer, P. D.; Gale, P. A. *Angew. Chem., Int. Ed. Engl.* **2001**, 40, 486–516.
8. Sessler, J. L.; Davis, J. M. *Acc. Chem. Res.* **2001**, 34, 989–997.
9. Best, M. D.; Tobey, S. L.; Anslyn, E. V. *Coord. Chem. Rev.* **2003**, 240, 3–15.
10. Sessler, J. L.; Camiolo, S.; Gale, P. A. *Coord. Chem. Rev.* **2003**, 240, 17–55.
11. Bondy, C. R.; Loeb, S. J. *Coord. Chem. Rev.* **2003**, 240, 77–99.
12. Choi, K.; Hamilton, A. D. *Coord. Chem. Rev.* **2003**, 240, 101–110.
13. Smith, B. D.; Lambert, T. N. *Chem. Commun.* **2003**, 2261–2268.

**Table 2.** X-ray experimental data for compound **15**

Formula	$C_{27}H_{35}N_3O_6$
Molecular weight	497.58
Crystal system	Monoclinic
Space group	$C2/c$
$a/\text{Å}$	25.6029(8)
$b/\text{Å}$	15.9471(6)
$c/\text{Å}$	14.1452(6)
$\alpha/^\circ$	90.0
$\beta/^\circ$	109.988(2)
$\gamma/^\circ$	90.0
$U/\text{Å}^3$	5427.5(4)
$Z$	8
$\mu/\text{mm}^{-1}$	0.086
$T/K$	153
Number of data measured	4604
Number of data with $I > 2\sigma(I)$	2199
$R$	0.110
$R_w$	0.245

14. Kirk, K. L. *Biochemistry of the Elemental Halogens and Inorganic Halides*; Plenum: New York, 1991.
15. He, M. X.; Wang, S.; Downey, H. F.; *Am J. Physiol.* **1997**, *272*, H1333–H1341.
16. Feranchak, A. P.; Roman, R. M.; Schwiebert, E. M.; Fitz, J. G. *J. Biol. Chem.* **1998**, *273*, 14906–14911.
17. Alberts, B. *Molecular Biology of the Cell*, 2nd ed.; Garland: New York, 1989; pp 301–304.
18. Kaplan, R. S. *J. Membr. Biol.* **2001**, *179*, 165–183.
19. Anderson, M. P.; Gregory, R. J.; Thompson, S.; Souza, D. W.; Paul, S.; Mulligan, R. C.; Smith, A. E.; Welsh, M. J. *Science* **1991**, *253*, 202–205.
20. Simon, D. B.; Bindra, R. S.; Mansfield, T. A.; Nelson-Williams, C.; Mendonca, E.; Stone, R.; Schurman, S.; Nayir, A.; Alpay, H.; Bakkaloglu, A.; Rodriguez-Soriano, J.; Morales, J. M.; Sanjad, S. A.; Taylor, C. M.; Pilz, D.; Brem, A.; Trachtman, H.; Griswold, W.; Richard, G. A.; John, E.; Lifton, R. P. *Nat. Genet.* **1997**, *17*, 171–178.
21. Piwon, N.; Gunther, W.; Schwake, M.; Bosl, M. R.; Jentsch, T. J. *Nature* **2000**, *408*, 369–373.
22. Yoshida, A.; Taniguchi, S.; Hisatome, I.; Royaux, I. E.; Green, E. D.; Kohn, L. D.; Suzuki, K. *J. Clin. Endocrinol. Metabol.* **2002**, *87*, 3356–3361.
23. Kleerekoper, M. *Endocrinol. Metab. Clin. North Am.* **1998**, *27*, 441–452.
24. Schwartz, B.; Drueckhammer, D. G. *J. Am. Chem. Soc.* **1995**, *117*, 11902–11905.
25. Beck, B.; Proscenc, M.-H.; Brintzinger, H.-H. *J. Mol. Catal. A: Chem.* **1998**, *128*, 41–52.
26. Clark, J. F.; Clark, D. L.; Whitener, G. D.; Schroeder, N. C.; Strauss, S. H. *Environ. Sci. Tehnol.* **1996**, *30*, 3124–3127.
27. Christensen, T. H.; Kjeldsen, P.; Bjerg, P. L.; Jensen, D. L.; Christensen, J. B.; Baun, A.; Albrechtson, H. J.; Heron, C. *Appl. Geochem.* **2001**, *16*, 659–718.
28. Dutzler, R.; Campbell, E. B.; Cadene, M.; Chait, B. T.; MacKinnon, R. *Nature* **2002**, *415*, 287–294.
29. Atanas, V.; Koulov, A. V.; Timothy, N.; Lambert, T. N.; Rameshwer Shukla, R.; Mahim Jain, M.; Middleton Boon, J. M.; Bradley, D.; Smith, B. D.; Hongyu Li, H.; Sheppard, D. N.; Jean-Baptiste Joos, J.-B.; Clare, J. P.; Davis, A. P. *Angew. Chem. Int. Ed.* **2003**, *43*, 4931–4933.
30. Nishizawa, S.; Bühlmann, P.; Iwao, M.; Umezawa, Y. *Tetrahedron Lett.* **1995**, *36*, 6483–6486.
31. Sasaji, S.-i.; Mizuno, M.; Naemura, K.; Tobe, Y. *J. Org. Chem.* **2000**, *65*, 275–283.
32. Cho, E. J.; Moon, J. W.; Ko, S. W.; Lee, J. Y.; Kim, S. K.; Yoon, J.; Nam, K. C. *J. Am. Chem. Soc.* **2003**, *125*, 12376–12377.
33. Pratt, M. D.; Beer, P. D. *Polyhedron* **2003**, *22*, 649–653.
34. Lee, D. H.; Lee, H. Y.; Hong, J.-I. *Tetrahedron Lett.* **2002**, *43*, 7273–7276.
35. Mei, M.; Wu, S. *New J. Chem.* **2001**, *25*, 471–475.
36. Hall, A. J.; Achilli, L.; Manesiotis, P.; Quaglia, M.; De Lorenzi, D.; Sellergren, B. *J. Org. Chem.* **2003**, *68*, 9132–9135.
37. Kelly, T. R.; Kim, M. H. *J. Am. Chem. Soc.* **1994**, *116*, 7072–7080.
38. Sessler, J. L.; Cyr, M. J.; Lynch, V.; McGhee, E.; Ibers, J. A. *J. Am. Chem. Soc.* **1990**, *112*, 2810–2813.
39. Sato, T.; Konno, H.; Tanaka, Y.; Kataoka, T.; Nagai, K.; Wasserman, H. H.; Ohkuma, S. *J. Biol. Chem.* **1998**, *273*, 21455–21462.
40. Ohkuma, S.; Sato, T.; Okamoto, M.; Matsuya, H.; Arai, K.; Kataoka, T.; Nagai, K.; Wasserman, H. H. *Biochem. J.* **1998**, *334*, 731–741.
41. Fürstner, A. *Angew. Chem. Int. Ed.* **2003**, *42*, 3582–3603.
42. Sessler, J. L.; Berthon-Gelloz, G.; Gale, P. A.; Camiolo, S.; Anslyn, E. V.; Anzenbacher, P.; Furuta, H.; Kirkovits, G.; Lynch, V.; Maeda, H.; Morosini, P.; Scherer, M.; Shriver, J.; Zimmerman, R. S. *Polyhedron* **2003**, *22*, 2963–2983.
43. Gale, P. A.; Sessler, J. L.; Král, V. *Chem. Commun.* **1998**, 1–8.
44. Lee, C.-H.; Na, H.-K.; Yoon, D.-W.; Won, D.-H.; Cho, W.-S.; Lynch, V. M.; Shevchuk, S. V.; Sessler, J. L. *J. Am. Chem. Soc.* **2003**, *125*, 7301–7306.
45. Anzenbacher, P.; Try, A. C.; Miyaji, H.; Jurisíková, K.; Lynch, V. M.; Marquez, M.; Sessler, J. L. *J. Am. Chem. Soc.* **2000**, *122*, 10268–10272.
46. Sessler, J. L.; Anzenbacher, P.; Shriver, J. A.; Jurisíková, K.; Miyaji, H.; Lynch, V. M.; Marquez, M. *J. Am. Chem. Soc.* **2000**, *122*, 12061–12062.
47. Levitskaia, T. G.; Marquez, M.; Sessler, J. L.; Shriver, J. A.; Vercouter, T.; Moyer, B. A. *Chem. Commun.* **2003**, 2248–2249.
48. Sessler, J. L.; An, D.; Cho, W.-S.; Lynch, V. *Angew. Chem. Int. Ed.* **2003**, *42*, 2278–2281.
49. Sessler, J. L.; An, D.; Cho, W. S.; Lynch, V. *J. Am. Chem. Soc.* **2003**, *125*, 13646–13647.
50. Bucher, C.; Zimmerman, R. S.; Lynch, V.; Sessler, J. L. *J. Am. Chem. Soc.* **2001**, *123*, 9716–9717.
51. Sessler, J. L.; Zimmerman, R. S.; Bucher, C.; Král, V.; Andioletti, B. *Pure Appl. Chem.* **2001**, *73*, 1041–1057.
52. Sessler, J. L.; Cho, W.-S.; Dudek, S. P.; Hicks, L.; Lynch, V. M.; Huggins, M. T. *J. Porph. Phthaloc.* **2003**, *7*, 97–104.
53. Black, C. B.; Andioletti, B.; Try, A. C.; Ruiperez, C.; Sessler, J. L. *J. Am. Chem. Soc.* **1999**, *121*, 10438–10439.
54. Mizuno, T.; Wei, W.-H.; Eller, L. R.; Sessler, J. L. *J. Am. Chem. Soc.* **2002**, *124*, 1134–1135.
55. Kerkovits, G. J.; Zimmerman, R. S.; Huggins, M. T.; Lynch, V. M.; Sessler, J. L. *Eur. J. Org. Chem.* **2002**, 3768–3778.
56. Sessler, J. L.; Maeda, H.; Mizuno, T.; Lynch, V. M.; Furuta, H. *Chem. Commun.* **2002**, 862–863.
57. Sessler, J. L.; Pantos, G. D.; Katayev, E.; Lynch, V. M. *Org. Lett.* **2003**, *5*, 4141–4144.
58. Sessler, J. L.; Maeda, H.; Mizuno, T.; Lynch, V. M.; Furuta, H. *J. Am. Chem. Soc.* **2002**, *124*, 13474–13479.
59. Sessler, J. L.; Andioletti, B.; Anzenbacher, P.; Black, C.; Eller, L.; Furuta, H.; Jursíková, K.; Maeda, H.; Marquez, M.; Mizuno, T.; Try, A. 2,3-Dipyrrolylquinoxaline-based Anion Sensors. *Fundamentals and Applications of Anion Separations*; Moyer, B. A., Singh, R. P., Eds.; Kluwer Academic/Plenum: New York, 2004; pp 71–85.
60. Schmidtchen, F. P. *Org. Lett.* **2002**, *4*, 431–434.
61. Yoon, D.-W.; Hwang, H.; Lee, C.-H. *Angew. Chem., Int. Ed.* **2002**, *41*, 1757–1759.
62. Warriner, C. N.; Gale, P. A.; Light, M. E.; Hursthouse, M. B. *Chem. Commun.* **2003**, 1810–1811 and references therein.
63. Anzenbacher, P.; Tyson, D. S.; Jursíková, K.; Castellano, F. N. *J. Am. Chem. Soc.* **2002**, *124*, 6232–6233.
64. Anzenbacher, P.; Aldakov, D. *Chem. Commun.* **2003**, 1394–1395.
65. Liao, J.-H.; Chen, C.-T.; Chou, H.-T.; Cheng, C.-C.; Chou, P.-T.; Fang, J.-M.; Slanina, Z.; Chow, T. J. *Org. Lett.* **2002**, *4*, 3107–3110.
66. Vega, I. E. D.; Camiolo, S.; Gale, P. A.; Hursthouse, M. B.; Light, M. E. *Chem. Commun.* **2003**, 1686–1687 and references therein.

67. Schmuck, C.; Bicker, V. *Org. Lett.* **2003**, 4579–4581 and references therein.
68. Aoyagi, Y.; Mizusaki, T.; Ohta, A. *Tetrahedron Lett.* **1996**, 37, 9203–9206.
69. Connors, K. A. *Binding Constants*; Wiley: New York, 1997.
70. Anzenbacher, P.; Jurisíková, K.; Sessler, J. L. *Am. Chem. Soc.* **2000**, 122, 9350–9351.

# Selective metal ion recognition using a fluorescent 1,8-diquinolynaphthalene-derived sensor in aqueous solution

Gilbert E. Tumambac, Charlene M. Rosencrance and Christian Wolf\*

Department of Chemistry, Georgetown University, 37th and O Streets, Washington, DC 20057 USA

Received 9 March 2004; revised 24 June 2004; accepted 21 July 2004

Available online 24 August 2004

**Abstract**—The use of *anti*-1,8-bis(2,2'-diisopropyl-4,4'-diquinolyl)naphthalene, **1**, for metal ion-selective fluorescence recognition has been investigated. Employing CuCl<sub>2</sub>, ZnCl<sub>2</sub>, FeCl<sub>2</sub>, and FeCl<sub>3</sub> in fluorescence titration experiments of **1** revealed formation of a bluegreen light emitting bimetallic complex. A dramatic red-shift of the fluorescence maximum of **1** and metal ion-selective quenching was observed in the presence of Cu(II), Fe(II), and Fe(III)chlorides in acetonitrile. By contrast, addition of ZnCl<sub>2</sub> was found to result in fluorescence enhancement, whereas Cu(I) did not induce any significant fluorescence change of **1**. The sensor was found to undergo highly ion-selective fluorescence quenching in aqueous solution. Screening of main group and transition metal ions showed excellent selectivity for FeCl<sub>3</sub> even in the presence of competing metal ions.

© 2004 Elsevier Ltd. All rights reserved.

## 1. Introduction

Because of the increasing demand in environmental and clinical sciences for fluorosensors that are capable of differentiating between metal ions and their oxidation states the development of sensor molecules for the detection of alkali, alkaline earth, and transition metals has recently received considerable attention.<sup>1</sup> Based on our previous studies with selectively substituted 1,8-dipyridynaphthalenes<sup>2</sup> and 1,8-diacridynaphthalenes,<sup>3</sup> we assumed that incorporation of 2-isopropylquinolyl groups into the *peri*-positions of naphthalene would afford a rigid and fluorescent bidentate ligand capable of selective metal ion recognition. Highly selective chemosensors for detection of Hg(II) and Zn(II) ions in aqueous solutions have recently been reported.<sup>4</sup> Herein, we wish to describe the design and fluorescence behavior of *anti*-1,8-bis(2,2'-diisopropyl-4,4'-diquinolyl)naphthalene, **1**, a new chemosensor for highly selective recognition of Fe(III) in aqueous solution (Fig. 1).

## 2. Results and discussion

The incorporation of two quinolyl rings into the *peri* positions of naphthalene requires two consecutive Stille or Suzuki cross-coupling steps of a 1,8-dihalonaphthalene and 2 equiv of a quinolyl-derived stannane or boronic acid, respectively. The major obstacle of the formation of highly

congested **1** is the severe steric hindrance in the second cross-coupling reaction of intermediate 1-bromo-8-(2-isopropyl-4-quinolyl)naphthalene (Scheme 1). Screening of various catalysts including Pd(PPh<sub>3</sub>)<sub>4</sub>, PdCl<sub>2</sub>(dppf), Pd<sub>2</sub>(dba)<sub>3</sub>/P(*t*-Bu)<sub>3</sub>, and [(*t*-Bu)<sub>2</sub>P(OH)]<sub>2</sub>PdCl<sub>2</sub> and optimization of reaction conditions revealed that **1** can be formed by CuO-promoted<sup>5</sup> Pd-catalyzed Stille cross-coupling in remarkable yields. Thus, cross-coupling of 2-isopropyl-4-trimethylstannylquinoline, **2**, and 1,8-dibromonaphthalene, **3**, in the presence of 10 mol% of Pd(PPh<sub>3</sub>)<sub>4</sub> and 2 equiv of CuO in DMF gave *anti*-1,8-bis(2,2'-diisopropyl-4,4'-diquinolyl)naphthalene, **1**, in 36% yield after purification by chromatography and recrystallization from ethanol (Scheme 1).

The space filling model of sensor **1** obtained by PM3 computations shows the unique structure of this highly congested bidentate ligand (Fig. 1). The antiparallel

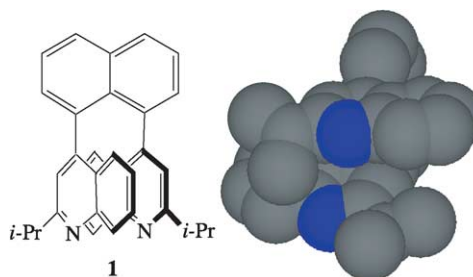
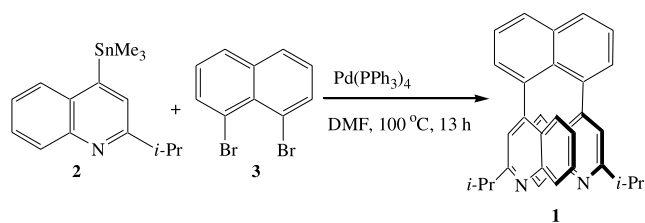


**Figure 1.** Structure and space filling model of 1,8-diquinolynaphthalene **1**. Hydrogens are omitted for clarity.

**Keywords:** Stille coupling; Fluorosensor; Metal ion sensing.

\* Corresponding author. Tel.: +1-202-687-3468; fax: +1-202-687-6209; e-mail: cw27@georgetown.edu





**Scheme 1.** Reagents and conditions: 10 mol% Pd(PPh<sub>3</sub>)<sub>4</sub>, 4 equiv CuO, DMF, 100 °C, 13 h, ratio: 2/3=3:1.

quinolyl moieties are almost perpendicular to the naphthalene ring. To minimize steric interactions, through-space Coulomb repulsion, and dipole–dipole interactions the two quinolyl groups are twisted and slightly splayed away from each other. The spatial arrangement of the 2-isopropylquinolyl rings thus creates a well-defined binding environment for metal ion-selective recognition. Our fluorescence studies revealed an emission maximum of 380 nm for the *syn*- and *anti*-isomers of **1** but different quantum yields. The quantum yield of *syn*-**1** and *anti*-**1** were determined as 2.0 and 11.6%, respectively. Because of its enhanced fluorescence we decided to employ *anti*-**1** in metal ion sensing studies. The majority of fluorescent chemosensors reported to date exhibit a chelating group physically separated from a fluorophore by a spacer.<sup>6</sup> However, smaller sensors such as *anti*-**1** may afford superior cell permeability properties and are therefore particularly interesting with respect to biomedical applications.

Fluorescence titrations using **1** and various transition metals were performed in acetonitrile at room temperature. We observed a striking change in the emission spectrum of the sensor in the presence of equimolar amounts of Cu(II), Fe(II), and Fe(III) chloride. Addition of these metal salts to a solution of *anti*-**1** was found to result in the formation of a bluegreen light emitting complex with a red-shifted emission maximum of 520 nm. Increasing the metal ion concentration did not result in any further shift of the emission maximum. By contrast, the fluorescence spectrum of diquinolyl naphthalene **1** exhibiting a maximum at 380 nm did not change significantly upon addition of Cu(I) and Zn(II) (Fig. 2). The remarkable difference in the fluorescence maximum and intensity of the sensor molecule

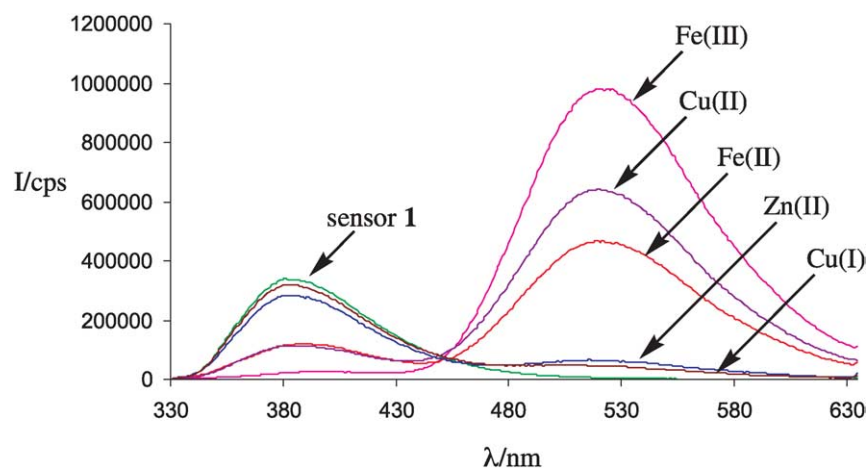


**Figure 2.** Fluorescence of *anti*-**1** in the presence of Cu(I), Cu(II), Zn(II), Fe(II), and Fe(III) in acetonitrile. The concentration of *anti*-**1** was  $4.3 \times 10^{-5}$  M and the metal ion concentration was  $1.0 \times 10^{-4}$  M. Excitation wavelength: 320 nm.

in the presence of Cu(I) and Cu(II) thus provides a new venue for real-time detection of the oxidation state of copper salts.

In addition to the remarkable red-shift of the fluorescence maximum of *anti*-**1** induced by CuCl<sub>2</sub>, FeCl<sub>2</sub>, and FeCl<sub>3</sub>, at approximately equimolar concentrations and by ZnCl<sub>2</sub> when employed in high excess, we observed metal ion-selective quenching and enhancing effects. Fluorescence titration experiments showed that CuCl does not significantly enhance the fluorescence signal at 520 nm even at high excess, whereas addition of CuCl<sub>2</sub>, ZnCl<sub>2</sub>, FeCl<sub>2</sub>, and FeCl<sub>3</sub> gave non-linear Stern–Völmer plots. Titration with FeCl<sub>2</sub> and FeCl<sub>3</sub> resulted in strong fluorescence at 520 nm, which reached a maximum at a metal ion-sensor ratio of approximately 4:1 and 3:1, respectively. A further increase in metal ion excess was found to decrease the fluorescence intensity and ultimately caused quenching indicating co-existence of different complex species in solution (Fig. 3).

Fluorescence titration experiments using CuCl<sub>2</sub> revealed formation of a 2:1 complex, which corresponds to a mol fraction of Cu(II) of 0.67 (Fig. 4). Because of the geometry of the diquinolyl naphthalene framework exhibiting cofacial hetaryl rings, the sensor affords two remote quinolyl nitrogens with a lone electron pair available for metal ion coordination in the hetaryl plane (Fig. 1). Apparently, both quinolyl nitrogens can undergo metal ion coordination, which results in the formation of a Cu(II)<sub>2</sub>-**1** complex.

Interestingly, Zn(II) remains a strong enhancer of the fluorescence signal at 520 nm at high concentration, whereas Cu(II), Fe(II), and Fe(III) induce fluorescence quenching at high metal ion/sensor ratios (Fig. 5). Notably, very effective quenching was observed at high Fe(III)-sensor ratio (Fig. 6). The sigmoidal quenching curve observed at high Fe(III)/*anti*-**1** ratio indicates that different quenching mechanisms and cooperative metal ion recognition might be operative.<sup>7</sup>

The selective fluorescence response of sensor **1** opens a new venue for real-time analysis of transition metal ions. The different fluorescence response of the sensor to Cu(I) and Cu(II) allows differentiation of the oxidation states of

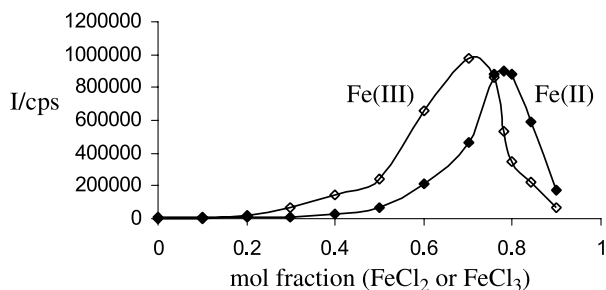


**Figure 3.** Fluorescence enhancement of *anti-1* induced by  $\text{FeCl}_2$  and  $\text{FeCl}_3$ . The concentration of *anti-1* was  $4.3 \times 10^{-5}$  M. Excitation wavelength: 320 nm, emission wavelength: 520 nm.

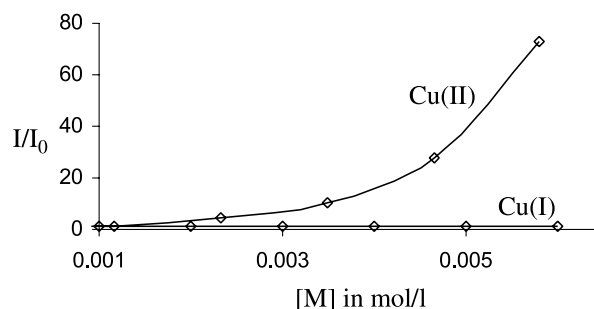


**Figure 7.** Stern-Völmer plot of *anti-1* in the presence of  $\text{CuCl}$  and  $\text{CuCl}_2$  (ratio metal ion/*anti-1* > 10). The concentration of *anti-1* was  $4.3 \times 10^{-5}$  M. Excitation wavelength: 320 nm, emission wavelength: 520 nm.

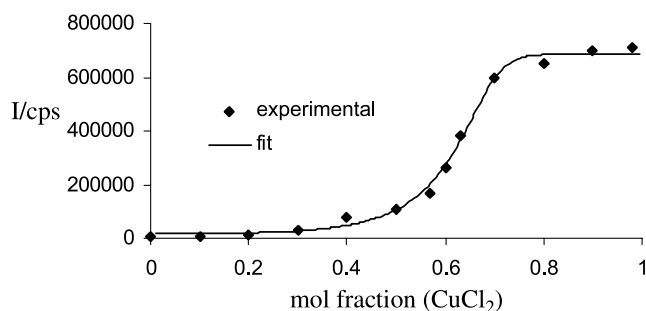


**Figure 4.** Fluorescence titration of *anti-1* using  $\text{Cu(II)}$ . The concentration of *anti-1* was  $4.3 \times 10^{-5}$  M. Excitation wavelength: 320 nm, emission wavelength: 520 nm.

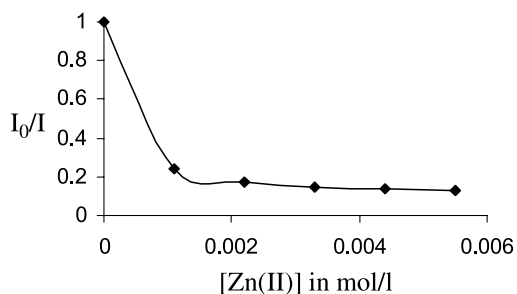


**Figure 5.** Stern-Völmer plot of *anti-1* in the presence of  $\text{ZnCl}_2$ . The concentration of *anti-1* was  $4.3 \times 10^{-5}$  M. Excitation wavelength: 320 nm, emission wavelength: 520 nm.

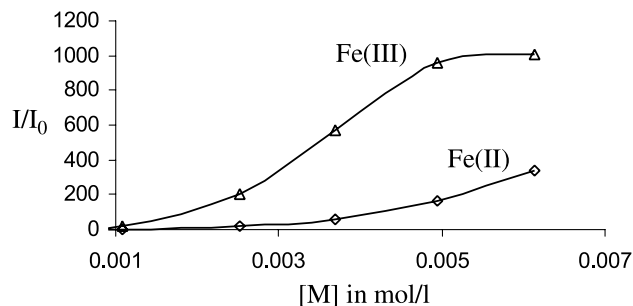


**Figure 6.** Stern-Völmer plot of *anti-1* in the presence of  $\text{FeCl}_2$  and  $\text{FeCl}_3$  (ratio metal ion/*anti-1* > 10). The concentration of *anti-1* was  $4.3 \times 10^{-5}$  M. Excitation wavelength: 320 nm, emission wavelength: 520 nm.

copper (Fig. 7). The fluorescence quenching observed with  $\text{CuCl}_2$ ,  $\text{FeCl}_2$ , and  $\text{FeCl}_3$  at high excess is probably a result of photo-induced electron transfer. Because this quenching mechanism is not available for  $d^{10}$ -metal complexes,  $\text{Cu(I)}$  and  $\text{Zn(II)}$  do not provide additional relaxation pathways for excited *anti-2* and are therefore inefficient quenchers. Fluorescent enhancement induced by binding to  $\text{Zn(II)}$  or other transition metals has been attributed to enhanced conformational restriction upon metal complexation.<sup>8</sup>

We then employed sensor **1** in water/acetonitrile to assess its use in aqueous solutions. The fluorescence spectrum of **1** in the presence of metal ions was found to afford maxima at 390 and 520 nm in a 1:1 water/acetonitrile (v/v) solution (Fig. 8). Screening of a broad variety of main group and transition metal chlorides revealed efficient fluorescence quenching by  $\text{FeCl}_3$ . It is noteworthy that ferric and ferrous chloride reduce the fluorescence maximum at 520 nm, whereas  $\text{Na(I)}$ ,  $\text{K(I)}$ ,  $\text{Ca(II)}$ ,  $\text{Cr(II)}$ ,  $\text{Mn(II)}$ ,  $\text{Co(II)}$ ,  $\text{Ni(II)}$ ,  $\text{Cu(I)}$ ,  $\text{Cu(II)}$ ,  $\text{Zn(II)}$ ,  $\text{Cd(II)}$ , and  $\text{Hg(II)}$  do not show any significant quenching. The quenching effects on the fluorescence maximum at 390 nm is even more dramatic. We observed that addition of  $\text{Fe(III)}$  to an aqueous solution of **1** decreases the emission intensity to less than 2%. The fluorescence intensity at 390 nm decreased to approximately 30% in the presence of  $\text{Cr(II)}$  and  $\text{Fe(II)}$ , whereas other metal ions do not show any significant effects (Fig. 9). Moreover, excellent selectivity for  $\text{Fe(III)}$  was found in the presence of  $\text{Cr(II)}$ ,  $\text{Mn(II)}$ ,  $\text{Cu(I)}$ , and  $\text{Zn(II)}$ . The highly selective quenching of 1,8-diquinolylnaphthalene **1** by ferric and ferrous chloride in aqueous solutions may be utilized for the diagnosis of various iron-related diseases. The determination of iron levels in blood serum and other body fluids is indispensable for the study and treatment of nutritional and metabolic diseases that result in low or high iron levels. Iron metabolism disorders have been reported to cause iron-deficiency anemia and hemochromatosis which might ultimately cause liver cancer, liver cirrhosis, arthritis, diabetes or heart failure.<sup>9</sup> Recent studies have linked late-onset neurodegenerative disorders such as Parkinson's disease to elevated iron levels.<sup>10</sup> The monitoring iron levels in blood serum and cell extracts has become an integral part of the diagnosis and treatment of cancer because tumor cells require iron to grow and proliferate. Iron also plays a crucial role in important infectious diseases such as malaria.<sup>11</sup>

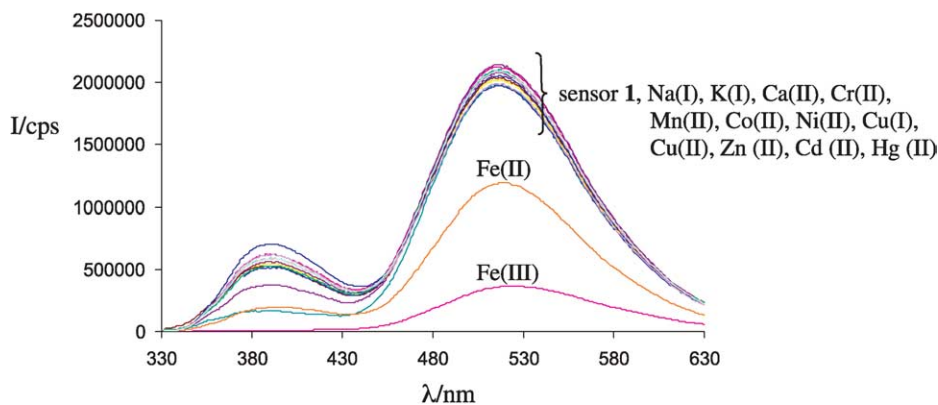


**Figure 8.** Fluorescence spectrum of **1** in the absence and presence of various metal ions in water/acetonitrile (1:1). The concentration of *anti*-**1** was  $4.3 \times 10^{-5}$  M. Metal ion concentration:  $10^{-3}$  M. Excitation wavelength: 320 nm.

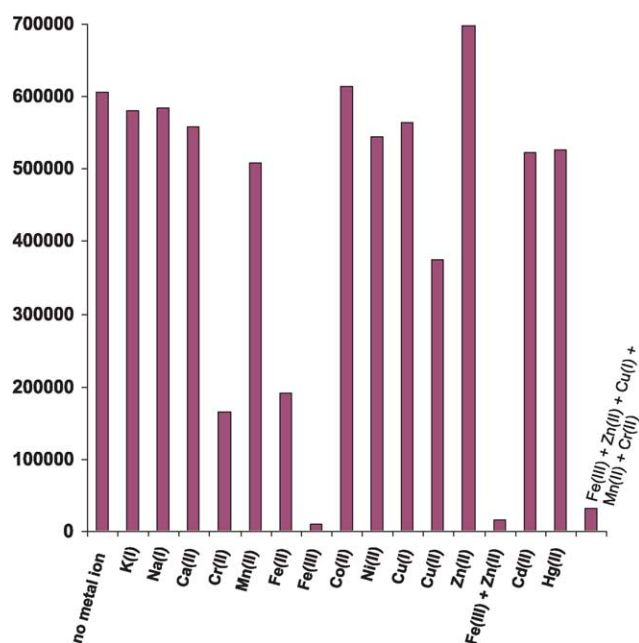


**Figure 9.** Fluorescence intensity of **1** in water/acetonitrile. The concentration of *anti*-**1** was  $4.3 \times 10^{-5}$  M. Metal ion concentration:  $10^{-3}$  M. Excitation wavelength: 320 nm, emission wavelength: 390 nm.

### 3. Conclusion

1,8-Diquinolynaphthalene **1** was found to exhibit a complex fluorescence behavior in the presence of transition metals. A significant red-shift of the fluorescence maximum of **1** was observed upon addition of approximately equimolar amounts of Cu(II), Fe(II), and Fe(III) in acetonitrile and attributed to the formation of a bimetallic complex. Quenching and non-linear Stern–Völmer plots indicating co-existence of different metal complexes of **1** were observed at high excess of these metal ions. By contrast, CuCl did not induce quenching or a red-shift of the fluorescence maximum of **1** and ZnCl<sub>2</sub> was found to enhance the red-shifted emission maximum at high concentration. The highly Fe(III)-selective quenching of the fluorescence maxima in aqueous solution makes **1** an attractive sensor for trace analysis and diagnosis of iron-related diseases. The Fe(III)-selective quenching was

insensitive to the presence of Cr(II), Mn(II), Cu(I), and Zn(II).

## 4. Experimental

### 4.1. General

All commercially available reagents and solvents were used without further purification. Sensor **1** was purified by flash chromatography on SiO<sub>2</sub> (particle size 0.032–0.063 mm). NMR spectra were obtained at 300 MHz (<sup>1</sup>H NMR) and 75 MHz (<sup>13</sup>C NMR) using CDCl<sub>3</sub> as the solvent. Chemical shifts are reported in ppm relative to TMS. Fluorescence experiments were conducted using degassed solutions and a Fluoromax-2 spectrometer from Instruments S.A. Inc. The quantum yield of each isomer of **1** was determined in acetonitrile following a procedure described by Jones and co-workers.<sup>12</sup> The diquinoline isomers were excited at 320 nm and relative integrated intensities of the emission spectra were compared to naphthalene which has a quantum yield of 0.2 in acetonitrile.

**4.1.1. Preparation of anti-1,8-bis(2,2'-diisopropyl-4,4'-diquinolyl)naphthalene, 1.** To a solution of 1,8-dibromonaphthalene, **3**, (0.3 g, 1.0 mmol), Pd(PPh<sub>3</sub>)<sub>4</sub> (130 mg, 10 mol%) and CuO (0.30 g, 4.0 mmol) in 10 mL of anhydrous DMF was added 2-isopropyl-4-trimethylstannylquinoline, **2**, (1.0 g, 3.0 mmol) in 5 mL of DMF. The reaction was stirred at 100 °C for 13 h, cooled to room temperature, quenched with aqueous NH<sub>4</sub>OH, and extracted with diethyl ether. The combined organic layers were washed with H<sub>2</sub>O, dried over MgSO<sub>4</sub> and concentrated under vacuum. Purification by flash chromatography (hexanes/EtOAc/Et<sub>3</sub>N = 100:20:1) and crystallization from ethanol gave **1** (168 mg, 0.36 mmol, 36%) as white crystals.

$\delta_{\text{H}}$  (CDCl<sub>3</sub>) 0.80 (d,  $J=6.9$  Hz, 6H), 0.98 (d,  $J=6.9$  Hz, 6H), 2.34 (sept,  $J=6.9$  Hz, 2H), 6.34 (s, 2H), 7.18 (dd,  $J=1.1, 8.2$  Hz, 2H), 7.23–7.29 (m, 4H), 7.54 (ddd,  $J=1.4, 6.7, 8.4$  Hz, 2H), 7.62 (dd,  $J=7.1, 8.2$  Hz, 2H), 7.87 (d,  $J=8.5$  Hz, 2H), 8.13 (dd,  $J=1.4, 8.4$  Hz, 2H).  $\delta_{\text{C}}$  (CDCl<sub>3</sub>) 21.4, 21.5, 36.4, 120.2, 120.4, 125.6, 125.7, 126.9, 128.7, 129.7, 129.9, 130.7, 131.5, 134.7, 136.1, 147.1, 148.2, 165.8. EI/MS:  $m/z$  466 (100%, M<sup>+</sup>), 451 (94, M<sup>+</sup> – Me), 436 (5, M<sup>+</sup> – 2Me), 423 (23, M<sup>+</sup> – *i*-Pr), 253 (5,

M<sup>+</sup>-isopropylquinoly). LC/APCI/MS: *m/z* 467 [100%, (M+H)<sup>+</sup>]. Anal. Calcd for C<sub>34</sub>H<sub>30</sub>N<sub>2</sub>: C, 86.70; H, 7.68; N, 5.62. Found: C, 86.27; H, 7.23; N, 5.87.

### Acknowledgements

C.W. gratefully acknowledges the National Science Foundation for a CAREER award (CHE 0347368).

### References and notes

- (a) Unob, F.; Asfari, Z.; Vicens, J. *Tetrahedron Lett.* **1998**, *39*, 2951–2954. (b) Purrello, R.; Gurrieri, S.; Lauceri, R. *Coord. Chem. Rev.* **1999**, *192*, 683–706. (c) Leray, I.; Valeur, B.; O'Reilly, F.; Jiwan, J.-L. H.; Soumillion, J.-P.; Valeur, B. *Chem. Commun.* **1999**, 795–796. (d) Valeur, B.; Leray, I. *Coord. Chem. Rev.* **2000**, *205*, 3–40. (e) de Silva, A. P.; Fox, D. B.; Huxley, A. J. M.; Moody, T. S. *Coord. Chem. Rev.* **2000**, *205*, 41–57. (f) Deo, S.; Godwin, H. A. *J. Am. Chem. Soc.* **2000**, *122*, 174–175. (g) Singh, A.; Yao, Q.; Tong, L.; Still, C. W.; Sames, D. *Tetrahedron Lett.* **2000**, *41*, 9601–9605. (h) Prodi, L.; Montalti, M.; Zaccaroni, N.; Dallavalle, F.; Folesani, G.; Lanfranchi, M.; Corradini, R.; Pagliari, S.; Marchelli, R. *Helv. Chim. Acta* **2001**, *84*, 690–706. (i) Burdette, S. C.; Walkup, G. K.; Spingler, B.; Tsien, R. Y.; Lippard, S. *J. Am. Chem. Soc.* **2001**, *123*, 7831–7841. (j) Baxter, P. N. W. *Chem. Eur. J.* **2002**, *8*, 5250–5264. (k) Chao, C.-T.; Huang, W.-P. *J. Am. Chem. Soc.* **2002**, *124*, 6246–6247. (l) Yang, N. C.; Jeong, J. K.; Suh, D. H. *Chem. Lett.* **2003**, *32*, 40–41. (m) Grabchev, I.; Chovelon, J.-M.; Qian, X. *New J. Chem.* **2003**, *27*, 337–340. (n) Zheng, Y.; Gattas-Asfura, K. M.; Li, C.; Andreopoulos, F. M.; Pham, S. M.; Leblanc, R. M. *J. Phys. Chem. B* **2003**, *107*, 483–488. (o) Kim, J. S.; Noh, K. H.; Lee, S. H.; Kim, S. K.; Yoon, J. *J. Org. Chem.* **2003**, *68*, 597–600. (p) Clark, M. A.; Duffy, K.; Tibrewala, J.; Lippard, S. *J. Org. Lett.* **2003**, *5*, 2051–2054.
- (a) Wolf, C.; Ghebremariam, B. T. *Synthesis* **2002**, 749–752. (b) Wolf, C.; Ghebremariam, B. T. *Tetrahedron: Asymmetry* **2002**, *13*, 1153–1156. (c) Wolf, C.; Tumambac, G. *J. Phys. A* **2003**, *107*, 815–817.
- Wolf, C.; Mei, X. *J. Am. Chem. Soc.* **2003**, *125*, 10651–10658.
- (a) Gunnlaugsson, T.; Lee, T. C.; Parkesh, R. *Org. Biomol. Chem.* **2003**, *1*, 3265–3267. (b) Moon, S. Y.; Cha, N. R.; Kim, Y. H.; Chang, S.-K. *J. Org. Chem.* **2004**, *69*, 181–183.
- Gronowitz, S.; Bjoerk, P.; Malm, J.; Hoernfeldt, A.-B. *J. Organomet. Chem.* **1993**, *460*, 127–129.
- (a) de Silva, A. P.; Gunaratne, H. Q. N.; Gunnlaugsson, T.; Huxley, A. J. M.; McCoy, C. P.; Rademacher, J. T.; Rice, T. E. *Chem. Rev.* **1997**, *97*, 1515–1566. (b) Pearson, A. J.; Xiao, W. *J. Org. Chem.* **2003**, *68*, 5361–5368. (c) Pearson, A. J.; Xiao, W. *J. Org. Chem.* **2003**, *68*, 5369–5376 and references therein.
- Glass, T. E. *J. Am. Chem. Soc.* **2000**, *122*, 4522–4523 and references therein.
- (a) McFarland, S. A.; Finney, N. S. *J. Am. Chem. Soc.* **2001**, *123*, 1260–1261. (b) Xia, W.-S.; Schmehl, R. H.; Li, C.-J.; Mague, J. T.; Luo, C.-P.; Guldi, D. M. *J. Phys. Chem. B* **2002**, *106*, 833–843. (c) McFarland, S. A.; Finney, N. S. *J. Am. Chem. Soc.* **2002**, *124*, 1178–1179.
- (a) Trinder, D.; Macey, D. J.; Olynyk, J. K. *Int. J. Mol. Med.* **2000**, *6*, 607–612. (b) Burkitt, M. J.; Milne, L.; Raafat, A. *Clin. Sci.* **2001**, *100*, 239–247. (c) Brugnara, C. *Clin. Chem.* **2003**, *49*, 1573–1578. (d) Leong, W.; Loennerdal, B. *J. Nutr.* **2004**, *134*, 1–4.
- (a) Bharath, S.; Hsu, M.; Kaur, D.; Rajagopalan, S. A.; Julie, K. *Biochem. Pharmacol.* **2002**, *64*, 1037–1048. (b) Beard, J. *J. Nutr.* **2003**, *133*, 1468S–1472S.
- (a) O'Neill, P. M.; Bray, P. G.; Hawley, S. R.; Ward, S. A.; Park, B. K. *Pharmacol. Ther.* **1998**, *77*, 29–58. (b) Blauer, G.; Akkawi, M.; Fleischhacker, W.; Hiessboeck, R. *Chirality* **1998**, *10*, 556–563. (c) Egan, T. J.; Hunter, R.; Kaschula, C. H.; Marques, H. M.; Misplon, A.; Walden, J. *J. Med. Chem.* **2000**, *43*, 283–291.
- Jones, G.; Jackson, W. R.; Choi, C.-Y. *J. Phys. Chem.* **1985**, *89*, 294–300.

# Heavy metal complexation by *N*-acyl(thio)urea-functionalized cavitands: synthesis, extraction and potentiometric studies

Marta M. Reinoso García,<sup>a</sup> Willem Verboom,<sup>a,\*</sup> David N. Reinhoudt,<sup>a</sup> Elzbieta Malinowska,<sup>b</sup> Mariusz Pietrzak<sup>b</sup> and Dorota Wojciechowska<sup>b</sup>

<sup>a</sup>Laboratory of Supramolecular Chemistry and Technology, MESA<sup>+</sup> Research Institute, University of Twente, PO Box 217, 7500 AE Enschede, The Netherlands

<sup>b</sup>Department of Analytical Chemistry, Faculty of Chemistry, Warsaw University of Technology, Noakowskiego 3, 00-664 Warsaw, Poland

Received 9 January 2004; revised 25 June 2004; accepted 19 August 2004

Available online 18 September 2004

**Abstract**—The synthesis and binding properties of resorcinarene-based cavitands functionalized with *N*-acylthiourea moieties towards different cations are described. Extraction studies with metal (Pb<sup>2+</sup>, Cu<sup>2+</sup>, Ag<sup>+</sup>, Hg<sup>2+</sup>, Cd<sup>2+</sup>, Eu<sup>3+</sup>, Fe<sup>3+</sup>, K<sup>+</sup>, Na<sup>+</sup>, and Ca<sup>2+</sup>) picrates and the incorporation in ion selective electrodes (ISEs), show that there is more than a 40% increase of the Ag<sup>+</sup> extraction for *N*-acylthiourea ionophores (**2**, **3**, and **8**) in comparison with *N*-benzoyl-*N'*-benzylthiourea (**9**). Ionophore **8**, which has a C<sub>3</sub> chain between the platform and the ionophore, extracts two times more Cu<sup>2+</sup> than the more rigid one (**2**). Stoichiometry studies showed for ligand **2** a ligand/metal ratio of 1:1, while for model compound **9** a ratio of 1:2 was found. Potentiometric studies of electrodes revealed that cavitands **2**, **3**, and **8** induce a significantly different selectivity pattern compared to the cation-exchanger used, as well as model compound **9**. Especially, a considerable enhancement of the selectivity towards Ag<sup>+</sup> and Pb<sup>2+</sup> over K<sup>+</sup>, Ca<sup>2+</sup>, and Na<sup>2+</sup> ions was observed. © 2004 Elsevier Ltd. All rights reserved.

## 1. Introduction

*N*-Acylthioureas represent an important class of ionophores which are already known for a long time as metal chelating agents.<sup>1</sup> They are very useful for the removal of heavy metal cations from waste water<sup>2</sup> and as selective extractants for separation<sup>3</sup> and concentration of precious metal cations such as Pd<sup>2+</sup> and Pt<sup>2+</sup>.<sup>4</sup> Several groups have reported their strong binding with Cu<sup>2+</sup>.<sup>5,6</sup> *N*-acylthioureas have also been used as ionophores in ion selective electrodes for the detection of Pb<sup>2+</sup>, Hg<sup>2+</sup>, and Cd<sup>2+</sup>.<sup>7</sup>

Complexation of transition and heavy metal cations is favored by the presence of soft donor atoms such as nitrogen, sulfur or phosphorus, but also ligands containing the harder oxygen atoms can bind these cations. *N*-acylthioureas have sulfur, nitrogen and oxygen as donor atoms, allowing them to act as monodentate sulfur donors, bidentate oxygen and sulfur, or oxygen and nitrogen donors. They can also coordinate through the keto- or enol-thione

form, depending of the ligands, the metal ions, and counter anions present.<sup>8</sup>

For the coordination of a metal ion more than one *N*-acylthiourea ligand is necessary. In the literature many examples are known of preorganization of ligating sites on a molecular platform, giving rise to improved complexation properties.<sup>9</sup> Appropriately functionalized calix[4]arenes<sup>10,11</sup> are being used for the complexation of alkali and alkaline earth metal ions and to a lesser extent heavy and transition metal ions.<sup>12</sup>

In this paper we describe our results of the use of the more rigid resorcinarene-based cavitand platform<sup>13</sup> for the attachment of *N*-acyl(thio)urea ligating sites. The complexation, extraction, and sensing behavior of the resulting ionophores (Chart 1) will be discussed.

## 2. Results and discussion

### 2.1. Synthesis

Reaction of tetrakis(aminomethyl)cavitand<sup>14</sup> (**1**) with ethoxycarbonyl isothiocyanate in chloroform gave *N*-acylthiourea derivative **3** in 69% yield (Scheme 1). In the <sup>1</sup>H

**Keywords:** Heavy metals; Complexation; Cavitands; Ion selective electrodes.

\* Corresponding author. Tel.: +31-53-4892977; fax: +31-53-4894645; e-mail: w.verboom@utwente.nl



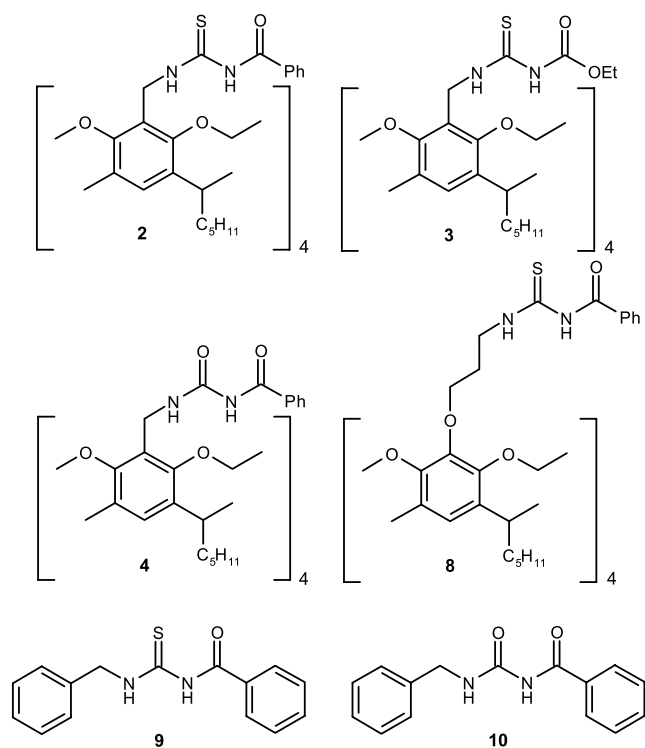
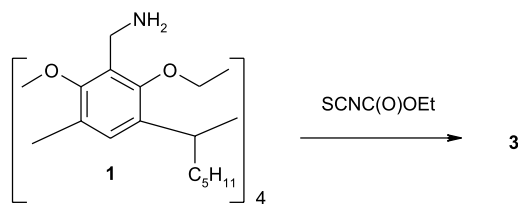


Chart 1. *N*-Acyl(thio)urea derivatives.



Scheme 1.

NMR spectrum the benzylic methylene hydrogens shifted upfield from  $\delta$  3.61 to  $\delta$  4.75 due to the introduction of a thiocarbonyl group.

In order to study the influence of a longer spacer between the platform and the ligating site, tetrahydroxycavitand<sup>15</sup> (**5**) was reacted with 3-bromopropylphthalimide in the presence of NaH as a base in DMF to give tetrakis[(phthalimido)propoxy]cavitand (**6**) in 65% yield. Subsequent removal of the phthalimido groups with hydrazine hydrate and reaction of the resulting tetrakis(aminopropoxy)cavitand (**7**) with

benzoyl isothiocyanate gave cavitand **8** in 50% yield (Scheme 2). In the <sup>1</sup>H NMR spectrum the methylene group adjacent to the nitrogen shifts from  $\delta$  3.25 in **7** to  $\delta$  3.93 in **8**.

In all the cases the introduction of the ligating sites clearly followed from the mass spectra and satisfactory elemental analyses. The other ionophores used, viz. **2**,<sup>16</sup> **4**,<sup>16</sup> **9**,<sup>17</sup> and **10**<sup>18</sup> were prepared by literature procedures.

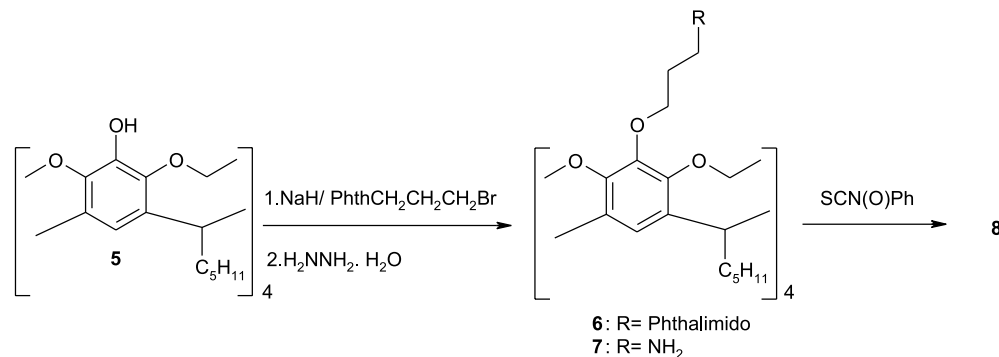
## 2.2. Liquid–liquid extraction

With the different *N*-acyl(thio)urea containing ionophores, **2**, **3**, **4**, **8**, **9**, and **10** extraction experiments were performed with various heavy metal ions according to the standard picrate extraction method.<sup>14,19</sup> The results, expressed as a percentage of extracted cation (%*E*), are summarized graphically in Figure 1.

All tetrafunctionalized compounds exhibit high extraction values for Ag<sup>+</sup>, especially the *N*-acylthiourea derivatives **2**, **3**, and **8**. The extraction levels are higher than those observed for other sulphur-containing calix[4]arene-based ionophores.<sup>20</sup> Moreover, ionophores **2**, **3**, and **8** display high Ag<sup>+</sup>/Pb<sup>2+</sup> selectivities:  $S_{Ag^+/Pb^{2+}} = 26.3, 42.4,$  and  $52.6$ , respectively, in comparison with values of 11.4 and 8.1 reported for *p*-*tert*-butyldihomooxalix[4]arene and a *p*-*tert*-butylcalix[4]arene with phenylketones as ligating sites, respectively.<sup>21</sup>

Surprisingly, both tetrakis[(benzoylthioureido)methyl]cavitand **2** and the corresponding model compound **9** have more or less the same extraction profile. However, tetrakis[(benzoylthioureido)propoxy]cavitand **8**, only having a longer spacer than **2**, is able to extract twice the amount of Cu<sup>2+</sup> than **2** (29%) and model compound **9** (22%). It is striking that **8** extracts two times more Hg<sup>2+</sup> than Cd<sup>2+</sup>, since these cations have a similar ionic radius.<sup>22</sup> Apparently, the slightly improved extraction properties come from the higher flexibility of the ligating sites, rather than the preorganization.

In the case of compound **4** preorganization clearly plays a role in the complexation of the alkali and alkaline earth metal ions as follows from comparison of the data of **4** and model compound **10**. Model compound **10** shows almost no extraction of K<sup>+</sup> (3%) and Ca<sup>2+</sup> (4%), and only 15% of Na<sup>+</sup> was extracted, whereas **4** is able to extract K<sup>+</sup> (37%),



Scheme 2.

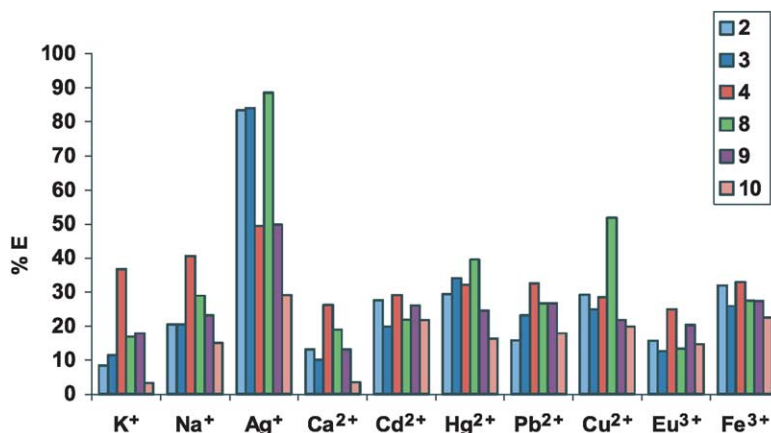


**Figure 1.** Extraction results of *N*-acyl(thio)urea derivatives. Conditions:  $[L]_{o,i} = 10^{-3}$  M;  $[M^{n+}]_{w,i} = 10^{-3}$  M;  $[LiPic]_w = 10^{-4}$  M;  $[HNO_3]_w = 10^{-3}$  M; pH 3.

$Na^+$  (41%) and  $Ca^{2+}$  (26%) in substantially higher percentages. However, in general, **4** extracts the different cations more or less to the same extent.

The stoichiometry coefficient  $p$  was determined using Eq. 1 taking into account that only one complex is present and that the metal is unassociated in the aqueous phase.

$$\log D = \log K_{ex} + n \log [Pic^-]_{aq} + p \log [L]_{org} \quad (1)$$

The representation of  $\log D$  versus  $\log [L]$  should be linear with a slope of  $p$ , where  $p$  indicates the number of ligand molecules involved per cation in the extracted species. Plots of  $\log D$  versus  $\log [L]$  for the extraction of  $Cu^{2+}$  by compound **2** and model compound **9** are given in Figure 2. For the complexation of **2** with  $Cu^{2+}$  the plots are linear with slopes close to one, in agreement with the formation of 1:1 complexes. In the case of model compound **9** the slope is close to 2 indicating the formation of 1:2 complexes, which is in agreement with the reported complexation behavior.<sup>23</sup> The same stoichiometries were obtained for  $Pb^{2+}$ .

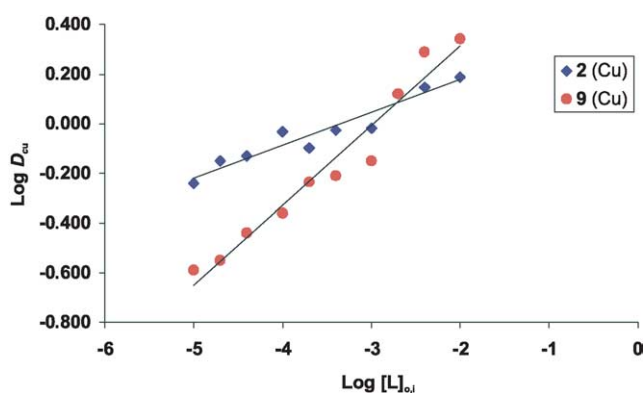


**Figure 2.** Plots of  $\log D_{Cu^{2+}}$  versus  $\log [L]_{o,i}$  of **2** and **9**. Conditions:  $[Cu^{2+}]_{w,i} = 10^{-4}$  M;  $[LiPic]_w = 10^{-3}$  M;  $[HNO_3] = 10^{-3}$  M; pH 3.

### 2.3. Potentiometric studies

The *N*-acylthiourea derivatives **2**, **3**, **8**, and **9** were examined as ionophores in *o*-NPOE/PVC membranes containing also 30% mol of lipophilic anionic additives. To obtain unbiased  $K_{i,j}^{pot}$  values, the calibration plots for various cations were collected starting from the most discriminating ones.<sup>24</sup> The preliminary selectivity order for each ionophore was

established after the preliminary screening of the electrode selectivities. The electrodes exhibited a Nernstian or near-Nernstian response in pure solutions of the moderate and highly discriminating cations, at least within the range  $10^{-3}$ – $10^{-1}$  M. When a flattening (or a reversing) of the calibration curves was observed, the selectivity coefficients were obtained from the Nernstian part of the response curve at lower activities.

The logarithmic values of the selectivity coefficients calculated for  $Pb^{2+}$  as the primary cation ( $\log K_{Pb,i}^{pot}$ ) are presented in Figure 3. Comparison of the results obtained for membranes containing *N*-acylthiourea derivatives and those for membranes containing only ion-exchanger (KTFPB) revealed that ionophores **2**, **3**, **8**, and **9** induce selectivities significantly different from the so-called Hofmeister series. This indicates that the compounds studied are capable of selective interactions with cations within the polymeric membrane phase. The incorporation of *N*-acylthiourea cavitands **2**, **3** or **8** into a polymeric membrane containing KTFPB led to dramatic changes in the electrode selectivity for  $Pb^{2+}$  over  $Na^+$ ,  $K^+$ , and  $Ca^{2+}$  ions. A less pronounced improvement of the selectivity over  $Na^+$  and  $Ca^{2+}$  could be seen in the case of model compound **9**.

Due to the fact that compounds **2**, **3**, **8**, and **9** possess a soft ligating C=S group it was expected that they might exhibit complexation properties toward soft metal cations. Indeed, electrodes with membranes based on *N*-acylthiourea ionophores showed an enhanced selectivity towards  $Ag^+$  compared to membranes with cation-exchanger. Moreover, the selectivity varied depending on the architecture of the *N*-acylthiourea derivative. The largest value of  $\log K_{Pb,Ag}^{pot}$  was determined for ionophore **3**. It was also found that the electrodes with membranes containing ionophores (except for compound **3**) provided an increased selectivity towards  $Cu^{2+}$  compared to membranes without ionophore. At this point it should be stressed that the value of  $\log K_{Pb,Cu}^{pot}$  for the electrodes based on **8** is only roughly estimated, because during the very first calibration in copper nitrate solutions the electrodes responded to  $Cu^{2+}$  ion in a super-Nernstian fashion. Moreover, after 24 h contact of the membrane with  $10^{-2}$  M copper nitrate solution, the electrode lost its initial selectivity and the response to  $Cu^{2+}$ .

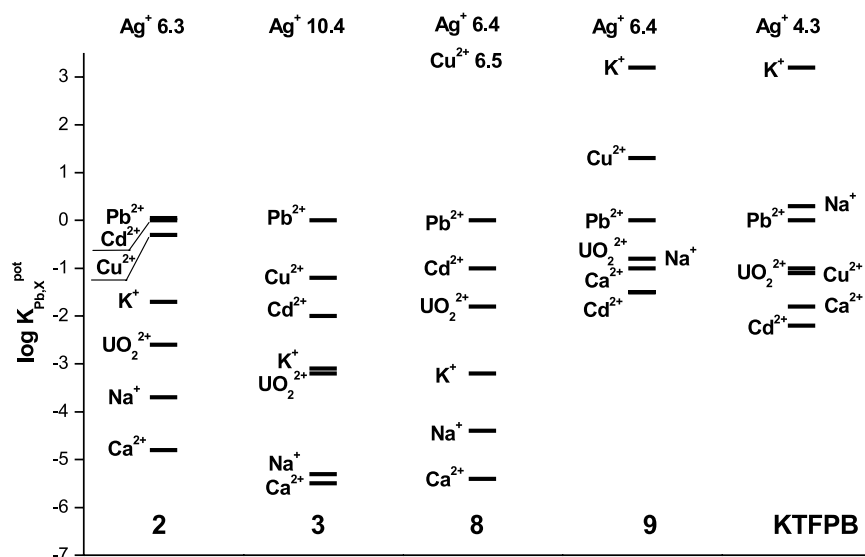


**Figure 3.** Selectivity coefficients for electrodes prepared with PVC/*o*-NPOE (1:2) membranes containing compounds **2**, **3**, **8**, **9**, and lipophilic sites (KTFPB) as well as membranes with ion-exchanger only.

**Table 1.** Formal complex formation constants,  $\log \beta_{IL_n}$ ,<sup>a</sup> obtained with ionophores **2**, **3**, **8**, and **9** in PVC/*o*-NPOE (1:2) membranes, using the segmented sandwich method

Cation	$\log \beta_{IL_n}$ , Membrane			
	<b>2</b> <sup>b</sup> /KTFPB	<b>3</b> <sup>b</sup> /KTFPB	<b>8</b> <sup>b</sup> /KTFPB	<b>9</b> <sup>c</sup> /KTFPB
Pb <sup>2+</sup>	8.9	11.6	11.4	8.8
Cd <sup>2+</sup>	10.3	11.8	9.8	7.4
Cu <sup>2+</sup>	8.1	12.4	(18.7) <sup>d</sup>	11.3
Ag <sup>+</sup>	7.2	10.1	8.0	6.4
Na <sup>+</sup>	4.9	4.9	4.4	5.3
UO <sub>2</sub> <sup>2+</sup>	5.4	10.3	8.9	8.4

<sup>a</sup> Standard deviations  $\leq 0.3$  (from at least three replicate measurements).

<sup>b</sup> The stoichiometry of the ion–ionophore complexes was assumed to be 1:1.

<sup>c</sup> The stoichiometry of the ion–ionophore complexes was assumed to be 1:2.

<sup>d</sup> Standard deviation  $\leq 1.3$  (from at least three replicate measurements).

Anionic response was observed in solutions more concentrated than  $10^{-3}$  M. This could indicate very strong and irreversible complexation of Cu<sup>2+</sup> by **8** or unidentified interactions between Cu<sup>2+</sup> and the *N*-acylthiourea ligating sites leading, for example, to changes in Cu<sup>2+</sup> oxidation state or changes in ionophore structure (the membranes become slightly greenish). Interestingly, this type of behavior has not been noted for other *N*-acylthiourea ionophores studied in this work. However, a similar phenomenon was observed before for azothiacycrown ethers.<sup>25</sup>

It is well established that selectivity coefficients for neutral carrier-based membranes are typically related to the differences in the free energies of solvation of the ions in the sample and membrane phase, the stability constants of the ion–ionophore complexes in the membrane, and the concentrations of the ionophore and ionic sites in the membrane.<sup>26</sup> However, the main factor that is primarily responsible for the selectivity of polymeric membrane electrodes is the selectivity of ion–ionophore interactions that can be expressed by relative stability constants of complexes formed by an ionophore with primary and interfering ions within the membrane phase.

The complex formation constants were determined by means of the segmented sandwich method.<sup>27</sup> The values of the complex formation constants for ionophores **2**, **3**, **8**, and **9** and chosen cations are collected in Table 1.<sup>†</sup> It was found that cavitand **3** with [–NH–C(S)–NHC(O)OEt] groups forms slightly stronger complexes than the one with [–NH–C(S)–NHC(O)Ph] moieties (**2**) with most of the examined cations. This can be explained by the fact that ethoxycarbonyl moieties interact stronger than phenylcarbonyl groups with hard and soft Lewis acids.<sup>28</sup> In addition, the ethoxy substituents are smaller and more flexible than the –C(O)Ph moieties.<sup>29</sup>

The complex formation constants,  $\log \beta_{ML}$ , for **8** with Pb<sup>2+</sup> and especially Cu<sup>2+</sup> are significantly larger than those for **2** (Table 1). This indicates that the presence of a longer spacer (–C<sub>3</sub>H<sub>6</sub>– in **8** vs –CH<sub>2</sub>– in **2**) might create a better architecture of the cavity for complexation of these cations. However, the value of  $\log \beta_{CuL}$  is given in brackets and

<sup>†</sup> It should be noted that no direct correlation can be made between the extraction data (Fig. 1) and the formation constants (Table 1), since in the first case the partitioning coefficient of the cations involved has to be taken into account.

should be treated as an approximation. This is due to the fact that the reproducibility of the potential measurements was much worse than in other cases ( $\Delta \log \beta_{\text{CuL}} \leq \pm 1.3$ ) and, as mentioned above, electrodes with membranes doped with **8** did not exhibit a linear response to the logarithm of the  $\text{Cu}^{2+}$  activity in sample solutions.

For ionophores **2** and **9**, additional membranes with a different amount of the ionophore (5–100 mmol/kg) and constant content of anionic additives (1 mmol/kg) were prepared in order to check the stoichiometry of the complexes formed with chosen cations ( $\text{Cu}^{2+}$  and  $\text{Pb}^{2+}$ ).

The results obtained for  $\text{Cu}^{2+}$  are illustrated in Figure 4. The linear relationships between the EMF and logarithmic values of free ionophore concentration suggest that one sort of complexes is predominant in the membrane.<sup>30</sup> The slope of the regression line close to 30 mV indicates a 1:1 **2**- $\text{Cu}^{2+}$  complexation, while in the case of **9**- $\text{Cu}^{2+}$  a complexation with 1:2 stoichiometry can be expected (the slope is close to 60 mV). The same behavior was found in the case of  $\text{Pb}^{2+}$ .

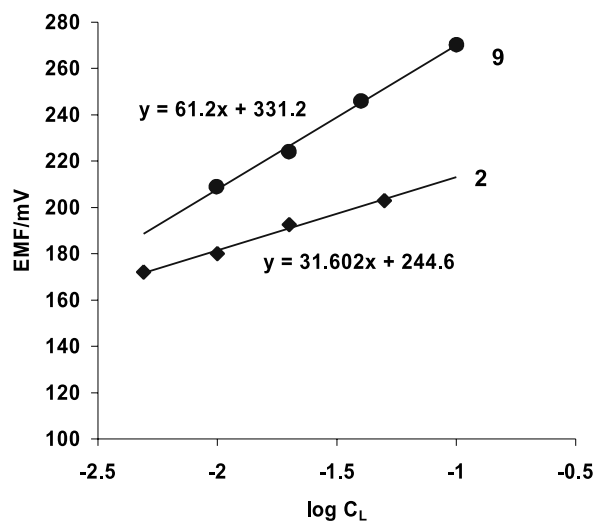


Figure 4. Dependence of the sandwich membrane electrodes' potential values on the content of ionophore: **2** and **9**.

Comparison of the relative values of the stability constants,  $\log \beta_{\text{ML}}$ , and the hydrophobicity of the cations with the respective selectivity coefficients,  $\log K_{\text{Pb,M}}^{\text{pot}}$ , reveals that the stronger  $\text{Cu}^{2+}$  interference (higher values of  $\log K_{\text{Pb,M}}^{\text{pot}}$ ) for membranes with ionophores **8** and **9** as well as the  $\text{Ag}^+$  interference in the case of the membrane containing **3** are related to a higher affinity of these ionophores to  $\text{Cu}^{2+}$  or  $\text{Ag}^+$  than to  $\text{Pb}^{2+}$  compared to cavitand **2** (see  $\log \beta_{\text{ML}}$  for  $\text{Cu}^{2+}$  or  $\text{Ag}^+$  vs  $\text{Pb}^{2+}$ ).

### 3. Conclusion

We have demonstrated that *N*-acylthiourea tetrafunctionalized cavitands are reasonable to good ionophores for the extraction and detection of soft metal ions with a preference for  $\text{Ag}^+$ . The attachment of four *N*-acylthiourea moieties to a molecular platform clearly improves the complexation behavior. In the case of ionophores **2**, **3**, and **8** a 40%

increase of the  $\text{Ag}^+$  extraction was observed, compared with the corresponding model compound **9**. The importance of flexibility of the ligating sites clearly follows from the different complexation behavior of ionophores **2** and **8**, only differing in length of the spacer between the platform and the ligating site. The latter ionophore shows a very good affinity for  $\text{Cu}^{2+}$ . In all cases there is a good correlation between the liquid–liquid extraction and ISE data.

## 4. Experimental

### 4.1. General

NMR experiments were performed using a Varian Unity 300 WB NMR spectrometer operating at 300 and 100 MHz for the  $^1\text{H}$  and  $^{13}\text{C}$  nuclei, respectively. All spectra were recorded in  $\text{CDCl}_3$ . Residual solvent protons were used as internal standard and chemical shifts are given in ppm relative to tetramethylsilane (TMS). Fast atom bombardment (FAB) mass spectra were measured on a Finnigan MAT 90 spectrometer using *m*-nitrobenzyl alcohol (NBA) as a matrix. All solvents were purified by standard procedures. All other chemicals were analytically pure and were used without further purification. All reactions were carried out under an inert argon atmosphere. Melting points (uncorrected) of all compounds were obtained on a Reichert melting point apparatus.

**4.1.1. Tetrakis[(ethoxycarbonylthioureido)methyl]cavitand **3**.** A solution of tetrakis(aminomethyl)cavitand **1** (150 mg, 0.16 mmol) and ethoxycarbonyl isothiocyanate (252 mg, 0.96 mmol) in acetonitrile (10 mL) was stirred overnight at room temperature. The white precipitate was filtered off and dried in vacuo to afford **3** (160 mg, 69%), mp 143–146 °C; FAB-MS:  $m/z$  1457.0 ( $[\text{M} + \text{H}]^+$ , calcd 1457.0);  $^1\text{H}$  NMR ( $\text{CDCl}_3$ )  $\delta$  9.86 (s, 4H,  $\text{CH}_2\text{NHCO}$ ), 7.93 (s, 4H,  $\text{CSNHCO}$ ), 7.05 (s, 4H, ArH), 6.01 (d, 4H,  $J=7.3$  Hz,  $\text{OCH}_2\text{O}$ ), 4.75–4.80 (m, 12H, ArCHAR,  $\text{ArCH}_2\text{NH}$ ), 4.41 (d, 4H,  $J=7.3$  Hz,  $\text{OCH}_2\text{O}$ ), 4.21 (q, 8H,  $J=7.3$  Hz,  $\text{OCH}_2$ ), 2.18–2.23 (m, 8H,  $\text{CH}_2$ ), 1.27–1.45 (m, 36H,  $\text{CH}_2 + \text{CH}_3$ ), 0.94 (t, 12H,  $J=6.2$  Hz,  $\text{CH}_3$ );  $^{13}\text{C}$  NMR ( $\text{CDCl}_3$ )  $\delta$  176.8, 151.8, 150.5, 136.3, 120.0, 118.4, 98.4, 61.0, 38.4, 30.1, 28.2, 20.7, 12.3, 12.2. Anal. calcd for  $\text{C}_{72}\text{H}_{96}\text{N}_8\text{O}_{16}\text{S}_4$ : C, 59.32; H, 6.64; N, 7.69; S, 8.80. Found: C, 59.16; H, 6.51; N, 7.75; S, 8.75.

**4.1.2. Tetrakis(phthalimidopropoxy)cavitand **6**.** A suspension of tetrol **5** (500 mg, 0.57 mmol) and NaH (219 mg, 9.12 mmol) in dry DMF (50 mL) was heated for 30 min at 65 °C. Subsequently, bromopropylphthalimide (3 g, 11.4 mmol) was added and heating was continued for 3 days at 90 °C. After removal of the solvent, the residue was dissolved in EtOAc (25 mL), whereupon 1 N HCl was added till pH 7. The solution was washed with water ( $3 \times 25$  mL) and brine ( $1 \times 25$  mL) and dried over  $\text{MgSO}_4$ . Evaporation of the solvent gave a brown oil, which was further purified by flash chromatography ( $\text{SiO}_2$ , EtOAc/hexanes, 1:2) to afford pure **6** (373 mg, 65%) as a white solid, mp 150–153 °C; FAB-MS:  $m/z$  1629.7 ( $[\text{M} + \text{H}]^+$ , calcd 1629.3);  $^1\text{H}$  NMR ( $\text{CDCl}_3$ )  $\delta$  7.82–7.86 and 7.69–7.73 (2m, 4+4H, ArH), 6.79 (s, 4H, ArH), 5.90 (d, 4H,  $J=7.0$  Hz,  $\text{OCH}_2\text{O}$ ), 4.70 (t, 4H,  $J=8.0$  Hz, ArCHAR), 4.43



(d, 4H,  $J=7.0$  Hz, OCH<sub>2</sub>O), 4.02 (t, 8H,  $J=5.8$  Hz, OCH<sub>2</sub>), 3.91 (t, 8H,  $J=5.4$  Hz, CH<sub>2</sub>N), 2.14–2.19 and 2.04–2.13 (2m, 8+8H, CH<sub>2</sub>+CH<sub>2</sub>), 1.27–1.42 (m, 24H, CH<sub>2</sub>), 0.91 (t, 12H,  $J=6.9$  Hz, CH<sub>3</sub>); <sup>13</sup>C NMR (CDCl<sub>3</sub>)  $\delta$  167.7, 147.7, 143.8, 138.3, 133.3, 131.7, 122.6, 113.5, 99.0, 70.5, 36.5, 34.9, 31.6, 29.4, 28.9, 27.1, 22.1, 13.6. Anal. calcd for C<sub>96</sub>H<sub>100</sub>N<sub>4</sub>O<sub>20</sub>: C, 70.75; H, 6.18; N, 3.44. Found: C, 70.78; H, 6.40; N, 3.17.

**4.1.3. Tetrakis(aminopropoxy)cavitand 7.** A solution of **6** (608 mg, 0.38 mmol) and hydrazine hydrate (247 mg, 7.7 mmol) in a 9:1 mixture of EtOH (27 mL) and THF (3 mL) was refluxed overnight. After addition of concentrated HCl (0.5 mL) refluxing was continued for another hour. Upon cooling of the reaction mixture 2 M NaOH was added till pH 10 to give a precipitate. The precipitate was filtered off and was washed with H<sub>2</sub>O (5 mL). The residue was dissolved in CH<sub>2</sub>Cl<sub>2</sub> (15 mL) and the resulting solution was dried over MgSO<sub>4</sub>. Evaporation of the solvent gave **7** (248 mg, 58%), mp 188–190 °C; FAB-MS:  $m/z$  1109.7 ([M+H]<sup>+</sup>, calcd 1109.7); <sup>1</sup>H NMR (CDCl<sub>3</sub>)  $\delta$  7.71–7.73 (m, 8H, NH<sub>2</sub>), 6.69 (s, 4H, ArH), 6.18 (d, 4H,  $J=7.8$  Hz, OCH<sub>2</sub>O), 4.64 (t, 4H,  $J=8.0$  Hz, ArCHAr), 4.47 (d, 4H,  $J=8.0$  Hz, OCH<sub>2</sub>O), 4.07 (t, 8H,  $J=5.1$  Hz, OCH<sub>2</sub>), 3.25–3.33 (m, 8H, CH<sub>2</sub>N), 2.02–2.21 (m, 8+8H, CH<sub>2</sub>+CH<sub>2</sub>), 1.27–1.42 (m, 24H, CH<sub>2</sub>), 0.84 (t, 12H,  $J=7.3$  Hz, CH<sub>3</sub>). Anal. calcd for C<sub>64</sub>H<sub>92</sub>N<sub>4</sub>O<sub>12</sub>·3CH<sub>2</sub>Cl<sub>2</sub>: C, 57.47; H, 7.34; N, 4.00. Found: C, 57.14; H, 7.10; N, 4.12.

**4.1.4. Tetrakis[(benzoylthioureido)propoxy]cavitand 8.** A solution of **7** (200 mg, 0.18 mmol) and benzoyl isothiocyanate (227.5 mg, 1.44 mmol) in chloroform (10 mL) was stirred at room temperature for 3 days. The solution was washed with H<sub>2</sub>O (2×20 mL) and dried over MgSO<sub>4</sub>. The solvent was removed in vacuo and the crude product was purified by flash chromatography (SiO<sub>2</sub>, CH<sub>2</sub>Cl<sub>2</sub>/hexanes 3:2) to give **8** (159 mg, 50%) as a yellowish solid, mp 90–92 °C; FAB-MS:  $m/z$  1761.5 ([M+H]<sup>+</sup>, calcd 1761.7); <sup>1</sup>H NMR (CDCl<sub>3</sub>)  $\delta$  9.02 (s, 4H, NH), 7.80 (d, 8H,  $J=8.1$  Hz, ArH), 7.30–7.64 (m, 12H, ArH), 6.83 (s, 4H, ArH), 5.93 (d, 4H,  $J=7.2$  Hz, OCH<sub>2</sub>O), 4.74 (t, 4H,  $J=8.4$  Hz, ArCHAr), 4.50 (d, 4H,  $J=6.9$  Hz, OCH<sub>2</sub>O), 4.04 (t, 8H,  $J=5.1$  Hz, OCH<sub>2</sub>), 3.93 (q, 8H,  $J=5.4$  Hz, CH<sub>2</sub>N), 2.15–2.20 (m, 8H, CH<sub>2</sub>), 2.08 (q, 8H,  $J=5.4$  Hz, CH<sub>2</sub>), 1.27–1.42 (m, 24H, CH<sub>2</sub>), 0.91 (t, 12H,  $J=6.9$  Hz, CH<sub>3</sub>); <sup>13</sup>C NMR (CDCl<sub>3</sub>)  $\delta$  179.9, 166.8, 148.3, 144.2, 138.9, 133.4, 132.0, 129.1, 127.0, 114.3, 99.8, 71.1, 43.4, 37.0, 32.1, 29.9, 28.8, 27.7, 22.7, 14.1. Anal. calcd for C<sub>96</sub>H<sub>112</sub>N<sub>8</sub>O<sub>16</sub>S<sub>4</sub>: C, 65.43; H, 6.41; N, 6.36; S, 7.28. Found: C, 64.60; H, 6.15; N, 6.75; S, 7.05.

## 4.2. Picrate extractions

**4.2.1. Solutions.** The 10<sup>-4</sup> M salt stock solutions were prepared by dissolving the required amounts of the appropriate metal nitrate M<sup>n+</sup>(X<sup>-</sup>)<sub>n</sub> and LiPic in 10<sup>-3</sup> M HNO<sub>3</sub> adjusting the total volume of the solution to 100 mL using volumetric glassware. The pH of the solutions was close to pH 3, and adjusted to pH 3 by adding small amounts of LiOH. The metal picrate solutions were prepared in situ in the stock solutions. The 10<sup>-3</sup> M stock solutions of the ligands were prepared by dissolving the appropriate amount of ligands in 20 mL of CH<sub>2</sub>Cl<sub>2</sub>.

**4.2.2. Procedure.** Equal volumes (1.0 mL) of the organic and the aqueous solutions were transferred into a stoppered glass vial and stirred at ambient temperatures (about 23 °C) for 17 h. The solutions were disengaged by centrifugation (1600 rpm for 10 min). The concentration of picrate ion in the aqueous and organic phase was determined spectrophotometrically ( $\lambda_{\max}=355$  nm). Each measurement was repeated three times. Blank experiments showed that no picrate extraction occurred in the absence of ionophore. The percentage of the cation extracted into the organic phase (%E = E × 100%), defined as the ratio of the activity in the organic phase (A<sub>o</sub>) and the total activity in both the organic and the aqueous phase (A<sub>w</sub>), is expressed by the following equation:

$$\%E = (A_o / (A_o + A_w)) 100\% \quad (2)$$

## 4.3. Potentiometric measurements

**4.3.1. Reagents.** The membrane components potassium tetrakis[3,4-bis(trifluoromethyl)phenyl]borate (KTFPB), 2-nitrophenyl octyl ether (*o*-NPOE), high molecular weight poly(vinyl chloride) (PVC), and tetrahydrofuran (THF, distilled prior to use) and all salts were purchased from Fluka (Ronkonkoma, NY). Aqueous solutions were obtained by dissolving the appropriate salts in Nanopure purified water.

**4.3.2. Membrane preparation.** The polymeric membranes used for the determination of stability constants contained ionophore (20 mmol/kg) and KTFPB (2 mmol/kg) in PVC/*o*-NPOE (1:2 by weight) polymeric matrix (total 140 mg), unless otherwise indicated in the text. The membrane components were dissolved in freshly distilled THF (1.4 mL). The solution was placed in a glass ring (22 mm i.d.) mounted over a glass plate and then covered with another glass plate to slow down the solvent evaporation. After 24 h, the resulting membrane (of the approximate thickness 130–140  $\mu$ m) was peeled from the glass plate and discs of 7 mm diameter were cut out.

The procedure for the preparation of polymeric membranes evaluated for the potentiometric ion response was similar to that described above. The total amount of membrane components was 200 mg and the membranes consisted of 1 wt% of ionophore, 30 mol% of KTFPB and PVC/*o*-NPOE (1:2 by weight).

**4.3.3. Potentiometric response to cations and selectivity measurements.** Membrane discs were mounted in conventional ISE electrode bodies (Type IS 561; Philips, Eindhoven, The Netherlands) for electromotive force (EMF) measurements. All measurements were performed at ambient temperature (22 ± 1 °C) using a galvanic cell of the following type: Ag/AgCl(s)/3 M KCl/1 M CH<sub>3</sub>COOLi/sample/ion-selective membrane/0.001 M NaCl solution/AgCl(s)/Ag. The EMF values were measured using a custom made 16-channel electrode monitor. Details of this equipment have been described previously.<sup>31</sup>

The performance of the electrodes was examined by measuring the EMF for aqueous solutions of examined cations over the concentration range of 10<sup>-7</sup>–10<sup>-1</sup> M.



Potentiometric selectivity coefficients were determined by the separate solution method (SSM) according to the procedure described in literature.<sup>32</sup> Selectivity coefficient  $K_{I,J}^{\text{pot}}$  values were obtained from adequate, unbiased  $E^0$  measurements for each cation, based on the equation:

$$K_{I,J}^{\text{pot}} = \exp\left\{\frac{z_I F}{RT}(E_J^0 - E_I^0)\right\} \quad (3)$$

where  $R$ ,  $T$ , and  $F$  are the gas constant, absolute temperature, and the Faraday constant, respectively. The charge of primary ion,  $I$ , is indicated as  $z_I$  and potentials obtained by an extrapolation of the linear part of calibration curve to log  $a = 0$  for primary and interfering ions are put as  $E_I^0$  and  $E_J^0$ , respectively.

Activity coefficients were calculated according to the Debye–Hückel approximation.<sup>33</sup>

**4.3.4. Potentiometric determination of stability constants.** The measurement setup was the same as described above. Experiments were carried out according to the procedure described in Ref. 27a,b. Two sets of membranes were prepared: membranes with and without ionophore. A series of 7 mm i.d. membrane discs were cut from the parent membranes, and these disks were conditioned over 2–3 days in appropriate salt solutions ( $10^{-1}$  M NaCl,  $10^{-2}$  M CuCl<sub>2</sub>,  $10^{-2}$  M CdCl<sub>2</sub>,  $5 \times 10^{-3}$  M PbCl<sub>2</sub>,  $10^{-3}$  M AgNO<sub>3</sub>).

To determine the stability constants for a given ionophore and a given cation, two measurements, for a membrane without ionophores and then for a sandwich membrane, were carried out. The sandwich membrane was made, after drying of individual membranes, by attaching of the membrane with ionophore to the membrane without ionophore. The segmented membrane was then mounted into a Philips electrode body (membrane with ionophore faced the sample solution) and immediately immersed into an appropriate salt solution (identical as for conditioning of the membrane). The potential was recorded as the mean of the last minute of a 10 min measurement period in the test solution. The potential of the electrodes with sandwich membranes remained free of diffusion-induced drifts for 20–50 min, depending on the ionophore incorporated within the membrane and the ion measured. The membrane potential values  $\Delta\text{EMF}$  were calculated by subtracting the cell potential for a membrane without ionophore from that of the sandwich membrane. The formation constant,  $\beta_{\text{IL}_n}$ , was calculated from Eq. 4:<sup>27a,b</sup>

$$\beta_{\text{IL}_n} = \left(L_T - \frac{n}{z_I} R_T^-\right)^{-n} \exp\left(\frac{z_I F}{RT} \Delta\text{EMF}\right) \quad (4)$$

where  $n$  is the complex stoichiometry,  $L_T$  and  $R_T^-$  are the concentrations of ionophore and ionic site additives in the membrane, respectively.

#### Acknowledgements

The Twente group gratefully acknowledges the financial support from the EEC for the synthesis and the extraction part of this work (contract FIKW-CT-2000-00088).

#### References and notes

- Siedler, J. *J. Prakt. Chem.* **1880**, *21*, 140.
- (a) Schwarzer, M.; Schuster, M. *Anal. Chim. Acta* **1996**, *328*, 1–11. (b) Ringmann, S.; Schuster, M. *Chem. Tech.* **1997**, *49*, 217–226. (c) Sandor, M.; Geistmann, F.; Schuster, M. *Anal. Chim. Acta* **1999**, *388*, 19–26. (d) Sandor, M.; Geistmann, F.; Schuster, M. *Anal. Chim. Acta* **2003**, *486*, 11–19.
- El Aamrani, F. Z.; Kumar, A.; Cortina, J. L.; Sastre, A. M. *Anal. Chim. Acta* **1999**, *382*, 205–213.
- Koch, K. R. *Coord. Chem. Rev.* **2001**, *216–217*, 473–488.
- (a) Richer, R.; Beyer, L.; Kaiser, J. Z. *Anorg. Allg. Chem.* **1980**, *461*, 67. (b) Cernak, J.; Chomic, J.; Kutschy, P.; Svrčinova, D.; Dzurilla, M. *Inorg. Chim. Acta* **1991**, *181*, 85–92.
- (a) Guillon, E.; Déchamps-Olivier, I.; Mohamadou, A.; Barbier, J. P. *Inorg. Chim. Acta* **1998**, *268*, 13–19. (b) Resch, U.; Rurack, K.; Bricks, J. L.; Slominski, J. L. *J. Fluoresc.* **1997**, *7*, 231S–233S.
- Otazo-Sánchez, E.; Pérez-Marín, L.; Estevéz-Hernández, O.; Rojas-Lima, S.; Alonso-Chamarro, J. *J. Chem. Soc., Perkin Trans. 2* **2001**, 2211–2218.
- Yuan, Y. F.; Wang, J. T.; Gimeno, M. C.; Laguna, A.; Jones, P. G. *Inorg. Chim. Acta* **2001**, *324*, 301–317 and references therein.
- Arnaud-Neu, F.; Böhmer, V.; Dozol, J. F.; Gruttner, C.; Jakobi, R. A.; Kraft, D.; Mauprivez, O.; Rouquette, H.; Schwing-Weill, M. J.; Simon, N.; Vogt, W. *J. Chem. Soc., Perkin Trans. 2* **1996**, 1175–1182.
- Talanova, G.; Elkarim, N. S. A.; Talanov, V. S.; Bartsch, R. A. *Anal. Chem.* **1999**, *71*, 3106–3109.
- Arena, G.; Contino, A.; Longo, E.; Sciotto, D.; Sgarlata, C.; Spoto, G. *Tetrahedron Lett.* **2003**, *29*, 5415–5418.
- Wieser, C.; Dieleman, C. B.; Matt, D. *Coord. Chem. Rev.* **1997**, *165*, 93–161.
- Timmerman, P.; Verboom, W.; Reinhoudt, D. N. *Tetrahedron* **1996**, *52*, 2663–2704.
- Boerrigter, H.; Verboom, W.; Reinhoudt, D. N. *J. Org. Chem.* **1997**, *62*, 7148–7155.
- Barret, E. S.; Irwin, J. L.; Turner, P.; Sherburn, M. S. *J. Org. Chem.* **2001**, *66*, 8227–8229.
- Malinowska, E.; Górski, Ł.; Wojciechowska, D.; Reinoso-García, M. M.; Verboom, W.; Reinhoudt, D. N. *New J. Chem.* **2003**, *27*, 1440–1445.
- (a) Van der Groot, H.; Schepers, M. J. P.; Sterk, G. J.; Timmerman, H. *Eur. J. Med. Chem. Chim. Ther.* **1992**, *5*, 511–517. (b) Ma, D.; Xia, C.; Jiang, J.; Zhang, J.; Tang, W. *J. Org. Chem.* **2003**, *68*, 442–451.
- Nakagawa, Y.; Wheelock, C. E.; Morisseau, C.; Goodrow, M. H.; Hammock, B. G.; Hammock, B. D. *Bioorg. Med. Chem.* **2000**, *8*, 2663–2673.
- Moore, S. S.; Tarnowski, T. L.; Newcomb, M.; Cram, D. J. *J. Am. Chem. Soc.* **1977**, *99*, 6398–6405.
- Yordanov, A. T.; Whittlesey, B. R.; Roundhill, D. M. *Inorg. Chem.* **1998**, *37*, 3526–3531.
- Marcos, P. M.; Ascenso, J. R.; Segurado, M. A. P.; Pereira, J. L. C. *J. Incl. Phenom.* **2002**, *42*, 281–288.
- Marcus, Y. *Ion Properties*; Marcel Dekker: New York, 1997; pp 47–48.
- Beyer, L.; Hoyer, E.; Liebscher, J.; Hartmann, H. *Z. Chem.* **1981**, *21*, 81–91.
- (a) Bakker, E.; Bühlman, P.; Pretsch, E. *Chem. Rev.* **1997**, *97*, 3083–3132. (b) Bakker, E. *Anal. Chem.* **1997**, *69*, 1061–1069.
- Wyglądacz, K.; Malinowska, E.; Szczygelska-Tao, J.; Biernat, J. F. *J. Incl. Phenom.* **2001**, *39*, 309–314.

26. Bakker, E.; Pretsch, E.; Bühlman, P. *Anal. Chem.* **2000**, *72*, 1127–1133.
27. (a) Mi, Y.; Bakker, E. *Anal. Chem.* **1999**, *71*, 5279–5287. (b) Qin, Y.; Mi, Y.; Bakker, E. *Anal. Chim. Acta* **2000**, *421*, 207–220. (c) Shultz, M. M.; Stefanowa, O. K.; Mokrow, S. B.; Mikhelson, K. N. *Anal. Chem.* **2002**, *74*, 510–517. (d) Mikhelson, K. N.; Bobacka, J.; Ivaska, A.; Lewenstam, A.; Bochenska, M. *Anal. Chem.* **2002**, *74*, 518–527.
28. Gutmann, V. *Coordination Chemistry in Non-aqueous Solvents*; Springer: New York, 1971.
29. Stoikov, I. I.; Omran, O. A.; Solovieva, S. E.; Latypov, S. K.; Enikeev, K. M.; Gubaidullin, A. T.; Antipin, I. S.; Kononov, A. I. *Tetrahedron* **2003**, *59*, 1469–1476.
30. Shultz, M. M.; Stefanowa, O. K.; Mokrow, S. B.; Mikhelson, K. N. *Anal. Chem.* **2002**, *74*, 510–517.
31. Brzózka, Z. *Pomiary, Automatyka, Kontrola* **1988**, *9*, 197.
32. Bakker, E.; Pretsch, E.; Buhlman, P. *Anal. Chem.* **2002**, *72*, 1127–1133.
33. Meier, P. C. *Anal. Chim. Acta* **1982**, *136*, 363–368.

# Fluorophore-linked zinc(II)dipicolylamine coordination complexes as sensors for phosphatidylserine-containing membranes

C. Lakshmi, Roger G. Hanshaw and Bradley D. Smith\*

Department of Chemistry and Biochemistry and The Walther Center for Cancer Research, University of Notre Dame, 251 Nieuwland Hall, Notre Dame, IN 46556-5670, USA

Received 19 February 2004; revised 8 July 2004; accepted 19 August 2004

Available online 15 September 2004

**Abstract**—A series of  $Zn^{2+}$ -2,2'-dipicolylamine ( $Zn^{2+}$ -DPA) coordination complexes with an attached NBD fluorophore are synthesized and evaluated as fluorescent sensors. The sensors do not respond to vesicles composed of zwitterionic phosphatidylcholine, but the NBD fluorescence emission is enhanced in the presence of anionic vesicles. A sensor with two  $Zn^{2+}$ -DPA units and a hydrophilic tris(ethyleneoxy) linker produced a larger emission enhancement than an analogue with a butyl linker, and titration with 1:1 POPC:POPS vesicles lead to an apparent phospholipid association constant of  $5.3 \times 10^4 M^{-1}$ . The sensor can detect the presence of vesicles containing as little as 5% phosphatidylserine. The sensing effect apparently requires a membrane surface because the sensors do not respond to a phosphatidylserine derivative that is monodispersed in aqueous solution.

© 2004 Elsevier Ltd. All rights reserved.

## 1. Introduction

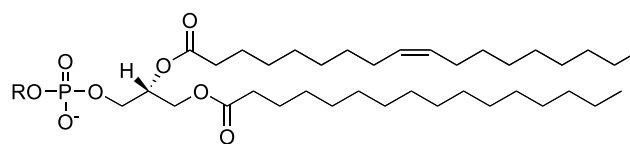
New and improved assays for the *in vitro* and *in vivo* detection of apoptosis (programmed cell death) would be a useful contribution to research in cell biology and clinical medicine. Current methods used in detecting apoptosis focus on changes in cytosolic biochemical events, degradation of cell nuclear material, and changes in the cell plasma membrane structure.<sup>1–4</sup> Each assay has its own inherent advantages and shortcomings. For example, monitoring of cytosolic caspase activity and detection of nucleic acid fragmentation are classic assays for apoptosis.<sup>5–8</sup> However, these processes often occur too late in the apoptosis process to allow other important events to be

**Keywords:** Molecular recognition; Phospholipid binding; Phosphate recognition; Chemosensor; Apoptosis; Phospholipid asymmetry; Phosphatidylserine.

**Abbreviations:** DHPC, 1,2-dihexanoyl-*sn*-glycero-3-phosphocholine; DHPS, 1,2-dihexanoyl-*sn*-glycero-3-[phospho-L-serine]; NBD, 7-nitro-1,3-benz-2-oxa-1,3-diaza-4-yl; PC, phosphatidylcholine; POPA, 1-palmitoyl-2-oleoyl-*sn*-glycero-3-phosphate; POPC, 1-palmitoyl-2-oleoyl-*sn*-glycero-3-phosphocholine; POPG, 1-palmitoyl-2-oleoyl-*sn*-glycero-3-phosphoglycerol; POPS, 1-palmitoyl-2-oleoyl-*sn*-glycero-3-[phospho-L-serine]; PS, phosphatidylserine; TEO, tris(ethyleneoxy); TES, *N*-tris[hydroxymethyl]methyl-2-aminoethanesulfonic acid.

\* Corresponding author. Tel.: +1-574-631-8632; fax: +1-574-631-6652; e-mail: smith.115@nd.edu

detected. Monitoring the appearance of phosphatidylserine (PS, Fig. 1) on a cell surface is a more suitable assay for the early stages of apoptosis.<sup>9–11</sup> PS is maintained almost exclusively in the inner monolayer of the plasma membrane of healthy animal cells, but a scrambling effect is initiated early in apoptosis which results in externalization of PS.



Formula for R	Phospholipid
-H	POPA
-CH <sub>2</sub> CH <sub>2</sub> N(CH <sub>3</sub> ) <sub>3</sub> <sup>+</sup>	POPC
-CH <sub>2</sub> CH(NH <sub>3</sub> <sup>+</sup> )COO <sup>-</sup>	POPS
-CH <sub>2</sub> CH(OH)CH <sub>2</sub> OH	POPG

**Figure 1.** Head group structure of common phospholipids.

Detection of externalized PS is currently achieved using annexin V, a member of a class of  $Ca^{2+}$ -dependent phospholipid binding proteins.<sup>12,13</sup> Annexin V exhibits high affinity for PS, and binding of fluorescent labeled annexin V (e.g., annexin-FITC) to the cell surface is currently used in microscopic and flow cytometric assays for the detection of apoptosis. However, use of annexin V is not without limitations. PS binding by annexin V is a  $Ca^{2+}$ -dependent process, which raises the concern of

activation of non-specific  $\text{Ca}^{2+}$ -dependent phospholipid scramblases within the membrane bilayer when  $\text{Ca}^{2+}$ -rich annexin binding buffers are used. Further, the protein is susceptible to degradation and exhibits slow binding kinetics.<sup>14,15</sup> Low molecular weight synthetic mimics of annexin V that bind rapidly to PS-enriched membrane surfaces in a  $\text{Ca}^{2+}$ -independent manner would be an attractive alternative.

An X-ray crystal structure of an annexin–glycero-phosphoserine complex shows that the phosphoserine head group is coordinated to one of the four canonical binding sites of the protein through two bridging  $\text{Ca}^{2+}$  ions.<sup>16</sup> This picture suggested to us that synthetic metal complexes with appropriate charge, geometry, and spatial orientation may bind to the head group of anionic phospholipids preferentially over zwitterionic phospholipids. In other words, rationally designed coordination complexes may be useful as mimics of annexin V. Several phosphate chemosensors with  $\text{Zn}^{2+}$ -coordinated binding sites have been described in the literature.<sup>17–19</sup> For example, Hamachi and co-workers recently described an anthracene-based sensor with two zinc dipicolylamine ( $\text{Zn}^{2+}$ -DPA) units (Fig. 2).<sup>20</sup> The sensor binds to the dianionic phosphotyrosine groups in phosphorylated peptides with association constants of up to  $10^7 \text{ M}^{-1}$ .

We subsequently demonstrated that this sensor, which we call PSS-380, can be used to detect the presence of anionic phospholipids, specifically PS, on the surface of vesicles and cells.<sup>21</sup> While the fluorescence emission of PSS-380 was unchanged upon treatment with vesicles composed entirely of zwitterionic phosphatidylcholine (PC), a 10-fold increase in fluorescence emission was observed upon addition of anionic vesicles composed of 1:1 POPC:POPS (Fig. 1). PSS-380 was successfully used to detect apoptosis in Jurkat cells treated with camptothecin (an apoptosis inducing agent) via fluorescence microscopy and flow cytometry. Although PSS-380 is an attractive alternative to annexin V-FITC, its wavelength of excitation (380 nm) is in the UV range, which is not compatible with the lasers in most flow cytometers. Replacing the anthracene unit with fluorophores that absorb at longer wavelengths would alleviate this drawback.

In an effort to develop second generation sensors, we have chosen to pursue a modular design which allows us to

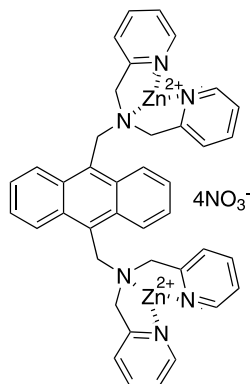


Figure 2. Structure of PSS-380.

systematically alter the three molecular components shown in Figure 3: the PS binding group, the linker, and the fluorophore. Herein, we report the design and synthesis of the first examples of this series, namely, coordination complexes 1–4 (Fig. 4). The design retains the  $\text{Zn}^{2+}$ -DPA affinity units, attached in a meta orientation to a phenyl ring,<sup>18</sup> which is in turn linked to a 7-nitrobenz-2-oxa-1,3-diaza-4-yl (NBD) fluorophore. The NBD fluorophore is excited at 470 nm and exhibits a broad emission centered at 530 nm, which limits its use in microscopy and flow cytometry applications; nevertheless, its environmental sensitivity makes it useful for the mechanistic experiments performed here.

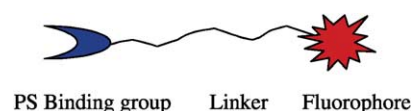


Figure 3. Modular design of PS sensor.

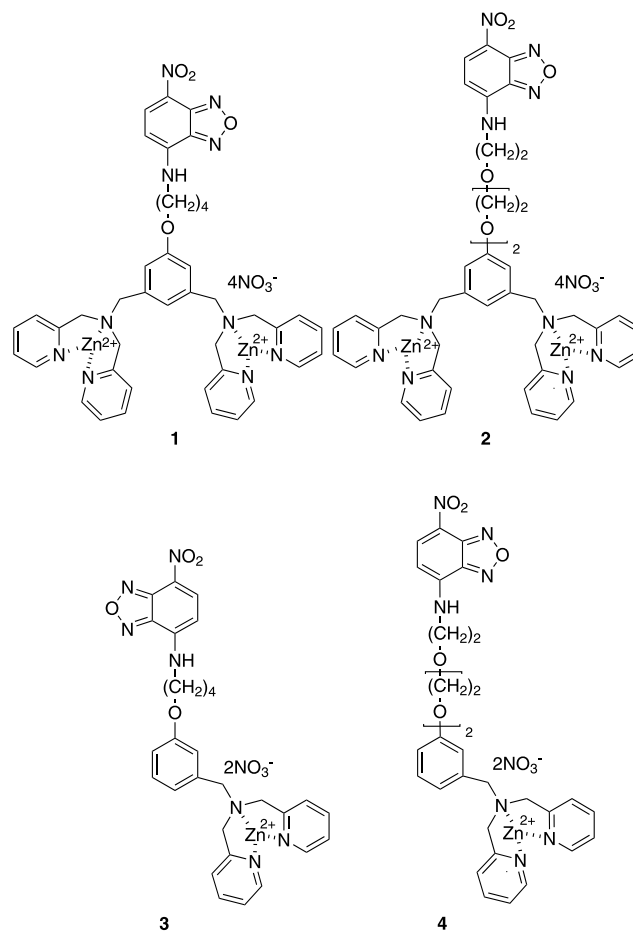


Figure 4. Coordination complexes 1–4 as potential PS sensors.

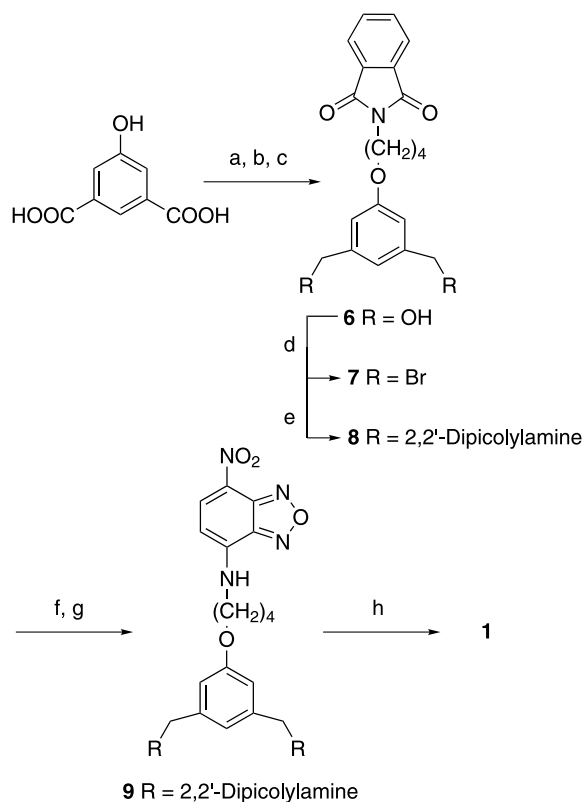
We examined two types of linkers, butyl (relatively hydrophobic) and tris(ethyleneoxy) (TEO, relatively hydrophilic), anticipating that upon binding, the nature of the linker may influence the interaction between the fluorophore and the bilayer membrane. We illustrate how sensor

response to PS-enriched membrane surfaces is altered by changes in the number of  $\text{Zn}^{2+}$ -DPA binding units, as well as the structure of the linker.

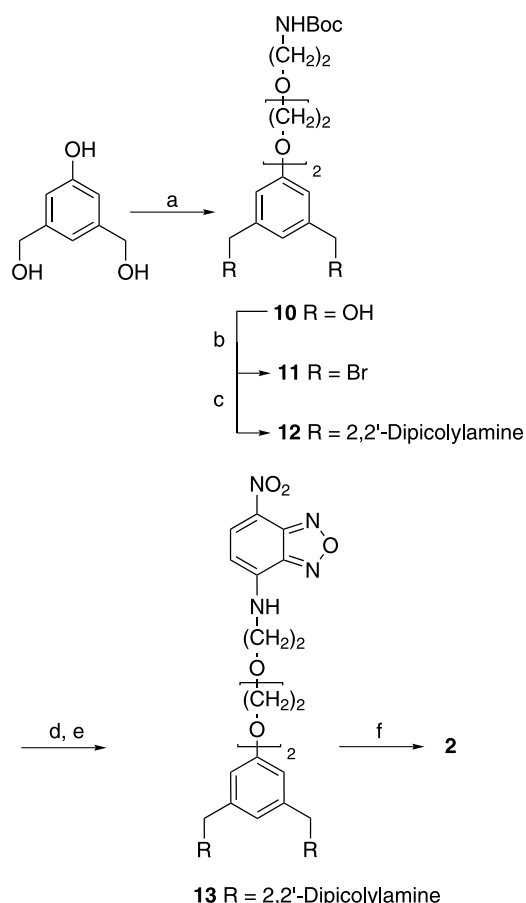
## 2. Results and discussion

### 2.1. Synthesis

The synthesis of **1** was achieved in eight steps starting from commercially available 5-hydroxyisophthalic acid (Scheme 1). The butyl linker was attached to 3,5-bis(hydroxymethyl)phenol,<sup>22,23</sup> using *N*-(4-bromobutyl)phthalimide and  $\text{K}_2\text{CO}_3$  in acetonitrile, and the product converted in high yield to the corresponding dibromide **7** using  $\text{CBr}_4$  and  $\text{Ph}_3\text{P}$ . The zinc binding groups were introduced in the next step by treating **7** with DPA in the presence of  $\text{K}_2\text{CO}_3$  in DMF. The phthalimide protecting group was removed using hydrazine hydrate and the resulting amine was treated with NBD-Cl in the presence of  $\text{K}_2\text{CO}_3$  in dry THF to afford **9** in 70% yield. The complexation of **9** with  $\text{Zn}(\text{NO}_3)_2$  in methanol/water mixture was quantitative and the complex was used for the binding studies without further purification. Compound **2**, with a TEO linker was synthesized using a similar synthetic strategy (Scheme 2). In addition, the syntheses of control compounds **3** and **4**, each with one  $\text{Zn}^{2+}$ -DPA unit are depicted in Schemes 3 and 4.



**Scheme 1.** (a) EtOH, concd  $\text{H}_2\text{SO}_4$ , reflux, (96%); (b)  $\text{LiAlH}_4$ , THF, 0 °C to rt, (96%); (c) *N*-(4-bromobutyl)phthalimide,  $\text{K}_2\text{CO}_3$ , acetonitrile, reflux, (90%); (d)  $\text{CBr}_4$ ,  $\text{Ph}_3\text{P}$ ,  $\text{CH}_2\text{Cl}_2$ , (89%); (e) 2,2'-dipicolylamine,  $\text{K}_2\text{CO}_3$ , DMF, (91%); (f) hydrazine hydrate,  $\text{CH}_2\text{Cl}_2/\text{EtOH}$ , reflux, (90%); (g) NBD-Cl,  $\text{K}_2\text{CO}_3$ , THF (70%); (h) zinc nitrate, MeOH/ $\text{H}_2\text{O}$ , (100%).

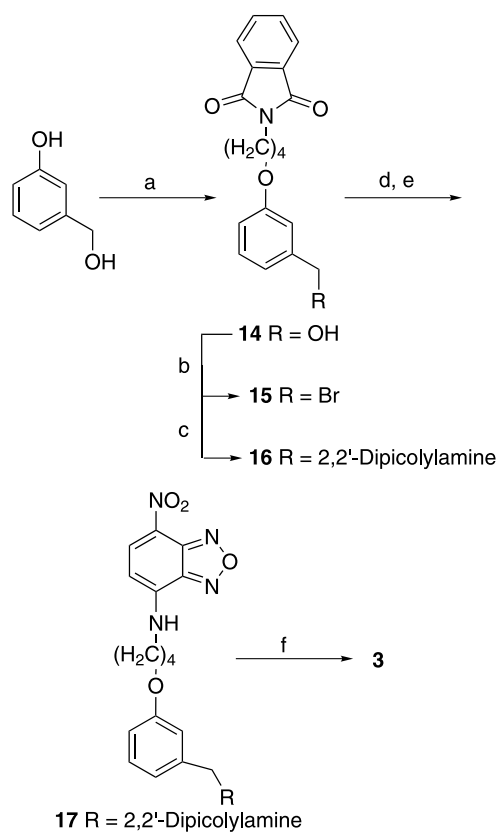


**Scheme 2.** (a) *N*-Boc-{2-[2-(2-bromoethoxy)-ethoxy]-ethyl} monoamine,  $\text{K}_2\text{CO}_3$ , acetonitrile, reflux (89%); (b)  $\text{CBr}_4$ ,  $\text{Ph}_3\text{P}$ ,  $\text{CH}_2\text{Cl}_2$  (70%); (c) 2,2'-dipicolylamine,  $\text{K}_2\text{CO}_3$ , DMF (87%); (d) TFA,  $\text{CH}_2\text{Cl}_2$  (85%); (e) NBD-Cl,  $\text{K}_2\text{CO}_3$ , THF (70%); (f) zinc nitrate, MeOH/ $\text{H}_2\text{O}$  (100%).

### 2.2. Evaluation of vesicle sensing properties

The ideal candidate for apoptosis detection via externalized PS should have a strong affinity for anionic PS embedded in a membrane that is primarily composed of zwitterionic phospholipids. The sensor binding, however, must not disrupt the membrane structure. The effect of **1** on membrane integrity was measured in two ways. The first was vesicle leakage, where **1** was found to be incapable of inducing bilayer permeabilization. Specifically, addition of **1** at concentrations up to 10  $\mu\text{M}$  to vesicles composed of either 100% POPC or 1:1 POPC:POPS failed to induce carboxyfluorescein leakage. Furthermore, **1** and **2** do not penetrate into vesicles. This was proved by adding sensors **1** or **2** at concentrations up to 2.0 mol% to a dispersion of vesicles (25  $\mu\text{M}$  total phospholipid) consisting either of 100% POPC or 1:1 POPC:POPS. Subsequent addition of the membrane-impermeable reducing agent sodium dithionite at 2 h after sensor addition resulted in greater than 95% quenching of fluorescence. The near total quenching of NBD fluorescence by sodium dithionite indicates that **1** and **2** do not cross the vesicle membrane and become protected from chemical reduction. The ability of **1** and **2** to bind to PS-enriched membranes (see below) and not disrupt the membrane structure establishes the utility of the *meta*-aryl bis ( $\text{Zn}^{2+}$ -DPA) unit as a PS affinity group in modular designs of PS-sensors.

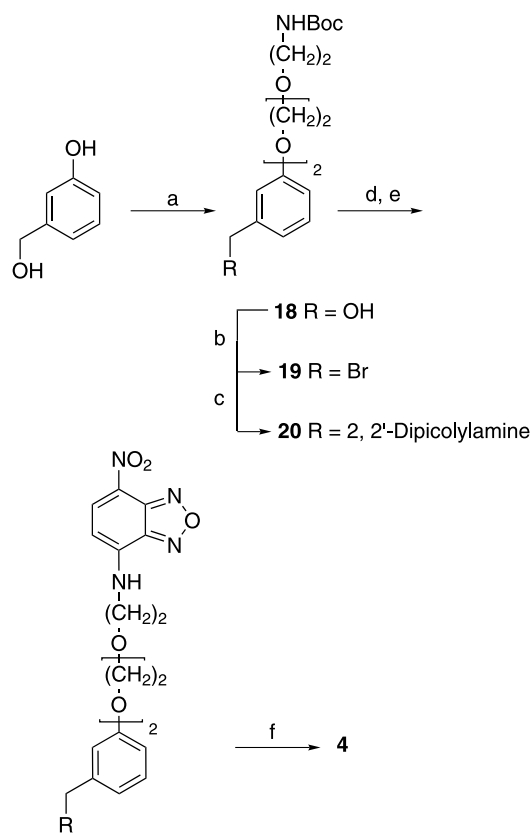




**Scheme 3.** (a) *N*-(4-Bromobutyl)phthalimide,  $K_2CO_3$ , acetonitrile, reflux (67%); (b)  $CBr_4$ ,  $Ph_3P$ ,  $CH_2Cl_2$  (85%); (c) 2,2'-dipicolylamine,  $K_2CO_3$ , DMF (93%); (d) hydrazine hydrate, EtOH/ $CH_2Cl_2$ , reflux (90%); (e) NBD-Cl,  $K_2CO_3$ , THF (72%); (f) zinc nitrate, MeOH/ $H_2O$  (100%).

The NBD fluorophore is known to exhibit an enhancement in fluorescence intensity upon transfer from a polar environment to an apolar environment.<sup>24,25</sup> Thus, the fluorescence emission from sensors **1** and **2** was expected to increase upon binding to the surface of a bilayer membrane. Indeed, titration of both sensors with anionic vesicles produced moderate to large fluorescence enhancements. While such an enhancement is not a necessary feature for employment in apoptosis detection, the observed NBD fluorescence enhancement upon membrane binding provides insight into the interactions between the sensor and the membrane surface. The titration experiments involved addition of unilamellar vesicles composed of 1:1 POPC:POPS, 1:1 POPC:POPA, 1:1 POPC:POPG, or 100% POPC to a 1  $\mu M$  solution of **1** or **2**. The resulting isotherms (Fig. 5) were fitted to a 1:1 binding model, which allowed calculation of apparent phospholipid binding constants.<sup>†</sup> With sensors **1** and **2**, the order of binding affinities to vesicles was 1:1 POPC:POPS > 1:1 POPC:POPG ~ 1:1 POPC:POPA  $\gg$  100% POPC (Table 1). The sensors were not expected to bind the zwitterionic POPC head group, and this titration was performed as a control to determine specificity of the sensors for anionic PS. Although **1** binds to

<sup>†</sup> At this point it is not known if the sensors induce lateral phospholipid aggregation; however, control experiments showed that the meta-aryl bis ( $Zn^{2+}$ -DPA) unit does not promote phospholipid transmembrane flip flop. The binding constants in Tables 1 and 2 are considered apparent because they do not consider  $Zn^{2+}$  dissociation from the DPA units in **1** and **2** in the absence of vesicles.



**21** R = 2, 2'-Dipicolylamine

**Scheme 4.** (a) *N*-Boc-2-[2-(2-bromoethoxy)-ethoxy]-ethyl monoamine,  $K_2CO_3$ , acetonitrile, reflux (89%); (b)  $CBr_4$ ,  $Ph_3P$ ,  $CH_2Cl_2$  (65%); (c) 2,2'-dipicolylamine,  $K_2CO_3$ , DMF (87%); (d) TFA,  $CH_2Cl_2$  (85%); (e) NBD-Cl,  $K_2CO_3$ , THF (76%); (f) zinc nitrate, MeOH/ $H_2O$  (100%).

anionic vesicles with slightly higher binding constants than **2**, the more important sensing property is the difference in emission intensity for anionic vesicles versus 100% POPC. In this case, the response with sensor **2** is much more selective. For example, when the total phospholipid concentration is 60  $\mu M$ , the emission of butyl-linked sensor **1** with 1:1 POPC:POPS vesicles is about two times that observed with 100% POPC vesicles, whereas, the intensity ratio with the TEO-linked sensor **2** is about five.

Sensors **1** and **2** only respond to membrane-bound phospholipids, as evidenced by the lack of response to the short acyl chain phospholipids, dihexanoylphosphatidylcholine (DHPC) and dihexanoylphosphatidylserine (DHPS), which exist as monomeric dispersions in aqueous media. For example, addition of DHPC (100  $\mu M$ ) or a 1:1 mixture of DHPC:DHPS to a 1  $\mu M$  solution of **2** results in no detectable increase in NBD fluorescence intensity (data not shown).

The effect of only one  $Zn^{2+}$ -DPA unit in the sensor structure was evaluated using control compounds **3** and **4**. Vesicles composed of 100% POPC or 1:1 POPC:POPS were added to a 1  $\mu M$  solution of **3** or **4**. As in the case above, the emission of butyl-linked sensor **3** with 1:1 POPC:POPS vesicles (60  $\mu M$  phospholipid) is about two times that observed with 100% POPC vesicles, whereas the intensity

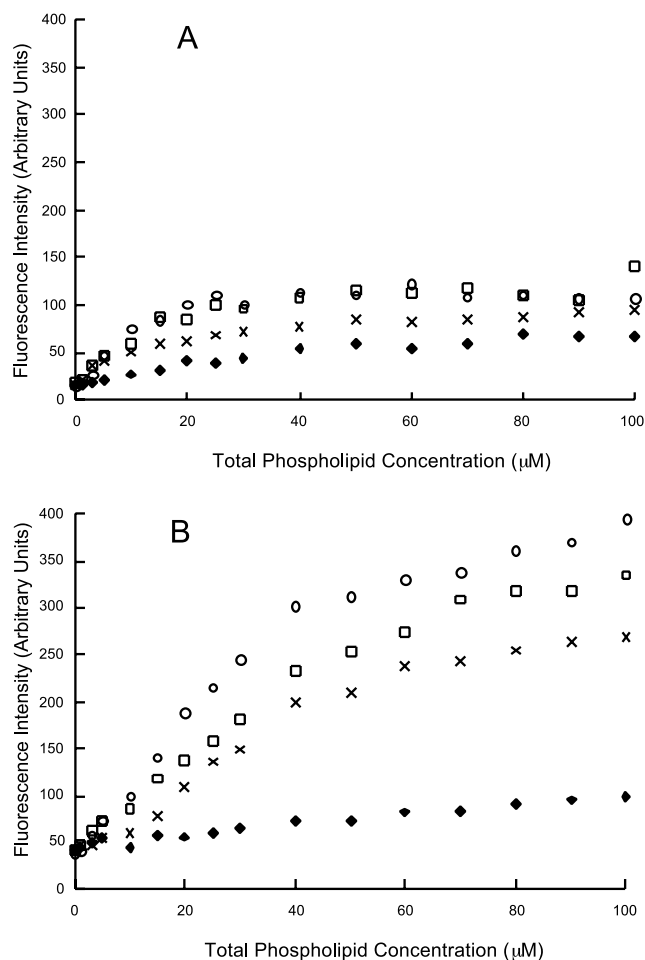


**Figure 5.** Fluorescence intensity upon addition of vesicles to a 1  $\mu\text{M}$  solution of **1** or **2** in 5 mM TES buffer, 145 mM NaCl, pH 7.4 at 25  $^{\circ}\text{C}$ . (A) Addition of 1:1 POPC:POPS ( $\circ$ ), 1:1 POPC:POPG ( $\square$ ), 1:1 POPC:POPA ( $\times$ ), or 100% POPC ( $\blacklozenge$ ) to **1**. (B) Addition of 1:1 POPC:POPS ( $\circ$ ), 1:1 POPC:POPG ( $\square$ ), 1:1 POPC:POPA ( $\times$ ), or 100% POPC ( $\blacklozenge$ ) to **2**.

ratio with TEO-linked sensor **4** is about five. Thus, it is clear that the hydrophilic TEO-linker is more useful for detecting PS-containing membranes over PC-only membranes. The emission of sensor **2** with two  $\text{Zn}^{2+}$ -DPA units is significantly higher than that obtained with **4**, indicating that the second  $\text{Zn}^{2+}$ -DPA unit increases the polar interactions that produce a stronger response to PS-containing membranes.

The Hamachi group has measured association constants for the two  $\text{Zn}^{2+}$  in PSS-380 and found  $K_1 \sim 7 \times 10^6 \text{ M}^{-1}$  and  $K_2 \sim 7 \times 10^4 \text{ M}^{-1}$ .<sup>26</sup> It is reasonable to think that sensors **1–4** have similar  $\text{Zn}^{2+}$  association constants which means that at 1  $\mu\text{M}$ , the sensor concentration used in this study, a

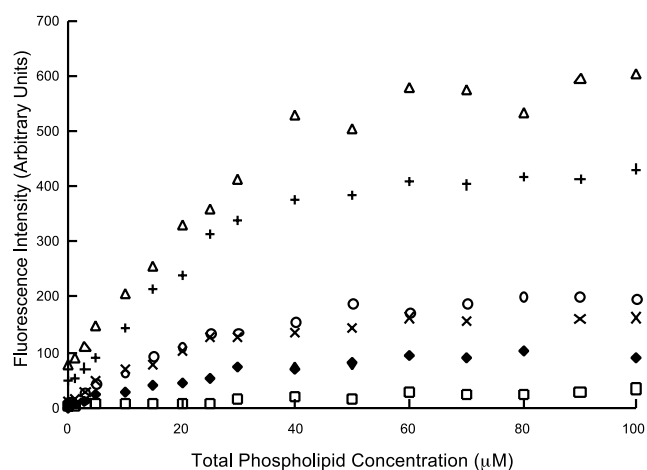


**Figure 6.** Fluorescence intensity of a 1  $\mu\text{M}$  solution of either **3** or **4** upon addition of phospholipid vesicles consisting of 100% POPC ( $\blacklozenge$  for **3**,  $\square$  for **4**), or 1:1 POPC:POPS ( $\circ$  for **3**,  $\times$  for **4**) in 5 mM TES buffer, 145 mM NaCl, pH 7.4 at 25  $^{\circ}\text{C}$ . For comparison, the fluorescence intensity for **2** upon addition of vesicles composed of 1:1 POPC:POPS is represented by ( $+$ ). Fluorescence intensity of **2** upon addition of vesicles composed of 1:1 POPC:POPS in the presence of 1  $\mu\text{M}$   $\text{Zn}(\text{NO}_3)_2$  is denoted by ( $\Delta$ ). All experiments were reproduced at least three times.

significant fraction of **1** and **2** may exist as the corresponding mononuclear  $\text{Zn}^{2+}$  complexes. To test if  $\text{Zn}^{2+}$  dissociation induces a measurable effect on sensor performance, the titration of sensor **2** with 1:1 POPC:POPS vesicles was repeated in the presence of 1  $\mu\text{M}$   $\text{Zn}(\text{NO}_3)_2$ . The resulting titration isotherm (Fig. 6) shows a 20% increase in fluorescence enhancement, but no measurable change in binding constant. This is consistent with an equilibrium picture that converts a less responsive mononuclear  $\text{Zn}^{2+}$  form of sensor **2** into a more responsive binuclear  $\text{Zn}^{2+}$  form.

The PS sensitivity of sensor **2** was evaluated by conducting additional titration experiments with POPC vesicles enriched with various amounts of POPS. Specifically, a solution of **2** (1  $\mu\text{M}$ ) was titrated with vesicles composed of POPC and 0–50% POPS (Fig. 7). The emission response of **2** increases with increasing fraction of PS, until about 20% PS, after which there is a plateau. This trend is also reflected by the apparent binding constants listed in Table 2. The data in Figure 7 shows that sensor **2** can readily detect the presence of bilayer membranes containing 5% PS. It is worth noting that this is approximately the fraction of PS that is externalized during the early-to-intermediate stages of cell apoptosis.<sup>27</sup>

In conclusion, we have shown that coordination complexes with  $\text{Zn}^{2+}$ -DPA units do not respond to anionic

**Table 1.** Sensor/phospholipid binding constants ( $K_a$ )

Sensor	$K_a \times 10^4 (\text{M}^{-1})^a$			
	100% POPC	1:1 POPC:POPS	1:1 POPC:POPG	1:1 POPC:POPA
<b>1</b>	<1	23.3 $\pm$ 1.7	14.2 $\pm$ 3.8	11 $\pm$ 6.0
<b>2</b>	<1	5.3 $\pm$ 2.0	2.0 $\pm$ 0.5	2.0 $\pm$ 0.3
<b>3</b>	<1 <sup>b</sup>	11.5 $\pm$ 5.5	—	—
<b>4</b>	<1 <sup>b</sup>	7.7 $\pm$ 3.3	—	—

<sup>a</sup> Values are average of at least three independent measurements.

<sup>b</sup> Values are average of two independent measurements.

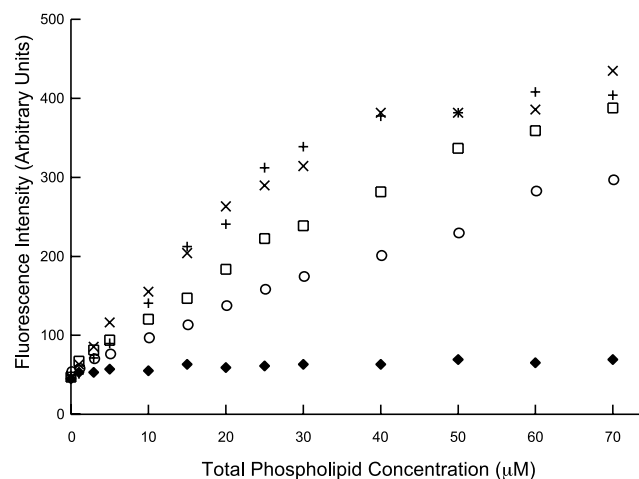


**Figure 7.** Fluorescence intensity of **2** (1  $\mu\text{M}$ ) upon addition of POPC vesicles enriched with 0% ( $\blacklozenge$ ), 5% ( $\circ$ ), 10% ( $\square$ ), 20% ( $\times$ ), or 50% ( $+$ ) POPS in 5 mM TES buffer, 145 mM NaCl, pH 7.4 at 25  $^{\circ}\text{C}$ .

**Table 2.** Sensor **2**/phospholipid binding constants ( $K_a$ ) for vesicles with varying PS content

	95:5 POPC:POPS	90:10 POPC:POPS	80:20 POPC:POPS	50:50 POPC:POPS
$K_a \times 10^4 \text{ (M}^{-1}\text{)}^a$	$1.0 \pm 0.3$	$2.2 \pm 0.5$	$5.7 \pm 0.5$	$5.3 \pm 2.0$

<sup>a</sup> Values are averages of at least three independent measurements.

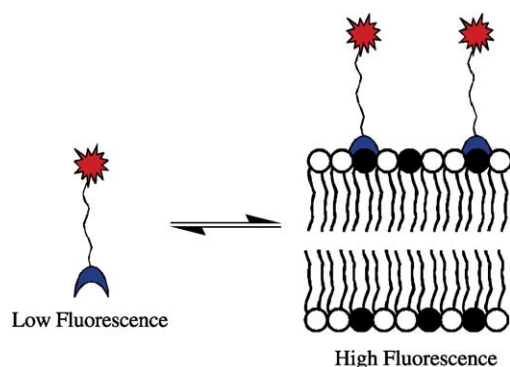


**Figure 8.** Sensing of PS-containing membranes. PS is represented with filled head group, PC is unfilled head group.

phospholipids (such as PS) when they are monodispersed in aqueous solution, but there is a significant fluorescence enhancement when the anionic phospholipids are part of a vesicle membrane (Fig. 8). The magnitude of the enhancement depends on the structure of the linker between the  $\text{Zn}^{2+}$ -DPA affinity units and the NBD fluorophore. The more hydrophilic TEO linker produces a sensor with significantly enhanced emission response to anionic PS-enriched membranes compared to zwitterionic PC-only membranes. The results reported here show that the NBD fluorophore can be used as a probe for rapid testing of new sensor designs, and for investigating fundamental questions in molecular recognition at the membrane surface. Future studies will determine if analogous sensors with more practically useful fluorophores can detect PS externalization and cell apoptosis.

### 3. Experimental

#### 3.1. Synthesis

**3.1.1. Synthesis of compound 6.** 3,5-Bis-hydroxymethyl phenol (1.06 g, 6.88 mmol), *N*-(4-bromobutyl)phthalimide (2.13 g, 7.57 mmol) and  $\text{K}_2\text{CO}_3$  (4.75 g, 34.4 mmol) were mixed in acetonitrile and refluxed for 24 h. The reaction mixture was cooled to room temperature and the solvent removed. The residue was redissolved in  $\text{CH}_2\text{Cl}_2$  and the insoluble residue filtered off. The filtrate was washed with water, dried over  $\text{MgSO}_4$  and the solvent removed under vacuum. The pure product was obtained as a semi-solid after purification on a silica column using EtOAc. Yield 90%;  $^1\text{H}$  NMR (300 MHz,  $\text{CDCl}_3$ ):  $\delta$  1.82–1.88 (br, 4H), 3.73–3.78 (m, 2H), 3.99–4.03 (m, 2H), 4.63 (s, 4H), 6.81 (s, 2H), 6.90 (s, 1H), 7.70–7.73 (m, 2H), 7.83–7.85 (m, 2H);  $^{13}\text{C}$  NMR (75 MHz,  $\text{CDCl}_3$ ):  $\delta$  25.3, 26.6, 37.7, 64.7, 67.3, 112.0, 117.5, 123.2, 132.1, 133.9, 143.0, 159.2, 168.5.

**3.1.2. Synthesis of compound 7.** To a solution of compound **6** (3.05 g, 8.62 mmol) and  $\text{CBr}_4$  (6.3 g, 18.96 mmol) in dry  $\text{CH}_2\text{Cl}_2$  at 0  $^{\circ}\text{C}$ , was slowly added  $\text{Ph}_3\text{P}$  (4.85 g, 18.52 mmol) in dry  $\text{CH}_2\text{Cl}_2$ . The reaction mixture was stirred at room temperature overnight. The reaction mixture was concentrated under vacuum and the pure product obtained as a white solid after silica gel chromatography (EtOAc/hexanes (1:1)). Yield 89%;  $^1\text{H}$  NMR (300 MHz,  $\text{CDCl}_3$ ):  $\delta$  1.86–1.89 (m, 4H), 3.78 (m, 2H), 4.00 (m, 2H), 4.42 (s, 4H), 6.83 (m, 2H), 6.98 (br, 1H), 7.71–7.74 (m, 2H), 7.84–7.87 (m, 2H);  $^{13}\text{C}$  NMR (75 MHz,  $\text{CDCl}_3$ ):  $\delta$  25.4, 26.6, 33.0, 37.7, 67.4, 115.3, 121.9, 123.3, 132.2, 134.1, 139.7, 159.4, 168.5.

**3.1.3. Synthesis of compound 8.** Compound **7** (1 g, 2.08 mmol), and  $\text{K}_2\text{CO}_3$  (1.44 g, 10.4 mmol) were mixed in dry DMF. 2,2'-Dipicolylamine (1.04 g, 5.21 mmol) was added and the reaction mixture stirred overnight. The DMF was removed and the residue dissolved in  $\text{CHCl}_3$ . The insoluble residue was filtered off. The filtrate was washed with water, brine and dried over  $\text{MgSO}_4$ . Solvent was removed and the residue chromatographed on a neutral alumina column using  $\text{CHCl}_3$  as eluent to afford the pure product. Yield 91%;  $^1\text{H}$  NMR (300 MHz,  $\text{CDCl}_3$ ):  $\delta$  1.85 (br, 4H), 3.62 (s, 4H), 3.74–3.79 (m, 10H), 3.97 (m, 2H), 6.84 (s, 2H), 7.04 (s, 1H), 7.08–7.13 (m, 4H), 7.57–7.64 (m, 8H), 7.67–7.70 (m, 2H), 7.81–7.84 (m, 2H), 8.48–8.50 (m, 4H);  $^{13}\text{C}$  NMR (75 MHz,  $\text{CDCl}_3$ ):  $\delta$  25.6, 26.9, 37.8, 58.7, 60.2, 67.2, 113.6, 121.6, 122.1, 122.9, 123.3, 132.2, 134.1, 136.6, 140.8, 149.1, 159.2, 159.9, 168.6; FAB MS  $m/z$  718  $[\text{M}+\text{H}^+]$ .

#### 3.1.4. Synthesis of compound 9.

**3.1.4.1. Generation of free amine from compound 8.** Compound **8** (0.550 g, 0.77 mmol) was dissolved in a mixture of  $\text{CH}_2\text{Cl}_2$  and EtOH (25:75). Hydrazine hydrate

(0.074 g, 2.31 mmol) was added and refluxed for 1 h. The solvent was removed and the residue dissolved in  $\text{CH}_2\text{Cl}_2$ . The insoluble residue was removed by filtration. The filtrate was collected, solvent removed under high vacuum to afford the free amine as a semi-solid. The free amine was directly used in Section 3.1.4.2 without further purification. Yield (90%);  $^1\text{H}$  NMR (300 MHz,  $\text{DMSO}-d_6$ ):  $\delta$  1.60–1.70 (m, 2H), 1.76–1.84 (m, 2H), 2.78–2.83 (m, 2H), 3.28 (br, 2H), 3.63 (s, 4H), 3.79 (s, 8H), 3.93–3.97 (m, 2H), 6.23 (s, 2H), 7.05 (s, 1H), 7.10–7.14 (m, 4H), 7.56–7.64 (m, 8H), 8.48–8.50 (m, 4H).

**3.1.4.2. Preparation of compound 9.** Amine (0.75 g, 1.28 mmol) and  $\text{K}_2\text{CO}_3$  (0.88 g, 6.4 mmol) was stirred in dry THF under Ar atmosphere. NBD-Cl (0.28 g, 1.41 mmol) dissolved in dry THF was slowly added and the reaction mixture stirred in dark for 36 h. The reaction mixture was filtered to remove the  $\text{K}_2\text{CO}_3$  and concentrated under vacuum. The dark green semi-solid obtained was dissolved in  $\text{CH}_2\text{Cl}_2$ , washed with water, brine and dried over  $\text{MgSO}_4$ . The crude product was purified on an alumina column using  $\text{CHCl}_3$  as eluent. Yield 70%;  $^1\text{H}$  NMR (300 MHz,  $\text{CD}_3\text{OD}$ ):  $\delta$  1.86 (br, 4H), 3.52 (s, 6H), 3.66 (s, 8H), 3.98 (m, 2H), 6.20 (d,  $J=9$  Hz, 1H), 6.73 (s, 2H), 6.92 (s, 1H), 7.13–7.18 (m, 4H), 7.54–7.68 (m, 8H), 8.30–8.33 (m, 5H);  $^{13}\text{C}$  NMR (75 MHz,  $\text{CDCl}_3$ ):  $\delta$  25.6, 26.7, 43.9, 58.6, 60.1, 67.3, 98.7, 113.7, 113.9, 122.2, 122.3, 123.0, 136.6, 140.7, 140.9, 144.2, 144.5, 149.2, 158.8, 159.9, 168.3; FAB MS  $m/z$  751  $[\text{M}+\text{H}^+]$ .

**3.1.5. Synthesis of compound 1.** A methanolic solution of compound 9 (0.187 g, 0.25 mmol) and an aqueous solution of zinc nitrate (0.1521 g, 0.512 mmol) were mixed and stirred for 0.5 h. The solvent was removed and the residue lyophilized to afford the complex 1 in quantitative yield.

**3.1.6. Synthesis of compound 10.** 3,5-Bis-hydroxymethyl phenol (1.35 g, 8.74 mmol), *N*-Boc- $\{2-[2-(2\text{-bromoethoxy})\text{-ethoxy}]\text{-ethyl}\}$  monoamine (3.0 g, 9.61 mmol) and  $\text{K}_2\text{CO}_3$  (6.63 g, 48.05 mmol) were mixed in acetonitrile and refluxed for 24 h. The reaction mixture was then cooled to room temperature and the solvent removed. The residue was dissolved in  $\text{CH}_2\text{Cl}_2$  and the insoluble residue filtered off. The filtrate was washed with water and dried over  $\text{MgSO}_4$ . The pure product was obtained as a semi-solid after purification on a silica column using EtOAc. Yield 89%;  $^1\text{H}$  NMR (300 MHz,  $\text{CDCl}_3$ ):  $\delta$  1.44 (s, 9H), 3.05–3.30 (br, 2H), 3.30 (br, 2H), 3.45–3.50 (m, 2H), 3.55–3.70 (m, 4H), 3.78 (m, 2H), 4.05 (m, 2H), 4.53 (s, 4H), 5.20 (br, 1H), 6.73 (s, 2H), 6.83 (s, 1H);  $^{13}\text{C}$  NMR (75 MHz,  $\text{CDCl}_3$ ):  $\delta$  28.6, 40.8, 60.6, 65.1, 67.6, 70.0, 70.5, 71.0, 79.6, 112.3, 117.9, 143.1, 156.3, 159.4.

**3.1.7. Synthesis of compound 11.** Synthesized according to procedure given in Section 3.1.2. Yield 70%;  $^1\text{H}$  NMR (300 MHz,  $\text{CDCl}_3$ ):  $\delta$  1.44 (s, 9H), 3.34 (m, 2H), 3.56 (m, 2H), 3.64–3.67 (m, 2H), 3.71–3.74 (m, 2H), 3.85–3.88 (m, 2H), 4.15–4.18 (m, 2H), 4.43 (s, 4H), 5.00 (br, 1H), 6.90 (s, 2H), 7.01 (s, 1H);  $^{13}\text{C}$  NMR (75 MHz,  $\text{CDCl}_3$ ):  $\delta$  28.6, 33.0, 40.0, 67.6, 69.7, 70.5, 71.0, 115.6, 122.6, 140.0, 159.0.

**3.1.8. Synthesis of compound 12.** Synthesized according to procedure given in Section 3.1.3. Yield 87%;  $^1\text{H}$  NMR

(300 MHz,  $\text{CDCl}_3$ ):  $\delta$  1.42 (s, 9H), 3.32 (m, 2H), 3.54 (m, 2H), 3.63–3.66 (m, 6H), 3.70–3.73 (m, 2H), 3.80 (s, 8H), 3.86 (m, 2H), 4.14 (m, 2H), 5.05 (br, 1H), 6.89 (s, 2H), 7.07 (s, 1H), 7.10–7.15 (m, 4H), 7.56–7.65 (m, 8H), 8.49–8.52 (m, 4H);  $^{13}\text{C}$  NMR (75 MHz,  $\text{CDCl}_3$ ):  $\delta$  28.6, 40.6, 58.8, 60.3, 67.4, 70.0, 70.5, 70.9, 113.8, 121.9, 122.2, 122.9, 136.6, 140.8, 149.2, 159.1, 160.0; FAB MS  $m/z$  748  $[\text{M}+\text{H}^+]$ .

### 3.1.9. Synthesis of compound 13.

**3.1.9.1. Generation of free amine from 12.** Compound 12 (1.073 g, 1.43 mmol) was dissolved in 6.9 mL of 50% TFA in dry  $\text{CH}_2\text{Cl}_2$  at 0 °C under  $\text{N}_2$  atmosphere. The reaction mixture was stirred at room temperature for 2 h. After removing TFA, the residue was taken in  $\text{CH}_2\text{Cl}_2$  and neutralized with satd  $\text{Na}_2\text{CO}_3$ . The aqueous layer was extracted with  $\text{CH}_2\text{Cl}_2$  (3  $\times$  20 mL) and the combined organic layer dried over  $\text{MgSO}_4$ . The solvent was removed under vacuum to yield the free amine (85%), which was directly used for the next step.

**3.1.9.2. Synthesis of compound 13.** Synthesized according to procedure given in Section 3.1.4.2. Yield 70%;  $^1\text{H}$  NMR (300 MHz,  $\text{CDCl}_3$ ):  $\delta$  3.64 (br, 6H), 3.74–3.78 (m, 12H), 3.85–3.92 (m, 4H), 4.16–4.19 (m, 2H), 6.11 (d,  $J=8.7$  Hz, 1H), 6.85 (s, 2H), 7.07 (s, 1H), 7.11–7.20 (m, 5H), 7.55–7.64 (m, 8H), 8.39 (d,  $J=8.7$  Hz, 1H), 8.49–8.51 (m, 4H);  $^{13}\text{C}$  NMR (75 MHz,  $\text{CDCl}_3$ ):  $\delta$  43.9, 58.7, 60.2, 67.5, 68.5, 70.1, 70.8, 71.1, 98.9, 113.8, 122.0, 122.2, 122.9, 128.7, 130.7, 136.5, 136.6, 140.7, 144.1, 144.4, 149.2, 158.9, 159.8; FAB MS  $m/z$  811  $[\text{M}+\text{H}^+]$ .

**3.1.10. Preparation of compound 2.** Synthesized according to the procedure given in Section 3.1.5.

**3.1.11. Synthesis of compound 14.** 3-Hydroxy benzyl-alcohol (1 mmol), *N*-(4-bromobutyl)phthalimide (1.01 mmol) and  $\text{K}_2\text{CO}_3$  (5 mmol) were mixed in acetonitrile and refluxed for 12 h. The work up and purification were done according to procedure given in Section 3.1.1. Yield 67%;  $^1\text{H}$  NMR (300 MHz,  $\text{CDCl}_3$ ):  $\delta$  1.96–2.05 (m, 4H), 2.39 (br, 1H), 3.91 (m, 2H), 4.15 (t,  $J=5.7$  Hz, 2H), 4.80 (s, 2H), 6.93–6.96 (m, 1H), 7.05–7.07 (m, 2H), 7.36–7.41 (m, 1H), 7.85–7.89 (m, 2H), 7.96–8.01 (m, 2H);  $^{13}\text{C}$  NMR (75 MHz,  $\text{CDCl}_3$ ):  $\delta$  25.4, 26.7, 37.7, 65.2, 67.2, 113.0, 113.8, 119.2, 123.3, 129.6, 132.1, 134.1, 142.8, 159.2, 168.6.

**3.1.12. Synthesis of compound 15.** Compound 14 (1 mmol),  $\text{CBr}_4$  (1.1 mmol) were dissolved in dry  $\text{CH}_2\text{Cl}_2$  and  $\text{Ph}_3\text{P}$  (1.05 mmol) dissolved in dry  $\text{CH}_2\text{Cl}_2$  slowly added over a period of 15 min. The reaction mixture was stirred at room temperature for 12 h. The solvent was removed and the residue chromatographed on a silica column using gradient elution with EtOAc/Hex (1:1). Yield 85%;  $^1\text{H}$  NMR (300 MHz,  $\text{CDCl}_3$ ):  $\delta$  1.83–1.92 (m, 4H), 3.78 (m, 2H), 4.00 (m, 2H), 4.45 (s, 2H), 6.79–6.83 (m, 1H), 6.90 (m, 1H), 6.94–6.96 (m, 1H), 7.20–7.25 (m, 1H), 7.70–7.75 (m, 2H), 7.84–7.87 (m, 2H);  $^{13}\text{C}$  NMR (75 MHz,  $\text{CDCl}_3$ ):  $\delta$  25.6, 26.8, 33.8, 37.9, 67.4, 114.9, 115.3, 121.5, 123.5, 130.0, 132.4, 134.2, 139.5, 159.4, 168.7.

**3.1.13. Synthesis of compound 16.** Compound 15 (1 mmol),  $\text{K}_2\text{CO}_3$  (5 mmol) and 2,2'-dipicolylamine (1.2 mmol) were

mixed in dry DMF under N<sub>2</sub> atmosphere and the reaction mixture stirred for 5 h. The work up and purification were carried out according procedure given in Section 3.1.3. Yield 93%; <sup>1</sup>H NMR (300 MHz, CDCl<sub>3</sub>): δ 1.86–1.91 (m, 4H), 3.67 (s, 2H), 3.75–3.79 (m, 2H), 3.83 (s, 4H), 3.97–4.01 (m, 2H), 6.74–6.77 (m, 1H), 6.97–7.00 (m, 2H), 7.12–7.23 (m, 3H), 7.59–7.74 (m, 6H), 7.83–7.87 (m, 2H), 8.51–8.53 (m, 2H); <sup>13</sup>C NMR (75 MHz, CDCl<sub>3</sub>): δ 25.6, 26.9, 37.9, 58.6, 60.0, 67.3, 113.3, 115.3, 121.4, 122.3, 123.2, 123.4, 129.5, 132.3, 134.2, 136.8, 149.1, 159.3, 168.7.

**3.1.14. Synthesis of compound 17.** Synthesized according to procedure given in Section 3.1.4. Yield 72%; <sup>1</sup>H NMR (300 MHz, DMSO-*d*<sub>6</sub>): δ 1.83 (br, 4H), 3.54 (br, 2H), 3.60 (s, 2H), 3.70 (s, 4H), 4.01 (m, 2H), 6.42 (d, *J*=9 Hz, 1H), 6.68–6.81 (m, 1H), 6.95–6.97 (m, 2H), 7.19–7.26 (m, 3H), 7.56 (d, *J*=7.5 Hz, 2H), 7.75–7.80 (m, 2H), 8.47–8.49 (m, 3H), 9.58 (m, 1H); <sup>13</sup>C NMR (75 MHz, DMSO-*d*<sub>6</sub>): δ 24.4, 26.1, 43.0, 57.3, 59.0, 66.9, 99.1, 113.0, 114.7, 120.7, 122.2, 122.5, 129.3, 136.6, 137.9, 140.1, 144.2, 144.4, 145.2, 148.8, 158.6, 158.9; FAB MS *m/z* 540 [M+H<sup>+</sup>].

**3.1.15. Preparation of Zn complex 3.** A methanolic solution of compound 17 (1 mmol) and an aqueous solution of zinc nitrate (1.025 mmol) were mixed and stirred for 0.5 h. The solvent was removed and the residue lyophilized to afford the complex 3 in quantitative yield.

**3.1.16. Synthesis of compound 18.** 3-Hydroxy benzylalcohol (1 mmol), *N*-Boc-{2-[2-(2-bromoethoxy)-ethoxy]-ethyl} monoamine (1.01 mmol) and K<sub>2</sub>CO<sub>3</sub> (5 mmol) were mixed in acetonitrile and refluxed for 12 h. The work up and purification were done according to procedure given in Section 3.1.6. Yield 89%; <sup>1</sup>H NMR (300 MHz, CDCl<sub>3</sub>): δ 1.46 (s, 9H), 2.01 (br, 1H), 3.32 (m, 2H), 3.56–3.58 (m, 2H), 3.61–3.76 (m, 4H), 3.87–3.90 (m, 2H), 4.12–4.20 (m, 2H), 4.65–4.69 (m, 2H), 5.09 (br, 1H), 6.85–6.88 (m, 1H), 6.95 (m, 2H), 7.26–7.31 (m, 1H); <sup>13</sup>C NMR (75 MHz, CDCl<sub>3</sub>): δ 28.6, 40.8, 65.4, 67.6, 70.0, 70.5, 71.0, 79.6, 113.3, 114.1, 119.6, 129.8, 143.0, 156.3, 159.3.

**3.1.17. Synthesis of compound 19.** Synthesized according to procedure given in Section 3.1.12. Yield 65%; <sup>1</sup>H NMR (300 MHz, CDCl<sub>3</sub>): δ 1.43 (s, 9H), 3.20 (br, 2H), 3.55 (m, 2H), 3.63–3.66 (m, 2H), 3.70–3.74 (m, 2H), 3.85–3.88 (m, 2H), 4.13–4.17 (m, 2H), 4.46 (s, 2H), 5.01 (br, 1H), 6.84–6.88 (m, 1H), 6.95–7.00 (m, 2H), 7.23–7.27 (m, 1H); <sup>13</sup>C NMR (75 MHz, CDCl<sub>3</sub>): δ 28.7, 33.7, 40.7, 67.7, 70.0, 70.6, 71.0, 115.1, 115.5, 121.8, 130.1, 139.4, 156.2, 159.2.

**3.1.18. Synthesis of compound 20.** Synthesized according to procedure given in Section 3.1.13. Yield 87%; <sup>1</sup>H NMR (300 MHz, DMSO-*d*<sub>6</sub>): δ 1.35 (s, 9H), 3.03–3.09 (m, 2H), 3.32–3.40 (m, 2H), 3.50–3.53 (m, 2H), 3.56–3.60 (m, 4H), 3.71–3.75 (m, 6H), 4.05–4.08 (m, 2H), 6.75–6.83 (m, 2H), 6.97–7.00 (m, 2H), 7.21–7.28 (m, 3H), 7.57–7.60 (m, 2H), 7.76–7.82 (m, 2H), 8.48–8.50 (m, 2H); <sup>13</sup>C NMR (75 MHz, DMSO-*d*<sub>6</sub>): δ 28.2, 39.7, 57.3, 59.1, 66.9, 68.9, 69.2, 69.5, 69.9, 112.9, 114.6, 120.8, 122.2, 122.4, 129.3, 136.6, 140.4, 148.8, 155.6, 158.5, 159.1.

**3.1.19. Synthesis of compound 21.** Synthesized according to procedure given in Section 3.1.9. Yield 76%; <sup>1</sup>H NMR

(300 MHz, DMSO-*d*<sub>6</sub>): δ 3.59–3.72 (m, 16H), 4.01–4.04 (m, 2H), 6.44 (d, *J*=9 Hz, 1H), 6.75–6.78 (m, 1H), 6.94–6.97 (m, 2H), 7.18–7.26 (m, 3H), 7.56 (d, *J*=7.8 Hz, 2H), 7.75–7.80 (m, 2H), 8.45–8.49 (m, 3H), 9.44 (br, 1H); <sup>13</sup>C NMR (75 MHz, DMSO-*d*<sub>6</sub>): δ 43.4, 57.3, 59.0, 66.9, 68.0, 69.0, 69.9, 99.5, 112.8, 114.6, 120.8, 122.2, 122.4, 129.3, 136.6, 137.8, 140.3, 144.4, 145.3, 148.8, 158.4, 159.1; FAB MS *m/z* 600 [M+H<sup>+</sup>].

**3.1.20. Synthesis of compound 4.** Synthesized according to procedure given in Section 3.1.15.

## 3.2. Vesicle preparations

All lipids were purchased from Avanti Polar Lipids, Inc. (Alabaster, AL) and stored as 10 mg/mL stock solutions in CHCl<sub>3</sub> at –20 °C. Lipids were added in the appropriate ratios to a 10 mL round bottom flask and solvent removed by rotary evaporation. Residual solvent was removed under oil pump vacuum for ≥ 1 h. Dried lipid was then rehydrated in TES buffer (5 mM TES, 145 mM NaCl, pH 7.4). A glass pyrex ring was added to the flasks to ensure complete removal of lipid from the flask walls, and then flasks were vortexed vigorously. The resulting lipid dispersion was then extruded approximately 30 times through a 19 mm diameter polycarbonate membrane with 200 nm pore diameter. All vesicles were prepared at room temperature and used the same day.

## 3.3. Fluorescence spectroscopy

All fluorescence spectroscopy was performed on a Perkin Elmer LS50B fluorimeter with FT WinLab software using standard 1×1×5 cm<sup>3</sup> cuvettes. NBD fluorescence was measured using excitation and emission wavelengths of 470 and 530 nm, respectively. A 515 nm cutoff filter was used in all NBD acquisitions. Carboxyfluorescein fluorescence was measured with monochromator excitation and emission wavelengths of 495 and 520 nm, respectively, with an open filter. All measurements were performed at 25 °C without degassing of samples.

## 3.4. Carboxyfluorescein leakage

Vesicles of the appropriate composition were prepared as described, with the following exceptions. Lipids were rehydrated after drying with TES buffer (5 mM TES, 100 mM NaCl, pH 7.4) containing 50 mM (5–6)carboxyfluorescein. Following extrusion, vesicles were separated from excess carboxyfluorescein using a Sephadex G-45 column. The fluorescence intensity of a 3 mL sample of 50 μM vesicles was monitored for 400 s. At time 100 s, an appropriate volume of a 1 mM solution of 1 in TES buffer was added to the cuvette, followed by Triton X-100 detergent (0.5%) at time 300 s. Zero and 100% leakage was determined from the initial fluorescence and the fluorescence after addition of detergent, respectively.

## 3.5. Vesicle titrations

Stock solutions of compounds 1, 2, 3 or 4 were diluted in TES buffer to a final concentration of 1 μM in a 5 mL cuvette. With stirring, aliquots of 10 mM phospholipid



vesicles of the appropriate composition were sequentially added to the solution to give the desired phospholipid concentration over the range 0–100  $\mu\text{M}$ . After each addition, the fluorescence intensity was measured after a twenty-second incubation. Curves of fluorescence intensity ( $\lambda_{530}$ ) versus available phospholipid concentration (taken as 60% of the total phospholipid concentration) were generated and fitted to a 1:1 binding model.<sup>28</sup> An iterative curve-fitting method yielded the apparent binding constants listed in Tables 1 and 2, all of which represent the average of at least three independent measurements.

### 3.6. Sensor permeation

To a 45 mL solution of 25  $\mu\text{M}$  phospholipid vesicles composed either of 100% POPC or 1:1 POPC-POPS, compound **1** or **2** was added to a final concentration of either 0.5 or 2.0 mol%. A 3.0 mL aliquot of the resulting solution was removed at predetermined intervals over a two-hour period and placed in a 5 mL cuvette. Fluorescence intensity of each aliquot was monitored over a 200 s interval. At 50 s, sodium dithionite was added to the cuvette to a final concentration of 55 mM. At 150 s, 0.2% octaethylene glycol monododecyl ether was added to disrupt vesicle membranes and expose any internalized NBD-labeled compounds to the aqueous environment.

### Acknowledgements

This work was supported by the National Institutes of Health, the Department of Defense, and the Phillip Morris External Research Program.

### References and notes

- Sgonc, R.; Gruber, J. *Exp. Gerontol.* **1998**, *33*, 525–533 and references cited therein.
- Gorczyca, W. *Endocr-Relat. Cancer* **1999**, *6*, 17–19.
- Brauer, M. *Prog. Neuro-Psychoph.* **2003**, *27*, 323–331.
- Waterhouse, N. J.; Trapani, J. A. *Cell Death Differ.* **2003**, *10*, 853–855.
- Stadelmann, C.; Lassmann, H. *Cell Tissue Res.* **2000**, *301*, 19–31.
- Lecoeur, H. *Exp. Cell Res.* **2002**, *277*, 1–14.
- Laxman, B.; Hall, D. E.; Bhojani, S. B.; Hamstra, D. A.; Chenevert, T. L.; Ross, B. D.; Rehemtulla, A. *Proc. Natl. Acad. Sci. U.S.A.* **2002**, *99*, 16551–16555.
- Bivèn, K.; Erdal, H.; Hägg, M.; Ueno, T.; Zhou, R.; Lynch, M.; Rowley, B.; Wood, J.; Zhang, C.; Toi, M.; Shoshan, M. C.; Linder, S. *Apoptosis* **2003**, *8*, 263–268.
- Koopman, G.; Kuijten, R. M. J.; Keehnen, R. M. J.; Pals, S. T.; van Oers, M. H. J. *Blood* **1994**, *84*, 1415–1420.
- Vermes, I.; Haanen, C.; Steffens-Nakken, H.; Reutelingsperger, C. *J. Immunol. Methods* **1995**, *184*, 39–51.
- van Engeland, M.; Nieland, L. J. W.; Ramaekers, F. C. S.; Schutte, B.; Reutelingsperger, C. P. M. *Cytometry* **1998**, *31*, 1–9.
- Liemann, S.; Huber, R. *CLMS, Cell. Mol. Life Sci.* **1997**, *53*, 516–521.
- Gerke, V.; Moss, S. E. *Physiol. Rev.* **2002**, *82*, 331–371.
- Kamp, D.; Sieberg, T.; Haest, C. W. M. *Biochemistry* **2001**, *40*, 9438–9446.
- Zweifach, A. *Biochem. J.* **2000**, *349*, 255–260.
- Sairjo, M. A.; Concha, N. M.; Dedman, J. R.; Seaton, B. A. *Nat. Struct. Biol.* **1995**, *2*, 968–974.
- Czarnik, A. W. *Acc. Chem. Res.* **1994**, *27*, 302–308.
- Matsuda, S.; Ishikubo, A.; Kuzuya, A.; Yashiro, M.; Komiyama, M. *Angew. Chem., Int. Ed.* **1998**, *37*, 3284–3286.
- Lee, D. H.; Im, J. H.; Son, S. U.; Chung, Y. K.; Hong, J. I. *J. Am. Chem. Soc.* **2003**, *125*, 7752–7753.
- Ojida, A.; Mito-oka, Y.; Inoue, M.; Hamachi, I. *J. Am. Chem. Soc.* **2002**, *124*, 6256–6258.
- Koulov, A. V.; Stucker, K. A.; Lakshmi, C.; Smith, B. D. *Cell Death Differ.* **2003**, *10*, 1357–1359.
- Ashton, R. A.; Anderson, D. W.; Brown, C. L.; Shipway, A. N.; Stoddart, J. F.; Tolley, M. S. *Chem. Eur. J.* **1998**, *4*, 781–795.
- Delphine, F.; Gutierrez, N. M.; del Pilar, M.; Jean-Francois, G.; Michael, L.; Cornie, S.; Patrick, M.; Jean-Louis, G.; Benoit, H.; Daniel, G.; Jean-Francois, N. *Helv. Chim. Acta* **2002**, *85*, 288–319.
- Lancet, D.; Pecht, I. *Biochemistry* **1977**, *16*, 5150–5157.
- Lin, Su.; Struve, W. S. *Photochem. Photobiol.* **1991**, *54*, 361–365.
- Ojida, A.; Mito-oka, Y.; Sada, K.; Hamachi, I. *J. Am. Chem. Soc.* **2004**, *126*, 2454–2463.
- Borisenko, G.; Matsura, T.; Liu, S.; Tyurin, V. A.; Jainfei, J.; Serinkan, F. B.; Kagan, V. E. *Arch. Biochem. Biophys.* **2003**, *413*, 41–52.
- Xie, H.; Wu, S. *J. Chem. Soc., Perkin Trans. 2* **1999**, 2751–2754.